UNIVERSITEIT VAN PRETORIA
UNIVERSITY OF PRETORIA
YUNIBESITHI YA PRETORIA

Functional consequences of the inhibition of Malaria S-adenosylmethionine decarboxylase as a key regulator of polyamine and methionine metabolism

By

Salome Smit

Submitted in partial fulfillment of the requirements for the degree
Philosophiae Doctor

in the Faculty of Natural and Agricultural Science
Department of Biochemistry
University of Pretoria
Pretoria
South Africa

SUPERVISOR: Prof L Birkholtz
Department of Biochemistry, University of Pretoria

CO-SUPERVISOR: Prof AI Louw
Department of Biochemistry, University of Pretoria

November 2010

Acknowledgements

I acknowledge with gratitude the following people and institutions:

My supervisor, Prof Lyn-Marie Birkholtz for her guidance and especially her patience during the duration of this study.

Prof Braam Louw for insightful discussions.

The malaria team for their ideas and support for the duration of this study. It is hard to single out anybody but a special thanks to Katherine and Esmare for their willingness to always help with anything. Also a special word of thanks to Jeff for designing the Agilent probes and Shaun for helping with HPLC work. Sandra for her willingness to always help with anything.

Dr Franz Birkholtz that were always willing to help with the drawing of blood for parasites despite his rooms being full of patients, it is much appreciated.

Dr Dalu Mancama from CSIR Biosciences for access to the MS laboratory and instruments.

Dr Stoyan Stochev from CSIR Biosciences for his help with the multitude of mass spectrometry experiments and analysis that were done.

Dr Isabelle Florent from Museum National d'Histoire Naturelle, Paris in France for the kind donation of the *Pf*A-M1 antibody.

Prof Choukri Ben Mamoun from the Department of Genetics and Developmental Biology, University of Connecticut, USA for the kind donation of the *Pf*PEMT antibody.

My parents for love and support and patience.

Lord, for giving me the capacity to endeavor such a project in my life.

Bursaries from funding authorities that has enabled me to continue with my studies: The University of Pretoria for a Doctoral post-graduate bursary, National Research Foundation for a NRF Prestigious Doctoral Bursary and the South African Malaria Initiative for awarding me a bridging fund to complete this PhD.

Summary

Malaria presents a global health risk that is becoming increasingly difficult to treat due to increased resistance of both the parasite and mosquito to all known drugs. Identification of novel drug targets are therefore essential in the fight against malaria. Polyamines are small flexible polycations that are represented by three basic polyamines. The interaction of polyamines with various macromolecules may lead to stabilisation of DNA, regulation of transcription, replication, and also have an important role in cellular differentiation, proliferation, growth and division. Therefore, disruption of polyamine biosynthesis presents a unique drug target worth exploiting. Polyamine biosynthesis in *P. falciparum* is regulated by a unique bifunctional S-adenosylmethionine decarboxylase/ornithine decarboxylase (AdoMetDC/ODC) complex, which is unique to *P. falciparum* and differs completely from human polyamine biosyntehsis. The inhibition of AdoMetDC induces spermidine and subsequent spermine depletion within the parasite that ultimately results in cell cycle arrest. A functional genomics approach was used within this study to identify a global response of the parasite due to the inhibition of AdoMetDC with the irreversible inhibitor, MDL73811.

The proteomics approach was optimised for conditions specific to our laboratory with regard to protein extraction, Plasmodial protein quantification, spot detection and finally protein identification by mass spectrometry (MS). This methodology resulted in reliable spot detection and achieved a 95% success rate in MS/MS identification of protein spots. Application of this methodology to the analyses of the Plasmodial ring and trophozoite proteomes ultimately resulted in the identification of 125 protein spots from the Plasmodial ring and trophozoite stages, which also confirmed stage specific protein production. Various protein isoforms were present which may be of significant biological importance within the Plasmodial parasite during development in the intraerythrocytic developmental cycle.

Subsequent application of the 2-DE methodology to the proteome of AdoMetDC inhibited parasites resulted in the identification of 61 unique Plasmodial protein groups that were differentially affected by the inhibition of AdoMetDC in 2 time points. The transcriptome of AdoMetDC inhibited parasites were also investigated at 3 time points. Investigation into the transcriptome revealed the differential regulation of 549 transcripts, which included the differential regulation of polyamine specific transcripts. Inhibition of AdoMetDC provided a unique polyamine specific transcriptomic signature profile that demonstrated unique interactions between AdoMetDC inhibition and folate biosynthesis, redox metabolism and cytoskeleton biogenesis. The results presented provide evidence that the parasite responds to AdoMetDC inhibition by the regulation of

the transcriptome and proteome in an attempt to alleviate the effects of AdoMetDC inhibition. Further analyses of the metabolome also provided evidence for the tight regulation of the AdoMet cycle. Overall, this study demonstrated important functional consequences as a result of AdoMetDC inhibition.

Table of Contents

Acknowledgements ..... **i**

Summary ..... **ii**

Table of Contents ..... **iv**

List of Figures ..... **viii**

List of Tables ..... **xi**

List of Abbreviations ..... **xiii**

CHAPTER 1 ..... **1**

Introduction **1**

1.1 The statistics *1*

1.2 The economic burden of malaria *3*

1.3 History of malaria *4*

1.4 Life cycle *4*

1.5 Pathogenesis *6*

1.6 Eradication efforts against malaria *8*
1.6.1 Insecticide resistance – the use of spraying and bed nets 10
1.6.2 Vaccines 10

1.7 Currently used drugs and drug resistance *11*
1.7.1 Chloroquine 12
1.7.2 Antifolates 14
1.7.3 Artemisinin 15

1.8 New drug targets *20*

1.9 Polyamines *22*
1.9.1 Polyamine synthesis 23

1.10 The "omics" era *26*
1.10.1 Transcriptomics 26
1.10.2 Proteomics 27
1.10.3 The Metabolome, kinome and interactome 28

1.11 The use of functional genomics to validate drug targets *28*

1.12 Objective *29*
1.12.1 Aims: 30
1.12.2 Papers resulting from the work presented within this dissertation 30
1.12.2 Conferences attended 31

CHAPTER 2 ..... **32**

Proteomic profiling of *P. falciparum* through improved, semi-quantitative two-dimensional gel electrophoresis **32**

2.1 Introduction *32*
2.1.1 Minimum information about a proteomics experiment 33
2.1.2 Liquid chromatography mass spectrometry and protein arrays used for proteomics 33

2.1.3 Plasmodial and parasite proteomics ... 34

2.2 Methods ... *37*
2.2.1 Blood collection ... 37
2.2.2 Thawing of parasites ... 37
2.2.3 Daily maintenance of parasites ... 37
2.2.4 Synchronisation ... 38
2.2.5 Culturing of parasites for proteomics ... 38
2.2.6 Protein preparation ... 39
2.2.7 Protein quantification ... 39
2.2.8 SDS-PAGE gels ... 41
2.2.9 Two-dimensional gel electrophoresis (2-DE) ... 41
2.2.10 Staining of 2-DE gels ... 42
2.2.11 Image Analysis of 2-DE gels by PD Quest ... 44
2.2.12 2-DE spot identification by tandem mass spectrometry ... 45
2.2.13 Submitting MS/MS data to the MASCOT database ... 46

2.3 Results ... *47*

A: Optimisation of Plasmodial proteins for 2-DE ... *47*
2.3.1 Protein concentration determination of Plasmodial proteins ... 47
2.3.2 Stain performance on SDS-PAGE using standard protein markers ... 48
2.3.3 Stain performance on 2-DE using Plasmodial proteins ... 49
2.3.4 Filtering of trophozoite data ... 51
2.3.5 Compatibility of the 4 stains with MALDI-TOF MS/MS ... 51

B: Application of 2-DE optimised method on the Plasmodial ring and trophozoite stages ... *53*
2.3.6 2-DE analysis of the Plasmodial proteome ... 53
2.3.7 Comparison of ring, trophozoite and schizont proteome ... 59
2.3.8 Comparison of proteomic data with transcript levels ... 61
2.3.9 Differential expression of isoforms ... 62

2.4 Discussion ... *64*
2.4.1 Optimisation of Plasmodial proteins for 2-DE ... 64
2.4.2 Application of 2-DE optimised method on the Plasmodial ring and trophozoite stages ... 67

Chapter 3 ... **71**

Proteome consequences of *P. falciparum* AdoMetDC inhibition with MDL73811 ... **71**

3.1 Introduction ... *71*
3.1.1 Plasmodial perturbation studies investigated by proteomics ... 71
3.1.2 Perturbation of polyamine metabolism on the proteome ... 73

3.2 Methods ... *74*
3.2.1 Malaria SYBR Green I-based fluorescence (MSF) assay for IC_{50} determination ... 74
3.2.2 Morphology study ... 74
3.2.3 Culturing for the proteomic time study ... 75
3.2.4 Protein preparation ... 75
3.2.5 Protein quantification by 2-D Quant kit ... 76
3.2.6 SDS-PAGE gels ... 76
3.2.7 1-DE SDS-PAGE spot identification by LC-ESI-MS/MS ... 76
3.2.8 Two-dimensional gel electrophoresis (2-DE) and staining ... 77
3.2.9 Image Analysis of 2-DE gels by PD Quest ... 78
3.2.10 2-DE spot identification by tandem mass spectrometry ... 79
3.2.11 Western blots ... 79

3.3 Results ... *81*
3.3.1 IC_{50} determination of MDL73811 ... 81
3.3.2 Morphological evaluation of *P. falciparum* 3D7 inhibited by MDL73811 over a complete life cycle ... 81
3.3.3 SDS-PAGE analysis of perturbed parasites and functional analysis of differentially regulated bands ... 83

3.3.4 2-DE analysis of AdoMetDC inhibited parasites ... 88
3.3.5 Protein identification of differentially affected protein spots from the AdoMetDC inhibited proteome ... 92
3.3.6 1-DE SDS-PAGE and 2-DE gels as complementary proteomic techniques ... 100
3.3.7 Hierarchical clustering of differentially expressed proteins from the proteome. ... 100
3.3.8 Functional classification of the differentially affected proteins identified from the proteome. ... 101
3.3.9 Changes in protein abundance in the proteome of AdoMetDC inhibited parasites over time. ... 104
3.3.10 Validation of differential proteomic data ... 106

3.4 Discussion ... 108

CHAPTER 4 ... 115

Transcriptional responses of *P. falciparum* to inhibition of AdoMetDC with MDL73811 ... 115

4.1 Introduction ... 115
4.1.1 Transcriptomic perturbation studies in other organisms ... 115
4.1.2 Microarray platforms ... 116
4.1.3 Experimental design and normalisation methods ... 117
4.1.4 Minimum information about a microarray experiment (MIAME) ... 118
4.1.5 Transcriptomic perturbation studies in Plasmodial parasites ... 119
4.1.6 Polyamine perturbation studies on Plasmodial parasites ... 120

4.2 Methods ... 122
4.2.1 Culturing of parasites for transcriptomics ... 122
4.2.2 RNA isolation from cultured parasites ... 122
4.2.3 RNA integrity determination ... 123
4.2.4 cDNA synthesis from RNA ... 123
4.2.5 cDNA labelling for hybridisation ... 124
4.2.6 Slide assembly and sample preparation for oligonucleotide hybridisation ... 125
4.2.7 Post-hybridisation, washing and slide scanning ... 126
4.2.8 Data analysis ... 126
4.2.9 Validation of microarray results with qRT-PCR ... 129

4.3 Results ... 130
4.3.1 RNA quality assessment ... 130
4.3.2 Microarray preparation ... 131
4.3.3 Normalisation of data ... 132
4.3.4 Pearson correlations of the three time points ... 137
4.3.5 Data analysis of differentially expressed transcripts ... 137
4.3.6 Biological classification of differentially expressed transcripts ... 140
4.3.7 Hierarchical clustering of the AdoMetDC inhibited transcripts ... 143
4.3.8 Transcript regulation of polyamine-specific transcripts followed over all 3 time points ... 146
4.3.9 Identification of uniquely affected Plasmodial pathways as a result of AdoMetDC inhibition ... 147
4.3.10 Interactions of the AdoMetDC inhibited transcriptome ... 149
4.3.11 Comparison of AdoMetDC inhibited transcriptome dataset to the transcriptomes of inhibited AdoMetDC/ODC and inhibited spermidine synthase ... 152
4.3.12 Comparison of AdoMetDC inhibited transcriptome dataset to other *P. falciparum* perturbation data ... 154
4.3.13 Validation of microarray results with real-time PCR ... 158

4.4 Discussion ... 160

Chapter 5 ... 168

Characterisation of specific metabolic responses identified in the transcriptomic and proteomic investigations of AdoMetDC inhibition in *P. falciparum* ... 168

5.1 Introduction ... 168
5.1.1 Transcriptional and translational control ... 168

5.1.2 DNA methylation 169
5.1.3 Regulation of AdoMet levels 170

5.2 Methods 171
5.2.1 Culturing of parasites for the determination of the methylation status 171
5.2.2 gDNA isolation from *P. falciparum* for the determination of the methylation status 171
5.2.3 South-Western immunoblot for methylation detection 172
5.2.4 Determination of polyamine-specific transcripts by the addition of methionine to parasite cultures 172
5.2.5 RNA isolation and cDNA synthesis of the metabolite treated parasites 173
5.2.6 Quantitative real-time PCR of methionine-treated parasites 173
5.2.7 Metabolite extractions for S-adenosylmethionine (AdoMet) and S-adenosylhomocysteine (AdoHcy) 173
5.2.8 Malaria SYBR Green I-based fluorescence (MSF) assay for synergy determination 174
5.2.10 Primer design 176

5.3 Results 177
5.3.1 Methylation status of *Pf*AdoMetDC inhibited parasites 177
5.3.2 Determination of AdoMet and AdoHcy metabolite levels upon inhibition of AdoMetDC 178
5.3.3 Polyamines and the folate pathway 178
5.3.4 Methionine perturbation of parasites 182
5.3.5 Comparison of transcriptomic and proteomic data 183

5.4 Discussion 187

CHAPTER 6 193

Concluding discussion 193

References 203

Appendix A-E

List of Figures

Figure 1.1: Estimated worldwide deaths (in millions) from malaria in 2006 2

Figure 1.2: Distribution of *P. falciparum* 3

Figure 1.3: The Plasmodial life cycle. 5

Figure 1.4: Timeline of some of the most important milestones in the fight against malaria. 9

Figure 1.5: Proposed mechanism of action of quinoline-based drugs. 14

Figure 1.6: Proposed mechanism of action of anti-folate drugs. 15

Figure 1.7: Proposed mechanism of action of artemisinin based drugs. 17

Figure 1.8: Chemical structures of the polyamines, putrescine, spermidine and spermine. 22

Figure 1.9: Polyamine metabolism in mammalian cells and in *Plasmodium* 23

Figure 1.10: Polyamine content of erythrocytes. 25

Figure 1.11: Structure of MDL73811 25

Figure 1.12: The phaseograms of the IDC of three Plasmodial strains depicted over a 48 hour period 27

Figure 1.13: Functional genomics workflow 29

Figure 2.1: The state of proteomic publications per year as on ISI Web of Science. 35

Figure 2.2: Comparison of 4 different protein concentration determination methodologies 47

Figure 2.3: Comparison of standard proteins on SDS PAGE gels using 4 different stains. 49

Figure 2.4: Comparison of Plasmodial proteins on 2-DE gels using 4 different stains. 50

Figure 2.5: Plot of the total trophozoite proteome 51

Figure 2.6: 2-DE of the rings and trophozoites stage *P. falciparum* indicating identified proteins. 54

Figure 2.7: Venn diagram of 3 stages investigated by proteomics in *P. falciparum*. 60

Figure 2.8: Proteins that are differentially regulated in the *P. falciparum* ring and trophozoite stage proteomes. 62

Figure 2.9: Isoforms of proteins that are differentially regulated in the *P. falciparum* 63

Figure 3.1: A concentration response curve for the IC_{50} determination of MDL73811. 81

Figure 3.2: Morphology study of *Pf*3D7 parasites over a 48 hour life cycle. 83

Figure 3.3: 1-DE SDS-PAGE gels for the soluble and insoluble protein fractions. 85

Figure 3.4: The difference between a real protein spot and a dust speckle. 89

Figure 3.5: Creation of the master image used for detection of differentially affected proteins. 89

Figure 3.6: Determination of differentially affected protein spots..... 90

Figure 3.7: Differential protein spot abundance determined by PD Quest. 92

Figure 3.8: The MS spectra of s-adenosylmethionine synthase. 93

Figure 3.9 A: Master images of the Tt_1 (16 HPI) with the differentially affected protein spots. 95

Figure 3.9 B: Master images of the Tt_2 (20 HPI) with the differentially affected protein spots..... 96

Figure 3.10: Correlation between Plasmodial proteins identified from 2 complimentary proteomic approaches..... 100

Figure 3.11: Hierarchical clustering of the differentially affected spots..... 101

Figure 3.12: GO annotation for the regulated spots of both time points..... 102

Figure 3.13: Differential regulation of proteins over time in the AdoMetDC inhibited proteome..... 105

Figure 3.14: 2-DE Western blot of phosphoethanolamine N-methyltransferase. 106

Figure 3.15: 1-DE western blot validation of the protein abundance of M1-family aminopeptidase. 107

Figure 4.1: Microarray designs for time course experiments. 117

Figure 4.2: Common reference design used for the inhibition of AdoMetDC. 125

Figure 4.3: Transcriptomic sampling points. 130

Figure 4.4: Assessment of RNA purity and integrity from the *P. falciparum* RNA. 131

Figure 4.5: The 60-mer Agilent array for one UTt_3 and one Tt_3. 132

Figure 4.6: Red and green background images of slide Tt_3 array8..... 133

Figure 4.7: Boxplot data after Loess normalisation and Gquantile..... 134

Figure 4.8: Boxplots of Robust Spline normalisation 135

Figure 4.9: RG density plots after Robust Spline and Gquantile normalisation..... 136

Figure 4.10: MA plot of Tt_3 array 6 before and after normalisation of the data. 136

Figure 4.11: Log_2-distribution ratios and volcanoplots of the 3 time points investigated..... 138

Figure 4.12: Functional classification of regulated transcripts according to their GO terms. 140

Figure 4.13: A tight cluster (r =0.949) containing polyamine-related transcripts..... 144

Figure 4.14: Hierarchical clustering of polyamine-specific and oxidative stress transcripts. 145

Figure 4.15: Fold change of polyamine-specific transcripts over the 3 time points. 147

Figure 4.16: Polyamine and methionine metabolism affected by AdoMetDC inhibition..... 149

Figure 4.17: Correlation between transcript data from the AdoMetDC inhibited transcriptome dataset, co-inhibition of AdoMetDC/ODC and SpdS inhibition..... 152

Figure 4.18: Comparisons between the differentially affected transcriptomes of the AdoMetDC inhibited transcriptome dataset, febrile temperature perturbation, CQ inhibition and artesunuate inhibition. 155

Figure 5.1: Determination of gDNA methylation (5mC) in AdoMetDC inhibited parasites. 177

Figure 5.2: Metabolite levels of AdoMet and AdoHcy after AdoMetDC inhibition. 178

Figure 5.3: The combined influence of folate-free media and the irreversible AdoMetDC inhibitor MDL73811. 179

Figure 5.4: A dose response curve for the IC_{50} determination of MDL73811 and PYR. 180

Figure 5.5: A dose response curve for the determination of possible interactions between MDL73811 and PYR. 181

Figure 5.7: qRT-PCR of methionine treated parasites. 183

Figure 5.8: Venn diagram of similarities between the transcriptomic and proteomic data sets. 184

Figure 5.9: Correlation between transcript and protein abundance 186

Figure 6.1: Functional consequences of polyamine depletion induced by AdoMetDC inhibition. 201

List of Tables

Table 1.1: Summary of currently used drugs. 18

Table 1.2: Summary of potential new drug targets. 21

Table 2.1: Program settings used for Virsonic sonifier 39

Table 2.2: The IEF focusing steps used for the 13cm IPG, pH 3-10 L strips. 42

Table 2.3: Scan settings used on PD Quest and the Versadoc 3000 for the 4 stains used 44

Table 2.4: Comparative stain analysis for Plasmodial proteins analysed with 1-D SDS PAGE. 48

Table 2.5: Comparative stain analysis for Plasmodial proteins analysed with 1-D as well as 2-DE SDS PAGE. 52

Table 2.6: List of proteins identified by tandem mass spectrometry for late rings and early trophozoites 55

Table 2.7: Table of the proteins shared between each of the 3 life stages. 61

Table 3.1: The IEF focusing steps used for 18cm IPG, pH 3-10 L strips. 77

Table 3.2: Spot selection criteria for the 2 time points 78

Table 3.3: Differentially affected bands from AdoMetDC inhibited parasites identified from SDS-PAGE 86

Table 3.4: Data obtained from PD Quest 7.1.1 after spot detection of both the UT and T gels for t_1 and t_2. 91

Table 3.5: The total number of differentially affected protein spots for the 2 time points 92

Table 3.6: Protein spots identified by MS/MS for the AdoMetDC inhibited proteome at Tt_1 and Tt_2 97

Table 3.7: Biological functions of the differentially regulated proteins identified from the 2-DE gels 103

Table 4.1: Parameters set for automated spot detection using GenePix. 127

Table 4.2: Pearson correlations of the *Pf*AdoMetDC inhibited transcriptome data. 137

Table 4.3: The 25 most increased and decreased transcripts for AdoMetDC inhibited parasites. 139

Table 4.4: Biological functions of some of the differentially regulated transcripts for AdoMetDC. 141

Table 4.5: Unique metabolic pathway identification of the data from the inhibition of AdoMetDC. 148

Table 4.6: The top 20 interacting partners for AdoMetDC, and AdoMet synthase. 151

Table 4.7: Shared transcripts from the AdoMetDC inhibited transcriptome dataset, the co-inhibited AdoMetDC/ODC dataset and the inhibition of SpdS. 153

Table 4.8: Five transcripts shared between all of the perturbation studies. 156

Table 4.9: Unique transcripts associated with AdoMetDC perturbation. 157

Table 4.10: Nine of the unique transcripts only found in polyamine-regulated parasites. 158

Table 4.11: Comparison of microarray data with real-time PCR data. 159

Table 5.1: Existing primers 182

Table 5.2: Additional primers designed for determination of polyamine specificity 182

Table 5.3: Similar transcripts obtained for both the transcriptomic and proteomic data. 184

List of Abbreviations

µg	Microgram
µl	Microliter
1-DE	One-dimensional gel electrophoresis
2-DE	Two-dimensional gel electrophoresis
4mC	N4-methylcytosine
5mC	5-methylcytosine
6mA	N6-methyladenine
A	Adenosine
ACT	Artemisinin-based combination therapy
AdoHcy	S-adenosyl-L-homocysteine
AdoMet synthase	S-adenosylmethionine synthase
AdoMetDC	S-adenosylmethionine decarboxylase
AdoMetDC/ODC	S-adenosylmethionine decarboxylase/Ornithine decarboxylase
AHC	S-adenosyl-L-homocysteine hydrolase
AM	Artemether
AMA	Apical membrane antigen
Arg	Arginine
ART	Artemisinin
AS	Artesunate
ATP	Adenosine triphosphate
Ave	Average
AVQ	Atovaquone
BCA	Bicinchoninic acid
BSA	Bovine Serum Albumin
C	Cytosine
CAPS	3-(cyclohexylamino)-1-propane sulfonic acid
CCB	Colloidal Coomassie Blue
CG	Cycloguanil
CHAPS	3-[(3-cholamidopropyl) dimethylammonio]-1-propane sulfonate
CPG	Chlorproguanil
CpG	Cytosine Guanine dinucleotide with connecting phosphodiester bond
CQ	Chloroquine
CSP	Circumsporozoite protein
Ct	Cycle threshold of the real-time amplification cycle
CV	Coefficient of variation
Cyclo	Cyclophillin
Cys	Cysteine
Da	Daltons
DALY	Disability adjusted life years
dcAdoMet	Decarboxylated AdoMet
DDT	Dichloro-diphenyl-trichloroethane
DFMO	DL-α-difluoromethylornithine
DHA	Dihydroartemisinin
DHFR	Dihydrofolate reductase
DHFR/TS	Dihydrofolate reductase/thymidylate synthetase
DHPS	Dihydropteroate synthetase
DIGE	Differential gel electrophoresis
DNA	Deoxyribonucleic acid
DS	Dapsone

EBA	Erythrocyte binding antigens
EDTA	Ethylenediamine tetra-acetic acid
eIF	Eukaryotic translation initiation factor
EMSA	Electrophoretic mobility shift assay
ESI	Electrospray ionisation
f	Forward primer
Fa-	Folic acid deficient
Fa+	Folic acid containing
FACS	Fluorescence activated cell sorting
FC	Fold change
FIC	Fractional inhibitory concentration
FIKK	A novel *Apicomplexa*-specific group of eukaryotic protein kinase-related proteins
FPP XI	Ferriprotoporphyrin IX
FTICR MS	Fourier transform ion cyclotron resonance mass spectrometry
g	Gram
G3PDH	Glyceraldehyde-3-phosphate dehydrogenase
GDH	Glutamate dehydrogenase
gDNA	Genomic DNA
GDP	Gross Domestic Product
GO	Gene ontology
h	hour
HA	Hyaluronic acid
HAART	Highly active antiretroviral therapy
HAT	Histone acetyltransferases
Hb	Hemoglobin
HC	Homocysteine
HCCA	4-hydroxy-α-cyanocinnamic acid
HDAC	Histone deacetylase
HDP	Hemoglobin derived products
HF	Halofantrine
HH4	Histone H4
HIV	Human Immunodeficiency Virus
HK	Hexokinase
HPI	hours post-invasion
HPLC	High-performance liquid chromatography
HPPK	Hydroxymethylpterin pyrophosphokinase
hPrx-2	human peroxiredoxin-2
HS	Homospermidine
Hsp	Heat shock protein
IC_{50}	Median Inhibitory concentration
ICAM	Intracellular adhesion molecule 1
ICAT	Isotope coded affinity tag
IDA	Information Dependant Acquisition
IDC	Intraerythrocytic developmental cycle
IEF	Iso-electrical focusing
IFN-γ	Interferon gamma
IL	Interleukin
Ile	Isoleucine
IMAC	Immobilised metal-ion affinity chromatography
iNOS	Inducible nitric oxide
IPG	Immobilsed polyacrylamide gel

IPT	Intermittent preventive treatment in pregnancy
iRBC	Infected red blood cell
IRS	Indoor residual spraying of insecticide
ITN	Insecticide treated nets
K	Thousand
kDa	Kilo daltons
L	Linear
l	litre
LC-ESI/MS	Liquid chromatography-electrospray ionisation/mass spectrometry
LDC	Lysine decarboxylase
LDH	Lactate dehydrogenase
LF	Lumefantrine
LLIN	Long lasting insecticidal nets
LOD	Limit of detection
LTα	Lymphotoxin alpha
M	Molar
MADIBA	Micro Array Data Interface for Biological Annotation
MALDI–TOF MS	Matrix assisted laser desorption/ionization time-of-flight mass
MAP	Malaria Atlas Project
MAQC	MicroArray Quality Control
MDG	Millennium development goal
MDL73811	5'-[(Z)-4-Amino-2-butenyl]methylamino]-5'-deoxyadenosine
mdr	Multi-drug resistance gene
Met	Methionine
mg	Milligram
MIAME	Minimum information about a microarray experiment
MIAPE	Minimum information about a proteomics experiment
MIM	Multilateral Initiative on Malaria
ml	Milliliter
MQ	Mefloquine
Mr	Molecular weight
mRNA	Messenger ribonucleic acid
MS	Mass spectrometry
MS/MS	Tandem mass spectrometry
MSF	Malaria SYBR Green I-based fluorescence assay
MSP	Merozoite surface protein
MTA	5'-Methylthioadenosine
MTI	5'-Methylthioinosine
MudPIT	Multi-dimensional protein identification techniques
n/a	Not applicable
NADPH	Reduced nicotinamide adenine dinucleotide phosphate
NCBI	National Center for Biotechnology Information
ng	Nanogram
NKT	Natural killer T-cells
nm	Nanometers
NMR	Nuclear magnetic resonance
NTD	Neglected tropical disease
OAT	Ornithine aminotransferase
ODC	Ornithine decarboxylase
PABA	*p*-aminobenzoic acid
PAGE	Polyacrylamide gel electrophoresis

PBS	Phosphate-buffered saline
PCA	Perchloric acid
PEMT	Phosphoethanolamine N-methyltransferase
PEXEL	*Plasmodium* export element
Pf	*Plasmodium falciparum*
*Pf*3D7	*Plasmodium falciparum* choloroquine sensitive strain 3D7
*Pf*CRT	*Plasmodium falciparum* chloroquine resistance transporter
*Pf*EMP-1	Erythrocyte membrane protein-1
*Pf*HB3	Plasmodium falciparum pyrimethamine resistant
Pfmdr1	*Plasmodium falciparum* multiple drug resistant protein
*Pf*PR	*Plasmodium falciparum* parasite rate
*Pf*RBL	*Plasmodium falciparum* reticulocyte binding like
PG	Proguanil
Pgh	P-glycoprotein homologue
pi	Post invasion
pI	Isoelectric point
PK	Pyruvate kinase
PLP synthase	Pyridoxal-5-phosphate synthase
PMF	Peptide mass fingerprint
PNP	Purine nucleoside phosphorylase (uridine phosphorylase)
ppm	Parts per million
PPQ	Piperaquine
PQ	Primaquine
pt	Post treatment
PTM	Post-translational modifications
PVM	Parasite vacuolar membrane
PYR	Pyrimethamine
QN	Quinine
qRT-PCR	Semi-quantitative reverse transcription polymerase chain reaction
Q-TOF MS	Quadrupole-time-of-flight mass spectrometer
r	Reverse primer
R^2	Correlation coefficient of a regression line
RESA	Ring infected erythrocyte surface antigen
RIN	RNA integrity number
RNA	Ribonucleic acid
RP-HPLC	Reversed phase-high performance liquid chromatography
RPS4	Ribosomal protein S4
RQI	RNA Quality Indicator
rRNA	Ribosomal RNA
s	Second
SAGE	Serial analysis of gene expression
SDS-PAGE	Sodium dodecyl sulphate polyacrylamide gel electrophoresis
SDX	Sulfadoxine
SELDI-TOF/MS	Surface-enhanced laser desorption ionisation-time-of-flight/mass
SEM	Standard error of the mean
SERCA	Sarco/endoplasmic reticulum calcium –dependent ATPase
SP	Sulfadoxine/Pyrimethamine combination therapy
SpdS	Spermidine synthase
SSH	Suppression subtractive hybridization
STRING	Search Tool for the Retrieval of Interacting Genes/Proteins
T	Treated
t_1	Time point 1
t_2	Time point 2

t_3	Time point 3
TEMED	N,N,N',N'-tetramethyl-ethylenediamine
THF	Tetrahydrofolate
TIM	Triosephosphate isomerase
Tm	Melting temperature
TNF	Tumor necrosis factor
Tris	Tris(hydroxymethyl)-aminomethane
TS	Thymidylate synthetase
Tt_1	Treated time point 1
U	Units
UN	United Nations
UNDP	United Nations Development Program
UNICEF	United Nations Children's Fund
US	United States
UT	Untreated
UTt_1	Untreated time point 1
UV	Ultraviolet
v/v	Volume per volume
Vhrs	Volt hours
VTS	Vacuolar transport signal
W	Watts
w/v	Weight per volume
WHO	World Health Organisation

CHAPTER 1

Introduction

"It hides in the dark, silent, waiting… Then as dusk approaches it strikes – fast! Deadly! Malaria is a killer! In Africa, it is one of the worst serial killers of all time..."

1.1 The statistics

Worldwide, there are 109 malaria endemic countries as surveyed in 2008, with 45 of these in Africa. In 2006, 3.3 billion people were at risk of contracting malaria of which 1.2 billion people reside in Africa. Two hundred and forty-seven million people were infected with malaria in 2008 resulting in 1 million deaths, with 91% of these in Africa and 85% due to children younger than 5 years of age (Figure 1.1) (World Malaria Report 2008). In Africa, a child dies every 30 seconds due to the devastating impact of malaria (Greenwood *et al.*, 2005). In eastern Uganda, children can expect to be infected with malaria once every 2 months, even with the use of bednets and artemisinin combination therapies (ACT's) (Price, 2000) and in the rest of Africa a child can have an average of 1.6 to 5.4 clinical episodes of malaria fever every year (World Malaria Report 2008). This is clearly in stark contrast to the Millennium Development Goals (MDG) that were adopted by 189 nations and signed by 147 heads-of-state and governments during the United Nations (UN) Millennium Summit in September 2000. The MDG's 8 goals include the eradication of hunger and poverty, provision of primary education, gender equality, improved maternal health and reduction in child mortality, to combat various diseases like Human Immunodeficiency Virus (HIV) and malaria, environmental sustainability and finally the development of global partnerships. Of particular interest is MDG goal 6, which aims to reduce malaria infection and mortality, and especially child mortality by 2015.

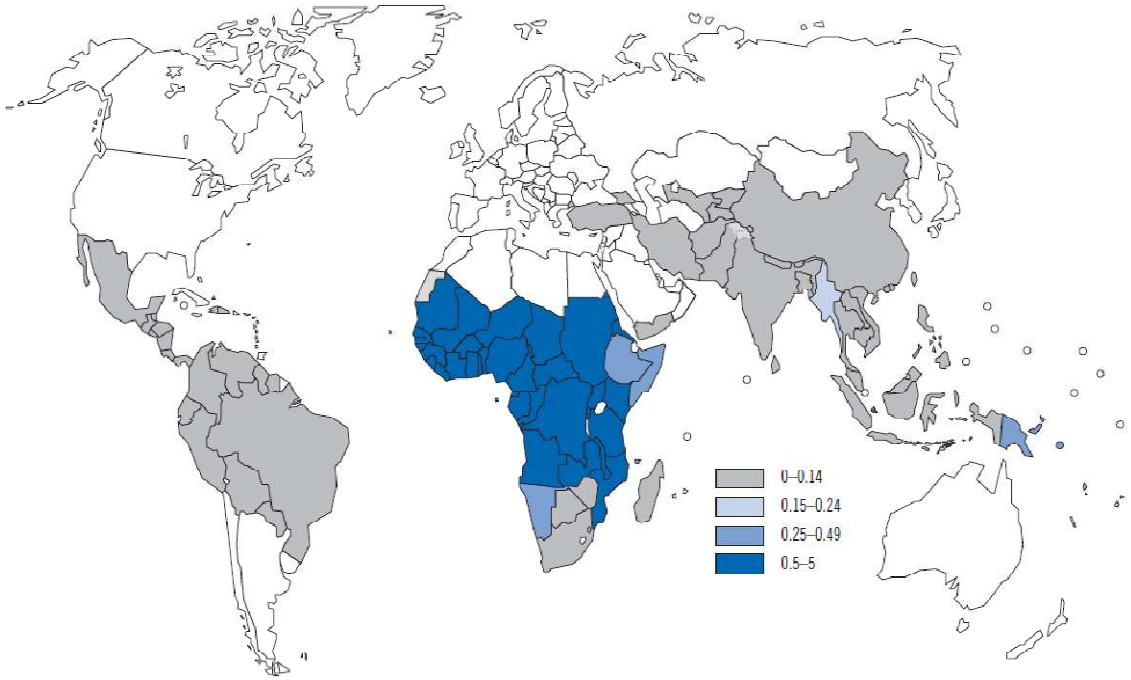

Figure 1.1: Estimated worldwide deaths (in millions) from malaria in 2006 as given by the 2008 WHO report (www.who.int).

A global map of endemicity of malaria is lacking since WHO maps only provide estimations of malaria incidence (Figure 1.1). The Malaria Atlas Project (MAP) generated a total of 8938 *P. falciparum* parasite rate (*Pf*PR) surveys, of which 7953 passed the strict criteria to be included in a global database. This data was captured from 1985 until currently (2010), of which more than 50% of the data is representative from 2000 onward. This database is currently used to predict malaria endemicity and incidence with geographic visualisation (Figure 1.2) (Hay *et al.*, 2009, Guerra *et al.*, 2008, Guerra *et al.*, 2007). In the future, it is aimed to also produce a map on *P. vivax* endemicity, but unfortunately data for this is still lacking (Hay *et al.*, 2009).

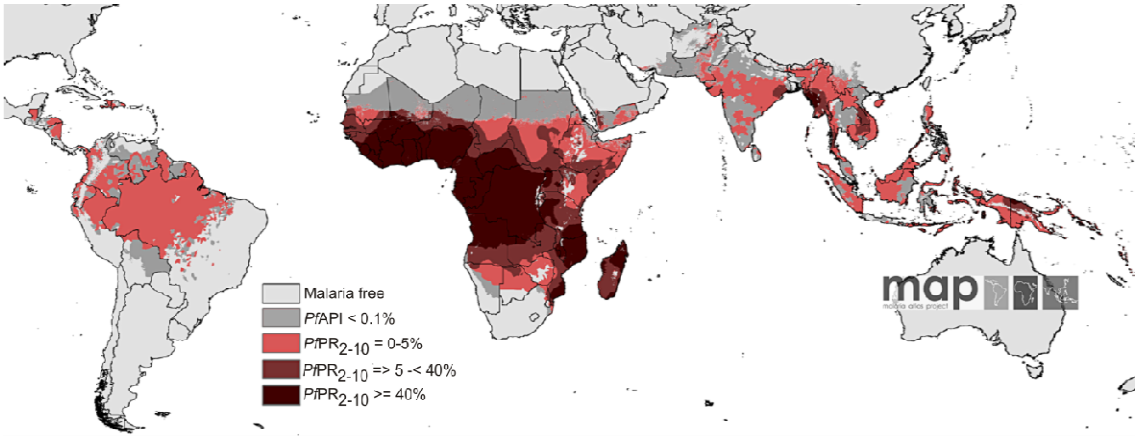

Figure 1.2: Distribution of *P. falciparum* (Hay *et al*., 2009).

The map is categorized as low risk *Pf*PR_{2-10} ≤ 5%, light red; intermediate risk *Pf*PR_{2-10} > 5 to 40%, medium red; and high risk *Pf*PR_{2-10} ≥40%, dark red. Unstable risk areas is medium grey where *Pf*API < 0.1 per 1000 pa or no risk in light grey. All red areas are representative of *Pf*API > 0.1 per 1000 pa. *Pf*API is the *P. falciparum* annual parasite incidence. *Pf*PR_{2-10} is *P. falciparum* prevalence rate corrected to the 2-10 year age group

1.2 The economic burden of malaria

During the rainy season in the province of Garki, Nigeria, a person would be bitten an average 174 times per night by mosquitoes of the genera *Anopheles gambiae* (Gallup J.L. & Sachs J.D., 2001). In Kou Valley in Burkina Faso, a person would be bitten 158 times per night by *A. gambiae*, with the average total mosquito bites reaching an astounding 35 000 per year (Gallup J.L. & Sachs J.D., 2001). Even with these horrible statistics, most people neither have bednets nor do they have proper prophylaxis, and are therefore constantly reinfected with malaria. This has a direct economic impact on mostly already poverty stricken countries, as people are unable to work or go to school, therefore resulting in an overall reduction in productivity (Greenwood *et al.*, 2005). It is not surprising that the 33 richest countries are malaria free (Gallup J.L. & Sachs J.D., 2001). The economic burden of malaria can be seen in the fact that the Gross Domestic Product (GDP) in endemic countries can decrease by as much as 1.3% per year.

Reasons for the deterioration of malaria in some parts of Africa may be attributed to environmental changes like climate instability, global warming, war and civil disturbances, increasing travel around the world, HIV infection, increasing drug resistance, and increasing insecticide resistance (Tatem *et al.*, 2006, Greenwood & Mutabingwa, 2002, Greenwood, 2002). However, in recent years, 7 out of 45 African countries and 22 countries outside of Africa, with small populations with active interventions were able to reduce the total number of malaria cases and malaria related deaths when compared to data from 2000. Four African countries, Eritrea, Rwanda, Sao Tome and Principe, as well as Zanzibar in Tanzania, were able to reduce their malaria burden by 50% between

2000-2007 by means of aggressive malaria control. A huge success story is the United Arab Emirates, which was the first malaria endemic country since the 1980's to be certified malaria free by the WHO, and now forms part of the 92 malaria free countries around the world. Of the 109 countries affected by malaria, 82 are in the control stage of malaria elimination, 11 countries are in pre-elimination, 10 in elimination stages and 6 countries are preventing re-introduction of malaria (World Malaria Report 2008).

1.3 History of malaria

Malaria has been known as a killer disease for centuries with Hippocrates already describing fevers, mostly correlating to swamps, hence the Italian name *"mal' aria"* meaning "bad air". Ancient Romans were affected by malaria due to the marshes around Rome (Gardiner D.L. *et al.*, 2005). The first challenge to the miasma theory (stench from decaying matter) came from Louis Pasteur and Robert Koch who demonstrated that microbes were responsible for certain diseases. Later, this was followed by Edwin Klebs and Corrado Tommasi-Crudeli who claimed in 1879 the isolation of "*Bacillus malariae"* as causative agent for malaria, although this theory was soon disregarded (Guillemin, 2002). In 1880, Alphonse Laveran (1845-1922) observed the first malaria gametocyte in the blood of a French soldier in Algeria, a discovery that won him the Nobel Prize in 1907. In 1897, Ronald Ross (1857-1932) identified *Plasmodium* parasites within the *Anopheles* mosquito and demonstrated that malaria is transmitted from an infected mosquito to the human host. This achievement won him Knighthood and the Nobel Prize in 1902 (Hagan & Chauhan, 1997). The final piece of the puzzle came from Short and Garnham who in 1948, described schizonts in the livers of monkeys and thereby completed the life cycle of *Plasmodium* (Gardiner D.L. *et al.*, 2005).

1.4 Life cycle

Malaria is caused by the protozoan parasite, *Plasmodium,* that occurs in 4 major disease causing species: *P. vivax, P. malariae, P. falciparum,* and *P. ovale. P. falciparum* is the most virulent, and causes the most severe form of malaria (Carter & Mendis, 2002). Recent findings has established the enzoonotic transmission of the simian malaria parasite *P. knowlesi,* that was previously only found in nature in macaques, to humans (Bronner *et al.*, 2009). The Plasmodial parasite has a complex life cycle that consists of both a vertebrate and invertebrate host. Malaria is transmitted by the bite of female *Anopheles* mosquitoes, occurring mainly between sunrise and sunset. Unfortunately, Africa is home to some of the most effective malaria vectors including *A. gambiae* and *A. funestus* (Mons B. *et al.*, 1997). The highest risk of contracting malaria is at the end of the rainy season or soon thereafter as this is also the time when the mosquito vectors are most

abundant. When an infected female mosquito takes a blood meal, malaria sporozoites are released from the saliva into the subcutaneous tissue of the human host (Figure 1.3 B).

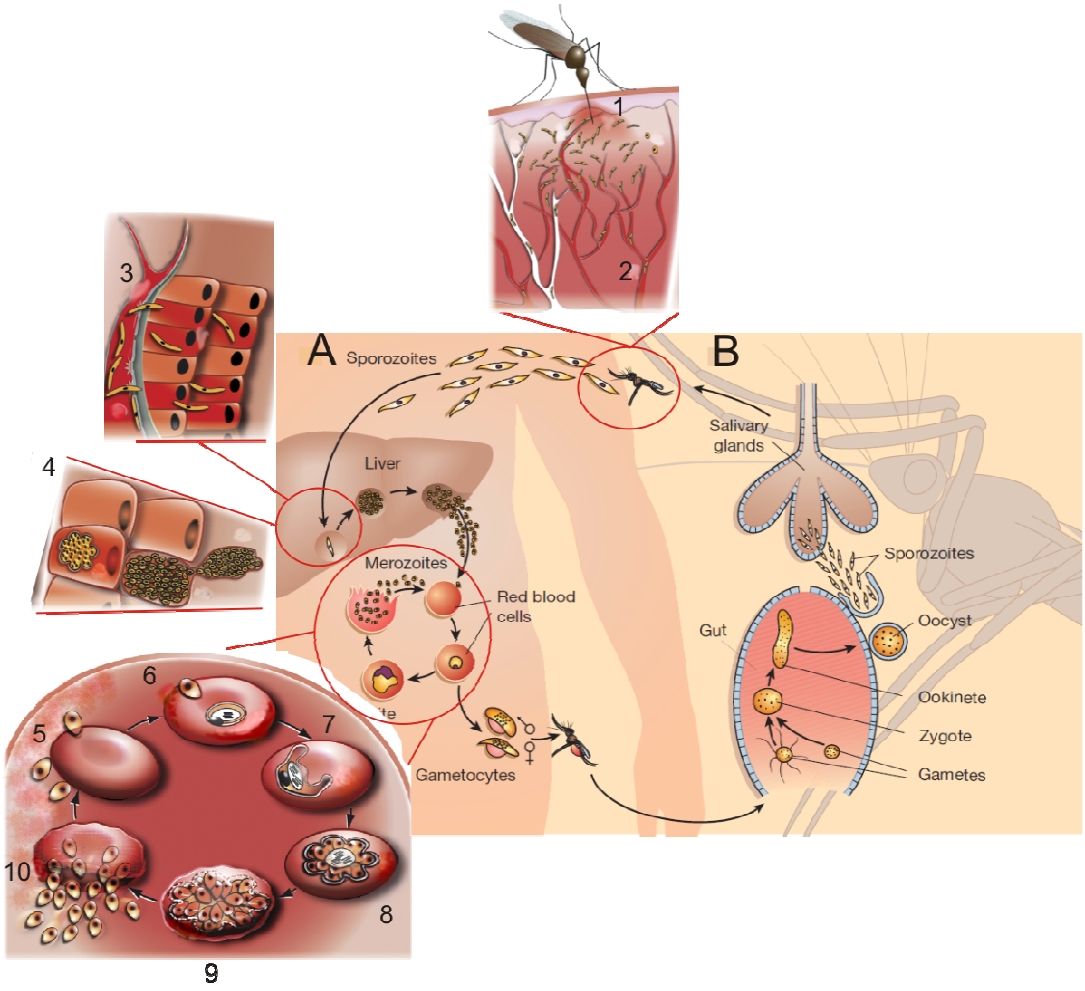

Figure 1.3: The Plasmodial life cycle. Compiled from (Wirth, 2002, Silvie *et al.*, 2008).

A: The asexual life cycle in the human host. B: The sexual life cycle in the mosquito. 1: Intradermal sporozoite injection when the female mosquito takes a blood meal. 2: Sporozoites migrate to the blood vessels to be distributed through the blood circulation. 3: Sporozoites invade the hepatocytes in the liver. 4: The parasites mature and multiply in the liver to ultimately release merozoites in membrane-shielded merosomes. 5: Start of the intraerythrocytic developmental cycle by the invasion of an erythrocyte by a merozoite. 6: Ring stage. 7: Trophozoite stage. 8: Schizont stage. 9: Preparation to release merozoites from the erythrocyte. 10: Merozoite egress. The released merozoites will then re-invade an erythrocyte to start the intraerythrocytic developmental cycle again.

The sporozoites progress to the liver where they will invade hepatocytes and develop into schizonts. This hepatocytic incubation period of malaria is 7 to 15 days but may also take up to 3 months (Silvie *et al.*, 2008). *P. vivax* is able to produce hypnozoites that can reside within the liver for months therefore causing malaria relapses months or sometimes years after infection. Usually, after 6 to 10 days, the schizonts will multiply and discharge 10 000 to 30 000 merozoites from the hepatocytes into the bloodstream (Yu *et al.*, 2008). The merozoites will invade erythrocytes where they will multiply within their 48 hour asexual life cycle. This intraerythrocytic development cycle

(IDC) consists of the development into the ring stage, followed by the trophozoite stage and finally the schizont stage in which the parasite will prepare itself for re-invasion of erythrocytes by the production and release of 8-32 merozoites (Figure 1.3 A) (Bozdech *et al.*, 2003, Bannister *et al.*, 2000). This cycle will continue until the death of the host occurs or death of the parasites due to drug treatment or immune responses of the human host. A proportion of the asexual parasites will develop into sexual gametocytes, which can be taken up by another mosquito when it bites an infected human host (Wirth, 2002). Within the mosquito gut, the gametocytes will differentiate into male and female gametes that can fuse to form a zygote, which is the only diploid stage in an otherwise mainly haploid life cycle. In the mosquito midgut, the zygote differentiate into an ookinete and finally matures into a sporozoite-filled oocyst (Wirth, 2002). The oocyst migrates out of the mosquito gut to release sporozoites that are able to migrate to the mosquito salivary gland therefore enabling the mosquito to infect a human host and completing the life cycle of the Plasmodial parasite (Sinden & Billingsley, 2001).

1.5 Pathogenesis

The most common symptoms of malaria include fevers, chills, headaches, muscular aching, weakness, vomiting, coughing, diarrhoea, abdominal pain and may therefore be commonly mistaken for flu (Clark & Cowden, 2003). Early diagnosis and treatment can be life saving and therefore it is important that travellers to malaria endemic areas monitor their health after visits to malaria areas and seek medical advice once they fall ill (World Malaria Report 2008). The rupture of infected erythrocytes and invasion of new erythrocytes is also the main cause of pathogenesis. Uncomplicated malaria has a cyclical occurrence with coldness, followed by rigor and fever as well as sweating every 48 hours corresponding to the lysis of infected erythrocytes and the release of merozoites and subsequent re-invasion of new erythrocytes.

Merozoites that are released into the bloodstream to invade erythrocytes do not pierce the erythrocyte but forms a deep invagination that encloses the parasite within the parasite vacuolar membrane (PVM) (Garcia *et al.*, 2008). Invasion can be divided into several stages that include initial adhesion, re-orientation of the merozoite apical surface, junction formation, generation of the PVM and movement of the merozoite into the parasite vacuole, sealing of the parasite vacuole, discharge of granules onto the parasite vacuole, and finally merozoite transformation into ring stage parasites (Iyer *et al.*, 2007). Initial adhesion is mediated mainly by merozoite surface protein-1 (MSP-1) that is an integral membrane protein on the surface of merozoites (Cowman & Crabb, 2002). Initial attachment to the erythrocyte by MSP-1, is followed by re-orientation of the merozoite apical end towards the erythrocyte surface which is mediated by apical membrane

antigen-1 (AMA-1). Duffy binding proteins and reticulocyte binding-like (*Pf*RBL) proteins are important for junction formation (Cortes, 2008), while entry into the parasite vacuole is mediated by the erythrocyte binding antigens (Silvie *et al.*, 2008).

Knob formation seems essential for erythrocyte adhesion by rosetting as well as sequestering, and is one of the major disease complications associated with clinical episodes of malaria that include impaired microvascular flow, hypoxia, reduced metabolite exchange, and cerebral malaria (Garcia *et al.*, 2008, Starnes *et al.*, 2009). The occurrence of rosetting and sequestration is one of the major differences between *P. falciparum* and *P. vivax*, since erythrocytes infected with *P. vivax* cannot sequester and therefore also does not result in the life-threatening symptoms associated with *P. falciparum.* Rosetting and sequestering is mediated due to the export of erythrocyte membrane protein-1 (*Pf*EMP-1) to the surface of the erythrocyte to protect the parasite against the host immune responses. *Pf*EMP-1 is able to bind various receptors, that include intracellular adhesion molecule 1 (ICAM), E-selectin, CD36, CD31, and hyaluronic acid (HA) ultimately resulting in rosetting and sequestration of infected erythrocytes (Artavanis-Tsakonas *et al.*, 2003).

Severe malaria will cause a 100% mortality rate if left untreated and even when treated still results in 15% mortality (World Malaria Report 2008). Symptoms of severe malaria include amongst others, splenomegaly, severe headaches, cerebral ischemia, cerebral malaria, hepatomegaly, hypoglycemia, and hemoglobinuria with renal failure, and finally coma and death (de Ridder *et al.*, 2008). High risk individuals include pregnant woman and children as well as travellers. Severe malaria has many similarities to sepsis, and for this reason sepsis has been used as a model in elucidating the pathogenesis of malaria as disease (Mackintosh *et al.*, 2004). “Malaria toxin” is released upon lysis of the erythrocytes due to merozoite release. This “malaria toxin” is identified as glycosylphosphatidylinositol (GPI) which subsequently induces the release of tumor necrosis factor (TNF) to activate a network of cytokines to mediate cellular defence, resulting in illness of the host (Grau *et al.*, 1989). Production of pro-inflammatory cytokines is central to malaria as disease with many of these mediators also active in various infectious diseases. Disease pathology as a result of cytokine induction include fever, hypoglycaemia, bone marrow depression, coagulopathy, hypotension, and the possible destruction of infected erythrocytes (Clark & Cowden, 2003). Both lymphotoxin (LTα) and TNF will induce high levels of IL-6 and induce arginine dependent nitric oxide (NO) production by inducible nitric oxide synthase (iNOS) which is able to kill parasites (Anstey *et al.*, 1996). Cytokine-mediated protection against malaria is mediated by the action of macrophages that are able to generate nitric oxide as a reactive oxygen species resulting in the

stimulation of T-cells. Cerebral malaria is typically associated with increased mRNA and protein levels of TNF, IL-2 and LTα (Brown *et al.*, 1999, Engwerda *et al.*, 2002).

Malaria in pregnant women poses a severe health risk to both mother and the unborn child. One of the main reasons is the fact that infected erythrocytes from the placenta bind specifically to chondroitin sulphate A (Fried *et al.*, 2006, Ricke *et al.*, 2000), compared to ICAM and CD36 in adults (Maubert *et al.*, 1998, Ricke *et al.*, 2000, Rogerson *et al.*, 2007). During normal pregnancy the cytokine balance is shifted towards a Th2-type response to ensure a safe pregnancy, while in malaria infected pregnancies the balance is shifted towards Th1 as a result of the malarial infection. Malarial infection increases the levels of TNFα, IFNγ, IL1β and IL-2 which severely affects the risk of stillbirths, abortions and congenital malaria (Rogerson *et al.*, 2007).

Children under the age of 5 and immuno compromised individuals are also at risk of severe malaria. Severe malaria in children may often result in anaemia, learning impairments and brain damage (World Malaria Report 2008). In Africa, the severity of malarial infections is worsened even further by the extremely high incidence of HIV infections that affect both children and adults. A susceptible immunity and impaired cytokine response poses a risk of severe complications and death due to malarial infection (Rogerson *et al*., 2007, de Ridder *et al.*, 2008). This is worsened even more by the fact that there seems to exist an antagonistic interaction between certain antimalarials and the various antiretroviral protease inhibitors commonly used for HIV infection (He *et al.*, 2009).

1.6 Eradication efforts against malaria

World War II was followed with huge malaria eradication efforts across all continents. These programmes made extensive use of insecticides like dichloro-diphenyl-trichloroethane (DDT) and antimalarials like chloroquine as prophylaxis (Hemingway J., 2004). By the 1950's, malaria was eliminated from Australia, Europe, and the USA (Figure 1.4). Unfortunately, these early eradication efforts failed in Africa and Asia. Today, various malaria eradication efforts have been renewed. One such an effort is the "Roll Back Malaria" partnership, a global partnership initiated by WHO, United Nations Development Programme **(**UNDP), The United Nations Children's Fund (UNICEF), and the World Bank in 1998. The aim of the "Roll Back Malaria" partnership is to work with national governmental organisations and private companies to enable the reduction of the human and socio-economic burden of malaria. This is done mainly by the provision of bednets and the necessary malarial drugs in rural areas affected by the harsh impact of malaria. To combat malaria,

the WHO recommend the use of long lasting insecticidal nets (LLIN), ACT's, indoor residual spraying of insecticides (IRS) and intermittent preventive treatment (IPT) during pregnancy.

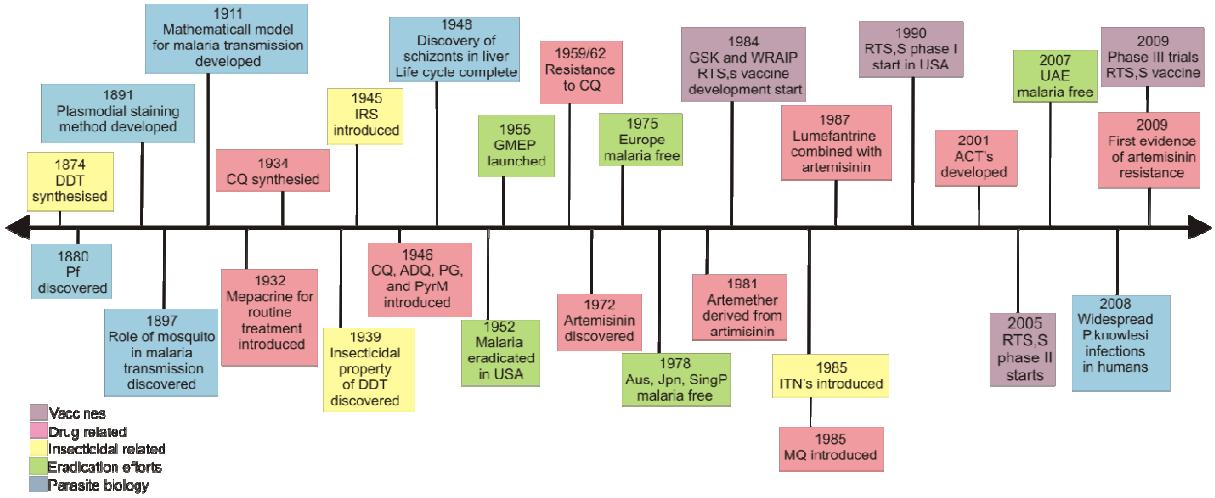

Figure 1.4: Timeline of some of the most important milestones in the fight against malaria.
Created from (Vangapandu *et al*., 2007, Hyde, 2005, WHO)

The South African Department of Health currently recommends mefloquine (MQ), doxycyclin or atovaguone/proguanil as appropriate chemoprophylaxis for use in South Africa . The Centre for Disease Control recommends the use of atovaquone/proguanil, doxycycline, chloroquine (CQ) or MQ (only in areas without CQ and MQ resistance) or primaquine, as chemoprophylaxis depending on which malaria endemic country is to be visited . Compliance is essential when taking chemoprophylaxis. MQ has to be taken weekly, at least 1 week before entering a malaria area and 4 weeks after leaving the malaria area. Doxycyclin has to be taken daily 2 days before entering a malaria area and continue for 4 weeks after leaving the malaria area. Atovaquone-proguanil is preferred for shorter stays since it needs to be taken daily 2 days before entering a malaria area and continued for 7 days after leaving the malaria area. The choice of prophylaxis depends on various factors that include the age and weight of a patient, medical conditions, and activities that the patient will embark on like scuba diving. For female patients it is also necessary to consider if the patient is pregnant or breastfeeding . No antimalarial prophylactic regimen gives complete protection, but it may be useful to alleviate the severity of the illness. Chemoprophylaxis and treatment of *P. falciparum* malaria is becoming difficult due to increasing resistance of the parasite to all known drugs. This is also the reasoning for the WHO to establish the "ABCD of Malaria Protection" (World Malaria Report 2008).

- Awareness of the risk of malaria
- Avoid being Bitten
- Chemoprophylaxis
- Diagnosis and treatment as soon as possible

1.6.1 Insecticide resistance – the use of spraying and bed nets

The main purpose of IRS is to reduce transmission of malaria from the mosquito to its human host by elimination of the vector found within houses. Unfortunately, a huge challenge is the increase in resistant mosquitoes to existing insecticides, especially DDT, and against the pyrethroids. Insecticide treated nets (ITN) may assist in the prevention of malaria infection, since it is able to reduce transmission of malaria from the mosquito to the human host. In 2000, only 1.7 million children living in malaria endemic countries had access to ITN's, but this number has now increased to 20.3 million children in 2007. Unfortunately, this still leaves 89.6 million (81.5%) children without nets and extremely vulnerable to infection (Noor *et al.*, 2009). In 18 African countries surveyed by the WHO, it was determined that 34% of households owned an ITN of which 23% children and 27% pregnant woman slept under (World Malaria Report 2008). Unfortunately, this still leaves 66% of African households without an ITN and therefore at an increased risk of contracting malaria.

1.6.2 Vaccines

Another step toward the eradication of malaria is through the development of an effective malaria vaccine. The ideal vaccine must be able to provide complete immunity against the disease or prevent severe disease and death. Unfortunately, genetic variability of the parasite is hampering vaccine development. Four stages of the parasite life cycle has been targeted as possible vaccine candidates including the pre-erythrocytic (when infected with sporozoites), the human hepatic stage, the erythrocytic and the gametocyte stages (Graves & Gelband, 2006). Vaccines directed towards the pre-erythrocytic stages aim to completely prevent infection while blood stage vaccines aim to reduce and hopefully eliminate parasites upon infection. Gametocyte vaccines on the other hand aim to prevent transmission of the parasite to the vector. The most advanced pre-erythrocytic vaccine to date is the RTS,S/AS01 vaccine developed by GlaxoSmithKline in a process that has already started in 1984 at the Walter Reed Army Institute of Research (Ballou, 2009) (Figure 1.4). It consists of the antigenic C-terminus of the parasite's circumsporozoite protein (CSP) fused to the hepatitis B surface antigen and is expressed in the form of virus-like particles in *Saccharomyces cerevisiae*. Phase I and Phase IIa clinical trials on Gambian adults (Bojang *et al.*, 2009), 2022 Mozambiquean children aged 1-4 years (Sacarlal *et al.*, 2008) as well as infants (Aponte *et al.*, 2007) used the AS02 oil-in-water adjuvant system and showed promising protection by RTS,S against malaria infection. The AS02 adjuvant was replaced with the RTS,S/AS01 which contains liposomes as adjuvant, and applied in Kenya and Tanzania with over 800 infants between 5-17 months and showed 55% efficacy over a follow-up period of 8 months (Bejon *et al.*, 2008b, Bejon

et al., 2008a). The previously used AS02-adjuvant was well tolerated, but the new AS01-adjuvant had similar safety with higher humoral immunogenicity, a favourable Th1 cell immune response and a trend towards higher vaccine immunogenicity (Kester *et al.*, 2009, Lell *et al.*, 2009). RTS,S/AS01 given in three doses, rather than a single dose, provided better results in Ghanaian and Gabonese children (Owusu-Agyei *et al.*, 2009, Lell *et al.*, 2009). Phase III clinical trials for RTS,S/AS01 started in May 2009 and include sites in Kenya, Tanzania, Malawi, Mozambique, Gabon, Ghana, and Burkina Faso. Should results be promising, the product could only be ready for recommendation and registration at the earliest by 2014 (World Malaria Report 2008).

Other vaccine candidates have also been pursued over time but with less success to date than that obtained with RTS,S/AS01. Asexual blood stage vaccines aim to protect against malaria as disease rather than the infection, but has been less successful to date. Various MSP's have been investigated as vaccine candidates with little success in clinical trials conducted to date in Kenya and Mali. Another vaccine, the Combination B vaccine (MSP/RESA), consisting of two merozoite surface proteins together with a ring infected erythrocyte surface antigen (RESA) showed good immunogenicity and is being investigated further (Graves & Gelband, 2006). Another joint venture by Walter Reed Army Institute of Research and GlaxoSmithKline resulted in the FMP2.1 (AMA-1/AS02) vaccine candidate which showed host immunity and safety in phase I trials (Polhemus *et al.*, 2007, Spring *et al.*, 2009) and is presently in phase II trials in Mali. The FMP2.1/AS02 (A) vaccine candidate consists of FMP2.1 which is a recombinant protein based on AMA-1 from *P. falciparum* strain 3D7. Another approach to vaccine development is transmission blocking vaccines that are based on the prevention of sporozoite development in the mosquito salivary glands. Various surface protein antigens are in development but is hampered by the problematic protein expression of these proteins. The use of irradiated attenuated *P. falciparum* sporozoites is also underway in phase I trials, but may pose safety, technical and logistical problems (Ballou, 2009).

1.7 Currently used drugs and drug resistance

Antimalarial drugs are probably the cornerstone of the malaria elimination effort with the use of ITN's and IRS strengthening the efforts against combating malaria. Unfortunately, the harsh reality is that even with these efforts, people living in endemic malaria areas will still contract malaria and without cheap and affective drugs, many more people will succumb to the devastating effect of malaria. The problem is compounded by the lack of new antimalarials. The tragedy is that all existing antimalarial drugs are actually only derivatives of certain core structures and can be grouped into three main classes; the quinolines (quinine, chloroquine, mefloquine, primaquine), the anti-folates (sulfadoxine, pyrimethamine) and the most recent drugs, the artemisinin derivatives

(artemisinin, artemether, dihydroartemisinin) (Na-Bangchang & Karbwang, 2009). Certain antibiotics (doxycyclin, clindamycin) also display antimalarial properties. There is an increasing spread of drug and insecticide resistance due to the evolutionary pressure put on both the mosquito and the parasite. The Thai-Cambodian border is historically the first site of emerging resistance to antimalarials, and has now also seen the first signs of resistance to treatment with artemisinin (Noedl *et al.*, 2008). This could result in a tragedy for all malaria endemic countries and as rightfully noted by Prof Ogobaro Doumbo during the 5th MIM Conference, Nairobi, Kenya, 2009: *"Artemisinin resistance is a Tsunami coming into Africa"*. The development of resistance to currently used drugs may be due to several factors that include the overuse of antimalarial drugs, inadequate therapeutic treatments of infections, parasite adaptability at genomic and metabolic levels and fast proliferation rates of the parasite that allows new generations to be formed in a very short time (Hyde, 2007, Olliaro & Taylor, 2003). The mechanisms of resistance to these drugs involve the modification of drug transport systems, increased synthesis of inhibited enzymes (Nirmalan *et al.*, 2004b), an increase in enzymes that can inactivate the drug and finally the use of alternative pathways (Vangapandu *et al.*, 2007). Unfortunately, except for the folate drugs, both the mode-of-action as well as the mechanism of resistance is poorly understood (Na-Bangchang & Karbwang, 2009).

1.7.1 Chloroquine

Chloroquine (CQ) is part of the quinoline family of drugs and was synthesized in 1934. Also part of the quinoline family is quinine (QN) which is extracted from cinchona bark and was one of the first antimalarial drugs. CQ provided antimalarial treatment for 8 decades and was the cornerstone of malaria eradication in the 1950's and 1960's (Figure 1.4). The main advantage of CQ was its fast action against the blood stages, low toxicity, good bio-availability and pharmacokinetics as well as its low production cost, therefore making it the ideal drug for Africa (Santos-Magalhaes & Mosqueira, 2010). Unfortunately, to its disadvantage, CQ has a very long half life (1-2 months) which may be one of the reasons for the emergence of resistance to CQ, which was first observed in 1962 in Thailand, and later in Africa (Gregson A. & Plowe C.V., 2005, Na-Bangchang & Karbwang, 2009) (Table 1.1). The mode-of-action of CQ is based on the accumulation of the drug within the food vacuole, which will eventually interfere with the polymerisation of toxic heme monomers into hemozoin, which is part of the parasite's detoxification process. CQ enters the food vacuole (pH of ~4.5-5.0) possibly by diffusion and then accumulates within the food vacuole due to pH trapping of the protonated drug at the low pH within the food vacuole (Figure 1.5). CQ will then form a complex with heme ferriprotoporphyrin IX which ultimately leads to the toxic effect of the

drug on the parasite (Vangapandu et al., 2007). CQ resistance occurs due to mutations in the *Pf*crt gene (located on chromosome 7) that expresses the chloroquine resistance transporter (*Pf*CRT), a transmembrane protein located on the digestive vacuole. Mutations of this gene were also found in CQ resistant field isolates (Djimde *et al.*, 2001). Modification in the P-glycoprotein homologue (Pgh1) gene is also implicated in CQ and mefloquine (MQ) resistance (Santos-Magalhaes & Mosqueira, 2010). It is an analogue of glycoproteins found in cancer cells that function as pumps to expel cytotoxic drugs (Le Bras & Durand, 2003). Therefore, CQ resistant strains are proposed to accumulate less CQ within the parasite.

MQ and halofantrine (HF) were developed by the US Army and are both aryl amino alcohol derivatives of quinine (Figure 1.5). They are all blood stage specific and acts on hemoglobin digestion probably similarly to the mode-of-action of CQ (Vangapandu *et al.*, 2007). QN accumulates in the food vacuole and therefore inhibits the formation of hemozoin biocrystals, hence leading to the formation of toxic heme within the parasite (Figure 1.5). QN has traditionally been used to treat cerebral malaria despite its toxicity when given intravenously and may also lead to serious cardiovascular or central nervous system toxicity. Complacency is also associated with QN since it must be taken orally three times daily for seven days therefore resulting in rapid resistance development to QN by the parasite (Na-Bangchang & Karbwang, 2009). MQ, which also induces the formation of toxic heme complexes within the parasite food vacuole, was developed during the Vietnam War to treat US soldiers (Figure 1.5). Side effects associated with MQ include nausea, vomiting, diarrhoea, and several severe neurological effects that include hallucinations, sleep disturbances, psychosis and delirium (Table 1.1). Primaquine (PQ) is a schizontocide used for prophylaxis against all types of malaria. It is active against schizonts and gametocytes and in *P. vivax* is able to prevent malaria relapse due to the presence of hypnozoites. Unfortunately, it is a very toxic drug with adverse side effects that includes anorexia, cramps, chest weakness, and anaemia (Santos-Magalhaes & Mosqueira, 2010) (Table 1.1). The mechanism of resistance to QN has not been elucidated. MQ resistance seems to be associated with mutations in the *Pf*mdr1 gene resulting in increased drug efflux (Vangapandu *et al.*, 2007).

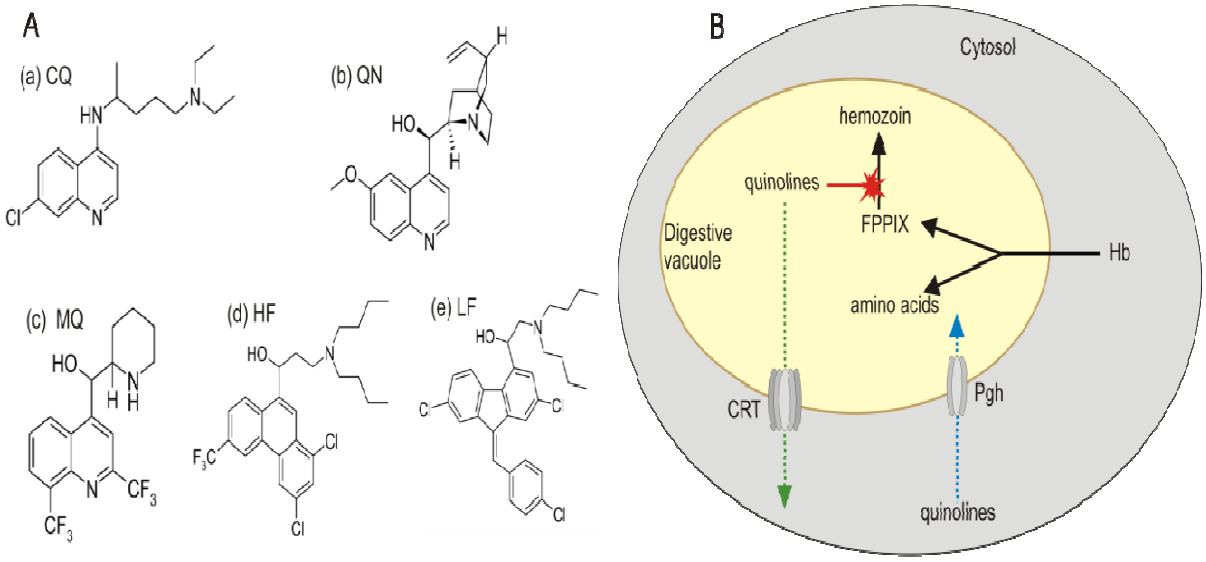

Figure 1.5: Proposed mode-of-action of quinoline-based drugs. Compiled from (Schlitzer, 2008, Hyde, 2007, Djimde *et al.*, 2001)

A: Structures of various quinoline drugs. (a) Chloroquine (CQ), (b) Quinine (QN), (c) Mefloquine (MQ), (d) Halofantrine (HF), (e) Lumefantrine (LF). B: Proposed mode-of-action of quinoline based drug. Quinolines prevent the formation of hemozoin (as indicated in red) during hemoglobin digestion within the food vacuole of the parasite. The proposed mechanism of resistance is also indicated in blue and green. Mutations in Pgh transporter protein will result in reduced import of CQ, while mutations in the *Pfcrt* gene will result in the *Pf*CRT transporter protein having increased ability to expel CQ from the food vacuole, therefore resulting in decreased CQ levels within the parasite food vacuole and therefore decreased efficiency.

1.7.2 Antifolates

Sulfadoxine/Pyrimethamine combination therapy (SP) has been used to replace CQ in many African countries. Unfortunately, due to the slow elimination of the drug, resistance soon prevailed (Na-Bangchang & Karbwang, 2009) (Table 1.1). Sulfadoxine (SDX) inhibits the dihydroopteroate synthase (DHPS) domain of the hydroxymethylpterin pyrophosphokinase/dihydropteroate synthase (HPPK/DHPS) bifunctional enzyme complex (Figure 1.6). DHPS is only found in the parasite and not in the human host, therefore making it a good target. Pyrimethamine (PYR), proguanil and cycloguanil (CG) are able to inhibit dihydrofolate reductase (DHFR) activity of the dihydrofolate reductase/thymidylate synthetase (DHFR/TS) bifunctional enzyme complex, and are able to bind more strongly to the DHFR enzyme from the parasite than that of its human orthologue. Anti-folates attack all stages of the parasite in the erythrocytic cycle and can inhibit the early development stages in the liver and mosquito (Vangapandu *et al.*, 2007). These drugs are able to block DNA replication in the parasite by blocking the synthesis of folates that are necessary for DNA metabolism. Resistance to PYR, CG and chlorocycloguanil are as a result of point mutations in the DHFR enzyme, while mutations in the DHPS gene are responsible for resistance to the sulfa-drugs (Na-Bangchang & Karbwang, 2009, Bacon *et al.*, 2009).

The atovaquone/proguanil combination was only introduced in 1997 as a prophylaxis and has a mechanism of synergy that is not yet fully understood (Table 1.1). Atovaquone (AVQ) is a structural analogue of coenzyme Q that plays a role in the electron transport chain (Figure 1.6). It works on the principle that blockage is obtained from the iron-sulfur protein that is required for electron transfer to cytochrome c1 from ubihydroquinone that is bound to the cytochrome b within complex III. Inhibition with this drug will result in the membrane potential changing and ultimately leading to arrest of parasite respiration and a lack of pyrimidine biosynthesis, with the added advantage that this drug does not affect the human mitochondria. Resistance occurs due to specific point mutations in cytochrome b (Hyde, 2007).

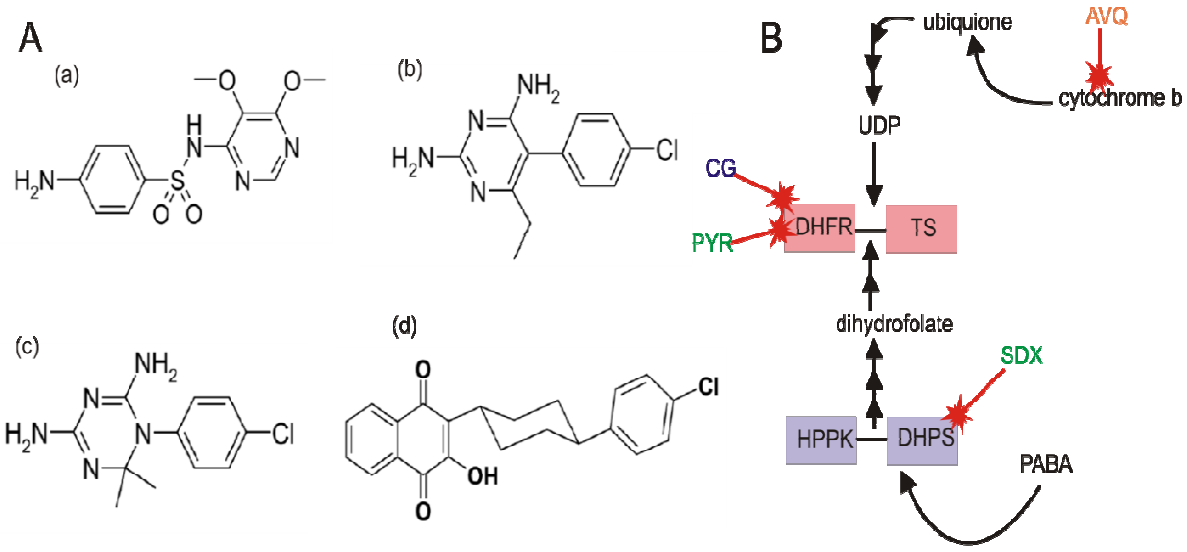

Figure 1.6: Proposed mode-of-action of anti-folate drugs. Compiled from (Hyde, 2007, Schlitzer, 2008, Le Bras & Durand, 2003).

A: Structures of various anti-folate drugs. (a) Sulfadoxine (SDX), (b) Pyrimethamine (PYR), (c) Cycloguanil (CG), (d) Atovaquone (AVQ). B: Proposed mode-of-action of anti-folate drugs. Drug target indicated in red. PYR and CG inhibits the activity of DHFR resulting in tetrahydrofolate depletion within the parasite. SDX inhibits the activity of DHPS resulting in dihydropteroate depletion within the parasite. AVQ is a prophylactic drug only and disrupts the membrane potential of the parasite. Resistance to PYR, CG and SDX are obtained by point mutations within their respective drug targets.

1.7.3 Artemisinin

The only currently effective drug is artemisinin and derivatives thereof. Artemisinin derivatives are used in clinical applications and are predominantly used in combination with other drugs (Hyde, 2005). The advantage of artemisinin is its short half live, and therefore unlikely resistance development, although the first signs of resistance to artemisinin has been reported in Western Cambodia (Noedl *et al.*, 2008) (Table 1.1). This calls for urgent containment measures, since

recrudescence is already seen in 30% of patients receiving artemisinin as a mono-therapy in Cambodia compared to 10 % in North-Western Thailand (Dondorp *et al.*, 2009).

Artemisinin was first extracted from the Chinese plant *Artemisia annua*, more commonly known as sweet wormwood or "qinghao", and was used by Chinese herbal medicine practitioners for at least 2000 years. The naturally occurring compound has poor bio-availability and therefore derivatives have been made. The most important artemisinin derivatives are artesunate, artemether, arteether and dihydroartemisinin (Meshnick S.R., 2002) of which sodium artesunate is the most effective derivative being able to reduce parasite numbers ~10^4-fold in 48 hours (Hyde, 2007). Artemisinin is a fast acting drug that acts on all forms of the blood stages as well as gametocytes, but not on the liver stage or transmission to the mosquito. Due to the rapid increase in antimalarial drug resistance by the parasite, the WHO recommends the use of ACT's rather than mono-therapy for the treatment of malaria (World Malaria Report 2008). An ACT will include an artemisinin-based drug in combination with another antimalarial drug in order to prevent development of resistance to the artemisinin drugs that are currently the last line of defence against malaria. The principle entails that the parasites that may escape the fast acting artemisinin are then killed by the slower acting partner. The WHO recommends the following therapeutic options for ACT-based treatment of uncomplicated and severe *falciparum* malaria: artemether/lumefantrine; artesunate/amodiaquine; artesunate/sulfadoxine/pyrimethamine (only in areas with sulfadoxine/pyrimethamine efficacy); artesunate/mefloquine; and, dihydroartemisinin/piperaquine. These ACT's should be administered for at least 3 days for an optimum effect. Absorption of the ACT's are also enhanced when administered in combination with a fatty meal (WHO Guidelines for the treatment of malaria, 2010). The use of ACT's have impacted positively on the malaria situation, since at least 40 countries in Africa now prefer the use of ACT's for first line treatment of malaria. Two-hundred and fifty million treatments of CoArtem® (artesunate/lumefantrine) were delivered to Africa at the end of July 2009 in the fight against malaria. The combined use of CoArtem (artemether/lumefantrine combination therapy) and increased efforts of IRS together with the provision of ITN's have resulted in a 66% decrease in malaria-related deaths in Zambia. Similarly in Kwa-Zulu Natal, South Africa, the use of CoArtem as first line treatment in combination with renewed vector control efforts resulted in a 97% decrease in malaria-related deaths in 2003 (Barnes *et al.*, 2009). CoArtem has few adverse side effects and also claims safety during pregnancy although this may be somewhat controversial (Falade & Manyando, 2009) (Table 1.1).

Two possible modes-of-action for artemisinin have been proposed, although it seems that both mechanisms depend on the activation of the peroxide group that will form free radicals (Figure 1.7).

The first proposed mechanism is that artemisinin interferes with sarco/endoplasmic reticulum calcium-dependent ATPase (SERCA). Upon treatment with artemisinin, Fe^{2+} is activated which will enable the inhibition of the SERCA-like *Pf*ATP6 ATPase transporter. *Pf*ATP6 is the only SERCA-type Ca^{2+} ATPase in the parasite and is completely inhibited by artemisinin. SERCA maintains the Ca^{2+} ion concentrations that play a role in signalling and post-translational processing of proteins. Artemisinin binds to *Pf*ATP6 by hydrophobic interactions allowing cleavage of the peroxide bridge by iron that will then generate carbon-centred radicals ultimately resulting in enzyme inhibition and parasite death (Eckstein-Ludwig *et al.*, 2003, Krishna *et al.*, 2006). The second proposed mechanism is the production of reactive species. The heme or iron catalyses the peroxide bridge of the drug causing the formation of free radicals that will ultimately lead to protein alkylation (de Ridder *et al.*, 2008, Vangapandu *et al.*, 2007). Resistance may be by mutations in the *Pf*atp6 gene (Jambou *et al.*, 2005).

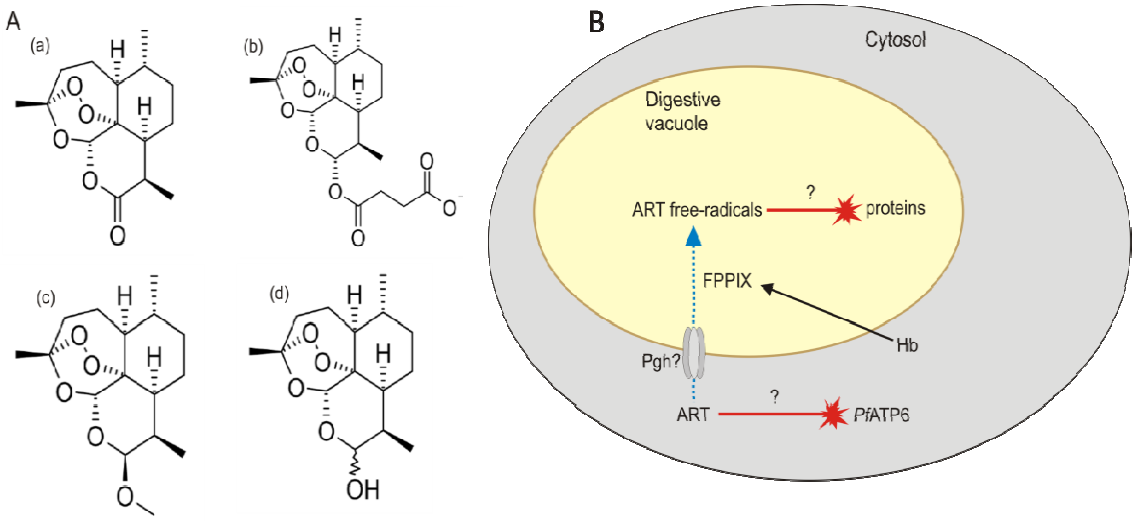

Figure 1.7: Proposed mode-of-action of artemisinin based drugs. Compiled from (Hyde, 2007, Schlitzer, 2008, de Ridder *et al.*, 2008, Jambou *et al.*, 2005)

A: Structures of various artemisinin based drugs. (a) Artemisinin (ART), (b) Artesunate, (c) Artemether, (d) Dihydroartemisinin. B: Proposed mode-of-action of artemisinin based drugs. The first proposed mode-of-action is by interference with *Pf*ATP6, while the second proposed mode-of-action is by the production of radicals that will damage parasite proteins. Resistance occurs due to mutations in the *Pf*atp6 gene.

The reality of the current malaria situation is that parasite resistance to drugs is on the increase. The problem at the moment is that there is no replacement drug available in the near future, and the possibility of a vaccine may be a reality but still far in the future. The availability of the *Plasmodium* genome (Gardner *et al.*, 2002) may impact on the quality of human health but needs to be exploited. It may provide a basic understanding of the *Plasmodium* parasite, and this may be used to develop effective vaccines, new drugs and improved diagnostics (Duraisingh M. *et al.*, 2006).

Table 1.1: Summary of currently used drugs. Compiled from (de Ridder *et al*., 2008, Vangapandu *et al.,* 2007, Jambou *et al*., 2005, Hyde, 2007, Schlitzer, 2008, Le Bras & Durand, 2003, Djimde *et al*., 2001)

Drug	Pharma name	Discover	Half life	Mw (g/mol)	Formulae	Cellular Target	Advantages	Disadvantages	Prophylaxis or treatment
Quinolines									
Chloroquine	Resochin Dawaquin Daramal	1934	1-2 months	436.0	$C_{18}H_{26}ClN_3$	Heme metabolism	Fast acting in erythrocytic stage, hydrophilic, good bio-availability, cheap	Macular retinopathy, widespread resistance, itching	Both
Quinine	Quininmax Aflukin	1633	~18 h	324.4	$C_{20}H_{24}N_2O_2$	Heme metabolism	Fast action in erythrocytic stage, hydrophilic, oral route, good bio-availability	Not well tolerated, adverse side effects, hypoglycemia, neurotoxicity	Treatment
Mefloquine	Lariam	1963	2 to 4 weeks	378.3	$C_{17}H_{16}F_6N_2O$	Heme metabolism	Potent in RBC stage	Severe neuropsychiatric reactions, depression, “suicide”, long half-life	Mostly prophylaxis
Amodiaquine	Camoquine Flavoquine		5.2 ± 1.7 min	355.9	$C_{20}H_{22}ClN_3O$	histamine N-methyltransferase inhibitor	Effective against CQ resistant strains	Hepatoxic No longer marketed in US	Treatment
Halofantrine	Halfan	1960s	6 to 10 days	500.4	$C_{26}H_{30}Cl_2F_3NO$	Withdrawn from market	oral	cardiac arrhythmias only for treatment due to erratic absorption and toxicity	Treatment
Anti-folates									
Pyrimethamine	Daraprim	1951	96 h	248.71	$C_{12}H_{13}ClN_4$	Folate synthesis inhibition of DHFR	Oral use, prophylaxis and treatment	may deplete folic acid in humans	Both
Sulfadoxine			150-200 h	310.33	$C_{12}H_{14}N_4O_4S$	Structural analog of PABA inhibits DHPS	Oral use, prophylaxis and treatment		Both
Antibiotics									
Doxycycline	Vibramycin Monodox Doxyhexal	1960s	18-22 h	444.43	$C_{22}H_{24}N_2O_8$	Impairment of apicoplast genes resulting in abnormal cell division	Used for prostatitis, sinusitis, syphilis, chlamydia, in malaria prophylaxis	Delayed antimalarial effect, slow acting	Prophylaxis
Artemisnins									
Artemesinin, Dihydroartemesinin, Artesunate, artemether			30 min			Inhibits *Pf*ATP6 outside food vacuole	Safe, well tolerated, fast acting, gametocytocidal, schizonticidal, no wide spread resistance	dose dependent, short half life, low bio-availability, poor water solubility	Treatment only
Combinations									
Artemether (AM)-lumefantrine (LM)	CoArtem® Lumerax	1987	LM 4-6 days, AM 30 min AM 20mg, LM 120mg			Many targets, heme metabolism, protein metabolism	Well-tolerated, meet WHO criteria for safety and quality	Expensive, not for use during pregnancy	Treatment
Pyrimethamine	Fansidar		100 - 231 h SDX, 54 - 148 h PYR,			Synergistic action against	synergistic action,	Not for use in pregnancy,	Treatment,

(PYR)-sulfadoxine (SDX)	Laridox		SDX 500mg, PYR 25mg	folate biosynthesis	schizonticidal, blood stages, effective against CQ resistance	skin reactions	no longer prophylaxis
Chlorproguanil (CPG)-dapsone (DS)	LapDap	1980s	CPG 12 h, DS 20 h CPG 80 mg, 100 mg DS	Synergistic on folate biosynthesis CP inhibits DHFR and DS inhibits DHPS	Fast elimination times, lower tendency towards resistance	Toxicity at high concentrations	
Dihydroartemisinin(DHA) - Piperaquine Phosphate (PPQ)	Duo-Cotecxin		DHA 2 h, PPQ 9 days DHA 40mg, PPQ 320mg	Synergistic combination	active against the asexual forms, schizonts, gametocytes oral, good for resistant strains	Only orally, nausea, diarrhoea, loss of appetite, not during pregnancy	Treatment
Artesunate (AS) - Mefloquine (MQ)	Artequin		AS 30 min and MQ 21 days AS 200 mg, MQ 250 mg	Schizonticidal action	Oral, good for resistant strains, good tolerability, short treatment duration	Side effects on nervous and digestive system	Treatment
Artesunate (AS) - Amodiaquine	ASAQ Larimal	2007	AS 30 min and ADQ 6 min AS 100 mg and ADQ 270 mg	Schizonticidal action	Affordable, effective against erythrocytic stages	Dizziness, itching, headache, photosensitivity	Treatment
Artesunate (AS) Pyrimethamine (PYR)-sulfadoxine (SDX)	Artidox		100 - 231 h SDX, 54 - 148 h PYR, AS 30 min AS 50 mg, SDX 500mg, PYR 25mg	AS has schizonticidal action SP has synergistic action against folate biosynthesis	Oral use	Not during pregnancy, abdominal pain, nausea	Treatment
Atovaquone (AV) - Proguanil (PG)	Malarone, Melanil	1997	AV 2-3 days PG weeks 250 mg AV, 100 mg PG	Synergistic combination, folate biosynthesis and pyrimidines	Short usage period	Prophylaxis only	Prophylaxis only

1.8 New drug targets

The first step in drug discovery is the identification of novel drug targets that are absolutely essential for parasite survival (Na-Bangchang & Karbwang, 2009). An important point for consideration during drug discovery is the fact that the parasite resides inside the erythrocyte and that a successful drug should be able to cross multiple membranes (Santos-Magalhaes & Mosqueira, 2010). Ideally, an antimalarial should be selective, curative and have no toxicity for the human host, have good oral bio-availability, and allow short treatment duration in order to avoid complacency. Drug development can be broken down into 4 main steps that include target identification, target validation, identification of lead inhibitors, and optimisation of those inhibitors regarding their pharmacological and toxicological properties. A drug target is validated when it is proven to be essential for growth and survival (Cowman & Crabb, 2003). Target selectivity is indicated by sequence differences between parasite and host or absence in the host. The *Pf*DHFR gene shares only 27% homology with its human counterpart with the majority of divergence occurring in the active site (Yuvaniyama *et al.*, 2003). This results in the extremely tight binding of PYR to *Pf*DHFR. The apicoplast is a plastid-like organelle related to the chloroplast found in plants and is the major centre for fatty acid metabolism, isoprenoid and heme synthesis which are not found in the human host (McLeod *et al.*, 2001). Specific pathways that can be targeted include the shikimate pathway which is not present in mammalians and is therefore a target worth exploiting. Seven enzymes are involved within this pathway that converts erythrose-4-phosphate and phosphoenolpuruvate to chorismate, which is then utilized by various other pathways including the production of p-aminobezoic acid (pABA) utilized in the folate pathway (Table 1.2). Secondly, the Plasmodial protein farnesyltransferase (*Pf*PFT) is active in the isopreniod biosynthesis and plays a role in post-translational modifications. PFT inhibitors have been used in the treatment of human cancers and are therefore worth exploiting. The parasite also has its own antioxidant enzymes to protect it from oxidative stress and include 3 enzymes (superoxide dismutase, glutathione peroxidase and catalase), which together with the redox enzymes can be viable drug targets (Muller, 2004) (Table 1.2).

Polyamine metabolism is a target in cancer therapy as well as in some other parasitic diseases and is therefore worth exploiting in the Plasmodial parasite (Muller *et al.*, 2008, Clark *et al.*, 2010), and is discussed in more detail in the following section.

Table 1.2: Summary of potential new drug targets. Compiled from (Jana & Paliwal, 2007, Vangapandu *et al.*, 2007, Olliaro & Yuthavong, 1999, Fatumo *et al.*, 2009)

Target/pathway	Enzymes	Inhibitor	DIndex[a]	Reference
Polyamine biosynthesis	S-adenosyl-L-homocysteine hydrolase Adenosine deaminase Spermidine synthase AdoMetDC ODC	Neplanocin A Coformycin Cyclohexalamine MDL73811 DFMO	0.8 1 0.6 0.8 0.8	(Kitade *et al.*, 1999, Shuto *et al.*, 2002) (Tyler *et al.*, 2007) (Haider *et al.*, 2005) (Wright *et al.*, 1991) (Berger, 2000)
Vitamine B synthesis	Pyridoxal kinase	Aminphylline	n/d	(Delport *et al.*, 1990)
Apicoplast	Fab H Fab I	Thiolactomycin Triclosan	n/d n/d	(He *et al.*, 2004) (McLeod *et al.*, 2001)
Shikimate pathway	5-enolpyruvyl shikimat 3-phosphate synthase Chorismate synthase	Glyphosphate 6-S-fluoroshikimate	0 0.6	(McConkey, 1999) (McRobert *et al.*, 2005)
Hemoglobin metabolism/proteases	Plasmepsin I, II, Falcipains	Leupeptin, pepstatin Vinyl sulfones, chalcones	0.8 0.6	(Coombs *et al.*, 2001) (Rosenthal *et al.*, 1996)
Pyrimidine synthesis, electron transport	DHODase Thymidylate synthase	Pyrazofurin 5-fluoroorotate	1 1	(Biagini *et al.*, 2003) (Jiang *et al.*, 2000)
Purine salvage, DNA/RNA	HGPRT Topoisomerase I DNA topoisomerase II	Allopurinol Irinotecan Levofloxacin	n/d 1 0.8	(Sarma *et al.*, 1998) (Azarova *et al.*, 2007) (Kicska *et al.*, 2002)
Glycolysis	Hexokinase	Brefeldin A	0.6	(Wanidworanun *et al.*, 1999, Kumar & Banyal, 1997)
Transporters	Hexose transporter	O-3-hexose derivatives	0.4	(Joet *et al.*, 2003)
Isoprenoid biosynthesis	DOXP reductoisomerase Protein farnesyltransferase	Fosmidomycin FTI-2153	0 n/d	(Nallan *et al.*, 2005) (Ohkanda *et al.*, 2001)
Redox system/ oxidant defense	Thioredoxin reductase Gamma-GCS GST Glutathione reductase	5,8-dihydroxy-1,4-naphtoquinone Buthionine sulfoximine Hemin Selenocysteine	0.9 0.6 0.6 0.9	(Luersen *et al.*, 2000) (Meierjohann *et al.*, 2002) (Fritz-Wolf *et al.*, 2003) (Muller, 2004)
Mitochondrial system	Cytochrome c oxidoreductase	Atovaquone	n/d	(Krungkrai *et al.*, 1997)
Membrane biosynthesis	Phospholipid biosynthesis	G25	n/d	(Roggero *et al.*, 2004)
Protein kinases	Various protein kinases	Xestoquinone	n/d	(Doerig & Meijer, 2007)

[a]DIndex is the druggability index given by the TDR database (www.tdrtargets.org). The DIndex is a composite score consisting of a weighted normalised sum in order to predict the likelihood of a protein being druggable. The DIndex values range from 0 to 1. A larger score is an indication that the protein is more likely to be a druggable target. n/d: not determined. HGPRT: hypoxanthine-guanine-xanthine phosphoribosyltransferase, DOXP: 1-deoxy-D-xylose-5-phosphate, GCS: glutamylcysteine synthetase, Fab H: β-ketoacyl-ACP synthase III, Fab I: enoyl-ACP reductase, DOHDase: dihydroorotate dehydrogenase. GST: glutathione S-transferase. CDK: Cyclin dependent protein kinases. AdoMetDC: S-adenosylmethionine decarboxylase. ODC: Ornithine decarboxylase.

1.9 Polyamines

Polyamines are small flexible polycations that are represented by 3 basic polyamines which include the diamine putrescine (1,4-diaminopropane), the tri-amine spermidine [N-(3-aminopropyl)-1,4-diaminobutane] and the tetra-amine spermine [N,N'-bis(3-aminopropyl)-1,4-butanediamine] (Figure 1.8). At physiological pH, these polyamines are positively charged and are therefore capable of electrostatic interaction with nucleic acids, DNA, RNA and proteins (Heby *et al.*, 2007) (Figure 1.8). The interaction of polyamines with various macromolecules may lead to stabilisation of DNA, and the regulation of transcription and replication. Polyamines also have a very important role in cellular differentiation, proliferation, growth and division (Pignatti C. *et al.*, 2004, Geall A.J. *et al.*, 2004, Assaraf Y.G. *et al.*, 1987).

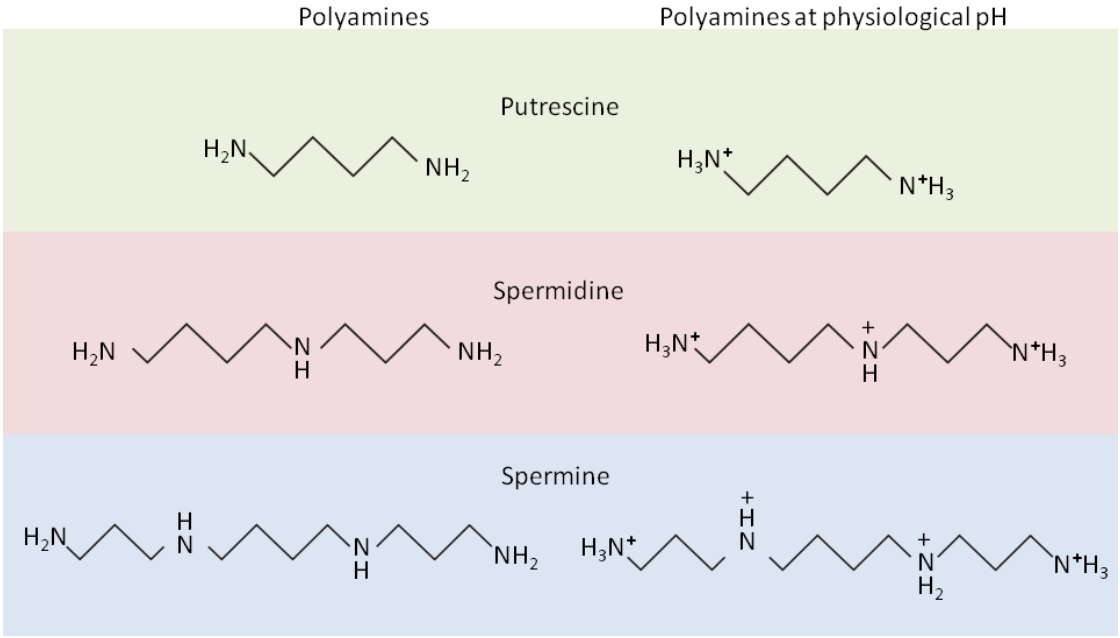

Figure 1.8: Chemical structures of the polyamines, putrescine, spermidine and spermine.
The 3 major polyamines at their uncharged states as well as at physiological pH when they are cationic.

In mammalian cells, the cell cycle is regulated by polyamines which are able to affect cell cycle check points and cyclin degradation (Pignatti C. *et al.*, 2004). The depletion of polyamines results in cell cycle arrest at the G1 phase of the cell cycle due to the accumulation of p21 and p27. Polyamines are also said to play a role in cell death and apoptosis. There is increasing evidence that polyamines, cell cycle regulation and apoptosis are closely connected. This is also one of the major issues in cancer research. When polyamine biosynthesis is inhibited by DL-α-difluoromethylornithine (DFMO), apoptosis will be induced by the release of cytochrome c from the mitochondria (Pignatti C. *et al.*, 2004). Complete polyamine depletion will result in an induction of caspase activation and subsequent induction of apoptosis (Pignatti C. *et al.*, 2004).

1.9.1 Polyamine synthesis

Polyamine metabolism in mammalian cells uses methionine and arginine as precursors which will then undergo a series of reactions for the formation of the 3 polyamines (Figure 1.9). The polyamine synthetic enzymes in mammalian cells are regulated at the transcriptional, translational and post-translational levels (Muller *et al.*, 2001). ODC activity is regulated by antizyme, which is also able to promote degradation of ODC. The polyamine biosynthetic enzymes are also prone to feedback inhibition of their products. Polyamine metabolism in mammalian cells are more complex than polyamine metabolism within the Plasmodial parasite since various enzymes are present within the mammalian cells that are absent from the parasite. Polyamines can be converted back by interconversion pathways that involve cytosolic N1-acetyltransferase and polyamine oxidase that are specific to spermidine and spermine.

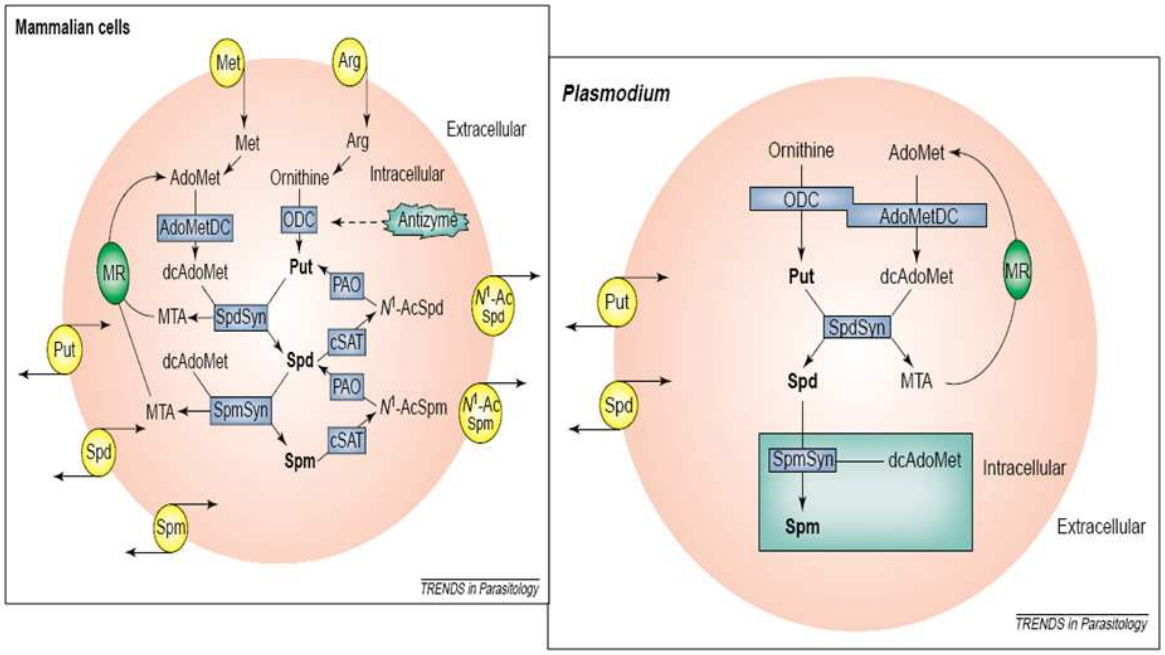

Figure 1.9: Polyamine metabolism in mammalian cells and in *Plasmodium* (Muller S. *et al.*, 2001).
The difference between mammalian cells and that of *Plasmodium* is the bifunctional AdoMetDC/ODC in *Plasmodium* and the simpler polyamine pathway. Ornithine acts as the substrate for ornithine decarboxylase (ODC) which produces putrescine (put). S-adenosylmethionine (AdoMet) is the substrate for S-adenosylmethionine decarboxylase (AdoMetDC) to form decarboxylated AdoMet (dcAdoMet). SpdSyn: Spermidine synthase, Spd: spermidine, spm: spermine, MR: methionine recycling.

In *P. falciparum*, arginase produces ornithine from arginine. Ornithine acts as the substrate for ornithine decarboxylase (ODC) which produces putrescine by the decarboxylation of ornithine. Methionine is utilised by S-adenosylmethionine synthase (AdoMet synthase) in the production of S-adenosylmethionine (AdoMet) which in turn is the substrate for S-adenosylmethionine decarboxylase (AdoMetDC). AdoMetDC decarboxylates AdoMet to form decarboxylated AdoMet (dcAdoMet) of which the aminopropyl group is then donated to spermidine synthase that will add

this to putrescine to form spermidine and ultimately spermine. No spermine synthase activity has been demonstrated in *Plasmodium* but it is assumed that spermidine synthase is able to produce low levels of spermine within the parasite (Haider *et al.*, 2005).

Polyamine metabolism in Plasmodial parasites are controlled by the rate-limiting decarboxylase activities of both AdoMetDC and ODC. An interesting property of Plasmodial polyamine metabolism is the fact that AdoMetDC and ODC form a unique bifunctional Plasmodial AdoMetDC/ODC complex (*Pf*AdoMetDC/ODC) with a molecular mass of 330 kDa (Muller *et al.*, 2000). *Pf*AdoMetDC/ODC is linked by a hinge and contains parasite specific inserts. Both *Pf*AdoMetDC and *Pf*ODC are able to function independently (Wrenger *et al.*, 2001), although specific inserts have been identified that is important in the modulation of enzyme activity and domain interactions within the parasite (Birkholtz *et al.*, 2004). Feedback regulatory mechanisms have been identified for *Pf*ODC which is regulated by putrescine (Wrenger *et al.*, 2001), but putrescine has no regulatory effect on the activity of *Pf*AdoMetDC (Wells *et al.*, 2006). This is in contrast to *Trypanosoma cruzi* in which putrescine activates AdoMetDC (Clyne *et al.*, 2002). This suggests that polyamine metabolism within Plasmodial parasites are probably regulated by the activities and interactions within the bifunctional *Pf*AdoMetDC/ODC complex (Clark *et al.*, 2010).

Another unique difference between mammalian and *P. falciparum* AdoMetDC/ODC is the fact that the Plasmodial bifunctional enzyme has a very long half-life of about 2 hours compared to 15 min of the mammalian counterpart (Muller *et al.*, 2001). This long half-life of *Pf*AdoMetDC/ODC has also been determined in Trypanosomes and is therefore worth exploiting (Wrenger *et al.*, 2001). The AdoMetDC activity within Trypanosomes is tightly regulated by prozyme, a property unique to Trypanosomes (Willert & Phillips, 2008). Both prozyme identified in Trypanosomes and antizyme identified in mammalians are absent in *Plasmodia.*

High levels of polyamines are often associated with highly proliferating cells like Plasmodial parasites and constitutes 14% of the Plasmodial metabolome, and is therefore the major metabolite present within the Plasmodial parasite (Teng *et al.*, 2009, Olszewski *et al.*, 2009). The host erythrocytes have no polyamine machinery and have therefore trace amounts of polyamines when they are uninfected. Upon invasion of the erythrocytes the polyamine content within the infected erythrocyte is altered due to the activities of the *Pf*AdoMetDC/ODC enzyme. Similar to the increase in *Pf*AdoMetDC/ODC activity an increase in polyamines can be observed during infection of an erythrocyte (Das Gupta *et al.*, 2005) (Figure 1.10).

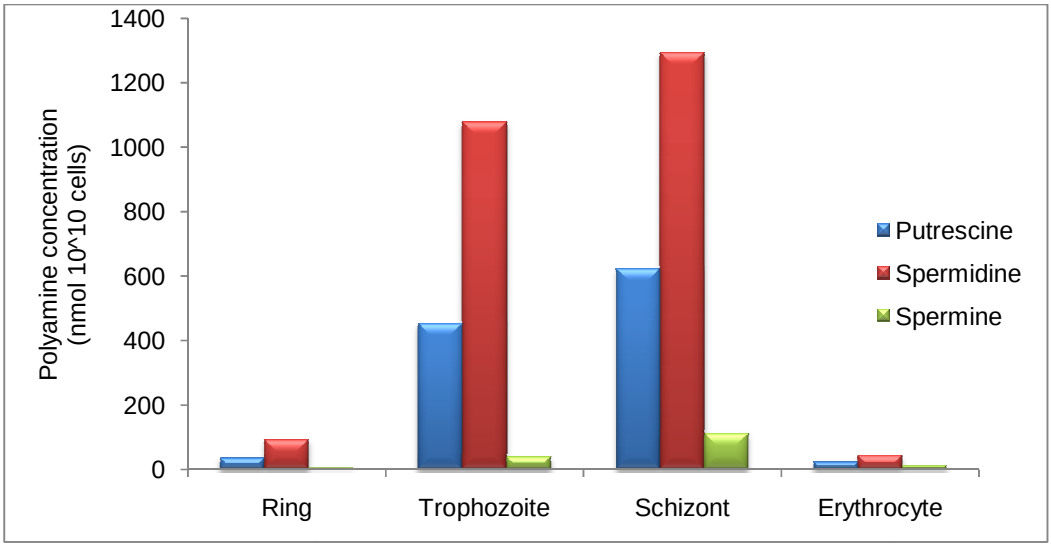

Figure 1.10: Polyamine content of erythrocytes. Adapted from (Das Gupta *et al.*, 2005)
A graph depicting the increase in polyamine levels when a erythrocyte is infected with *P. falciparum*. The metabolite levels of spermine, spermidine and putrescine all increase more than a 1000-fold upon infection of an erythrocyte.

Mice infected with *T. brucei* were treated with the AdoMetDC inhibitor 5'-([(Z)-4-amino-2-butenyl]methylamino)-5'-deoxyadenosine (MDL73811) (Figure 1.11) and were subsequently cured from infection (Bitonti *et al.*, 1990). MDL73811 is a potent irreversible inhibitor of AdoMetDC and were effective against *T. brucei rhodesiense* infected mice (Bacchi *et al.*, 1992b). Similarly to the effectiveness of polyamine depletion with MDL73811 in Trypanosomes, polyamine depletion in *Leishmania* resulted in parasite death (Singh *et al.*, 2007) and the polyamine biosynthetic enzymes were subsequently validated as drug targets in *L. donovani* (Boitz *et al.*, 2009).

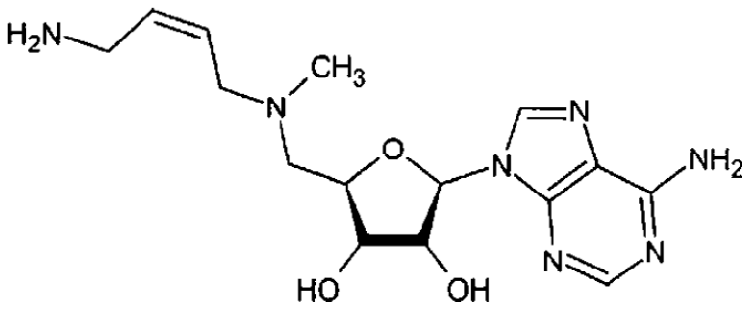

Figure 1.11: Structure of MDL73811

The bifunctional *Pf*AdoMetDC/ODC is considered one of the top 20 drug targets and is highly druggable with a druggable index of 0.8 (max 1) according to the TDR database (Table 1.2). It is therefore of utmost importance that these unique features of *Pf*AdoMetDC/ODC are exploited with the aim to validate this protein as a drug target.

1.10 The "omics" era

Research is currently dominated by the "omics" boom, and the wealth of information that are being made available. With the completion of the *Plasmodium* genome (Gardner *et al.*, 2002), as well as the *Anopheles* genome (Holt R.A., 2002), the hope has been on finding a vaccine for malaria or finding a novel drug target. The *P. falciparum* 3D7 nuclear genome is composed of 22.8 megabases (Mb) that are distributed among 14 chromosomes ranging in size from approximately 0.643 to 3.29 Mb, with an overall A+T composition of 80.6% (Gardner *et al.*, 2002). The availability of the genome sequence has opened the way for application of functional genomics. Functional genomics attempts to answer questions on the function of genes and proteins by a genome wide approach using high-throughput methods like transcriptomics, proteomics and metabolomics.

1.10.1 Transcriptomics

Microarray data for *P. falciparum* has been published on the IDC (Bozdech *et al.*, 2003) sexual gametocytes (Young J.A. *et al.*, 2005), as well as the comparative gene expression profiles of the IDC for 3D7, Dd2 and HB3 (Llinas *et al.*, 2006). The IDC transcript profile was established by monitoring transcripts every hour over the complete 48 hour life cycle of the parasite. This transcriptional profile revealed that 60% of the transcriptome is transcriptionally active during the IDC with a unique "just-in-time" manufacturing process by which the genes are only transcribed once they are needed (Bozdech *et al.*, 2003). Therefore, a transcript is generally only expressed for a period of 0.75 to 1.5 cycles over the 48 hour life period of the parasite (Bozdech *et al.*, 2003). Only a few transcripts are expressed throughout the life cycle of the parasite. Cross comparison of 3 Plasmodial strains revealed that the transcripts between 3D7, Dd2 and HB3 share more than 80% similarity (Llinas *et al.*, 2006). The transcripts of all 3 strains are also expressed and regulated remarkably similar to each other (Figure 1.12). The *in vivo* transcriptome derived from *P. falciparum* infected patients revealed similarities to the *in vitro Pf*3D7 ring stage transcriptome, with a major difference being the over expression of surface proteins in the *in vivo* data (Daily *et al.*, 2004). Various malarial drug perturbation studies have been investigated on a global transcriptome level and will be discussed in more detail in Chapter 4.

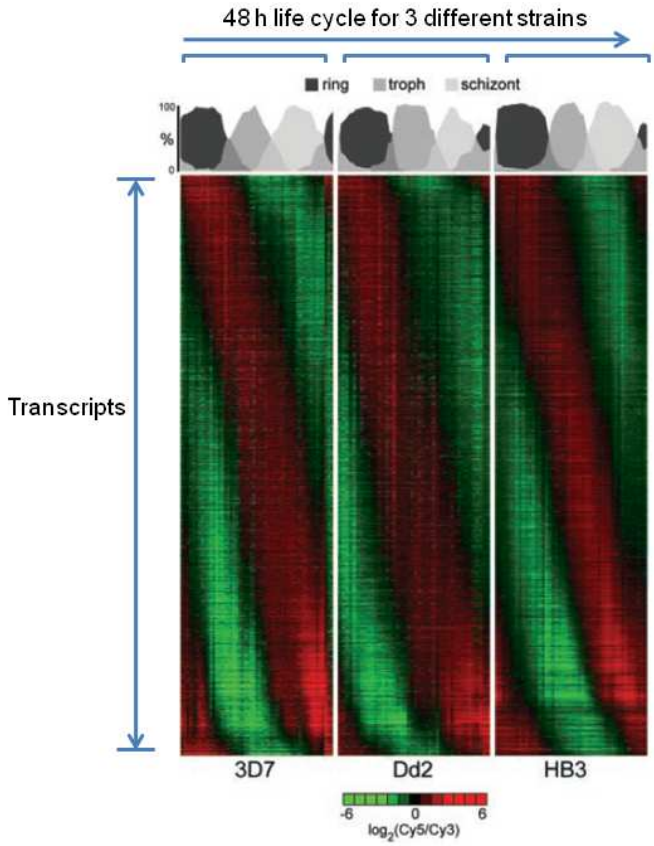

Figure 1.12: The phaseograms of the IDC of 3 Plasmodial strains depicted over a 48 hour period (Llinas *et al.*, 2006).

The phaseograms depicts the "just-in-time" expression of transcripts only when they are needed. The picture is representative of *P. falciparum* strain 3D7, *P falciparum* strain Dd2 and *P. falciparum* strain HB3. Red is indicative of transcripts with increased abundance ("switched on"), while green is indicative of transcripts with decreased abundance ("switched off").

1.10.2 Proteomics

Integration of microarray data with proteomic data will further our understanding of molecular mechanisms and regulation. Proteomic data is of utmost importance since it is able to provide a blue print of the functional units within a cell at any given moment in time. Similar to microarray data, the whole proteome of the different stages of *Plasmodium* has been characterised (Lasonder *et al.*, 2002), with additional Plasmodial life stages classified that include trophozoites, merozoites, sporozoites and gametocytes (Florens *et al.*, 2002). Proteome data for *P. berghei* and *P. chabaudi*, (Hall *et al.*, 2005) as well as *P. falciparum* ItG, A4, C24 and 3D7 strains are available (Wu Y. & Craig A., 2006). Plasmodial proteomic advances and Plasmodial perturbation studies investigated with proteomics will be discussed in more detail in Chapters 2 and 3.

1.10.3 The Metabolome, kinome and interactome

The Plasmodial interactome has been created and can be accessed at PlasmoMAP for interactive information regarding the interactome (Date & Stoeckert, 2006). Recently, clusters within the interactome has also been determined and revealed the importance of especially the ring and schizont stages (Wuchty *et al.*, 2009). The Plasmodial kinome identified a total of 65 genes encoding the protein kinase family within Plasmodial parasites (Ward *et al.*, 2004). The most interesting observation was the identification of the FIKK family of kinases which consists of 20 unique enzymes that are only found in apicomplexa. All these FIKK kinases contain a unique PEXEL sequence targeting proteins carrying this for transport to the erythrocyte membrane. Plasmodial parasites contain about 85-100 protein kinases which accounts for 1.1-1.6% of the total Plasmodial proteome. In contrast to Plasmodial parasites, humans have about 2% protein kinases (Doerig *et al.*, 2008). The Plasmodial metabolome is still relatively unknown with only 2 metabolome investigations to date. The Plasmodial metabolome was investigated using two-dimensional nuclear magnetic resonance (2-D NMR) (Teng *et al.*, 2009). Various extraction methods were investigated with more than 50 metabolites that were quantitated. Another metabolome investigation used LC-MS to determine metabolite levels of the Plasmodial parasite (Olszewski *et al.*, 2009).

1.11 The use of functional genomics to validate drug targets

With the completion of the genome for *P. falciparum* it sparked renewed hope for a novel drug target, although it was soon realised that the gene sequence alone cannot predict the gene activity and ultimately the gene and protein function (Chanda & Caldwell, 2003). Target validation entails identification of all the parasite proteins and processes that are affected and related to the efficacy of the particular drug in question (Figure 1.13). Targets that are unique to parasites and differ from host proteins are ideal, but parasite metabolism, drug binding to the target, and drug uptake should also be considered. A drug target can only be validated if the target is essential to growth with two validation strategies that can be followed. The first is genetically, by knock-out or knock-down or chemically, by inhibition of a specific protein (Cowman & Crabb, 2003). A gene can only be regarded as essential when the organism cannot survive without it (Freiberg & Brotz-Oesterhelt, 2005). The “omics” technologies alone does not provide sufficient information and for a complete understanding of the physiology and pathogenicity of organisms, integration between all the components of “omics” technologies are needed to gain maximal understanding of an particular organism (Hegde *et al.*, 2003, Birkholtz *et al.*, 2008b).

The transcriptome and proteome are both dynamic entities that changes rapidly in response to environmental changes, and therefore mining of both the transcriptome and the proteome may reveal valuable insight into the parasite response upon perturbation (Freiberg *et al.*, 2004). The application of functional genomics has proved successful in the elucidation of the mode-of-action of various anti-microbial agents (Scherl *et al.*, 2006, Pietiainen *et al.*, 2009). As such, functional genomics has proved indispensable in the mode-of-action determination of the drugs, isoniazid and ethionamide, against *Mycobacterium tuberculosis* (Wilson *et al.*, 1999, Fu & Shinnick, 2007, Boshoff *et al.*, 2004). Functional genomic investigations are currently contributing to the identification and validation of new drug targets to exploit in the fight against malaria (Birkholtz *et al.*, 2008b).

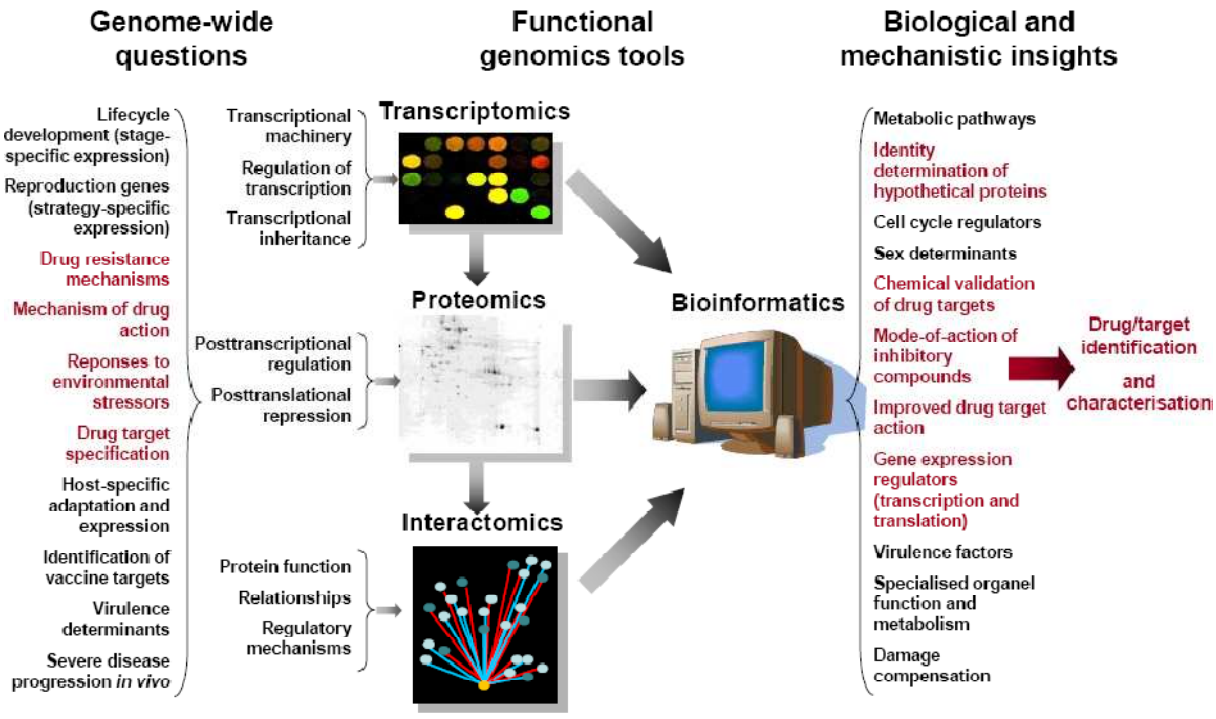

Figure 1.13: Functional genomics workflow (Birkholtz *et al.*, 2006).

The proposed workflow for Plasmodial functional genomics. Transcriptomics, proteomics and interactomics should be integrated to obtain biological and mechanistic insights into the functioning of Plasmodial parasites.

1.12 Objective

The objective of this study was the analysis of drug induced expression differences in the transcriptome and proteome of *P. falciparum* to allow the chemical validation of *Pf*AdoMetDC as a drug target.

1.12.1 Aims:

a) Morphological assessment of *Pf*AdoMetDC inhibited parasites over the complete life cycle to determine morphological time of parasite arrest.

b) Proteome profile analysis of *Pf*AdoMetDC inhibited parasites.

c) Transcriptome profile analysis of *Pf*AdoMetDC inhibited parasites.

d) Determination of the effect of polyamine depletion on the methylation status in *Pf*AdoMetDC inhibited parasites.

e) Determination of the biological relevance of the drug-induced expression changes in *P. falciparum* as a result of AdoMetDC inhibition.

Chapter 2 provides a description of an optimised 2-DE proteomic approach and application of this optimised 2-DE proteomic approach to characterise proteins within the late ring and early trophozoite stages of *P. falciparum* strain 3D7.

Chapter 3 describes the application of the optimised 2-DE proteomic approach to determine the proteomic response of Plasmodial parasites upon inhibition of AdoMetDC.

Chapter 4 is an investigation into the transcriptomic response of *P. falciparum* using oligonucleotide microarrays after the inhibition of AdoMetDC with MDL73811.

In chapter 5, further characterisation of specific metabolic responses identified in the transcriptomic and proteomic investigations of AdoMetDC-inhibited *P. falciparum* is described. This chapter includes an investigation into specific metabolites as well as determination of the methylation status of the parasite upon AdoMetDC inhibition as well as possible synergistic interactions. Finally, comparisons are made between the transcript and proteome to determine possible regulatory mechanisms.

Chapter 6 is the concluding discussion which integrates the knowledge gained from the transcriptomic and proteomic investigations and highlights the scientific contribution made within this study.

1.12.2 Papers resulting from the work presented within this dissertation

a) Smit, S., S. Stoychev, A. I. Louw & L. Birkholtz (2010) Proteomic profiling of *Plasmodium falciparum* through improved, semiquantitative two-dimensional gel electrophoresis. *J Proteome Res* **9**: 2170-2181.

b) Clark, K., J. Niemand, S. Reeksting, S. Smit, A. C. van Brummelen, M. Williams, A. I. Louw & L. Birkholtz (2010) Functional consequences of perturbing polyamine metabolism in the malaria parasite, *Plasmodium falciparum*. *Amino Acids* **38**: 633-644.

c) Smit, S., Clark K., Louw A.I., Birkholtz L. Functional genomic investigations into inhibited Plasmodial AdoMetDC and ODC reveals polyamine specific regulatory mechanisms. (Manuscript in preparation)

1.12.3 Conferences attended

1.12.3.1 Oral presentations

a) Smit S., Louw A.I., Birkholtz L. (2010) Functional consequences of the inhibition of Plasmodial S-adenosylmethionine decarboxylase as a key regulator of polyamine metabolism. 6th Biennial Symposium on Polyamines in Parasites, 3-6 August 2010, Phalaborwa, South Africa.

b) Smit S., Louw A.I., Birkholtz L. (2009) A functional genomic approach to investigate the effect of polyamine depletion induced by the inhibition of S-adenosylmethionine decarboxylase in the human malaria parasite. 5th Multilateral Initiative on Malaria (MIM) Pan-African Malaria Conference, 2-6 November 2009, Kenyatta International Conference Centre, Nairobi, Kenya.

1.12.3.2 Posters

a) Smit S., Louw A.I., Birkholtz L. (2009) An extensive proteomic view after inhibition of S-adenosylmethionine decarboxylase in *Plasmodium falciparum*. European Science Foundation Europe-Africa Frontier Research Conference Series Infectious Diseases: From Basic to Translational Research, 4 – 9 April 2009, The Cape Winelands, South Africa.

b) Smit S., Louw A.I., Birkholtz L. (2008) Analysis of the malaria parasite proteome after inhibition of S-adenosylmethionine decarboxylase resulting in polyamine depletion. 2nd SA Proteomics & Genomics Conference, 03 - 05 March 2008, University of the Western Cape, South Africa.

CHAPTER 2

Proteomic profiling of *P. falciparum* through improved, semi-quantitative two-dimensional gel electrophoresis

Work presented in this chapter was published as follows: Smit, S., S. Stoychev, A. I. Louw & L. Birkholtz, (2010) Proteomic profiling of *Plasmodium falciparum* through improved, semiquantitative two-dimensional gel electrophoresis. *J Proteome Res* **9**: 2170-2181.

"Two D, or not two D: that is the question:
Whether 'tis nobler in the mind to suffer
The streaks and blobs of intractable proteins
Or to take chips against a sea of genes
And by comparing, find them that
hold the bitter taste of disease and death."

(Fey & Larsen, 2001)

2.1 Introduction

Proteomics enables the direct study of the proteome in which sets of proteins occur together in a particular biological state at a particular time. One of the workhorses for proteomic applications has been bottom-up proteomics that include the use of differential expression detected on two-dimensional gel electrophoresis (2-DE) gels followed by mass spectrometry (MS) identification. Bottom-up proteomics is the process in which proteins and their post-translational modifications (PTM's) are identified and characterised by separating the proteins first, followed by proteolytic digestion prior to MS analysis. 2-DE was first introduced in the mid 1970's by O'Farrell (O'Farrell, 1975). In recent years the technology has gone from strength to strength and is now widely employed to assess proteomes of various organisms in a variety of applications that include proteome mapping, differential regulation of perturbation studies and detection of PTM's. Application of 2-DE technology has several visible properties which is irreplaceable and include good resolution of abundant proteins, information on quantity, detection of PTM's, immediate information on approximate pI and molecular weight values (Lopez, 2000). Despite these advantages the reality is that 2-DE is limited to high abundance proteins while the dynamic proteome within a cell range from 7-12 orders of magnitude. Furthermore, 2-DE also has bias towards soluble proteins and mid-range molecular weight and pI proteins (Ong & Pandey, 2001).

2.1.1 Minimum information about a proteomics experiment

To avoid discrepancies in the reporting of proteomic data minimum information about a proteomics experiment (MIAPE) (Taylor *et al.*, 2007) was established similar to minimum information about a microarray experiment (MIAME) (Brazma *et al.*, 2001) for transcriptomic data. The general criteria for reporting of data and the collection of metadata include sufficiency and practicality. Basically, sufficient information should be given to allow the reader to understand and to critically evaluate the data and repetition of experiments should be achievable to most laboratories (Taylor *et al.*, 2007). For 2-DE, guidelines exist on study design and sample generation, in which the origin of the samples together with sample processing and number of replicates should be reported (Gibson *et al.*, 2008). For the separation of samples and sample handling, fractionation, manipulation, storage as well as sample transport should be discussed. For gel electrophoresis the separation methods, stain, visualisation and image acquisition methods should be specified as well as all the information regarding image analysis (Gibson *et al.*, 2008). Spot identification by mass spectrometry require information on the generation of the peak list, sample handling, the informatics used, the search engine, spectra submitted, peptide matching, database used for identification purposes and quality control measures (Binz *et al.*, 2008, Taylor *et al.*, 2008). Considering the huge amount of proteomic data that is published each year, it is of utmost importance that data that are being reported in the public domain are standardised.

2.1.2 Liquid chromatography mass spectrometry and protein arrays used for proteomics

Liquid chromatography mass spectrometry (LC-MS) has an advantage of being able to analyse complex peptide mixtures that include soluble proteins as well as membrane-, trans-membrane-, and integral proteins. Commonly used MS based methods for quantification include isotope coded affinity tags (ICAT) and isobaric tags (iTRAQ) (Shiio & Aebersold, 2006, Aggarwal *et al.*, 2006). ICAT is dependent on the number of cysteine residues, which is of relative low abundance in the Plasmodial proteome (Sims & Hyde, 2006, Nirmalan *et al.*, 2004a) and would thus not be ideal to use. Labelling of peptides with iTRAQ targets primary amines and enables the simultaneous analyses and identification as well as quantification of proteins. iTRAQ uses 4 specific amine tags enabling the simultaneous detection of up to 4 different samples (Aggarwal *et al.*, 2006). Using iTRAQ, all types of proteins can be determined but it may have a slight bias against the more acidic proteins due to fewer arginine and lysine residues (Aggarwal *et al.*, 2006). Another setback of iTRAQ is the delayed sample mixing (Sims & Hyde, 2006). Metabolic labelling techniques has proved to be superior for Plasmodial proteins (Nirmalan *et al.*, 2004a). The method employed the use of labelled isoleucine added to *in vitro* cultures, with the added advantage that cultures could be

mixed immediately in equal ratios, but unfortunately a major setback is that the labeled isoleucine is extremely expensive. Overall, a major disadvantage with regard to MS-based methods is the lack of effective search algorithms and databases that may complicate and increase analysis time of data (Aggarwal *et al.*, 2006, Sims & Hyde, 2006, Nesvizhskii *et al.*, 2007).

Other technologies that can be applied to the analysis of the proteome include protein microarrays, which have been applied for identification, quantification and functional analysis in basic and applied proteomics (MacBeath, 2002, Poetz *et al.*, 2005). There is no absolute correlation between the mRNA expression level and the corresponding protein expression (Gygi *et al.*, 1999). Similarly it is impossible to correlate the protein state purely by investigation of the protein expression level (Poetz *et al.*, 2005). Protein arrays are able to analyse the function of the proteome by investigating binding partners and target proteins therefore providing a functional classification of the protein and its interacting partners. Surface-enhanced laser desorption/ionisation-time-of-flight/mass spectrometry (SELDI-TOF/MS) is able to employ a surface-based fractionation of proteins therefore separating protein mixtures and their binding properties (Gast *et al.*, 2006). Basically, proteins are captured on surfaces and then separated based on their biophysical properties which is then followed by TOF/MS to identify the proteins and expression profiles (Weinberger *et al.*, 2000, Merchant & Weinberger, 2000).

2.1.3 Plasmodial and parasite proteomics

The Plasmodial proteome is multifaceted and stage-specific, indicating a high degree of specialisation at the molecular level to support the biological and metabolic changes associated with each of the life cycle changes (Shock *et al.*, 2007, Sims & Hyde, 2006). Post-translational modifications are employed as a mechanism to regulate protein activity during the parasite's life cycle (Nirmalan *et al.*, 2004a) and certain proteins are predicted to act as controlling nodes that are highly interconnected to other nodes and thus results in a highly specialised interactome (Wuchty *et al.*, 2009, Birkholtz *et al.*, 2008b). These enticing properties motivate studies focused on in-depth characterisation of the Plasmodial proteome including regulatory mechanisms and the ability to respond to external perturbations. Analysis of the schizont stage proteome reinforced the notion that both post-transcriptional and post-translational mechanisms are involved in the regulation of protein expression in *P. falciparum* (Foth *et al.*, 2008).

Due to the >80% A+T-richness of the Plasmodial genome (Gardner *et al.*, 2002), the resultant Plasmodial proteome contains proteins in which long hydrophobic stretches and amino acid repeats (notably consisting of lysine and asparagine) are found. Moreover, the proteins from this parasite

are comparatively large, non-homologous and highly charged with multiple isoforms within the parasite (Birkholtz *et al.*, 2008a). These properties have confounded analyses of the Plasmodial proteome, including the recombinant expression of Plasmodial proteins (Mehlin *et al.*, 2006, Vedadi *et al.*, 2007). Few studies attempted to describe the Plasmodial proteome, which is predicted to have about 5300 proteins of which ~60% are hypothetical and un-annotated (Foth *et al.*, 2008, Gelhaus *et al.*, 2005, Makanga *et al.*, 2005). The last decade has experienced an explosion in proteomic studies with an exponential growth in proteomic publications, unfortunately it seems that Plasmodial proteomics has been left behind (Figure 2.1).

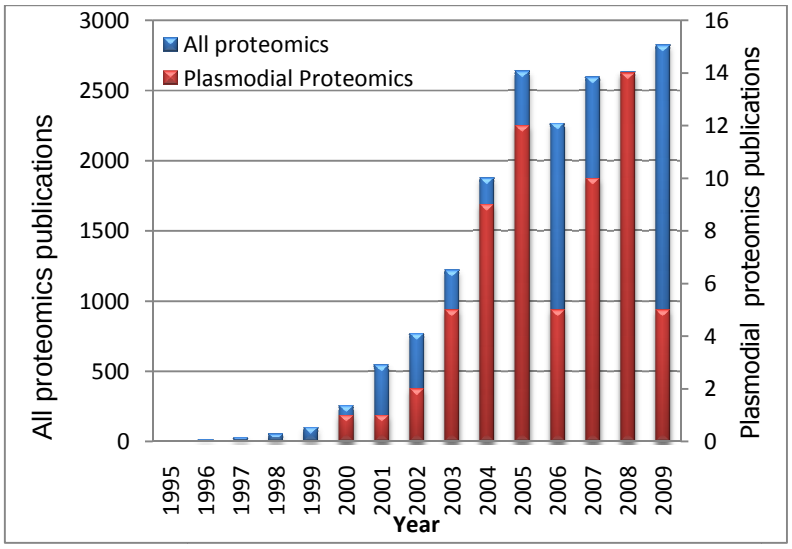

Figure 2.1: The state of proteomic publications per year as on ISI Web of Science.

Search criteria was according to title (proteom* AND (plasmodium* or malaria*) and publication year. Date last searched 02/12/2009.

Proteomics of most protozoan parasites is a fast evolving field. Early in the development of the 2-DE methodology for *Leishmania*, it was recognized that this parasite needs an efficient lysis buffer for 2-DE for optimal spot detection of the Leishmanial proteins (Acestor *et al.*, 2002). Five years later *L. amazonensis* proteins were used to demonstrate the efficiency of liquid phase isoelectric focusing (IEF) in combination with 2-DE to improve proteins detected in the acidic and basic ranges (Brobey & Soong, 2007). The 2-DE proteomic map of the protozoan parasite *Trypanosoma cruzi*, which is responsible for Chagas disease in humans, include 26 identified spots that corresponded to 19 unique protein groups accounting for 27% isoforms (Paba *et al.*, 2004).

A striking feature was that the majority of the spots remain similar throughout all the life stages and therefore the progression of the parasite is due to the expression of a limited number of proteins

(Paba *et al.*, 2004). Similarly, another protozoan parasite *T. brucei,* which causes sleeping sickness, was investigated with 2-DE. A large scale 2-DE proteomic study of the procyclic form of *T. brucei* identified 2000 spots that related to 700 proteins which included various isoforms due to PTM's (Jones *et al.*, 2006). Uncommon protozoan parasites characterised with 2-DE include the first 2-DE reference map of *Trichomonas vaginalis*, in which 116 spots that related to 67 different proteins, representative of 42% isoforms were identified (De Jesus *et al.*, 2007). The importance of PTM's was demonstrated for this parasite, since PTM's may regulate protein function in the cells by altering their localisation, interaction or activity. N-terminal acetylation was seen for actin, while deamidation of certain proteins has been associated with protein turnover, development and aging (De Jesus *et al.*, 2007). The yeast *(Saccharomyces cerevisiae)* proteome map has been in progress for 10 years, with a total of 716 proteins successfully identified that consists of 32% isoforms (Perrot *et al.*, 1999, Perrot *et al.*, 2009).

Compared to other protozoan parasites, the reported efficacy of 2-DE to analyse the Plasmodial proteome is relatively poor since only a low number of protein spots could be detected with various protocols and stains (Makanga *et al.*, 2005, Gelhaus *et al.*, 2005, Panpumthong & Vattanaviboon, 2006, Radfar *et al.*, 2008, Wu & Craig, 2006). The highest number of spots detected to date on Plasmodial 2-DE gels with silver staining is only 239 (Panpumthong & Vattanaviboon, 2006) and recently, a total of 345 spots were detected for 4 time points in the Plasmodial schizont stage using two-dimensional differential gel electrophoresis (2-D DIGE) (Foth *et al.*, 2008), of which only 54 protein spots were identified. This clearly illustrates the need for an optimised protocol including extraction, quantification and detection methods. This chapter details such an optimised 2-DE protocol, which was applied to the analysis of the Plasmodial proteome in the ring and trophozoite stages. Firstly, established methodology was optimised with regard to protein extraction, quantification, detection and finally MS identification is described. Once the protocol was established, it was applied to the analyses of the soluble Plasmodial proteome.

2.2 Methods

2.2.1 Blood collection

Type O^+ blood was collected in a blood bag (Fenwal Primary container with citrate phosphate glucose adenine anticoagulant, 70 ml anticoagulant for the collection of 500 ml blood, Adcock Ingram) which was left overnight at 4°C in the bag after collection. The following morning the blood was transferred to a sterile plastic container and kept for use at 4°C for 4-5 weeks. Erythrocytes were collected from the bottom of the container and washed by adding an equal amount of phosphate buffered saline (PBS, 137 mM NaCl, 2.7 mM KCl, 10mM phosphate, pH 7.4) to the erythrocytes and centrifugation at 2500×*g* for 5 min. The supernatant were aspirated and the step repeated at least another 4 times until there was no visible buffy coat left. The washed erythrocytes were then resuspended in an equal volume of culture media (RPMI 1640 media (Sigma), supplemented with 0.4% (w/v) D-glucose (Sigma), 50 mg/l hypoxanthine (Sigma), 48 mg gentamycin (Sigma), buffered with 12 mM HEPES (Sigma) and 21.4 mM sodium bicarbonate (Merck) per litre of MilliQ water (double distilled, de-ionised, 0.22 µM filter sterilised) and finally the addition of 0.5% (w/v) Albumax II (Gibco) for complete culture media) for use in all experimental procedures to follow.

2.2.2 Thawing of parasites

The chloroquine-sensitive *P. falciparum* 3D7 (*Pf*3D7) parasites were thawed from parasite stock solutions stored at -180°C in liquid nitrogen. Parasites were thawed at 37°C for 5 min after which 0.2 ml of 12% (w/v) NaCl was added, mixed, followed by the addition of 1.8 ml of 0.6% (w/v) NaCl. The parasites were then centrifuged at 2500×*g* for 5 min and resuspended in 30 ml culture media and 1.5 ml packed erythrocytes was added to obtain a 5% hematocrit. The resuspended parasites were finally gassed using a special gas mixture containing 5% CO_2, 5% O_2 and 90% N_2 (Afrox), before being placed in a shaking incubator at 37°C and 58 revolutions per minute (rpm). Thawed parasites were never used for longer than 2 months to prevent possible genetic alterations.

2.2.3 Daily maintenance of parasites

*Pf*3D7 parasites were maintained *in vitro* in 75 cm^3 Cellstar culture flasks (Greiner bio-one) in human O^+ erythrocytes in culture media (Trager & Jensen, 1976). The culture media of the parasites were changed daily by transferring the cultures to a sterile 50 ml tube which was then centrifuged at 2500×*g* for 5 min. The culture media was then aspirated and the remaining parasite-containing pellet was resuspended in pre-heated fresh culture media. The resuspended parasites were then transferred back into a 75 cm^3 Cellstar culture flask and gassed for 30 s with the special gas

mixture. The flasks were sealed air-tight before being placed back into the 37°C incubator. On every second day, when the parasites were in the trophozoite stage the parasite culture were either divided into several flasks or parasites were removed from the original flask in order to maintain the parasitemia at 5%. Fresh erythrocytes were also added to maintain the hematocrit at 5%. Parasites were monitored daily through light microscopy of Giemsa stained thin blood smears. Giemsa's Azur Eosin methylene blue solution (Merck) was diluted 1:5 in proprietary buffer for staining blood smears pH 6.4 (Merck). Slides were incubated for 3 min before investigation by light microscopy to determine the parasitemia. Slides were analysed using a Nikon light microscope at 1000× magnification under oil immersion. At least 10 fields of 100 erythrocytes each were examined for the determination of parasite progression.

2.2.4 Synchronisation

Synchronisation was done using a modified sorbitol method of Lambros and Vanderberg (Lambros & Vanderberg, 1979). Parasites mostly in the ring stage, were centrifuged at 2500×*g* for 5 min, after which the supernatant were aspirated. Three volumes 15% (w/v) sorbitol were added to the parasite pellet, resuspended and incubated at 37°C for 5 min. This was followed by the addition of 6 volumes of 0.1% (w/v) glucose, mixed, and incubated for 5 min at 37°C. After incubation the mixture was centrifuged at 2500×*g* for 5 min, the supernatant removed and the synchronised parasite pellet resuspended in culture media and a 5% hematocrit. Parasites were always synchronised for 3 consecutive cycles (6 times in total, always 8 h apart once in the morning and later in the afternoon). The morning synchronisation is done to remove parasites that are still schizonts and the afternoon synchronisation is to remove trophozoites. This is done to ensure that the parasites that fall out of the ring stage window is removed thus resulting in better synchronisation with a smaller window.

2.2.5 Culturing of parasites for proteomics

*Pf*3D7 parasites were maintained *in vitro* in human O^+ erythrocytes in culture media and monitored daily through light microscopy of Giemsa stained thin blood smears as described in section 2.2.3. Before treatment could commence the parasites were always synchronised for 3 consecutive cycles (6 times in total, always 8 h apart once in the morning and later in the afternoon) as described in section 2.2.4. Thirty millilitres of *Pf*3D7 parasite cultures at 8% parasitemia and 5% hematocrit were used per gel to establish the proteomics methodology. Saponin was added to a final concentration of 0.01% (v/v) followed by incubation on ice for 5 min to lyse the erythrocytes. Parasites were collected by centrifugation at 2500×*g* for 15 min at room temperature, and washed in PBS at 16 000×*g* for 1 min at 4°C. This step was repeated at least 4 times until the supernatant was

clear instead of 3 times as previously reported (Nirmalan *et al.*, 2004a). The parasite pellet was stored at –80°C until use, but never stored for longer than 30 days. For the analyses of proteomes of different developmental stages of the parasites, parasites were harvested from 60 ml cultures at 16 hours post invasion (HPI) (late rings) and 20 HPI (early trophozoites).

2.2.6 Protein preparation

Parasite pellets were suspended in 500 µl lysis buffer as described by Nirmalan *et al.* (8 M urea, 2 M thiourea, 2% CHAPS, 0.5% (w/v) fresh DTT and 0.7% (v/v) ampholytes, pH 3-10 linear) (Nirmalan *et al.*, 2004a). Samples were pulsed-sonicated on a Virsonic sonifier with microtip for 20 s with alternating pulsing (1 s pulse, 1 s rest) at 3 W output with 1 min cooling steps on ice (to prevent foaming and carbamylation) and repeated 6 more times (Table 2.1).

Table 2.1: Program settings used for Virsonic sonifier

Process time	10 s
Pulsar on	1 s
Pulsar off	1 s
Power	3 W
Total time	20 s
Microtip	Yes
Pulsed	Yes

Sonication was followed by centrifugation at 16 000×*g* for 60 min at 4°C, after which the protein-containing supernatant was used in subsequent 2-DE.

2.2.7 Protein quantification

Four different protein quantification methods were tested on the samples obtained using 2 BSA standard curves in each of the methods: firstly, BSA in 0.9% saline, and secondly, BSA in the Plasmodial lysis buffer, each containing the same amount of protein for analysis.

2.2.7.1 Bradford method

The Bradford method is based on the principle that the dye binds mainly to basic and aromatic amino acids. Upon binding of the dye to the protein the dye is converted into the stable un-protonated blue form that can be detected at 595 nm (Bradford, 1976). The Quick Start™ Bradford dye method (Bio-Rad) was used for protein determination at an absorbance of 595 nm with a Multiskan Ascent spectrophotometer (Thermo Labsysytems).

2.2.7.2 Lowry

The Lowry method is based on the Biuret reaction in which peptide bonds react with Cu^{2+}. Under alkaline conditions the copper will react with the Folin Ciocalteau reagent giving a blue colour that can be detected at 660 nm. The reaction is also partially dependent on aromatic amino acids (Lowry *et al.*, 1951). The Lowry method used a reaction mixture containing solution A (2% (w/v) $NaCO_3$, 2% (w/v) NaOH, 10% (w/v) Na_2CO_3), solution B (2% (w/v) $CuSO_4.5H_2O$), and solution C (0.5% (w/v) potassium tartrate). Two hundred microlitres of the reaction mixture was added to each protein sample, mixed and incubated for 15 min at room temperature. Six hundred microlitres of Folin Ciocalteau reagent (1:10, FC reagent and H_2O) were added and incubated at room temperature for 45 min in the dark. Absorbance was measured at 660 nm.

2.2.7.3 Protein quantification by the BCA method

The BCA method uses bicinchoninic acid (BCA) as the detection reagent for Cu^{+} which is formed when Cu^{2+} is reduced by protein in an alkaline environment. A purple coloured reaction product is formed by the chelation of 2 molecules of BCA with one Cu^{+} ion, and can be measured at 562 nm. The colour formation is due to the macromolecular structure of the protein, the number of peptide bonds and the presence of 4 amino acids (cysteine, cystine, tryptophan, tyrosine) (Smith *et al.*, 1985). The commercially available Micro BCA™ Protein assay kit (Pierce) was used. In short, a working solution was prepared and added to the protein standards and then incubated for 2 h at 37ºC. The plate was left to cool to room temperature for approximately 30 min, before the absorbance was measured at 550 nm.

2.2.7.4 Protein quantification by 2-D Quant kit

The 2-D Quant kit quantitatively precipitates protein, leaving the interfering substances in solution. It is based on the specific binding of copper ions to proteins. The precipitated proteins are resuspended in a copper containing solution of which the unbound copper is then measured with a colorimetric agent at 480 nm. The colour density is inversely related to the protein concentration. The commercially available 2-D Quant Kit (GE Healthcare) was used according to the manufactures instructions with a few modifications. In short, a standard curve containing 6 dilutions (0, 10, 20, 30, 40, 50 µg) was prepared using the 2 mg/ml BSA stock solution provided by the kit. Varying volumes of Plasmodial proteins (2.5, 5, 7.5, 10, 15 µl) were used to determine the protein concentration of each Plasmodial sample. 500 µl precipitant were added to each tube, vortexed and left to incubate for 3 min at room temperature, followed by 500 µl of co-precipitant and mixed by

inversion immediately upon addition. Samples were centrifuged at 16 000×*g* for 15 min at 4°C. The supernatants were decanted and centrifuged for 3 min at 16 000×*g*, 4°C. The remaining supernatant was removed by pipette, before the addition of 100 µl of a copper containing solution followed by 400 µl MilliQ water and mixing each tube. This was followed by the addition of 1 ml working solution to each tube, which was mixed immediately upon addition to ensure rapid mixing, before proceeding to the next tube. The tubes were then incubated for 20 min at room temperature, before the absorbance was measured at 492 nm.

2.2.8 SDS-PAGE gels

Low molecular weight markers (GE Healthcare) were diluted in reducing buffer (0.06 M Tris-glycine, 2% (w/v) SDS, 0.1% (v/v) glycerol, 0.05% (v/v) β-mercaptoethanol and 0.025% (v/v) bromophenol blue, pH 6.8), to provide a total protein concentration range of 1250 ng to 9.7 ng and individual protein concentrations ranging from 100 ng to 0.6 ng. Equal amounts of markers were loaded onto 4 different 12.5% SDS-PAGE gels and the gels were subsequently stained with either Colloidal Coomassie, silver, SYPRO Ruby (Molecular Probes) or Flamingo Pink (Bio-Rad) stains. The gels were scanned on a Versadoc 3000 and analysed using Quantity One 4.4.1 (Bio-Rad). The Rf values and the intensities of each band were compared, and used to determine the limit of detection and linearity.

2.2.9 Two-dimensional gel electrophoresis (2-DE)

For 2-DE, the protein concentration was determined with the 2-D Quant kit. Two hundred micrograms of protein in rehydration buffer (8 M urea, 2 M thiourea, 2% (w/v) CHAPS). 0.5% (w/v) DTT and 0.7% (v/v) IPG Buffer (pH 3-10 Linear) was applied to a 13 cm IPG, pH 3-10 L strip. First dimensional isoelectric focusing (IEF) was performed on an Ettan IPGphore Isoelectric Focusing Unit (GE Healthcare), and commenced with a 10 h active rehydration step. Isoelectric focusing time followed an alternating gradient and step and hold protocol and was always allowed to proceed to a total of 18 500 Volt-hours, that completed within 15 h. The complete IEF focusing steps is given in Table 2.2.

Table 2.2: The IEF focusing steps used for the 13cm IPG, pH 3-10 L strips.

Step	Voltage limit (V)	Time or Volt hour (h) or (V-h)	Gradient
1	30 V	10:00 h	Step and hold[a]
2	200 V	0:10 h	Gradient[b]
3	200 V	0:15 h	Step and hold
4	500 V	0:15 h	Gradient
5	500 V	0:15 h	Step and hold
6	2 000 V	0:15 h	Gradient
7	2 000 V	0:30 h	Step and hold
8	8 000 V	0:30 h	Gradient
9	8 000 V	14 500 V-h	Step and hold
Total		18 500 V-h	

[a] Step and hold $V\text{-}h = h \times V$ Equation 2.1

[b] Gradient $V\text{-}h = h \times \frac{(V\ previous\ step + V\ new\ step)}{2}$ Equation 2.2

Following IEF, the IPG strips were equilibrated for 10 min each in SDS equilibration buffer (50 mM Tris-glycine, pH 6.8, 6 M urea, 30% (v/v) glycerol, 2% (w/v) SDS, 0.002% bromophenol blue) containing 2% DTT, and then incubated in 2.5% iodoacetamide. Finally, the strip was placed in SDS electrophoresis running buffer (0.25 M Tris-HCl, pH 8.3, 0.1% SDS, 192 mM glycine) for 10 min as a final equilibration step. Second dimensional separation was performed by placing the IPG strips on top of the 10% SDS PAGE gel (Hoefer SE 600), covered with 1% agarose dissolved in SDS electrophoresis running buffer. Separation was performed at 80 V at 20°C until the bromophenol blue front reached the bottom of the gel. The gels were then fixed in the appropriate fixing solution for each specific stain (see below). For proteomic analyses of the different developmental stages of *P. falciparum*, 400 µg protein was applied to 18 cm IPG strips for separation and subsequently stained with Flamingo Pink.

2.2.10 Staining of 2-DE gels

Fluorescent stains often present with problematic background as the sensitivity of the stain also enables staining of dust particles and any impurity present within the gel or solutions used during the preparation and staining of the gel. For this reason, special care was taken during 2-DE preparation to avoid dust, to wash all glassware with special care and take extra special precaution to avoid contamination of the sample. The buffers and the stain used were filtered to ensure good quality gels and data.

2.2.10.1 Flamingo Pink staining of 2-DE gels

Flamingo Pink is a fluorescent stain that is a dilute alcoholic solution of an organic dye that binds to denatured protein. It is non-fluorescent in solution, but becomes strongly fluorescent when bound to protein. Gels were fixed overnight in 40% (v/v) ethanol, 10% (v/v) acetic acid, and subsequently in 200 ml Flamingo Pink working solution (diluted 1:9 with Milli-Q water as per the manufacturer's instructions) and incubated with gentle agitation in the dark for 24 h, to increase the sensitivity of the stain. The gels were washed in 0.1% (w/v) Tween-20 for 30 min to reduce background. Finally the gels were rinsed in Milli-Q water twice before scanning on the Versadoc 3000. All gels were stored in Flamingo Pink at 4°C until use for MS.

2.2.10.2 Silver staining of 2-DE gels

Silver binds to the amino acid side chains usually the sulfhydryl and carboxyl groups, in which the silver is reduced to metallic silver on the protein. The silver is then deposited on the gel to give a black and brown colour. Gels were fixed in 45% (v/v) methanol, 5% (v/v) acetic acid overnight, followed by sensitising for 2 min in 0.02% (w/v) sodium thiosulfate, and rinsing with Milli-Q water twice. 200 ml ice cold 0.1% (w/v) silver nitrate was added and incubated at 4°C for 30 min, rinsed twice with Milli-Q water and developed in fresh 2% (w/v) sodium carbonate with 0.04% (v/v) formaldehyde. Development was stopped by adding 1% (v/v) acetic acid (Jensen *et al.*, 1999). All gels were stored in 1% (v/v) acetic acid at 4°C in airtight containers until use for MS.

2.2.10.3 SYPRO Ruby staining of 2-DE gels

SYPRO Ruby is a fluorescent stain that consists of an organic and ruthenium component that binds non-covalently to the proteins (Berggren *et al.*, 2000). Gels were fixed in 10% (v/v) methanol, 7% (v/v) acetic acid overnight. The fixing solution was replaced with 200 ml SYPRO Ruby stain (used undiluted as supplied by the manufacturer) and the gels were incubated with agitation for 24 h in the dark, to increase sensitivity. After staining, the gels were washed for 60 min with 10% (v/v) methanol, 7% (v/v) acetic acid to reduce fluorescent background. Finally, the gels were rinsed twice with MilliQ water before scanning on the Versadoc 3000. Gels were stored in SYPRO Ruby at 4°C until use for MS.

2.2.10.4 Colloidal Coomasie Blue (CCB) staining of 2-DE gels

Colloidal Coomassie Brilliant Blue G250 stock solution (2% (v/v) phosphoric acid, 10% (w/v) ammoniumsulfate, and 0.1% (v/v) Coomassie Brilliant Blue G250) was diluted (4:1) with methanol just before use. The gels were immersed in the Colloidal Coomassie solution and left shaking overnight. Gels were rinsed with 25% (v/v) methanol, 10% (v/v) acetic acid before destaining with 25% (v/v) methanol, until the background was clear (Neuhoff *et al.*, 1988). Gels were then scanned on the Versadoc 3000, and stored in 1% (v/v) acetic acid at 4°C until use for MS.

2.2.11 Image Analysis of 2-DE gels by PD Quest

All the gels were scanned using the VersaDoc 3000 image scanner (Bio-Rad) and the appropriate software from the PD Quest™ 7.1.1 Software package (Bio-Rad). Scan settings for each of the 4 stains is given in Table 2.3.

Table 2.3: Scan settings used on PD Quest and the Versadoc 3000 for the 4 stains used

Stain	CBB	Silver	SYPRO Ruby	Flamingo Pink
Light application	Clear white TRANS	Clear white TRANS	520 LP UV TRANS	520 LP UV TRANS
Gain	0.5× Gain	0.5× Gain	4× Gain	4× Gain
Bin	1 × 1 Bin	1 × 1 Bin	1 × 1 Bin	1 × 1 Bin
Total exposure	3 s	3 s	30 s	120 s
Start exposure	0.5 s	0.5 s	5 s	30 s
Nr of exposures	6 (1 image taken every 0.5 s)	6 (1 image taken every 0.5 s)	6 (1 image taken every 5 s)	6 (1 image taken every 15 s)

For the method optimisation protocol, gel image analysis was performed using PD Quest 7.1.1 (Bio-Rad). All 8 gels were filtered using the Filter Wizard. Spot detection was performed on the gels by automated spot detection. The display of the gels stained with SYPRO Ruby and Flamingo Pink was inverted for easier comparisons with the gels stained with CCB and silver. Additional manual settings for spot detection were sensitivity (2.22), size scale (5) and min peak (1244). For proteomic analyses of the different developmental stages of *P. falciparum*, 400 µg protein was applied to 18 cm IPG strips for separation and subsequently stained with Flamingo Pink and scanned using the Versadoc 3000 as described below. PD Quest 7.1.1 was used to identify the number of spots on each of the gels that were done for the ring and trophozoite 2-DE proteomes (8 gels for each stage). First, all images were cropped to the same dimensions (1.59 Mb, 933 × 893 pixels, 303.7 × 290.7 mm) and filtered using the salt setting (light spots on dark background) of the Filter Wizard. The Spot Detection Wizard was used to automatically detect spots on the selected master image by manual identification of a small spot, faint spot and large spot. Additional settings

for spot detection were manually selected for sensitivity (5.31 for rings and 4.35 for trophozoites), size scale 5.0 (both), min peak (808 for rings and 4712 for trophozoites). After automated matching of all the gels, every spot was manually verified to determine correctness of matching.

2.2.12 2-DE spot identification by tandem mass spectrometry

MS is an analytical technique that measures the motion of charged particles (usually +1 for MALDI-TOF) in an electric field. The particle or peptide is ionised and is then separated according to its mass:charge ratio (m/z) which is then compared to a database containing theoretical mass values for the peptides of specific proteins. Unfortunately, it is possible that the mass of a particular peptide may be similar to another peptide of an unrelated protein, and therefore the use of MS/MS to obtain partial amino acid sequences are of utmost importance. The PMF are analysed in the first chamber and then one peptide at a time is allowed into the second collision chamber where it is fragmented with nitrogen gas to produce daughter ions which are then used to obtain an amino acid sequence. During this MS/MS fragmentation, low collision energy is used to fragment the peptide ion at each amide bond along the peptide backbone, hence yielding a peptide sequence. Upon fragmentation of the peptide two complimentary ion series can be obtained that include the b-ion series and the y-ion series (Roepstorff & Fohlman, 1984). The b-ion series will contain the N-terminal amino acid and is therefore the total residue mass of the amino acid, while the y-ion series will contain the C-terminus of the amino acid and is the total mass with an additional mass of 19 (18 for the presence of water and +1 Da for the ionising proton). Since a tryptic digestion was done the y_1-ion will always be either Arg with a mass of 175.1 Da or Lys with a mass of 147.1 Da.

For comparative purposes mostly the same 39 spots (154 in total) covering a wide range on the gels as well as low molecular weight markers were cut from each of the 4 differently stained gels, dried and stored at -20°C. The silver stained samples were first destained with 30 mM potassium ferricyanide and 100 mM sodium thiosulfate to remove the silver before proceeding to wash steps (Gharahdaghi *et al.*, 1999). All gel pieces were cut into smaller cubes and washed twice with water followed by 50% (v/v) acetonitrile for 10 min each. The acetonitrile was replaced with 50 mM ammonium bicarbonate and incubated for 10 min, repeated twice, except for CCB samples, which had an additional wash step to ensure complete removal of the dye. All the gel pieces were then incubated in 100% acetonitrile until they turned white. This was followed by another ammonium bicarbonate, acetonitrile wash step as above, after which the gel pieces were dried *in vacuo*. Gel pieces were digested with 20 µl of a 10 ng/µl trypsin solution at 37°C overnight. Resulting peptides were extracted twice with 70% acetonitrile for 30 min, and then dried and stored at -20°C. Dried peptides were dissolved in 10% (v/v) acetonitrile, 0.1% (v/v) formic acid and mixed with saturated

alpha-cyano-4-hydroxycinnamic acid before being spotted onto a MALDI sample plate. Experiments were performed using Applied Biosystems QSTAR-ELITE, Q-TOF mass spectrometer with oMALDI source installed. Laser pulses were generated using a Nitrogen laser with intensities between 15 and 25 µJ depending on sample concentration and whether single MS or MS/MS experiments were performed. First, single MS spectra were acquired for 15-30 s. The 50 highest peaks from the MS spectra were automatically selected for MS/MS acquisition. Tandem spectra acquisition lasted 4-8 min depending on sample concentration. Argon was used as cooling gas in Q0 and collision gas in Q2. The collision energy was first optimised using a 9 peptide mixture covering the scan range of 500–3500 Da and then automatically set during MS/MS experiments using the Information Dependent Acquisition (IDA) function of the Analyst QS 2.0 software. The instrument was calibrated externally, in TOF-MS mode, via a two point calibration using the peptides Bradykinin 1-7 and Somatostatin 28 ($[M+H]^+$ = 757.3992 Da and 3147.4710 Da, respectively).

2.2.13 Submitting MS/MS data to the MASCOT database

Data was submitted in MASCOT (www.matrixscience.com). The list of PMF's and the peptide sequence data (amino acid sequences for the 50 highest peptide peaks) was submitted to MASCOT using the MS/MS ion search utility that uses uninterpreted MS/MS data from one or more peptides for identification of the protein. The National Centre for Biotechnology Information non-redundant (NCBInr database, April 2009) was selected for protein identification and is a composite non-identical protein and nucleic acid database. Taxonomy was set to search all entries, using the NCBI database (April 2009). The enzyme used to obtain peptides was specified as trypsin, and allowed 1 missed cleavage. Fixed modifications were specified as carbamidomethyl (C) due to the use of iodoacetmide during sample preparation, and variable modifications were selected as oxidation (M) for possible methionine oxidation. Peptide tolerance was set to 50 parts per million (ppm, determined by MS calibration) and the MS/MS tolerance was set at 0.6 Da. The peptide charge was set to +1 since the MS used was a MALDI-TOF and would thus usually generate only singly charged ions. Finally, the instrument was selected as a MALDI-TOF-TOF and the data format was selected as Mascot generic. The final ion score is the probability that the observed match is a random event. Protein scores of more than 45 was considered as significant for identification of the protein ($p<0.05$).

2.3 Results

A: Optimisation of Plasmodial proteins for 2-DE

2.3.1 Protein concentration determination of Plasmodial proteins

Semi-quantitative proteomic analysis requires highly specific protein quantification procedures, to ensure the application of equal amounts of material in all downstream applications. In this study, 4 different methodologies were evaluated in their accuracy to determine Plasmodial protein concentration. The standardly used Bradford method achieved high correlation (R^2 = 0.9971) for proteins dissolved in a saline buffer, but was not compatible with the composition of the lysis buffer (Figure 2.2 A).

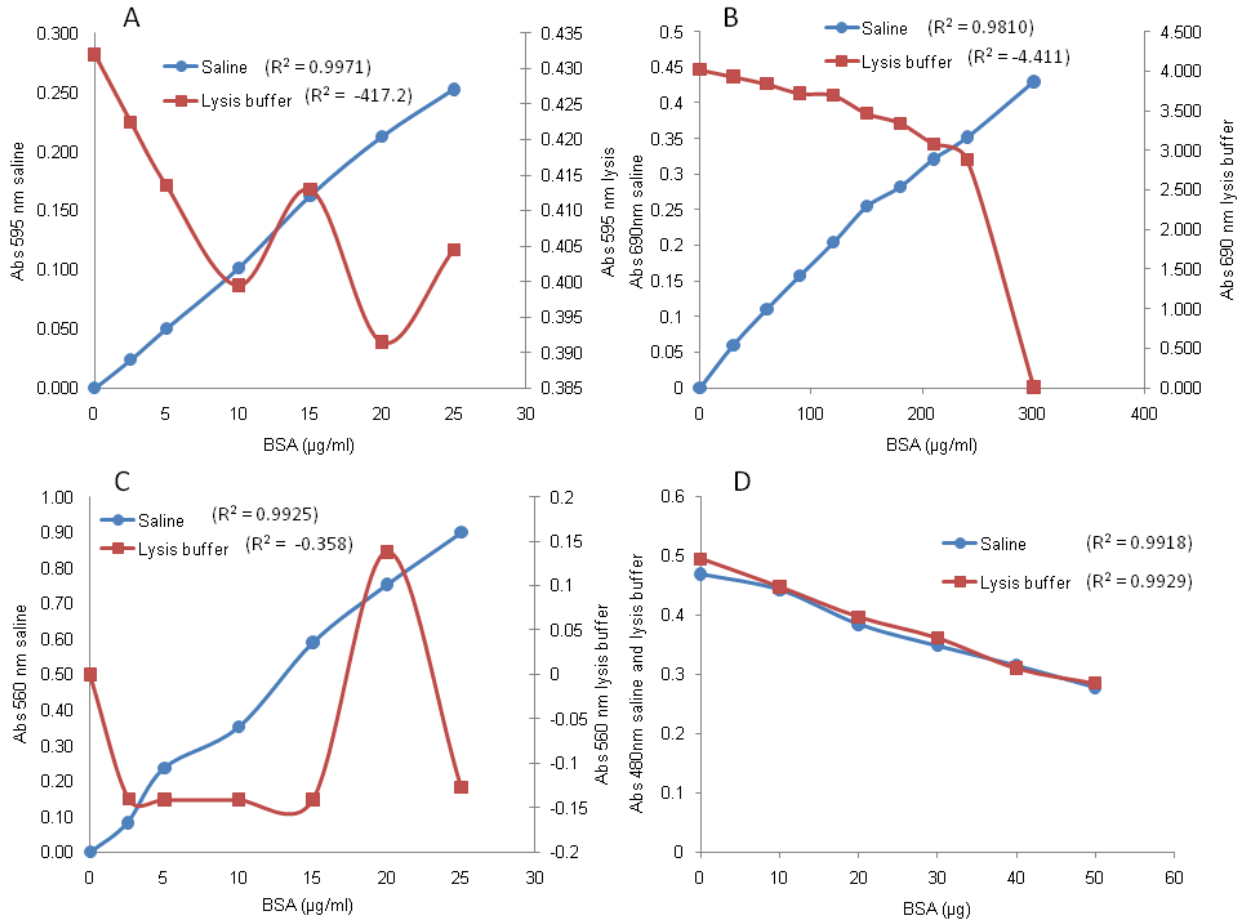

Figure 2.2: Comparison of 4 different protein concentration determination methodologies

(A) Bradford method, R^2 = 0.9971 for saline (——●——), R^2 = -417.2 for lysis buffer (--- ---), (B) Lowry method, R^2 = 0.981 for saline (——●——), R^2 = -4.411 for lysis buffer (--- ---), (C) BCA method R^2 = 0.9925 for saline (——●——), R^2 = -0.358 for lysis buffer (--- ---), (D) 2-D Quant kit, R^2 = 0.9918 for saline (——●——), R^2 = 0.9929 for lysis buffer (--- ---). (——●——) Saline standard curve, (--- --) lysis buffer standard curve. No secondary axis is necessary for 3.2 D from the 2-D Quant kit since both the saline and lysis buffer standard curves gave similar results.

Similar results can be seen for Lowry and the BCA method (Figure 2.2 B and C). The 2-D Quant kit was able to give both similar as well as accurate data for the saline (R^2 = 0.9918) and lysis buffer (R^2 = 0.9929) standard curves (Figure 2.2 D). The 2-D Quant kit was used as the method of protein quantification in all determinations to follow.

2.3.2 Stain performance on SDS-PAGE using standard protein markers

In order to determine the sensitivity and performance of various protein stains, a 2-fold serial dilution was made of a standard molecular weight marker, and then loaded quantitatively onto 4 different SDS-PAGE gels and subsequently stained with 4 different stains: Colloidal Coomassie Blue (CCB), silver stain, SYPRO Ruby and Flamingo Pink (Figure 2.3). The 4 gels were compared by using Quantity One to determine the sensitivity and linear regression constant of each individual stain (Table 2.4).

Table 2.4: Comparative stain analysis for Plasmodial proteins analysed with 1-D SDS PAGE.

Stain	LOD[a] (ng)	R^2
CCB	25-90	0.89
Silver	10-90	0.83
SYPRO	1-90	0.97
Flamingo	1-90	0.97

[a]Limit of detection (LOD) is defined as the minimum amount of protein that could be detected on the SDS-PAGE gel with a specific stain.

Both Sypro Ruby and Flamingo Pink achieved similar results, as both were able to detect as little as 1 ng of protein, and were linear with R^2 = 0.97. CCB was the least sensitive of the 4 stains with a detection limit of 25 ng and linearity of R^2 = 0.89. Silver stain was able to detect a minimum of 10 ng but has a very poor linear range of R^2 = 0.83, and would thus not be ideal to use for quantitation.

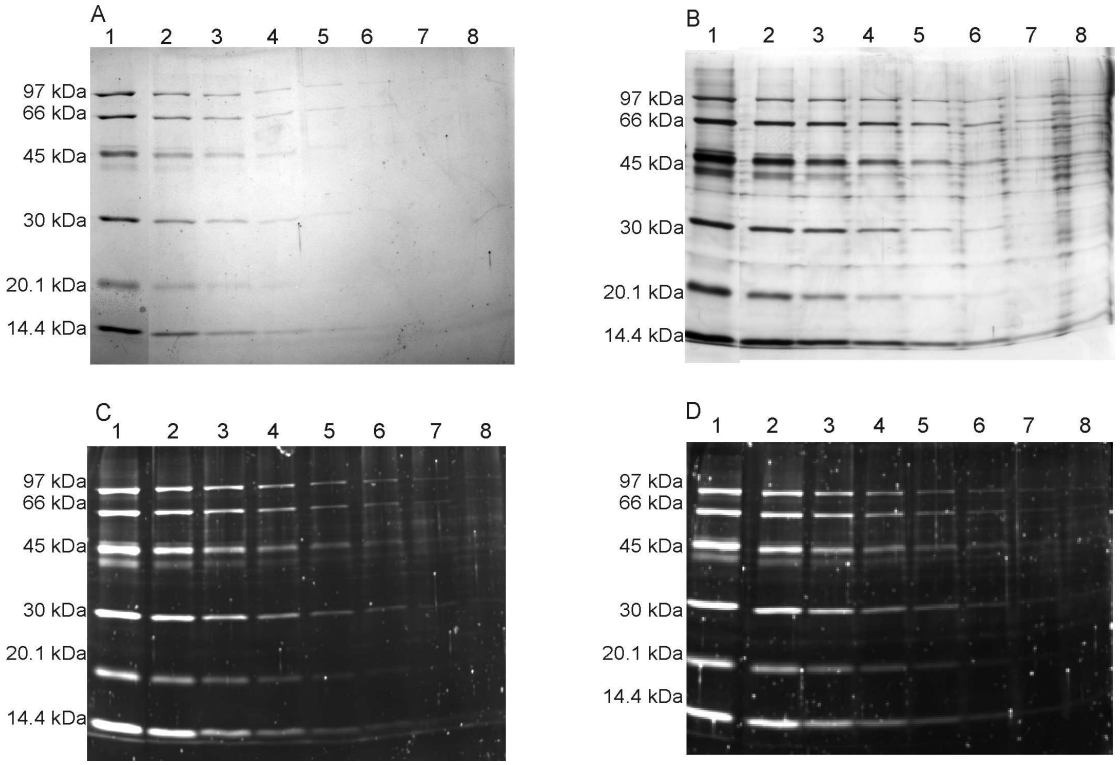

Figure 2.3: Comparison of standard proteins on SDS PAGE gels using 4 different stains.

Two fold dilutions of a standard molecular weight marker were loaded similarly onto each gel. (A) Colloidal coomassie blue, (B) MS-compatible silver stain, (C) SYPRO Ruby, (D) Flamingo Pink. The total protein per lane is: lane (1) 1250 ng, (2) 625 ng, (3) 312.5 ng, (4) 156.3 ng, (5) 78 ng, (6) 39 ng, (7) 19 ng, (8) 9.7 ng. Bands from the top to the bottom are: Phosphorylase b, 97 kDa, Albumin, 66 kDa, Ovalbumin, 45 kDa, Carbonic anhydrase, 30 kDa, Trypsin inhibitor, 20.1 kDa, Alpha-lactalbumin, 14.4 kDa

2.3.3 Stain performance on 2-DE using Plasmodial proteins

These 4 stains were subsequently tested on the proteome of Plasmodial proteins after 2-DE. All the samples were pooled to one sample and used for all 8 gels that were run. This is to ensure that gels are only judged on staining performance and not on possible sample differences. The concentration was determined using the 2D Quant kit as above (Figure. 2.2 D). Two hundred microgram protein was loaded onto each 13 cm IPG strip (pH 3-10 L). Duplicate 2-DE analysis were performed for all 4 stains used (n = 2 per stain, n = 8 in total) and spot analyses were performed with PD Quest. The CCB stain performed poor in detection with an average of 126 spots detected, markedly less than any of the other 3 stains tested (Table 2.5).

The MS-compatible silver stain is a highly sensitive stain able to detect proteins in their low nanogram levels (Berggren *et al.*, 2000) and was also superior within this study in terms of sensitivity with an average of 420 spots detected (Figure 2.4). However, the poor linearity and spurious artefacts associated with silver staining of 2-DE could lead to unreliable results when

groups of gels with differentially expressed proteins are compared (Table 2.6) (Berggren *et al.*, 2000).

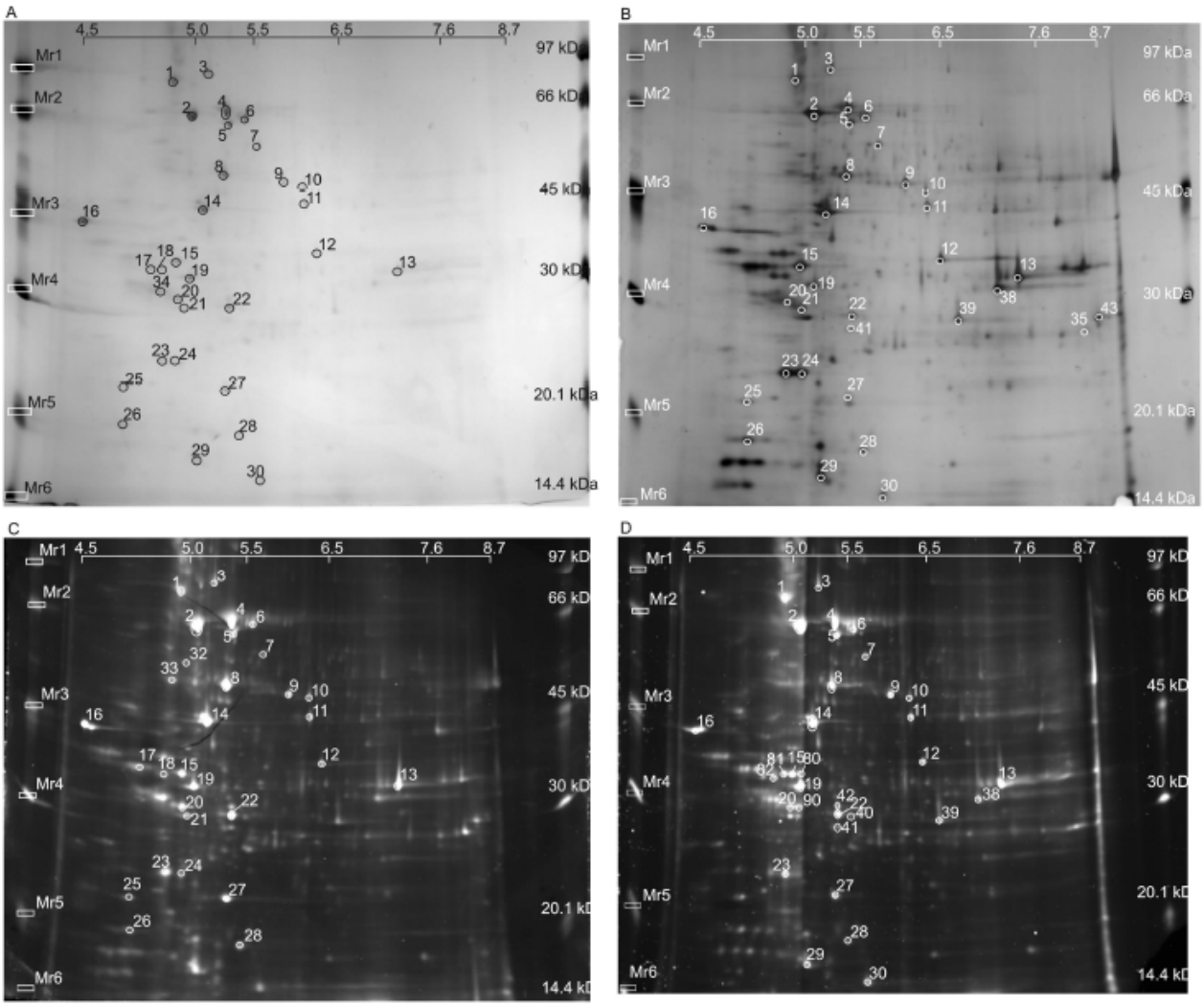

Figure 2.4: Comparison of Plasmodial proteins on 2-DE gels using 4 different stains.

Two-hundred micrograms of *Pf*3D7 proteins were loaded onto 13 cm IPG pH 3-10L strips for 2-DE analysis. After electrophoresis, the gels were stained with (A) Colloidal Coomassie Blue, (B) MS compatible silver stain, (C) SYPRO Ruby, (D) Flamingo Pink. The number of spots was determined using PD Quest 7.1.1 with n = 2 for each individual stain. About 39 similar spots were cut from each of the stained gels to determine the MS efficiency. The identified spots are marked on the gels. All MS data for the identified spots can be obtained in Appendix A as supplementary tables A-D.

SYPRO Ruby only detected 235 spots on the 2-DE gels. This loss in sensitivity is in sharp contrast to the results that were obtained for SYPRO Ruby when tested on the molecular weight markers when it had similar sensitivity to Flamingo Pink. It has also been shown that Flamingo Pink is highly consistent in the number and array of spots detected, and has little gel to gel variability (Harris *et al.*, 2007). In this study Flamingo Pink was able to detect 349 spots.

2.3.4 Filtering of trophozoite data

The total Plasmodial trophozoite proteome is predicted to contain 1029 proteins (Florens *et al.*, 2002, Aurrecoechea *et al.*, 2008) (PlasmoDB 6.0), which spans a wide molecular weight range and pI with different degrees of solubility. Filtering of this dataset to represent the conditions used in this study for 2-DE resulted in the identification of 443 Plasmodial trophozoite proteins that should be detectable on a standard 2-DE gel in the molecular weight range of 10-110 kDa with a pI range of 4-9. Unfortunately, these 443 Plasmodial proteins that should be detectable on 2-DE out of the total 1029 trophozoite proteins accounts for only 41% of the total trophozoite proteome (Figure 2.5). Silver detected 420 protein spots which accounts for 95% (420 out of 443) of the 2-DE detectable proteome as per our calculations. However, this does not take the possibility of protein isoforms being present within these protein spots. Similarly, Flamingo Pink detected 79% (349 out of 443), SYPRO Ruby 53% (235 out of 443) and CCB 28% (126 out of 443) of the detectable 2-DE proteome as with our calculations.

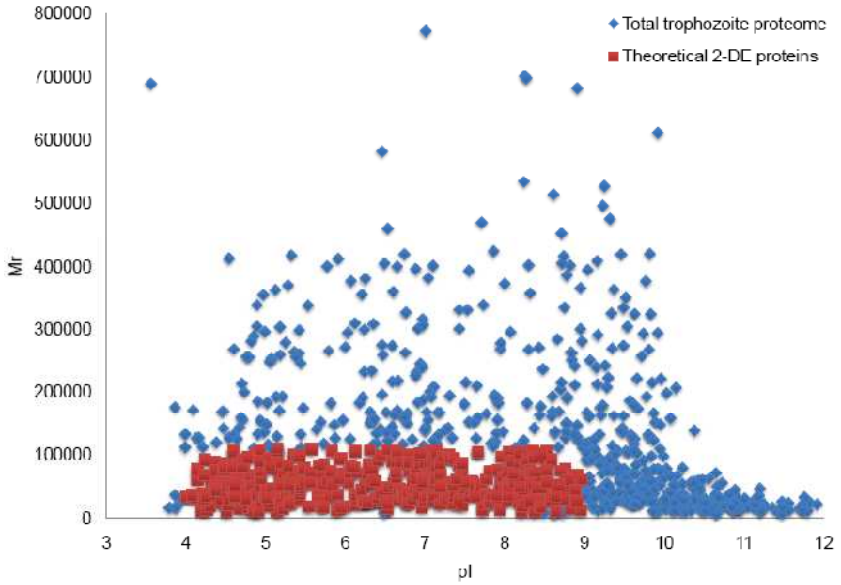

Figure 2.5: Plot of the total trophozoite proteome

The diamond shapes (blue) represent a computer generated plot of the total trophozoite proteome as given in PlasmoDB 6.0. The squares (red) are proteins that are detectable on 2-DE gels, within the range of 10-110 kDa, and a pI of 4-9 as per our calculations.

2.3.5 Compatibility of the 4 stains with MALDI-TOF MS/MS

In order to assess the overall MS-compatibility of the 4 staining methods, approximately 39 spots of each of the 4 individual gels were selected, consisting of 33 Plasmodial proteins each (Figure 2.4, 1-33) and 6 standard molecular weight marker proteins (Figure 2.4, marked Mr1 to Mr6), summarised in Table 2.5 (2-DE trophozoite analysis of stains). The spots were prepared for MS as described in the methods section, with the exception that for CCB samples an additional wash step was

incorporated to ensure that the dye is washed out, although some of the very highly abundant spots still had a faint blue colour despite this extra wash step. The silver stained samples were first destained to remove all the silver from the gel pieces (Gharahdaghi *et al.*, 1999). Proteins were identified when a significant Mascot score was obtained and further criteria of at least 5 peptides and sequence coverage of at least 10% was achieved (Appendix A). This was done to increase the MS/MS identification confidence. A summary of the precise number of spots that were cut for each of the different stains and the number of spots identified by tandem MS for each stain as well as the success rate for each stain and overall success rate is shown in Table 2.5.

Table 2.5: Comparative stain analysis for Plasmodial proteins analysed with 1-D as well as 2-DE SDS PAGE. Spot detection and MS identification rates are included for each of the 4 different stains, analysed on duplicate gels each (n=2).

Stain	Spots detected (PD Quest)	Nr cut for MS	Nr identified by MS	Identification success rate (%)
CCB	126	37	35	95
Silver	420	39	33	85
SYPRO	235	39	33	85
Flamingo	349	39	37	95
Total	**1130**	**154**	**138**	**90[a]**

[a] =average

Silver staining resulted in the least number of positive identifications (33 out of 39 selected spots). Similar to silver staining SYPRO Ruby resulted in the identification of 33 out of 39 spots. The best results were obtained with CCB (35 out of 37 tested) and Flamingo Pink (37 positive identifications out of 39 tested). The high success rate was due to the fact that tandem MS were performed on all of the samples.

B: Application of 2-DE optimised method on the Plasmodial ring and trophozoite stages

2.3.6 2-DE analysis of the Plasmodial proteome

After the successful establishment of a reliable protein quantification method, linear staining and good MS identification, the methodology could now be applied to the Plasmodial early trophozoite proteome as proof-of-principle. The parasites were harvested in the late ring and the early trophozoite stages and 400 µg of the protein containing supernatants were applied to 18 cm IPG strips pH 3-10 L. Linear IPG strips were used since this would enable similar increments between the pH values, and therefore give an overall view of the proteome spanning a wide pI range. Spots were analysed using PD Quest after which the spots were manually cut and prepared for MS analysis. The spots selected for analysis of the ring and trophozoite proteomes included spots of various intensities covering the whole 2-DE range (pI 4-9, and Mr 13-135 kDa). The normalised intensities of these spots ranged from 58 to a maximum of 9734 with 1963 as the average intensity per spot. Normalisation was done to correct for inconsistencies that may occur between gels that are not due to differential expression of spots but are rather due to experimental errors like inconsistency in staining and pipetting. Normalistion is of utmost importance for the determination of differentially regulated spots. The normalisation method entails removing starurated spots (flagged as invalid) and then averaging the intensities of a single spot between the comparative technical repeated gels. This is done for every single valid spot for all technical repeated gels. For the ring stage proteome analysis, 77 spots were selected for MS identification and 63 spots were selected for the trophozoite stage. The spots that were positively identified are marked in Figure 2.6 and the MS data is given in Table 2.6 A and B. The identified proteins all had significant MASCOT scores, at least 5 peptides identified, and sequence coverage of at least 10% each (Table 2.6 A and B).

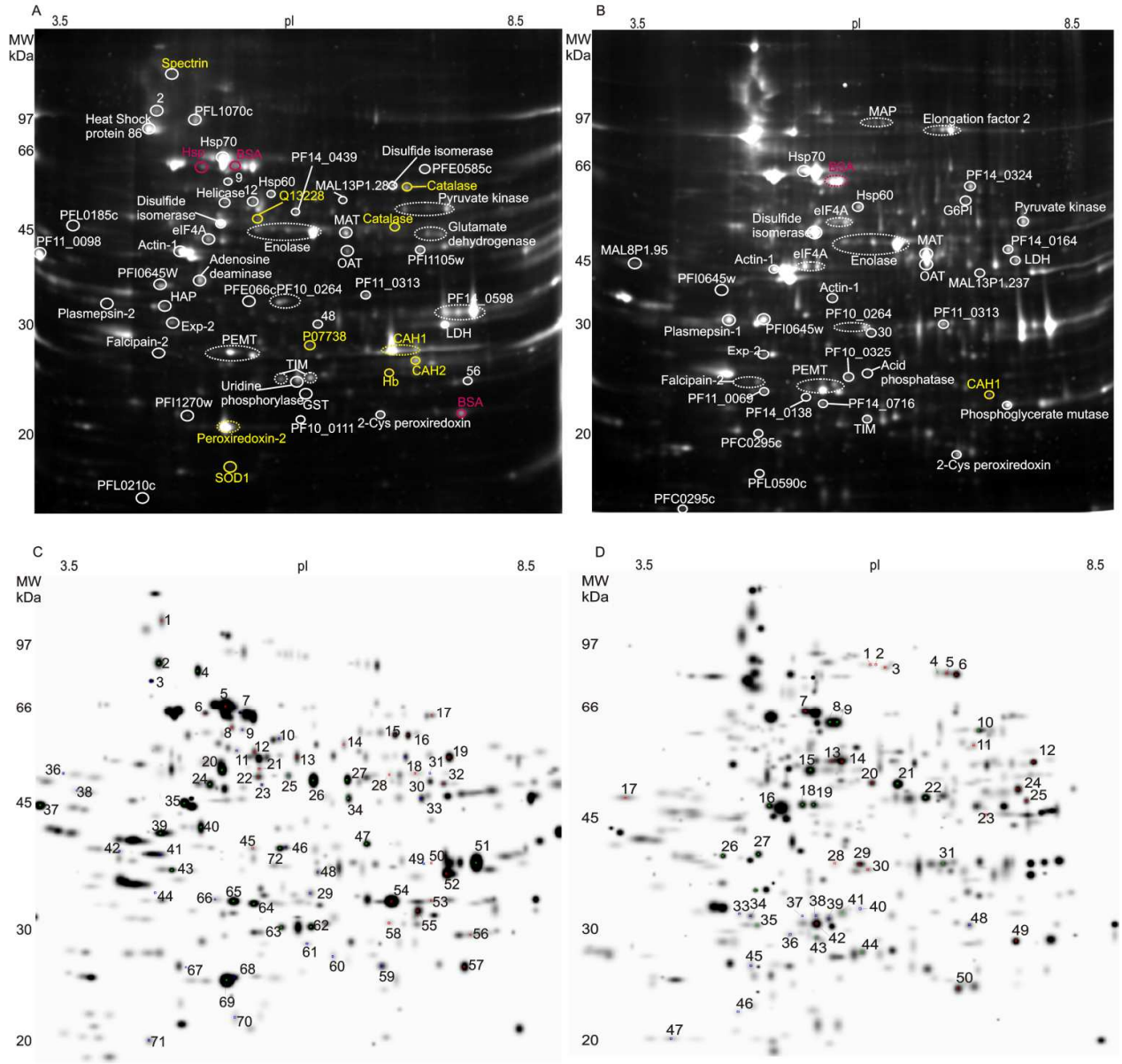

Figure 2.6: 2-DE of the rings and trophozoites stage *P. falciparum* indicating identified proteins.

2-DE of Plasmodial ring-stage proteome (A) and its master image (C) compared to the 2-DE of early trophozoites stage proteome (B) and its corresponding master image (D). Master images were created by PD Quest as representative of all the 2-DE gels performed for each of the time points and contains spot information of a total of eight 2-DE gels. Plasmodial proteins are marked in white, human proteins are marked in yellow and bovine proteins are marked in red. Isoforms are encircled with dotted lines. The representing master images are also marked with identified proteins and all positively identified proteins are listed in Table 1 A and B.

Table 2.6: List of proteins identified by tandem mass spectrometry for late rings and early trophozoites

Spot nr[a]	Transcript trend[b]	PlasmoDB ID	Name	Mr (obtained) Da	pI (PlasmoDB)	Mascot Score MS/MS[c]	Seq Cover[d]	Match[e]
(A) Proteins identified for late rings								
60	Up	□□□□□□□□	20S proteasome beta subunit, putative	30862	5.18	150	9	4
59	↔	PF14_0368	2-Cys peroxiredoxin	21964	6.65	540	59	8
46	↔	PF10_0264	40S ribosomal protein, putative (1)	30008	5.91	152	11	3
72	↔	PF10_0264	40S ribosomal protein, putative (2)	30008	5.91	146	14	4
35	↔	PFL2215w	Actin-I	42022	5.27	627	33	10
40	Up	PF10_0289	Adenosine deaminase, putative	42895	5.41	573	38	15
29	—	—	Bisphosphoglycerate mutase *(Homo sapiens)*	30027	6.1	441	46	10
53	—	—	Carbonic anhydrase 1 *(Homo sapiens)*	28778	6.63	531	50	8
54	—	—	Carbonic anhydrase 1 *(Homo sapiens)*	28620	6.65	845	58	11
55	—	—	Carbonic anhydrase 2 *(Homo sapiens)*	28802	6.63	320	30	7
16	—	—	Catalase *(Homo sapiens)*	59816	6.95	659	29	15
28	—	—	Catalase *(Homo sapiens)*	59816	6.95	425	22	9
15	Up	MAL8P1.17	Disulfide isomerase, putative (1)	55808	5.56	693	35	15
20	Up	MAL8P1.17	Disulfide isomerase, putative (2)	55808	5.56	1005	41	17
6	—	—	dnaK-type molecular chaperone hsc70 *(Bos Taurus)*	71454	5.37	579	20	11
24	—	PF14_0655	eIF4A	45624	5.48	580	36	16
11	↔	PFB0445c	eIF4A-like helicase, putative (1)	52647	5.68	589	26	10
12	↔	PFB0445c	eIF4A-like helicase, putative (2)	52647	5.68	251	13	6
37	Up	PF11_0098	Endoplasmic reticulum-resident calcium binding protein	39464	4.49	1135	59	17
4	Up	PFL1070c	Endoplasmin homolog, putative	95301	5.28	298	14	10
22	Up	PF10_0155	Enolase (1)	48989	6.21	313	18	7
23	Up	PF10_0155	Enolase (2)	48989	6.21	373	18	7
25	Up	PF10_0155	Enolase (3)	48989	6.21	414	27	11
26	Up	PF10_0155	Enolase (4)	48989	6.21	1000	40	16
71	↔	PFL0210c	Eukaryotic initiation factor 5a, putative	17791	5.42	159	27	4
43	↔	PF14_0678	Exported protein 2	33619	5.1	379	26	8
44	↔	PF11_0165	Falcipain 2	56405	7.12	212	12	6
30	Down	PF14_0164	Glutamate dehydrogenase (NADP+) (1)	53140	7.48	283	17	8
31	Down	PF14_0164	Glutamate dehydrogenase (NADP+) (2)	53140	7.48	212	15	6
32	Down	PF14_0164	Glutamate dehydrogenase (NADP+) (3)	53140	7.48	497	30	13
61	—	PF14_0187	Glutathione s-transferase	24888	5.97	47	11	2

49	Up	PF14_0598	Glyceraldehyde-3-phosphate dehydrogenase (1)	37068	7.59	302	25	7
50	Up	PF14_0598	Glyceraldehyde-3-phosphate dehydrogenase (2)	37068	7.59	131	11	3
51	Up	PF14_0598	Glyceraldehyde-3-phosphate dehydrogenase (3)	37068	7.59	810	47	14
56	—	PF11_0183	GTP binding nuclear protein Ran	24974	7.72	485	55	12
41	Down	PF14_0078	HAP protein	51889	8.05	645	34	13
5	↔	PF08_0054	Heat shock 70 kDa protein	74382	5.51	1378	34	23
3	↔	PF07_0029	Heat shock protein 86	86468	4.94	1153	25	24
58	—	—	Hemoglobin subunit beta *(Homo sapiens)*	16112	6.75	294	43	6
10	Up	PF10_0153	Heat shock protein 60 kDa	62911	6.71	870	37	19
13	↔	PF14_0439	Leucine aminopeptidase, putative	68343	8.78	172	14	7
52	↔	PF13_0141	Lactate dehydrogenase	34314	7.12	611	43	12
14	↔	MAL13P1.283	MAL13P1.283 protein	58506	6.09	261	10	6
17	↔	PFE0585c	Myo-inositol 1-phosphate synthase, putative	69639	7.11	454	25	14
36	Down	PFL0185c	Nucleosome assembly protein 1, putative	42199	4.19	293	16	7
34	Up	PFF0435w	Ornithine aminotransferase	46938	6.47	589	27	11
68	—	—	Peroxiredoxin-2 *(Homo sapiens)*	21918	5.67	515	41	10
69	—	—	Peroxiredoxin-2 *(Homo sapiens)*	21918	5.67	664	43	11
64	Up	MAL13P1.214	Phosphoethanolamine N-methyltransferase, putative (1)	31309	5.43	871	50	14
65	Up	MAL13P1.214	Phosphoethanolamine N-methyltransferase, putative (2)	31309	5.43	935	50	14
66	Up	MAL13P1.214	Phosphoethanolamine N-methyltransferase, putative (3)	31309	5.43	252	22	5
33	Up	PFI1105w	Phosphoglycerate kinase	45569	7.63	214	15	5
42	↔	PF14_0077	Plasmepsin 2	51847	5.35	72	6	3
48	↔	MAL8P1.142	Proteasome beta-subunit	31080	6.00	212	22	7
2	—	PFF0940c	Putative cell division cycle protein 48 homologue, putative	90690	4.95	303	10	7
18	Up	PFF1300w	Putative pyruvate kinase (1)	56480	7.50	633	28	15
19	Up	PFF1300w	Putative pyruvate kinase (2)	56480	7.50	732	37	16
67	—	PFI1270w	Putative uncharacterized protein PFI1270w	24911	5.49	327	26	6
47	↔	PF11_0313	Ribosomal phosphoprotein P0	35002	6.28	430	36	9
27	Up	PFI1090w	S-adenosylmethionine synthetase	45272	6.28	863	40	14
21	—	—	Selenium binding protein 1 *(Homo sapiens)*	52928	5.93	140	12	6
7	—	—	Serum albumin *(Bos Taurus)*	71274	5.82	620	24	15
57	—	—	Serum albumin *(Bos Taurus)*	71274	5.82	510	16	10
38	—	—	Solute carrier family 4, anion exchanger, member 1 *(Homo sapiens)*	101987	5.13	189	7	4
1	—	—	Spectrin alpha chain *(Homo sapiens)*	282024	4.98	889	24	9
70	—	—	Superoxide dismutase *(Homo sapiens)*	16154	5.70	219	37	4

39	↔	PFI0645w	Translation elongation factor 1 beta	32121	4.94	208	24	7
62	↔	PF14_0378	Triosephosphate isomerase (1)	27971	6.02	490	43	10
63	↔	PF14_0378	Triosephosphate isomerase (2)	27971	6.02	430	38	9
45	Up	PFE0660c	Purine nucleoside phosphorylase, putative (1)	27525	6.07	315	31	8
63	Up	PFE0660c	Uridine phosphorylase, putative (2)	27525	6.07	572	35	10
8	—	PF13_0065	V-type proton ATPase catalytic subunit A (1)	69160	5.51	291	19	10
9	—	PF13_0065	V-type proton ATPase catalytic subunit A (2)	69160	5.51	184	13	7
			(B) Proteins identified for late rings					
50	↔	PF14_0368	2-Cys peroxiredoxin	21964	6.65	504	72	11
45	Down	PFC0295c	40S ribosomal protein S12, putative (1)	15558	4.67	85	14	2
47	Down	PFC0295c	40S ribosomal protein S12, putative (2)	15558	4.67	217	36	5
28	↔	PF10_0264	40S ribosomal protein, putative (1)	30008	5.91	27	11	3
29	↔	PF10_0264	40S ribosomal protein, putative (2)	30008	5.91	267	24	8
40	Up	PF14_0036	Acid phosphatase, putative	35972	6.3	63	5	2
51	↔	PFL2215w	Actin-1 (1)	42272	5.17	81	36	12
16	↔	PFL2215w	Actin-1 (2)	42022	5.27	455	36	9
38	↔	PFL2215w	Actin-1 (3)	42022	5.27	225	14	5
48	—	—	Carbonic anhydrase 1 *(Homo sapiens)*	28620	6.65	70	20	4
15	Up	MAL8P1.17	Disulfide isomerase precursor, putative	55808	5.56	883	38	16
18	Up	PF14_0655	eIF4A (1)	45624	5.28	353	30	12
19	Up	PF14_0655	eIF4A (2)	45624	5.48	326	23	12
13	↔	PFB0445c	eIF4A-like helicase, putative (1)	52647	5.68	320	23	8
14	↔	PFB0445c	eIF4A-like helicase, putative (2)	52646	5.68	62	42	14
5	↔	PF14_0486	Elongation factor 2 (1)	94546	6.36	91	4	4
6	↔	PF14_0486	Elongation factor 2 (2)	94546	6.78	657	26	18
20	↔	PF10_0155	Enolase (1)	48989	6.21	408	32	10
21	↔	PF10_0155	Enolase (2)	48989	6.21	949	36	12
30	—	PFD0615c	Eryhrocyte membrane protein 1 (fragment)	13608	6.96	51	38	7
33	↔	PF11_0165	Falcipain 2 (1)	56481	7.9	47	23	10
34	↔	PF11_0165	Falcipain 2 (2)	55928	7.49	56	24	11
11	↔	PF14_0341	Glucose-6-phosphate isomerase	67610	6.78	61	28	14
24	Down	PF14_0164	Glutamate dehydrogenase (NADP+)	53140	7.48	336	28	11
39	↔	PF10_0325	Haloacid dehalogenase-like hydrolase, putative	33220	5.62	180	27	6
7	↔	PF08_0054	Heat shock 70 kDa protein	74382	5.33	861	33	18
52	Up	PF10_0153	Heat shock protein 60 kDa	62911	6.71	128	38	21
35	Up	PF11_0069	Hypothetical protein	32112	4.91	55	13	3

36	Up	PF14_0138	Hypothetical protein	23889	5.49	53	9	2
23	Up	MAL13P1.237	Hypothetical protein MAL13P1.237	42475	7.14	574	37	13
17	Down	MAL8P1.95	Hypothetical protein MAL8P1.95	37933	4.13	385	25	8
10	↔	PF14_0324	Hypothetical protein, conserved	66415	6.63	66	7	4
25	Up	PF13_0141	Lactate dehydrogenase	34314	7.12	100	12	3
1	↔	MAL13P1.56	M1 family aminopeptidase (1)	126552	7.3	102	26	23
2	↔	MAL13P1.56	M1 family aminopeptidase (2)	126552	6.68	124	26	25
3	↔	MAL13P1.56	M1 family aminopeptidase (3)	126552	7.3	107	27	23
22	Up	PFF0435w	Ornithine aminotransferase	46938	6.47	637	29	12
37	Up	MAL13P1.214	Phosphoethanolamine N-methyltransferase, putative (1)	31043	5.28	69	9	2
38	Up	MAL13P1.214	Phosphoethanolamine N-methyltransferase, putative (2)	31043	5.28	261	26	6
41	Up	MAL13P1.214	Phosphoethanolamine N-methyltransferase, putative (3)	31309	5.28	177	22	5
42	Up	MAL13P1.214	Phosphoethanolamine N-methyltransferase, putative (4)	31309	5.28	722	48	13
49	↔	PF11_0208	Phosphoglycerate mutase, putative	28866	8.3	401	36	10
26	Down	PF14_0076	Plasmepsin-1	51656	6.72	540	35	12
43	↔	PF14_0716	Proteosome subunit alpha type 1, putative	29218	5.51	268	31	6
46	—	PFL0590c	P-type ATPase, putative	135214	6.13	54	18	16
12	Up	PFF1300w	Putative pyruvate kinase	56480	7.5	101	51	16
31	↔	PF11_0313	Ribosomal phosphoprotein P0	35002	6.28	121	13	3
22	Up	PFI1090w	S-adenosylmethionine synthetase	45272	6.28	480	32	10
8	—	—	Serum albumin *(Bos Taurus)*	71274	5.82	466	24	15
9	—	—	Serum albumin *(Bos Taurus)*	71274	5.82	822	36	21
27	↔	PFI0645w	Translation elongation factor 1 beta	32121	4.94	488	35	9
44	Up	PF14_0378	Triosephosphate isomerase	27971	6.02	183	22	6

Proteins identified are sorted alphabetically according to name with isoforms grouped together and the number of isoforms per protein is marked in brackets. [a]Spot number corresponds to marked spots on the master image of ring stage parasites. [b]Trend of transcripts regulation from 16-20 HPI as acquired from the IDC database (http://malaria.ucsf.edu/comparison/index.php) for each of the identified proteins. (↔) indicates unchanged transcript levels and (—) is indicative that result is not applicable. [c]Mascot scores are based on MS/MS searches and is only taken when the score is significant ($p<0.05$). [d]Sequence coverage is given by Mascot for detected peptide sequences. [e]Matched is the number of peptides matched to the particular protein

In this study any spot on the 2-DE gel that was cut out and identified by MS is referred to as a protein spot. Unique Plasmodial protein groups represent Plasmodial proteins that may contain more than one isoform but are still grouped into one unique protein group. A protein isoform is when more than one spot was identified as the same protein as a result of PTM's. For example in the ring stage 4 different spots on the 2-DE gel were identified as enolase due to the presence of various PTM's. Therefore, this will be representative of 1 unique protein group which is enolase, but 4 protein isoforms. This nomenclature will be used throughout this chapter as well as in Chapter 3. For the ring stage proteome 73 protein spots were positively identified out of 77 spots subjected to MS/MS, while for the trophozoite proteome 57 protein spots were positively identified out of 63 spots subjected to MS/MS (Table 2.7 A and B). Of the 73 protein spots identified in the ring stage proteome, 57 protein spots were from Plasmodial origin, and consisted of 41 unique Plasmodial protein groups and protein isoforms were representative of an additional 28% (16 isoforms) of these Plasmodial protein spots. The trophozoite proteome consists of 52 protein spots identified by MS of which 49 protein spots were from Plasmodial origin. Of these, 29% (14 protein spots) additionally accounted for isoforms from the 35 unique Plasmodial protein groups.

2.3.7 Comparison of ring, trophozoite and schizont proteome

The earlier release of the schizont proteome by 2-DIGE (Foth *et al.*, 2008) prompted investigation of the late ring and early trophozoite stage proteomes with 2-DE. A total of 54 protein spots were identified in the schizont proteome (Foth *et al.*, 2008). Upon filtering of the schizont protein identifications it was observed that only 24 unique Plasmodial protein groups were identified. The ring and trophozoite data from this study was compared to the schizont data and it was determined that only 9 unique Plasmodial protein groups were shared between all 3 life stages of the parasite (Figure 2.7 and Table 2.7). Nineteen unique Plasmodial protein groups were shared between the ring and trophozoite stages, 14 unique Plasmodial protein groups shared between the ring and schizont and 11 shared between the trophozoite and schizont stages.

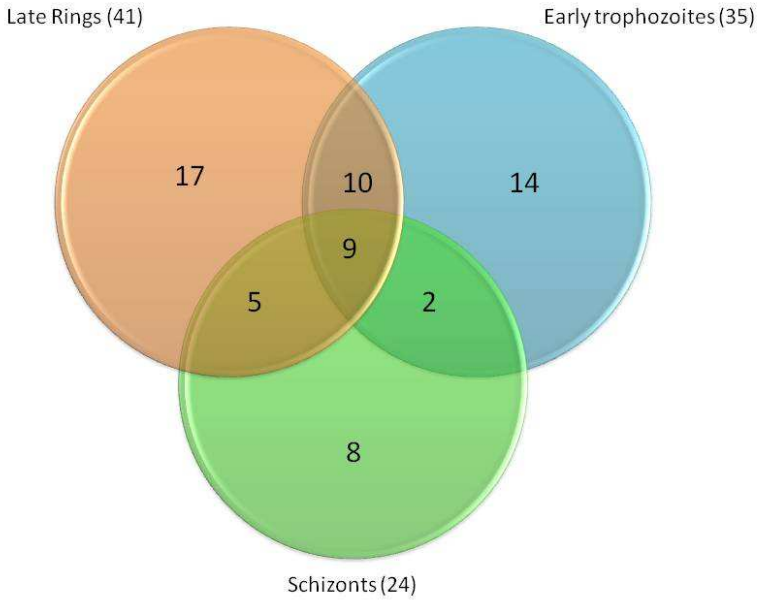

Figure 2.7: Venn diagram of 3 stages investigated by proteomics in *P. falciparum*.

Seventeen ring stage proteins, 14 trophozoite proteins and 8 schizont stage proteins were not shared in any way between the 3 life stages. The unique Plasmodial protein groups shared between the ring, trophozoite and schizont life cycle stages are given in Table 2.7. A total of 26 proteins are shared which consist of 24 ring proteins shared, 21 trophozoite proteins shared and only 16 schizont stage proteins that are shared.

Table 2.7: Table of the proteins shared between each of the 3 life stages.

Unique Plasmodial protein groups only (occurrence in more than one of the stages) excluding human proteins and isoforms.

PlasmoDB ID	Annotation	R	T	S
MAL13P1.214	Phosphoethanolamine N-methyltransferase, putative	Y	Y	Y
MAL13P1.56	M1-family aminopeptidase		Y	Y
MAL8P1.17	Disulfide isomerase precursor, putative	Y	Y	
PF08_0054	Heat shock 70 kDa protein	Y	Y	Y
PF10_0153	Hsp60	Y	Y	Y
PF10_0155	Enolase	Y	Y	Y
PF10_0264	40S ribosomal protein, putative	Y	Y	
PF10_0289	Adenosine deaminase, putative	Y		Y
PF10_0325	Hypothetical protein, conserved		Y	Y
PF11_0165	Falcipain 2 precursor	Y	Y	
PF11_0313	Ribosomal phosphoprotein P0	Y	Y	
PF13_0141	L-lactate dehydrogenase	Y	Y	
PF14_0164	NADP-specific glutamate dehydrogenase	Y	Y	
PF14_0368	2-Cys peroxiredoxin	Y	Y	Y
PF14_0378	Triose-phosphate isomerase	Y	Y	Y
PF14_0655	RNA helicase-1, putative	Y	Y	Y
PF14_0678	Exported protein 2	Y		Y
PFB0445c	Helicase, putative	Y	Y	Y
PFE0660c	Uridine phosphorylase, putative	Y		Y
PFF0435w	Ornithine aminotransferase	Y	Y	
PFF1300w	Pyruvate kinase, putative	Y	Y	
PFI0645w	EF-1B	Y	Y	
PFI1090w	S-adenosylmethionine synthetase, putative	Y	Y	
PFI1270w	Hypothetical protein	Y		Y
PFL0210c	Eukaryotic initiation factor 5a, putative	Y		Y
PFL2215w	Actin	Y	Y	Y
Total		**24**	**21**	**16**

2.3.8 Comparison of proteomic data with transcript levels

Comparison of the protein levels from the ring and trophozoite proteomes to the IDC transcript profile demonstrated distinct similarities between transcript production profiles (obtained from PlasmoDB 6.0 www.plasmodb.org)(Aurrecoechea *et al.*, 2008) and protein levels (Table 2.6 A-B). Proteins that increased in abundance from rings to trophozoites mostly exhibited a corresponding increase in transcript level when compared to IDC data (Figure 2.8, Table 2.6). Enolase, S-adenosylmethionine synthase (AdoMet synthase), ornithine aminotransferase (OAT), uridine phosphorylase (PNP) and disulfide isomerase all demonstrated an increase in abundance of both the transcript and protein expression levels. Similarly, eIF4A-like helicase and ribosomal phosphoprotein P0 all exhibited unchanged transcript and protein expression levels from ring to trophozoite stage parasites. Actin-1 was one of the few exceptions in which transcript levels remained constant from ring to trophozoite stage parasites whilst protein levels were increasing. Similarly, the transcript levels of 2-Cys peroxiredoxin remained constant over the two time points whilst the protein was decreased.

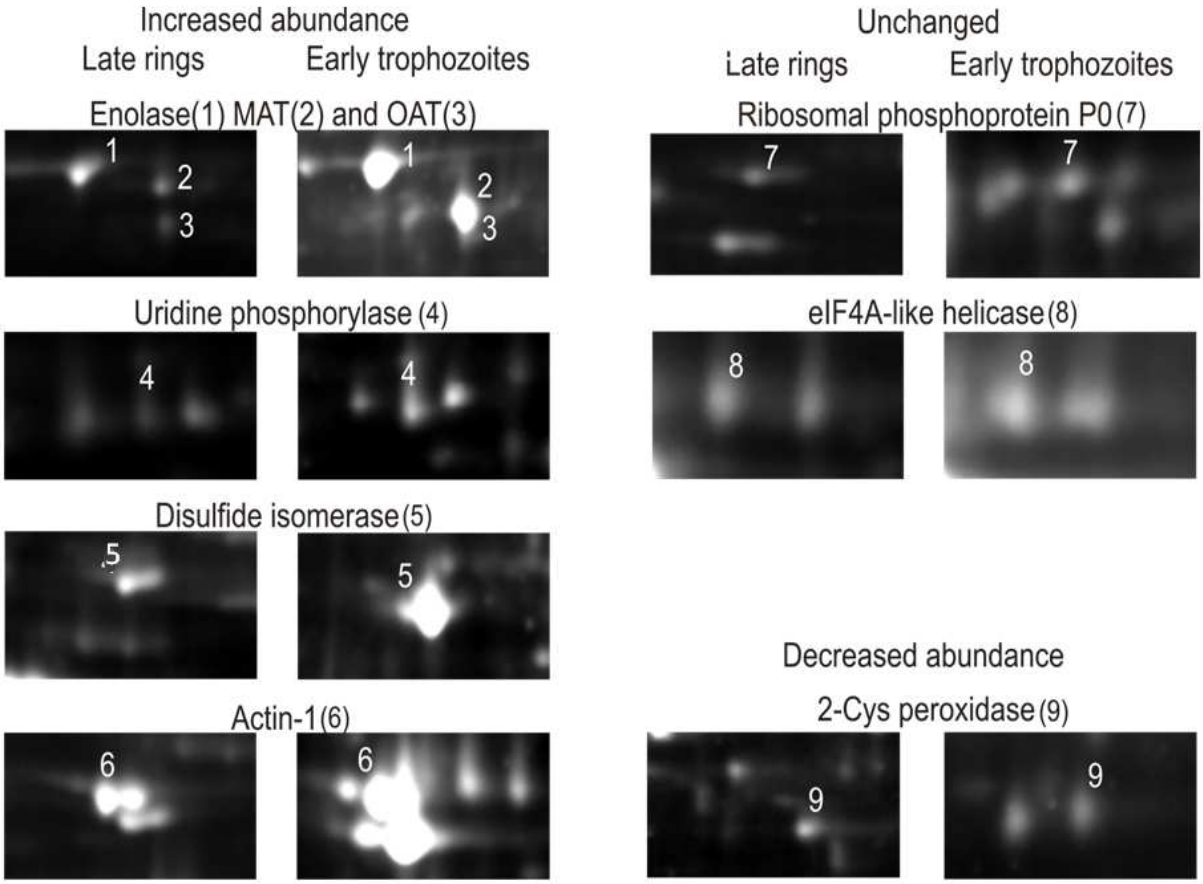

Figure 2.8: Proteins that are differentially regulated in the *P. falciparum* ring and trophozoite stage proteomes.

Numbers are indicative of protein spot that is indicated. MAT: S-adenosylmethionine synthase, OAT: ornithine aminotransferase

2.3.9 Differential expression of isoforms

Of the nineteen identified Plasmodial proteins shared between the ring and trophozoite stages of the parasite, several proteins appear as isoforms (Figure 2.9, isoforms are also marked in Figure 2.6 and Table 2.6 A-B). Moreover, some of these protein isoforms display differential regulation from the ring to trophozoite stages (Figure 2.9). An increase in both transcript as well as protein expression levels were determined for the 4 enolase and phosphoethanolamine N-methyltransferase (PEMT) isoforms and the 3 glyceraldehyde-3-phosphate dehydrogenase (G3PDH) isoforms. The transcript levels of pyruvate kinase (2 isoforms) increased over the specified period, but the protein expression levels for both isoforms declined. The transcript levels for both triosephosphate isomerase (TIM, 2 isoforms) and eIF4A (2 isoforms) remained constant during this period but the corresponding proteins increased in abundance. For glutamate dehydrogenase (3 isoforms) the transcript level decreased but the protein level remained constant from the ring to the trophozoite stages. Unchanged transcript and protein levels were detected for eIF4A-like helicase (2 isoforms).

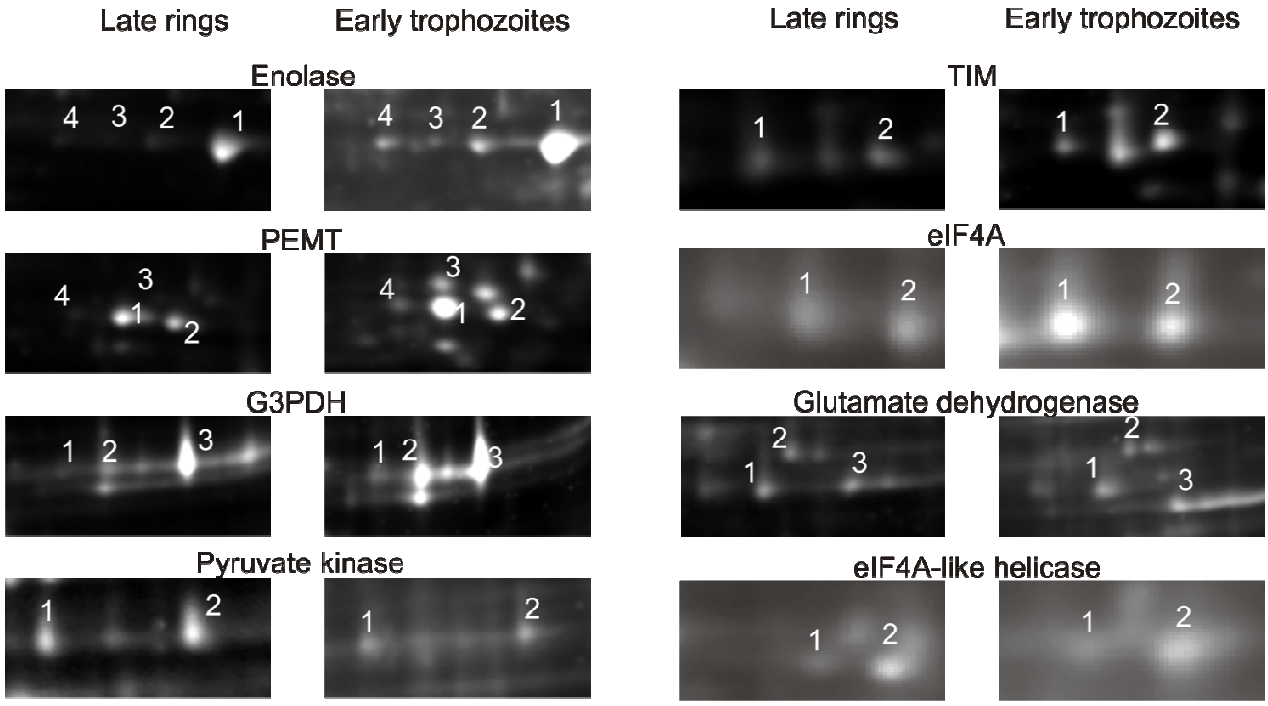

Figure 2.9: Isoforms of proteins that are differentially regulated in the *P. falciparum* ring and trophozoite stage proteomes.

The numbers are indicative of the number of isoforms per protein that were detected. Enolase, PEMT, and G3PDH, TIM and eIF4A all increase in protein abundance from the ring to the trophozoite stage. Pyruvate kinase decreased in protein abundance from rings to trophozoites, while glutamate dehydrogenase and eIF4A-like helicase remained unchanged over the specified time in protein expression levels. PEMT: phosphoethanolamine methyltransferase, TIM: triosephosphate isomerase, G3PDH: glyceraldehyde-3-phosphate dehydrogenase.

2.4 Discussion

2.4.1 Optimisation of Plasmodial proteins for 2-DE

The ability of 2-DE to provide a snapshot of the proteome at any particular time, is a distinct advantage for a multistage organism such as *Plasmodium*. The 2-DE technique remains the most widely used for proteomic investigation techniques (Wang *et al.*, 2009) due to several advantageous properties such as good resolution of abundant proteins as well as information on protein size, quantity and isoforms with post-translational modifications or different pIs (Lopez, 2000). However, 2-DE gels are biased to the detection of relatively high abundant proteins as well as soluble and mid-range molecular weight proteins (Ong & Pandey, 2001). Besides the visual advantages of 2-DE in comparing protein levels, proteins are differentially stained due to their specific chemical and physical properties, which necessitates careful selection of the staining method in terms of its sensitivity, reproducibility, ease of use and cost-effectiveness. Most importantly, the stain should be compatible with downstream applications such as MS. This chapter describes an improved protocol for the detection and identification of Plasmodial proteins separated by 2-DE, which was then also subsequently applied to identify the proteome of the Plasmodial ring and trophozoites stages.

The analysis of the Plasmodial proteome by 2-DE has been hampered by numerous technical constraints. Plasmodial proteins are notoriously insoluble, comparatively large, non-homologous and highly charged (Birkholtz *et al.*, 2008a) and therefore necessitates the use of optimised lysis buffers to ensure maximal solubility of these proteins for 2-DE. The lysis buffer described by Nirmalan *et al.*, is able to solubilise a large proportion of Plasmodial proteins. In this study, the combination of using 5-fold less saponin, increased washing steps and shorter sonication cycles (with prolonged cooling in between cycles), contributed to the absence of hemoglobin on the 2-DE gels in the 14 kDa range and enabled the detection of proteins in the range of pH 8-9 that was previously cumbersome in Plasmodial 2-DE. The use of this lysis buffer however, precludes the use of traditional methods of protein concentration determination.

A two-pronged approach was used in this study to determine the most effective and reproducible detection and staining method for Plasmodial proteins. Firstly, the effect of the extraction medium on standard protein determination methods was established as well as the sensitivity of staining methods to detect gel-separated molecular weight standards and secondly, for comparative purposes the sensitivity and reproducibility of these staining methods to detect Plasmodial proteins on 2-DE gels. Four different methodologies were evaluated to determine Plasmodial protein concentrations in the lysis buffer used for the protein extraction. The standard Bradford method as well as the

Lowry and BCA methods was found to be incompatible with the lysis buffer. The 2-D Quant kit conversely provided reproducible and comparable data for both the saline (R^2 = 0.9918) and lysis buffer (R^2 = 0.9929) standard curves, most likely due to the quantitative protein precipitation step by which any other interfering substances in the lysis buffer are also removed. Although various Plasmodial proteomic studies have employed the Bradford method (Makanga *et al.*, 2005, Panpumthong & Vattanaviboon, 2006), the present study confirms recent reports of the reliability of the 2-D Quant method (Foth *et al.*, 2008, van Brummelen *et al.*, 2009).

A second caveat in semi-quantitative proteomics is the sensitivity of the staining method used for the detection of protein spots after 2-DE. The sensitivity, performance, and linear regression constants of 4 different staining methods were compared in this study with quantitative 1-D analyses of standard molecular weight markers. Four different SDS-PAGE gels were individually stained with Colloidal Coomassie Blue (CCB), MS-compatible silver stain, SYPRO Ruby and Flamingo Pink, and compared by using Quantity One 4.4.1 to determine the detection limits. CCB was the least sensitive of the 4 stains and had relatively poor linearity (R^2 = 0.89). The MS-compatible silver stain was able to detect a minimum of 10 ng but has a very poor linear range (R^2 = 0.83). The fluorescent stains, SYPRO Ruby and Flamingo Pink, thus seem superior to CCB and silver in both sensitivity and dynamic linear quantification range of standard protein molecular weight markers. Coomassie Brilliant Blue is one of the most commonly used stains for detection of highly abundant proteins, and has been widely employed since its discovery in the 1960's. The more sensitive Colloidal Coomassie Blue (CCB) stain used here is a enhanced modification of the Coomassie Brilliant Blue stain and has a detection limit similar to that of silver staining but with the added advantage of limited background noise (Neuhoff *et al.*, 1988). It has an average linear dynamic range, is easy to use, cheap, has little protein to protein variation and is MS compatible (Berggren *et al.*, 2000). Silver staining is labour-intensive and can easily saturate during staining, and is generally not MS compatible due to the addition of cross linkers and fixatives such as gluteraldehyde and formaldehyde. Silver staining relies on salt or complex formation involving sulfhydryl and carboxyl groups of amino acid side chains. The formaldehyde and gluteraldehyde (not used in this case) can attach covalently to the proteins and alkylate alpha and epsilon amino groups of proteins, thus limiting down-stream applications and reducing the MS quality and the amount of peptides that can be obtained (Lin *et al.*, 2008). In this study a good identification rate (85%) were obtained, which may be due to the ferricyanide destaining step that reacts with the sodium thiosulfate to form a water soluble complex, that can be removed from the gel pieces, hence reducing background interference (Gharahdaghi *et al.*, 1999). Various MS compatible silver stains have been developed which omits gluteradehyde, but unfortunately this usually results in reduced

sensitivity (Gharahdaghi *et al.*, 1999, Shevchenko *et al.*, 1996). Another problem with silver quantitation of spots is the formation of a donut effect on the gel image, with the edges of the spot darker than the middle and ultimately creates problems during analysis of spots (Winkler *et al.*, 2007). This effect was not seen in the silver stained gels here.

Fluorescent stains have been developed with seemingly similar sensitivity to silver as well as being MS-compatible, which include the earlier SYPRO Orange and SYPRO Red (Steinberg *et al.*, 1996b, Steinberg *et al.*, 1996a), and the currently commonly used SYPRO Ruby stain (Berggren *et al.*, 2000). SYPRO Ruby is a fluorescent ruthenium-based stain that binds non-covalently to proteins in gels, and can be used to stain refractory proteins like glycoproteins and lipoproteins without staining nucleic acids. SYPRO Ruby has good photo-stability, cannot over stain proteins, and has a good detection limit and linear dynamic range, as well as being MS-compatible (Berggren *et al.*, 2000, Yan *et al.*, 2000 (a)). Despite several advantages that are associated with SYPRO Ruby (Berggren *et al.*, 2000, Yan *et al.*, 2000 (a)), SYPRO Ruby was only able to detect 235 Plasmodial protein spots after 2-DE with a MS identification rate of 85% (33/39). These results are in sharp contrast to those obtained with standard protein molecular weight markers and indicate that SYPRO Ruby is not an appropriate stain to use with Plasmodial proteins. It may be due to the fact that SYPRO Ruby dye binds to the proteins in such a way that it interferes with ionisation and identification and hence reduces the chance of a positive identification (Lanne & Panfilov, 2005). New generation fluorescent stains such as Flamingo Pink are reported to be able to detect proteins across the full range of molecular weights and isoelectric points separated on 2-DE with little gel-to-gel variability (Harris *et al.*, 2007), good linear dynamic range and MS-compatibility. These properties seem to be supported by the results of this study since 79% (349/443) of the Plasmodial trophozoite proteome predicted by our calculations were detected on 2-DE. The most promising results concerning protein identification were obtained with CCB and Flamingo Pink, which both had MS/MS success rates in excess of 90% (CCB had positive identification for 35 out of 37 proteins subjected to MS/MS and Flamingo Pink had positive identification for 37 out of 39 proteins subjected to MS/MS). The MS-compatibility of CCB is well documented (Winkler *et al.*, 2007, Lauber *et al.*, 2001), but literature evidence for the MS-compatibility of Flamingo Pink is still lacking. However, for the Plasmodial proteins investigated here, Flamingo Pink was superior to the other standard stains regarding its ability to provide excellent MS/MS identification rates (95% success). This suggests that Flamingo Pink may the preferable stain as far as Plasmodial proteomics are concerned but this may also be generally true for proteome analyses due to its superior detection and identification of proteins after 2-DE.

2-DE based analyses of the Plasmodial proteome is hampered by contaminating hemoglobin derived products (HDP) (Nirmalan *et al.*, 2007), possibly as a result of the thiourea/sonication steps during the extraction of Plasmodial proteins, and the resultant destabilization of hemozoin. Typically, these HDPs are observed as an intense smear focused around pI 7-10 with varying molecular weights. The less harsh sonication steps used in this study combined with extensive wash steps (to remove hemoglobin) and 5-fold less saponin, resulted in discrete spots identified in the 2-DE based Plasmodial proteome described here. Very little background and smearing were observed here compared to other Plasmodial proteome studies (Nirmalan *et al.*, 2004a, Makanga *et al.*, 2005, Panpumthong & Vattanaviboon, 2006, Aly *et al.*, 2007) enabling the identification of several proteins in the pI 7.5-9 and 14 kDa range (Figure 2.4, e.g. LDH, G3PDH, Adenylate kinase). Moreover, the protocol used here makes it unnecessary to use additional fractionation steps to remove contaminating high pI fractions (Nirmalan *et al.*, 2007) or two-step extraction procedures (Panpumthong & Vattanaviboon, 2006). Furthermore, the use of the 2-D Quant kit provided the only means of protein concentration determination for Plasmodial proteins in the lysis buffer. Finally, Flamingo Pink proved to be superior with regard to sensitivity as far as detection of spots on 2-DE is concerned and provided excellent MS/MS compatibility for Plasmodial proteins.

2.4.2 Application of 2-DE optimised method on the Plasmodial ring and trophozoite stages

The successful establishment of an optimised 2-DE method allowed the comprehensive analyses of the Plasmodial proteome during its IDC. Due to the just-in-time nature of transcript production per life cycle stage in the parasite, and little delay between transcript and protein production, the majority of this parasite's proteins are relatively life cycle specific (Le Roch *et al.*, 2004). Proteins are therefore expressed over 0.75 to 1.5 times of a life cycle (Bozdech *et al.*, 2003). Highly synchronized parasites were used where proteins were isolated from either >98% pure ring stage or conversely trophozoite stage proteins. For the ring-stage parasite proteome, an average of 328 spots were detected on 2-DE with Flamingo Pink staining, and of these spots, 73 protein spots were identified by MS/MS. An average of 272 spots were detected on 2-DE with Flamingo Pink staining for the trophozoite proteome, of which 52 protein spots were positively identified by MS/MS, resulting in a total of 125 protein spots identified (out of 140 analysed) in the late ring and trophozoite proteomes. These results confirmed the high MS success rate (90%) that was achieved by applying the optimised methodology to the analyses of the Plasmodial proteome. Of the 73 proteins spots identified in the ring stage proteome, 57 proteins spots were from Plasmodial origin, and consisted of 41 unique Plasmodial protein groups, where some groups contained multiple

isoforms of the same protein. The trophozoite proteome consists of 52 protein spots identified by MS of which 49 protein spots were from Plasmodial origin. Therefore, protein isoforms represented ~28% of the total number of Plasmodial protein spots identified. From this data, it is clear that protein isoforms are prominent within both the ring and trophozoite stages and may play an important role in Plasmodial protein regulation. Similarly, this has also been demonstrated on 2-DE proteome maps for other protozoan parasites that also highlighted the importance of isoform detection and PTM's that regulate protein function (De Jesus *et al.*, 2007, Brobey & Soong, 2007, Jones *et al.*, 2006). The significance of isoforms is further exemplified in a 2-DE proteomic study of *T. brucei* where the absence of a single protein isoform was associated with drug resistance (Foucher *et al.*, 2006).

Comparison of the positively identified proteins groups from the ring (41 Plasmodial proteins) and trophozoite (35 Plasmodial proteins) stage proteomes to those of the schizont stage proteome (24 Plasmodial proteins) (Foth *et al.*, 2008) revealed only 9 proteins (~9%) which were shared between all three stages. These include proteins involved in a variety of biological processes such as glycolysis, protein folding, oxidative stress and the cytoskeleton. Nineteen (19) proteins are shared between the ring and trophozoite stage whilst only 11 proteins were shared between the trophozoite and schizont. However, 14 proteins are shared between the ring and schizont stage parasites suggesting differentiation of the schizont stage proteins in preparation for the next round of invasion by the merozoites and the formation of the subsequent ring stage parasites. The remaining 39% of the proteins (39 proteins, 31 proteins from ring and trophozoite stage and 8 from schizont stage) were not shared between the different life stages of the parasite, consistent with stage-specific production of proteins (and their transcripts) due to tightly controlled mechanisms within the parasite (Bozdech *et al.*, 2003).

Comparison of the protein levels from the ring and trophozoite proteomes to the IDC transcript profile demonstrated distinct similarities between transcript production profiles (obtained from PlasmoDB 6.0 www.plasmodb.org) and their corresponding protein levels as determined in our study. Proteins that were up-regulated from rings to trophozoites mostly exhibited a corresponding increase in transcript level when compared to IDC data, with only a few exceptions illustrated, that could indicate possible differential regulation of these proteins at a post-transcriptional/translational level. Mostly the results emphasised the general observation of correspondences between transcript and protein levels in *P. falciparum* (Le Roch *et al.*, 2004). Several isoforms were also detected that displayed differential regulation from the ring to trophozoite stages. These examples, demonstrate

the complexity of post-transcriptional and post-translational regulation in the *P. falciparum* proteome.

Post-translational modification of proteins in *P. falciparum* has also been observed in the schizont stage proteome (Foth *et al.*, 2008) similar to what has been detected within this study. Post-translational modifications of Plasmodial proteins include at least phosphorylation (Pal-Bhowmick *et al.*, 2007, Wu *et al.*, 2009), glycosylation (Davidson *et al.*, 1999, Gowda & Davidson, 1999, Yang *et al.*, 1999, Davidson & Gowda, 2001), acetylation (Miao *et al.*, 2006) and sulfonation (Medzihradszky *et al.*, 2004). The lateral shift of the eIF4A-like helicase isoforms in this study suggests phosphorylation or sulfonation as potential modifications (Kinoshita *et al.*, 2009, Thingholm *et al.*, 2009). However, only 2 isoforms of this protein were observed in the trophozoite stage compared to five in the schizont stage, indicating additional regulatory mechanisms e.g. increased phosphorylation in later stages of the parasite (Wu *et al.*, 2009) consistent with the proposed involvement of this protein in controlling developmentally regulated protein expression. Enolase seems to undergo post-translational modifications to produce 5 isoforms in *P. yoelii*, 7 isoforms in the *P. falciparum* schizont stages (Foth *et al.*, 2008, Pal-Bhowmick *et al.*, 2007) and 4 isoforms as described here. However, enolase phosphorylation was not reported in the *P. falciparum* phospho-proteome (Wu *et al.*, 2009). Some of these enolase-isoforms have also been detected in nuclei and membranes in *P. yoelii* and therefore suggests moonlighting functions including host cell invasion, stage-specific gene expression (*Toxoplasma*), stress responses and molecular chaperone functions (Pal-Bhowmick *et al.*, 2007). The biological significance of these isoforms is not yet fully understood, but it clearly emphasises the need for further in-depth investigations of post-transcriptional and post-translational modifications to further our understanding of the biological regulatory mechanisms within the Plasmodial parasite.

This is the first Plasmodial proteome study in which the 2-DE proteomic process was optimised in detail, from sample preparation through to spot identification with MS/MS. This resulted in a more detailed description of the Plasmodial proteome due to the removal of some contaminating hemoglobin without additional fractionation steps or extraction procedures. The fluorescent stain, Flamingo Pink, proved superior to the other stains tested and resulted in the detection of 79% of the predicted trophozoite proteome after 2-DE and achieved exceptional protein identification by MS. The reproducibility of the methods described here makes it highly expedient for the analysis of differentially expressed Plasmodial proteins. The application of the optimised 2-DE method allowed the characterisation of 2-DE proteomes of the ring and trophozoite stages of *P. falciparum*, which showed that some proteins are differentially regulated between these life cycle stages and included

the identification of a significant number of protein isoforms. These results emphasise the importance of post-translational modifications as regulatory mechanisms within this parasite. Application of this methodology will be demonstrated in Chapter 3 where the proteome of AdoMetDC inhibited parasites will be investigated.

Chapter 3

Proteome consequences of *P. falciparum* AdoMetDC inhibition with MDL73811

3.1 Introduction

The proteome is more complex than the genome, since a single gene can give rise to several protein isoforms, and therefore proteomics tries to directly determine the level of gene products present in a cell, usually in the form of proteins (Ong & Mann, 2005). Biological processes are mainly controlled by proteins and their interacting partners which will determine the protein function. Many factors apart from mRNA abundance determine the protein levels and include PTM's and mRNA decay mechanisms (Ong & Mann, 2005), therefore increasing the complexity of the proteome. Various protein isoforms can be created all with different functions within the cell. PTM's are the chemical reactions by which a newly synthesised polypeptide is converted into a functional protein either by addition of a chemical group or by proteolytic cleavage (Canas *et al.*, 2006). It is considered that the goals of protein expression profiling is to increase identification and quantification of components that are unique to a particular life stage or of a particular diseased state (Johnson *et al.*, 2004). This property therefore makes proteomics ideal to study the life stages of the Plasmodial parasites as well as the response of the parasite to a specific perturbation.

3.1.1 Plasmodial perturbation studies investigated by proteomics

The first Plasmodial proteomic study was a large scale high accuracy mass spectrometric analyses of various Plasmodial life stages (Lasonder *et al.*, 2002). A total of 1289 proteins were identified of which 714 were related to the asexual blood stages of mainly trophozoites and schizonts. A further 931 proteins were identified that were related to gametocytes and 645 proteins related to gametes. Of the 1289 proteins identified between all the life stages, it was determined that a total of 350 proteins were shared between all 3 stages investigated (Lasonder *et al.*, 2002). Another large scale proteome investigation was done using multidimensional protein identification technology (MudPIT) (Florens *et al.*, 2002). A total of 2415 parasite proteins were identified that related to the trophozoite, merozoite, sporozoite and gametocyte proteome of *P. falciparum* strain 3D7. Of these, only 152 (6%) proteins were shared between all 4 stages, indicative of stage-specific protein production (Florens et al., 2002).

The first 2-DE proteomic study established a 2-DE protocol for quantitative protein determination by the incorporation of heavy and light isoleucine into the media and therefore into the proteins under investigation (Nirmalan *et al.*, 2004a). The isoleucine labelled proteins can then be identified and quantified by mass spectrometry (MS). The protein abundance of selected proteins under PYR pressure was also investigated (Nirmalan *et al.*, 2004a). Two-dimensional gel electrophoresis has subsequently been used to determine the differences between 4 *P. falciparum* laboratory strains using metabolic labelling (Wu & Craig, 2006). Possible differences in cyto-adherence between the strains were determined and can be exploited for possible future drug development (Wu & Craig, 2006). The effect of the active ingredients in CoArtem (artemether and lumefantrine) was also investigated by 2-DE (Makanga *et al.*, 2005). Drug-specific effects were determined for both lumefantrine and artemether, which was associated with an increased protein abundance of specific proteins under drug pressure from one compound but the opposite effect with the other compound (Makanga et al., 2005). Parasites challenged with an endoperoxide-containing compound was investigated by 2-DE and revealed the increased protein abundance of 12 protein spots and decreased protein abundance of 14 protein spots of which only 15 protein spots were from Plasmodial origin (Aly *et al.*, 2007).

The mode-of-action of CQ was investigated by the use of 2-DE (Radfar *et al.*, 2008). The oxidised protein status of proteins was determined since it was hypothesised that CQ produces oxidative stress within the parasite. A total of 79 protein spots were identified which represented 41 unique proteins (Radfar et al., 2008). The mode-of-action of CQ was also investigated on CQ-resistant and CQ-sensitive strains using surface enhanced laser desorption ionisation-time of flight (SELDI-TOF) MS analysis (Koncarevic *et al.*, 2007). Hierarchical clustering of the data revealed clear patterns associated with CQ-sensitive and CQ-resistant strains, therefore revealing vital information on the mode of resistance to chloroquine. Further analysis revealed 10 possible CQ-resistance markers (Koncarevic *et al.*, 2007). In another CQ based study, the effect of CQ and artemisinin on Plasmodial parasites were determined using isoleucine-based SILAC in combination with MudPIT (Prieto *et al.*, 2008). The proteome of CQ treated parasites revealed oxidative proteins while artemisinin did reveal changes in the ATP vacuolar synthase subunits. Interestingly, the multiple drug resistant protein *(Pfmdr1)* was up-regulated in both CQ and artemisinin treatment reiterating its involvement in parasite resistance (Prieto *et al.*, 2008). Forty-one proteins were up-regulated, while 14 proteins were down-regulated with CQ treatment and 38 proteins were up-regulated and 8 were down-regulated with artemisinin treatment.

3.1.2 Perturbation of polyamine metabolism on the proteome

Co-inhibition of AdoMetDC/ODC in *P. falciparum* resulted in the identification of 6 differentially affected proteins (van Brummelen *et al.*, 2009). Of these, S-adenosylmethionine synthase (AdoMet synthase) had decreased protein abundance, while the protein abundance of ornithine aminotransferase (OAT) and pyridoxal-5'-phosphate (PLP) synthase increased. These polyamine specific proteins reveal some compensatory mechanisms. The regulation of ornithine may be a compensatory effect in order to homeostatically control the levels of ornithine that may be toxic to the parasite in high levels, while the decreased protein abundance of AdoMet synthase may be an attempt to maintain AdoMet levels within the parasite (van Brummelen et al., 2009). This study was followed by the determination of the proteome of cyclohexylamine inhibited spermidine synthase (Becker *et al.*, 2010). This investigation revealed the differential regulation of 38 spots over 3 time points of which 21 protein spots could be identified by MS. Four of the identified proteins were related to polyamine metabolism and included OAT (PFF0435w), AdoMet synthase (PFI1090w), purine nucleoside phosphorylase (PNP)(PFE0660c) and adenosine deaminase (PF10_0289), all of which were down-regulated (Becker et al., 2010).

This chapter investigates the proteome of *P. falciparum* AdoMetDC inhibited with MDL73811 with the 2-DE approach that was established in Chapter 2. The proteome was first investigated by SDS-PAGE in which 29 unique Plasmodial protein groups were identified by LC-MS/MS. This was followed by the determination of the proteome of MDL73811 inhibited parasites by 2-DE in which 91 protein spots were identified which accounts for 46 unique Plasmodial protein groups that were identified at two time points, and included the differential regulation of several polyamine-related proteins.

3.2 Methods

3.2.1 Malaria SYBR Green I-based fluorescence (MSF) assay for IC_{50} determination

The SYBR green assay was developed to be easy to use, cheap, and have robust performance and speed (Smilkstein *et al.*, 2004). The assay is based on the principle that the dye binds to DNA and since erythrocytes do not contain DNA or RNA only the parasite DNA will be stained (Bennett *et al.*, 2004). The SYBR Green dye has a very strong affinity for DNA and once bound to the DNA will fluoresce (Bennett et al., 2004, Smilkstein et al., 2004). Parasite cultures were centrifuged at 3000×*g* for 5 min to obtain a pellet that will be used for experimental procedures. First, the parasitemia was determined by counting parasites on Giemsa stained thin smears in at least 10 different microscopic fields containing about 100 erythrocytes each (10×100). The cultures were then diluted to 1% parasitemia and 2% hematocrit in culture media. A sterile 96-well plate was used for the assays to follow. The first column of the plate was filled with only culture media (300 µl) and not used as part of the IC_{50} determination due to the possibility of edge effects. The second column contained 0.5 µM CQ as a negative control (300 µl), and represented total inhibition of parasite and hence no parasite growth. This was followed by the positive control that contained parasites in drug-free media (300 µl). The next 8 columns contained a serial dilution of the drug starting at the highest concentration of 16 µM MDL73811 (in PBS) to the lowest concentration of 0.125 µM MDL73811. The plate was then placed into a gas chamber and gassed for 2 min, before being placed in a 37ºC incubator for 96 h. On the day of the assay, SYBR green buffer was prepared by adding 2 µl of SYBR green (Invitrogen) in 10 ml lysis buffer (20 mM Tris, pH 7.5; 5 mM EDTA; 0.008 % (w/v) saponin; 0.08 % (v/v) Triton X-100) and kept in the dark. One hundred microlitres of the SYBR green lysis buffer was pipetted into each of the wells of a 96-well black fluorescence plate (Nunc) followed by 100 µl of resuspended, treated parasites. The plate was then incubated for 1 h in the dark at room temperature before the fluorescence was measured using the Fluoroskan Acent FL Fluorimeter (Thermo LabSystems) at excitation of 485 nm and emission at 538 nm (integration time of 1000 ms). Data were analysed using SigmaPlot 9.0 to determine the IC_{50} of MDL73811 against *Pf*3D7.

3.2.2 Morphology study

To determine the morphological time of parasite arrest induced by the drug MDL73811, a morphological study was done using Giemsa stained blood smears as described earlier (Section 2.2.3). MDL73811 was dissolved in PBS, and filtered using a 0.22 µm Ministart syringe filter.

Aliquots were stored at -20°C until use. Parasites were treated with 10 µM MDL73811 (10×IC_{50}) just before or during invasion. A similar amount of PBS was added to the control parasite cultures to eliminate any possible effect of PBS on the parasites. A blood smear was made every 2-5 h to morphologically follow the parasite during the intraerythrocytic cycle and was continued for a total of 60 h. Slides were analysed using a Nikon light microscope at 1000× magnification under oil immersion. At least 10 fields of 100 erythrocytes each were examined for the determination of parasite progression.

3.2.3 Culturing for the proteomic time study

*Pf*3D7 parasites were maintained *in vitro* in human O^+ erythrocytes in culture media as described in chapter 2 section 2.2.3. Parasites were monitored daily through light microscopy of Giemsa stained thin blood smears as described in section 2.2.3. Before treatment could commence the parasites were always synchronised for 3 consecutive cycles (6 times in total, always 8 h apart once in the morning and later in the afternoon) as described in section 2.2.4. A starting parasite culture (in the schizont stage) at 2% parasitemia, 5% hematocrit was treated with 10 µM MDL73811 at invasion after which the parasitemia increased to 10% in both the treated and untreated samples in the ring stage. A small scale morphology study was always conducted at the same time, and used as a positive control to ensure parasite arrest at ~26 h as the drug takes effect in the treated parasite culture. Sixty milliliters of *Pf*3D7 parasites at 10% parasitemia and 5% hematocrit were used per gel and harvested at 16 HPI (time point 1, t_1) and 20 HPI (t_2), and contained 4 biological replicates for each time point. 10% (w/v) Saponin was added to the infected erythrocytes to a final concentration of 0.01% (v/v), and incubated on ice for 5 min to lyse the erythrocytes and release the parasites. Parasites were collected by centrifugation at 2500×*g* for 15 min, and washed at least 4 times in 1 ml PBS at 16 000×*g* for 1 min until the supernatant was clear (Smit *et al.*, 2010). The parasite pellet was stored at –80°C until further use, but never stored for longer than 30 days.

3.2.4 Protein preparation

The 4 parasite pellets were pooled and then suspended in 500 µl lysis buffer as described by Nirmalan *et al.* (8 M urea, 2 M thiourea, 2% CHAPS, 0.5% (w/v) fresh DTT and 0.7% (v/v) ampholytes) (Nirmalan *et al.*, 2004a). Samples were pulsed-sonicated as described in section 2.2.6. Sonication was followed by centrifugation at 16 000×*g* for 60 min at 4°C, after which the protein-containing supernatant was used in subsequent 1-D SDS-PAGE and 2-DE and the remaining pellet was also used for 1-D SDS-PAGE (see following sections).

3.2.5 Protein quantification by 2-D Quant kit

The commercially available 2-D Quant Kit (GE Healthcare) was used according to the manufactures instructions with a few modifications as described in Chapter 2 section 2.2.7.4.

3.2.6 SDS-PAGE gels

Sixty micrograms of the supernatant containing proteins were dissolved in reducing buffer (0.06 M Tris-HCl, 2% (w/v) SDS, 0.1% (v/v) glycerol, 0.05% (v/v) β-mercaptoethanol and 0.025% (v/v) bromophenol blue, pH 6.8), boiled for 5 min before loading equal amounts of protein onto a 12.5% SDS-PAGE gel (Hoefer SE600, 16×18 cm). Similarly the pellet proteins were also dissolved in reducing buffer but were boiled for 10 min and vortexed vigorously to dissolve the pellet proteins before being loaded onto the 12.5% SDS-PAGE gels (Hoefer SE600, 16×18 cm). The gels were allowed to run until the bromophenol blue front reached the bottom of the gel. The gels were then removed from the glass plates and immersed in Colloidal Coomassie solution and left shaking overnight. The gels were rinsed with 25% methanol, 10% acetic acid before destaining with 25% methanol, until the background was clear (Neuhoff *et al.*, 1988). The gels were scanned on a Versadoc 3000 and analysed using the Quantity One 4.4.1.

3.2.7 1-DE SDS-PAGE spot identification by liquid chromatography electrospray ionization tandem mass spectrometry (LC-ESI-MS/MS)

The bands of interest were cut from each of the 4 SDS-PAGE gels, dried and stored at -20°C. Each gel piece was cut into smaller cubes and washed twice with water followed by 50% (v/v) acetonitrile for 10 min each. The acetonitrile was replaced with 50 mM NH_4HCO_3 and incubated for 10 min, repeated 3 times until the gel pieces was clear and free from CCB. The gel pieces were incubated in 100% acetonitrile until they turned white. This was followed by another NH_4HCO_3, acetonitrile wash step, after which the gel pieces were dried *in vacuo*. Gel pieces were digested with 10 ng/µl trypsin at 37°C overnight. Resulting peptides were extracted twice with 70% acetonitrile for 30 min, and then dried and stored at -20°C. Trypsin digested samples extracted from gel-plugs were re-suspended in 100 µl 0.5% acetonitrile, 0.5% formic acid and centrifuged at 16 000×*g*, 4°C for 15 min. Samples were analysed on an Agilent 1100 HPLC system equipped with capillary and nano-LC pumps coupled to a QSTAR ELITE mass spectrometer. Sample (1-2 µg) were de-salted on a Symmetry C18 trap column (0.18×23.5 mm) for 20 min at 20 µl/min using 0.5% acetonitrile/0.5% formic acid. Peptides were separated on a NanoEase XBridge C18 column (0.1×50 mm) connected to the trap column via 6-port switching valve. Peptide elution was achieved

using a flow-rate of 800 nl/min with a gradient: 0-10% B in 1 min, 10-30% B in 30 min, 30-50% B in 5 min, 50-100% B in 1 min; 100% B for 10 min (A: 2% acetonitrile, 0.5% formic acid; B: 98% acetonitrile, 0.5% formic acid). Nano-spray was achieved using a MicroIonSpray head assembled with a New Objective, PicoTip emitter (o.d. 360 µm; i.d. 75 µm; tip i.d. 15 µm). An electrospray voltage of 2.5-3.0 kV was applied to the emitter. The QSTAR ELITE mass spectrometer was operated in Information Dependant Acquisition (IDA) using an Exit Factor of 2.0 and Maximum Accumulation Time of 2.5 s. MS scans were acquired from m/z 400 to m/z 1600 and the 3 most intense ions were automatically fragmented in Q2 collision cells using Nitrogen as the collision gas. Collision energies were chosen automatically as function of m/z and charge. Protein identification was performed using the Paraghon™ algorithm *Thorough* search in Protein Pilot. An identification confidence of 95% was selected during searches with a False Discovery Rate (FDR) determined for the experiment.

3.2.8 Two-dimensional gel electrophoresis (2-DE) and staining

Four hundred micrograms of protein in rehydration buffer was applied to an 18 cm IPG, pH 3-10 L strip as described in section 2.2.9. First dimensional IEF commenced with a 10 h active rehydration step and followed an alternating gradient and step and hold protocol that was always allowed to proceed to a total of 35 000 Volt-hours, that completed within 17 h. The complete IEF focusing steps is given in Table 3.1.

Table 3.1: The IEF focusing steps used for 18cm IPG, pH 3-10 L strips.

Step	Voltage limit (V)	Time or Volt hour (h) or (V-h)	Gradient
1	30 V	10:00 h	Step and hold
2	200 V	0:10 h	Gradient
3	200 V	0:20 h	Step and hold
4	500 V	0:20 h	Gradient
5	500 V	0:20 h	Step and hold
6	2 000 V	0:20 h	Gradient
7	2 000 V	0:45 h	Step and hold
8	8 000 V	1:40 h	Gradient
9	8 000 V	24 000 V-h	Step and hold
Total		35 000 V-h	

IPG strips were equilibrated and placed on top of the 10% SDS-PAGE gel and covered with 1% agarose as described in section 2.2.9. Separation was performed at 80 V at 20°C until the bromophenol blue front reached the bottom of the gel. The gels were then fixed overnight in 40% (v/v) ethanol, 10% (v/v) acetic acid. After an overnight fixing step the gels were subsequently stained in 200 ml Flamingo Pink working solution and incubated with gentle agitation in the dark

for 24 h, to increase the sensitivity of the stain as described in section 2.2.10.1. All gels were stored in Flamingo Pink at 4°C until use for MS.

3.2.9 Image Analysis of 2-DE gels by PD Quest

PD Quest 7.1.1 was used to identify the number of spots on each of the 16 gels (4 untreated and 4 treated per time point) that were done for the 2 time points as was done in section 2.2.11. First, all images were cropped to the same dimensions (1.59 Mb, 933 × 893 pixels, 303.7 × 290.7 mm). The images were then filtered using the Filter Wizard, with the following settings that were manually incorporated by the user: the salt setting (light spots on dark background) was chosen since the fluorescent stain will show the spots as bright spots with a black background, outlier (chosen according to gaussian curve calculated by software) and filter size 3 × 3 was set to filter the image. The gel with the most spots and least streaks were then manually selected as the master image. Automated spot detection was performed by the Spot Detection Wizard and manually selecting a small spot, faint spot and large spot as the minimum and maximum spot selection criteria. The Spot Detection Wizard was also set to eliminate horizontal- and vertical streaking, subtract the background according to the floating ball method (automatically determined by the software), perform smoothing using a 3 × 3 filter according to the power mean filter type (suggested by the software). Additional settings for both t_1 and t_2 were manually selected for spot detection and are given in Table 3.2. After automatic matching of the 8 gels, every spot were manually verified to determine correctness of matching. Finally, reports were created to display information on the number of spots regulated for both time points.

Table 3.2: Spot selection criteria for the 2 time points

Settings	t_1	t_2
Scan area (mm)	366.0 × 336.7	308.6 × 293.3
Pixel size (µm)	390.6 × 390.6	325.5 × 325.5
Sensitivity	5.31	4.35
Size scale	5	5
Min peak	808	4712
Vertical radius	55	43
Horizontal radius	35	39
Large spot size	34 × 54	34 × 54
Floating ball radius	35	39
Smoothing	Power mean (3 × 3)	Power mean (3 × 3)

3.2.10 2-DE spot identification by tandem mass spectrometry

The spots of interest were cut from each of the gels and pooled, dried and stored at -20°C. The gel pieces were then prepared for MALDI-TOF MS/MS as described in section 2.2.12. The peak lists for each gel piece was then submitted to MASCOT as described in section 2.2.13.

3.2.11 Western blots

The protein containing lysates from the treated and untreated samples were quantitatively loaded onto a 12.5% SDS-PAGE gel with an initial voltage of 30 V for 30 min followed by 100 V until the bromophenol blue front had reached the bottom of the gel and electrophoresis was stopped. The gel was removed from the glass plates and then equilibrated for 5 min in 10 mM (3-(cyclohexylamino)-1-propanesulfonic acid (CAPS), pH 9.0. The membrane was cut to size and activated for 15 s in methanol and then placed in 10 mM CAPS to equilibrate.

Filter paper was equilibrated in 10 mM CAPS and then placed on a transfer cell. This was followed by the PVDF membrane and the gel placed on top of the membrane followed by another 5 layers of equilibrated filter paper. The blot proceeded for 45 min at 10 V. After blotting, the membrane was blocked overnight in blocking buffer (3% (w/v) BSA, 0.5% (v/v) Tween in PBS) at 4°C.

The gel was stained overnight in colloidal coomassie blue as described in chapter 2 section 2.2.10.4. This was done to ensure that complete transfer of all the proteins did occur. The next morning, the blocking buffer was removed and replaced with the primary antibody (1:4000) in wash buffer (1% (w/v) BSA, 0.5% (v/v) Tween in PBS) for 1 h at 37°C. This was followed by washing of the membrane with wash buffer for 10 min at 37°C, repeated 6 times. The membrane was then incubated with the secondary antibody (1:10 000) in wash buffer for 1 h at 37°C. Once again, this was followed by washing of the membrane and repeated 6 times. Finally, the membrane was incubated for 5 min with equal volumes (4 ml each) of Luminol/Enhancer solution (Pierce) and stable peroxidase solution (Supersignal West Pico Chemiluminescent substrate, Pierce). This works on the principle that the horseradish peroxidase enzyme that is conjugated to the antibody generates a hydroxide ion that gives rise to the transition of luminal to 3'-aminophthalate with the concurrent emission of light. The excess reagent was drained and then the membrane was exposed to Hyperfilm ECL X-ray film (Pierce) for 30 s in the dark. The X-ray were developed for 1 min in Universal Paper developer (Illford), rinsed briefly in water and then fixed for 3 min with Rapid Paper Fixer (Illford). The film was again rinsed in water and left to dry before being scanned on the Versadoc-3000 using Quantity One 4.4.1 (Bio-Rad), with the following settings: Densitometry, X-

ray film, Clear white TRANS, 0.5× Gain and 1×1 Bin. The density (ODu/mm^2) of each spot on the X-ray film was calculated using Quantity One and then the ratio of UT/T were calculated. The primary antibody for M1-family aminopeptidase (M1-AP) was a kind gift from Dr Isabelle Florent from Museum National d'Histoire Naturelle, Paris, France. The primary antibody for phosphoethanolamine N-methyltransferase (PEMT) was a kind gift from Prof Choukri Ben Mamoun from the Department of Genetics and Developmental Biology, University of Connecticut, USA.

3.3 Results

3.3.1 IC_{50} determination of MDL73811

Before a full scale proteomic investigation could be attempted, the IC_{50} of MDL73811 against the CQ sensitive *P. falciparum* parasite 3D7 strain (*Pf*3D7) had to be determined and was done using the Malaria SYBR Green I-based fluorescence (MSF) assay. A *Pf*3D7 parasite culture at 1% parasitemia, 2% hematocrit was used for each of the assays and incubated for 96 h before SYBR Green could be added to determine the fluorescence and ultimately the IC_{50} for MDL73811. Figure 3.1 illustrates the sigmodial graph of the IC_{50} determination for *Pf*3D7 treated with MDL73811.

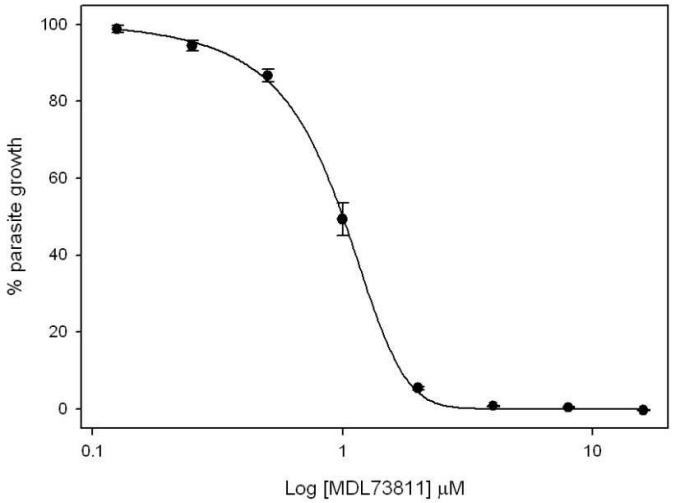

Figure 3.1: A concentration response curve for the IC_{50} determination of MDL73811.
Error bars are representative of the SEM, n = 4. R^2=0.99, IC_{50} = 0.96 µM ± 0.16 µM

An IC_{50} of 0.96 µM ± 0.16 µM were obtained for MDL73811 against the CQ sensitive *Pf*3D7 strain. Successful establishment of the IC_{50} of MDL73811 prompted the evaluation of the morphological impact of MDL73811 on the parasites. *Pf*3D7 parasites were treated with a concentration of 10 µM MDL73811 (~10×IC_{50}). This high concentration of MDL73811 against *Pf*AdoMetDC is used to ensure that parasites do not escape drug pressure, and were used for all experimental procedures to follow (Van Brummelen, 2009).

3.3.2 Morphological evaluation of *P. falciparum* 3D7 inhibited by MDL73811 over a complete life cycle

The entire Plasmodial life cycle was monitored morphologically over a 48 h period. *Pf*3D7 were treated just before invasion of erythrocytes. The media was changed every 12 h to minimise the negative influence of lactic acid on parasite growth. Morphological examination of the parasites

microscopically occurred at 2-3 hourly intervals (Figure 3.2 A and B). The complete morphological assessment of control parasites (untreated, UT) and 10 µM MDL73811-treated (T) parasites over a complete lifecycle of 48 h was followed (Figure 3.2). Both UT and T parasites remained morphologically similar from invasion (0 hours post-invasion, HPI) through the ring stage (0-18 HPI) and the early trophozoite stage (18-25 HPI) (Figure 3.2 A). This is further iterated by Figure 3.2 B which shows that the representative graphs of both UT and T parasites were identical during the ring and early trophozoite stages. Morphological arrest of MDL73811-treated parasites occurred between 25 and 30 HPI (Figure 3.2 A). According to the IDC transcriptome, the *Pf(adometdc/odc)* transcript is produced from 12 to 36 HPI with maximum expression at 24 HPI (Bozdech *et al.*, 2003). It is also within this period of maximum transcript expression of *Pf(adometdc/odc)* that the morphological arrest occurs. At 30 HPI the UT parasites differentiated into schizonts, while the T parasites clearly remained in the trophozoite stage without any further differentiation and remained in the trophozoite stage indefinitely (Figure 3.2 B). It is also visible that after 32 HPI the MDL73811-treated parasites became picnotic and remains picnotic over the rest of the life cycle and does not re-invade new erythrocytes (Figure 3.2 A). The MDL73811-treated parasites did not progress to a new life cycle and consequently did not form new ring stage parasites unlike the UT parasites that started a new life cycle after 48 h by releasing merozoites that invaded new erythrocytes that will ultimately form new ring stage parasites. This morphological assessment of the MDL73811-treated parasites furthered the notion that MDL73811 acts as a cytostatic drug even at concentrations of 10 µM MDL73811 (Van Brummelen, 2009).

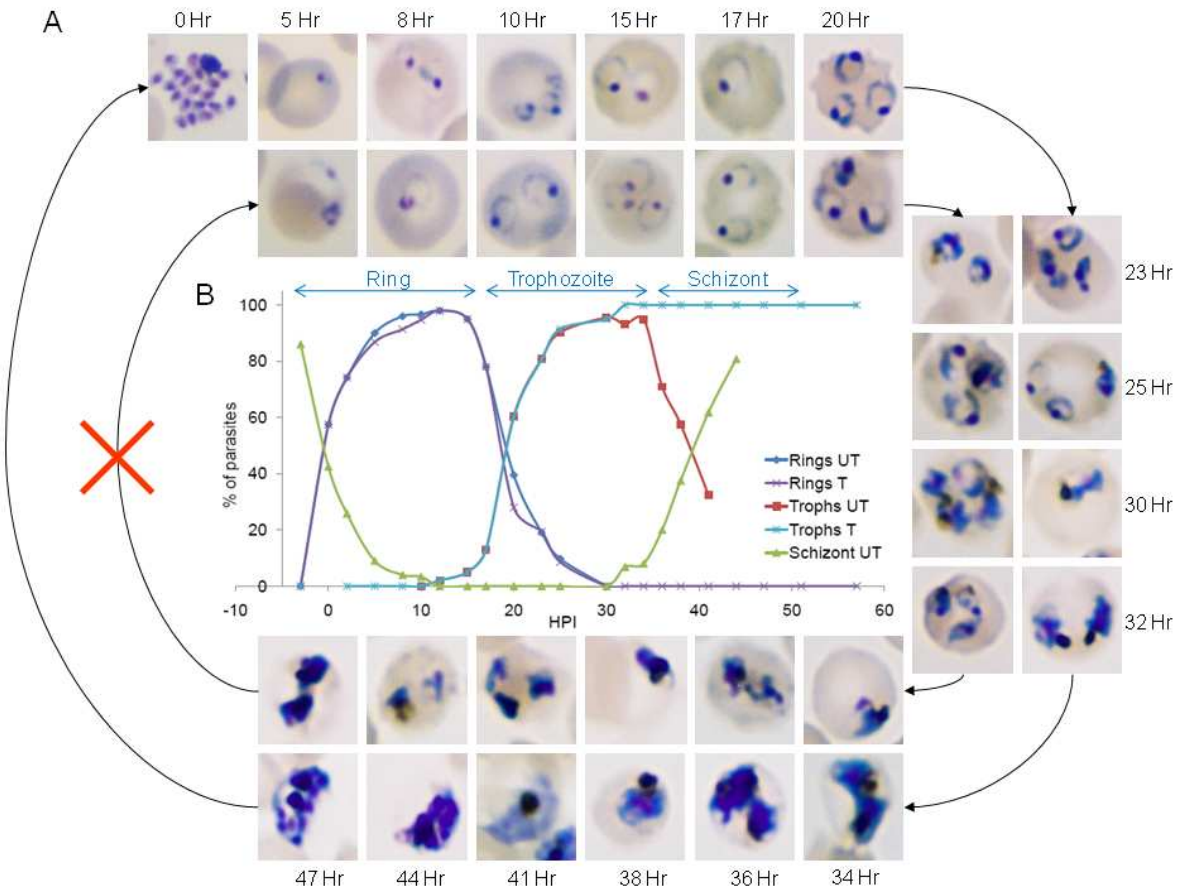

Figure 3.2: Morphology study of *Pf*3D7 parasites over a 48 hour life cycle.

(A)The outside of the circle illustrates the untreated parasites that will progress through schizogeny to develop into merozoites at approximately 46-52 hours and will ultimately invade new erythrocytes. The inside circle demonstrates the MDL73811-treated parasites, which will not develop into new merozoites, since these treated parasites are arrested during schizongeny from about 25 hours onwards. (B) A graphical illustration of the morphological arrest of MDL73811-treated and untreated *Pf*3D7 parasites. The light blue line is the trophozoite stage of the MDL73811-treated parasites that persist as trophozoites and does not develop into schizonts.

3.3.3 SDS-PAGE analysis of perturbed parasites and functional analysis of differentially regulated bands from 1-DE SDS-PAGE gels

Due to the fact that the transcript for *Pf*AdoMetDC/ODC is produced from 12 to 36 HPI with maximum transcript expression at 24 HPI (Bozdech *et al.*, 2003) and the morphological assessment that showed that morphological arrest of the MDL73811-treated parasites occurs between 25-30 HPI (Figure 3.2 A and B). Two time points (16 HPI (t_1) and 20 HPI (t_2)) were chosen that were before morphological arrest of the MDL73811-treated parasites and relating to the time at which the transcript for *Pf(adometdc/odc)* should already be expressed by the parasites and therefore the MDL73811 could take effect on *Pf*AdoMetDC. The perception was also that because these 2 time points were before a visible morphological arrest the 2 time points would be representative of drug

specific parasite response rather than life cycle differences. Therefore, the UT and T parasites were harvested at 16 HPI and 20 HPI for the proteomic study. The protein-containing supernatant and the insoluble protein pellet of both time points were run on SDS-PAGE gels to determine if differential protein expression did occur. Figure 3.3 is a representation of the 4 SDS-PAGE gels that each is representative of 1 biological replicate that were loaded in quadruplet. For both time points, 60 µg of the soluble protein-containing supernatant was loaded onto the SDS-PAGE gels. Due to the insoluble nature of the protein pellet the protein concentration could not be reliably determined and therefore 60 µl of each protein pellet were loaded onto the SDS-PAGE gels. All 4 gels were stained with Colloidal Coomassie Blue.

The SDS-PAGE gels were analysed using Quantity One 4.4.1 to detect possible differentially affected bands between the treated and untreated samples. Differentially affected bands were detected in both the soluble and insoluble fractions for the 2 time points, of which 17 bands were selected, and prepared for MS analysis (Figure 3.3, labelled numerically from 1-17). Since SDS-PAGE separation is limited to only molecular weight, it is extremely likely that one band may consist of various proteins of similar molecular weights. This is one of the essential reasons for separating the extracted peptides from each band of the SDS-PAGE gels with a reverse phase column before being identified by electrospray ionisation tandem mass spectrometry (ESI-MS/MS). The peptides and partial sequences were searched by Protein Pilot™ to identify the proteins present within each of the bands. The identified bands and their corresponding proteins are given in Table 3.3.

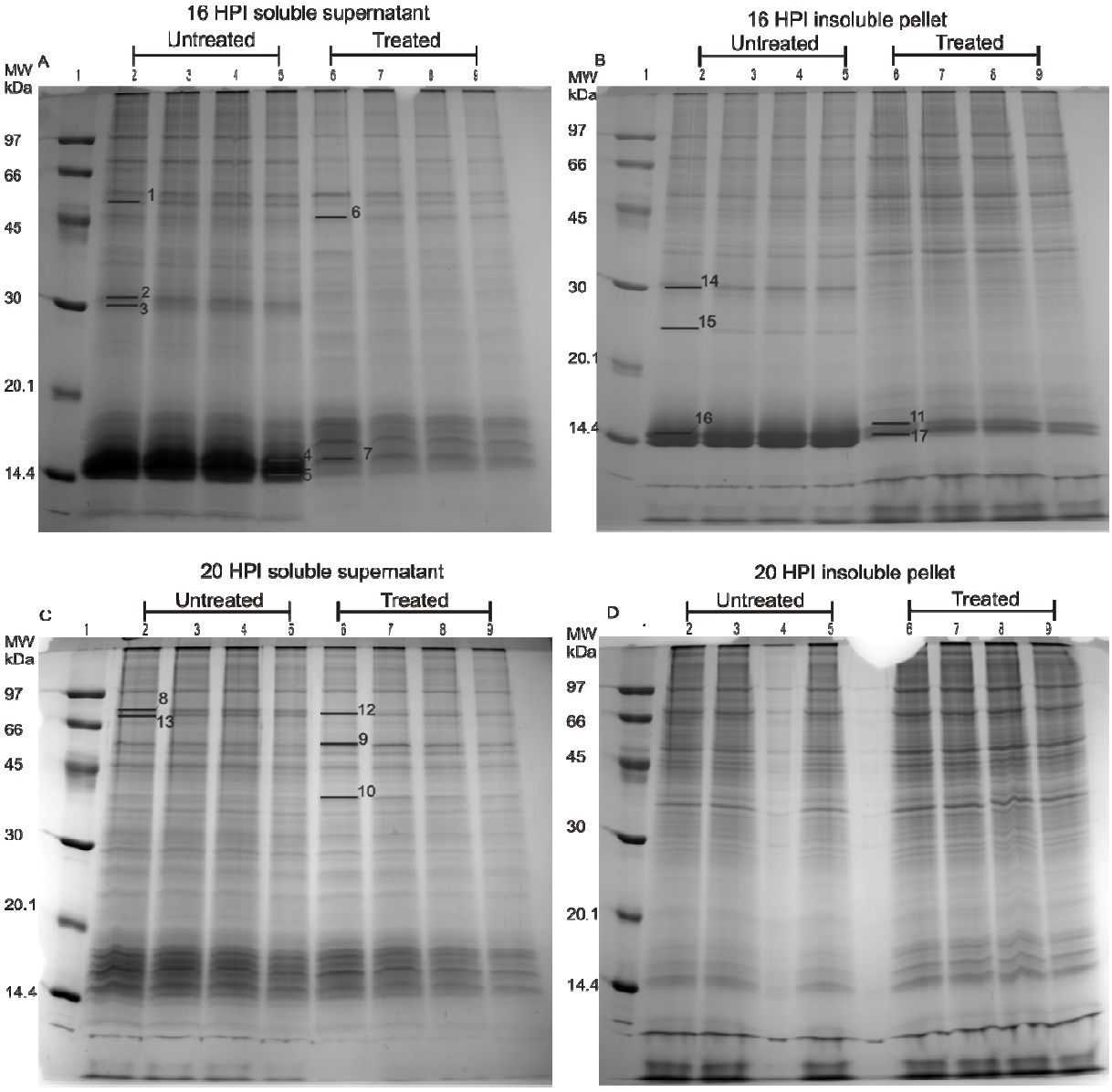

Figure 3.3: 1-DE SDS-PAGE gels for the soluble and insoluble protein fractions from the 2 time points investigated.

(A) 16HPI soluble supernatant, (B) 16 HPI insoluble pellet, (C) 20 HPI soluble supernatant, (D) 20 HPI insoluble pellet. Lanes are marked with numbers 1-9 on top of each gel. Lane 1 is always the molecular weight marker. Lanes 2-5 are the untreated samples and lanes 6-9 are the treated samples. Differentially affected bands that were used for MS analysis is marked on the gels with numbers 1-17.

Table 3.3: Differentially affected bands from AdoMetDC inhibited parasites identified from SDS-PAGE by LC-ESI-MS/MS

Band nr[a]	FC[b]	Accession nr[c]	PlasmoDB ID[d]	Name	MW	pI	Score[e]	%Cov[f]
				(A) Up-regulated bands				
6	1.4	Q8I431	PFE0350c	60S ribosomal subunit protein L4/L1, putative	46212	11.2	11.39	13.87
		Q8I4X0	PFL2215w	Actin I	41821	5.27	9.46	15.69
		Q8IJC6	PF10_0272	Ribosomal protein L3, putative	44222	10.89	5.64	9.59
9	2	Q8IJD0	PF10_0268	Merozoite capping protein 1	43936	10.45	11.68	15.27
		Q9TY94	PFB0445c	Helicase, putative pf	52224	5.84	11.68	2.41
10	3.5	Q8IDR9	PF13_0228	40S ribosomal subunit protein S6, putative	35385	11.19	4.63	8.50
				(B) Down-regulated bands				
1	-1.8	Q27727	PF10_0155	Enolase	48678	6.54	14.75	23.09
		Q8I0P6	PF13_0305	Elongation factor 1-alpha	48959	9.6	13.39	18.96
		Q8IL88	PF14_0359	Hypothetical protein	48470	7.2	1.69	
2	-18	P00915	—	Carbonic anhydrase 1 *(Homo sapiens)*	28870	6.59	14.96	36.78
		Q8IDQ9	MAL13P1.214	Phosphoethanolamine N-methyltransferase, putative	31043	5.28	3.5	5.26
		Q8IM10	PF14_0083	Ribosomal protein S8e, putative	25051	10.65	3.41	13.76
		Q8IIU8	PF11_0065	Ribosomal protein S4, putative	32355	10.55	2.33	3.55
		Q8I3T9	PFE0845c	60S ribosomal subunit protein L8, putative	28000	11.18	2.13	5.00
3	-6	P68871	—	Hemoglobin subunit beta *(Homo sapiens)*	15998	6.74	9.1	32.65
		P00915	—	Carbonic anhydrase 1 *(Homo sapiens)*	28870	6.59	5.71	13.03
4	-5	P68871	—	Hemoglobin subunit beta *(Homo sapiens)*	15998	6.74	0.02	84.83
		P02042	—	Hemoglobin delta chain *(Homo sapiens)*	16055	7.84	7.39	58.22
		Q7JSX6	PF11_0061	Histone H4, putative	11456	11.8	4.34	22.33
		Q8IIV1	PF11_0062	Histone H2B	13125	10.96	3.24	12.82
5	-3.4		—	Hemoglobin alpha chain *(Homo sapiens)*			0	82.14
		Q7JSX6	PF11_0061	Histone H4, putative	11456	11.8	6.16	33.01
		Q8ILN8	PF14_0205	Ribosomal protein S25, putative	15741	10.42	3.05	15.56
		Q8IIV1	PF11_0062	Histone H2B	13125	10.96	0	12.82
7	-5	P68871	—	Hemoglobin subunit beta *(Homo sapiens)*	15998	6.74	14.74	43.54
		Q7JSX6	PF11_0061	Histone H4, putative	11456	11.8	8.66	33.98
		Q8IIV1	PF11_0062	Histone H2B	13125	10.96	0	12.82
8	-1.3	P16452	—	Erythrocyte membrane band 4.2 protein *(Homo sapiens)*	77009	8.39	0	16.78
		Q8IB24	PF08_0054	Heat shock 70 kDa protein	73916	5.33	0	0.00
12	-1.3	Q8IB24	PF08_0054	Heat shock 70 kDa protein	73916	5.33	25.75	21.86

		Q8I2X4	PFI0875w	Heat shock protein	72388	4.93	7.73	6.13
13	-3.1	Q8IB24	PF08_0054	Heat shock 70 kDa protein	73916	5.33	20.58	13.44
		Q8I2X4	PFI0875w	Heat shock protein	72388	4.93	6.25	6.13
14	-3.9	P00915	—	Carbonic anhydrase 1 *(Homo sapiens)*	28870	6.59	19.7	44.44
		Q8IDQ9	MAL13P1.214	Phosphoethanolamine N-methyltransferase, putative	31043	5.28	6.76	18.05
		P00921	—	Carbonic anhydrase II *(Bos taurus)*	29114	6.41	3.58	10.77
		P00918	—	Carbonic anhydrase 2 *(Homo sapiens)*	29246	6.87	2.73	7.34
15	-3.4	P32119	—	Peroxiredoxin-2 *(Homo sapiens)*	21892	5.66	4.57	4.57
16	-4.4	P68871	—	Hemoglobin subunit beta *(Homo sapiens)*	15998	6.74	0.04	93.20
11	-4.4	P68871	—	Hemoglobin subunit beta *(Homo sapiens)*	15998	6.74	0	57.93
		Q7JSX6	PF11_0061	Histone H4, putative	11456	11.8	5.68	22.33
		Q8I467	PFE0165w	Actin depolymerizing factor, putative	13741	7.94	2.06	10.66
17	-0.9		—	CS185522 NID *(Homo sapiens)*			48.19	53.16
		Q7JSX6	PF11_0061	Histone H4, putative	11456	11.8	8.09	33.98
		Q8I5C5	PFL1420w	Macrophage migration inhibitory factor homolog, putative	12845	6.43	4.69	21.55

Proteins identified are sorted numerically according to the band number. [a]Band number corresponds to marked bands in Figure 3.5. [b]FC is the fold change for regulation of each differentially regulated band as determined by Quantity One 4.1.1 and is the intensity ratio for T/UT. All values given are significant ($p<0.05$).[c]Accession number is obtained from the SwissProt UniProt database. [d]PlasmoDB ID is obtained from the PlasmoDB 6.0 database. [e]Score is based on MS/MS searches done by the Protein Pilot™ software for LC-MS/MS. A score of more than 2.0 is considered significant ($p<0.05$). [f]Sequence coverage is given by Protein Pilot for detected peptide sequences.

Of the 17 bands that were cut for LC-ESI-MS/MS analysis, a total of 45 proteins were identified within these bands. This correlates to 29 unique proteins, of which 20 are unique Plasmodial proteins. Eleven of the unique Plasmodial proteins had a pI above 9.6 and would therefore normally not be detected on 2-DE due to the pI constraints associated with 2-DE. Of these 11 proteins, 7 proteins were ribosomal proteins that ranged in pI from 10-11.2, while the other 4 proteins included elongation factors and histone proteins that ranged in pI from 9.6 to 11.8 (Table 3.3). From the original 17 bands that were cut for MS-identification, 3 bands had an increased abundance and correlated to 6 proteins identified, while 13 bands had decreased abundance which correlated to 36 proteins identified. One band used for MS-identification showed no change in differential abundance between the treated and untreated samples and consisted of 3 identified proteins. It should be noted that although the bands are differentially regulated this is not necessarily true for all of the proteins that are identified for that particular band. This is because a band consists of more than 1 protein of which only 1 may be differentially regulated in abundance and the other proteins may be unchanged in abundance.

3.3.4 2-DE analysis of AdoMetDC inhibited parasites

The results obtained from SDS-PAGE analysis of both soluble and insoluble proteins fractions from AdoMetDC inhibited parasites confirmed the feasibility of the presence of differentially regulated proteins. This prompted the 2-DE analyses of the soluble proteins over 2 time points to enable a more comprehensive proteomic view of the overall protein regulation induced by the inhibition of AdoMetDC. For first dimensional IEF separation, each of the sixteen 18 cm IPG strips was loaded with 400 µg total protein each and run overnight before being placed on large format gels for second dimensional separation to achieve maximal spot separation. The gels were then stained with Flamingo Pink, scanned using the Versadoc 3000 scanner and finally analysed using PD Quest 7.1.1 to determine statistically significant differences between UT and T samples.

PD Quest program is able to distinguish between a protein-related spot and background dust speckles and automatically removes speckles from the dataset. This was also manually determined for all spots reported on each of the gels where speckles have very distinguishable sharp peaks, and protein-related spots have nice gaussian shapes and are therefore easily distinguished (Figure 3.4).

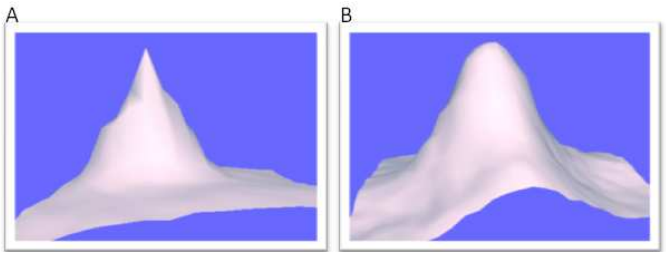

Figure 3.4: The difference between a real protein spot and a dust speckle.
A: speckle, B real protein spot.

Spots were detected by automated detection and matching by the software. All the spots detected and matched were manually verified to limit the possibility of false positive spot matching. A master image was created from the 8 gels (4 × UTt_1 and 4 × Tt_1 gels) present within the first time point (t_1) (Figure 3.5). Similarly a master image containing all the spot information for all 8 gels for the second time point (t_2) was also created (not shown).

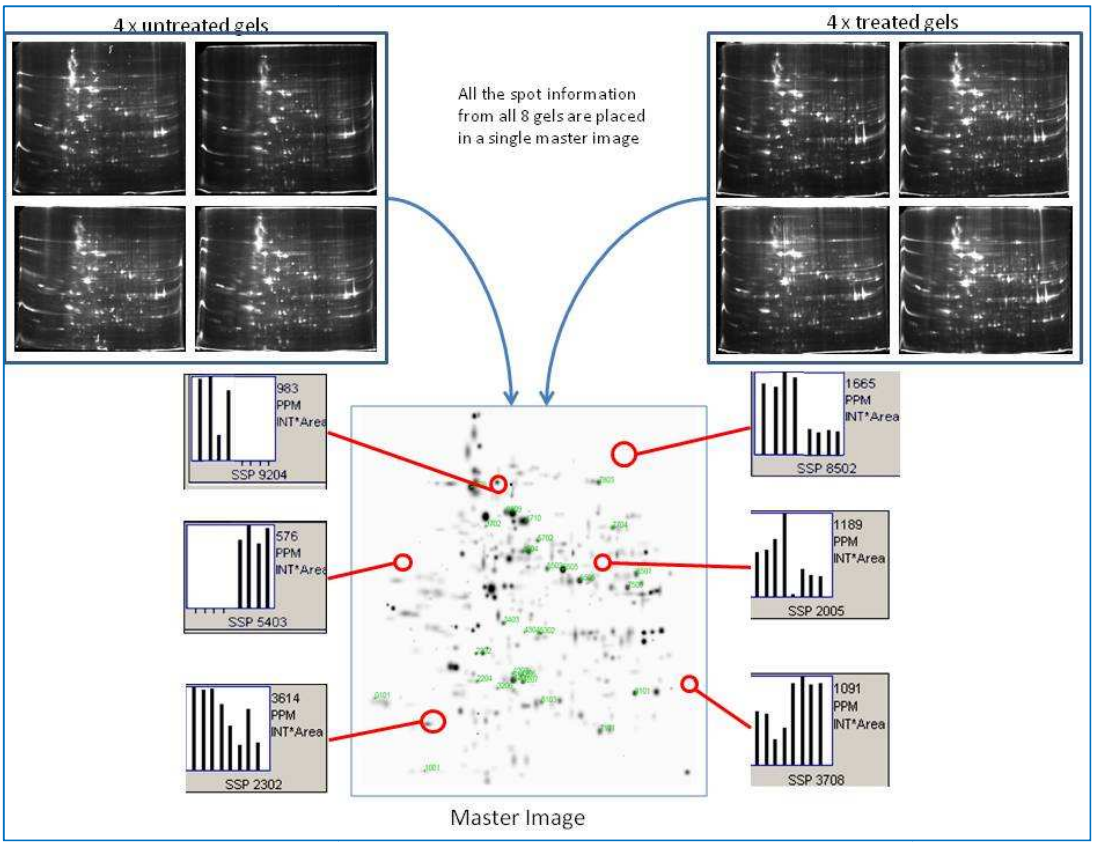

Figure 3.5: Creation of the master image used for detection of differentially affected proteins.
The spot information of the 4 UT gels and the 4 T gels are combined into a single master image that contains all the spot information on all 8 gels it consists of. The user can then select any spot on the master image and a graph will appear that will give information of the exact same spot in all of the 8 different gels that the master image consists of. Therefore for SSP9204 the master image contains information that the spot is only present in each of the 4 UT gels and completely absent in all of the 4 T gels. Each bar represents the normalised intensity for the specific spot from each of the 8 gels.

The master image contains all the spot information for both the untreated as well as the treated gels. The master image is used to obtain all the information needed for differentially affected protein spots. Basically, the master image is used to answer questions asked by the user on differential regulation of spots (Figure 3.6).

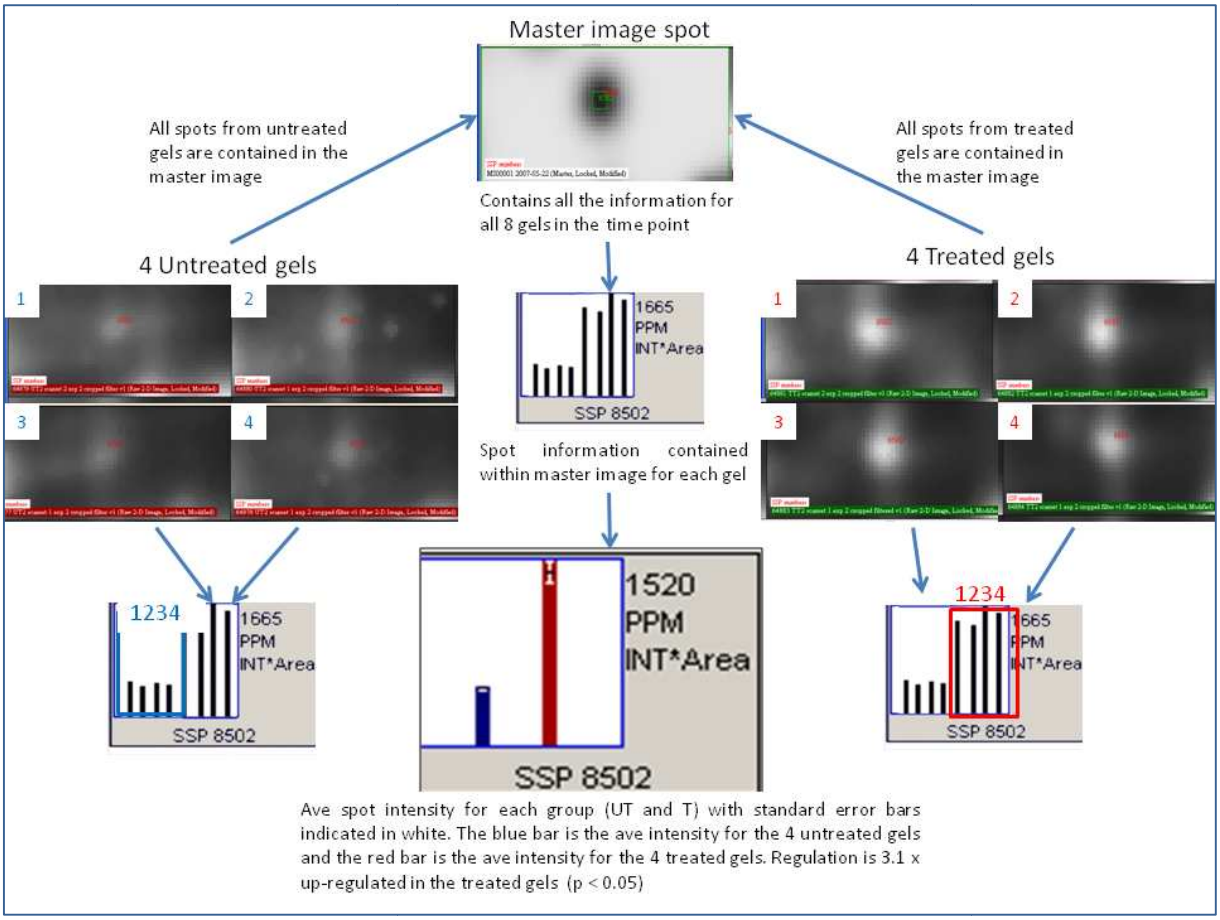

Figure 3.6: Determination of differentially affected protein spots between the treated and untreated groups using the master image.

The master image contains a single spot with the information from the single spot from each of the 4 T and 4 UT gels (numbered 1-4 in blue for UT and 1-4 in red as T). The master image then is able to give the information in graphical form for a specific spots, in which each of the 8 gels is represented as a different bar on the graph (marked 1-4 in blue on the bar graphs for UT samples and correlate to gel number, and similarly for the T samples marked in red on the bar graphs and gel images. Finally, for differential protein abundance determination the 4 values of the UT samples are taken as an average (blue bar), which is similarly done for the treated sample (red bar). A standard error is also calculated and given as a white error bar on each of the graphs. This is then used to determine differential protein abundance ($p < 0.05$).

The master image is created from all 8 gels. Therefore, if a spot in present within all 8 gels (4 × UTt_1 and 4 × Tt_1 gels) then the master image contains only a single spot in similar position on its image, but that spot contains the information for all 8 spots from the 8 gels. This information contained for each spot can be extracted from the master image and converted to graph format. The bars on the graph represent each of the 8 gels with the first 4 bars representative of the UT sample

and the last 4 bars representative of the T samples (Figure 3.6). To determine differentially affected protein spots ($p < 0.05$), the average value is taken and together with a standard error-of-the-mean to determine significance of protein spots between the 2 groups.

A summary of the data for both time points are given in Table 3.4. A good gel match rate (number of spots that are matched for each individual gel) of 96-98% was achieved for t_1 and t_2. The master match rate was 88% for t_1 and 58% for t_2. The master match rate is defined as the matching number of spots of each individual gel to the number of spots contained within the master image. The high match rate obtained for t_1 indicates that the differences observed between the T and UT samples are relatively small. The lower master match rate for t_2 is indicative of progression of the UT samples when compared to the T samples due to AdoMetDC inhibition. When even later time points were to be investigated the discrepancies between the UT and the T sample would increase due to life cycle stage differences, hence resulting in an even lower match rate. The correlation coefficient for t_1 between the T and UT groups was 0.719 while for t_2 it decreased to 0.664.

Table 3.4: Data obtained from PD Quest 7.1.1 after spot detection of both the UT and T gels for t_1 and t_2.

Condition	t_1	t_2
Master image spot count	369	450
UT vs T group corr coeff	0.719	0.664
Ave match rate per gel	98% ± 0.7[a]	96% ± 1.8[a]
Ave master match rate	88% ± 4.4[a]	58% ± 6.0[a]
Ave spots per gel	325	272

[a]Match rates are given as an average of all eight gels per time point with the standard deviation.

For statistical purposes, replicate groups were created in which the 4 gels of the UT samples are grouped together as the UT group and similarly for the 4 gels from the T samples. The information contained within the master image is then used to ask questions to the master image. This is usually done to determine spots that are differentially affected ($p<0.05$) between the 2 groups. Both graphical and numerical data can be obtained for each regulated spot and are given in a report. Figure 3.7 depicts a graphical representation of spot quantification where this protein spot was increased 3.1-fold in the T group compared to the UT group. Each of the bars given on the graph contains the information for all 4 gels of that specific group (UT blue bar vs T red bar), and are statistically significant.

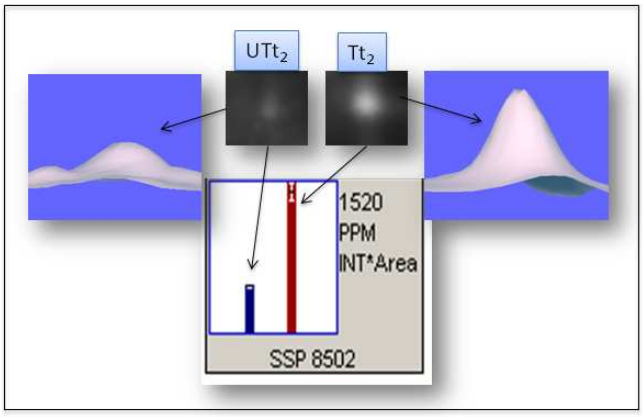

Figure 3.7: Differential protein spot abundance determined by PD Quest.

SSP 8502 is the number given to the spot by the software. This spot is increased 3.1-fold in protein abundance in Tt_2 as compared to UTt_2. The spots as seen on the 2-DE gels are on top of the figure with the white spot on the black background. To the sides of each of the two spots are a 3-D representation of the spots and the graphs for the spots are given at the bottom of the figure. The blue bar represents the UTt_2 group that contains all the information for the 4 gels within this group. The red bar is representative of the 4 gels within the Tt_2 group.

In a similar fashion as described above, the total number of differentially affected protein spots for both time points was determined and is given in Table 3.5. A total of 55 spots were identified as differentially regulated in Tt_1 ($p<0.05$). This indicates that 17% (55/325) of the proteome of AdoMetDC inhibited parasites are differentially affected within the first time point (late rings). For the second time point, 64 (52 + 7 + 5) spots fulfilled the criteria of $p<0.05$ according to the student t-test. Therefore, Tt_2 resulted in 24% (64/272) of the AdoMetDC inhibited proteome to be affected. Therefore in total, 119 protein spots were identified as differentially affected in the AdoMetDC inhibited proteome.

Table 3.5: The total number of differentially affected protein spots for the 2 time points

Regulation type	t_1	t_2
Present only in T[a]	0	7
Absent only in T[a]	0	5
Differentially regulated spots[b]	55	52
Total nr of differentially regulated spots	**55**	**64**

[a]These are spots that are only present in either the T or UT group. [b]Spots that are at differentially regulated and considered as significant ($p<0.05$) according to the student t-test.

3.3.5 Protein identification of differentially affected protein spots from the AdoMetDC inhibited proteome

The differentially affected protein spots identified by the software were subsequently cut from the gels and prepared for MALDI-Q-TOF MS/MS analysis. For identification of each of the protein spots, a PMF was first obtained from the protein, which was immediately followed by MS/MS analysis of the 50 highest peaks from the PMF for that particular protein. An example of a PMF and

the MS/MS data obtained for AdoMet synthase is given in Figure 3.8. A series of peptides were obtained that ranged from 600 – 3400 Da. From this range of peptides, the peptide with a m/z value of 1401.8 was used to illustrate the effect of MS/MS in which the amino acid sequence could now be obtained. The collision gas is used in the collision chamber of the MALDI-Q-TOF to fragment the peptide into its different amino acids. From Figure 3.8 B it can be seen that the y_1-ion is arginine (R) since it has a m/z value of 175.1, and was expected since trypsin cleaves at either lysine or arginine residues. Each amino acid has a specific mass and therefore by analysing the MS/MS spectra (Figure 3.8 B), the amino acid sequence can be obtained from the spectra, which in this case is a peptide that consists of 15 amino acids that are marked y_1 to y_{15} or b_1 to b_{15} (Figure 3.8 C). Protein scores of more than 45 was considered as significant for identification of the protein ($p<0.05$).

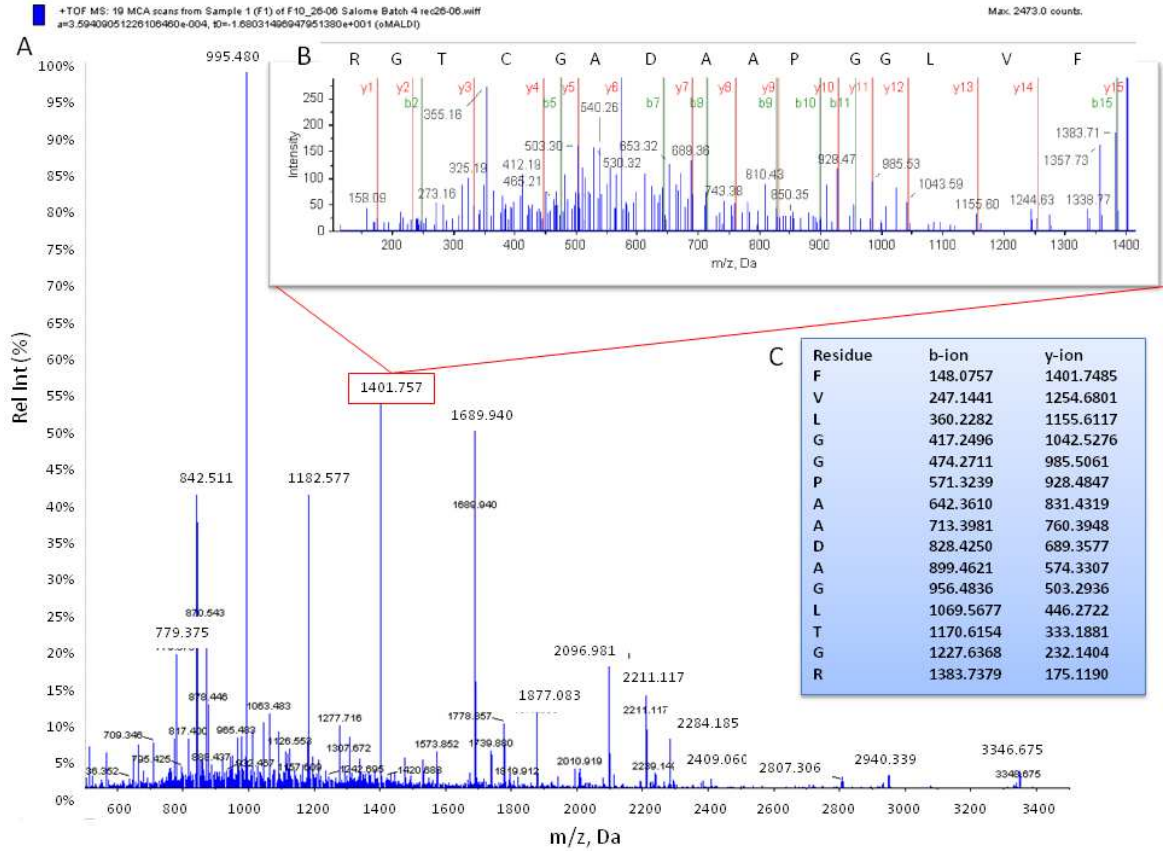

Figure 3.8: The MS spectra of S-adenosylmethionine synthase.

The bottom of the figure is a representation of a PMF that was obtained. The insert depicts the amino acid sequence (FVLGGPAADAGCTGR) of a single PMF peak (1401.757) as determined by MS/MS with the values of both the b- and y-ions and the masses of each. A protein score of 863 were obtained in the MS-ion search mode of MASCOT. Sequence coverage of 40% was obtained for this protein and the amino acid sequences of 14 peptides were used for scoring.

In a similar way as described above, the differentially affected protein spots identified by PD Quest for Tt_1 and Tt_2 were cut and trypsinised before being subjected to MALDI-Q-TOF MS/MS and finally the MS-spectra submitted to MASCOT for protein identification. Differentially affected protein spots that were positively identified by MS/MS analyses are depicted in Figure 3.9 for both Tt_1 and Tt_2. The differential fold-change of each identified protein spot as well as the MW, pI, MS/MS scores is given in Table 3.6. To minimise the possibility of false positive identifications, a protein was only considered to have a positive identification if the protein score was more than 45 ($p<0.05$), together with at least 10% sequence coverage, with at least 5 peptides for each particular protein.

Of the 119 differentially regulated spots that were identified for Tt_1 and Tt_2 (Table 3.6), a total of 91 protein spots were identified of which 53 protein spots were from Tt_1 and 38 protein spots were from Tt_2. For the first time point (Tt_1) 25 protein spots were identified by MS/MS to have increased protein abundance together with 28 protein spots that had decreased protein abundance. This accounts for a total of 15 Plasmodial protein spots with increased protein abundance of which 14 were unique Plasmodial protein groups. Amongst the 28 decreased abundance protein spots, 23 were unique Plasmodial proteins. A total of 20 protein spots had increased protein abundance (15 unique Plasmodial proteins) and 12 protein spots (6 unique Plasmodial proteins) had decreased protein abundance in Tt_2, together with 6 protein spots that were either absent or present in only one of the samples (either UTt_2 or Tt_2). Therefore, the 91 protein spots identified by MS/MS consisted of 75 Plasmodial protein spots (82% Plasmodial protein spots) and finally accounted for a total of 46 unique Plasmodial protein groups over the 2 time points (Table 3.6).

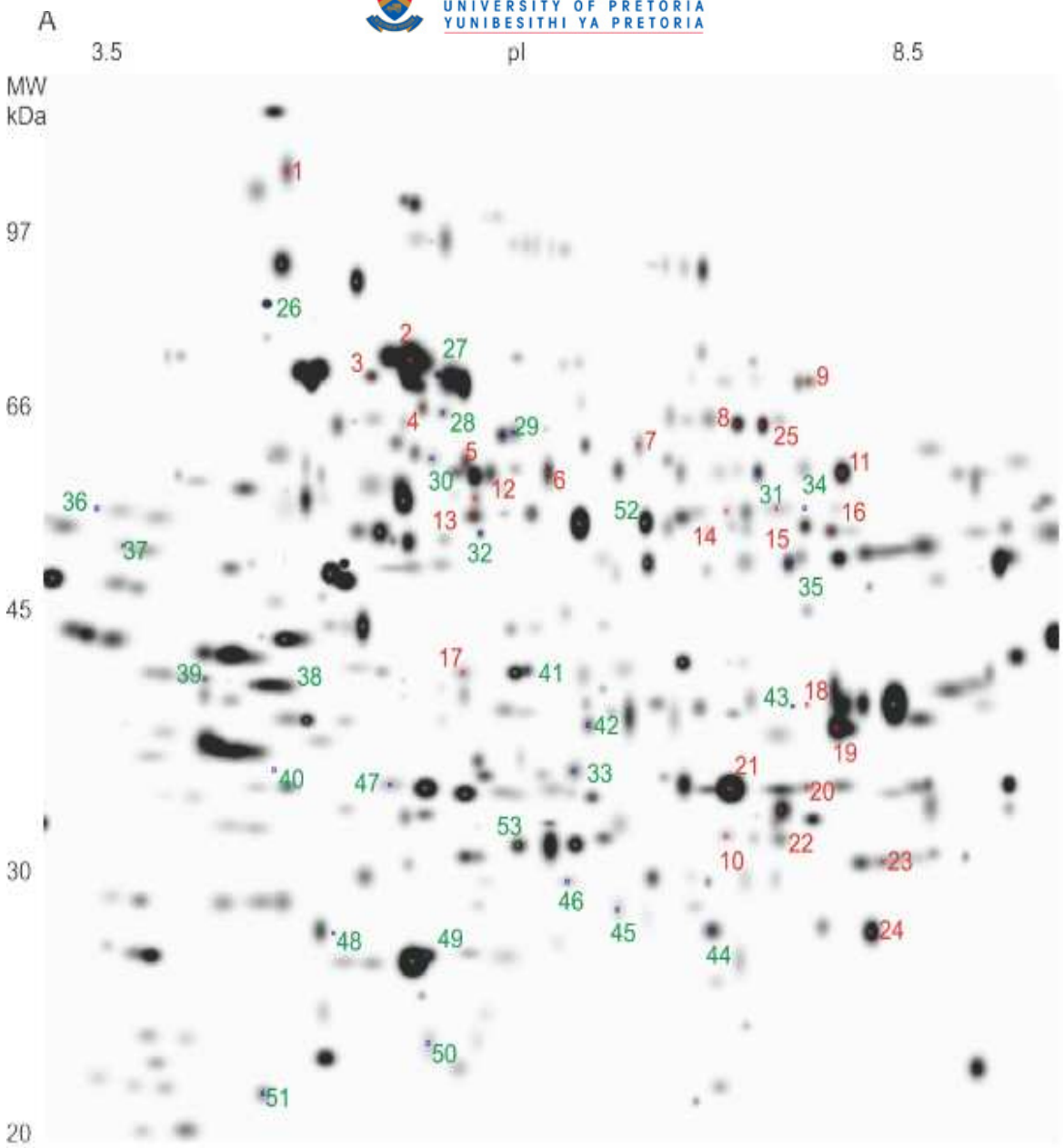

Figure 3.9 A: Master images of the Tt_1 (16 HPI) with the differentially affected protein spots that were identified indicated.

Numbers given in red is indicative of increased protein abundance of the protein spots while green is decreased protein abundance of protein spots. The numbers correspond to the numbers given in Table 3.6.

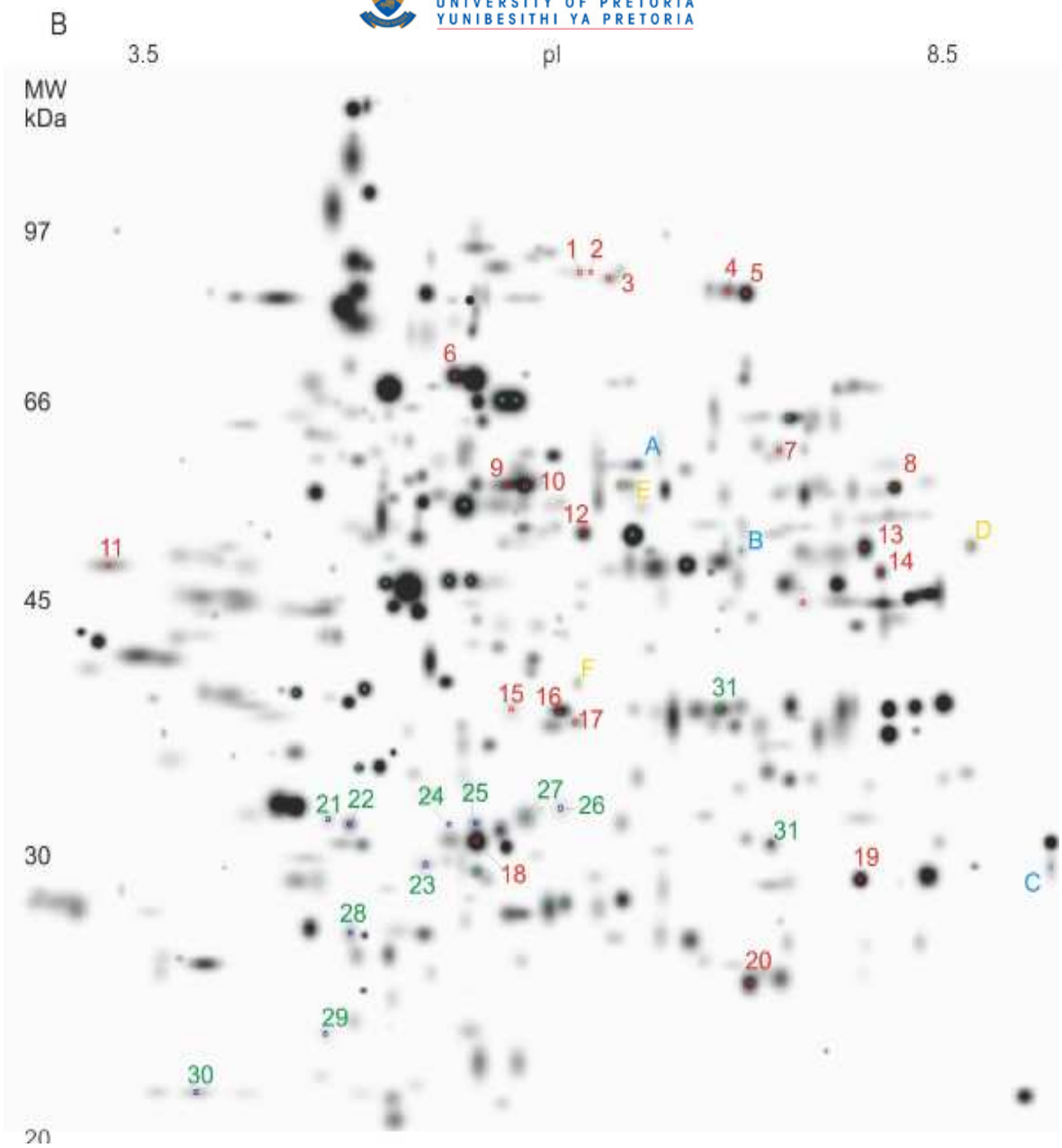

Figure 3.9 B: Master images of the Tt_2 (20 HPI) with the differentially affected protein spots that were identified indicated.

Numbers given in red is indicative of increased protein abundance of the protein spots while green is decreased protein abundance of protein spots. Protein spots that were only detected in one of either the T or UT sample were only found in Tt_2 and are marked A-F, with blue indicative of spots that are present in Tt_2 and yellow indicative of spots that were absent in Tt_2. The numbers correspond to the numbers given in Table 3.6.

Table 3.6: Protein spots identified by MS/MS for the AdoMetDC inhibited proteome at Tt_1 and Tt_2.

Spot nr[a]	FC[b]	Accession nr[c]	Plasmo DB[d]	Name	Mr	pI	Mascot score MS/MS[e]	Seq cover[f]	Match[g]
(A) Protein spots with increased protein abundance Tt_1									
20	18.0	P00915	—	Carbonic anhydrase 1 *(Homo sapiens)*	28778	6.63	531	50	8
21	1.7	P00915	—	Carbonic anhydrase 1 *(Homo sapiens)*	28620	6.65	845	58	11
22	1.5	P00918	—	Carbonic anhydrase 2 *(Homo sapiens)*	28802	6.63	320	30	7
14	3.3	P04040	—	Catalase *(Homo sapiens)*	59816	6.95	425	22	9
25	1.6	P04040	—	Catalase *(Homo sapiens)*	59816	6.95	659	29	15
8	2.2	Q8I6S6	MAL8P1.17	Disulfide isomerase, putative	55808	5.56	693	35	15
5	2.2	Q9TY94	PFB0445c	eIF4A-like helicase, putative	52647	5.68	251	13	6
13	2.0	Q27727	PF10_0155	Enolase	48989	6.21	313	18	7
15	5.1	O96940	PF14_0164	Glutamate dehydrogenase ($NADP^+$) (1)	53140	7.48	283	17	8
16	2.1	O96940	PF14_0164	Glutamate dehydrogenase ($NADP^+$) (2)	53140	7.48	497	30	13
18	2.2	Q8T6B1	PF14_0598	Glyceraldehyde-3-phosphate dehydrogenase	37068	7.59	131	11	3
23	2.1	P38545	PF11_0183	GTP-binding nuclear protein ran/tc4	24974	7.72	485	55	12
2	2.7	Q8IB24	PF08_0054	Heat shock 70 kDa protein	74382	5.51	1378	34	23
3	3.5	P19120	—	Heat shock 70 kDa protein *(Bos taurus)*	71454	5.37	579	20	11
10	1.3	P68871	—	Hemoglobin subunit beta *(Homo sapiens)*	16112	6.71	870	37	19
6	1.4	Q8IL11	PF14_0439	Leucine aminopeptidase, putative.	68343	8.78	172	14	7
19	1.5	Q71T02	PF13_0141	L-lactate dehydrogenase	34314	7.12	611	43	12
7	1.3	Q8IDC7	MAL13P1.283	MAL13P1.283 protein	58506	6.09	261	10	6
9	10	Q8I3Y8	PFE0585c	Myo-inositol 1-phosphate synthase, putative	69639	7.11	454	25	14
11	1.3	Q8IJ37	PFI1300w	Putative pyruvate kinase	56480	7.5	732	37	16
12	2.8	Q13228	—	Selenium binding protein 1 *(Homo sapiens)*	52928	5.93	140	12	6
24	1.8	P02769	—	Serum albumin *(Bos taurus)*	71274	5.82	510	16	10
1	2.0	P00915	—	Spectrin alpha chain, erythrocyte *(Homo sapiens)*	282024	4.98	889	24	9
17	1.6	Q8I3X4	PFE0660c	Purine nucleoside phosphorylase, putative	27525	6.07	412	47	9
4	2.0	Q03498	MAL13P1.271	V-type ATPase, putative	69160	5.51	291	19	10
(B) Protein spots with decreased protein abundance Tt_1									
45	-1.8	Q8IJT1	PF10_0111	20S proteasome beta subunit, putative	30862	5.18	150	9	4
44	-1.4	Q9N699	PF14_0368	2-Cys peroxiredoxin	21964	6.65	540	59	8
41	-2.3	Q8IJD4	PF10_0264	40S ribosomal protein, putative	30008	5.91	152	11	3
33	-1.4	P07738	—	Bisphosphoglycerate mutase *(Homo sapiens)*	30027	6.1	461	43	10
30	-3.5	Q9TY94	PFB0445c	eIF4A-like helicase	52647	5.68	589	26	10
32	-4.1	Q27727	PF10_0155	Enolase	48989	6.21	373	18	7

51	-10.0	Q8I603	PFL0210c	Eukaryotic initiation factor 5a, putative	17791	5.42	159	27	4
40	-7.0	Q8I6U4	PF11_0165	Falcipain 2	56405	7.12	212	12	6
34	-2.2	O96940	PF14_0164	Glutamate dehydrogenase (NADP+)	53140	7.48	212	15	6
46	-1.6	Q8MU52	PF14_0187	Glutathione s-transferase	24888	5.97	47	11	2
43	-2.8	O96369	PF14_0598	Glyceraldehyde-3-phosphate dehydrogenase	37068	7.59	302	25	7
38	-2.0	Q8IM15	PF14_0078	HAP protein	51889	8.05	645	34	13
26	-3.5	Q8IC05	PF07_0029	Heat shock protein 86	86468	4.94	1153	25	24
29	-2.7	Q8IJN9	PF10_0153	Hsp60	62911	6.71	870	37	19
36	-4.7	Q8I608	PFL0185c	Nucleosome assembly protein 1, putative	42199	4.19	293	16	7
49	-2.9	P32119	—	Peroxiredoxin-2 *(Homo sapiens)*	21918	5.67	515	41	10
47	-1.5	Q8IDQ9	MAL13P1.214	Phosphoethanolamine N-methyltransferase, putative	31309	5.43	252	22	5
35	-1.5	P27362	PFI1105w	Phosphoglycerate kinase	45569	7.63	214	15	5
39	-2.2	Q8I6V3	PF14_0077	Plasmepsin 2	51847	5.36	72	6	3
42	-1.4	Q9U570	MAL8P1.142	Proteasome beta-subunit	31080	6.00	212	22	7
31	-1.3		PFF1300w	Putative pyruvate kinase	56480	7.5	633	28	15
48	-3.3	Q8I2Q0	PFI1270w	Putative uncharacterized protein PFI1270w	24911	5.49	327	26	6
52	-1.3		PFI1090w	S-adenosylmethionine synthetase	45272	6.28	863	40	14
27	-3.4		—	Serum albumin *(Bos taurus)*	71274	5.82	620	24	15
37	-4.2	Q4KKW9	—	Solute carrier family 4, anion exchanger, member 1 *(Homo sapiens)*	101978	5.13	189	7	4
50	-1.7	P00441	—	Superoxide dismutase *(Homo sapiens)*	16154	5.7	219	37	4
53	-1.8	Q8I3X4	PFE0660c	Purine nucleoside phosphorylase, putative	27525	6.07	572	36	10
28	-3.2	Q03498	MAL13P1.271	V-type ATPase, putative	69160	5.51	184	13	7
				(C) Protein spots with increased protein abundance Tt_2					
20	1.9	Q9N699	PF14_0368	2-Cys peroxiredoxin	21964	6.65	504	72	11
15	3.6	Q8IJD4	PF10_0264	40S ribosomal protein, putative (1)	29856	6.15	27	11	3
16	1.6	Q8IJD4	PF10_0264	40S ribosomal protein, putative (2)	30008	5.91	267	24	8
9	5.9	Q97TY94	PFB0445c	eIF4A-like helicase, putative (1)	52647	5.68	320	23	8
10	2.1	Q97TY94	PFB0445c	eIF 4A-like helicase, putative (2)	52646	5.68	62	42	14
4	4.7	Q8IKW5	PF14_0486	Elongation factor 2 (1)	94545	6.36	96	4	4
5	2.0	Q8IKW5	PF14_0486	Elongation factor 2 (2)	94546	6.78	657	26	18
12	1.4	Q8IJN7	PF10_0155	Enolase	48989	6.21	408	20	7
17	11.1	Q95W62	PFD0615c	Eryhrocyte membrane protein 1 (fragment)	13608	6.96	51	38	7
7	8.9	Q8ILA4	PF14_0341	Glucose-6-phosphate isomerase	67610	6.78	61	28	14
13	2.0	O96940	PF14_0164	Glutamate dehydrogenase (NADP+)	53140	7.48	336	28	11
6	2.2	Q8IB24	PF08_0054	Heat shock 70 kDa protein	74382	5.33	861	33	18
11	8.0	Q8IAW8	MAL8P1.95	Hypothetical protein MAL8P1.95	37933	4.13	385	25	8

14	3.1	Q71T02	PF13_0141	Lactate dehydrogenase	34000	8.5	100	12	3
1	8.1	Q8IEK1	MAL13P1.56	M1 family aminopeptidase (1)	126552	7.3	102	26	23
2	2.4	Q8IEK1	MAL13P1.56	M1 family aminopeptidase (2)	126552	6.68	124	25	25
3	4.6	Q8IEK1	MAL13P1.56	M1 family aminopeptidase (3)	126552	7.3	107	23	23
18	1.7	Q8IDQ9	MAL13P1.214	Phosphoethanolamine N-methyltransferase, putative	31309	5.28	722	48	13
19	1.3	Q8IIG6	PF11_0208	Phosphoglycerate mutase, putative	28866	8.3	401	36	10
8	2.3	Q8IJ37	PFF1300w	Putative pyruvate kinase	56480	7.5	101	51	16
				(D) Protein spots with decreased protein abundance Tt_2					
28	-1.6	O97249	PFC0295c	40S ribosomal protein S12, putative (1)	15558	4.9	85	14	2
30	-1.9	O97249	PFC0295c	40S ribosomal protein S12, putative (2)	15558	4.9	217	36	5
26	-2.1	Q8IM55	PF14_0036	Acid phosphatase, putative	35824	5.98	63	5	2
27	-1.4	Q8I4X0	PFL2215w	Actin-1 (1)	42272	5.27	359	22	7
32	-2.0	Q8I4X0	PFL2215w	Actin-1 (2)	42272	5.17	81	42	12
31	-2.4	P00915	—	Carbonic anhydrase 1 *(Homo sapiens)*	28620	6.65	70	20	4
21	-24.0	Q8I6U4	PF11_0165	Falcipain 2, putative (1)	56481	7.9	47	23	10
22	-2.3	Q8I6U4	PF11_0165	Falcipain-2, putative (2)	55804	7.49	56	24	11
23	-3.3	Q8ILV5	PF14_0138	Hypothetical protein	23889	5.49	53	9	2
24	-3.8	Q8IDQ9	MAL13P1.214	Phosphoethanolamine N-methyltransferase, putative (1)	31043	5.43	69	9	2
25	-1.8	Q8IDQ9	MAL13P1.214	Phosphoethanolamine N-methyltransferase, putative (2)	31043	5.28	177	22	5
29	-2.6	Q8I5T3	PFL0590c	P-type ATPase, putative	135214	6.13	54	18	16
				(E) Protein spots that were either present or absent in Tt_2					
A	On	Q8IDJ8	PF13_0262	Lysine tRNA ligase (EC 6.1.1.6)	68003	7.02	100		17
B	On	S51042		tat binding protein homolog malaria parasite	49859	6.86	52		12
C	On	Q8IDC6	MAL13P1.284	Pyrroline-5-carboxylate reductase (EC 1.5.1.2)	28816	8.13	61		9
D	Off	AAN36874	PF14_0261	Proliferation associated protein 2g4 putative	43327	7.54	63		12
E	Off	Q6LF74	PFF1155w	Hexokinase (EC 2.7.1.1)	56081	6.72	44		10
F	Off	Q8IKW5	PF14_0486	Elongation factor 2	94545	6.36	74		17

Proteins identified are sorted alphabetically according to name with isoforms grouped together and the number of isoforms per protein is marked in brackets next to the protein name. [a]Spot number corresponds to marked spots on the master image of ring stage parasites. [b]FC is the fold change for protein abundance of each spot either increased (+ value) or decreased (- value) compared to the untreated sample as determined by PD Quest 7.1.1. All values given are significant ($p<0.05$). [c]Accession number is obtained from the SwissProt UniProt database. [d]PlasmoDB ID is obtained from the PlasmoDB 6.0 database. [e]Mascot scores are based on MS/MS ion searches and is only taken when the score is significant ($p<0.05$). [f]Sequence coverage is given by Mascot for detected peptide sequences. [g]Matched is the number of peptides matched to the particular protein.

3.3.6 1-DE SDS-PAGE and 2-DE gels as complementary proteomic techniques to obtain maximal proteome information

A total 46 unique Plasmodial protein groups were identified with 2-DE as differentially affected in addition to the 20 unique Plasmodial protein groups identified using a 1-DE approach (Section 3.3.3). Of these 66 unique Plasmodial protein groups, only 5 unique Plasmodial protein groups were shared between the 2 approaches followed (Figure 3.10). These include heat shock protein 70 kDa (PF08_0154), enolase (PF10_0155), PEMT (MAL13P1.214), eIF4A-like helicase protein (PFB0445c) and actin-1 (PFL2215w). The 15 Plasmodial proteins that were identified with only 1-DE would not normally be detected on 2-DE due to the pI and molecular weight constraints associated with the use of 2-DE. Similarly, 41 Plasmodial protein groups were only detected on the 2-DE gels, which proves its superior separation ability. The use of both 1-DE and 2-DE therefore complemented the proteins that could be identified.

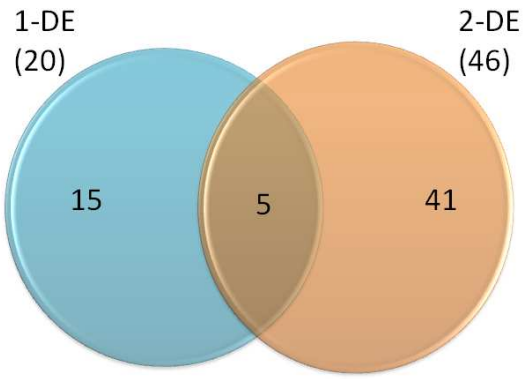

Figure 3.10: Correlation between Plasmodial proteins identified from 2 complimentary proteomic approaches.

3.3.7 Hierarchical clustering of differentially expressed proteins from the proteome of AdoMetDC inhibited parasites.

Hierarchical clustering of the differentially affected proteins identified by MS was performed for both time points (Figure 3.11). Only 2 clusters were obtained for the AdoMetDC inhibited proteome dataset because the T sample was always compared to the UT sample in order to determine differential regulation of the spots or proteins, therefore a differentially regulated spot has either increased or decreased abundance. Interestingly, the polyamine-related proteins and oxidative stress proteins tended to cluster together (Figure 3.11, marked in red and blue).

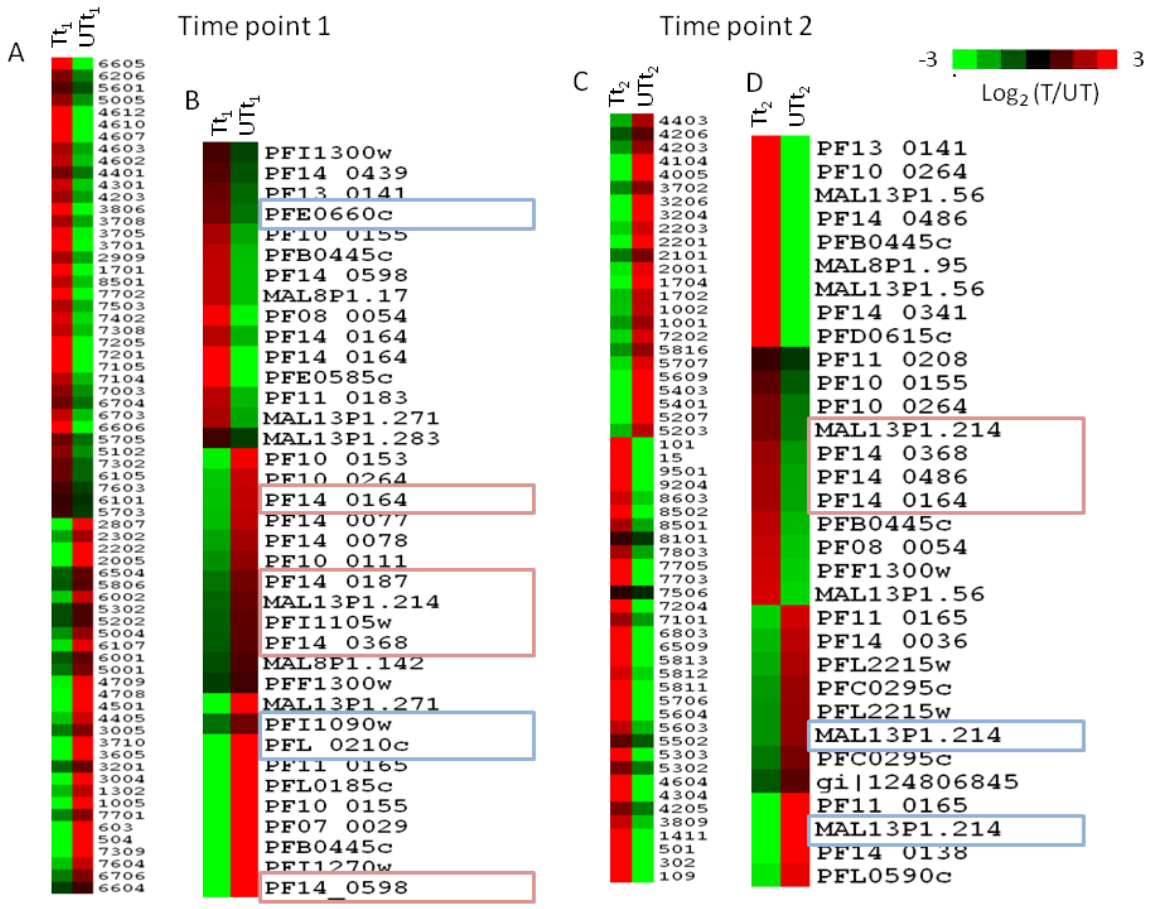

Figure 3.11: Hierarchical clustering of the differentially affected spots and identified proteins from AdoMetDC inhibition for two time points.

(A)All the differentially affected spots from t_1. (B) Clustering of the identified proteins from t_1. (C) All the differentially affected spots from t_2. (D) Clustering of the identified proteins from t_2. The pink blocks are representative of mostly oxidative stress proteins and the blue blocks are representative of mostly polyamine-related proteins. Unregulated spots were not included into the hierarchical clustering of any of the time points.

3.3.8 Functional classification of the differentially affected proteins identified from the proteome of AdoMetDC inhibited parasites.

The 46 unique Plasmodial protein groups were sorted according to their GO annotations that were obtained from PlasmoDB 6.0, and then grouped into their respective GO functions (Table 3.7, Figure 3.12). Each protein was only grouped into a single category despite the fact that some proteins may be representative of more than one GO annotation. The functional GO groupings were validated with MADIBA (www.bi.up.ac.za/MADIBA/).

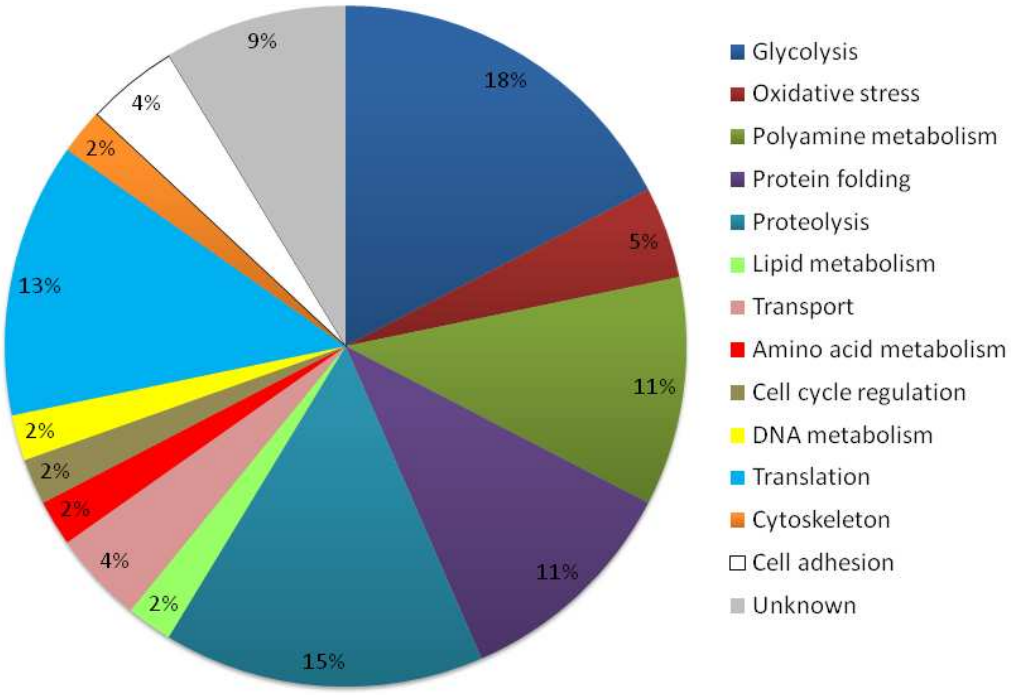

Figure 3.12: GO annotation for the regulated spots of both time points.
GO annotations were obtained from PlasmoDB 6.0 and classified according to biological process in MADIBA.

Only 9% (4/46 proteins) of the AdoMetDC inhibited proteome dataset that was identified by MS was regarded as hypothetical proteins with unknown functions. This is probably due to the small portion of unique Plasmodial protein groups that were identified (46 proteins). Of the 46 unique Plasmodial protein groups identified by MS, 18% were associated with glucose metabolism. Some of the other groups that were highly represented included protein folding (11%), polyamine metabolism (11%), proteolysis (15%), translation (13%) and oxidative stress (5%). Polyamine and methionine metabolism included 5 differentially expressed proteins. Of these 5 unique Plasmodial proteins groups that were differentially affected, 3 proteins had increased protein expression and included PNP (PFE0660c, 1.6-fold), pyrroline-5-carboxylate reductase (MAL13P1.284, present in Tt_2) and 1 isoform of PEMT (MAL13P1.214, 1.7-fold). Two other isoforms of PEMT both had decreased transcription (-1.5-fold and -3.8-fold respectively). The protein expression of AdoMet synthetase (PFI1090w, -2.3-fold), eukaryotic initiation factor 5a (eIF5A, PFL0210c, -10-fold) and another protein isoform of PNP (PFE0660c, -1.8-fold) had decreased abundance in the first time point (Figure 3.9 and Table 3.7). Unfortunately, in the second time point, AdoMet synthase and OAT which is in close proximity of each other on the 2-DE gel overlapped and were saturated possibly due to the increased protein abundance of OAT and could therefore not be quantitated.

Some of the other proteins that were differentially affected included eIF4A-like helicase protein (PFB0445c) that was detected as 2 isoforms at Tt_1 (2.2-fold and -3.5-fold) and 1 isoform at Tt_2 (5.9-fold) and seemed to be gradually increased in abundance over time. Several heat shock proteins were detected at both time points that included heat shock protein 70 kDa (PF08_0054, 2.7-fold Tt_1 and 2.2-fold Tt_2) that were increased in abundance at both time points, heat shock protein 86 (PF07_0029, -3.5-fold) and heat shock protein 60 (PF10_0153, -2.7-fold) that were both decreased in abundance at Tt_1 (Table 3.7).

Table 3.7: Biological functions of the differentially regulated proteins identified from the 2-DE gels from the AdoMetDC inhibited proteome.

PlasmoID[a]	Product name	Time point[b]	FC[c]	Min exp time HPI[d]	Max exp time HPI[d]
	Glycolysis				
PF10_0155	Enolase (1)	t_1	2	38	16
PF10_0155	Enolase (2)	t_1	-4.1	38	16
PF14_0598	Glyceraldehyde-3-phosphate dehydrogenase (1)	t_1	2.2	42	27
PF14_0598	Glyceraldehyde-3-phosphate dehydrogenase (2)	t_1	-2.8	42	27
PF13_0141	Lactate dehydrogenase	t_1	1.5	42	26
PFI1105w	Phosphoglycerate kinase	t_1	-1.5	38	19
PFF1300w	Putative pyruvate kinase	t_1	-1.3	41	26
PF10_0155	Enolase	t_2	1.4	38	16
PF14_0341	Glucose-6-phosphate isomerase	t_2	8.9	37	16
PF13_0141	Lactate dehydrogenase	t_2	3.1	42	26
PF11_0208	Phosphoglycerate mutase, putative	t_2	1.3	38	11
PFF1300w	Putative pyruvate kinase	t_2	2.3	41	26
	Polyamine metabolism				
PFE0660c	Purine nucleoside phosphorylase, putative (1)	t_1	1.6	4	22
PFE0660c	Purine nucleoside phosphorylase, putative (1)	t_1	-1.8	4	22
PFI1090w	S-adenosylmethionine synthetase	t_1	-1.3	12	32
MAL13P1.214	Phosphoethanolamine N-methyltransferase, putative	t_1	-1.5	10	33
PFL0210c	Eukaryotic initiation factor 5a, putative	t_1	-10	42	26
MAL13P1.214	Phosphoethanolamine N-methyltransferase, putative (1)	t_2	-3.8	10	33
MAL13P1.214	Phosphoethanolamine N-methyltransferase, putative (2)	t_2	1.7	10	33
MAL13P1.284	Pyrroline-5-carboxylate reductase	t_2	10		
	Protein folding				
MAL13P1.283	MAL13P1.283 protein	t_1	1.3	36	18
MAL8P1.17	Disulfide isomerase, putative	t_1	2.2	43	32
PF10_0153	Hsp60	t_1	-2.7	1	21
PF07_0029	Heat shock protein 86	t_1	-3.5	46	22
PF08_0054	Heat shock 70 kDa protein	t_1	2.7	42	23
PF08_0054	Heat shock 70 kDa protein	t_2	2.2	42	23
	Proteolysis				
PF10_0111	20S proteasome beta subunit, putative	t_1	-1.8		
PF11_0165	Falcipain 2	t_1	-7	36	19
PF14_0078	HAP protein	t_1	-2	38	19
PF14_0439	Leucine aminopeptidase, putative.	t_1	1.4	1	19
PF14_0077	Plasmepsin 2	t_1	-2.2	38	18
MAL8P1.142	Proteasome beta-subunit	t_1	-1.4	1	31
PF11_0165	Falcipain 2	t_2	-24	36	19
MAL13P1.56	M1 family aminopeptidase (1)	t_2	8.1	33	17
MAL13P1.56	M1 family aminopeptidase (2)	t_2	4.6	33	17

MAL13P1.56	M1 family aminopeptidase (3)	t_2	2.4	33	17
	Lipid metabolism				
PFE0585c	Myo-inositol 1-phosphate synthase, putative	t_1	10	10	34
	Proton transport				
MAL13P1.271	V-type ATPase, putative (1)	t_1	2	35	24
MAL13P1.271	V-type ATPase, putative (2)	t_1	-3.2	35	24
	Amino acid metabolism				
PF14_0164	Glutamate dehydrogenase (NADP+) (1)	t_1	5.1	28	43
PF14_0164	Glutamate dehydrogenase (NADP+) (2)	t_1	-2.2	28	43
PF14_0164	Glutamate dehydrogenase (NADP+) (3)	t_2	2	28	43
	Cell cycle regulation				
PF11_0183	GTP-binding nuclear protein ran/tc4	t_1	2.1	42	30
	DNA metabolism				
PFB0445c	eIF4A-like helicase, putative (1)	t_1	2.2	41	16
PFB0445c	eIF4A-like helicase, putative (2)	t_1	-3.5	41	16
PFL0185c	Nucleosome assembly protein 1, putative	t_1	-4.7	23	46
PFB0445c	eIF4A-like helicase, putative	t_2	5.9	41	16
	Translation				
PF10_0264	40S ribosomal protein, putative	t_1	-2.3	41	11
PFC0295c	PFC0295c	t_2	-1.6	41	11
PF10_0264	40S ribosomal protein, putative	t_2	3.6	41	11
PF14_0486	Elongation factor 2	t_2	4.7	46	17
	Oxidative stress				
PF14_0368	2-Cys peroxiredoxin	t_1	-1.4	41	26
PF14_0187	Glutathione s-transferase	t_1	-1.6	37	21
PF14_0368	2-Cys peroxiredoxin	t_2	1.9	41	26
	Hypotheticals				
PFI1270w	Putative uncharacterized protein PFI1270w	t_1	-3.3		
PF14_0036	PF14_0036	t_2	-2.1	2	18
MAL8P1.95	Hypothetical protein MAL8P1.95	t_2	8	37	18
	Cytoskeleton				
PFL2215w	Actin I	t_2	-1.4	15	39
	Cell adhesion				
PF14_0138	Hypothetical protein	t_2	-3.3	11	31
PFD0615c	Eryhrocyte membrane protein 1 (fragment)	t_2	11.1	31	46
	Cation transport				
PFL0590c	P-type ATPase, putative	t_2	-2.6	28	41

Proteins are sorted according to their GO classifications. [a]PlasmoDB ID is obtained from the PlasmoDB 6.0 database. [b]Time point is the time point at which the specific protein is differentially expressed. [c]FC is the fold change for protein abundance of each spot either increased (+ value) or decreased (- value) compared to the untreated sample as determined by PD Quest 7.1.1. All values given are significant ($p<0.05$). [d]The maximum and minimum transcript expression times for each of the proteins as given in the PlasmoDB 6.0 database. Isoform identified in a time point is given in brackets.

3.3.9 Changes in protein abundance in the proteome of AdoMetDC inhibited parasites over time.

The protein abundance of some of the differentially regulated proteins in the AdoMetDC inhibited proteome was investigated over time (Tt_1 and Tt_2), to determine a possible trend in protein expression. Some of the proteins that are closely involved in methionine and polyamine biosynthesis were investigated over time and could be divided into 3 main groups (Figure 3.13).

Proteins that increased in abundance over time, included 2-Cys peroxiredoxin (PF14_0368), heat shock protein 60 kDa (PF10_0153), pyruvate kinase (PFF1300w) and pyrroline-5-carboxylate reductase (MAL13P1.284) (Figure 3.13 A). The other proteins decreased in abundance over time and were therefore grouped together which included heat shock protein 70 (PF08_0054), adenosine deaminase (PF10_0289) and PNP (PFE0660c) (Figure 3.13 B). Three protein isoforms were identified for PEMT (MAL13P1.214) of which 1 isoform increased in abundance, while the other 2 isoforms that were identified for PEMT (MAL13P1.214) decreased in abundance over time (Figure 3.13 C). Polyamine-related proteins that were not included in the groups were eIF5A (PFL0210c) and AdoMet synthase (PFI1090w) that both had decreased protein abundance at Tt_1, but could not be identified at Tt_2. Together, this regulation of protein abundance indicates that AdoMetDC inhibition does influence the parasite over time, with the majority of the detected polyamine-related proteins having decreased protein abundance over time. Comparisons between transcript and protein abundance and possible transcriptional regulatory mechanisms will be discussed in more detail in Chapter 5.

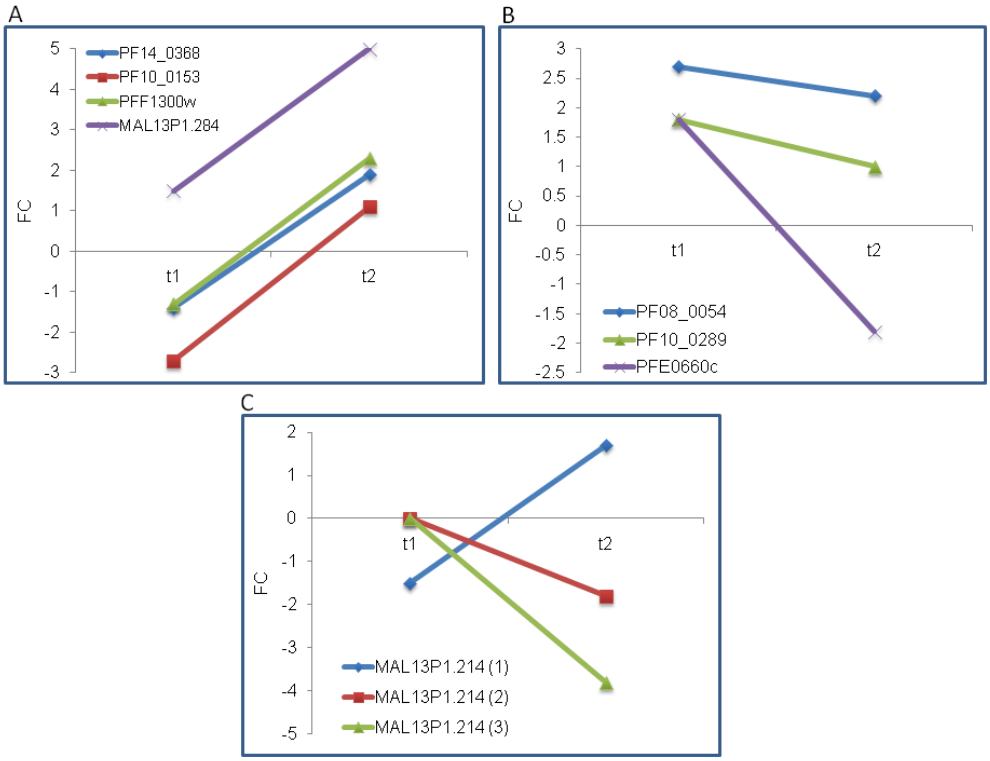

Figure 3.13: Differential regulation of proteins over time in the AdoMetDC inhibited proteome.

(A)Proteins that increased in abundance over time and include 2-Cys peroxiredoxin (PF14_0368), heat shock protein 60 kDa (PF10_0153), pyruvate kinase (PFF1300w), pyrroline-5-carboxylate reductase (MAL13P1.284). (B) Proteins that decreased in abundance over time and include heat shock protein 70 (PF08_0054), adenosine deaminase (PF10_0289), purine nucleoside phosphorylase (PFE0660c). (C) Three isoforms of phosphoethanolamine N-methyltransferase (MAL13P1.214) that changed in abundance over time.

3.3.10 Validation of differential proteomic data

To validate the 2-DE data, selective western blot analysis was performed on PEMT and M1-family aminopeptidase. Even though Flamingo Pink is a fluorescent stain that is semi-quantitative and has good linearity, it is of utmost importance to validate proteomic data with a sensitive and accurate method to confirm protein levels obtained from the 2-DE gels. The 2-DE gels and 2-DE western blot analysis showed clearly that PEMT consists of several isoforms that are grouped in close proximity of each other (Figure 3.14).

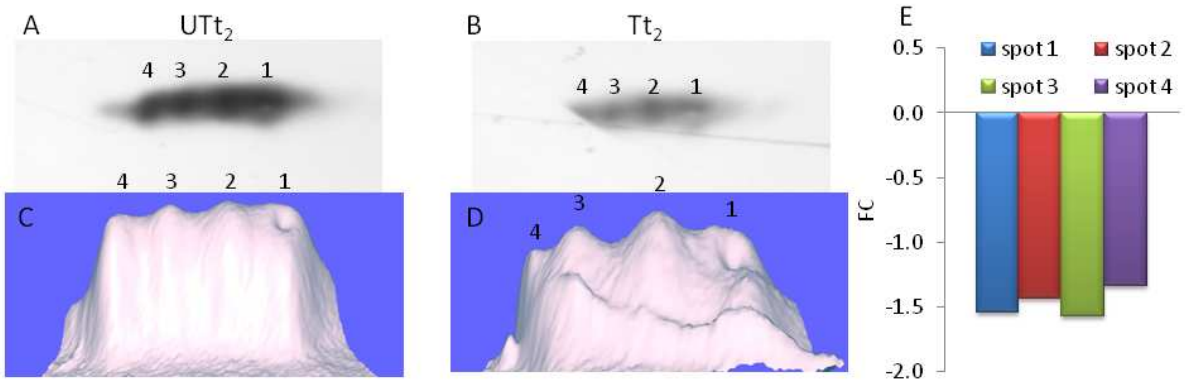

Figure 3.14: 2-DE Western blot of phosphoethanolamine N-methyltransferase.

The 3-D images were created by PD Quest. 2-DE was done on 13 cm IPG strips pH3-10 L, and run on a 16x18 cm gel. (A) The immunoblot for UTt_2, (B) immunoblot for Tt_2, (C) 3-D image of the spots in A, (D) 3-D image of the spots in B. The numbers on top of the spots is indicative of the number of isoforms detected. (E) The fold change calculated for each of the 4 different isoforms. All isoforms have decreased protein abundance. The intensity of each of the spots was determined using PD Quest. The fold change was then calculated for each individual spot to determine differential regulation of each of the 4 spots detected.

The 2-DE western blot of PEMT confirmed the decreased abundance of the protein in the treated sample as well as the existence of at least 4 isoforms that could be detected. All 4 isoforms decreased in protein abundance (spot 1: -1.6-fold, spot 2: -1.4-fold, spot 3: -1.6-fold, and spot 4: -1.3-fold) according to the 2-DE western blot. 2-DE analysis of PEMT revealed 3 protein isoforms of PEMT that was identified by MS/MS (Figure 3.9 and Table 3.6). Two isoforms decreased in protein abundance in Tt_2 (-3.8-fold and -1.7-fold) and 1 protein isoform had an increase in protein abundance (1.7-fold). The AdoMetDC inhibited 2-DE gels for Tt_2 were done on 18 cm IPG strips while the 2-DE western blot for validation was done on a 13 cm IPG strip. The 2-DE gels for the AdoMetDC inhibited proteome revealed a cluster of 6 spots in close proximity of which 3 were used for MS identification and subsequently identified as PEMT. The difference in separation power between the 2 strips could be the reason that 4 isoforms were detected on the 2-DE western blot since some of the protein isoforms and spots may overlap.

Three isoforms of M1-family aminopeptidase was detected in Tt_2 all with increased protein abundance according to the 2-DE analysis (Figure 3.9 and Figure 3.15). Therefore, the increased protein abundance that was determined for M1-family aminopeptidase in Tt_2 by 2-DE was also validated by 1-DE western blot analysis. Depicted in Figure 3.15 is the conventional 1-DE western blot that confirmed the increased protein expression determined on the 2-DE gels for the AdoMetDC inhibited proteome. Since only 1-DE western blot was done the data was analysed using Quantity One 4.4.1 by determination of the intensity of each band. The blot showed increased protein abundance for the Tt_2 sample compared to UTt_2, which was therefore sufficient for the validation of the proteomic results.

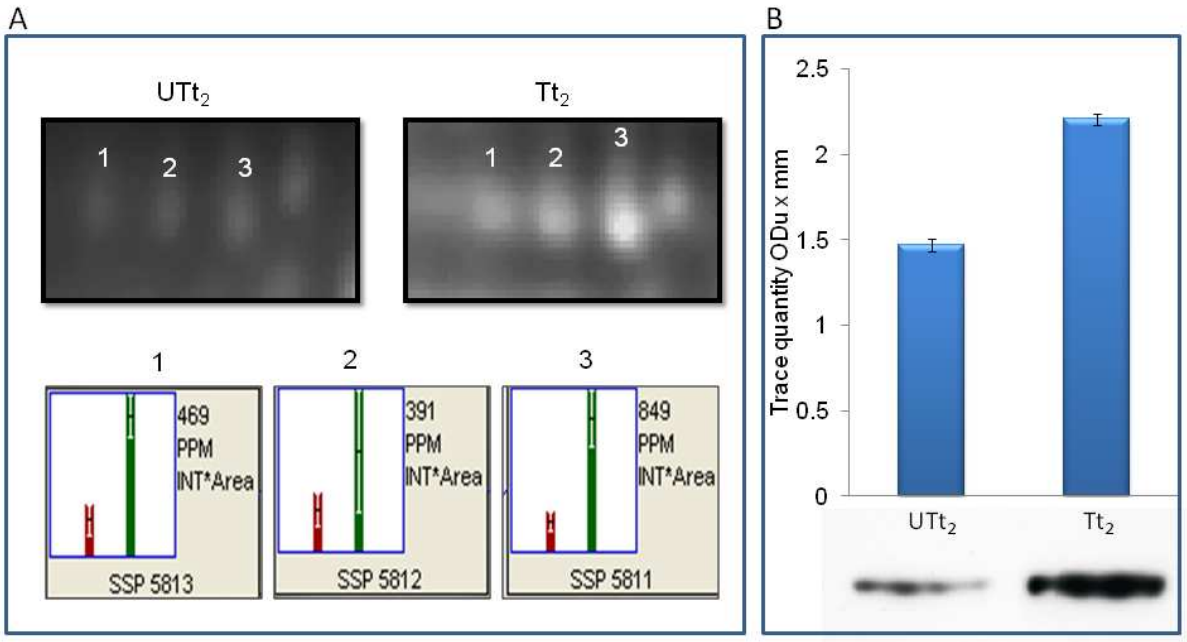

Figure 3.15: 1-DE western blot validation of the protein abundance of M1-family aminopeptidase that was detected on 2-DE at Tt_2.

A: The 3 M1-family aminopeptidase isoforms identified on the 2-DE gel with MS/MS. The 3 M1-family aminopeptidase isoforms are marked on the representative gels with the numbers 1-3. Spot number 1 has a fold change of 8.1, spot number 2 has a fold change of 2.4 and spot number 3 has a fold change of 4.6. At the bottom of the figure is the corresponding PD Quest data for each of the 3 isoforms. The PD Quest data indicates the red bar as the average intensity for the spot for UTt_2 and the green bar as the corresponding spot for Tt_2. The data are representative of 4 gels each for the T and UT gels, and the error bars are represented by the SEM. B: Graphical representation of the immunoblot data obtained. At the bottom of the graphs are the immunoblot showing UTt_2 and Tt_2. The data are for 2 immunoblots and the error bars are representative of SEM.

3.4 Discussion

An IC_{50} of 0.96 µM was determined for MDL73811 against a CQ sensitive strain of *P. falciparum* (*Pf*3D7) using the fluorescence based MSF assay. This is similar to previous results that made use of fluorescence activated cell sorting (FACS) in which an IC_{50} of 0.8 µM was determined (Van Brummelen, 2009). Another study, in which a [^{3}H]hypoxanthine assay was used, the IC_{50} of MDL73811 against *Pf*3D7 was determined to be 3µM (Das Gupta *et al.*, 2005), which is 3 times more than both the values obtained from different methodologies in our laboratory. The results obtained within this study supports the sensitivity of the SYBR green assay for DNA detection (Rengarajan *et al.*, 2002) especially in *Plasmodium*. A possible reason for the discrepancy between the IC_{50} obtained for MDL73811 during this study using the MSF-assay, and the IC_{50} of 3 µM obtained using the [^{3}H]hypoxanthine assay (Das Gupta *et al.*, 2005), may be the differences in incubation times for the assays. The [^{3}H]hypoxanthine assay is completed over a period of 48 h compared to the MSF-assay which spans over 96 h. The increased incubation time of the MSF-assay may therefore result in lower IC_{50}-values.

For all the experiments a dosage of 10 µM (~10×IC_{50}) MDL73811 was used as treatment. This high dosage was used due to the cytostatic nature of MDL73811 on the Plasmodial parasites, and to ultimately ensure complete arrest of all the parasites (Van Brummelen, 2009). The use of lower dosages of MDL73811 treatment in the ring stage, resulted in only incomplete arrest (Van Brummelen, 2009). This is due to the wide synchronisation window of 8-12 h. The MSF-assay used here to determine the IC_{50} of MDL73811, indicated complete arrest at the high concentration of 10 µM (~10×IC_{50}) MDL73811, and no parasite growth when performed over a 96 h period. The high concentration of MDL73811 (10 µM) is not toxic to the parasites, especially since in all the experiments performed within this study (Chapters 3, 4 and 5) the parasites were exposed to MDL73811 for only short periods of time, and therefore the MDL73811 only exert a cytostatic effect. The cytostatic nature of MDL73811 was also demonstrated previsiously with the use of propidium iodide stained parasites. Staining of MDL73811-treated parasites revealed no membrane permeability and therefore confirmed the cytostatic nature of MDL73811 (Van Brummelen, 2009) which can also be reversed by the addition of spermidine and spermine to MDL73811-treated parasites (Wright *et al.*, 1991).

After establishment of the IC_{50} of MDL73811 a morphology study commenced to determine the morphological point of parasite arrest. According to the IDC data the transcript of *Pf(adometdc/odc)* is already produced from about 12 HPI (morphologically in the ring stage) onwards with the maximum transcript production at 24 HPI (trophozoites) and transcript production levels decreasing

soon afterwards with the minimal transcript production at 53 HPI (schizont and merozoites stages). Observation of MDL73811-treated parasites revealed morphological arrest at about 25-30 HPI in the late trophozoite stage, when the drug inhibits the AdoMetDC domain of AdoMetDC/ODC. This was also demonstrated previously with the complete enzymatic inhibition of *Pf*AdoMetDC with 5 µM MDL73811 in which MDL73811-inhibited parasites revealed no decarboxylase activity in either the ring or late trophozoites stages but is also not toxic to the parasite (Van Brummelen, 2009).

Differential regulation of the proteome was observed in Tt_1 and Tt_2. This was especially illustrated by the fact that the correlation for UTt_1:Tt_1 was 0.719 compared to UTt_2:Tt_2 that was 0.664. Direct comparisons were made between the time points, although later time points would have prompted the use of the t_0 reference strategy (van Brummelen *et al.*, 2009) rather than the direct comparison employed here.

This proteomic study employed the use of both 1-DE and 2-DE gel-based methods to determine differentially regulated proteins. It was clearly illustrated that the use of both techniques were complementary to each other since only 5 unique Plasmodial protein groups were shared between the 1-DE AdoMetDC inhibited proteome data and the 2-DE AdoMetDC inhibited proteome data. This was somewhat unexpected since it would have been considered that more proteins would be shared between the 2 gel-based protein separation techniques employed. Although 1-DE does not have the powerful protein separation ability of 2-DE gels, the 1-DE approach does have the advantage that pI constraints do not impact on the proteins that are separated. This was illustrated in that the majority of the proteins that were detected in the 1-DE approach would never be detected on 2-DE due to the pI constraints associated with IPG strips. The pI of some of the identified proteins ranged from 9.6 to 11.8, and even with the use of extremely basic IPG strips it would have been difficult to detect such extremely basic proteins on 2-DE. Therefore, the use of complementary gel-based protein separation techniques as employed here proved an invaluable approach to obtain maximum information on the AdoMetDC inhibited proteome.

One of the proteins detected within this extreme pI range was histone H4 that was decreased in all of the bands. Another histone protein that was detected on the 1-DE gels and decreased in abundance was histone 2B. Histones form part of the nucleosome in eukaryotes and play an important role in chromatin packaging and structural organisation as well as regulation of all aspects of DNA function, which includes transcriptional control and DNA damage responses (Trelle *et al.*, 2009). The histone family consist of 4 histone classes that include H2A, H2B, H3 and

H4 which is regulated by PTM's that include acetylation, methylation, phosphorylation and ubiquitylation (Berger, 2002). These PTM's of the histones creates the "histone code" that may be recognised by transcription factors that will ultimately result in transcriptional responses (Strahl & Allis, 2000) or possible DNA repair (Wurtele & Verreault, 2006) and therefore epigenetic regulation and DNA metabolism control. The histone protein levels detected in the 1-DE AdoMetDC inhibited proteome does not reflect the histone PTM's and therefore only indicated protein abundances and not any type of PTM. Histones are in low abundance in ring and early trophozoite stages but increase in abundance in late trophozoite and schizont stages, which coincides with the parasite going through active DNA synthesis to prepare for schizogeny (Miao *et al.*, 2006). Since the AdoMetDC inhibited protein samples were harvested at 16 HPI and 20 HPI which is in the early trophozoite stages, it is therefore indicative of the sensitivity of the 1-DE coupled with LC-ESI/MS approach which were able to detect proteins that were in low abundance.

Various polyamine specific-proteins were identified within the AdoMetDC inhibited proteome. The protein levels of pyrroline-5-carboxylate reductase (MAL13P1.284) were increased in abundance with AdoMetDC inhibition, while the protein levels of eIF5A (PFL0210c) were decreased in abundance. The increased protein abundance of pyrroline-5-carboxylate reductase (MAL13P1.284) may be as an attempt to utilise L-glutamate-5-semialdehyde for conversion to proline. Closely linked to pyrroline-5-carboxylate reductase (MAL13P1.284) is OAT which is able to catalyse the reversible reaction from L-glutamate-5-semialdehyde into ornithine. Therefore, the regulation of OAT protein abundance may play a role on pyrroline-5-carboxylate reductase (MAL13P1.284) through the regulation of L-glutamate-5-semialdehyde and ornithine. The protein abundance of OAT remained unchanged in Tt_1 and could not be determined in Tt_2 due to the spots of OAT and AdoMet synthase that overlapped on the 2-DE gels. Therefore, the increase in abundance of pyrroline-5-carboxylate reductase (MAL13P1.284) remains unclear, and prompts further investigation into the metabolite levels within this pathway to elucidate the reason for increased protein abundance of pyrroline-5-carboxylate reductase (MAL13P1.284).

The protein abundance of eIF5A was decreased. Although putrescine is formed by ODC with the inhibition of AdoMetDC, its conversion to spermidine is prevented (Das Gupta *et al.*, 2005). The synthesis of eIF5A is dependent on the production of spermidine (Park *et al.*, 1981) and the decreased protein abundance of eIF5A may therefore be as a result of spermidine depletion due to AdoMetDC inhibition. Decreased expression of eIF5A may result in decreased protein synthesis for the parasite. The decreased protein abundance of eIF5A is similar to previous results which were obtained by the inhibition of *Pf*AdoMetDC with SAM486A (Blavid *et al.*, 2010). eIF5A is a unique

small acidic protein and is the only protein that contains the unique amino acid hypusine [N^{ε}-(4-amino-2-hydroxybutyl)lysine] (Park *et al.*, 1991, Park *et al.*, 1997). The spermidine dependent biosynthesis of hypusine in eIF5A is the most specific post-translational modification to date of which eIF5A hypusinylation is essential for eukaryotic cell proliferation (Park, 2006, Cooper *et al.*, 1982) and translational initiation for protein synthesis (Park *et al.*, 1991, Wolff *et al.*, 2007, Molitor *et al.*, 2004, Park, 2006).

Previously, cytostasis has been observed in spermidine-deprived L1210 cells after the inhibition of AdoMetDC and the cytostasis was attributed to the depletion of the hypusine-containing eIF5A (Byers *et al.*, 1994). Similarly, in human colon cancer cells polyamine-depletion also resulted in a cytostatic effect which was attributed to a decrease in protein synthesis as a result of decreased protein expression of eIF5A (Ignatenko *et al.*, 2009). eIF5A is transcribed throughout the *P. falciparum* lifecycle (Molitor *et al.*, 2004, Le Roch *et al.*, 2004, Bozdech *et al.*, 2003), emphasising the importance of this protein in the developmental stages of the malaria parasite (Kaiser *et al.*, 2007) and its involvement in cell proliferation within the parasite (Kaiser *et al.*, 2007, Kaiser *et al.*, 2003b, Kaiser *et al.*, 2003a). Therefore, eIF5A synthesis is dependent on spermidine levels, but it should be noted that only eIF5A protein abundance levels were determined within the AdoMetDC inhibited proteome and the protein abundance does not necessarily determine the hypusinilation of eIF5A which will determine the function of the eIF5A protein. Previous evidence suggests that AdoMetDC inhibition and subsequent spermidine depletion may result in decreased protein abundance of the functional eIF5A protein (Blavid *et al.*, 2010).

Other polyamine-related proteins that were identified during the 2-DE proteomic investigation of inhibited *Pf*AdoMetDC included PNP (PFE0660c), adenosine deaminase (PF10_0289), AdoMet synthase (PFI1090w) and PEMT (MAL13P1.214). The protein abundance of AdoMet synthase was decreased in Tt_1. Two protein isoforms was identified for PNP of which 1 was decreased and the other increased in abundance. Three protein isoforms was identified for PEMT of which 2 were decreased and 1 increased in abundance. Upon validation of the PEMT protein levels with 2-D immunoblotting it was determined that at least 4 protein isoforms exist for PEMT of which all of them had decreased protein expression. The western blot for PEMT was conducted on a 13 IPG strip while the 2-DE gels were performed using 18 cm IPG strips. It is therefore possible that even more isoforms do exist, since the 2-DE gels reveal a cluster of at least 6 protein spots in the range of PEMT that may all be PTM's of PEMT. More than 500 protein PTM's have been discovered, with new ones being added regularly as the technology improves (Krishna & Wold, 1993). The importance of PTM's has recently been demonstrated by the detection of several isoforms that have

differential expression (Nair *et al.*, 2008), which may also be the case for PEMT and PNP in the AdoMetDC inhibited proteome. Few regulatory motifs and transcription regulators have been uncovered in Plasmodial parasites (Coulson *et al.*, 2004) and since transcription within the parasite may be hard-wired (Ganesan *et al.*, 2008) it may suggest that post-transcriptional and post-translational mechanisms are regulating the parasite life cycle as well as have a role in invasion and egress (Chung *et al.*, 2009).

Several heat shock proteins were detected at both time points that included heat shock protein 70 (PF08_0054) that had increased protein abundance in both time points, while heat shock protein 86 (PF07_0029) and heat shock protein 60 (PF10_0153) had decreased protein levels at Tt_1. Heat shock proteins are encountered throughout the erythrocytic life stages of the parasite and can act as chaperones as well as enable the parasite to survive temperature fluctuations often associated with malarial infections (Misra & Ramachandran, 2009). Heat shock protein 70 (PF08_0054) has also been implicated in the transport of nuclear encoded proteins to the apicoplast (Foth *et al.*, 2003). It is therefore not surprising, that upon inhibition of AdoMetDC, the protein abundances of heat shock proteins 70 (PF08_0054) and 60 (PF10_0153) were increased over time from Tt_1 to Tt_2 to help the parasite cope with increased stress.

The protein abundance of actin-1 (PFL2215w) was decreased at Tt_2. In *Trichomonas vaginalis* a 2-DE approach determined that actin-1 consisted of 8 different isoforms which may enable the rapid changes in morphology associated with the parasite (De Jesus *et al.*, 2007). Recently, it has been determined in HeLa cells that polyamines are essential for microtubule formation, and as a consequence polyamine depletion would result in decreased microtubule formation (Savarin *et al.*, 2010). The results obtained with the AdoMetDC inhibited proteome therefore provide evidence that spermidine and spermine depletion as a result of AdoMetDC inhibition within Plasmodial parasites may also hinder microtubule formation.

The protein abundances of leucine aminopeptidase (PF14_0439) and 3 isoforms of the M1-family aminopeptidase (MAL13P1.56) were increased, while HAP protein (PF14_0078), plasmepsin-2 (PF14_0077) and 2 isoforms of falcipain-2 (PF11_0165) had decreased abundances. Elongation factor 2 (PF14_0486) was detected as 3 isoforms of which the protein abundance of 2 isoforms increased, while the other protein isoform had decreased protein abundance. All these proteins play a role in translation and protein synthesis either by providing amino acids from hemoglobin degradation for translation or by initiation of translation. Therefore the AdoMetDC inhibition is able to differentially affect proteins associated with protease activity as well as translation.

Various glycolytic proteins were identified at both time points and had both increased and decreased protein abundance. Hexokinase (PFF1155w) was either at undetectable protein levels or completely absent in the treated samples. The protein levels of phosphoglycerate kinase (PFI1105w) and glyceraldehyde-3-phosphate dehydrogenase (PF14_0598) was decreased in abundance, while pyruvate kinase (PFF1300w) consisted of various isoforms of which 1 had increased protein abundance and 1 had decreased protein abundance. Phosphoglycerate kinase (PFI1105w) and pyruvate kinase (PFF1300w) are the only enzymes able to produce ATP to provide energy during glycolysis (Roth *et al.*, 1988a). $NADP^+$-dependent glutamate dehydrogenase (GDH; PF14_0164) was detected as 3 isoforms. Two of these isoforms were increased in abundance at both Tt_1 and Tt_2, while the other isoform were decreased in abundance at both time points. GDH is present within all the stages of the intraerythrocytic life cycle of the parasite and is the major source of NADPH (Roth, 1990, Wagner *et al.*, 1998). Glycolysis is integral to parasite survival since the parasite relies on a constant supply of glucose and subsequently also imports large quantities of glucose into the erythrocyte for parasite utilisation (Saliba *et al.*, 2003). As a consequence of the large glucose utilisation of the parasite most of the glycolytic enzymes within the parasite are elevated to ensure that the energy needs of the parasite are met (Roth *et al.*, 1988b). Therefore, the AdoMetDC inhibited proteome revealed differential regulation of various isoforms of the glycolytic pathway, although the PTM's associated with the various isoforms needs further investigation to elucidate the functional state of the specific proteins.

T. brucei, T. cruzi and *Leishmania* does not contain catalase (Flohe *et al.*, 1999). *P. falciparum* is also devoid of catalase. The parasite is able to take up the human Cu/Zn SOD from its host to help with detoxification (Fairfield *et al.*, 1983 (b), Fairfield *et al.*, 1983 (a), Fairfield & Meshnick, 1984). Recently it has also been shown that human peroxiredoxin-2 is imported into the parasite cytosol and accounts for 50% of the overall thioredoxin peroxidase activity within the parasite (Koncarevic *et al.*, 2009). Once taken up into the parasite the human peroxiredoxin-2 was detected as 6 protein isoforms in all the intra-erythrocytic life stages of the parasite. CQ drug pressure of the parasites resulted in increased import of the human peroxiredoxin-2 to alleviate oxidative damage (Koncarevic et al., 2009). Previous drug perturbation proteomic studies also detected human peroxiredoxin-2, but it was considered as human contaminating proteins (Makanga et al., 2005, Gelhaus *et al.*, 2005). In the AdoMetDC inhibited proteome both human peroxiredoxin-2 and human Cu/Zn superoxide dismutase were identified by MS and both proteins had decreased protein abundance at Tt_1. Therefore, the decreased protein abundances of the 2 human proteins with AdoMetDC inhibition may be as a result of decreased import of the human proteins into the parasite

in an attempt to preserve energy. The decreased protein abundances of these 2 human proteins may therefore also result in a state of increased oxidative stress within the parasite.

The parasite is heavily dependent on an efficient detoxification system, since both the parasite and the host erythrocyte is under constant oxidative stress due to the presence of oxygen and iron (Muller, 2004). The protein abundance of GST (PF14_0187) was decreased at Tt_1, but increased in protein abundance at Tt_2. The parasite has only one copy of the GST gene (Srivastava *et al.*, 1999) and inhibition of GST would disturb the GSH-dependent processes within the parasite resulting in an increase in the concentration of FPP IX produced during hemoglobin digestion and hence enhanced cytotoxic levels (Deponte & Becker, 2005, Hiller *et al.*, 2006). The trend of increased protein abundance of GST over time may suggest an attempt by the parasite to detoxify toxic metabolites.

2-Cys peroxiredoxin (PF14_0368) was detected in the AdoMetDC inhibited proteome, with the protein abundance of this protein progressively increasing over the 2 time points. 2-Cys peroxiredoxin and 1-Cys peroxiredoxin form part of the thioredoxin superfamily proteins necessary for detoxification that include thioredoxin, glutaredoxin and plasmoredoxin of which plasmoredoxin is unique to Plasmodial parasites (Becker *et al.*, 2003). An increase in the abundances of both the transcript and protein of 2-Cys peroxiredoxin has been reported which was associated with increased oxidative stress within the parasite (Akerman & Muller, 2003). Therefore, the increased protein abundance of 2-Cys peroxiredoxin within the AdoMetDC inhibited proteome may be an attempt by the parasite to cope with the increased oxidative stress within the parasite.

From the AdoMetDC inhibited proteome data obtained at the 2 time points investigated it is proposed that the inhibition of AdoMetDC results in decreased hemoglobin digestion, decreased microtubule formation, differential regulation of glycolytic enzymes and regulation of the redox status of the parasite. The AdoMetDC inhibited proteome is therefore dynamic and able to respond to drug pressure exerted by MDL73811.

In the next chapter, the AdoMetDC inhibited transcriptome will be investigated. Even with the improved 2-DE applied here to the AdoMetDC inhibited proteome only 119 protein spots could be determined that were differentially affected. Therefore, the proteomic study for AdoMetDC inhibition remained limited to soluble proteins within the pI range of 3-10 and molecular weight of 15 to 120 kDa. In an attempt to obtain a more global view and a larger dataset the transcriptome will be investigated with the hope of finding more differentially affected transcripts.

CHAPTER 4

Transcriptional responses of *P. falciparum* to inhibition of AdoMetDC with MDL73811

4.1 Introduction

Microarray technologies consist of thousands of transcripts or even the whole genome on a single chip or array and enable expression profiling of differentially expressed transcripts that may be induced by a certain perturbation. This global overview of the response of organisms to any perturbation makes transcriptomic investigations by microarrays extremely promising technologies to deduce the mode-of-action of drugs (Brazas & Hancock, 2005). The ultimate aim of functional genomics is to increase the number of validated drug targets (Chanda & Caldwell, 2003). An advantage associated with transcriptomic investigations are the large number of data points, which is more than that of gel-based proteomics. Therefore, transcriptomics offer a larger data set and in combination with proteomics can provide a global picture of both the transcriptome and proteome.

4.1.1 Transcriptomic perturbation studies in other organisms

The wealth of information gained with the use of microarrays has been demonstrated in several research fields. Transcriptional responses have been determined for the effect of rapamycin on the immune response of human cell lines (Grolleau *et al.*, 2002), as well as the response of *Staphylococcus aureus* to glycopeptides (Scherl *et al.*, 2006). Similarly, the mode-of-action has also been determined for anti-fungal agents against *Saccharomyces cerevisiae* (Agarwal *et al.*, 2003), and various anti-microbial peptides against *S. aureus* (Pietiainen *et al.*, 2009). The information gained from these transcriptomic studies can then be used in the elucidation and design of new anti-microbial peptides and compounds that will not infer resistance to infection (Pietiainen *et al.*, 2009).

Tuberculosis research has employed microarrays under a variety of conditions to determine the transcriptional response of *Mycobacterium tuberculosis* to various drugs. Transcriptional investigations using Affymetrix array microarrays confirmed the mode-of-action of the tuberculosis drug isoniazid and ethionamide against *M. tuberculosis* (Wilson *et al.*, 1999, Fu, 2006). Signature profiles of the gene expression of isoniazid, thiolactomycin, and triclosan treated *M. tuberculosis*, elucidated that the expression of 21 transcripts were able to distinguish between the mode-of-action of these 3 drugs (Betts *et al.*, 2003). To aid in the identification of gene expression signature profiles of tuberculosis drugs a large scale microarray study was performed on *M. tuberculosis* to

determine the mode-of-action of tuberculosis drugs. A total of 430 microarrays were done for 75 known and unknown tuberculosis drugs to validate their mode-of-action and to provide fingerprint profiles of the transcriptomic response of *M. tuberculosis* to these drugs (Boshoff *et al.*, 2004). Ongoing studies employed the use of Affymetrix oligonucleotide GeneChips to determine the transcriptional response of highly resistant *M. tuberculosis* strains against isoniazid in order to determine the mode-of-resistance (Fu & Shinnick, 2007).

4.1.2 Microarray platforms

Various microarray platforms exist all with their own advantages and disadvantages. NimbleGen has several multiplex arrays which include a 4-plex format (4×72K) with 72,000 probes per array and a 12-plex format (12×135K). Ultra-high density NimbleGen arrays can contain between 385 000 and 2.1 million probes, resulting in the presence of multiple, unique probes. Eppendorf provides pathway-focused DualChip® microarrays that contains two identical microarrays, printed side-by-side, and makes use of Xmer probe technology that contains long sense DNA (200-400 nucleotides) to provide maximum signal and minimal background. Affymetrix has quartz Gene Chips that provide whole genome coverage for humans and contains 28,869 genes each represented by approximately 26 probes spread across the full length of the gene, ultimately resulting in a total of 764 885 distinct probes. These Gene Chips are produced by *in situ* manufacturing of short (25-mer) oligo's on glass by photolithography (Kreil *et al.*, 2005). Agilent provides custom printing of 60-mer oligo's on a slide in a base-by-base manner by a combination of inkjet technology and phosphoramidite chemistry (Wolber *et al.*, 2006). The principle of phosphoramidite chemistry relies on the reactive sites of the nucleotides that are blocked with chemical groups that can then be selectively removed with the progression of synthesis. This process therefore allows the addition of one base at a time in a controlled manner. Overall, this process allows more spots to be printed on an array due to the precision of inkjet printing, as well as better shaped spots (Wolber et al., 2006). Agilent slides were compared to custom microarrays using cDNA long length probes (800-2000 bp) (Hockley *et al.*, 2009). Although great overlap of genes were detected for both arrays, more differentially expressed genes were found using the Agilent slides (Hockley *et al.*, 2009). Overall, Agilent provides greater specificity and sensitivity due to the Agilent 60-mer design, and also provides the opportunity to investigate various organisms like *Plasmodium* with the custom array design. Comparisons between platforms are constantly being investigated together with validation of these results by quantitative real-time polymerase chain reactions (qRT PCR) (Hester *et al.*, 2009, Baumbusch *et al.*, 2008, Arikawa *et al.*, 2008, Wang *et al.*, 2006).

4.1.3 Experimental design and normalisation methods

Microarrays provide a technology for comparing the expression profiles of genes across the entire genome. The arrow annotation (Figure 4.1) used, was proposed by Kerr and Churchill in 2001(Kerr & Churchill, 2001). Each arrow is representative of a single microarray. The point of the array is indicative of the sample labelled with Cy3 (green channel), while the base of the arrow is representative of the sample labelled with Cy5 (red channel). The symbols are representative of the samples used for analysis (Kerr & Churchill, 2001).Various designs are possible for two colour arrays (Figure 4.1). The direct design is used to make direct comparisons between two samples (Figure 4.1 a). Dye swaps are often used in direct designs to compensate for possible dye bias that may exist. A variety of reference designs does exist (Figure 4.1 d, e, h) that include a single reference or a combined reference design.

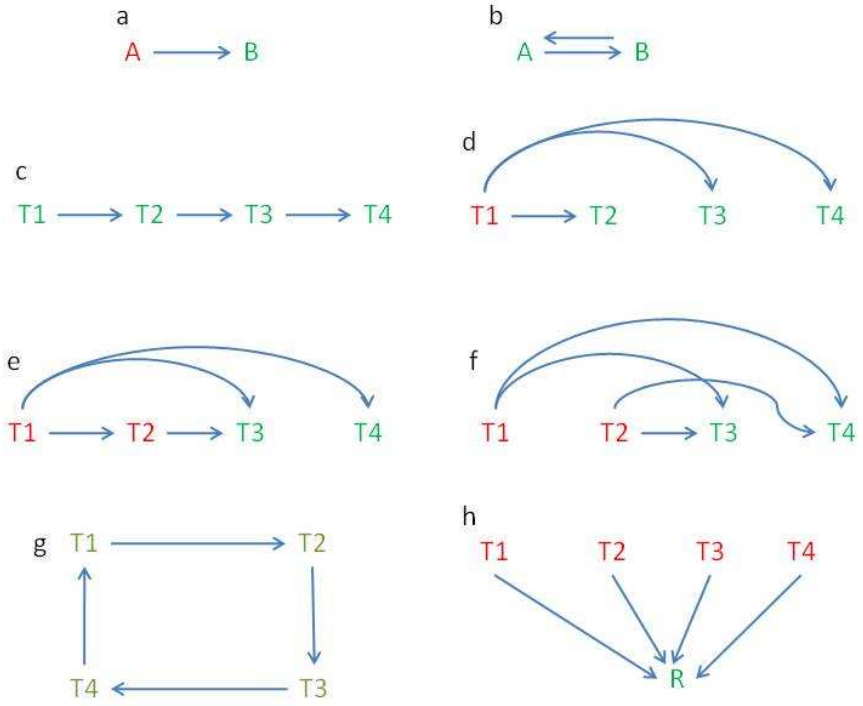

Figure 4.1: Microarray designs for time course experiments (Yang & Speed, 2002).
(a)Common design to use only one microarray, (b) dye swap design, (c) direct sequential design, (d) T1 as common reference, (e) T1 as common reference, (f) direct mixed design, (g) direct loop design, (h) common reference

The reference design is the most commonly used design (Dombkowski *et al.*, 2004, Churchill, 2002), which has the advantage of simplicity and the ease to add arrays, although to its disadvantage is limited experimental design (Kerr, 2003). The use of a reference design allows easy expansion of an experiment as long as each additional sample was included in the reference sample. Reference designs have higher variability than direct designs, but have the added advantage that all the comparisons that are made in reference designs are made with equal efficiency since the

samples are always compared to the same reference sample (Churchill, 2002). Therefore, in a reference design the differential abundance of any sample can be determined in relation to the other samples as long as all the samples that are compared were included within the reference sample.

Normalisation of microarray data is used to remove systematic bias and variation that is introduced into the sample by technical artefacts, though it is important to still maintain the important biological variations, therefore creating unbiased microarray variation between the samples that are to be analysed (Quackenbush, 2002, Oshlack *et al.*, 2007). Normalisation of microarray slides may also be used to compensate and correct for differences that exist in the microarray experimentation rather than the biological data (Smyth & Speed, 2003). Various normalisation methods exist for correcting microarrays and can be applied in two classes which include within-array normalisation which is normalisation of the M-values (log transformation of Cy3/Cy5) and between-array normalisation which is normalisation of the intensities ($\log_2$-ratios) to be comparable between all the arrays within the dataset (Smyth *et al.*, 2008). The M-value is defined as the log transformation of Cy3/Cy5 while the A-value is defined as the log transformation of the squared root of Cy3×Cy5. Linear model for microarray data (LIMMA) is a package for the analysis of microarray data and are used to obtain differentially regulated transcripts from the microarray data. Print-tip Loess is the default normalisation method used by LIMMA, but is generally unreliable when less than 150 spots per print-tip are used. Global Loess normalisation assumes that the majority of the oligo's is not differentially expressed, but does not assume that the number of up- and down-regulated genes is equal (Smyth *et al.*, 2008). Another option is Robust Spline normalisation which is an empirical Bayes compromise between print-tip and global Loess normalisation. It makes use of a 5-parameter regression spline that is used in place of the Loess curves (Smyth *et al.*, 2008). Within-array normalisation only affects the M-values and not the A-values. Normalisation of the A-values, which result in similar distribution across all arrays, makes use of quantiles that can correct for the individual red and green channels (Smyth *et al.*, 2008). R-quantile and G-quantile normalisation is useful for reference designs since R-quantile will normalise the samples labelled with red (Cy5), while G-quantile will normalise the samples in green (Cy3). Therefore, if the reference sample was labelled with Cy5 throughout in a reference design, it will be useful to use R-quantile for normalisation in order to correct the reference sample similarly across all arrays.

4.1.4 Minimum information about a microarray experiment (MIAME)

Microarray technology provides a large scale high-throughput method to investigate the transcriptional response of any organism to any stimuli. One of the drawbacks of microarray

analysis is the generation of large volumes of data and to maintain high standards of microarray analysis and to enable the comparison of microarray data between laboratories, it is necessary to set a standard for microarray data. The minimum information about a microarray experiment (MIAME) was established to ensure equivalent data to be reported for various microarrays (Brazma *et al.*, 2001). Three main levels of data reporting are important for microarray experiments and include the scan images which is the raw data, the quantitative output of the data, and the derived measurements (Brazma *et al.,* 2001). Detailed information regarding experimental design, sample preparation, hybridisation conditions, array type, array manufacturer, the number and size of the spots printed on the array as well as all the information regarding the generation of data should be given (Brazma *et al.,* 2001). For the reporting of such information various databases have been created to deposit microarray data. One such data repository is the National Centre for Biotechnology Information Gene Expression Omnibus (NCBI GEO, www.ncbi.nlm.nih.gov/geo) which provides an accession number that can be searched for easy access to all the relevant data.

4.1.5 Transcriptomic perturbation studies in Plasmodial parasites

The transcriptional response of Plasmodial parasites under CQ pressure analysed by serial analysis of gene expression (SAGE) revealed 100 regulated transcripts that included groups of transcripts involved in oxidative stress, hemoglobin digestion and proteins synthesis (Gunasekera *et al.*, 2003). Further, microarray investigations of Plasmodial parasites under CQ pressure revealed differential expression of 600 transcripts of which 41% were cell-cycle related (Gunasekera *et al.*, 2007). The transcriptome of doxycyclin-treated *P. falciparum* revealed a delayed death effect in which parasites were able to invade erythrocytes after the first cycle but died soon thereafter (Dahl *et al.*, 2006). This effect was most likely due to loss of the apicoplast function with loss of mitochondrion function as a secondary effect (Dahl *et al.,* 2006). Stress responses on the Plasmodial parasite elicited by febrile temperature (41^{o}C) commonly associated with malaria infections, identified 336 transcripts that were differentially regulated of which 162 (49%) had increased abundance and 173 (51%) decreased abundance (Oakley *et al.,* 2007). Severely affected transcripts were involved in stress responses, cell surface adhesion and, a large number of regulated transcripts containing a PEXEL sequence associated with protein export to the erythrocyte, therefore indicating a possible extrusion to the erythrocyte or even erythrocyte remodelling and parasite sequestration (Oakley *et al.,* 2007). Perturbation with artesunate resulted in 398 transcripts identified as differentially expressed of which 244 had increased abundance and 154 decreased abundance. The majority of the latter were classified as chaperones, transporters, kinases, and transcription activating proteins, oxidative stress and cell cycle regulation (Natalang *et al.*, 2008). The transcripts that displayed an

increase in transcript abundance contained a large number of export proteins and transporter transcripts which may result in drug resistance (Natalang et al., 2008). In one of two histone-related microarray studies, histone acetyltransferase was inhibited using anacardic acid which resulted in hypo-acetylation of histone H3 (Cui *et al.*, 2008). Of the 271 transcripts that were differentially expressed 207 were decreased and only 64 increased in abundance. This major decrease in transcript abundance is probably as a result of the hypo-acetylation which will lead to gene silencing and therefore have a pronounced effect on transcription (Cui *et al.*, 2008). In the other study, histone deacetylase activity was inhibited with apicidin which resulted in profound transcriptional changes within the parasites (Chaal *et al.*, 2010). Transcription factors were affected by the inhibition and especially schizont-stage genes were severely affected. Overall the inhibition of histone deacetylase resulted in complete de-regulation of the IDC transcriptional cascade (Chaal *et al.*, 2010). The most recent microarray study, the expression of genes in response to 20 different compounds resulted in arrest in the schizont stage (Hu *et al.*, 2010). A total of 3000 differentially affected transcripts were identified demonstrating that functionally related genes share transcription profiles even with all the different perturbations, since they may also share similar regulatory mechanisms that are associated with transcription rather than mRNA decay (Hu *et al.*, 2010).

4.1.6 Polyamine perturbation studies on Plasmodial parasites

The first polyamine depletion study on *Plasmodium* was done using suppression subtractive hybridization (SSH) in which pre-selected libraries were created and subsequently used for microarray analysis (Clark *et al.*, 2008). Plasmodial parasites were treated with DFMO to inhibit ODC and consequent putrescine depletion. Interesting polyamine-specific responses included the increased transcript abundance of OAT and hypoxanthine phosphoribosyltransferase (HPPRT) (Clark *et al.*, 2008). A follow-up study, the co-inhibition of AdoMetDC/ODC with DFMO and MDL73811, respectively induced total polyamine depletion (van Brummelen *et al.*, 2009), and revealed the differential regulation of 538 transcripts of which 171 had increased abundance and 377 decreased abundance. Treated parasites were arrested in the trophozoite stage while untreated parasites progressed through their life cycle, which therefore prompted the use of a t_0 reference time point to which the treated parasites best correlate. Analysis of the differentially regulated transcripts revealed a polyamine-related response with increased transcript abundance of OAT and lysine decarboxylase (LDC) and decreased abundance of AdoMet synthase (van Brummelen *et al.*, 2009). Inhibition of spermidine synthase (SpdS) with cyclohexylamine was also investigated at 3 time points and revealed the differential regulation of various polyamine-dependent transcripts (Becker *et al.*, 2010).

Microarray technologies enable the expression profiling of transcripts induced by perturbation. Given the advances in Plasmodial transcriptomics and the promising data obtained from 3 other polyamine depletion studies, the transcriptional response to inhibition of AdoMetDC with the irreversible inhibitor MDL73811, will be investigated in this chapter.

4.2 Methods

4.2.1 Culturing of parasites for transcriptomics

*Pf*3D7 parasites were maintained *in vitro* in human O^+ erythrocytes in culture media and monitored daily through light microscopy of Giemsa stained thin blood smears as described in Chapter 2 section 2.2.3. Before treatment could commence the parasites were always synchronised for 3 consecutive cycles (6 times in total, always 8 h apart once in the morning and later in the afternoon) as described in section 2.2.4. A starting parasite culture (in the schizont stage) at 2% parasitemia, 5% hematocrit was treated with 10 µM MDL73811 ($10\times IC_{50}$) at invasion after which the parasitemia increased to 10% in both the treated and untreated samples in the ring stage. Treatments were always done in duplicate cultures with 2 biological replicates for both treated and untreated samples. Cultures were split into 4 separate flasks of which 2 were the untreated parasites (control) and 2 were the MDL73811 treated parasites. Ten millilitres of parasite cultures at 10% parasitemia and 5% hematocrit were used per sample. A small scale morphology study was always conducted at the same time, and used as a positive control to ensure that complete inhibition (cell cycle arrest) of the *Pf*3D7 parasites did occur with the use of the MDL73811. At 3 different time points (t_1 = 16 hours post-invasion (HPI), t_2 = 20 HPI and t_3 = 26 HPI) cells were harvested by centrifugation at 2500×*g* for 5 min, followed by washing of the cell pellet twice with PBS. These time points were chosen due to the peak transcript production of AdoMetDC that occur between 18-40 HPI. The erythrocyte pellet containing the parasites was snap frozen and stored at -80°C until use.

4.2.2 RNA isolation from cultured parasites

RNA was isolated from untreated and treated *Pf*3D7 parasites for the 3 time points in an RNAse free environment using a combined RNeasy Mini Kit (QIAGEN) and TRI-Reagent (Sigma) method, with the incorporation of DNase I on-column digestion (QIAGEN). The RNA isolation procedure does not make use of saponin lysis of the erythrocytes, in order to prevent possible contamination of human and bovine RNA that may be released upon lysis of the erythrocytes. The tubes containing the frozen infected erythrocyte pellets were removed from -80°C and thawed. The pellet was loosened by flicking the tube, before the addition of 600 µl RLT lysis buffer (Proprietary, QIAGEN) to the pellet and mixed by vortexing. The mixture was transferred onto a QIA-Shredder column (QIAGEN) and centrifuged at 15 700×*g* for 2 min. The eluate of each QIA-Shredder column was divided into 2 equal parts and transferred to clean microfuge tubes. TRI-Reagent (600 µl) was added and mixed by vortexing after which the mixture was incubated at room temperature for 5 min. TRI-reagent contains phenol/guanidine that denatures proteins and therefore inhibits

possible RNAse activity. This was followed by the addition of 400 µl chloroform to each tube and vigorous vortexing. The chloroform separates the homogenate into an upper aqueous phase and a DNA interphase with the lower organic phase containing the denatured proteins. The chloroform containing mixture was incubated at room temperature for 10 min followed by centrifugation at 15 700×*g* for 15 min. The upper aqueous phase of each tube was transferred to clean microfuge tubes to which 700 µl of 70% (v/v) ethanol was added to precipitate the RNA. The mixtures in the two tubes that were split earlier were combined and 700 µl was loaded onto an RNeasy column and centrifuged at 8000×*g* for 15 s. This was repeated until all the sample was loaded onto a single column. Wash buffer RW1 (350 µl, proprietary, QIAGEN) was added and centrifuged at 8000×*g* for 15 s to wash the membrane containing the RNA. For the on-column DNase I digestion, 70 µl Buffer RDD (Proprietary, QIAGEN) was combined with a 10 µl aliquot of DNase I before the addition of this mixture directly onto the membrane. The membrane containing the DNase I mixture was incubated at room temperature for 15 min. The membrane was washed by the addition of 350 µl wash buffer RW1, centrifuged at 8000×*g* for 15 s followed by another two wash steps with 500 µl wash buffer RPE, and centrifuged at 8000×*g* for 15 s to remove all residual ethanol. The RNeasy column was placed in a clean 2 ml collection tube and centrifuged again at 15 700×*g* for 1 min to ensure that the membrane was dried completely and that absolutely no residual ethanol is present. The RNeasy column was transferred to another clean 2 ml microfuge tube, and 30 µl RNase free water was added directly onto the membrane and incubated for 2 min before centrifugation at 8000×*g* for 1 min to elute the RNA. The RNA concentration and purity was determined on the Gene Quant (GE Healthcare) and stored at -80°C until cDNA synthesis.

4.2.3 RNA integrity determination

The RNA integrity and purity was assessed using the Experion automated electrophoresis system (Bio-Rad). The RNA was prepared and run according to the manufacturer's instructions on a Lap-Chip microfluidic separation technology using a fluorescent sample detection method. All the gel-based steps which include sample preparation, staining, and destaining, imaging, band detection, and data analysis are automatically performed by the system (Delibato *et al.*, 2009).

4.2.4 cDNA synthesis from RNA

Due to the difficulty in isolating mRNA from *P. falciparum* parasites that is representative of the complete sample an approach was followed in which RNA was isolated from the parasites for cDNA synthesis (Bozdech *et al.*, 2003). A RNA reference pool was constructed by using 2 µg total RNA from each of the twelve samples resulting in a representative RNA reference pool. First strand

cDNA synthesis was initiated using 2 µg RNA of the reference or individual samples, 775 pmol random primer nonamer (Inqaba), 250 pmol OligodT (dT_{25}) (Inqaba) and incubated at 70°C for 10 min, followed by 10 min at 4°C. After this incubation step, 1.7 µl of the 10× aminoallyl dNTP mixture (10 mM dATP, 5 mM dCTP, 5 mM dGTP, 5 mM dTTP, 5 mM aminoallyl-dUTP), 6µl of the 5× SuperScript First-strand buffer, 10 mM DTT, 40 U rRNasin (RNAse Inhibitor, ProMega) and 340 U Superscript III Reverse Transcriptase (Invitrogen) were added, mixed and incubated at 42°C for 18-20 h for cDNA synthesis. The high amount of dNTPs allowed the synthesis of the A+T-rich cDNA of the Plasmodial genome. Contaminating RNA was removed by hydrolysis with the addition of 1 M NaOH, and 0.5 M EDTA, pH 8 to the reaction mixture and incubating at 65°C for 15 min. The cDNA were purified using the PCR Clean-up kit (Macherey-Nagel) and is based on the principle that the DNA binds to the silica matrix in the presence of choatropic salts. These salts are then removed by the addition of alcohol based buffers after which the DNA is eluted in water. In short, ten volumes of the binding buffer NT was added to the cDNA mixture and then transferred to a Nucleospin extract II column and incubated for 4 min on the column before centrifugation at 13 000×*g* for 1 min, followed by washing of the silica membrane. The cDNA was subsequently eluted by the addition of 30 µl pre-heated RNAse-free SABAX water (Adcock) (37°C) directly onto the membrane and incubated for 4 min before centrifugation at 13 000×*g* for 90 s to elute the cDNA. The cDNA concentration and purity was measured on a Nanodrop-1000 (Thermo).

4.2.5 cDNA labelling for hybridisation

cDNA (1.2–2 µg) for each of the individual samples were dried *in vacuo* and then resuspended in 2.5 µl SABAX water followed by the addition of 5 µl 0.2 M Na_2CO_3, pH 9.0 and 2.5 µl of the respective dye to each sample. The aminoallyl-dUTP incorporated during cDNA synthesis was used to couple the Cy-dyes to the samples. The reference pool was labelled with Cy3 (green) and the samples for each of the time points were labelled with Cy5 (red) using a common reference design (Figure 4.2).

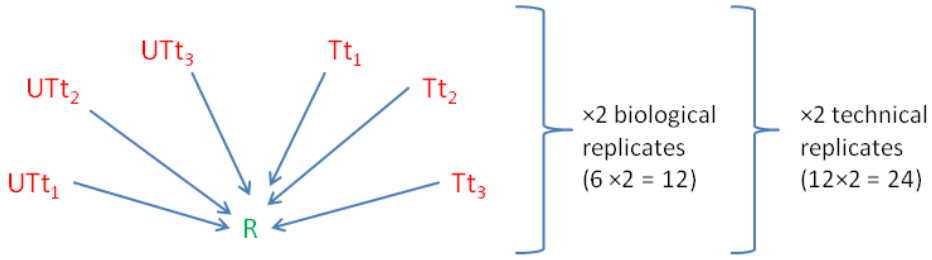

Figure 4.2: Common reference design used for the inhibition of AdoMetDC.
The reference was labelled with Cy3 (green) and all the samples were labelled with Cy5 (red). The reference sample contains equal amounts of all the samples and is therefore representative of all samples. 24 arrays were done in total since two biological replicates and two technical replicates of each sample were done.

The samples were incubated in a desiccator in the dark for 2 h at room temperature. This is done since the Cy-dyes used for labelling is sensitive to ozone degradation and because it is a fluorophore it is light sensitive. Excess dye was removed with the QIAquick PCR purification kit (QIAGEN). In short, 10 volumes of buffer PBI were added to the sample, mixed and applied directly onto a QIAquick column and incubated for 4 min before centrifugation for 1 min at 13 000×*g*. Three wash steps were performed by adding 500 µl Buffer PE followed by centrifugation at 13 000×*g* for 1 min, after which the membrane were dried. 30 µl pre-heated water (37°C) were applied directly onto the membrane and incubated for 4 min followed by elution at 13 000×*g* for 90 s. The dye incorporation and concentration were determined using the microarray setting on the Nanodrop-1000. The coupling efficiency was calculated (Equation 4.1), and should be at least 10 labelled nucleotides per 1000 nucleotides to proceed with hybridisation.

The coupling efficiency for each reaction was determined using the following formulae:

$$\text{Efficiency} = \frac{\text{pmol dye} \times 324.5\ \text{pg/mol}^*}{\text{ng DNA}} \qquad \text{Equation 4.1}$$

*324.5 pg/mol is the average mass of a dNTP

4.2.6 Slide assembly and sample preparation for oligonucleotide hybridisation

Equal amounts of the Cy5 labelled sample and Cy3 labelled reference pool (20 pmol each) were added in a PCR tube (40 pmol in total). For the 8×15K *P. falciparum* Agilent slides, 5 µl of the 10× Blocking buffer (Proprietary, Agilent), 1 µl of the 25× Fragmentation buffer (Proprietary, Agilent) and finally SABAX water to a total volume of 25 µl was added to the Cy-labelled samples. The mixture was incubated at 60°C for 30 min to fragment any remaining RNA. This was followed by the addition of 25 µl 2× GE hybridisation buffer (Proprietary, Agilent) to the sample mixture. It is important not to vortex this mixture as this will introduce bubbles, and should therefore be mixed by careful pipetting and then put on ice during array loading. 40 µl of each sample was loaded onto

each array to obtain a final sample concentration of 20 pmol. Care should be taken not to introduce bubbles as this might introduce problems during hybridisation. Before sample loading the slide is assembled by loading a gasket slide into the assembly chamber. The 40 µl sample was then loaded onto the gasket slide. The slide containing the printed arrays was placed on top of the gasket slide containing the samples. The arrays were sealed by tightening the screw onto the chamber. The chamber containing the arrays was placed in the hybridisation oven at 65°C for 17 h at a rotational speed setting of 10.

4.2.7 Post-hybridisation, washing and slide scanning

After hybridisation the array slide was removed from the chamber and disassembled in wash buffer 1 (Proprietary, Agilent). The slide was washed twice in pre-heated (37°C) wash buffer 2 (Proprietary, Agilent) for 1 min each. Finally the slide was dried in a centrifuge for 1 min after which it was scanned on an Axon GenePix 4000B scanner (Molecular Devices).

4.2.8 Data analysis

The original *P. falciparum* Operon Array containing 8089 70-mer gene probes was adapted to the 60-mer Agilent platform by Mr J Verlinden (J. Verlinden, MSc thesis in preparation). In short, all the unnecessary 'NULL' annotations and corresponding oligonucleotide sequences, used as controls specific to the Operon platform, were removed. The remaining 7004 oligonucleotides were adapted to the 60-mer Agilent platform by shortening their sequences using a 10-mer scanning window from both 3' and 5' ends and keeping the annealing temperature close to 65°C using the following equation:

$$*Tm = 64.9°C + 41°C\ (GC-16.4)/N \qquad \text{Equation 4.2}$$

*Tm is the annealing temperature for microarray hybridisation, GC is the number of G and C nucleotides in a target sequence, N is the total length of the sequence

The shortened sequences were validated by submitting the target sequence to NBLAST (www.ncbi.nlm.nih.gov/BLAST). All sequences submitted to NBLAST analysis had E-values below 10^{-6}. In addition to adapting the *P. falciparum* Operon Array, the most recent annotated form of the *P. falciparum* (strain 3D7) genome from PlasmoDB 5.4 (www.plasmodb.org) was used to design a new 60-mer based array to overcome ambiguities in previous annotations used for the Operon array dataset. The Agilent 60-mer probes were designed by submitting the FASTA files into ArrayOligoSelector (AOS) in order to design the 60-mer probes from the various target sequences

(http://arrayoligosel.sourceforge.net/). The designed target sequences were once again validated using NBLAST. The designed probes were then submitted to Agilent for printing of the slides.

Each array was analysed with Axon GenePix Pro 6.0 software (Molecular Devices). The spots of each array were analysed according to the criteria of the five parameters in Table 4.1 (parameter and function for the cut-off values). Spots not fulfilling the specified criteria were flagged and received a zero weight value (Table 4.1).

Table 4.1: Parameters set for automated spot detection using GenePix.

Parameter	Function[a]	Flag[b]	% of flagged spots[c]
Circularity of spots	[Circularity] < 40 Or [F Pixels] < 50	Bad	0
CV of scan channels	[F532 CV] > 400 Or [F635 CV] > 400	Bad	0.2 – 3.8
Intensity	[F532 Mean] < 150	Absent	15.2 – 36.9
Saturation	[F532 % Sat.] > 20 Or [F635 % Sat.] > 20	Bad	0.3 – 2.9
Signal to noise ratio	[SNR 532] < 3 And [SNR 635] < 3	Bad	19.8 – 45.4

Automated spot detection parameters used for GenePix to flag spots if they did not qualify according to the criteria set. [a]is the function used to set the criteria in GenePix. [b]flag is how the spot is marked as not useable. [c]the percentage range for each of the parameters set for the 24 arrays and is indicative of the percentage of spots that were flagged for each of the parameters. F Pixels is the minimum number of pixels for an intensity measurement. 532 nm is the red channel and 635 nm is the green channel. CV is the coefficient of variation. Circularity is a measure of the shape of the spot.

For further data analysis and identification of differentially expressed transcripts, the LIMMA (Smyth *et al.*, 2005b) and LIMMA-GUI (Wettenhall & Smyth, 2004) packages were used. This included the mArray package that provides alternative functions for reading and normalising spotted microarray data and overlaps with the LIMMA package, while LIMMA-GUI provides more graphical user interfaces. All these packages are from Bioconductor (www.bioconductor.com) and are freely available. Background correction was performed on all arrays with a subset of 50 (Ritchie *et al.*, 2007). Within-array normalisation made use of robust spline normalisation, followed by between-array normalisation making use of Gquantile normalisation due to the common reference that was used and always labelled with Cy3 in the green channel (Smyth & Speed, 2003). Pearson correlations were calculated for each of the time points. The differentially expressed transcripts were determined by comparing UTt_3 to Tt_3 and making use of the linear modelling approach (lmFit) and the empirical Bayes statistics (eBayes) (Smyth *et al.*, 2005a). All transcripts with a $\log_2$ ratio $\geq$ 0.75 or $\leq$ -0.75 and a p-value of less than 0.05 were considered as significant. This related to a fold change (FC) of 1.7 and -1.7. The FC is calculated from the $\log_2$ ratio in Microsoft EXCELL™ 2007 using the equation: FC = POWER(2, $\log_2$-value) Equation 4.3

Therefore, a $\log_2$-ratio of 1 is similar to a FC-value of 2 and a $\log_2$-ratio of 0.75 is equal to a FC-value of 1.7. The list of differentially regulated transcripts was submitted to PlasmoDB 6.0 (www.plasmodb.org) to obtain the GO terms of each of the transcripts. The transcripts were then

manually sorted according to their biological function and GO term and grouped together. Each group were submitted to MADIBA (www.bi.up.ac.za/MADIBA) to verify the GO terms and groupings. To determine the biological pathway most affected by the perturbation study all the differentially expressed transcripts were submitted to MADIBA to determine the significant metabolic pathway affected, together with a p-value as calculated by Fishers test (Fisher, 1935).
Hierarchical clustering was performed on all the data using CLUSTER 2.1.1 (http://rana.stanford.edu.software). Only data that had expression values in all of the time points were used for clustering to avoid blank spots upon clustering. Clustering of data was performed using average linkage clustering which indicates that the distances between transcripts are calculated on average vales and uncentered symmetric correlation which assumes that the average is zero. Clustering data was visualised in TREEVIEW 1.6 (www.EisenSoftware/ClusterTreeView/TreeView).

The STRING (Search Tool for the Retrieval of Interacting Genes/Proteins) 8.0 database covers 2.5 million proteins from 630 organisms (http://string.embl.de) (Jensen *et al.*, 2009). The curated database is able to provide a comprehensive view of protein-protein interactions (http://string.embl.de) (Jensen *et al.*, 2009) by experimental repositories, computational prediction methods and public text collections. STRING scores and weighs protein interactions. The basic interaction unit is the functional association which is specific and meaningful between two proteins that jointly contribute to the same functional process. AdoMetDC was submitted to the web-based programme to determine possible protein-protein interactions.

Finally, the differentially affected transcripts from the AdoMetDC-inhibited parasites were submitted to the *P. falciparum* interactome (www.plasmomap.org) (Date & Stoeckert, 2006, Wuchty *et al.*, 2009). The *P. falciparum* interactome was constructed *in silico* using Bayesian frameworks (Date & Stoeckert, 2006, Wuchty *et al.*, 2009).

Comparisons made between the AdoMetDC-inhibited data and the artesunuate, CQ, and febrile temperature studies as well as the comparisons made between the AdoMetDC-inhibited data and the co-inhibition study and spermidine synthase inhibition study was done using Microsoft EXCELL™ 2007. The PlasmoID identifiers of each study were submitted to the EXCELL™ worksheet. The VLOOKUP function in EXCELL™ was used to compare all the different studies at once and considered only if the PlasmoID was present or not.

4.2.9 Validation of microarray results with qRT-PCR

The treated and untreated cDNA from all the samples were diluted to 0.65 ng/µl with SABAX water for use in qRT-PCR. A standard curve was constructed from a dilution series of UTt_1 samples that contained the following dilutions: an undiluted sample, 1/10, 1/20, 1/50 and 1/100 dilutions. Cyclophillin was used as household transcript and used to construct the standard curve. The reactions were performed in a 384-well plate using the Lightcycler 480 (Roche). The total reaction volume was 10 µl and consisted of 5× KAPA SYBR FAST qPCR reaction mixture, 0.1625 ng/µl cDNA and 1 pmols each of both the forward and reverse primers for each individual reaction. The reaction mixture was pre-incubated at 95ºC for 10 min. This was followed by 48 amplification cycles that each consisted of denaturation at 95ºC for 10 s, annealing at 55ºC for 5 s and extension at 72ºC for 7 s. Fluorescence was detected at the end of each cycle. Amplification was followed by melting curve analysis to detect possible primer-dimers and to determine the specific melting temperature (TM) of each product. The thermal profile of melting curve analysis consisted of incubation at 95ºC for 5 s, 65ºC for 5 s and 95ºC for denaturation with continuous measurement of fluorescence. Finally the reaction mixture was cooled to 40ºC for 30 s. The fold change was calculated for each sample by comparing the untreated samples to the treated samples for each specific time point and then normalised to cyclophillin that remained unchanged in all 3 time points.

4.3 Results

4.3.1 RNA quality assessment

Parasite culture, *Pf*3D7 (10 ml) at 10% parasitemia were sampled at 3 time points (t_1: 16 HPI, t_2: 20 HPI, and t_3: 26 HPI) for RNA isolation and subsequent transcriptomic investigation of MDL73811-treated parasites (Figure 4.3). Figure 4.3 is a morphological representation of the parasites harvested at the 3 time points used for the transcriptomic investigation.

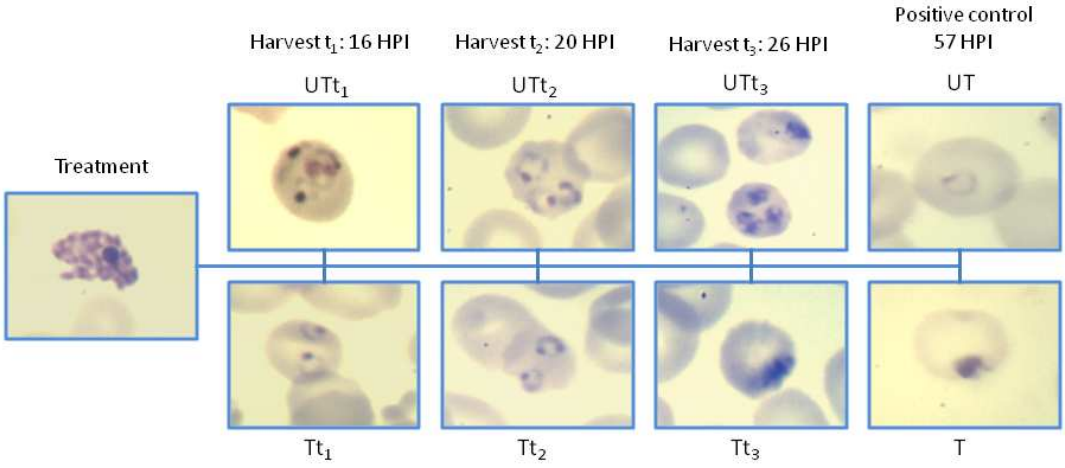

Figure 4.3: Transcriptomic sampling points.
Treatment with MDL73811 was done at invasion. Three time points were taken for the transcriptomic analysis (t_1: 16 HPI, t_2: 20 HPI, and t_3: 26 HPI). The positive control is included to ensure arrest of the MDL73811-treated parasites while the untreated parasites have progressed to a new life cycle with rings being formed.

The RNA integrity number (RIN) or RNA Quality Indicator (RQI) provides the most accurate and reproducible account of RNA integrity, and requires very small amounts of sample per run (Imbeaud et al., 2005). Three of the 12 RNA samples (UTt_3, Tt_3, and Tt_1) were therefore chosen randomly to run on the Experion system (Bio-Rad). All 3 samples (Ut_3, Tt_3 and Tt_1) had RQI values in excess of 9 indicating high quality, non-degraded RNA (Figure 4.4). The RQI number is based on 3 regions of the electropherogram and should be between 1 and 10, with 1 the most degraded, and 10 the most intact RNA. RQI values between 7 and 10 are considered as good intact RNA samples, but the compatibility of the RQI number with down-stream applications should be determined by the user (Buhlmann *et al.*, 2004).

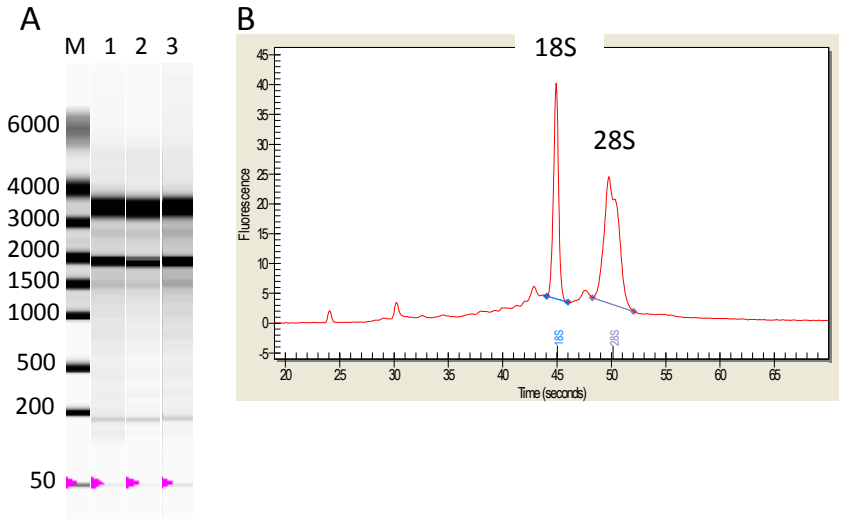

Figure 4.4: Assessment of RNA purity and integrity from the *P. falciparum* RNA that will be used for microarray analysis.

(A) Virtual gel image of RNA samples with lane 1: UTt_3(9.1; 1.47), lane 2: Tt_3(9.4; 1.5), lane 3: Tt_1(9.0; 1.49). RQI number is the first number given in brackets, followed by the 28S/18S ratio. (B) is representative of the electropherogram indicating the 18S and 28S rRNA subunits. No RNA degradation is visible since no peaks is found except the rRNA subunits as indicated.

The RNA electropherogram in Figure 4.4 illustrates the clearly distinguishable bands, the lack of smears, and the 28S rRNA subunit that has higher intensity than the 18S rRNA subunit therefore indicating good RNA quality (Copois *et al.*, 2007). Good RNA yields (ranging from 3 µg in the ring stage to 18 µg in the untreated trophozoite stages) were obtained and none of the RNA had any indication of either protein or DNA contamination and was therefore used for the microarray analysis to follow.

4.3.2 Microarray preparation

A Plasmodial Agilent microarray platform was used that enabled the simultaneous analysis of 8 different samples on a single slide (J. Verlinden, MSc thesis in preparation). Each of the slides used consisted of 8×15 K hybridisation chambers that could each be prepared for a different sample. The Agilent arrays required only 4 µg RNA per sample for a complete experiment. Figure 4.5 is an example of a typical Agilent array from *Pf*3D7 representing an untreated and treated array from time point 3. The 4 corners of each of the arrays contained several control spots that was used for assessment of hybridisation of the samples (Figure 4.5). The treated array has an overall yellowish colour that is associated with differences between the treated and untreated arrays (Van Brummelen, 2009). Also notice the differences on the enlarged inserts between the Tt_3 array which is yellowish

or green whereas the UTt_3 array has several yellow, green and red spots associated with the differential expression of transcripts as the parasite progress through its life cycle. Due to the use of the inkjet technology of the Agilent system all the spots are exactly the same size, which was previously tedious to achieve. Overall, the use of the Agilent arrays resulted in better quality microarray data, and confidence in analysis.

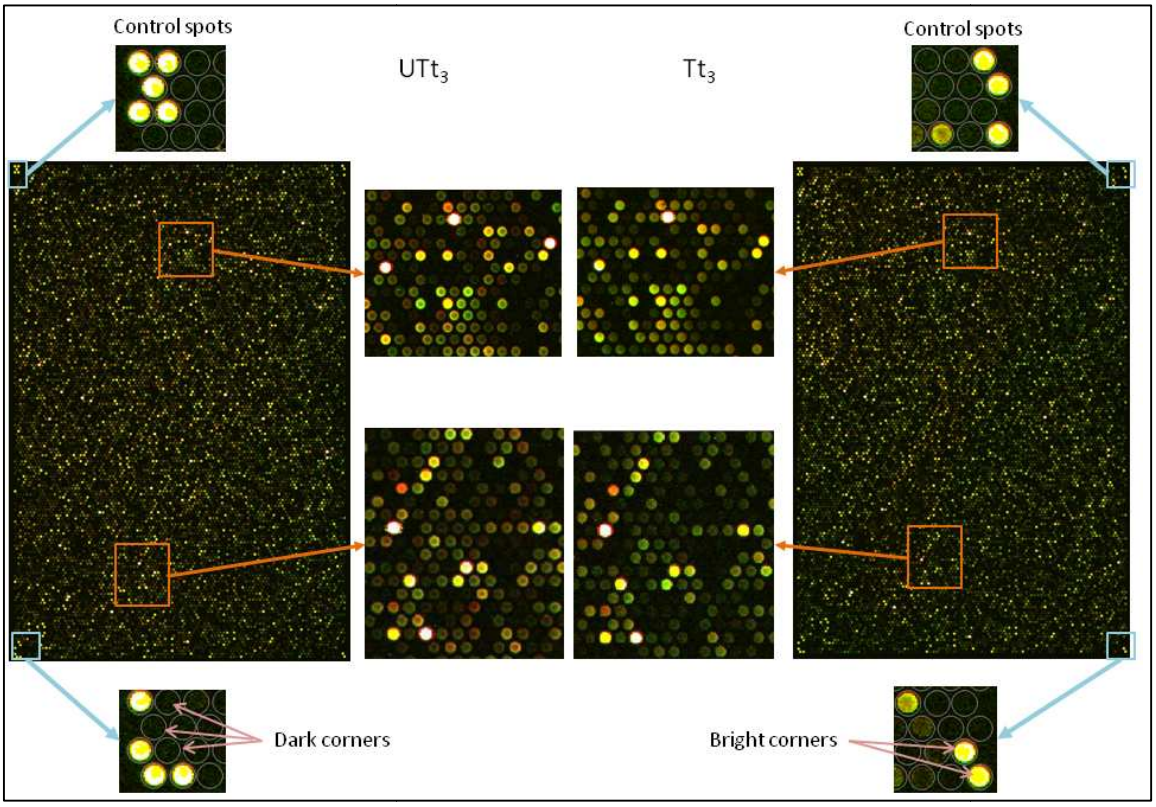

Figure 4.5: The 60-mer Agilent array for one UTt_3 and one Tt_3.

The control spots are incorporated in the corners of each array. Enlarged images from UTt_3 and Tt_3 (images in the middle indicate spot colour differences between the treated and untreated samples). Control spots are also added to each of the arrays and are in the four corners of each array as indicated. The yellow spots in the control boxes are indicative of the bright corners that should always be yellow and dark corners in which no cDNA have been hybridised to the slide.

4.3.3 Normalisation of data

The dataset comprised of 24 individual hybridisations and the first step is usually background correction, if necessary. As shown in Figure 4.6, some localized artefacts (at the top and at the edges) may occur on the arrays that only affect a specific channel and therefore needs correction. Artefacts localised in the green channel (indicated with blue arrows) are not seen in the red channel. The red channel has more speckling (indicated with grey arrow), probably due to insufficient washing and therefore also needed background correction.

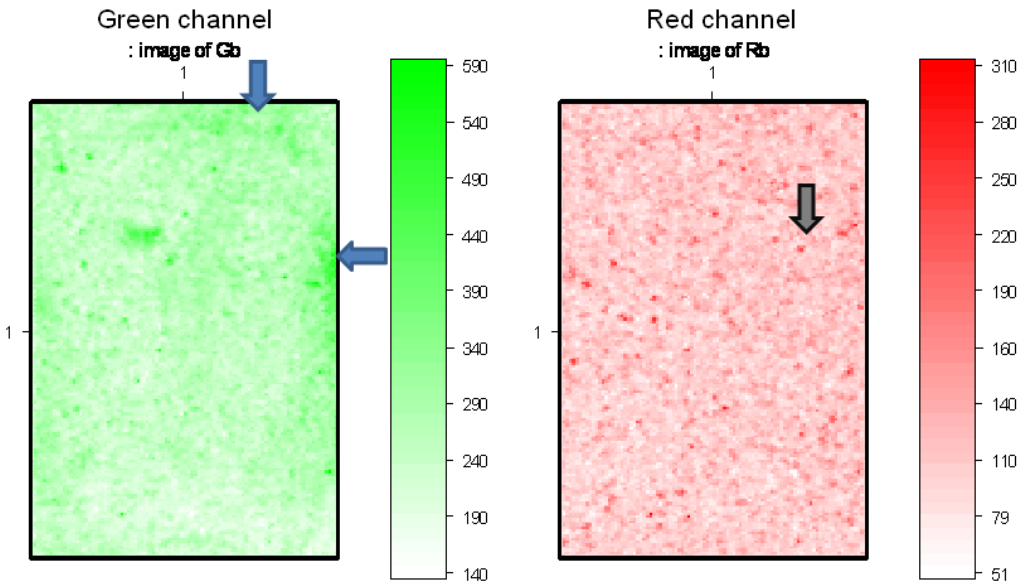

Figure 4.6: Red and green background images of slide Tt_3 array8.

An offset of 50 was used for background subtraction, which is the preferred methodology when microarrays are to be used for differential expression analysis (Smyth & Speed, 2003). Noise is reduced for each slide in every step that is performed and accordingly adjusts the foreground intensity for the background intensity. An important aspect of background subtraction necessary for differential expression analysis is the representation of only positive values on the array with low intensity spots and negative values that are converted to zero resulting in lower log-ratio variation as well as the stabilisation of the variability of the M-value as a function of intensity (Smyth et al., 2005b). The offset method for background subtraction has the benefit of providing small variability and more reliable data. Two normalisation strategies exist, which include within-array normalisation in which the M-value are normalised for each array separately to correct for dye effects, and between-array normalisation in which the intensities or log-ratios are normalised in order to be comparable across all the arrays that are compared (Chiogna *et al.*, 2009). Print-tip Loess normalisation is the standard within-array normalisation method, but is not applicable to Agilent slides, since these slides do not have print tips, and therefore Global Loess or Robust Spline would be more appropriate. Global Loess normalisation assumes that the majority of probes are not differentially regulated but inefficient normalisation was evident since various outliers were still visible within the data (Figure 4.7 A and B, indicated with arrows) and had a relative large amount of noise (Figure 4.7 C).

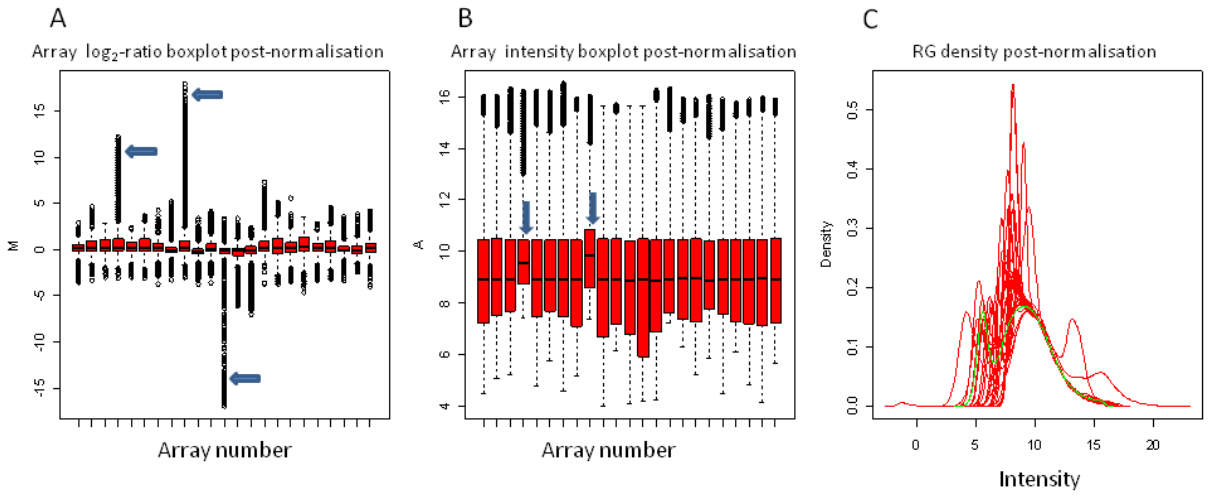

Figure 4.7: Boxplot data after Loess normalisation and Gquantile.

A: Boxplot of the log2-ratios after normalisation, B: Boxplot of the intensities for each array, C: Density plot after normalisation. Visible outliers are indicated with arrows.

The M-values of 3 slides were clear outliers (with values of 10, 15 and -15), while the other 21 slides had M-values ranging between -5 and 5 (Figure 4.7 A, marked with arrows). The RG density plot (Figure 4.7 C) appears erratic and not smooth after normalisation. Figure 4.7 B also indicates the large box sizes that will skew the dataset. The variation in box sizes poses a problem since the bigger boxes have a larger influence on the data than the smaller boxes (Smyth & Speed, 2003). Inefficient normalisation with Loess prompted the use of Robust Spline within-array normalisation method. Robust Spline is an empirical Bayes compromise between print-tip and global Loess normalisation, with 5-parameter regression splines used in place of the Loess curves. Robust Spline analysis resulted in more stable M-values between 4 and -4 and stable A-values (Figure 4.8 A and B), which is in stark contrast to the M-values of 15 obtained for Loess normalisation. Robust Spline filters were originally designed for surface texture analysis and are able to deal with outliers in data without affecting the mean data (Krystek, 2005).

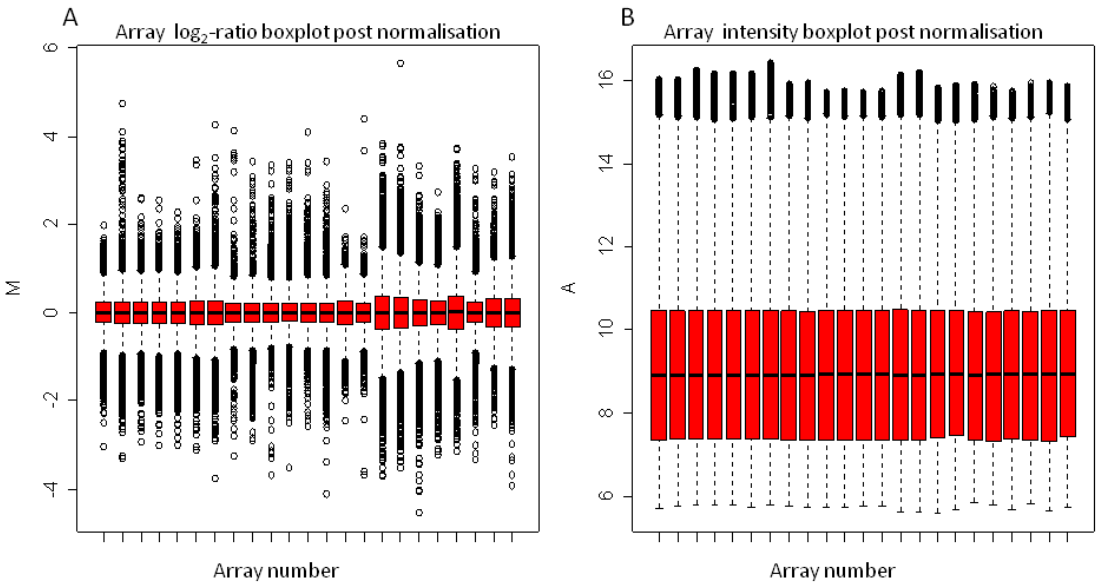

Figure 4.8: Boxplots of Robust Spline normalisation

A: All the boxes are centred on zero and are of similar sizes after normalisation indicating that all the boxes have a similar influence on the data. B: the spot intensities are all similar since all the boxes has the same A-value and are of equal size.

Dye differences may also play an important role and needs to be corrected. The dyes have various differences that include their chemistry, half-life, dynamic range, and susceptibility to degradation by ozone. Taken together all these differences may result in signal discrepancies and therefore it needs normalisation to produce similar signals from both dyes since it is assumed that the starting material for both dyes are similar (Meiklejohn & Townsend, 2005). Between-array normalisation normalises the individual (red and green) intensity values rather than the $\log_2$-ratios. It is also important for between-array normalisation that the background has been corrected to provide quality data.

Gquantile was used since all the reference samples were always labelled with Cy3 (green) and the different samples were always labelled with Cy5 (red). The use of a reference pool and labelling of the reference pool with only one dye may aid in normalisation (Kreil *et al.*, 2005). Therefore, the reference samples were all normalised to a single green line (Figure 4.9 B) since it is essentially the same reference used on all of the slides. As shown in Figure 4.9 the combination of Robust Spline and Gquantile produces a smooth density plot post-normalisation.

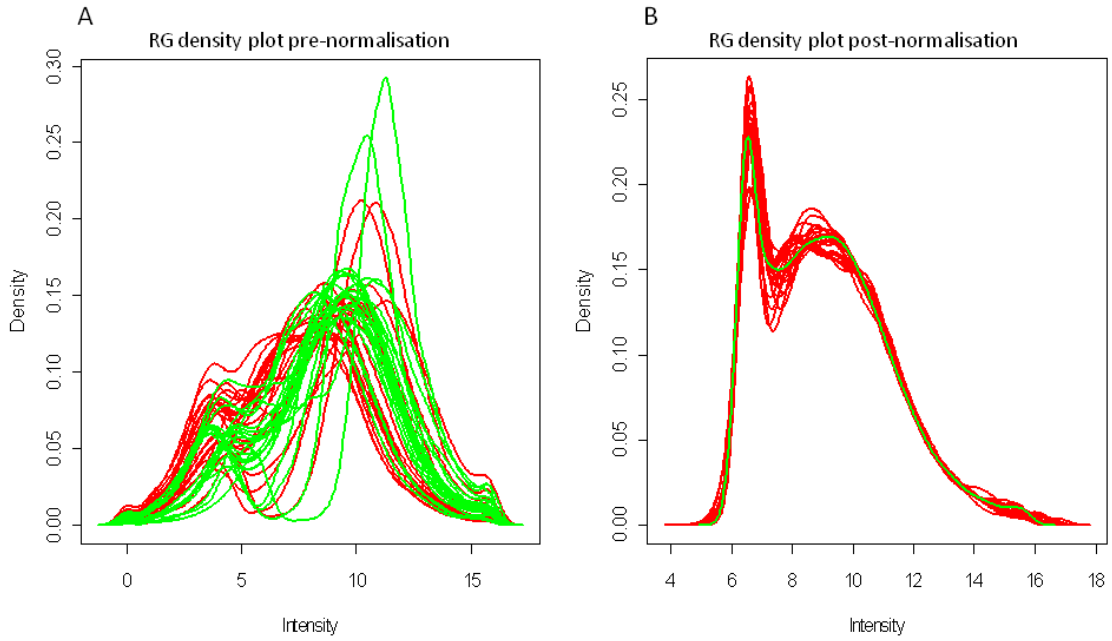

Figure 4.9: RG density plots after Robust Spline and Gquantile normalisation.
A: RG density plot pre-normalisation, B: RG density plot post normalisation with Robust Spline and Gquantile.

MA plots give an indication on the quality of the microarray data before and after normalisation. On MA plots the M-value should ideally be around zero and the ratios should ideally not be dependent on intensity (A-value). Upon normalisation of the data the MA-plots changed into more desirable data as the spots were concentrated around zero and is parallel to the intensity axis (A-value) (Figure 4.10 A and B). It is expected that there should be no variance between M and A, but this is not the case with small variances being detected in the relationship with M versus A. The variance of M is larger for small A-values, stable for the middle A-values and once again a slight reduction in variance in the larger A-values. This is one of the reasons that the MA plot does not give a straight line on M = 0.

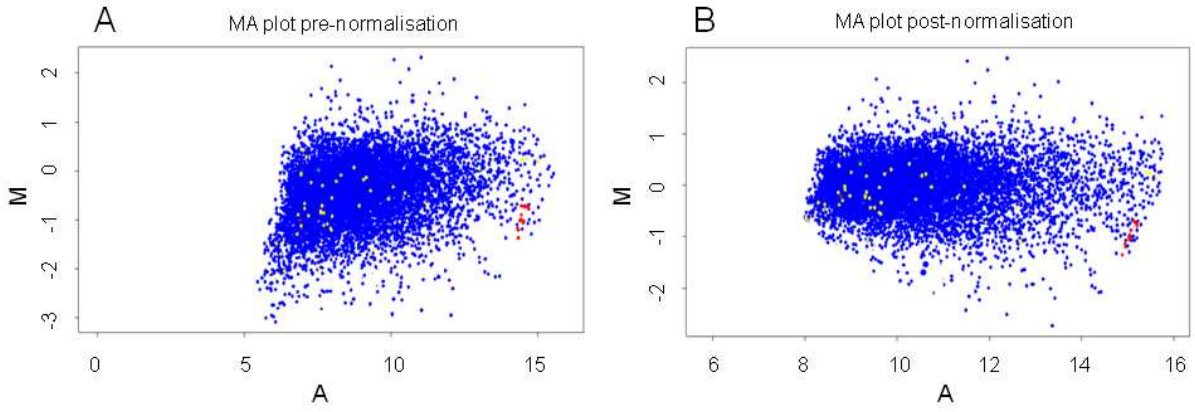

Figure 4.10: MA plot of Tt_3 array 6 before and after normalisation of the data.
(A) MA plot before any normalisation methods were employed, (B) MA plot after normalisation of the data.

4.3.4 Pearson correlations of the three time points

Spot finding was performed on all the arrays using GenePix 6.0, in which poor quality and saturated spots were removed from the dataset. Pearson correlations of all the valid spots present within the arrays were grouped into the 6 groups and compared (Table 4.2). The Pearson correlations were calculated after normalisation in LIMMA-GUI.

Table 4.2: Pearson correlations of the *Pf*AdoMetDC inhibited transcriptome data.

Comparison	Correlation (r)
UTt_1 : Tt_1	0.865
UTt_2 : Tt_2	0.608
UTt_3 : Tt_3	0.584
UTt_1 : Tt_2	0.396
UTt_1 : Tt_3	-0.327
UTt_2 : Tt_1	0.096
UTt_2 : Tt_3	0.212
UTt_1 : UTt_2	0.188
UTt_1 : UTt_3	-0.529
Tt_1 : Tt_3	-0.312
UTt_3 : Tt_1	-0.531

A Pearson correlation is observed between UTt_1 and Tt_1 (0.865) but progressively reduces to 0.584 between UTt_3 and Tt_3. This, as well as the anti-correlation detected between UTt_1 and Tt_3 (-0.327) and UTt_1 compared to UTt_3 (-0.529), indicate the progression of the parasite from the initial ring to the late trophozoite stages. Therefore, the early time points that were used within this study negate the use of the t_0 strategy due to the early time points taken (van Brummelen *et al.*, 2009) and allowed a direct comparison between time points for data analysis.

4.3.5 Data analysis of differentially expressed transcripts

A volcano-plot displays the fold changes as a measure of the statistical significance of the change (Smyth *et al.*, 2003). The volcano-plots for the data are given in Figure 4.11 A-C. Analysis of the first treated time point (UTt1:Tt1) did not result in the identification of any differentially expressed transcripts, and UTt_2:Tt_2 resulted in only a few differentially expressed transcripts that were significant ($p<0.05$). Time point 3 (UTt_3:Tt_3) resulted in the identification of 549 differentially expressed transcripts that consisted of 143 transcripts that had increased abundance and 406 transcripts with decreased abundance (Figure 4.11). The distribution of the $\log_2$-ratios for the differentially expressed transcripts from t_3 (UTt_3:Tt_3) indicated that the majority of the transcripts have a $\log_2$-ratio of about 1 (similar to a FC of 2).

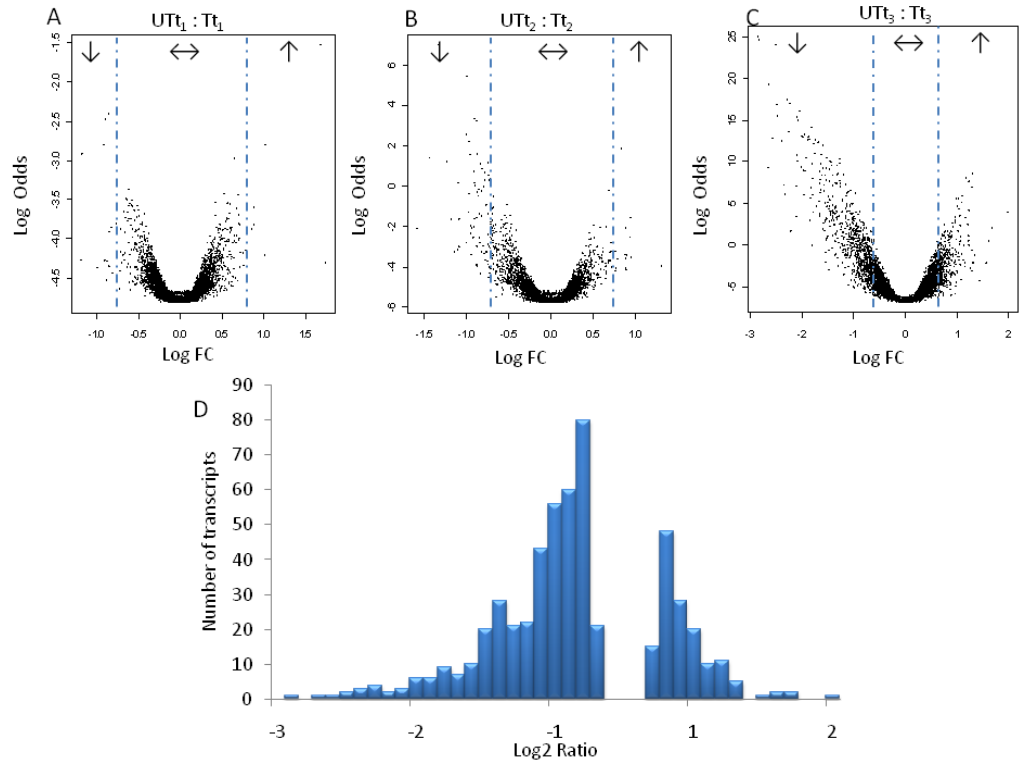

Figure 4.11: Log_2-distribution ratios and volcanoplots of the 3 time points investigated upon inhibition of AdoMetDC.

(A) t_1 (UTt_1:Tt_1), UTt_1 compared to Tt_1, resulted in no differentially expressed transcripts, (B) t_2 (UTt_2:Tt_2), UTt_2 compared to Tt_2, resulted in few differentially expressed transcripts, (C) t_3 (UTt_3:Tt_3), UTt_3 compared to Tt_3 resulted in 549 differentially expressed transcripts. (D) The distribution of log ratios for the differentially expressed transcripts from t_3. The log_2 ratio cut-off was ± 0.7, which relates to a fold change of ± 1.7.

The transcripts with decreased abundance represent ~74% (406/549) of the differentially expressed transcripts, while the transcripts with increased abundance are representative of ~24% (143/549) of the differentially regulated transcripts. The 25 most profoundly affected transcripts with a decrease in abundance are given in Table 4.3 and have a maximum fold change of -7.3 for α-tubulin which progressively decrease to -3.8 for a putative transporter. The increased abundance transcripts were less profound with the 25 most abundant transcripts having a fold change of 4.0 decreasing to a fold change of 2.2 (Table 4.3). A complete list of all 549 differentially regulated transcripts is available in Appendix B.

Table 4.3: The 25 most increased and decreased transcripts for AdoMetDC inhibited parasites.

Nr	PlasmoDB ID	Product Description	FC[a]	adj.P.Val[b]
		Decreased abundance		
1	PFI0180w	Alpha tubulin	-7.3	1.1E-11
2	PF11_0282	Deoxyuridine 5'-triphosphate nucleotidohydrolase, putative	-6.3	5.8E-06
3	PFI0905w	Probable protein, unknown function	-6.3	1.6E-09
4	PF13_0328	Proliferating cell nuclear antigen	-5.7	1.5E-11
5	PFI0135c	Serine repeat antigen 9 (SERA-9)	-5.6	1.2E-08
6	PF10_0154	Ribonucleotide reductase small subunit, putative	-5.4	1.1E-07
7	PF10_0084	Tubulin beta chain, putative	-5.2	3.5E-07
8	MAL13P1.214	Phosphoethanolamine N-methyltransferase	-5.1	2.5E-05
9	PFD0830w	□□□□nctional dihydrofolate reductase-thymidylate synthase	-4.9	1.1E-08
10	PF14_0443	Centrin-2	-4.9	8.8E-09
11	PFL1720w	Serine hydroxymethyltransferase	-4.8	1.6E-06
12	PF07_0065	Zinc transporter, putative	-4.8	1.8E-07
13	PFA0520c	Chromatin assembly factor 1 protein WD40 domain, putative	-4.7	1.1E-08
14	PF13_0032	Hydrolase, putative	-4.7	2.2E-03
15	PFF0510w	Histone H3	-4.3	5.2E-04
16	PFB0835c	Conserved Plasmodium protein, unknown function	-4.3	1.6E-06
17	PF13_0192	Conserved Plasmodium protein, unknown function	-4.2	5.5E-08
18	MAL13P1.303	Polyadenylate-binding protein, putative	-4.1	2.2E-08
19	PF10_0020	Alpha/beta hydrolase, putative	-4.1	4.8E-06
20	PFL2005w	Replication factor C subunit 4	-4.0	2.7E-07
21	PFF0630c	Conserved Plasmodium protein, unknown function	-4.0	2.7E-07
22	PF14_0053	Ribonucleotide reductase small subunit	-3.9	7.0E-06
23	PFL1670c	Conserved Plasmodium protein, unknown function	-3.9	7.2E-05
24	PF14_0309	Protein-L-isoaspartate O-methyltransferase beta-aspartate	-3.9	2.3E-07
25	PFA0245w	Transporter, putative	-3.8	7.0E-06
		Increased abundance		
1	PF13_0314	Conserved Plasmodium protein, unknown function	4.0	4.6E-04
2	PFB0115w	Conserved Plasmodium protein, unknown function	3.2	1.9E-03
3	PF14_0182	Hypothetical protein	3.2	7.4E-03
4	PFB0475c	Conserved Plasmodium protein, unknown function	3.1	7.2E-03
5	PFB0815w	Calcium-dependent protein kinase 1	3.0	4.0E-02
6	MAL13P1.328	DNA topoisomerase VI, B subunit, putative	2.8	1.3E-06
7	PFB0923c	Plasmodium exported protein, unknown function	2.5	1.8E-02
8	PF14_0698	Conserved Plasmodium protein, unknown function	2.5	3.4E-02
9	PF14_0015	Aminopeptidase, putative	2.5	3.3E-02
10	PFD0285c	Lysine decarboxylase, putative	2.5	8.6E-06
11	PFI1780w	Plasmodium exported protein (PHISTc), unknown function	2.5	3.1E-05
12	PF14_0017	Lysophospholipase, putative	2.4	3.4E-04
13	PFB0920w	DNAJ protein, putative	2.4	8.6E-03
14	PFD1175w	Serine/Threonine protein kinase, FIKK family	2.4	1.8E-05
15	PF10_0307	Conserved Plasmodium protein, unknown function	2.4	3.0E-04
16	MAL8P1.330	Conserved Plasmodium protein, unknown function	2.3	5.2E-03
17	PF10_0034	Conserved Plasmodium protein, unknown function	2.3	9.6E-06
18	PFA0130c	Serine/Threonine protein kinase, FIKK family, putative	2.3	1.0E-03
19	PF14_0018	Plasmodium exported protein (PHISTb), unknown function	2.3	1.2E-05
20	PFL1885c	Calcium/calmodulin-dependent protein kinase 2	2.2	3.2E-03
21	PF08_0118	Conserved Plasmodium protein, unknown function	2.2	3.4E-02
22	PF08_0060	Asparagine-rich antigen	2.2	4.5E-02
23	PF14_0703	Conserved Plasmodium protein, unknown function	2.2	7.3E-03
24	PFE0340c	Rhomboid protease ROM4	2.2	3.3E-02
25	PF08_0001	Plasmodium exported protein, unknown function	2.2	7.7E-05

[a]FC is representative of the fold change calculated from the $\log_2$-ratios given in LIMMA. [b]Adjusted p-value calculated by LIMMA to determine the statistical significance of transcripts and to avoid false positives with $p<0.05$ considered as significant.

4.3.6 Biological classification of differentially expressed transcripts

The 549 differentially regulated transcripts were sorted according to their biological functions and grouped according to their Gene Ontology (GO) annotations (Figure 4.12).

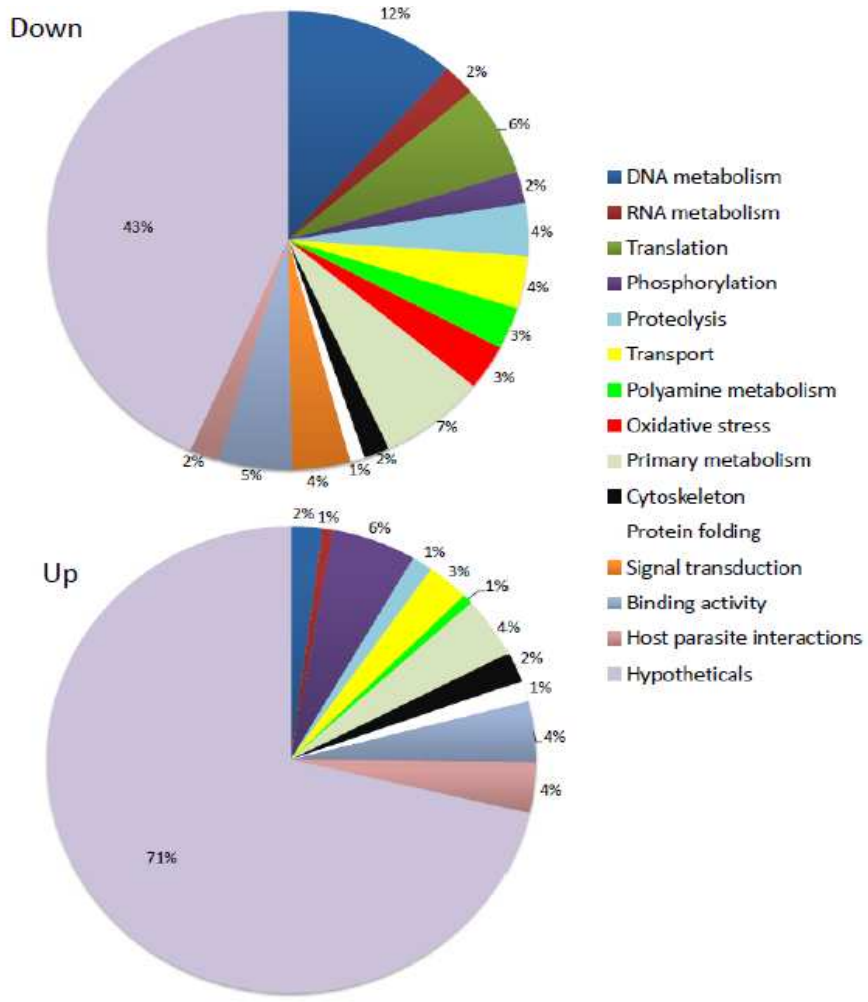

Figure 4.12: Functional classification of regulated transcripts according to their GO terms.
GO terms of differentially regulated transcripts were obtained from PlasmoDB 6.0 and classified according to their biological functions. Percentages were calculated from the total number of up- or down-regulated transcripts.

Of the 143 transcripts that had increased abundance, 6% of the transcripts are involved in phosphorylation. Primary metabolism, host-parasite interactions and binding activity each represented 4% of the biological functions, with transport represented by 3% of the differentially affected transcripts. The majority (71%) of the transcripts with increased abundances were hypothetical transcripts. The 406 transcripts that had decreased abundance consisted of 43% hypothetical transcripts. DNA metabolism (12%), translation (6%) and RNA metabolism (2%). Polyamine metabolism (3%) and oxidative stress (3%) also represented transcripts with decreased abundance. Transcripts associated with phosphorylation included 2% of the decreased transcripts.

Polyamine and methionine metabolism included the increased abundance (2.5-fold) of lysine decarboxylase (PFD0285c)(Table 4.4). Transcripts directly involved in methionine and AdoMet metabolism, AdoMet synthetase (PFI1090w; -2.3-fold) and adenosylhomocysteinase (PFE1050w; -2.1-fold), all had decreased abundance. Five methyltransferase transcripts associated with polyamine metabolism had decreased abundance of which phosphoethanolamine N-methyltransferase (-5.1-fold) were the most affected. The abundance of the transcript associated with polyamine metabolism, calcium/calmodulin-dependent protein kinase 2, had increased abundance (2.2-fold). Thirteen transcripts involved in oxidative stress and redox metabolism had decreased abundances (Table 4.4). Transcripts involved in folate and pyrimidine biosynthesis also had decreased abundances. Interestingly, the transcript of AdoMetDC was not differentially affected by inhibition with MDL73811, in contrast to the co-inhibition of AdoMetDC/ODC which resulted in 2-fold decreased abundance of the transcript (van Brummelen et al., 2009).

Table 4.4: Biological functions of some of the differentially regulated transcripts for AdoMetDC inhibited parasites according to their GO annotations.

PlasmoDB ID	Name	FC UTt_3:Tt_3	Min exp time HPI	Max exp time HPI
	Polyamine and Methionine metabolism			
PF10_0121	Hypoxanthine phosphoribosyltransferase	-1.7	4	26
PF10_0289	Adenosine deaminase, putative	-3.1	42	27
PFD0285c	Lysine decarboxylase, putative	2.5	1	17
PFE0660c	Purine nucleotide phosphorylase, putative	-3.0	4	22
PFE1050w	Adenosylhomocysteinase	-2.1	1	30
PFI1090w	S-adenosylmethionine synthetase	-2.3	12	32
PFL1475w	Sun-family protein, putative	-1.8	36	21
	Methyltransferases			
MAL13P1.214	Phosphoethanolamine N-methyltransferase	-5.1	10	33
PF14_0309	Protein-L-isoaspartate O-methyltransferase beta-aspartate methyltransferase, putative	-3.9	14	31
PF14_0526	Conserved Plasmodium protein, unknown function	-3.1	10	25
PF13_0016	Methyl transferase-like protein, putative	-1.9	1	26
PFL1775c	S-adenosyl-methyltransferase, putative	-1.7	8	27
	Potential polyamine associated effects			
PFL1885c	Calcium/calmodulin-dependent protein kinase 2	2.2	24	43
	Oxidative stress and redox metabolism			
PF08_0071	Fe-superoxide dismutase	-2.0	1	28
PF08_0131	1-cys peroxiredoxin	-2.7	8	26
PF14_0187	Glutathione S-transferase	-1.8	37	21
PF14_0192	Glutathione reductase	-2.2	8	22
PF14_0545	Thioredoxin, putative	-3.1		
PFL0595c	Glutathione peroxidase	-2.2	47	35
PF13_0353	NADH-cytochrome B5 reductase, putative	-2.1	14	33
PF14_0248	Ubiquinol-cytochrome c reductase hinge protein, putative	-1.8	14	37
PF14_0597	Cytochrome c1 precursor, putative	-3.2	11	35
PFI1170c	Thioredoxin reductase	-1.9	10	31
PFI1250w	Thioredoxin-like protein 2	-1.7		
PFL1550w	Lipoamide dehydrogenase	-2.3	15	38
PF11_0352	Protein disulfide isomerase	-1.8	12	32

	Folate and Pyrimidine metabolism			
PFD0830w	Bifunctional dihydrofolate reductase-thymidylate synthase	-4.9	47	35
PFL1720w	Serine hydroxymethyltransferase	-4.8	48	35
PF13_0140	Dihydrofolate synthase/folylpolyglutamate synthase	-1.8	10	31
PF13_0349	Nucleoside diphosphate kinase b, putative	-3.5	11	28
PF10_0154	Ribonucleotide reductase small subunit, putative	-5.4	11	32
PF14_0053	Ribonucleotide reductase small subunit	-3.9	10	32
PF14_0352	Ribonucleoside-diphosphate reductase, large subunit	-2.1	10	32
PFA0555c	UMP-CMP kinase, putative	-2.9		
MAL13P1.218	UDP-N-acetylglucosamine pyrophosphorylase, putative	-1.7	4	26
	Glycolysis			
PF10_0155	Enolase	-2.7	38	16
PF13_0141	L-lactate dehydrogenase	-1.9	42	26
PF14_0378	Triosephosphate isomerase	-1.7	1	26
PFF1300w	Pyruvate kinase	-1.7	41	26
	DNA replication			
PF11_0061	Histone H4	-3.4	14	37
PF11_0062	Histone H2B	-2.9	42	27
PF11_0117	Replication factor C subunit 5, putative	-1.8	10	28
PF11_0282	Deoxyuridine 5'-triphosphate nucleotidohydrolase, putative	-6.3	12	28
PF13_0095	DNA replication licensing factor MCM4-related	-3.1	12	37
PF13_0149	Chromatin assembly factor 1 subunit, putative	-2.9	11	35
PF13_0291	Replication licensing factor, putative	-2.5	11	32
PF14_0177	DNA replication licensing factor MCM2	-2.0	11	32
PF14_0254	DNA mismatch repair protein Msh2p, putative	-1.9	11	30
PFB0840w	Replication factor C, subunit 2	-3.4	13	30
PFD0685c	Chromosome associated protein, putative	-2.0	10	28
PFE0270c	DNA repair protein, putative	-3.5	12	31
PFE0450w	Chromosome condensation protein, putative	-2.6	10	30
PFE0675c	Deoxyribodipyrimidine photolyase, putative	-2.8	9	28
PFF0510w	Histone H3	-4.3		
PFF0865w	Histone H3	-1.8		
PFF1225c	DNA polymerase 1, putative	-2.0	10	30
PF14_0314	Chromatin assembly factor 1 P55 subunit, putative	2.0	24	40
PFI0235w	Replication factor A-related protein, putative	-2.1	8	32
	Transcription factors			
PF11_0241	Myb-like DNA-binding domain, putative	1.7	32	1
PFL0465c	Zinc finger transcription factor (krox1)	1.8		
PF14_0374	CCAAT-binding transcription factor, putative	1.7	20	43
	Translation			
PF14_0289	Mitochondrial ribosomal protein L17-2 precursor, putative	-3.6	10	26
PF14_0606	Mitochondrial ribosomal protein S6-2 precursor, putative	-2.2	15	45
PF14_0709	Mitochondrial ribosomal protein L20 precursor, putative	-2.1	36	44
PFB0645c	Mitochondrial large ribosomal subunit, putative	-2.3	11	24
PFC0675c	Mitochondrial ribosomal protein L29/L47 precursor, putative	-1.9	41	46
PFC0701w	Mitochondrial ribosomal protein L27 precursor, putative	-2.5	12	1
PFD0675w	Apicoplast ribosomal protein L10 precursor, putative	-2.9	11	35
PFI0890c	Organelle ribosomal protein L3 precursor, putative	-2.2	10	35
PFI1240c	Prolyl-t-RNA synthase, putative	-2.8	11	31
PFI1575c	Peptide release factor, putative	-2.7	10	28
	Cell cycle and cytokinesis			
PF13_0328	Proliferating cell nuclear antigen	-5.7	11	28
PFL1330c	Cyclin-related protein, Pfcyc-2	-2.7	14	36
PF11_0478	Kinesin-like protein, putative	2.1	21	35
PFE0165w	Actin-depolymerizing factor, putative	-2.2	14	36
PFI0180w	Alpha tubulin	-7.3	11	35

PFI1565w	Profilin, putative	-3.0	15	38
PFL0925w	Formin 2, putative	2.0		
PFL2215w	Actin I	-2.5	15	39
	Signal transduction			
MAL13P1.19	Peptidase, putative	-2.4	10	28
MAL13P1.205	Rab11b, GTPase	-1.9	48	35
PFE0690c	PfRab1a	-1.8	10	28
PFI0215c	Signal peptidase, putative	-1.8	10	33
PFI1005w	ADP-ribosylation factor-like protein	-2.0	21	41

4.3.7 Hierarchical clustering of the AdoMetDC inhibited transcripts

Hierarchical clustering of the AdoMetDC-inhibited transcripts was done using Gene Cluster to cluster the transcripts of UTt_3:Tt_3. Hierarchical clustering is able to join transcript data and cluster the data in groups that can be easily visualised. It compares the expression profile of each transcript and then form groups which represent transcripts that have similar expression profiles. This process of comparing all the transcripts within the dataset will continue until only one large cluster is present. Transcripts within close distance on the dendogram have similar expression profiles, while transcripts with larger distances between them on the dendrogram are less similar. Transcripts that are within a specific single cluster are then assumed to be co-regulated and functionally related to each other. A specific tight cluster (correlation of 0.949) containing 4 polyamine-related transcripts was revealed (Figure 4.13), adenosine deaminase (PF10_0289), adenosylhomocysteinase (PFE1050w), S-adenosylmethionine synthetase (PFI1090w) and phosphoethanolamine N-methyltransfease (MAL13P1.214). All of these transcripts increased in abundance from UTt_1 to UTt_3 under unchallenged conditions, but after inhibition of AdoMetDC these transcripts revealed decreased abundances in Tt_3 compared to UTt_3. Due to the lack of significant regulation of the transcript of AdoMetDC (PF10_0322), its transcript clustered separately from the other polyamine related transcripts and is therefore not shown in Figure 4.13.

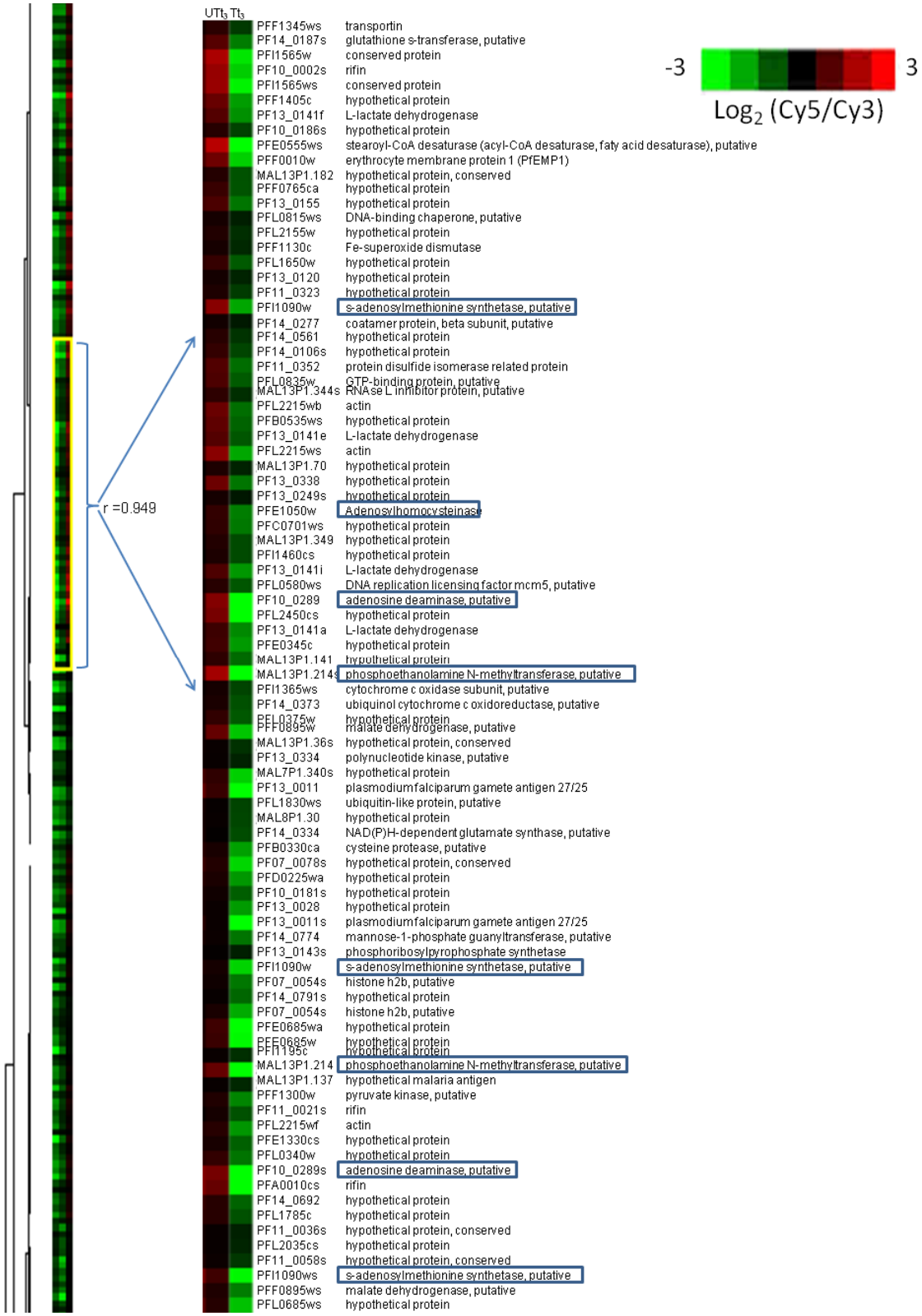

Figure 4.13: A tight cluster (r =0.949) containing polyamine-related transcripts.

A correlation coefficient of 0.949 was produced by hierarchical clustering of AdoMetDC-inhibited parasites and contained 8 polyamine-related transcripts that related to 4 unique transcript groups. These transcripts are blocked on the picture in blue. This cluster contains 91 transcripts that clustered together out of the total of 9966 transcripts that were detected on the slides.

Hierarchical clustering was performed on the polyamine-specific differentially regulated transcripts that were identified with the inhibition of AdoMetDC as well as some oxidative stress-related transcripts that were identified in Table 4.4 (Figure 4.14). Three tight clusters were identified from these transcripts [1-3]. The first cluster ([1] correlation of 0.88) resulted in clustering of mostly the methyltransferase-related transcripts. These transcripts have low expression in UTt_1, which then increased in abundance over time in the untreated samples (UTt_3). With the inhibition of AdoMetDC the transcripts from this cluster [1] remained low in abundances (Tt_3). The second [2] and third group [3] contained the majority of the polyamine and methionine-related transcripts. The second cluster ([2] correlation of 0.83) contained transcripts that had slightly increased expression in UTt_1, which increased even further in abundances at the untreated time points (UTt_3). Similar to the first cluster the treated sample (Tt_3) were indicative of transcriptional arrest since the transcripts in Tt_3 had lower abundances. The last cluster ([3] correlation of 0.88) contained the transcripts with low abundances in both Utt_1 and UTt_3, but increased abundances in Tt_3.

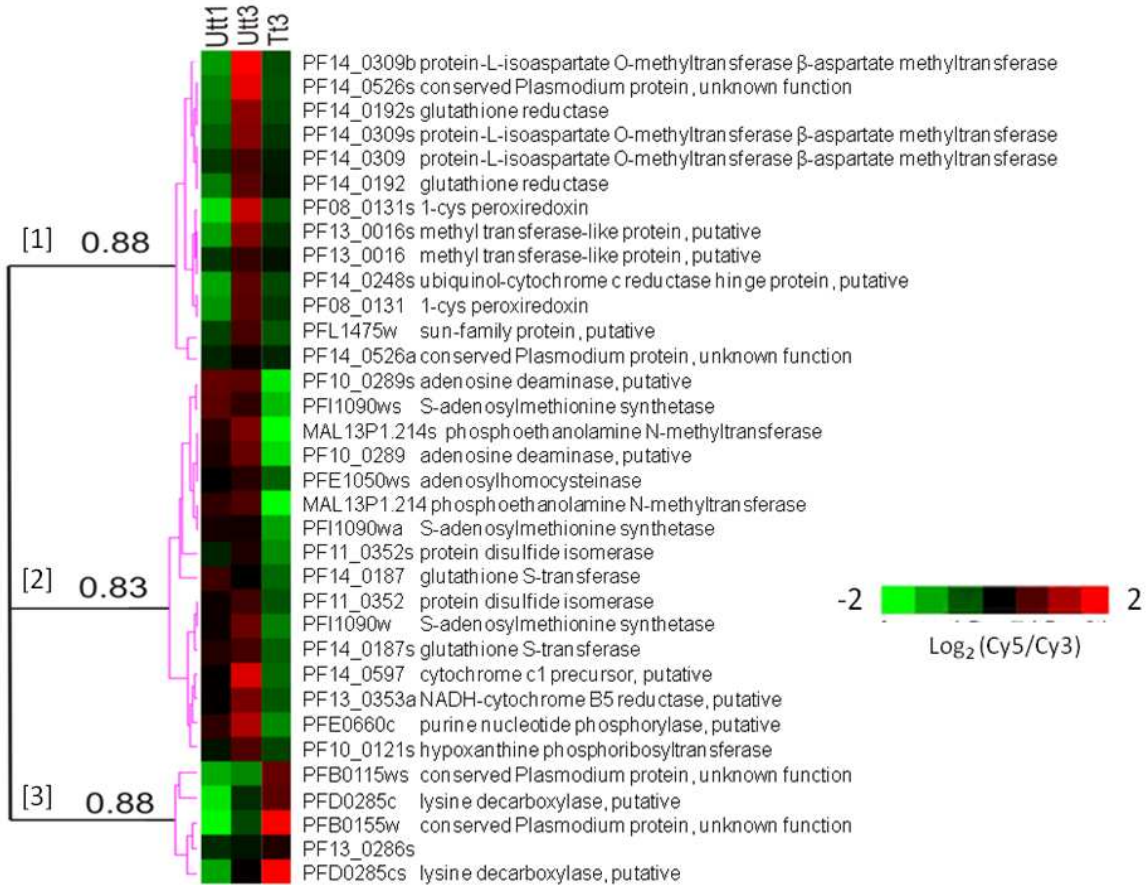

Figure 4.14: Hierarchical clustering of polyamine-specific and oxidative stress transcripts.
Three tight clusters exist for the polyamine and oxidative stress related transcripts.

4.3.8 Transcript regulation of polyamine-specific transcripts followed over all 3 time points

The differential regulation of polyamine-specific transcripts were analysed over the 3 time points by comparison of their FC over time (Figure 4.15). The fold change values obtained for UTt_1:Tt_1 and UTt_2:Tt_2 was not significantly differentially affected, but these fold changes could still be used to determine the trend of transcript abundances over time (Figure 4.15). At Tt_1 the majority of the transcripts are completely unaffected by the inhibition of AdoMetDC with MDL73811. At Tt_2 the majority of the transcripts were slightly affected by either a small increase or decrease in transcript abundance. In Tt_3 the differential regulation of the transcripts were more pronounced. Phosphoethanolamine N-methyltransferase (MAL13P1.214), methyl transferase-like protein (PF13_0016), hypoxanthine phosphoribosyltransferase (PF10_0121), S-adenosylmethionine synthetase (PFI1090w), sun-family protein (PFL1475w), S-adenosyl-methyltransferase (PFL1775c) all had decreased transcript abundance at Tt_1 which decreased further over time, and are therefore some of the transcripts that seem to be more severely affected by AdoMetDC inhibition. Adenosine deaminase (PF10_0289), protein-L-isoaspartate O-methyltransferase beta-aspartate methyltransferase (PF14_0309), adenosylhomocysteinase (PFE1050w), purine nucleotide phosphorylase (PFE0660c), conserved *Plasmodium* protein (PF14_0526) all had a positive fold change at Tt_1 which then gradually decreased over time and are therefore affected over time. Lysine decarboxylase (PFD0285c) and calcium/calmodulin-dependent protein kinase 2 (PFL1885c) transcript abundances both increased over time with AdoMetDC inhibition.

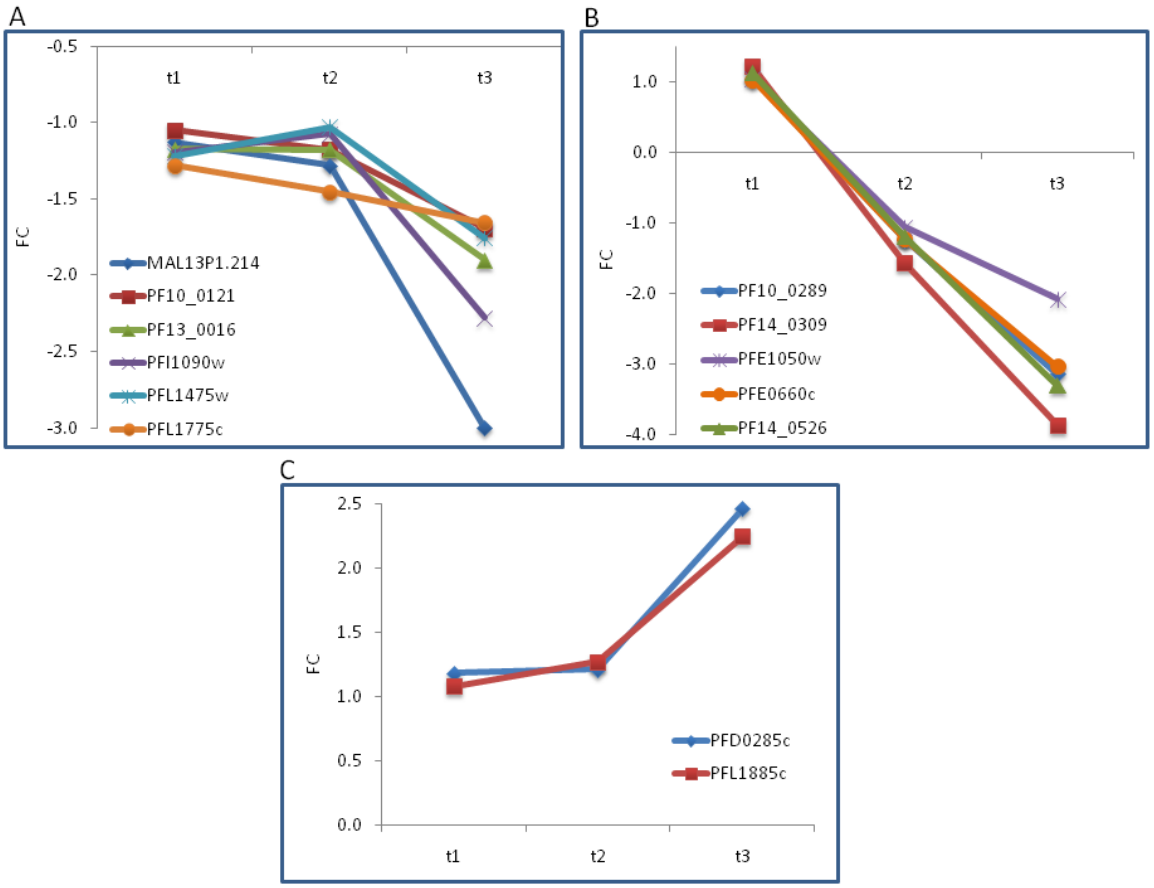

Figure 4.15: Fold change of polyamine-specific transcripts over the 3 time points.

(A)Include transcripts that have decreased transcript abundance which is the even further decreased over the 3 time points and include: MAL13P1.214: phosphoethanolamine N-methyltransferase, PF10_0121: hypoxanthine phosphoribosyltransferase, PF13_0016: methyl transferase-like protein, PFI1090w: S-adenosylmethionine synthetase, PFL1475w: sun-family protein, PFL1775c: S-adenosyl-methyltransferase, (B) Include transcripts which is high in abundance initially in Tt_1 but then decreases over time and include: PF10_0289: adenosine deaminase, PF14_0309: protein-L-isoaspartate O-methyltransferase beta-aspartate methyltransferase, PFE1050w: adenosylhomocysteinase, PFE0660c: purine nucleotide phosphorylase, PF14_0526: conserved *Plasmodium* protein, (C) Include transcripts that increase in abundances: PFD0285c: lysine decarboxylase, PFL1885c: calcium/calmodulin-dependent protein kinase 2.

4.3.9 Identification of uniquely affected Plasmodial pathways as a result of AdoMetDC inhibition

All 549 differentially expressed transcripts identified in the study were subjected to metabolic pathway identification in MADIBA (Law *et al.*, 2008). P-values for each of these pathways containing unique enzymes were calculated according to Fishers test (Fisher, 1935), therefore $p<0.05$ is representative of significance within the results. A unique enzyme according to MADIBA is defined as an enzyme that can only be classified into one specific pathway and not multiple pathways. A total of 49 pathways containing unique enzymes were detected, of which 27 pathways had only 1 unique enzyme, 8 pathways had 2 unique enzymes, 4 pathways had 3 unique enzymes, 5 pathways had 4 unique enzymes, and 5 pathways had 5 or more unique enzymes per pathway. Only

1 pathway, methionine and polyamine metabolism had a significant p-value of 0.0183 with 7 unique enzymes (Table 4.5 and Figure 4.16).

Table 4.5: Unique metabolic pathway identification of the data from the inhibition of AdoMetDC.

Pathway	p-value[a]	Nr of unique enzymes found[b]
Glycine, serine and threonine metabolism	0.9990	3
Methionine metabolism	0.9575	3
Selenoamino acid metabolism	0.7400	3
Pantothenate and CoA biosynthesis	0.8573	3
Citrate cycle (TCA cycle)	0.5503	4
Pyruvate metabolism	0.9982	4
Oxidative phosphorylation	0.2286	4
Glycerophospholipid metabolism	0.9827	4
Glutathione metabolism	0.6851	4
Glycolysis / Gluconeogenesis	0.8263	5
Lysine degradation	0.9600	5
Pyrimidine metabolism	0.9095	7
Purine metabolism	0.9929	9
Methionine and Polyamine Metabolic Pathway	0.0183*	7

[a]p-value is calculated by MADIBA according to the Fisher test and considered as significant if $p < 0.05$. [b]Unique enzymes determined for a specific pathway. * The only pathway with $p < 0.05$ that were considered as significant.

MADIBA identified methionine and polyamine metabolism as a pathway that was significantly affected with AdoMetDC inhibition. The differentially regulated transcripts associated with methionine and polyamine metabolism are given in Figure 4.16. The transcripts with decreased transcript abundance are indicated in green, while increased transcripts are indicated in red. Transcripts that are both up-stream and down-stream of AdoMetDC were affected including transcripts in the methionine cycle that had decreased transcript levels.

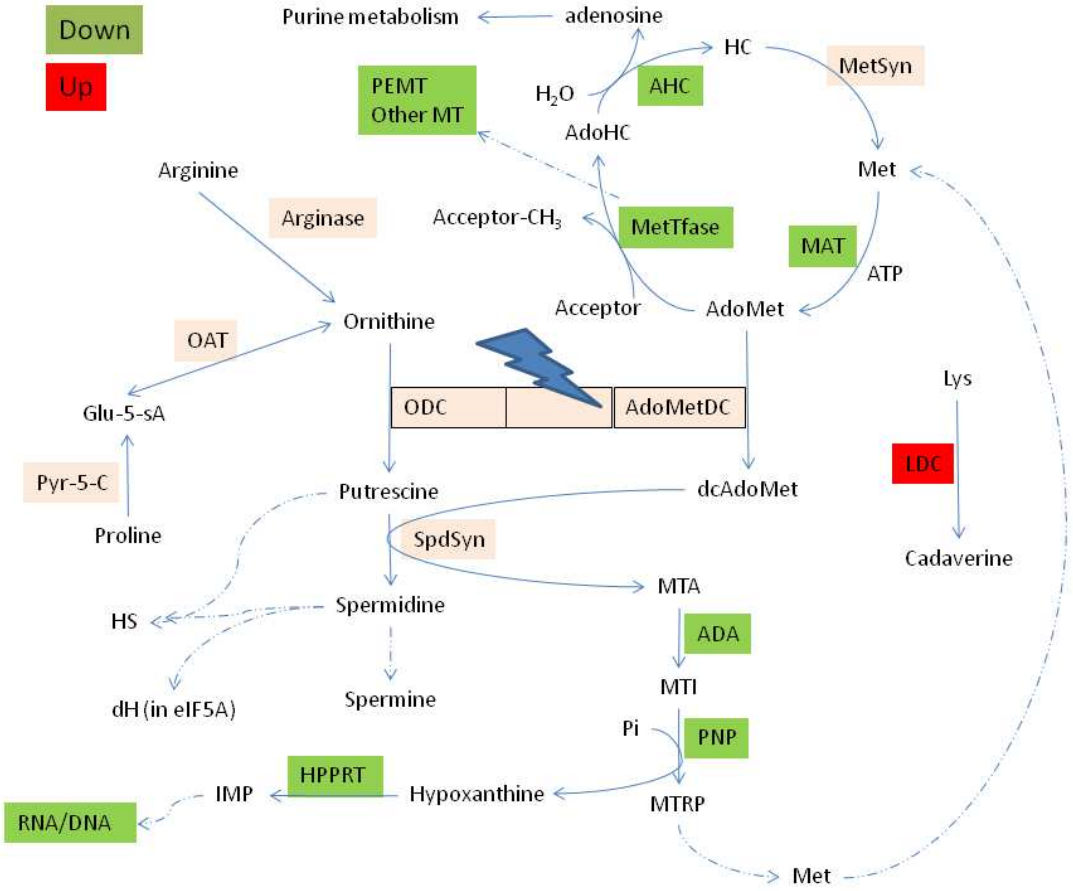

Figure 4.16: Polyamine and methionine metabolism affected by AdoMetDC inhibition.
Green is indicative of transcripts that have decreased abundance, while red is indicative of increased abundance of the transcripts. All other transcripts not affected by AdoMetDC inhibition within this pathway is marked in pink.

4.3.10 Interactions of the AdoMetDC inhibited transcriptome

The *P. falciparum* interactome was constructed *in silico* using Bayesian frameworks (Date & Stoeckert, 2006, Wuchty *et al.*, 2009). Submission of the AdoMetDC inhibited dataset to MADIBA indicated methionine and polyamine metabolism as a pathway that was significantly affected by AdoMetDC inhibition (Table 4.5). Due to the fact that the target was known within this study and to further iterate the enrichment for polyamine metabolism with AdoMetDC inhibition, the AdoMetDC inhibited dataset was investigated for possible AdoMetDC interacting partners (Van Brummelen, 2009). The interactome for the AdoMetDC inhibited dataset was determined *in silico* by comparison of the interactome database (PlasmoMAP)(Date & Stoeckert, 2006) and the AdoMetDC inhibited dataset. A total of 147 potential interacting partners for AdoMetDC were determined of which 41 (28%) were present in the AdoMetDC inhibited dataset (Table 4.6). The top 20 interacting partners for AdoMetDC included 11 transcripts (55%) from the AdoMetDC inhibited dataset of which 1-cys peroxiredoxin was one. Three other transcripts involved in

oxidative stress, glutathione reductase (PF14_0192), disulfide isomerase precursor, putative (MAL8P1.17), and ferredoxin (MAL13P1.95) were also present within the interactome of AdoMetDC, therefore establishing a possible link between AdoMetDC inhibition and oxidative stress. The complete list of interacting partners for AdoMetDC is given in Appendix C.

To determine if the 55% obtained for the top 20 interacting partners for the AdoMetDC inhibited transcriptome dataset was random, the interactome data from another unrelated bifunctional enzyme, dihydroopteroate synthase/hydroxymethylpterin pyrophosphokinase (DHPS/HPPK) was also compared to the data from the AdoMetDC inhibited transcriptome dataset (Appendix C). Unlike the interacting partners of AdoMetDC, only 19 out of a total of 164 (12%) possible interacting partners of DHPS/HPPK were present within the AdoMetDC inhibited transcriptome dataset. Interestingly, the DHPS/HPPK interactome only included hypoxanthine phosphoribosyltransferase (PF10_0121) that was also present within the AdoMetDC inhibited transcriptome dataset and is a polyamine related transcript. Therefore, these results indicate that the AdoMetDC inhibited transcriptome dataset is specific to proteins that may interact with AdoMetDC (Table 4.6 and Appendix C).

According to STRING 8.2 analysis functional binding partners of AdoMetDC included SpdS (PF11_0301), AdoMet synthase (PFI1090w) and a putative modification methylase-like protein (MAL7P1.151). Therefore these 3 functional binding partners of AdoMetDC were also subjected to *in silico* interactome analysis (PlasmoMAP) to determine if the high percentage of interacting partners that was determined for AdoMetDC was specific to AdoMetDC or if it is a polyamine-related process. Comparison of the AdoMetDC inhibited transcriptome dataset with the interactome for putative modification methylase-like protein (MAL7P1.151) revealed a total of 325 interacting partners of which only 20 (6%) were present within the AdoMetDC inhibited transcriptome dataset. Similarly, the comparison of the interactome data for SpdS and the AdoMetDC inhibited transcriptome dataset revealed that only 9 out of 95 (9%) interacting partners could be identified in the AdoMetDC inhibited transcriptome dataset. However, comparison of the interacting partners of AdoMet synthase to the AdoMetDC inhibited transcriptome dataset revealed that 84 out of 257 (33%) interacting partners were present within the AdoMetDC inhibited transcriptome dataset (Table 4.6 and Appendix C). The interactome of AdoMet synthase contained 6 oxidative stress transcripts that included NADH-cytochrome b5 reductase (PF13_0353), putative protein disulfide isomerase related protein (PF11_0352), putative disulfide isomerase precursor (MAL8P1.17), thioredoxin reductase (PFI1170c), glutathione peroxidase (PFL0595c), putative thioredoxin-related protein (PF13_0272). Although the interactome (PlasmoMAP) is an *in silico* datbase and needs

experimental verification the results may reveal a possible link between AdoMetDC and AdoMet synthase. The complete set of interactome binding partners for AdoMetDC, DHPS/HPPK and AdoMet synthase is given in Appendix C.

Table 4.6: The top 20 interacting partners for AdoMetDC, and AdoMet synthase.

Nr	PlasmoDB ID	Name	Score[x]	Present in diff affected transcriptome
		AdoMetDC[a]		
1	PF11_0317	Structural maintenance of chromosome protein, putative	9.53	
2	PFE0195w	P-type ATPase, putative	8.31	
3	PFA0390w	DNA repair exonuclease, putative	7.98	
4	MAL8P1.99	Hypothetical protein	6.62	Yes
5	PF11_0427	Dolichyl-phosphate b-D-mannosyltransferase, putative	6.62	
6	PF07_0129	ATP-dept. acyl-coa synthetase	6.62	Yes
7	PFA0590w	ABC transporter, putative	6.62	Yes
8	PF10_0260	Hypothetical protein	5.90	
9	PF13_0348	PfRhop148,Rhoptry protein	5.90	Yes
10	PF14_0053	Ribonucleotide reductase small subunit	5.70	Yes
11	PFD0685c	Chromosome associated protein, putative	4.71	Yes
12	PFC0125w	ABC transporter, putative	4.71	Yes
13	PF14_0709	Ribosomal protein L20, putative	4.71	Yes
14	PF08_0131	1-cys peroxidoxin	4.71	Yes
15	PF11_0117	□eplication factor C subunit 5, putative	4.71	Yes
16	PF11_0181	Tyrosine --tRNA ligase, putative	4.71	Yes
17	PFB0180w	5'-3' exonuclease, N-terminal resolvase-like domain, putative	4.71	
18	PFL2180w	50S ribosomal protein L3, putative	4.71	
19	PF14_0097	Cytidine diphosphate-diacylglycerol synthase	4.71	
20	PF14_0081	DNA repair helicase, putative	4.71	
		AdoMet synthase[b]		
1	PFE1345c	Minichromosome maintenance protein 3, putative	11.69	Yes
2	PFB0895c	Replication factor C subunit 1, putative	11.69	Yes
3	PFL0835w	GTP-binding protein, putative	8.31	
4	PFI1575c	Peptide release factor, putative	8.31	Yes
5	PF13_0095	DNA replication licensing factor mcm4-related	8.31	Yes
6	PF14_0177	DNA replication licensing factor MCM2	8.31	Yes
7	PFB0795w	ATP synthase F1, alpha subunit, putative	8.31	
8	PFE0450w	Chromosome condensation protein, putative	7.98	Yes
9	PFD0420c	Flap exonuclease, putative	7.98	
10	MAL13P1.96	Chromosome segregation protein, putative	7.98	
11	PFD0590c	DNA polymerase alpha	7.98	Yes
12	PFC0745c	Proteasome component C8, putative	6.62	
13	PF13_0061	ATP synthase gamma chain, mitochondrial precursor, putative	6.62	
14	PF07_0023	DNA replication licensing factor mcm7 homologue, putative	6.62	Yes
15	MAL8P1.128	Proteasome subunit alpha, putative	6.62	
16	PF13_0353	NADH-cytochrome b5 reductase, putative	5.96	Yes
17	MAL8P1.101	Hypothetical protein	5.96	Yes
18	PF14_0063	ATP-dependent Clp protease, putative	5.96	
19	PFI0240c	E1-E2_ATPase/hydrolase, putative	5.96	Yes
20	PF11_0249	Hypothetical protein	5.96	

[a]AdoMetDC top 20 interacting partners resulted in 11/20 hits (55%). [b]AdoMet synthase top 20 interacting partners resulted in 11/20 hits (55%). [x]Probability score predicted by the interactome database. Interactome data obtained from PlasmoMAP (http://www.cbil.upenn.edu/cgi-bin/plasmoMAP).

4.3.11 Comparison of AdoMetDC inhibited transcriptome dataset to the transcriptomes of inhibited AdoMetDC/ODC and inhibited spermidine synthase

Comparison of the AdoMetDC inhibited transcriptome dataset (549 transcripts) to the co-inhibition of AdoMetDC/ODC (dataset of 538 transcripts), revealed that 154 transcripts were shared between these two datasets (Figure 4.17). Of these 154 transcripts, 21% (34/154) had increased transcript abundance and 79% (122/154) had decreased transcript abundance with regard to the AdoMetDC inhibited transcriptome dataset. Comparison of the AdoMetDC inhibited transcriptome dataset to the differentially affected transcriptome of inhibited SpdS (dataset of 708 transcripts) revealed that 194 transcripts were shared between these 2 perturbation studies. Within these 194 shared transcripts, 76% (148/194) had decreased transcript abundance while 24% (46/194) had increased transcript abundance.

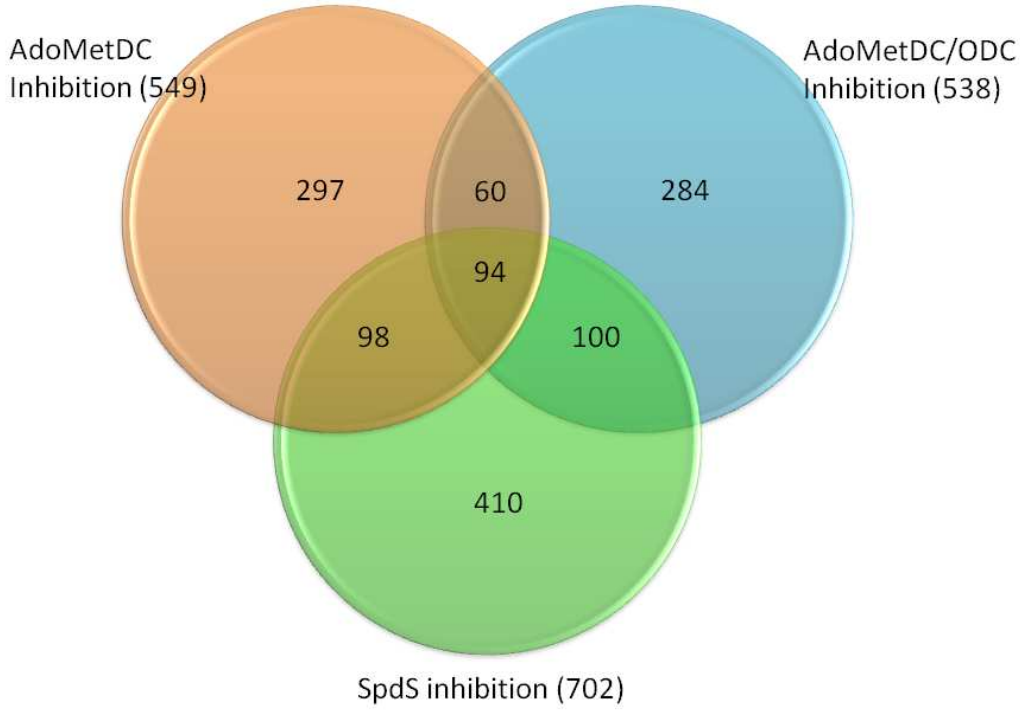

Figure 4.17: Correlation between transcript data from the AdoMetDC inhibited transcriptome dataset, co-inhibition of AdoMetDC/ODC and SpdS inhibition.

The total number of differentially affected transcripts for each of the 3 different studies is given in brackets next to the study name. In total, 94 transcripts were shared between all 3 studies.

In total, 94 transcripts were shared between all 3 polyamine-perturbation studies mentioned (Table 4.7 and Appendix D for full list of shared transcripts). Submission of these 94 shared transcripts to MADIBA did not reveal any metabolic pathway to be significantly affected according to Fishers

test. Of the transcripts that were shared between the AdoMetDC inhibited transcriptome dataset and at least one of the other polyamine-perturbation studies, 6 polyamine-related transcripts were similarly affected in all 3 polyamine-perturbation studies (Table 4.7). Adenosine deaminase (PF10_0289), purine nucleotide phosphorylase (PFE0660c), lysine decarboxylase-like protein (PFD0670c), phosphoethanolamine N-methyltransferase (MAL13P1.214), and pyridoxal 5'-phosphate synthase (PF14_0570) had decreased transcript abundances in all 3 polyamine-perturbation studies. AdoMet synthetase was only shared between the AdoMetDC inhibited transcriptome dataset and the co-inhibition of AdoMetDC/ODC, and was not regulated in the SpdS inhibited transcriptome. Only 2 of the polyamine-related transcripts that were shared in all 3 polyamine-perturbation studies had increased transcript abundances and included LDC (PFD0285c) and calcium/calmodulin-dependent protein kinase 2 (PFL1885c). Various oxidative stress-related transcripts were shared between all 3 polyamine-perturbation studies and all of these transcripts had decreased abundance. Similar results were obtained for folate metabolism, cell cycle regulation, transcription factors and the majority of transporters shared between all 3 polyamine-perturbation studies.

Table 4.7: Shared transcripts from the AdoMetDC inhibited transcriptome dataset, the co-inhibited AdoMetDC/ODC dataset and the inhibition of SpdS.

PlasmoDB ID	Name	Fold change		
		AdoMetDC	AO	SpdS
	Polyamine and Methionine metabolism			
PF10_0289	Adenosine deaminase, putative	-3.1	-2.4	-2.3
PFD0285c	Lysine decarboxylase, putative	2.5	2.8	2.4
PFE0660c	Purine nucleotide phosphorylase, putative	-3.0	-2.7	-3.6
PFE1050w	Adenosylhomocysteinase	-2.1	-1.5	
PFI1090w	S-adenosylmethionine synthetase	-2.3	-1.5	
PFD0670c	Lysine decarboxylase-like protein, putative	-2.0	-1.6	-3.1
	Methyltransferases			
MAL13P1.214	Phosphoethanolamine N-methyltransferase	-5.1	-2.7	-3.4
PF14_0309	Protein-L-isoaspartate O-methyltransferase beta-aspartate methyltransferase, putative	-3.9	-1.8	
PF14_0526	Conserved Plasmodium protein, unknown function	-3.1	-2.1	-2.0
	Potential polyamine associated effects			
PFL1885c	Calcium/calmodulin-dependent protein kinase 2	2.2	2.3	2.4
PF14_0570	Pyridoxal 5'-phosphate synthase, putative	-2.3	-2.2	-2.5
PF14_0200	Pantothenate kinase, putative	-1.7		-2.2
	Oxidative stress and redox metabolism			
PF08_0131	1-cys peroxiredoxin	-2.7	-2.8	-4.5
PF14_0187	Glutathione S-transferase	-1.8	-1.5	-2.1
PF14_0192	Glutathione reductase	-2.2	-1.7	-2.6
PF13_0353	NADH-cytochrome B5 reductase, putative	-2.1		-2.4
PFI1170c	Thioredoxin reductase	-1.9		-3.1
	Folate and Pyrimidine metabolism			
PFD0830w	Bifunctional dihydrofolate reductase-thymidylate synthase	-4.9	-1.6	-2.2
PF13_0349	Nucleoside diphosphate kinase b, putative	-3.5	-1.9	-4.4

PF10_0154	Ribonucleotide reductase small subunit, putative	-5.4	-1.5	-4.2
PF14_0053	Ribonucleotide reductase small subunit	-3.9	-1.4	-5.0
	Glycolysis			
PF13_0141	L-lactate dehydrogenase	-1.9	-1.5	-2.4
	DNA replication			
PF11_0117	Replication factor C subunit 5, putative	-1.8	-1.8	-4.5
PF11_0282	Deoxyuridine 5'-triphosphate nucleotidohydrolase, putative	-6.3	-2.9	-2.8
PF13_0291	Replication licensing factor, putative	-2.5	-1.2	-3.5
PF14_0254	DNA mismatch repair protein Msh2p, putative	-1.9	-1.4	-2.0
PFD0685c	Chromosome associated protein, putative	-2.0	-2.0	-2.0
PFE0675c	Deoxyribodipyrimidine photolyase, putative	-2.8	-1.5	-4.3
PFI0235w	Replication factor A-related protein, putative	-2.1	-1.8	-4.0
	Transcription factors			
PF11_0241	Myb-like DNA-binding domain, putative	1.7	1.8	2.1
PFL0465c	Zinc finger transcription factor (krox1)	1.8	2.0	
PF14_0374	CCAAT-binding transcription factor, putative	1.7	2.1	
PFL1900w	Transcription factor with AP2 domain(s), putative	-2.7	-1.4	-4.9
PF11_0404	Transcription factor with AP2 domain(s), putative	1.9		2.0
PF13_0097	Transcription factor with AP2 domain(s), putative	1.7		2.3
PFI1665w	Transcription factor with AP2 domain(s), putative	-1.9		-2.2
	Translation			
PF14_0709	Mitochondrial ribosomal protein L20 precursor, putative	-2.1	-1.9	-2.4
PFI0890c	Organelle ribosomal protein L3 precursor, putative	-2.2	-1.6	-2.7
	Cell cycle and cytokinesis			
PF13_0328	Proliferating cell nuclear antigen	-5.7	-1.9	-4.2
PFE0165w	Actin-depolymerizing factor, putative	-2.2	-2.0	-2.5
PFI0180w	α-tubulin	-7.3	-1.5	-4.5
PFI1565w	Profilin, putative	-3.0	-2.0	-2.2
	Transporters			
PFC0125w	ABC transporter, (TAP family), putative	-1.9	-1.9	-2.1
MAL13P1.23	CorA-like Mg^{2+} transporter protein, putative	1.8		2.0
PF14_0211	Ctr copper transporter domain containing protein, putative	-2.3		-3.4
PFI0240c	Cu^{2+} -transporting ATPase,	-1.9		-4.4
MAL8P1.32	Nucleoside transporter, putative	-2.8	-1.5	-3.0
PF14_0662	Nucleoside transporter, putative	1.8	1.8	
PFA0245w	Transporter, putative	-3.8	-1.3	
PFE0410w	Triose phosphate transporter	-1.7	-1.9	-2.5
PF07_0065	Zinc transporter, putative	-4.8	-2.2	-3.4

4.3.12 Comparison of AdoMetDC inhibited transcriptome dataset to other *P. falciparum* perturbation data

The 549 differentially affected transcripts from the AdoMetDC inhibited transcriptome dataset was compared to the transcriptomes of 5 other perturbation studies which included CQ inhibition (Gunasekera *et al.*, 2007, Gunasekera *et al.*, 2003), febrile temperature perturbation (Oakley *et al.*, 2007), artesunuate inhibition (Natalang *et al.*, 2008), anti-folate inhibition (Ganesan *et al.*, 2008) and the effect of 20 individual compounds on the transcriptome (Hu *et al.*, 2010). Microarray analysis of artesunate inhibition resulted in the differential regulation of 398 transcripts (Natalang et al., 2008). Of these, only 62 transcripts were shared between artesunate inhibition (398 transcripts)

and the AdoMetDC inhibited transcriptome dataset (549 transcripts). Anti-folate inhibition resulted in only 54 differentially regulated transcripts (Ganesan *et al.*, 2008) of which 9 were shared with the AdoMetDC inhibition transcriptome dataset. CQ inhibition resulted in 601 differentially affected transcripts (Gunasekera et al., 2007) of which 65 were shared with the AdoMetDC inhibited transcriptome dataset. The effect of febrile temperature perturbation on parasites resulted in 336 differentially affected transcripts (Oakley et al., 2007) of which 66 were shared with the AdoMetDC inhibited transcriptome dataset (Figure 4.18).

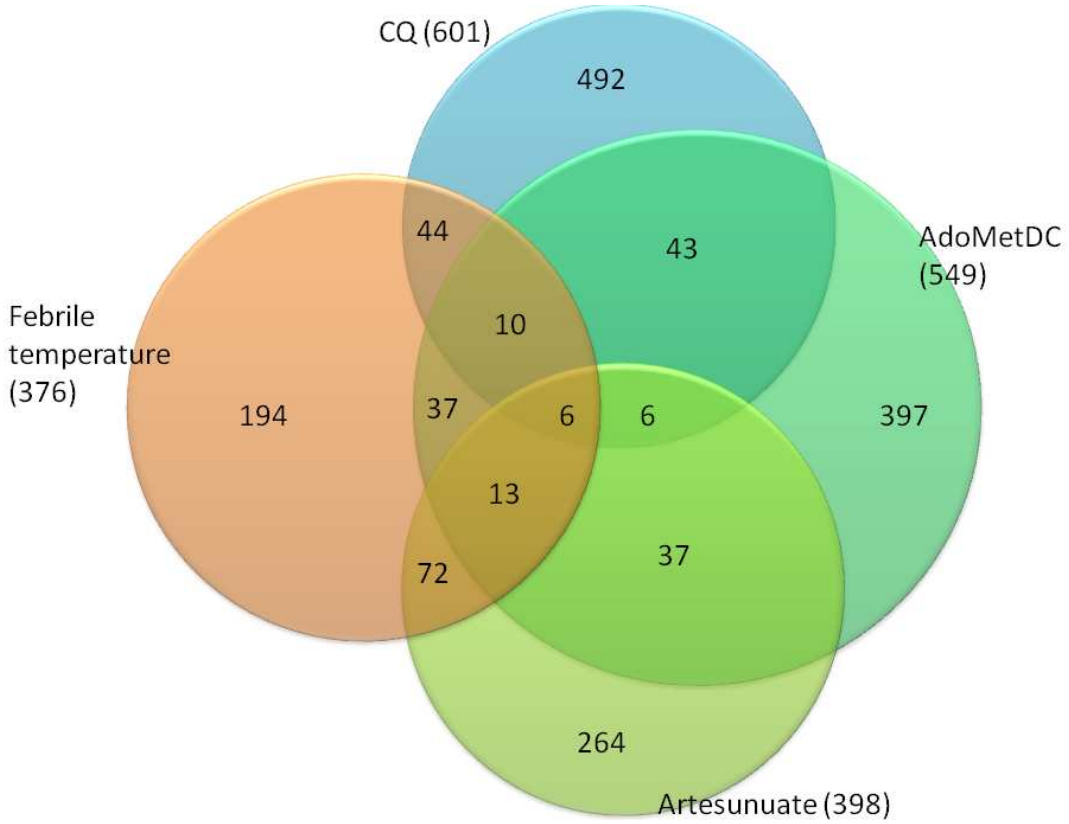

Figure 4.18: Comparisons between the differentially affected transcriptomes of the AdoMetDC inhibited transcriptome dataset, febrile temperature perturbation, CQ inhibition and artesunuate inhibition.

The total number of differentially affected transcripts for each of the 4 different studies is given in brackets next to the study name. In total, 6 transcripts were shared between all 4 studies. 6 transcripts were shared between the AdoMetDC inhibited transcriptome dataset, artesunuate inhibition, and CQ inhibition. 10 transcripts were shared between the AdoMetDC inhibited transcriptome dataset, febrile temperature perturbation and CQ inhibition. 13 transcripts were shared between the AdoMetDC inhibited transcriptome dataset, artesunuate inhibition, and febrile temperature perturbation. 37 transcripts were shared between the AdoMetDC inhibited transcriptome dataset and febrile temperature perturbation. 37 transcripts were shared between the AdoMetDC inhibited transcriptome dataset and artesunuate inhibition. 43 transcripts were shared between the AdoMetDC inhibited transcriptome dataset and CQ inhibition.

Parasites inhibited by 20 individual compounds in the schizont-stage resulted in the differential transcript regulation of 3125 transcripts (Hu, 2010) of which 430 were shared with the AdoMetDC inhibited transcriptome dataset. In total 466 transcripts from the AdoMetDC inhibited transcriptome

dataset were shared with at least one of the studies mentioned. Comparison of all the data from the above mentioned studies resulted in the identification of 5 transcripts shared between the AdoMetDC inhibited transcriptome dataset, artesunate inhibition, CQ inhibition, febrile temperature perturbation, and the 20 individual compounds data (Table 4.8). These 5 transcripts are therefore indicative of a general stress response by the parasite regardless of the perturbation. Of these 5 transcripts, only 4 were shared with the co-inhibition of AdoMetDC/ODC and inhibition of SpdS. The only transcript that was not shared within these studies was protein disulfide isomerase (PF11_0352).

Table 4.8: Five transcripts shared between all of the perturbation studies.

PlasmoID	Name	A	20 Comp	Temp	Artes	CQ
PF08_0060	Asparagine-rich antigen	2.2	n/a	2.1	2.4	n/a
PF11_0352	Protein disulfide isomerase	-1.8	n/a	-2.7	-1.9	n/a
PF14_0631	Conserved Plasmodium protein, unknown function	1.7	n/a	3.2	2.8	n/a
PF14_0758	Plasmodium exported protein (hyp17), unknown function	1.7	n/a	5.2	2.2	n/a
PFC0085c	Plasmodium exported protein, unknown function	1.8	n/a	4.3	2.7	n/a

A: AdoMetDC inhibition transcriptome dataset, 20 Comp: is the 20 individual compounds dataset, Temp: is the febrile temperature-perturbation dataset, Artes: Artesunuate inhibited dataset, CQ: CQ inhibited dataset. n/a is not available since the dataset provided only transcripts and not the fold changes.

Eighty three transcripts were identified that were unique to the AdoMetDC inhibited transcriptome dataset and not shared with any other published transcriptome analysis of *P. falciparum* after any other perturbation (Appendix E). These transcripts were sorted according to their GO terms (Table 4.9). Of the 83 unique transcripts, 32% (27/83) had increased transcript abundance and 68% (57/83) had decreased transcript abundance. Transcripts associated with DNA metabolism with increased transcript abundance included putative DNA topoisomerase VI B subunit (MAL13P1.328; 2.8-fold). Another transcript that was increased was kinesin-like protein (PF11_0478; 2.1-fold) and is associated with the cytoskeleton of the parasite. Various translation associated transcripts were identified that were all decreased, similarly for RNA metabolism and signal transduction. Interestingly, 3 polyamine-associated transcripts were unique and included phosphoetanolamine N-methyltransferase (MAL14P1.214; -5.1-fold), methyl transferase-like protein (PF13_0016; -1.9-fold) and a conserved protein (PF14_0526; -3.1-fold). Pyridoxal 5'-phosphate synthase (PF14_0570; -2.3-fold), associated with Vitamin B synthesis was also unique to the AdoMetDC inhibited transcriptome dataset and had decreased transcript abundance. Various exported proteins were also identified as unique for AdoMetDC perturbation and were mostly increased in transcript abundance.

Table 4.9: Unique transcripts associated with AdoMetDC perturbation.

PlasmoDB ID	Product Description	FC[a]
	DNA metabolism	
MAL13P1.328	DNA topoisomerase VI, B subunit, putative	2.8
PF14_0053	Ribonucleotide reductase small subunit	-3.9
PFL1180w	Chromatin assembly protein (ASF1), putative	-2.2
	Proteolysis	
PF13_0084	Ubiquitin-like protein, putative	1.7
PF14_0348	ATP-dependent Clp protease proteolytic subunit, putative	-2.0
	Translation	
PFC0675c	Mitochondrial ribosomal protein L29/L47 precursor, putative	-1.9
PFF0495w	Mitochondrial ribosomal protein L19 precursor, putative	-2.0
PF11_0113	Mitochondrial ribosomal protein L11 precursor, putative	-2.0
PFC0701w	Mitochondrial ribosomal protein L27 precursor, putative	-2.5
PFD0675w	Apicoplast ribosomal protein L10 precursor, putative	-2.9
	Phosphorylation	
PFC0485w	Protein kinase, putative	-1.7
PFF0260w	Serine/threonine protein kinase, Pfnek-5	-1.7
	Polyamine methionine metabolism	
PF13_0016	Methyl transferase-like protein, putative	-1.9
PF14_0526	Conserved Plasmodium protein, unknown function	-3.1
MAL13P1.214	Phosphoethanolamine N-methyltransferase	-5.1
	Primary metabolism	
PFI0960w	Dolichyl-diphosphooligosaccharide-protein glycosyltransferase, putative	-1.7
MAL13P1.220	Lipoate synthase, putative	-1.7
PFB0505c	3-oxoacyl-(acyl carrier protein) synthase III, putative	-2.1
	Cytoskeleton organization and biogenesis	
PF11_0478	Kinesin-like protein, putative	2.1
	RNA metabolic process	
MAL8P1.72	High mobility group protein	-1.7
PF13_0043	CCAAT-binding transcription factor, putative	-1.8
PFD0750w	Nuclear cap-binding protein, putative	-1.8
PF10_0313	Mitochondrial preribosomal assembly protein rimM precursor, putative	-1.9
	Signal transduction	
PF14_0317	Microsomal signal peptidase protein, putative	-1.7
PFI1005w	ADP-ribosylation factor-like protein	-2.0
	Coenzyme metabolic process	
MAL7P1.130	3-demethylubiquinone-9 3-methyltransferase, putative	-1.7
PF14_0570	Pyridoxal 5'-phosphate synthase, putative	-2.3
	Host parasite	
PFF0020c	Erythrocyte membrane protein 1 (PfEMP1)-like protein	1.7
PF07_0138	Rifin	-2.1
MAL7P1.23	RAP protein, putative	-1.7
PF11_0046	CPW-WPC family protein	-1.8
PF14_0297	Apyrase, putative	-2.0
MAL8P1.216	Rifin	-2.4
	Hypotheticals	
PFI1780w	Plasmodium exported protein (PHISTc), unknown function	2.5
PF14_0760	Plasmodium exported protein, unknown function	2.0
PF11_0514	Plasmodium exported protein (PHISTa), unknown function	2.0
PFF1535w	Plasmodium exported protein (hyp5), unknown function	1.9
PFF0075c	Plasmodium exported protein (PHISTb), unknown function	1.8
PFB0970c	Plasmodium exported protein, unknown function	1.7
MAL7P1.230	Hypothetical protein, pseudogene	1.7

Unique differentially expressed transcripts associated with the perturbation of AdoMetDC when compared to the Bozdech data, Artesunate, CQ, antifolate, and febrile temperatures. [a] Fold change of AdoMetDC perturbation.

To determine if the comparisons between the AdoMetDC perturbation and all the other perturbation studies mentioned had any significance, the 83 transcripts unique to the AdoMetDC inhibited transcriptome dataset were analysed with MADIBA to identify significant metabolic pathways. Methionine and polyamine metabolism were once again identified as significant ($p = 0.0638$ with $p<0.01$) for the 83 transcripts unique to the AdoMetDC inhibited transcriptome dataset. This is similar to the complete AdoMetDC inhibited transcriptome dataset in which methionine and polyamine metabolism were identified as the only significant ($p = 0.018$) metabolic pathways affected. Of the 83 unique transcripts that were identified for the AdoMetDC inhibited transcriptome dataset only 9 were shared with the co-inhibition of AdoMetDC/ODC and SpdS inhibition (Table 4.10) and may be unique to parasites in which polyamine metabolism were affected.

Table 4.10: Nine of the unique transcripts only found in polyamine-regulated parasites.

PlasmoID	Name	Fold Change[a]		
		A[b]	AO[c]	SpdS[d]
MAL13P1.214	Phosphoethanolamine N-methyltransferase	-5.1	-2.7	-3.4
MAL7P1.33	Conserved Plasmodium protein, unknown function	-2.6	-1.6	-2.2
MAL7P1.61	Hypothetical protein	1.7	-1.8	2.4
PF14_0053	Ribonucleotide reductase small subunit	-3.9	-1.4	-5.0
PF14_0297	Apyrase, putative	-2.0	-1.5	-2.1
PF14_0526	Conserved Plasmodium protein, unknown function	-3.1	-2.1	-2.0
PF14_0570	Pyridoxal 5'-phosphate synthase, putative	-2.3	-1.7	-2.5
PFB0953w	Plasmodium exported protein (hyp15), unknown function	-1.8	-1.3	-3.9
PFE0685w	Hypothetical protein	-2.6	-1.9	-3.5

[a]Fold change for each of the transcripts in each of the individual studies. [b]A: AdoMetDC inhibited transcriptome dataset. [c]AO: AdoMetDC/ODC co-inhibition. [d]SpdS: spermidine synthase inhibition.

4.3.13 Validation of microarray results with real-time PCR

The MicroArray Quality Control (MAQC) consortium has been established to evaluate the performance of several microarray and qRT-PCR platforms, which is crucial for comparisons between microarray data (Arikawa et al., 2008). Microarray validation consists of a selection of genes on the microarray that is not differentially regulated in order to use these genes as housekeeping genes for normalisation purposes (Abruzzo *et al.*, 2005).

To validate the microarray data from the AdoMetDC inhibited transcriptome dataset, 6 transcripts were selected and used for qRT-PCR. Cyclophillin was used as “housekeeping gene” since its transcript abundance remains relatively unchanged within the AdoMetDC inhibited transcriptome dataset. The qRT-PCR was done over the 3 time points and the fold change calculated to compare to the microarray results. Comparison of the FC for both the microarray Tt_3 and the qRT-PCR Tt_3

revealed similarities in the values obtained. The qRT-PCR data also show that during Tt_1 and Tt_2 the transcripts were not yet affected by the inhibition of AdoMetDC, which is similar to the data obtained from the microarray experiment for Tt_1 and Tt_2, and that the affected transcripts progress over time. SpdS was included in the validation process since it is a polyamine-related transcript, but was not differentially affected by AdoMetDC perturbation (Table 4.11).

Table 4.11: Comparison of microarray data with real-time PCR data.

Name	qRT-PCR FC			Micro-array FC
	Tt_1	Tt_2	Tt_3	Tt_3
PEMT	1.1	-1.7	-3.9	-5.0
AHC	1.0	-1.4	-1.9	-2.1
SpdS	1.1	1.1	1.2	nd
AdoMet synthase	-1.1	-1.8	-1.5	-2.3
LDC	1.2	1.1	2.4	2.5
HH4	-1.0	-1.3	-2.6	-3.4

PEMT: phosphoethanolamine N-methyltransferase, AHC: adenosylhomocysteinase, SpdS: spermidine synthase, AdoMet synthase: S-adenosylmethionine synthestase, LDC: lysine decarboxylase, HH4: histone H4. Nd is representative of a transcript not detected as regulated in the microarray data.

4.4 Discussion

Three time points were selected for RNA extraction for microarray analysis, in an attempt to span the maximum life stages in which the transcript for *Pf(adometdc/odc)* is available. According to the IDC the transcript of *Pf(adometdc/odc)* is produced from 12 to 36 HPI with maximum transcript expression of *Pf(adometdc/odc)* at 24 HPI (Bozdech *et al.*, 2003). The morphology study conducted in Chapter 3 also determined that morphological arrest occurs at 30 HPI and therefore earlier time points were needed before visible morphological arrest of the parasites occur.

Microarrays enable the analysis of thousands of genes on a single slide, and offer the promise of a wealth of information on the transcriptomic state of an organism at any particular moment in time. The use of the Plasmodial Agilent platform enables the simultaneous analyses of 8 samples on a single slide therefore reducing labour intensive hours and improving reproducibility. Overall, the use of the Agilent arrays resulted in better quality microarray data, and confidence in analysis (Hester *et al.*, 2009). This increased spot quality and the subsequent increased quality in the microarray data was also seen in our lab when the Agilent hybridised spots were compared to previously used in-house spotted Plasmodial arrays. The A+T-richness of the Plasmodial genome negates the use of amplification methods for microarrays (Bozdech *et al.*, 2003), therefore the 3-fold reduction in sample size needed per array on the Agilent platform is highly advantageous. The transcriptomic investigation of the AdoMetDC inhibited transcriptome employed a reference design (Figure 4.1), which enabled valid comparisons of data. The reference is a representative sample of equal amounts of each of the treated and untreated samples used at the 3 different time points. Synchronised parasite cultures were used during the transcriptomic investigation in order to determine drug-specific responses of the parasite and not life cycle-related responses.

Determination of the Pearson correlations at the 3 time points investigated for the AdoMetDC inhibited transcriptome revealed that Tt_1 and Tt_2 had only a few differentially expressed transcripts. The 2 early time points were harvested before any observable morphological difference between the treated and untreated parasite (Chapter 3). The later time point (Tt_3: 26 HPI) which correlates with the predicted maximum transcript expression of AdoMetDC (Bozdech *et al.*, 2003) did result in the identification of differentially affected transcripts as a result of AdoMetDC inhibition. The Pearson correlations indicated that the 3 time points used within the AdoMetDC inhibited transcriptome was early enough to enable direct comparisons between treated and untreated parasites and deemed the use of a t_0 strategy unnecessary. The relative t_0 strategy determines the point of transcriptional arrest within the parasite and then uses this point as reference for comparisons made between treated and untreated parasites. This strategy compensates for life and stage specific responses, and ensures that

only drug-specific responses are detected (Van Brummelen, 2009). The co-inhibition of AdoMetDC/ODC used 3 time points taken at 19 HPI, 27 HPI and 34 HPI. This is later than the time points used within this study for the AdoMetDC inhibited transcriptome, of which all 3 time points were in the early life cycle stages. Pearson correlations between all the time points confirmed the validity of directly comparing UTt_3 with Tt_3 for the AdoMetDC inhibited transcriptome. Further analyses of the data for UTt_3:Tt_3 subsequently revealed the differential regulation of 549 transcripts with AdoMetDC inhibition. MDL73811 is an irreversible inhibitor of AdoMetDC, and it is assumed to inhibit its effects from 24 HPI when the transcript for *Pf(adometdc/odc)* is maximally expressed at 24 HPI. Hierarchical clustering of all 3 time points of the AdoMetDC inhibited transcriptome confirmed that transcriptional arrest occurs at Tt_3 and that only a few differentially affected transcripts are present in Tt_1 and Tt_2. Analysis of the data with LIMMA-GUI identified 549 differentially expressed transcripts of which 143 transcripts (24%) had an increase in abundance and 406 transcripts (74%) had a decrease in abundance. Transcript differential expression levels ranged from 7-fold decreased to 4-fold increased transcript abundance, which is in agreement with most other microarray perturbation studies on *P. falciparum*

Methionine and polyamine metabolism were the only significantly affected pathways with 7 unique transcripts present within the AdoMetDC inhibited transcriptome dataset when analysed with MADIBA. This result clearly indicates the specificity of the AdoMetDC inhibited transcriptome dataset for polyamine-related responses of the parasite under AdoMetDC inhibition. All the transcripts associated with polyamine biosynthesis had decreased transcript abundances with the exception of lysine decarboxylase (PFD0285c) that had an increased transcript abundance (2.5-fold). Five methyltransferase transcripts associated with polyamine metabolism were also decreased in transcript abundance.

A comparison was made between the microarray data for the AdoMetDC inhibited transcriptome data (this study), AdoMetDC/ODC co-inhibition (Van Brummelen, 2009) and the inhibition of SpdS (Becker *et al.*, 2010). Comparison of these transcriptomic datasets revealed 154 transcripts that were shared between the AdoMetDC inhibited transcriptome dataset and the AdoMetDC/ODC co-inhibition study and 194 transcripts that were shared between the AdoMetDC inhibited transcriptome dataset and inhibition of SpdS. Ninety-four transcripts were shared between the 3 polyamine-affected transcriptomic studies. Transcripts with decreased abundance in these transcriptomic studies included adenosine deaminase, purine nucleotide phosphorylase, lysine decarboxylase-like protein, phosphoethanolamine N-methyltransferase and pyridoxal 5'-phosphate synthase. These transcripts may therefore be considered as signature transcripts for polyamine-

affected parasites. LDC and calcium/calmodulin-dependent protein kinase 2 had increased transcript abundance in all 3 polyamine-affected transcriptomic studies, suggesting that these 2 transcripts may be involved in compensatory mechanisms of the parasite to cope with polyamine-depletion.

The transcript of AdoMetDC/ODC was not differentially affected by inhibition with MDL73811, which corresponds to the cyclohexylamide perturbation of SpdS that also resulted in the transcript of AdoMetDC/ODC remaining unchanged. This is different to the co-inhibition data in which the transcript abundance of AdoMetDC/ODC decreased 2-fold (van Brummelen *et al.*, 2009) as well as the mono-functional inhibition of ODC, which also resulted in the transcript of AdoMetDC/ODC to decrease in abundance (K. Clark, unpublished data). The inhibition of AdoMetDC and SpdS would result in increased putrescine levels and the transcript abundance of AdoMetDC/ODC is maintained. With the mono-functional inhibition of ODC and the co-inhibition of AdoMetDC/ODC putrescine levels decrease, resulting in the abundance of the AdoMetDC/ODC transcript being decreased (Van Brummelen, 2009). It appears that putrescine may act as a transcriptional stabiliser for the transcript of AdoMetDC/ODC. Evidence for the regulation of *Pf*ODC activity by putrescine does exist (Wrenger *et al.*, 2001), but to date there is no evidence as to the transcriptional regulation of *Pf*AdoMetDC/ODC transcript by putrescine. Spermidine synthase was not differentially affected in any one of the 3 polyamine-affected transcriptomic studies. Therefore the transcript abundance of SpdS is not affected by the absence of any one of the polyamines. The regulatory role of SpdS within the polyamine pathway therefore needs further investigation.

Another measure of the specificity of the AdoMetDC inhibited transcriptome dataset was obtained by the comparison of the differentially affected transcripts from the AdoMetDC inhibited transcriptome, with those of the other Plasmodial perturbation studies. In total 466 transcripts from the AdoMetDC inhibited transcriptome dataset were shared with at least one of the studies mentioned. Only 5 transcripts were shared between all the different perturbation studies and are therefore indicative of general stress responses elicited by the parasites under exposure to unwanted external stimuli.

Comparison of the AdoMetDC data to the total of 4513 differentially expressed transcripts from the inhibition studies mentioned above revealed a total of 83 transcripts unique to only AdoMetDC inhibition (Table 4.9). Three transcripts were unique to polyamine metabolism and were all decreased in abundance, identifying polyamine and methionine metabolism as uniquely-affected pathways for the 83 unique transcripts submitted to MADIBA. The importance of these 83 unique

transcripts provides a specific transcriptomic signature profile for the AdoMetDC inhibited transcriptome. These specific transcriptomic signature profiles therefore can be utilised to determine the mode-of-action of unknown compounds, which has already been successfully applied in antimicrobial (Pietiainen *et al.*, 2009) and tuberculosis transcriptomic studies (Boshoff *et al.*, 2004).

The inhibition of AdoMetDC with MDL73811 resulted in the decreased transcript abundance of adenosine deaminase (PF10_0289), HPPRT (PF10_0121) and PNP (PFE0660c), and decreased dcAdoMet metabolite levels and conversely also in decreased spermidine and MTA levels and subsequently MTI. The absence of MTA as result of AdoMetDC-inhibition may result in the decreased transcript abundances observed for adenosine deaminase, PNP and HPPRT. These results indicate a co-dependency between polyamine metabolism and down-stream MTA and MTI metabolism.

The transcript of AdoMet synthase was decreased with the inhibition of AdoMetDC. AHC also had decreased transcript abundance and together with AdoMet synthase play an essential role in regulation of the methionine levels. AdoMet synthase produces AdoMet from methionine and is therefore an important link between polyamine biosynthesis and methionine metabolism. In Trypanosomes treated with MDL73811 there is a significant increase in AdoMet levels, which ultimately results in hypermethylation and parasite death (Goldberg *et al.*, 1997a). Trypanosomal AdoMet synthase is not inhibited by its own product (Goldberg *et al.*, 2000, Yarlett *et al.*, 1993). Similar to Trypanosomes, AdoMet synthase in Plasmodial parasites is also not feedback regulated by its product, AdoMet (Muller *et al.*, 2008), which may also lead to the expectation of increased AdoMet levels and consequent hypermethylation within the Plasmodial parasite as a mode-of-action for MDL73811. Methylation is dependent on the AdoMet:AdoHcy levels. An increase in AdoMet will result in hypermethylation, while an increase in AdoHcy will result in hypomethylation. However, the effect of the decreased transcript abundance observed for both AdoMet synthase and AHC may restore the balance of AdoMet and AdoHcy within methionine metabolism (Van Brummelen, 2009), but it does seems that in *P. falciparum* polyamine metabolism and methionine metabolism is closely linked. The effect of the decreased transcript abundance of both AdoMet synthase and AHC on the methylation status of Plasmodial parasites is unclear. Closely linked to the methionine metabolism and methylation cycle is methyltransferases. The majority of methyltransferases had decreased transcript abundances. In particular, PEMT had decreased transcript abundance and is uniquely-affected by AdoMetDC inhibition, the co-inhibition of AdoMetDC and inhibition of SpdS, but was not affected with the mono-functional inhibition of ODC or any other perturbation. Therefore, in the absence of spermidine and spermine, PEMT is

affected. These possible methylation regulatory mechanisms will be investigated further in Chapter 5.

Polyamine-related transcripts that remained unaffected by the inhibition of AdoMetDC include arginase and OAT. The transcript regulation of OAT could not be determined with microarray due to saturation of the spot on the microarray. Subsequent RT-PCR revealed that the transcript of OAT remained unchanged in abundance with AdoMetDC inhibition. Ornithine levels are also homeostatically regulated through the action of arginase (Olszewski *et al.*, 2009). Therefore, ornithine homeostasis is independent of polyamine metabolism. It should however be noted that it did seem like the protein abundance of OAT increased although this could not be measured in Tt2 of the proteomic study due to the spot for OAT and AdoMet synthase that overlapped and were saturated (Chapter 3).

Upon inhibition of AdoMetDC with MDL73811, 9 folate and pyrimidine metabolism transcripts displayed a decrease in transcript abundance. Folate and methionine metabolism is linked by the recycling of N5-methyl THF to methionine (Bistulfi *et al.*, 2009). In human prostate and colon cell lines, folate and polyamine pathways are connected since N-5,10-methylene THF can be converted to N-5-methyl THF, which plays a role in methionine metabolism in the conversion of homocysteine back into methionine (Bistulfi *et al.*, 2009). Folate depletion in prostate cells resulted in an imbalance of AdoMet levels due to the link between folate and methionine metabolism (Bistulfi *et al.*, 2009). Given the evidence in prostate cells, and the fact that 9 folate-related transcripts were decreased with AdoMetDC inhibition it is postulated that a link does exist between polyamine metabolism and folate metabolism within the Plasmodial parasite. This will be investigated further in Chapter 5.

Thirteen transcripts associated with oxidative stress and redox status of the parasite all had a decrease in transcript abundance (Appendix B). Some of these transcripts include 1-cys peroxiredoxin (PF08_0131), glutathione S-transferase (PF14_0187), glutathione reductase (PF14_0192), thioredoxin (PF14_0545) and thioredoxin reductase (PFI1170c). The parasite is exposed to a constant risk of oxidative stress since it resides in a pro-oxidant environment. The constant exposure to oxygen and iron from hemoglobin within the erythrocyte enables the formation of reactive oxygen species (ROS) via the Fenton reaction. It is therefore essential that the parasite needs an efficient anti-oxidant system to be able to deal with all these threats (Muller, 2004). The role of polyamines to protect against ROS is different to that of glutathionine probably as a result of the close association of polyamines with DNA, lipids and proteins (Rider *et al.*, 2007).

Polyamines are able to provide protection by several mechanisms that include possible direct scavenging of ROS, induction of DNA conformational changes and primary protection of DNA by close association with DNA (Rider *et al.*, 2007). The relationship between polyamines and oxidative stress presents two possible scenarios. The first is that polyamine depletion reduces anti-oxidant capacity thus promoting oxidative stress (Assimakopoulos *et al.*, 2010). The second scenario is that ROS act as messengers that regulate expression of enzymes implicated in polyamine synthesis (Assimakopoulos *et al.*, 2010). *E. coli* and yeast strains with reduced polyamines have increased sensitivity towards oxidative damage (Chattopadhyay *et al.*, 2003, Jung *et al.*, 2003, Chattopadhyay *et al.*, 2006). Various studies have shown that polyamines are able to protect against superoxide (Lovaas & Carlin, 1991), radiation (Chiu & Oleinick, 1997, Chiu & Oleinick, 1998) and fenton radicals (Ha *et al.*, 1998). As such, the high polyamine content of Plasmodial parasites during normal proliferation may therefore provide protection against oxidative stress.

The transcript abundance of thioredoxin (PF14_0545) and thioredoxin reductase (PFI1170c) were decreased. The thioredoxin interactome revealed that OAT, AdoMet synthase and AHC are all interacting partners of thioredoxin (Sturm *et al.*, 2009). Similarly, thioredoxin reductase is also a binding partner of AdoMet synthase (Sturm et al., 2009, Wuchty *et al.*, 2009). This provides a further link between polyamine biosynthesis and oxidative stress. AdoMet synthase, AHC and thioredoxin reductase all had decreased transcripts levels with AdoMetDC inhibition. Therefore, due to the absence or decreased abundance of the binding partners, the decreased transcript abundances may result in the deregulation of the redox status of the parasite. This also establishes a link between AdoMet synthase and consequent polyamine regulation and the redox status of the parasite.

Similarly, decreased spermidine and spermine with increased putrescine levels in rat brain resulted in the production of ROS (Assimakopoulos *et al.*, 2010). Putrescine in *E. coli* protected DNA against oxidative stress and also resulted in increased survival rates of the bacteria, with an increase in ODC and LDC activity to combat the effects of the oxidative stress exposure (Tkachenko & Shumkov, 2004 (b), Tkachenko, 2004 (a)). As such, this provides a direct link between polyamine biosynthesis and oxidative stress.

The transcript abundance of LDC was increased with polyamine depletion in the Plasmodial parasites in all polyamine-affected transcriptome studies. Induced LDC may result in lysine being converted to cadaverine. The functional importance of cadaverine to the survival of Plasmodial parasites in AdoMetDC-inhibited parasites is unclear. However, LDC is able to increase in response

to oxidative stress while its product; cadaverine acts as a radical scavenger of superoxide in *Vibrio vulnificus* (Kim *et al.*, 2006, Kang *et al.*, 2007). In a polyamine-depleted environment, mammalian SpdS is able to utilise cadaverine due to the presence of the diamine group (Pegg *et al.*, 1981). This was similarly shown in *E. coli* cells in which spermidine was subsequently available for eIF5A synthesis (Park *et al.*, 1991). The induction of LDC and consequent increased cadaverine levels have been determined to alleviate AdoMetDC and arginine decarboxylase inhibition in pea seedlings (Icekson *et al.*, 1986) as well as alleviate ODC inhibition in *P. falciparum* (Assaraf *et al.*, 1987). Therefore, the induction of LDC is a possible compensatory mechanism in response to AdoMetDC inhibition.

Three cyclin-associated transcripts with decreased abundance were identified and included putative cyclin related protein (PFL1335w; -2.4-fold), Pfcyc-2 cyclin-related protein (PFL1330c; -2.6-fold) and proliferating cell nuclear antigen (PF13_0328; -5.7-fold). Polyamines play a role during cell cycle progression by being able to degrade cyclin B1 mRNA in the eukaryotic G1-phase, therefore enabling cells to enter the S-phase of the cell cycle (Thomas & Thomas, 2001). Polyamine-depletion can also result in cell cycle arrest due to decreased stabilisation of cyclin D1 (Wallace *et al.*, 2003). Therefore, polyamines and the cell cycle have an involvement in cell proliferation, since cyclin-associated transcripts decreased in abundance upon AdoMetDC inhibition.

Recently, a link was established between polyamines and microtubules (Savarin *et al.*, 2010). Interestingly, various transcripts involved in cytoskeleton organisation and biogenesis was also uniquely affected in the AdoMetDC inhibited transcriptome dataset. The transcript abundance of actin and tubulin were severely decreased with AdoMetDC perturbation. The disruption of tubulin results in G2/M cell cycle arrest and the induction of apoptosis in tumour cells (Chen *et al.*, 2007). It may therefore be assumed that polyamines may play a role in stabilisation of these transcripts. Microtubules in Plasmodial parasites have an essential role in cell division, motility and preserving the structural integrity of the parasite (Naughton *et al.*, 2008). The transcripts of centrin-3 (PF10_0271; -2.8-fold) and centrin-2 (PF14_0443; -4.9-fold) were also decreased with AdoMetDC perturbation. These centrins play a role in the cell cycle and cell proliferation within the malaria parasite. The decreased transcript abundances of the centrins in the erythrocytic stages may result in attenuation of sporozoite stage and erythrocyte stage parasites as well as result in transmission-defiecient Plasmodial strains (Mahajan *et al.*, 2008). Therefore, the decreased transcript abundances of the various cytoskeleton associated transcripts as a result of AdoMetDC inhibition are indicative of cell cycle arrest in the Plasmodial parasite.

In this chapter the transcriptomic response of the Plasmodial parasite was investigated after AdoMetDC inhibition. Evidence was provided that the 549 differentially regulated transcripts provide information on drug-specific responses by the parasite. Polyamine biosynthesis was a pathway uniquely associated with the AdoMetDC inhibited transcriptome dataset, which revealed unique links between polyamine biosynthesis and methionine metabolism. Other interesting consequences of AdoMetDC inhibition included the link between polyamine-regulation (spermidine and spermine depletion) and oxidative stress, folate metabolism, cytoskeleton biogenesis and phosphorylation that may impact on regulation of the *P. falciparum* cell cycle.

Due to the "just-in-time" production of transcripts, the transcripts are only expressed as they are needed (Bozdech *et al.*, 2003). It is also a general notion that the protein levels will mimic transcript levels within the Plasmodial parasite (Daily *et al.*, 2004). In the following chapter the correlation between the transcript and proteins of the AdoMetDC inhibited datasets are compared. Furthermore, it should be noted that the transcript and protein expression levels does not necessarily indicate the activity of that specific enzyme, therefore further biological investigations are presented in Chapter 5.

Chapter 5

Characterisation of specific metabolic responses identified in the transcriptomic and proteomic investigations of AdoMetDC inhibition in *P. falciparum*

5.1 Introduction

The "omics" technologies as a stand alone do not always provide sufficient information for a complete understanding of the physiology and pathogenicity of an organism (Hegde *et al.*, 2003). It is therefore of utmost importance to integrate the "omics" technologies to gain maximal information in understanding a response of an organism upon any perturbation. Unfortunately, integration of transcriptomic and proteomic data is not always easy since a clear correlation between mRNA and protein abundance is not always the case (Gygi *et al.*, 1999). It is therefore of utmost importance to determine such possible regulatory mechanisms. Another important aspect of integration of all the "omic" data is to determine the biological significance of the data that were obtained. In order to determine the biological significance of the transcriptomic (Chapter 4) and the proteomic (Chapter 3) data that emerged from *Pf*AdoMetDC inhibition with MDL73811, several aspects were investigated further and include the possibility of hypermethylation as the mode-of-action of MDL7381. The interaction between AdoMetDC inhibition and the folate pathway was also further investigated. Finally, the metabolome was investigated to determine the regulation of metabolites within polyamine biosynthesis.

5.1.1 Transcriptional and translational control

mRNA abundance is not always proportional to protein expression due to RNA splicing and various protein modifications that include PTM's, protein degradation, protein turnover as well as differences between transcription and translation (Hegde et al., 2003, Griffin *et al.*, 2002, Gygi et al., 1999). In contrast to some other organisms, *P. falciparum* generally has good correlation between mRNA and protein levels although there might be a slight delay between mRNA and protein accumulation which is mostly regulated by post-transcriptional mechanisms (Le Roch *et al.*, 2004). The *P. falciparum* parasites utilises a process of stage-specific transcript production and therefore post-transcriptional regulation would form an integral part in regulation of transcriptional processes (Bozdech *et al.*, 2003). Investigation of transcription associated proteins within *P. falciparum* revealed 156 transcription associated proteins that may modulate mRNA and translation rates, which also suggests that protein expression is mainly regulated by post-transcriptional

mechanisms (Coulson et al., 2004). Post-transcriptional regulation may be a major mechanism of the control of gene expression within the parasite throughout the various life stages of the parasite (Ponts *et al.*, 2010). This process is highly co-ordinated and may also play a role in the adaptability of the parasite to environmental stresses (Mackinnon *et al.*, 2009). Translational repression is a post-transcriptional regulatory mechanism which also plays an important role in stage-specific transcript production of the malaria parasite and therefore also has a key role in parasite development (Mair *et al.*, 2006) especially in female gametocytes (Braks *et al.*, 2008).

5.1.2 DNA methylation

DNA methylation is a modification that includes the transfer of a methyl group from AdoMet to the 5'-carbon of cytosine creating the fifth DNA base, 5-methyl cytosine (5mC), which is widespread in CpG islands (Jones & Laird, 1999, Gitan *et al.*, 2002, Caiafa & Zampieri, 2005). CpG islands are 0.5-2 kb regions that are rich in cytosine-guanine dinucleotides and are found at the promoter region of some human genes (Caiafa & Zampieri, 2005). DNA methylation in eukaryotes may be involved in the regulation of gene expression by the methylation of transcription factor binding sites, induction of heterochromatin formation, as well as a possible defence mechanisms against molecular parasites (Oakeley E.J., 1999).

Disruption of polyamine synthesis can lead to increased DNA, protein and lipid methylation (Goldberg B. *et al.*, 1999). AdoMet plays an integral role in the production of polyamines and acts as a methyl donor for nearly all methylation reactions that include DNA and protein methylation. Initially, it was proposed that *P. falciparum* does not contain any DNA methylation sites such as 5mC and 6mA (Triglia *et al.*, 1992). This theory was later disregarded with the discovery that 5mC, but not 6mA may be present in *P. falciparum* (Hattman, 2005). However, this was again contradicted when LC-MS demonstrated the absence of 5mC in *P. falciparum* gDNA (Choi *et al.*, 2006).

The principle of DNA methylation detection is based on the observation that unmethylated cytosine is converted to uracil and leaves methylated cytosine as it is. This is done by the use of sodium-bisulfite, and was first observed in the 70's by Shapiro (Shapiro R. *et al.*, 1970a, Shapiro R. *et al.*, 1970b). Since then, developments have taken place to increase the speed and efficiency of the reaction. Bisulfite treatment of DNA has recently been modified to obtain high speed (Shiraishi M. & Hayatsu H., 2004), and easy methylation detection (Yang A.S. *et al.*, 2004). Other types of DNA methylation detection include the use of reverse phase HPLC or LC-MS of which both are considered to be extremely sensitive and good detection. Immunology can also be used for

detection of methylation. The DNA is denatured and then immobilized onto a DEAE membrane and incubated with monoclonal antibodies that are directed against m5C. The monoclonal antibody can then be detected by fluorescence. A two coloured microarray can also be used to quantitatively detect methylation within CpG islands using a methylation specific oligonucleotide microarray to potentially scan the whole genome for CpG methylation (Gitan et al., 2002).

In Trypanosomes the rate of protein methylation increases with the concentration of AdoMet (Goldberg B. et al., 1999). Inhibition of Trypanosomal AdoMetDC with the irreversible AdoMetDC inhibitor, MDL73811, will result in an elevation of the AdoMet levels, hence resulting in hypermethylation of DNA, proteins and lipids (Goldberg *et al.*, 1999, Goldberg *et al.*, 1997b). Protein methylation is increased 1.5-fold in Trypanosomes when MDL73811 is added for the inhibition of AdoMetDC and when DFMO is added for the inhibition of ODC (Goldberg B. *et al.*, 1997). In *T. brucei rhodesiense* an elevation in AdoMet levels is associated with cell death due to hypermethylation (Xiao *et al.*, 2009).

5.1.3 Regulation of AdoMet levels

Another factor that may have an impact on DNA methylation is the regulation of AdoMet and S-adenosyl-L-homocysteine (AdoHcy) levels. AdoMet is the universal methyl donor. Methionine is converted to AdoMet by the action of AdoMet synthase. AdoMet is decarboxylated by AdoMetDC in the formation of decarboxylated AdoMet (dcAdoMet) and spermidine which is essential for polyamine metabolism. AdoMet is also crucial for methylation reactions with the by-product of methylation being AdoHcy, which is rapidly degraded by AdoHcy hydrolase. AdoHcy, which is implicated in cardiovascular disease, inhibits methylation reactions by the down-regulation of the methyltransferases (Nakanishi *et al.*, 2001, Zinellu *et al.*, 2007). Therefore the AdoMet:AdoHcy ratio is of importance to DNA methylation, since high AdoMet levels will result in hypermethylation, but in the presence of high AdoHcy DNA hypomethylation will occur.

This chapter investigates the impact of *Pf*AdoMetDC inhibition with MDL73811 further. The methylation status and AdoMet homeostasis of Plasmodial parasites inhibited with MDL73811 is investigated. To further validate polyamine depletion as an essential drug target the effect of polyamine depletion is investigated on metabolite level as well as possible synergy within a folate depleted environment. Finally, the transcriptomic and proteomic data are combined in an effort to evaluate the regulatory mechanisms that may be induced upon *Pf*AdoMetDC inhibition with MDL73811.

5.2 Methods

5.2.1 Culturing of parasites for the determination of the methylation status of MDL73811 treated parasites over time

*Pf*3D7 parasites were maintained *in vitro* in human O+ erythrocytes in culture media and treated with 10 µM MDL78311 as described in section 2.2.3 and section 3.2.3. Parasites (5 ml) at 10% parasitemia and 5% hematocrit were used per sample and harvested at 4 time points (t_1 = 16 HPI, t_2 = 20 HPI, t_3 = 26 HPI, t_4 = 34 HPI) by centrifugation of the parasites at 2500×*g* for 5 min and then washed twice with PBS, after which the infected erythrocytes were stored at -80°C until use.

5.2.2 gDNA isolation from *P. falciparum* for the determination of the methylation status

The erythrocyte pellet (0.25 ml erythrocyte pellet from 5 ml culture) containing the parasites were used for gDNA isolation using the QIAquick DNA Blood Mini-Kit (QIAGEN) without saponin lysis. The kit is based on the principle that the infected erythrocytes are lysed by the addition of choatropic salts, followed by the removal of the cellular debris by filtration. The pellets were removed from -80°C and thawed before the addition of 20 µl Proteinase K (QIAGEN) to the blood pellets and then vortexed. This was followed by the addition of 40 µl RNase A (Fermentas) to degrade any remaining RNA by cleavage of phosphodiester bonds. This mixture was vortexed and then 200 µl Buffer AL (Proprietary, QIAGEN) was added, vortexed and incubated at 56°C for 10 min. Absolute ethanol (200 µl) were added, mixed and then transferred to the mini-spin column and centrifuged for 1 min at 13 000×*g*. The column was transferred to a clean microfuge tube before the addition of 500 µl buffer AW1 (Proprietary, QIAGEN) and centrifugation at 13 000×*g* for 1 min, followed by the addition of 500 µl buffer AW2 (Proprietary, QIAGEN) and centrifugation at 13 000×*g* for 3 min. This was followed by drying of the membrane by centrifugation at 13 000×*g* for 90 s before the addition of 200 µl SABAX water to the membrane which was incubated for 5 min before centrifugation at 8 000×g for 90 s. The gDNA concentration was measured on a Nanodrop-1000 using the ds DNA-50 setting for double-stranded DNA. This setting for double-stranded DNA uses an extinction coefficient of 50 ng-cm/µl for the determination of the DNA concentration. The 260/280 ratio measurement was also determined and was always above 1.8 in order to ensure DNA free of protein contamination.

5.2.3 South-Western immunoblot for methylation detection after MDL73811 treatment of Plasmodial parasites

The method followed was based on a previous method followed by Fisher *et al.*, 2004 for global methylation detection in *Entamoeba histolytica* (Fisher *et al.*, 2004). The Plasmodial gDNA for all 4 time points were denatured by boiling for 5 min and then cooled on ice for 5 min. Each sample (1000 ng) were loaded onto a positively charged nylon membrane (Roche) along with 10 µl of 0.01 M 5-methylcytidine (Sigma) as negative control. The Dotblotter (Bio-Rad) was used to spot samples onto the membrane under vacuum. After sample loading the membrane was cross-linked on a UV transiluminator light (Spectroline TC-312 A) at 312 nm for 3 min. The membrane was then placed into a re-sealable plastic bag and blocked overnight at 4°C in blocking buffer (2% (w/v) BSA in PBS). The next morning the blocking buffer was discarded and 1:5000 of the mouse anti-5-methylcytidine monoclonal IgG (AbD Serotec, Oxford, UK) was added to 10 ml wash buffer (2% (w/v) BSA, 0.1% Tween-20 in PBS) and incubated overnight at 25°C with gentle agitation. The next morning the membrane was washed 6 times with wash buffer for 10 min each before the addition of the goat anti-mouse IgG horse radish-peroxidase (HRP)-conjugate (1:1000) (AbD Serotec, Oxford, UK) in wash buffer and left to incubate for 1 h at 25°C. This was followed by 6 wash steps of 5 min each with wash buffer, 4 wash steps of 5 min each with 0.1% Tween-20 and finally 3 wash steps of 5 min each with PBS. Finally, the membrane was incubated for 5 min with equal volumes (4 ml each) of Luminol/Enhancer solution and stable peroxidase solution (Supersignal West Pico Chemiluminescent substrate). The excess reagent was drained, and the membrane was exposed to Hyperfilm ECL X-ray film (Pierce) for 30 s in the dark. The X-ray was developed for 1 min in Universal Paper developer (Illford), rinsed briefly in water, and then fixed for 3 min with Rapid Paper Fixer (Illford). The film was again rinsed in water and left to dry before being scanned on the Versadoc-3000 using Quantity One 4.4.1 (Bio-Rad), with the following settings: Densitometry, X-ray film, Clear white TRANS, 0.5× Gain and 1×1 Bin. The density of each spot on the X-ray film was calculated using Quantity One and then the ratio of UT/T were calculated.

5.2.4 Determination of polyamine-specific transcripts by the addition of methionine to parasite cultures

*Pf*3D7 parasites were maintained as described in section 2.2.3. A parasite culture of 5 ml were used during the treatments and done in biological duplicates. Treatment with methionine took place 4 HPI in the early ring stage, and harvested 24 h later in the trophozoite stage. A stock solution of methionine (100 mM) was dissolved in water before being added to the culture media. Methionine was analysed at 4 different concentrations (100 mM, 10 mM, 1 mM, 0.1 mM), and done in

duplicate. Parasites were harvested by centrifugation of the culture at 2500×*g* for 5 min and then washed twice with PBS, after which the infected erythrocytes were stored at -80°C until use.

5.2.5 RNA isolation and cDNA synthesis of the metabolite treated parasites

RNA was isolated from UT and T parasites in an RNAse free environment using a combined RNeasy Mini Kit (QIAGEN) and TRI-Reagent (Sigma) method, with the incorporation of DNase I on-column digestion (QIAGEN) as described earlier in Chapter 4 section 4.2.2. For the methionine-treated samples, 1 µg RNA was used for each individual sample. First strand cDNA synthesis was initiated using 1 µg RNA per sample, 25 pmol random primer nonamer (Inqaba), 15 pmol OligodT (dT_{25}) (Inqaba) and incubated at 65°C for 10 min, followed by 1 min at 4°C. After this incubation step, 6 µl 5× SuperScript First-strand buffer, 10 mM DTT, and 200 U Superscript III Reverse Transcriptase (Invitrogen) were added, mixed and incubated at 25°C for 5 min, 50°C for 1 h, 70°C for 15 min and then 4°C until use. Contaminating RNA was removed by hydrolysis with the addition of 1 M NaOH, and 0.5 M EDTA, pH 8 to the reaction mixture and incubating at 65°C for 10 min. The cDNA were purified using the PCR Clean-up kit (Qiagen). The cDNA was subsequently eluted by the addition of 30 µl pre-heated RNAse-free SABAX water (37°C) directly onto the membrane and incubated for 4 min before centrifugation at 13 000×*g* for 90 s to elute the cDNA. The cDNA concentration and purity was measured on a Nanodrop-1000 (Thermo).

5.2.6 Quantitative real-time PCR of methionine-treated parasites

cDNA from the methionine-treated (T_{met}) and untreated samples (UT_{met}) were diluted to 0.65 ng/µl with SABAX water for use in qRT-PCR. A standard curve was constructed from a dilution series of UT_{met} samples that contained the following dilutions: an undiluted sample, 1/10, 1/20, 1/50 and 1/100 dilutions. Lactate dehydrogenase (LDH) was used as household transcript and used to construct the standard curve. The reactions were performed in a 384-well plate using the Lightcycler 480 (Roche) as described in section 4.2.9. The fold change was calculated for each sample by comparing the UT_{met} samples to the T_{met} samples, and were then normalised to LDH that remained unchanged with methionine treatment.

5.2.7 Metabolite extractions for S-adenosylmethionine (AdoMet) and S-adenosylhomocysteine (AdoHcy)

Parasites were cultured *in vitro* and treated with 10 µM MDL73811 as described earlier in section 2.2.3 and 3.2.3. Two time points were taken (t_1:16 HPI, t_3:26 HPI). 20 ml cultures in triplicate were

used for each time point at 15% parasitemia and 5 % hematocrit. Cultures were centrifuged to a 1 ml pellet and the pellet was then washed 3 times with PBS and kept on ice. The pellet was transferred to a 2 ml microfuge tube. A portion of this pellet was diluted 1000-fold (1 µl of the pellet with 999 µl fixation solution) in fixation solution (4% (w/v) glucose, 10% (w/v) formaldehyde in a saline solution containing 10 mM Tris-HCl, 150 mM NaCl, 10 mM sodium azide, pH 7.3) that was used for Nebauer cell counting, and ultimately for normalisation of the cultures. A volume of 1 ml of a 10% perchloric acid (PCA) solution was added to the 1 ml pellet immediately after centrifugation and washing and vortexed vigorously to obtain a brownish colour before being placed at -70°C for at least 16 h. The samples were then thawed and again vortexed vigorously before being centrifuged at 16 000×*g* for 10 min at 4°C. The supernatant were removed to a clean microfuge tube and then filtered using a 0.22 µM HPLC filter (GE Healthcare) before 200 µl injections were made onto the HPLC and stored at -70°C until use. HPLC analyses were performed on a Waters HPLC equipped with a Waters 600 pump, Waters 996 Photodiode Array detector and a Waters 717 Plus autosampler. High performance liquid chromatography was performed with a 250 mm x 4.0 mm Luna C18 (2) 5 µm reverse-phase (RP) column (Phenomenex). A Guard-Pak™ Precolumn steel housing (Waters Corporation) with µBondapak C18 HPLC pre-column inserts (Waters Corporation) was connected in-line. Mobile phase A consisted of an aqueous solution of 8 mM octanesulfonic acid and 50 mM NaH_2PO_4, mobile phase B consisted of 100% methanol. Mobile phase C consisted of only MilliQ water and mobile phase D consisted of 95% acetonitrile. The column were equilibrated with 80% A: 20% B before each injection, and upon injection of the sample maintained for 8 min, before being changed to 60% A: 40% B and maintained for 13 min after which the gradient was changed back to 80% A: 20% B and maintained until the end of the run (35 min in total). Absorbance measurements were made a 254 nm.

5.2.8 Malaria SYBR Green I-based fluorescence (MSF) assay for synergy determination of folates and MDL73811

The MSF assay was performed as described earlier in Chapter 3 section 3.2.1. The first column of the sterile 96-well plate was filled with only culture media and not used as part of the IC_{50} determination due to the possibility of edge effects. The second column contained 0.5 µM CQ as a negative control, and represented total inhibition of parasite and hence no parasite growth. This was followed by the positive control that contained parasites in drug-free media. Folic acid were added to the folate-free media at normal physiological concentrations (23 nM) (Nduati *et al.*, 2008). This was also repeated with 1 µM MDL 73811 (IC_{50}) added to the folic acid concentration range. To determine the presence of possible drug interactions, *Pf*3D7 parasites were cultured in folic acid

deficient media containing pyrimethamine (PYR) and MDL73811. Pyrimethamine (Sigma) was added to folate-free media. A 10 mg/ml stock solution of PYR was prepared by dissolving 10 mg PYR in 1 ml DMSO, and then further diluted to a final concentration of 1.28 µM in PBS. The IC_{50} for PYR was determined before the synergism study could commence. Serial dilutions were made of both drugs as they were added together. The plate was then placed into a gas chamber and gassed for 2 min, before being placed in a 37°C incubator for 96 h. On the day of the assay, SYBR green buffer was prepared and added (100 µl) to each of the wells of a 96-well black fluorescence plate (Nunc) followed by 100 µl of resuspended treated parasites. The plate was then incubated for 1 h in the dark at room temperature before the fluorescence was measured using the Fluoroskan Acent FL Fluorimeter (Thermo LabSystems) at excitation of 485 nm and emission 538 nm (integration time of 1000 ms). Data were analysed using SigmaPlot 9.0 to determine the IC_{50} of MDL73811 and PYR against *Pf*3D7.

To determine possible synergism between MDL73811 and PYR in folate-free media the drugs were added to the *Pf*3D7 parasites in combination. The first column of the plate was filled with only culture media and not used as part of the IC_{50} determination due to the possibility of edge effects. The second column contained 0.5 µM CQ as a negative control, and represented total inhibition of parasite and hence no parasite growth. This was followed by the positive control that contained parasites in drug-free media. The next eight columns contained a serial dilution of the drug starting at the highest concentration of 16 µM MDL73811 to the lowest concentration of 0.125 µM MDL73811 and similarly, 120 nM PYR down to 0.23 nM for the lowest concentration. The plate was then placed into a gas chamber and gassed for 2 min, before being placed in a 37°C incubator for 96 h. The plate was then treated as described previously. Data were analysed using SigmaPlot 9.0 to determine the IC_{50} of MDL73811 against *Pf*3D7.

Another measure to determine synergism is by the calculation of the fractional inhibitory concentration (FIC) as given in equation 5.1 (Vivas *et al.*, 2007). For the calculation of the FIC value most studies use IC_{50} values, although a more accurate representation would be the use of IC_{90} or even IC_{99} values (Fivelman *et al.*, 2004). The combination of two drugs will indicate that a FIC value of <0.5 is considered as synergistic, since it indicative of a 4-fold decrease in minimum inhibitory concentration (MIC) (Fivelman et al., 2004). Synergy between two drugs can be defined as FIC ≤ 0.5, additivity/indifference is defined FIC >0.5 to 4, and antagonism is defined as an FIC < 4 (Fivelman et al., 2004, Hu *et al.*, 2002).

To calculate for possible interaction:

$$FIC50 = \left(\frac{IC50\ Drug\ A\ comb}{IC50\ Drug\ A\ alone}\right) + \left(\frac{IC50\ Drug\ B\ comb}{IC50\ Drug\ B\ alone}\right)$$ Equation 5.1

$$FIC50 = \left(\frac{IC50\ Pyr\ comb}{IC50\ Pyr\ alone}\right) + \left(\frac{IC50\ MDL73811\ comb}{IC50\ MDL73811\ alone}\right)$$

$$FIC50 = \left(\frac{7.2819\ nM}{14.1370\ nM}\right) + \left(\frac{0.9709\ \mu M}{0.9600\ \mu M}\right)$$

$$FIC50 = 0.515 + 1.011$$

$$FIC50 = 1.53$$

5.2.10 Primer design

Primers with melting points around 55°C and a product length of 150-170 were designed using Oligo 6.0. The Tm for the primers was calculated with Tm in the range of 55°C. Five primers were designed that include MAL13P1.214, PF11_0061, MAL13P1.56, PFE1050w, PFF1300w and are given in Table 5.2. Existing primers that were used are given in Table 5.1

Table 5.1: Existing primers used for proteomic validation

PlasmoDB ID	Set	Primer sequence (5' - 3')	Product length	Tm[a] (°C)
PFF0435w	OAT f	CAACTTTGGTCCATTCGTACC	165	58
	OAT r	GCTACACCTGGGAAATAACTATC		59
PF13_0141	LDH f	GATTTGGCTGGAGCAGATGTA	169	58
	LDH r	CAACAATAATAAAAGCATTTGGACAA		55
PFD0285c	LDC f	AGA GGG ATA TGG ATT GGT AGA	161	56
	LDC r	TTC TCT TCA TGT ATG ATA CAG TA		54
PF10_0322	AdoMetDC/ODC f	AATCAATTCCATGACGCTTATCTG	165	58
	AdoMetDC/ODC r	ACAATTCACCATTCCTGTATCTTC		58
PFE0505w	Cyclo f	AAT TCT TTG ACC ATC TTA ATC ATT C	167	55
	Cyclo r	CAA AAC AAT TTT ACT TCC TTG GGT TA		57
Pfi0320w	ARG f	CGT TTC CAT TAT TGG TTC TC	164	53
	ARG r	GTT TCA TTT CAT TAT CCC CAT TAT C		56
PFI1090w	SAMS f	TTT AGA TTA CAA AAC GGC AGA GAT AA	160	57
	SAMS r	AGG CAT ATA ATT CTC AGT TTC ATC AG		58

[a] $Tm = 69.3 + (0.41 \times \%GC) - \left(\frac{650}{Primer\ length}\right)$ (Rychlik et al., 1990) Equation 5.2

5.3 Results

5.3.1 Methylation status of *Pf*AdoMetDC inhibited parasites

The action of MDL73811 upon AdoMetDC in Trypanosomes were speculated to be through hypermethylation of nucleic acids or proteins, therefore resulting in parasite death (Bacchi *et al.*, 1992a). To investigate the possibility of hypermethylation of genomic DNA (gDNA) in Plasmodial parasites, gDNA of Plasmodial parasites were isolated and prepared for an immunoblot that is able to detect 5mC within gDNA (Fisher et al., 2004). Methylated RNA is able to interfere with detection of 5mC in gDNA and therefore RNA was removed from the samples with RNAse A. Four time points were chosen for the detection of possible methylation of gDNA in AdoMetDC inhibited samples to determine the possibility that methylation might increase over time. gDNA (1000 ng) for each time point was quantitatively loaded onto the positive nylon membrane (Figure 5.1 A). 5mC was detected in all 4 time points, but remained constant over time with no increase or decrease in the methylation status of the T or UT parasites (Figure 5.1). This is similar to the co-inhibition study done on AdoMetDC/ODC (Van Brummelen, 2009).

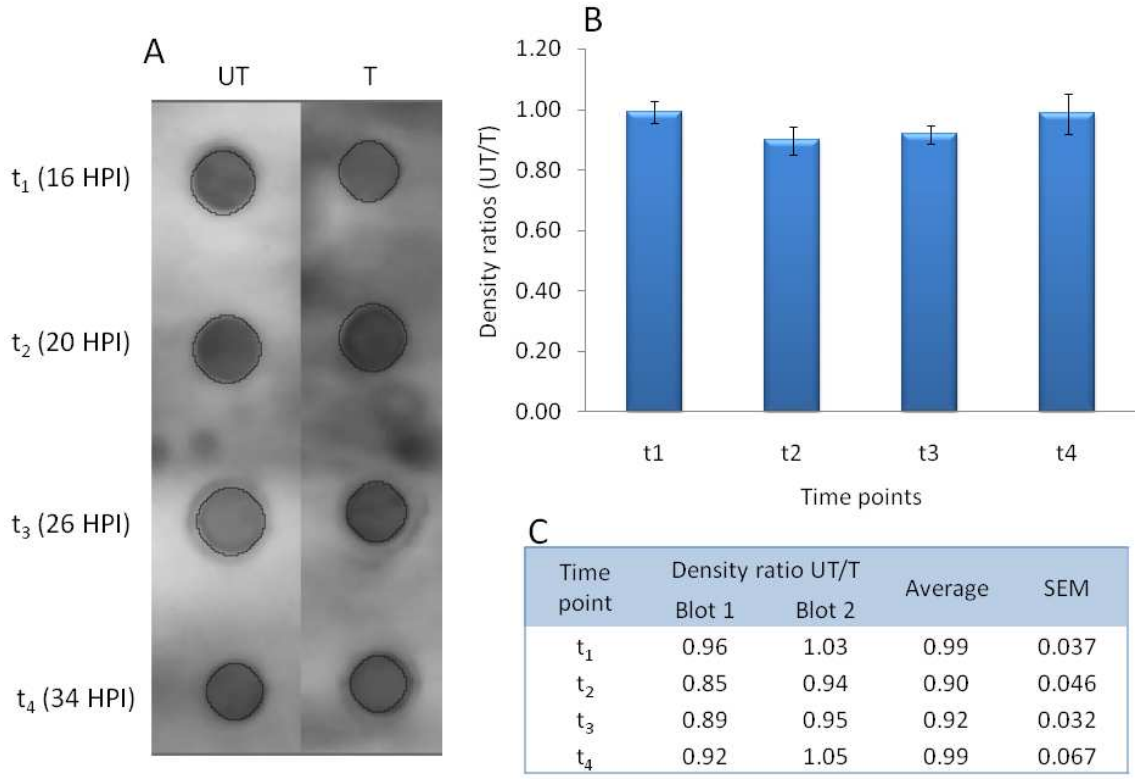

C

Time point	Density ratio UT/T Blot 1	Density ratio UT/T Blot 2	Average	SEM
t_1	0.96	1.03	0.99	0.037
t_2	0.85	0.94	0.90	0.046
t_3	0.89	0.95	0.92	0.032
t_4	0.92	1.05	0.99	0.067

Figure 5.1: Determination of gDNA methylation (5mC) in AdoMetDC inhibited parasites.

A: Immunoblot of quantitatively loaded gDNA from treated and untreated parasites over time. B: Density ratios of the four time points investigated, error bars are representative of SEM for 2 experiments. C: Table containing the data from the immunoblots. Average ratios of 2 individual biological replicates and blots. SEM is representative of standard error of the mean. Data were calculated from the density determined by Quantity One.

5.3.2 Determination of AdoMet and AdoHcy metabolite levels upon inhibition of AdoMetDC

The methylation status of an organism is usually controlled by the AdoMet:AdoHcy ratios (Goldberg et al., 1999), which prompted the determination of the AdoMet and AdoHcy metabolite levels in AdoMetDC inhibited parasites. The metabolite levels of AdoMet and AdoHcy, which is crucial in polyamine metabolism and methionine recycling, were determined by HPLC for 2 time points (t_1: 16 HPI and t_3: 26 HPI; Figure 5.2). No significant differential regulation of either AdoMet or AdoHcy could be determined when UTt_1 was compared to Tt_1 or UTt_3 compared to Tt_3 ($p<0.05$). This is similar to the co-inhibition of AdoMetDC/ODC, in which no significant differential regulation of either AdoMet or AdoHcy could be determined (Van Brummelen, 2009). This is also in support of the previous results that determined that no hypermethylation is present within the parasites (Section 5.3.1 and Van Brummelen 2009).

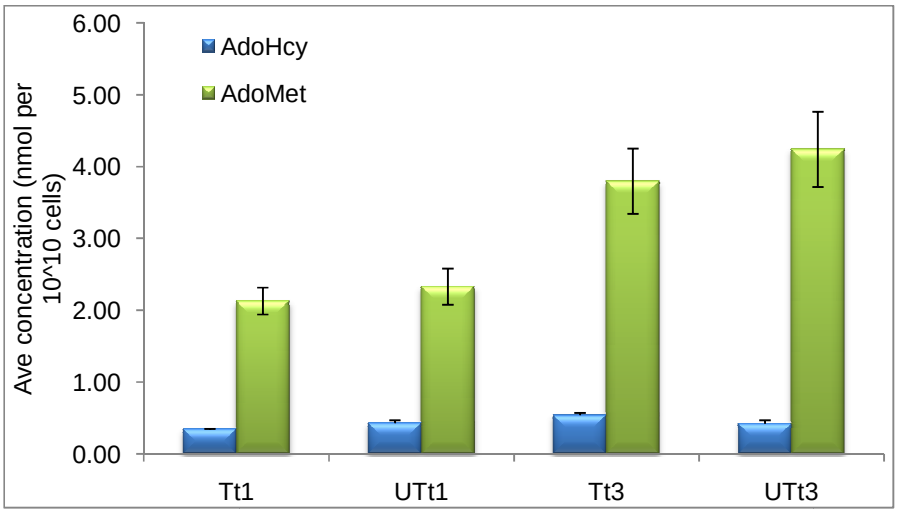

Figure 5.2: Metabolite levels of AdoMet and AdoHcy after AdoMetDC inhibition.
N=2 (biological replicates) and N=3 (technical replicates) for each time point. Error bars are representative of SEM, cells are normalised to the average cells per 10^{10} cells. t_1 is 16 HPI, t_3 is 26 HPI.

5.3.3 Polyamines and the folate pathway

It was determined in Chapter 4 that AdoMetDC inhibition resulted in decreased transcript abundance of various folate-related transcripts which therefore prompted further investigation. Folate depletion may result in an imbalance in AdoMet levels and ultimately an imbalance in polyamine biosynthesis (Bistulfi *et al.*, 2009). The effect of folate-free media and simultaneous inhibition of polyamines with MDL73811 were investigated using the MSF assay (Figure 5.3). The physiological concentration of folic acid in human erythrocytes is 23 nM (Nduati et al., 2008). In the presence of folate-free media the parasites had ~70% growth (therefore ~30% growth reduction) when compared to parasites in normal media (which is representative of 100% parasite growth)(Figure 5.3). The addition of 1 µM MDL73811 (IC_{50}) to the folate-free media and normal

media was done to determine the effect of simultaneous folate depletion and AdoMetDC inhibition on the growth of the parasites. Treatment with 1 µM MDL73811 in folate containing media resulted in 50% parasite inhibition (Figure 5.3) with is similar to the IC_{50} of MDL73811 which has already been determined previously (Chapter 3). Similarly, when parasites were treated with 1 µM MDL73811 in the presence of 2.3 µM folates 50% parasite inhibition was determined. When folate depleted media were supplemented with 2.3 µM folates growth was restored to about 75%. Parasites exposed to folate-free media and 1 µM MDL73811 had a ~75% reduction in parasite growth (Figure 5.3). This is also a 25% reduction in parasite growth when compared to 1 µM MDL73811 (IC_{50}) in folate containing media. Therefore, the combination of folate depletion and AdoMetDC inhibition with MDL73811 resulted in a further 25% reduction in parasite growth when compared to MDL73811 alone and therefore prompted an investigation in to possible synergistic mechanisms between folate depletion and AdoMetDC inhibition.

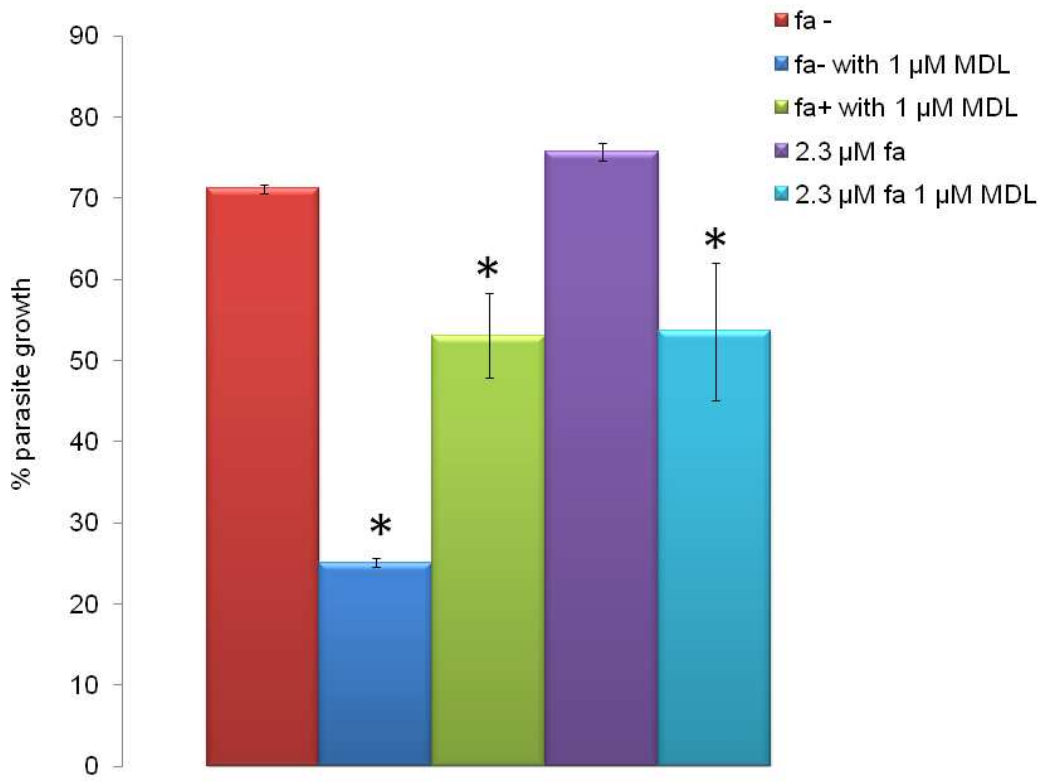

Figure 5.3: The combined influence of folate-free media and the irreversible AdoMetDC inhibitor MDL73811 on Plasmodial parasites.

MSF assay done in various concentrations of folic acid or folate free media but not pABA free media together with 1 µM MDL73811 at each concentration of folic acid. Data is representative of 2 biological replicates that were done in triplicate. Error bars are representative of SEM. Fa is folic acid. MDL is MDL73811. No fa is done in folate free, but not pABA free media without addition of folic acid to the media. A positive control is always included and is parasites in normal RPMI1640 media, and as a negative control, CQ is added to the parasites. * is indicative the treated sample compared to folate depleted samples with the student t-test $p < 0.05$.

The decreased parasite growth of the combination of AdoMetDC inhibition and folate depletion observed in Figure 5.3 prompted an investigation into possible synergistic interactions as a result of the combination of AdoMetDC inhibition and folate depletion. To further investigate this possibility, complete depletion of folates was desired for an effective experiment. Folate-free media still contained pABA that can be salvaged and utilised by *Pf*DHPS-HPPK for the production of folates. Therefore, the bifunctional enzyme DHFR-TS which is down-stream of DHPS-HPPK, and is responsible for folate production within the parasite was inhibited with PYR in an attempt to minimise pABA or folate salvage from the folate-depleted media. The IC_{50} of both PYR and MDL73811 in the presence and absence of folates were determined (Figure 5.4 A and B).

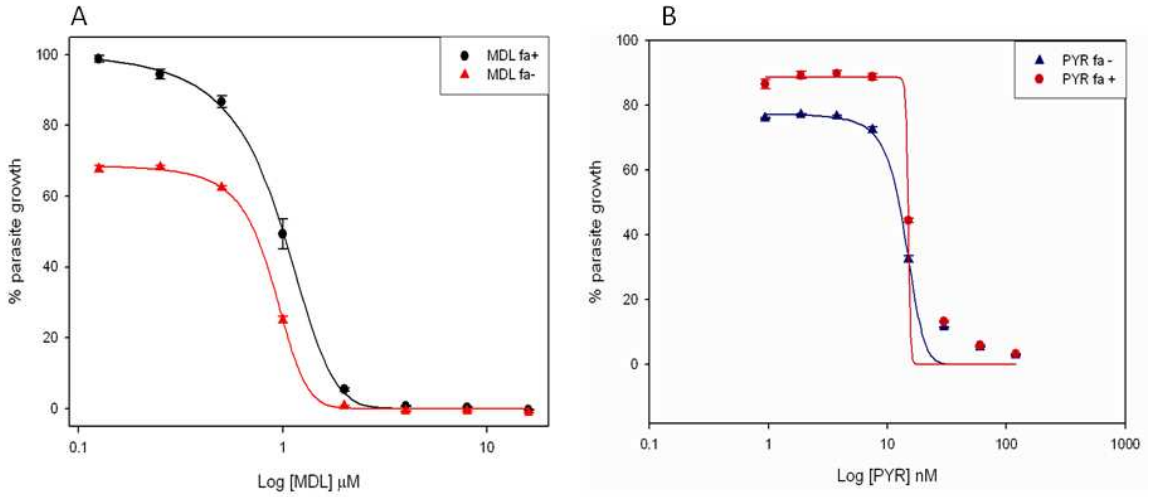

Figure 5.4: A dose response curve for the IC_{50} determination of MDL73811 and PYR in the presence and absence of folate free media.

(A)Error bars are representative of the SEM for 2 or 4 individual experiments done in triplicate. For folate free media (fa-) the R^2= 0.9990 and IC_{50} is 0.8979 µM with SEM representative of 4 experiments. For folate containing media (fa+) R^2= 0.9908 and the IC_{50} is 0.9600µM. (B)Error bars are representative of the SEM for 2 individual experiments done in triplicate. For folate free media (Fa-) the R^2= 0.9926 and IC_{50} is 14.1370 nM. For folate containing media (fa+) R^2= 0.9922 and the IC_{50} is 15.0031 nM.

The IC_{50} of PYR remained unchanged in both the presence and absence of folates (Figure 5.4 B). In the presence of folate-containing media the IC_{50} of PYR in the *Pf*3D7 strain were determined to be 15 nM, while in the absence of folate the IC_{50} of PYR was determined as 14.1 nM. The IC_{50} of MDL73811 in normal folate-containing media was determined as 0.96 µM, while in the absence of folates within the media the IC_{50} of MDL73811 was determined as 0.89 µM (Figure 5.4 A).

In order to determine if complete inhibition of folates had a synergistic effect on AdoMetDC inhibition, parasites were inhibited with both PYR and MDL73811 at varying concentrations. The dose response curve for the co-inhibition of parasites with both PYR and MDL73811 shifted to the left indicating possible synergistic effects of the 2 drugs in combination (Figure 5.5). For

antagonism the combination curve would have shifted to the right of the individual curves, and for additivity the combination curve would have been in the middle of the 2 individual curves (Van Brummelen, 2009, Fivelman *et al.*, 2004). Indeed, the IC_{50} of PYR changed from 14.1 nM to 7.3 nM in the presence of MDL73811, indicative of almost 50% reduction in IC_{50}-concentration needed for inhibition. This was not seen with MDL73811 for which the IC_{50} remained almost unchanged in the presence and absence of PYR.

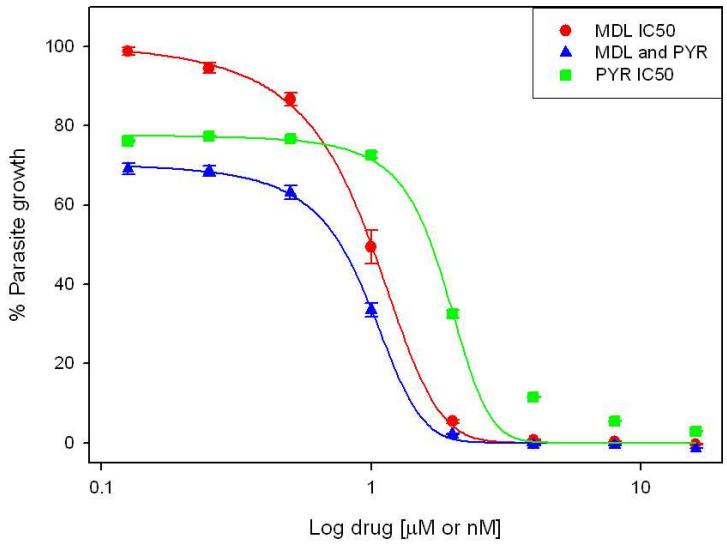

Figure 5.5: A dose response curve for the determination of possible interactions between MDL73811 and PYR in the absence of folates.

Error bars are representative of the SEM for 2 individual experiments done in triplicate. IC_{50} of MDL73811 alone is 0.9600 µM. IC_{50} of PYR alone is 14.1370 nM. In combination of both MDL73811 and PYR the IC_{50} of MDL73811 is 0.9709 µM and the IC_{50} of PYR is 7.2819 nM. The shift of the combination of drugs to the left is a possible indication of synergism/additive.

The determination of synergistic drug interactions depends on the methods chosen for investigation (Bonapace *et al.*, 2002). Time-kill analysis can be used to determine drug interaction in bacteria and is measured in time and log cfu/ml (Leonard *et al.*, 2008). However, the FIC measure is most commonly used (Equation 5.1) (Vivas *et al.*, 2007). Synergy between two drugs can be defined as FIC $\leq$ 0.5, additivity/indifference is defined FIC >0.5 to 4, and antagonism is defined as an FIC < 4 (Fivelman et al., 2004, Hu *et al.*, 2002).

Calculation of the FIC of both PYR and MDL73811 resulted in a FIC value of 1.53 which is indicative of additivity (Fivelman et al., 2004, Hu *et al.*, 2002). This is in contrast to the results obtained from the dose response curves that indicated possible synergism. This lack of possible synergism may be due to the lack of AdoMet:AdoHcy regulation as was determined in Section 5.3.2.

5.3.4 Methionine perturbation of parasites

Knowledge of stress responses can be useful in the elucidation of possible new drug targets, as these would be genes that should rather be avoided within this drug development process. Here, an attempt is made to induce stress responses upon the parasites in an effort to determine such stress genes particularly within polyamine metabolism. Transcripts that were specifically affected by AdoMetDC inhibition as was determined in Chapter 4 were selected to determine a polyamine specific or non-specific response. Primers were designed of transcripts affected to complement some of the already existing polyamine specific primers (Table 5.1 and Table 5.2).

Table 5.2: Additional primers designed for determination of polyamine specificity

PlasmoDB ID	Set	Primer sequence (5' - 3')	Product length	Tm (ºC)
MAL13P1.214	PEMT f	ACA TTC CTG GAA AAT AAT CAA TAT AC	168	55.3
	PEMT r	TCC TAA ACC AGA TCC GAT ATC		55.9
PF11_0061	Histone H4 f	GCA AGA AGA GGT GGT GTT AA	170	55.3
	Histone H4 r	CCT TGT CTT TTT AAG GAG TAT AC		55.3
MAL13P1.56	M1-AP f	GGC AAA ATA TGA CGT TAC AGT AAC	162	57.6
	M1-AP r	CCA GCT ACA ACA GCA AAT AAA TAA		58.1
PFE1050w	AHC f	AGA GCT ACC GAT TTT TTA ATA TC	155	53.5
	AHC r	CCT TCC ATT ACA GCT TGT ATA G		56.5
PFF1300w	Pyruvate kinase f	TTG GCA CAA AAA TTG ATG ATA TC	166	53.5
	Pyruvate kinase r	CTG AAA GCA TAA CAC AAT CAG TAC		57.6

Morphological evaluation of the addition of the 4 different Met concentrations to the *Pf*3D7 parasites revealed that in the presence of 0.1 mM, 1mM and 10 mM Met there is no visible morphological difference between the T_{met} and UT_{met} parasites. It does seem morphologically that the parasites treated with 100 mM Met are morphologically smaller than the other parasites at the trophozoite stage (Figure 5.6).

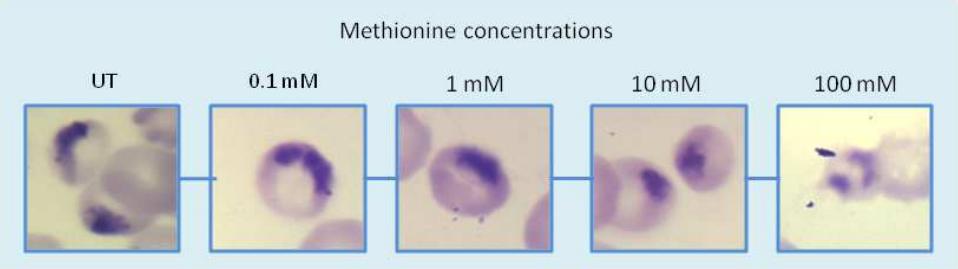

Figure 5.6: Morphological illustration of the various methionine concentrations on the parasites. Methionine was added in the early ring stage and the parasites were harvested 24 h later in the trophozoite stage.

The addition of Met had an influence on transcripts involved in polyamine metabolism similar to the inhibition of AdoMetDC with MDL73811 (Chapter 4). High concentrations of Met (100 mM) induced decreased transcript abundance of AdoMet synthase, AHC, HH4 and PEMT which was similarly determined with AdoMetDC inhibition with MDL73811 (Chapter 4). Transcripts with increased transcript abundance were LDC and arginase (Figure 5.7). In contrast to the high Met concentration that induced possible polyamine specific transcripts, the lower concentrations of methionine resulted in unchanged transcripts for all of the transcripts that were investigated. This may support the notion that AdoMet synthesis within the parasite may be homeostatically controlled and is under tight regulation possibly independent of polyamine metabolism.

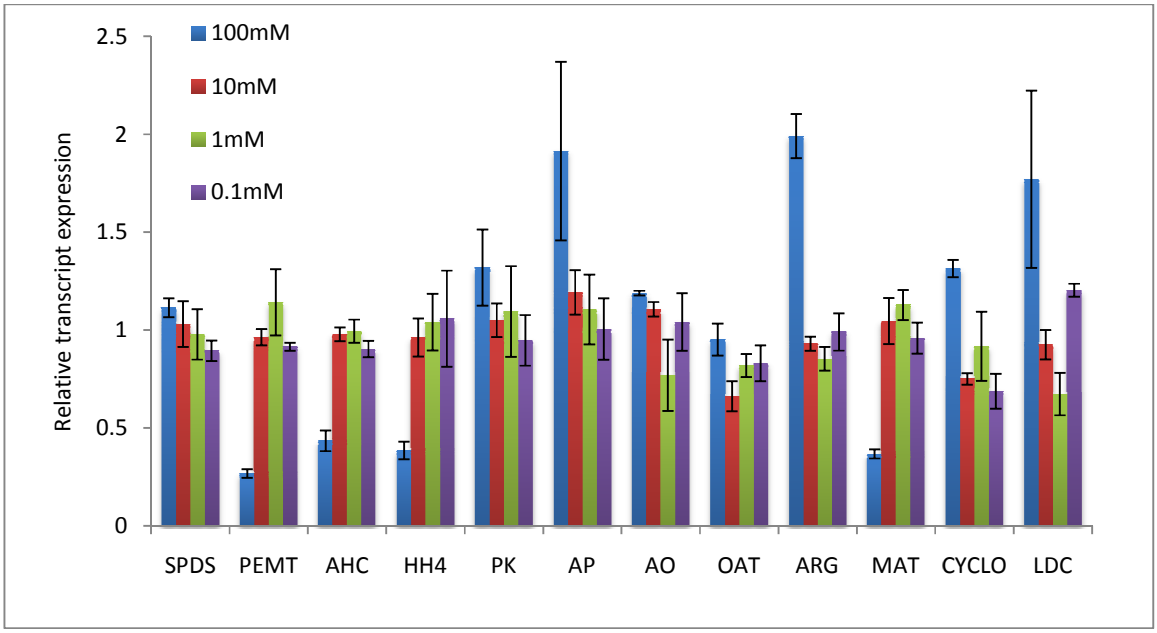

Figure 5.7: qRT-PCR of methionine treated parasites.

N=2 error bars representative of the SEM. All transcripts normalised to LDH. SPDS: spermidine synthase, PEMT: phosphoethanolamine N-methyltransferase, AHC: adenosylhomocysteinase, HH4: histone H4, PK: pyruvate kinase, AP: M1-family aminopeptidase, AO: AdoMetDC/ODC, OAT: ornithine aminotransferase, ARG: arginase, MAT: AdoMet synthase, CYCLO: cyclophillin, LDC: lysine decarboxylase.

5.3.5 Comparison of transcriptomic and proteomic data

Comparison of the transcriptomic and proteomic data revealed that 16 transcripts were similarly detected as proteins in the proteomic investigation (Table 5.3 and Figure 5.8). Therefore, 3% (16/549) of the transcripts that were identified as differentially regulated and 26% (16/61) of the differentially affected identified proteins were shared between the 2 technologies employed.

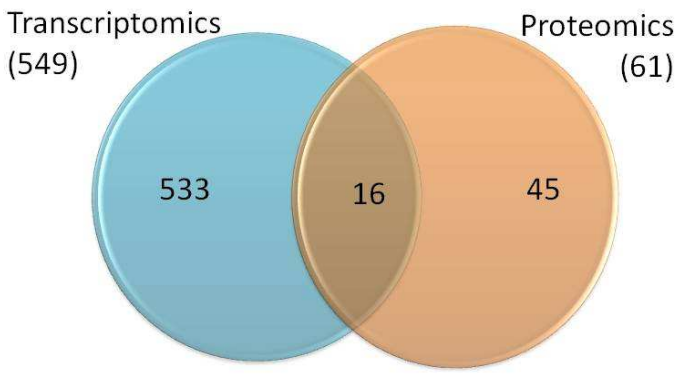

Figure 5.8: Venn diagram of similarities between the transcriptomic and proteomic data sets for the AdoMetDC perturbation.

In total 549 transcripts were determined to be differentially affected by AdoMetDC inhibition. In total, 61 unique protein groups were identified to be differentially regulated, when the 1-DE and 2-DE results were combined as a total proteomic study.

Of the 16 shared transcripts and proteins that were identified, 8 had a similar decreased abundance in both the transcript and protein (Table 5.3). Three proteins had multiple isoforms that were both increased and decreased in abundance and therefore not always similar to the transcript data and include MAL13P1.214, PF10_0155 and PFF1300w. Five proteins had increased protein abundance but had decreased transcript abundance (Table 5.3). These results are indicative of transcriptional and translational regulatory mechanisms within the parasite.

Table 5.3: Similar transcripts obtained for both the transcriptomic and proteomic data.

PlasmoDB ID	Name	Proteomics		Transcriptomics
		FC Tt_1	FC Tt_2	FC Tt_3
	Decreased abundance			
PF14_0138	hypothetical protein		-3.3	-1.8
PF14_0187	glutathione S-transferase	-1.6		-1.8
PFI1090w	s-adenosylmethionine synthetase, putative	-1.3		-2.3
PFI1270w	PFI1270w	-3.3		-2.9
PFL2215w	Actin		-1.4/-2.0	-2.5
PF11_0061	Histone H4, putative*	-5.0/-3.4		-3.4
PF11_0062	Histone H2B*	-5.0/-3.4		-2.9
PFE0165w	Actin depolymerising factor, putative*	-4.4		-2.2
	Increased abundance			
MAL13P1.283	TCP-1/cpn60 chaperonin family, putative	1.3		-1.7
PF08_0054	heat shock 70 kDa protein	2.7	2.7	-1.9
PF13_0141	L-lactate dehydrogenase	1.5	3.1	-1.9
PFE0660c	purine nucleotide phosphorylase, putative	1.6		-3.0
PFL1420w	Macrophage migration inhibitory factor homolog, putative*	0.9		-2.1
	Multiple isoforms			
MAL13P1.214	phosphoethanolamine N-methyltransferase, putative	-1.5	1.7/-3.8/ -1.8	-5.0
PF10_0155	Enolase	2.0/-4.1	1.4	-2.7
PFF1300w	pyruvate kinase, putative	1.3/-1.3	2.3	-1.7

Multiple entries for the proteomics data is separated by a dash, which is representative of various isoforms *Proteins identified for SDS-PAGE only.

Some of the polyamine specific proteins that were identified by MS/MS in Chapter 3 were compared to their transcript profiles that were obtained in Chapter 4. The fold change of the MDL73811-treated *Pf*3D7 parasites were plotted for both the transcripts (t_1 to t_3) as well as the proteins (t_1 to t_2) to determine possible regulatory mechanisms (Figure 5.9).

Adenosine deaminase (PF10_0289), AdoMet synthase (PFI1090w) and PNP (PFE0660c) all had transcript and protein abundance that decreased similarly over time, although it did seem that the protein abundance of adenosine deaminase (PF10_0289) does lag behind the transcript abundance in Tt_2 (Figure 5.9). This lag was also determined for Hsp70 (PF08_0054) which revealed a high protein abundance when compared to the transcript abundance although the protein abundance was slowly decreasing and therefore, also had a delay between transcript and protein abundance. Finally, it was determined that eIF5A (PFL0210c) had decreased transcript and protein abundance although the protein abundance was decreased dramatically from that of the transcript abundance (Figure 5.9). PEMT (MAL13P1.214) and enolase (PF10_0155) both had decreased transcript levels, but had various protein isoforms that were identified. Three protein isoforms were detected for PEMT (MAL13P1.214) of which 2 of these protein isoforms had decreased protein abundance similar to the transcript levels, with the other protein isoforms having increased protein abundance levels. Similarly for enolase (PF10_0155) 1 protein isoform had decreased protein levels but was lagging behind the transcript while the other protein isoform had increased protein abundance. Pyrroline-5-carboxylate reductase (MAL13P1.284) had unchanged transcript levels (+1-fold), but the protein abundance increased from Tt_1 to Tt_2. Similarly, 2-cys peroxiredoxin (PF14_0368) and Hsp60 (PF10_0153) also had unchanged transcript levels (-1-fold) that remained constant over the 3 time points with the protein abundance that also increased from Tt_1 to Tt_2. A decrease in transcript abundance with an increase in protein abundance was determined for GST (PF14_0187) and pyruvate kinase (PFI1300w).

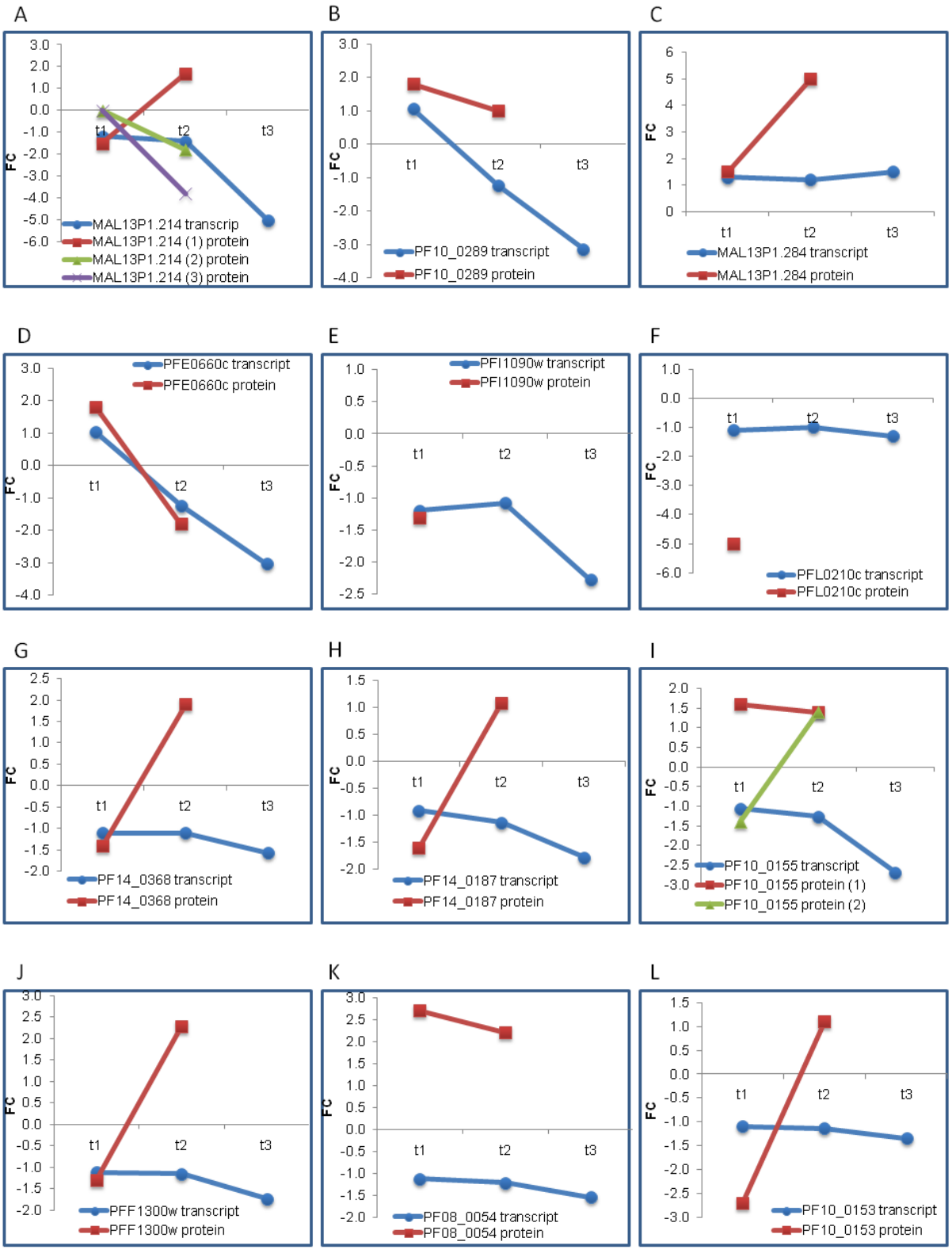

Figure 5.9: Correlation between transcript and protein abundance

A: phosphoethanolamine N-methyltransferase, B: adenosine deaminase, C: Pyrroline-5-carboxylate reductase, D: purine nucleotide phosphorylase, E: S-adenosylmethionine synthetase, F: Eukaryotic initiation factor 5a, putative, G: 2-Cys peroxiredoxin, H: Glutathione s-transferase, I: enolase, J: pyruvate kinase, K: heat shock protein 70 kDa, L: heat shock protein 60 kDa.

5.4 Discussion

Inhibition of AdoMetDC with MDL73811 resulted in the identification of gDNA methylation but no hypermethylation could be identified. MDL73811 inhibition of Trypanosome AdoMetDC revealed hypermethylation of nucleic acids and proteins, and concurrent parasite death due to the accumulation of AdoMet and subsequent interference with translational processes (Bacchi *et al.*, 1992a, Goldberg *et al.*, 1997a). Similar results of hypermethylation was obtained in the liver of rats fed with excess methionine (Bacchi et al., 1995). Hypermethylation of promoter genes and an increase in the mRNA expression of DNA methyltransferases is commonly associated with cancerous cells, although the correlation between DNA methylation and the mRNA expression of DNA methyltransferases are not always clear (Oh et al., 2007, Park et al., 2006). Hypermethylation is associated with various malignancies (Oh et al., 2007) and usually occurs in cancerous cells in which epigenetic control is the result of hypermethylation of the tumour suppressor genes (Chan *et al.*, 2008). Gene silencing is commonly associated with the occurrence of hypermethylation of genes (Chan *et al.*, 2008), although epigenetic control through 5mC methylation in Plasmodial parasites are contradictory (Choi *et al.*, 2006). Previously, it was determined that 5mC does not occur in Plasmodial parasites (Choi *et al.*, 2006). In contrast to these results, it was determined within this study that 5mC does exist within the Plasmodial parasites and that this 5mC does increase over time as the parasite progress through its life stages. In contrast to MDL73811 inhibition of AdoMetDC in Trypanosomes, hypermethylation was not detected with the inhibition of *Pf*AdoMetDC with MDL73811. This also corroborate with the lack of hypermethylation as determined in the co-inhibition of *Pf*AdoMetDC/ODC with MDL73811 and DFMO (Van Brummelen, 2009).

The AdoMet and AdoHcy metabolite levels were determined using HPLC in two different time points. It was observed that the AdoMet level does increase over time from 16 HPI to 26 HPI, but that this increase in AdoMet levels is similar in both the treated and untreated parasites. No significant changes could be detected in the AdoHcy metabolite levels. AdoMet plays an integral role in the production of polyamines and acts as a methyl donor for nearly all methylation reactions that include DNA and protein methylation. AdoHcy is the product formed after the methylation reaction and is rapidly degraded by AHC since high concentrations of AdoHcy is toxic to the parasite and will also result in down-regulation of the methyltransferases (Nakanishi et al., 2001). Therefore, the AdoMet:AdoHcy ratio is of importance within the parasites as this may result in hyper- or hypomethylation of DNA within the parasite. The transcript abundances of both AdoMet synthase and AHC were decreased as well as the protein abundance of AdoMet synthase. The unchanged metabolite levels of both AdoMet and AdoHcy together with decreased transcript and

protein abundances of AdoMet synthase and AHC may be a reason for the lack of hypermethylation with AdoMetDC inhibition. This was similarly determined with the co-inhibition of AdoMetDC/ODC (van Brummelen *et al.*, 2009). It therefore seems that in Plasmodial parasites the methionine cycle is in homeostasis and maintains AdoMet levels at a constant level, due to the decreased transcript and protein abundances of AdoMet synthase and AHC. This once again brings into question the regulatory role of AdoMet synthase as possible regulator of the entire AdoMet cycle as well as transcriptional regulatory mechanisms of AdoMet synthase.

In Chapter 4 a possible link between polyamine biosynthesis and the folate pathway was established with the decreased transcript abundance of various folate-related genes (DHFR-TS, DHFS-FPGS, serine hydroxymethyl transferase, NDPK) as a result of AdoMetDC inhibition. These transcriptomic results together with a recent finding that further iterated that polyamine biosynthesis does impact on folate metabolism in prostate cells and that folate depletion will result in imbalanced AdoMet levels (Bistulfi et al., 2009) prompted further investigation. The addition of MDL73811 in the absence of folates resulted in decreased parasite growth when compared to MDL73811 inhibition in media that does contain folates. To further establish a possible link between polyamines and folates the IC_{50}'s of both PYR and MDL73811 was determined in the presence and absence of folates. The IC_{50} of PYR remained unchanged regardless of the media used, but unlike PYR, the IC_{50} of MDL73811 was slightly reduced in the absence of folates. This prompted the determination of possible synergy determination between polyamine and folate depletion especially since a synergistic killing effect was established in human ovarian cancer cell lines depleted of both folate and polyamines (Marverti *et al.*, 2010). Although the combination of folate depletion and polyamine depletion resulted in reduced IC_{50}'s of both PYR and MDL73811, it was established that PYR and MDL73811 does not seem to act synergistically but rather have an additive effect, although further investigation is needed to confirm this. The lack of synergy between polyamine and folate depleted parasites may be due to the tight regulation of AdoMet levels that remained unchanged within MDL73811-treated parasites. Folate depletion of human cells impacts on the AdoMet pool and may result in epigenetic damage (Pogribny et al., 1995). N-5-methyl THF is essential in the recycling of homocysteine back into methionine and THF. Low folate as a result of decreased folate-related transcripts with the inhibition of AdoMetDC may therefore prevent the recycling of homocysteine into methionine and ultimately AdoMet (Pogribny *et al.*, 1995, Sohn *et al.*, 2003).

Met is important in protein synthesis and the production of AdoMet (Reguera et al., 2007). The addition of Met had an influence on transcripts involved in polyamine metabolism similar to

MDL73811. Both MDL73811 and Met resulted in a decrease of transcript levels for PEMT, AHC and histone H4. Met is essential for protein synthesis but also as substrate for the production of AdoMet which is crucial for polyamine biosynthesis and transmethylation reactions (Goldberg *et al.*, 2000, Bacchi et al., 1995). Met is present in low levels and supplementation with Met may be optimal for parasite growth (Liu et al., 2006). Met is needed for the initiation of protein synthesis, polyamine synthesis, and is the precursor for AdoMet via AdoMet synthase within polyamine metabolism. Notably, it was determined that with the addition of high Met concentrations, the transcript level of AdoMet synthase was decreased similar to inhibition of AdoMetDC with MDL73811. This indicates that AdoMet synthase may become saturated with Met, and in response induce transcriptional repression of the enzyme. This was not seen at lower Met concentrations. Excess levels of methionine can suppress the methylation cycle by causing a reduction in the AdoMet:AdoHcy ratio, that inhibits transmethylation reactions (Dunlevy et al., 2006). This may be a reason for the lack of hypermethylation with inhibition of AdoMetDC in Plasmodial parasites. Therefore, the similarities observed for the addition of high Met concentrations and the inhibition of AdoMetDC with MDL73811 could indicate that AdoMet synthase is transcriptionally regulated by Met, similar to the regulation of Plasmodial phosphoetanolamine N-methyltransferase by choline (Witola & Ben Mamoun, 2007).

Comparison of the transcriptomic and the proteomic studies revealed that only 16 proteins were identified with both technologies. This low number is probably due to the large amount of transcripts that can be identified with the use of microarrays compared to 2-DE in which far less proteins could be identified. Comparison of the transcript and protein abundances for the shared proteins revealed some interesting observations. *T cruzi* metabolism is mainly controlled by post-transcriptional and post-translational control (Clayton, 2002, Carrillo et al., 2007, Kahana, 2007), while previously it was reported that *P. falciparum* is mainly controlled by post-transcriptional regulation and that there is generally good correlation between mRNA and protein levels (Le Roch *et al.*, 2004). This was not always the case with the inhibition of AdoMetDC, which did reveal correlation between transcript and protein abundances of some of the proteins but it seemed that the majority did not correlate well. This corroborate with the notion that mRNA abundance is not always proportional to protein expression due to post-transcriptional modifications, RNA splicing, post-translational modifications, protein degradation, protein turnover as well as differences between transcription and translation (Hegde et al., 2003, Griffin *et al.*, 2002, Gygi et al., 1999).

Various studies have been employed to determine the correlation between mRNA and protein abundance in which most found a lack of correlation between mRNA and protein abundance

(Anderson & Seilhamer, 1997, Gygi et al., 1999, Chen et al., 2002). In a study on *S. cerevisiae* the correlation of 678 loci were determined and also demonstrated poor correlation between mRNA and protein expression ratios (Washburn *et al.*, 2003). The majority of deviation was from the protein abundance that was altered but had unchanged mRNA. Interestingly, methionine metabolism had an almost perfect correlation between mRNA and proteins expression (Washburn *et al.*, 2003).

The regulation of mRNA half life is an important determination of gene expression levels and is essential for regulation of post-transcriptional control. The average mRNA decay half-life in *P. falciparum* increases with the progress of the parasite through its life cycle (Shock *et al.*, 2007). The average mRNA half-life of ring stage parasites is 9.5 min, which progressively increases to 20.5 min in trophozoites and 65.4 min in late schizonts. The cascade of gene expression seen in *P. falciparum* is unlike any other organism, and may provide clues that post-translational regulation may be a key in gene regulation although little is known on the regulation of this cascade or how it is maintained (Shock et al., 2007). mRNA abundance is the result of the rate at which mRNA is produced minus the rate at which it is decayed, with mRNA decay a extremely well regulated process rather than the degradation of all transcripts (Wang *et al.*, 2002). mRNA decay may also be related to protein function and the energy requirements of the growing parasites (Wang *et al.*, 2002, Garcia-Martinez *et al.*, 2004).

The inhibition of AdoMetDC with MDL73811 resulted in the identification of a few major groups regarding the correlation between transcript and protein abundance levels. The first group revealed that a change in the transcript levels was similarly seen in the protein levels and may therefore correlate to possible transcriptional mechanisms (Chen *et al.*, 2002). Basically, most of the transcripts displayed a decrease in transcript abundance which was similarly determined with a decrease in protein abundance although the decrease in protein abundance was sometimes associated with a delay. Proteins in this group included adenosine deaminase, AdoMet synthase, PNP, Hsp70, and eIF5A. The similarity of the transcript and protein abundance of *Pf*eIF5Adiffer from that of eIF5A in lung adenocarcinomas in which mRNA and protein abundance did not correlate due to higher protein expression indicative of a post-transcriptional or post-translational regulation mechanism (Chen *et al.*, 2003). It may therefore be that *Pf*eIF5A may be under transcriptional regulation or that it has other isoforms which has not yet been identified on the 2-DE gel and may therefore result in a change in protein abundance. The delay of the protein abundance that is observed in some of these proteins may be due to a delay in protein turnover, or slow degradation of the protein (Foth *et al.*, 2008). Post-transcriptional regulation may be a major mechanism of gene expression in *P. falciparum* since it is carried out by chromatin remodelling in

the various life stages (Ponts *et al.*, 2010). The ring stage plays an essential role in the regulation of gene expression since stress in the ring stage can initiate gametocytogenesis (Ponts *et al.*, 2010). Transcriptional regulation may also be mediated by co-regulation of genes through copy number variant regions that may play a role in gene regulation to genes that are distant from them (Mackinnon *et al.*, 2009). Overall, the process of transcription in *P. falciparum* is highly coordinated and co-regulation of transcription of adaptive genes may play a role in the ability of the parasite to adapt to environmental stresses (Mackinnon *et al.*, 2009).

Another group that was identified were proteins that revealed a decrease in transcript abundance but had an increase in protein abundance and included pyruvate kinase, MAL13P1.283, and GST. This may be due to some mechanism of translational repression, or protein turnover, or it may be that these proteins have various PTM's that have not yet been identified on the 2-DE gel and that these protein isoforms may resemble the transcript abundance (Foth *et al.*, 2008). It may also be due to a process of post-transcriptional gene silencing which seems to play a role in gene expression through translational repression (Hall *et al.*, 2005). Translational repression and mRNA turnover plays an important role in stage specific gene expression of the malaria parasite and therefore also has a key role in parasite development (Mair *et al.*, 2006).

2-Cys peroxiredoxin, pyrroline 5-carboxylate reductase, Hsp60 and 40S ribosomal protein all formed part of a group that revealed no change in transcript levels but an increase in protein abundance which is probably due to post-transcriptional regulation (Hegde *et al.*, 2003). Another possibility may be due to slow degradation or that the proteins may be resistant to degradation, or perhaps the protein lag behind the transcript and the decrease in protein abundance will be seen later (Foth *et al.*, 2008). This may also be similar to *Pf*DHFR-TS which is translationally regulated as it is able to bind to its own mRNA, therefore initiating the inhibition of its own translation (Zhang & Rathod, 2002). In the presence of an inhibitor, *Pf*DHFR-TS has no change in transcript level but has an increase in protein expression therefore releasing the translational restraints upon the protein (Nirmalan *et al.*, 2004b). It may therefore be concluded that upon inhibition of AdoMetDC and subsequent polyamine depletion 2-cys peroxiredoxin, pyrroline 5-carboxylate, hsp60 and 40S ribosomal protein may all be translationally regulated.

PEMT and enolase both had decreased transcript levels but had multiple protein isoforms. Some of the protein isoforms resembled the transcript abundance while other protein isoforms increased in protein abundance. This reveals some mechanisms of PTM's where different protein isoforms may have different functions (Foth *et al.*, 2008, Pal-Bhowmick *et al.*, 2007). Phosphoethanolamine N-

methyltransfearse is expressed throughout the life cycle of *P. falciparum* (Pessi *et al.*, 2004). It is a monomeric enzyme with a single catalytic domain of which the activity is inhibited by its own product phosphocholine (Pessi *et al.*, 2004). PEMT is regulated by metabolite-mediated transcriptional regulation and subsequently degraded by proteasomal regulation (Witola & Ben Mamoun, 2007), although the various post-translational modifications on the protein isoforms cannot be excluded and are often associated with differences that arise between the protein and mRNA abundance due to separate regulation of the multiple isoforms (Chen *et al.*, 2002).

Overall, it seems that upon polyamine depletion due to the inhibition of AdoMetDC in Plasmodial parasites the majority of regulatory mechanisms are controlled by post-transcriptional regulatory mechanisms. Post-translational modifications were also abundant in the proteome (Chapter 2 and 3) and may therefore also play a role in the regulation of protein isoforms. It can also be concluded that various post-transcriptional regulatory mechanisms exist and that combinations of these regulatory motifs regulate gene expression similar to previous reports (van Noort & Huynen, 2006).

CHAPTER 6

Concluding discussion

"We don't have perfect tools, but the tools we do have today if fully scaled up will have a profound effect"

Robert Newman (Director WHO Global malaria program)

Malaria is a killer disease transmitted by the protozoan parasite, *Plasmodium*. With the spread of increasing resistance to currently used drugs (Noedl *et al.*, 2008), insecticide resistance (Tatem *et al.*, 2006), the effect of global warming, global travel as well as the identification of enzoonotic species that are now able to infect humans (Bronner *et al.*, 2009), the need for new drugs are more urgent than ever. Unique differences between *P. falciparum* and eukaryotic cells must be exploited in order to identify novel drug targets. One such potential drug target is polyamine metabolism, which differs significantly from that of humans and is essential to parasite survival. *Plasmodium* polyamine metabolism includes a uniquely bifunctional AdoMetDC/ODC complex that regulates the biosynthesis of polyamines within the parasite. Functional genomics, as applied in this study to AdoMetDC inhibited malaria parasites, is an integral part of drug discovery to investigate the therapeutic potential of this bifunctional enzyme as an antimalarial drug target.

The general objective of this study was to determine the biological relevance and consequences of the inhibition of Plasmodial AdoMetDC with MDL73811 in order to chemically validate *Pf*AdoMetDC as a drug target. This question was answered with the use of a functional genomics approach in which both transcriptomics and proteomics were utilised in order to provide a picture of the global response of the parasite to AdoMetDC inhibition. Ideally, it is hoped that the use of the technologies associated with functional genomics will allow the ability to obtain the mode-of-action of drugs.

Due to the multistage life cycle of the Plasmodial parasite careful consideration were given to experimental design in order to obtain maximal information from the transcriptomic study. A reference design was employed that enabled the determination of the differential abundance of any sample in relation to the other samples (Kerr & Churchill, 2001). Three time points were investigated in the ring stage (16 HPI), early trophozoite stage (20 HPI) and the late trophozoite stage (26 HPI) in order to obtain the exact point of transcriptional arrest. The early time points used in this study allowed a direct comparison of the transcriptome and therefore negated the use of the t_0 reference strategy (van Brummelen *et al.*, 2009). Pearson correlations and hierarchical clustering confirmed the use of the direct comparison employed within this study and also confirmed that the

differentially affected transcripts are representative of drug-specific effects and not stage specific effects. A total of 549 transcripts were differentially affected by the inhibition of AdoMetDC with MDL73811.

The proteome does not always mimic the transcriptome, therefore to obtain a global picture of the response of the parasites to AdoMetDC inhibition the proteome were investigated using 2-DE. Due to the complexity and notorious nature of Plasmodial proteins, the proteins were solubilised in a potent lysis buffer. The nature of the lysis buffer negates the use of any traditional methods of protein quantification which is problematic for the determination of differentially regulated proteins. In order to overcome this problem, the existing Plasmodial 2-DE protocols (Nirmalan *et al.*, 2004a, Makanga *et al.*, 2005) were optimised for use in our laboratory. Optimisation included the use of the 2-D Quant kit for protein quantification to ensure that similar amounts of protein were used for both the treated and untreated samples, therefore enabling differential abundance analysis. The 2-DE protocol was also optimised to reduce hemoglobin contamination in the 14 kDa and pI 7-9 range by the addition of extra wash steps and softer sonication methods. Finally, the use of the fluorescent stain Flamingo Pink enabled a quantitative measure of proteins within the 2-DE gels. Application of this methodology to the ring and trophozoite stages of the parasite enabled the MS-identification of 125 protein spots. Interestingly, protein isoforms were a prominent feature of the spots that were identified and accounted for ~28% of the total number of Plasmodial protein spots identified in the ring and trophozoite stages. This clearly illustrates the prominent role of protein isoforms during Plasmodial protein regulation and the use of PTM's as a regulatory mechanism within the parasite. Furthermore, a comparison between the ring, trophozoite and schizont stages (Foth *et al.*, 2008) revealed that only 9 proteins were shared in all 3 stages, therefore indicative of stage specific protein production. This is similar to other MS-based studies on the various life stages of the parasites (Lasonder *et al.*, 2002, Florens *et al.*, 2002) in which stage specific production of proteins were also observed.

The optimised method described in Chapter 2 proved robust and reproducible in various applications of the Plasmodial proteome. This was demonstrated in Chapter 3 in which the proteome of AdoMetDC inhibited parasites were investigated and resulted in good spot detection and spot identification with MS. The consistency of this method was also demonstrated with the co-inhibition of AdoMetDC/ODC in which 400 spots were detected in each of the 3 time points investigated (Van Brummelen, 2009). The same optimised proteomics protocol was also used in 2 separate herbicide studies on the Plasmodial proteome (J. Verlinden MSc thesis in preparation, J. Snyman MSc thesis in preparation) in which good spot separation was achieved. Overall, the

optimised 2-DE methodology proved robust and is repeatable for different parasite applications. The established proteomic methodology was applied to the proteome of inhibited AdoMetDC to obtain a snapshot of the proteome at two time points (16 HPI and 20 HPI). Complementary proteomic techniques were employed that made use of both 1-D SDS-PAGE as wells as 2-DE to obtain maximal information from the proteome. This approach paid dividend in that 11 proteins were identified using the SDS-PAGE gels that would normally fall outside the 2-DE gel range and would have remained unidentified.

Unlike the transcriptome in which at least half of the transcripts are classified as hypothetical, this was not the case for the AdoMetDC inhibited proteome. Only 9% (4/46 proteins) of the total proteome that was identified was regarded as hypothetical proteins with unknown functions. This was probably due to the small portion of unique proteins that were identified (46 proteins) in comparison to the AdoMetDC inhibited transcriptome that contained 549 differentially expressed transcripts (Chapter 4). Another reason for the small number of hypothetical proteins was probably due to the fact that 2-DE was only representative of high abundance proteins and therefore the majority of these have already been characterised. Of the 46 identified proteins that were differentially expressed 18% were associated with glucose metabolism. Some of the other groups that were highly represented included protein folding (11%), polyamine metabolism (11%), proteolysis (15%), translation (13%) and oxidative stress (5%). These groups were also prominent in the differentially affected transcripts from the transcriptome, in which oxidative stress (3%), translation (6%) and polyamine metabolism (3%) were represented (Chapter 4). Therefore, AdoMetDC inhibition does affect certain key pathways that seem to be polyamine related or dependent on the presence of polyamines.

Evidence as to the possibility of post-transcriptional regulation was supported in this study in that 17% (55/325) of the ring and 24% (64/272) of the trophozoite proteome were differentially regulated which is in contrast to the transcriptome in which little regulation were detected within the first two time points. It should however be considered that the transcriptome and proteome samples were harvested independently from each other and therefore a possible time window exists. Ideally, the samples for the transcriptome and the proteome analysis should be harvested simultaneously to eradicate possible time errors that may develop and should be considered for all future functional genomics experiments.

Even though, a combination of proteomic gel-based techniques were employed relatively few proteins were identified in comparison to the transcriptome (549 differentially affected transcripts).

In total, 61 unique Plasmodial proteins were identified with the combination of 1-D SDS-PAGE and 2-DE. This re-iterated the use of complimentary proteomic techniques to obtain differentially expressed proteins (Nirmalan *et al.*, 2007). The use of MudPIT-based technologies would have allowed the identification of more proteins within the study, but with the disadvantage of the loss of protein isoforms. PTM's are employed as a mechanism to regulate protein activity during the parasite's life cycle (Nirmalan *et al.*, 2004a) and certain proteins are predicted to act as controlling nodes that are highly interconnected to other nodes and thus results in a highly specialised interactome (Wuchty *et al.*, 2009, Birkholtz *et al.*, 2008b). It is therefore of utmost importance to identify protein isoforms within the proteome and determine their regulatory functions. The use of 2-DE enabled the identification of various protein isoforms. Ideally, these protein isoforms should be investigated further in order to be able to distinguish between the different protein isoforms based upon their different PTM's. The identification of these different PTM's will also provide more clarity on the function of the protein and whether the isoform is an active protein or an inactive protein. In order to obtain more protein spots on the 2-DE gels fractionation techniques could also be considered. The proteome can be fractionated into different pI fractions before running the fraction on a 2-DE gel (Nirmalan *et al.*, 2007, Nirmalan *et al.*, 2008). This fraction will enable enhanced spot and protein determination within a specified pI range and provide a more detailed picture of the proteome. Organellar fractionation can also be considered to obtain proteins associated with a specific compartment of the parasite. These approaches will produce more protein spots and will also eliminate high abundance proteins therefore enabling the determination of low abundance protein profiles. This approach should be considered for future experiments, which will then enable the identification of both high (current approach) and low (fractionation) abundance proteins.

Both the transcriptome and the proteome of AdoMetDC inhibited *P. falciparum* parasites revealed inhibitor-induced differences. These differentially expressed genes and proteins include polyamine-related pathways, possible compensatory mechanisms, down-stream pathways as well as regulated proteins in other essential pathways within the parasite. Essential pathways associated with AdoMetDC inhibition included the folate pathway, oxidative stress and redox metabolism as well as cytoskeleton biogenesis. Polyamine metabolism is essential to parasite survival and depletion of the polyamines induced transcriptional arrest within the parasite.

Down-stream metabolic pathways that were severely affected by AdoMetDC inhibition included the decreased transcript abundances of adenosine deaminase, PNP and HPPRT. The protein of PNP was also decreased in abundance which confirmed the transcript levels. The decreased abundances

of these 3 transcripts are probably as a result of the decreased MTI due to the decreased dcAdoMetDC as a result of AdoMetDC inhibition. These 3 transcripts are therefore polyamine dependent and an absence of polyamines will result in their decreased abundances and will also impact on DNA and RNA metabolism.

Polyamine-related transcripts also revealed a decrease in transcript and protein abundance upon inhibition of AdoMetDC and include AdoMet synthase and adenosylhomocysteinase that are associated with methionine recycling. Despite the decreased transcript and protein abundances of both AdoMet synthase and AHC there were no alteration of the AdoMet levels. This is indicative of homeostasis and tight regulation of the AdoMet levels within the parasite. Trypanosomal AdoMet synthase is not feedback regulated by AdoMet which results in the significant increase in AdoMet levels and subsequent hypermethylation within Trypanosomal parasites and consequent parasite death (Muller *et al.*, 2008, Goldberg *et al.*, 2000, Yarlett *et al.*, 1993). It has been reported that Plasmodial AdoMet synthase is similar to the Trypanosomal AdoMet synthase and is not feedback regulated. The data that were obtained with the inhibition of *Pf*AdoMetDC is indicative of the contrary. The decreased transcript and protein abundances of AdoMet synthase and the lack of change in the AdoMet and AdoHcy metabolite levels and subsequent lack of hypermethylation with MDL73811 treatment suggests that AdoMet synthase plays an essential role during polyamine metabolism and is tightly regulated. It is therefore essential to determine the possible transcriptional regulatory mechanisms that may be involved with AdoMet synthase.

Phosphoethanolamine N-methyltransfease was identified as a unique transcript to AdoMetDC inhibition. Both the transcript and the various protein isoforms of PEMT were decreased in abundance with AdoMetDC inhibition. From the comparisons that were made it seems that PEMT is dependent on spermidine and spermine since the mono-functional inhibition of ODC did not identify PEMT as a differently regulated transcript. An interesting observation that was made from the polyamine-related transcripts that were identified is that it seems that these transcripts are under post-transcriptional control. The transcripts and proteins of AdoMet synthase, AHC, PNP and PEMT were all decreased and is therefore indicative of transcriptional and post-transcriptional control mechanisms. It may be that the transcripts of these proteins are stabilised by the presence of polyamines, therefore exerting transcriptional control on both the transcripts and the proteins.

The transcript of AdoMetDC was not differentially regulated by inhibition with MDL73811, which is in contrast to the co-inhibition of AdoMetDC/ODC that resulted in two-fold decreased abundance of the transcript (van Brummelen et al., 2009). An interesting observation would have been to

determine if the protein abundance of AdoMetDC was affected by the irreversible inhibition with MDL73811. This was attempted by western blot analysis of treated and untreated parasites but unfortunately the antibody demonstrated some unspecific binding and therefore no conclusive results could be made. A new antibody is currently under development from our laboratory, and once this task has been completed the AdoMetDC antibody could be used to determine if the protein abundance of AdoMetDC is differentially regulated with inhibition. This is an important validation step that is still lacking. Previously, it was determined that upon inhibition of the folate pathway the transcript levels remained constant, but that enzyme activity increased with a possible increase in the synthesis of new protein to combat the effect of the drug (Nirmalan *et al.*, 2004b).

Polyamine-related transcripts with increased transcripts included lysine decarboxylase and calcium/calmodulin-dependent protein kinase 2 (PFL1885c), and is indicative of possible compensatory mechanisms within the parasite as a response to polyamine depletion. Due to the large size of LDC the protein could not be detected on the 2-DE gels. It is assumed that during normal growth of the parasite lysine is converted to cadeverine by LDC although the precise role of cadaverine within the parasite remains unclear. Evidence in *Vibrio vulnificus* suggests an increase in LDC and cadaverine may enable protection against oxidative stress while its product; cadaverine acts as a radical scavenger of superoxide (Kim *et al.*, 2006, Kang *et al.*, 2007). In a polyamine-depleted environment cadaverine may also be utilised by SpdS therefore freeing the remaining spermidine for eIF5A synthesis and subsequent protein synthesis (Pegg *et al.*, 1981, Park *et al.*, 1991). It is therefore assumed that a similar situation exists in Plasmodial parasites in which the increased transcript abundance of LDC may be indicative of an attempt by the parasite to preserve protein synthesis by freeing spermidine for utilisation by eIF5A or that the increased transcript abundance of LDC and possible increase in cadaverine may provide protection against oxidative stress or possibly both.

The protein of eIF5A was decreased in abundance and would therefore result in decreased protein synthesis. The decreased protein abundance of eIF5A may suggest that cadaverine is not utilised by eIF5A but rather acts as a radical scavenger, but this needs confirmation within the Plasmodial parasite. The protein levels of pyrroline 5-carboxylate reductase increased in the treated samples and may therefore also be a polyamine-related response. The increased protein abundance of pyrroline 5-carboxylate reductase may suggest an attempt by the parasite to relieve the excess build-up of ornithine as a result of AdoMetDC inhibition and may also be a possible compensatory mechanism.

Calcium/calmodulin-dependent protein kinase 2 were increased as well as various FIKK kinases, calcium dependent protein kinase 1 and cAMP dependent protein kinase regulatory subunit were decreased in transcript abundance. In *P. falciparum*, calcium signalling pathway is able to control vital functions within the parasite especially the cell cycle, which corroborate with the increase in calcium throughout the life cycle of the parasite. Host melatonin regulates both calcium and cAMP which acts as second messengers in the Plasmodial life cycle. A rise in calcium will result in an increase in cAMP production which will further induce calcium release, although the exact mode-of-action of the calcium influx pathway remains elusive to date. This may indicate a role of the calcium/calmodulin-dependent protin kinase 2 and the various FIKK kinases in the regulation of the cell cycle and needs further investigation in the future.

Three key pathways seem to be affected by the inhibition of AdoMetDC and in comparison to other perturbation studies seems to be unique to polyamine perturbations. These pathways include the folate pathway, oxidative stress and cytoskeleton biosynthesis (Figure 6.1). Upon polyamine depletion a general decrease in folate-related transcripts was determined which may possibly result in a polyamine- and folate-depleted environment within the parasite. The connection between polyamine metabolism and folate synthesis has been established previously (Bistulfi *et al.*, 2009). Further investigation of folate and polyamine depletion revealed that in a folate and polyamine depleted environment the IC_{50}'s of both MDL73811 and PYR were decreased. The possibility of synergism between polyamine depletion and folate depletion was investigated and revealed an additive effect rather than a synergistic drug interaction. Polyamine and folate depletion in human ovarian cancer revealed a synergistic killing effect (Marverti *et al.*, 2010) which is in contrast to the results obtained for the Plasmodial parasites. This may be as a result of the differences between mammalian and Plasmodial polyamine metabolism, as well as the regulation of AdoMet which seem to exist within the parasite. Although it should be noted that the synergistic studies between PYR and MDL73811 needs further investigation. The advantage of eliminating 2 pathways is that it will reduce the possibility of resistance. Therefore the decreased transcript abundances obtained for both pathways and the additive effect of polyamine-and folate-depletion may indicate co-regulation of the pathways, but needs further investigation.

Another consequence of polyamine metabolism seems to be the interaction with oxidative stress (Figure 6.1). In the transcriptome various oxidative stress-related transcripts were all decreased possibly resulting in increased oxidative stress within the parasite. The thioredoxin interactome revealed that OAT, AdoMet synthase and AHC were all interacting partners of thioredoxin (Sturm *et al.*, 2009). Similarly thioredoxin reductase is also a binding partner of AdoMet synthase which

may ultimately result in a possible link between the tight regulation of the AdoMet cycle as well as regulation of the polyamine pathway (Sturm *et al.*, 2009, Wuchty *et al.*, 2009). The decreased transcript and protein abundance of AdoMet synthase may have an influence on thioredoxin reductase activity or protein expression, which may result in regulation of the redox status of the parasite. The increased transcript of LDC which may result in increased levels of cadaverine may also provide a clue as to the attempt of the parasite to relieve the induced oxidative stress by other pathways than the conventional redox metabolism. Two of the proteins associated with oxidative stress (2-cys peroxiredoxin and GST) revealed an increase in protein abundance over time despite the transcripts having decreased abundance, indicative of post-transcriptional control mechanism within the parasite. Another possibility is that the proteins can be resistant to degradation, or the protein lag behind the transcript and the decrease in protein abundance will be seen later (Foth *et al.*, 2008). This may also be similar to *Pf*DHFR-TS which is translationally regulated as it is able to bind to its own mRNA, therefore initiating the inhibition of its own translation (Zhang & Rathod, 2002). The influence of polyamine depletion on oxidative stress prompts further investigation to determine the oxidative status of the parasite after AdoMetDC inhibition. The functional genomics results indicate that AdoMetDC inhibition may result in an increased oxidative state within the parasite which may therefore reveal a clue as to the mode-of-action of MDL78311 within the Plasmodial parasite.

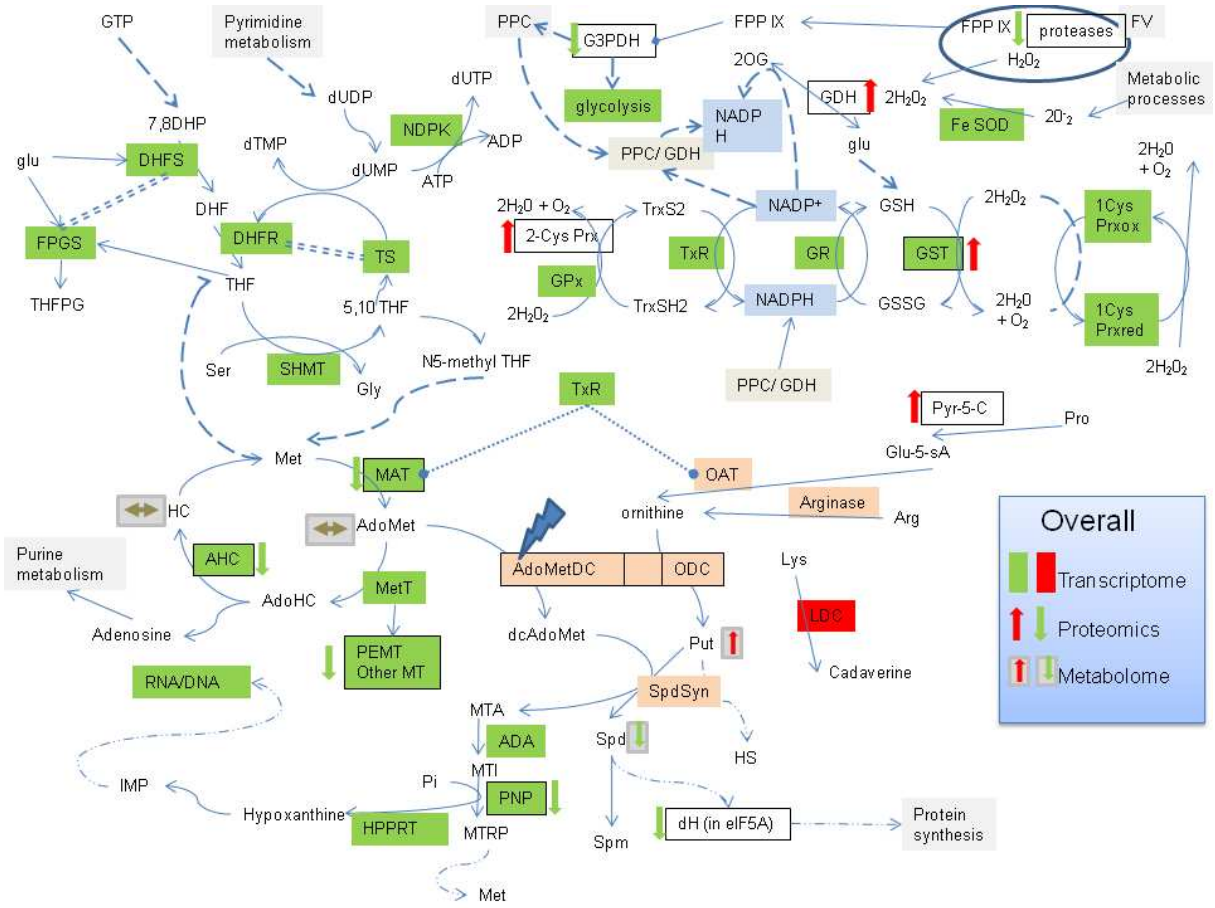

Figure 6.1: Functional consequences of polyamine depletion induced by AdoMetDC inhibition.
Green in indicative of corresponding decrease in transcript or protein while red is indicative of a corresponding increase in transcript or protein abundance. Names that are blocked with a black line is indicative of the change in protein, while transcripts are not blocked. For example: PNP denotes a decrease in both transcript and protein abundance, while HPPRT denotes a decrease in only the transcript.

Various transcripts involved in cytoskeleton organisation and biogenesis was also unique to the AdoMetDC dataset re-iterating the recent link that was established between polyamines and microtubules (Savarin *et al.*, 2010). The transcript abundance of actin and tubulin were severely decreased with AdoMetDC perturbation. The disruption in tubulin may suggest a link to cell cycle arrest in the G1-phase of the parasite. It may therefore be assumed that polyamines may play a role in stabilisation of these transcripts involved in the cell cycle and that upon polyamine depletion the majority of these transcripts may become destabilised resulting in parasite arrest. Investigations on the cell cycle are currently underway in our laboratory. It would be interesting to determine the role of polyamine depletion on microtubule formation and possible apoptosis within the parasite.

In conclusion, transcriptomics and proteomics as part of a functional genomics strategy provided the tools needed to investigate the global response of AdoMetDC inhibition on the parasite. Indeed, these tools are not perfect, but as shown throughout this study if they are scaled up and used

correctly, functional genomics can provide a profound effect on the drug discovery efforts. Here, it was demonstrated that inhibition of AdoMetDC does have a unique transcriptomic fingerprint. Furthermore, unique compensatory pathways were identified that provided clues as to the global effect of polyamine depletion on the parasite. Severely affected pathways like folate biosynthesis, oxidative stress and cytoskeleton biogenesis can be exploited further in combination with polyamine depletion to provide a more pronounced effect on the parasite. Another pathway that may also be considered for targeting in combination with polyamine depletion is protein kinases that were severely increased in abundance and may play an essential role in the cell cycle. Integration of functional genomics and systems biology were critical in the determination of uniquely affected pathways and possible regulatory mechanisms. Fortunately, the target was known within this study and it remains to be seen if a functional genomic approach in malaria parasites will be able to elucidate the mode-of-action of a compound with the same success as seen in tuberculosis and antibacterial research. This study revealed an in depth investigation into the transcriptome and proteome of AdoMetDC inhibited parasites and provided a novel contribution to the ongoing fight against malaria.

References

Centre for Disease Control (www.cdc.gov).

Department of Health South Africa (www.doh.gov.za).

Abruzzo, L. V., K. Y. Lee, A. Fuller, A. Silverman, M. J. Keating, L. J. Medeiros & K. R. Coombes, (2005) Validation of oligonucleotide microarray data using microfluidic low-density arrays: a new statistical method to normalize real-time RT-PCR data. *BioTechniques* **38**: 785-792.

Acestor, N., S. Masina, J. Walker, N. G. Saravia, N. Fasel & M. Quadroni, (2002) Establishing two-dimensional gels for the analysis of *Leishmania* proteomes. *Proteomics* **2**: 877-879.

Agarwal, A. K., P. D. Rogers, S. R. Baerson, M. R. Jacob, K. S. Barker, J. D. Cleary, L. A. Walker, D. G. Nagle & A. M. Clark, (2003) Genome-wide expression profiling of the response to polyene, pyrimidine, azole, and echinocandin antifungal agents in *Saccharomyces cerevisiae*. *J. Biol. Chem.* **278**: 34998-35015.

Aggarwal, K., L. H. Choe & K. H. Lee, (2006) Shotgun proteomics using the iTRAQ isobaric tags. *Brief. Funct Genomic Proteomic* **5**: 112-120.

Akerman, S. E. & S. Muller, (2003) 2-Cys peroxiredoxin PfTrx-Px1 is involved in the antioxidant defence of *Plasmodium falciparum*. *Mol. Biochem. Parasitol.* **130**: 75-81.

Aly, N. S. M., A. Hiramoto, H. Sanai, O. Hiraoka, K. Hiramoto, H. Kataoka, J. M. Wu, A. Masuyama, M. Nojima, S. Kawai, H. S. Kim & Y. Wataya, (2007) Proteome analysis of new antimalarial endoperoxide against *Plasmodium falciparum*. *Parasitol. Res.100*

Anderson, L. & J. Seilhamer, (1997) A comparison of selected mRNA and protein abundances in human liver. *Electrophoresis* **18**: 533-537.

Anstey, N. M., J. B. Weinberg, M. Hassanali, E. D. Mwaikambo, D. Manyenga, M. A. Misukonis, D. R. Arnelle, D. Hollis, M. I. McDonald & D. L. Granger, (1996) Nitric oxide in Tanzanian children with malaria: Inverse relationship between malaria severity and nitric oxide production nitric oxide synthase type 2 expression. *J. Exp. Med.* **184**: 557-567.

Aponte, J. J., P. Aide, M. Renom, I. Mandomando, Q. Bassat, J. Sacarlal, M. N. Manaca, S. Lafuente, A. Barbosa, A. Leach, M. Lievens, J. Vekemans, B. Sigaugue, M. C. Dubois, M. A. Demoitie, M. Sillman, B. Savarese, J. G. McNeil, E. Macete, W. R. Ballou, J. Cohen & P. L. Alonso, (2007) Safety of the RTS,S/AS02D candidate malaria vaccine in infants living in a highly endemic area of Mozambique: a double blind randomised controlled phase I/IIb trial. *Lancet* **370**: 1543-1551.

Arikawa, E., Y. Sun, J. Wang, Q. Zhou, B. Ning, S. L. Dial, L. Guo & J. P. Yang, (2008) Cross-platform comparison of SYBR (R) Green real-time PCR with TaqMan PCR, microarrays and other gene expression measurement technologies evaluated in the MicroArray Quality Control (MAQC) study. *BMC Genomics* **9**.

Artavanis-Tsakonas, K., J. E. Tongren & E. M. Riley, (2003) The war between the malaria parasite and the immune system: immunity, immunoregulation and immunopathology. *Clin. Exp. Immunol.* **133**: 145-152.

Assaraf, Y., J. Golenser, D. Spira, G. Messer & U. Bachrach, (1987) Cytostatic effect of DL-a-difluoromethylornithine against *Plasmodium falciparum* and its revearsal by diamines and spermidine. *Parasitol. Res.* **73**: 313–318.

Assaraf Y.G., L. Abu-Elheiga, D.T. Spira, H. Desser. & U Bachrach, (1987) Effect of polyamine depletion on macromolecular synthesis of the malarial parasite, *Plasmodium falciparum*, cultured in uman erythrocytes. *Biochem J.l* **242**: 221-226.

Assimakopoulos, S. F., D. Konstantinou, C. Georgiou & E. Chroni, (2010) Metabolism of polyamines and oxidative stress in the brain of cholestatic rats. *Amino Acids* **38**: 973-974.

Aurrecoechea, C., J. Brestelli, B. P. Brunk, J. Dommer, S. Fischer, B. Gajria, X. Gao, A. Gingle, G. Grant, O. S. Harb, M. Heiges, F. Innamorato, J. Iodice, J. C. Kissinger, E. Kraemer, W. Li, J. A. Miller, V. Nayak, C. Pennington, D. F. Pinney, D. S. Roos, C. Ross, C. J. Stoeckert Jr,

C. Treatman & H. Wang, (2008) PlasmoDB: a functional genomic database for malaria parasites. *Nucleic Acids Res.* **37**: D539-D543.

Azarova, A. M., Y. L. Lyu, C. P. Lin, Y. C. Tsai, J. Y. N. Lau, J. C. Wang & L. F. Liu, (2007) Roles of DNA topoisomerase II isozymes in chemotherapy and secondary malignancies. *Proc. Natl. Acad. Sci. U. S. A.* **104**: 11014-11019.

Bacchi, C. J., B. Goldberg, J. Garofalohannan, D. Rattendi, P. Lyte & N. Yarlett, (1995) Fate of soluble methionine in African Trypanosomes - effect of metabolic inhibitors. *Biochem. J.* **309**: 737-743.

Bacchi, C. J., B. Goldberg, N. Yarlett & J. Garofalo, (1992a) Protein methylation and S-adenosylmethionine methylation in *Trypanosoma brucei brucei*. *Mol. Biol. Cell* **3**: A177-A177.

Bacchi, C. J., H. C. Nathan, N. Yarlett, B. Goldberg, P. P. McCann, A. J. Bitonti & A. Sjoerdsma, (1992b) Cure of murine *Trypanosoma brucei rhodesiense* infections with an S-adenosylmethionine decarboxylase inhibitor. *Antimicrob. Agents Chemother.* **36**: 2736-2740.

Bacon, D. J., D. Tang, C. Salas, N. Roncal, C. Lucas, L. Gerena, L. Tapia, A. A. Llanos-Cuentas, C. Garcia, L. Solari, D. Kyle & A. J. Magill, (2009) Effects of Point Mutations in *Plasmodium falciparum* Dihydrofolate Reductase and Dihydropterate Synthase Genes on Clinical Outcomes and In Vitro Susceptibility to Sulfadoxine and Pyrimethamine. *Plos One* **4**.

Ballou, W. R., (2009) The development of the RTS,S malaria vaccine candidate: challenges and lessons. *Parasite Immunol.* **31**: 492-500.

Bannister, L. H., J. M. Hopkins, R. E. Fowler, S. Krishna & G. H. Mitchell, (2000) A Brief Illustrated Guide to the Ultrastructure of *Plasmodium falciparum* Asexual Blood Stages. *Parasitol. Today* **16**: 427-433.

Barnes, K. I., P. Chanda & G. Ab Barnabas, (2009) Impact of the large-scale deployment of artemether/lumefantrine on the malaria disease burden in Africa: case studies of South Africa, Zambia and Ethiopia. *Malaria J.* **8**.

Baumbusch, L. O., J. Aaroe, F. E. Johansen, J. Hicks, H. Sun, L. Bruhn, K. Gunderson, B. Naume, V. N. Kristensen, K. Liestol, A. L. Borresen-Dale & O. C. Lingjaerde, (2008) Comparison of the Agilent, ROMA/NimbleGen and Illumina platforms for classification of copy number alterations in human breast tumors. *BMC Genomics* **9**.

Becker, J. V. W., L. Mtwisha, B. G. Crampton, S. Stoychev, A. C. van Brummelen, S. Reeksting, A. I. Louw, L. M. Birkholtz & D. T. Mancama, (2010) *Plasmodium falciparum* spermidine synthase inhibition results in unique perturbation-specific effects observed on transcript, protein and metabolite levels. *BMC Genomics* **11**.

Becker, K., S. M. Kanzok, R. Iozef, M. Fischer & R. H. Schirmer, (2003) Plasmoredoxin, a novel redox-active protein unique for malarial parasites. *Eur. J. Biochem.* **270**: 1057-1064.

Bejon, P., J. Lusingu, A. Olotu, A. Leach, M. Lievens, J. Vekemans, S. Msham, T. Lang, J. Gould, M. C. Dubois, M. A. Demoitie, P. Vansadia, T. Carter, P. Njuguna, K. Kawuondo, S. Gesase, C. Drakeley, B. Savarese, T. Villafana, W. R. Ballou, J. Cohen, E. Riley, M. Lemnge, K. Marsh & L. von Seidlein, (2008a) Phase IIb, randomized, double-blind trial to assess the efficacy, safety and immunogenicity of the candidate malaria vaccine RTS,S/AS01 in Kenyan and Tanzanian children. *Am. J. Trop. Med. Hyg.* **79**: 26.

Bejon, P., J. Lusingu, A. Olotu, A. Leach, M. Lievens, J. Vekemans, S. Mshamu, T. Lang, J. Gould, M. Dubois, M. Demoitie, J. F. Stallaert, P. Vansadia, T. Carter, P. Njuguna, K. O. Awuondo, A. Malabeja, O. Abdul, S. Gesase, N. Mturi, C. J. Drakeley, B. Savarese, T. Villafana, W. R. Ballou, J. Cohen, E. M. Riley, M. M. Lemnge, K. Marsh & L. von Seidlein, (2008b) Efficacy of RTS,S/AS01E Vaccine against Malaria in Children 5 to 17 Months of Age. *New Engl. J. Med.* **359**: 2521-2532.

Bennett, T. N., M. Paguio, B. Gligorijevic, C. Seudieu, A. D. Kosar, E. Davidson & P. D. Roepe, (2004) Novel, rapid, and inexpensive cell-based quantification of antimalarial drug efficacy. *Antimicrob. Agents Chemother.* **48**: 1807-1810.

Berger, B. J., (2000) Antimalarial activities of aminooxy compounds. *Antimicrob. Agents Chemother.* **44**: 2540-2542.

Berger, S. L., (2002) Histone modifications in transcriptional regulation. *Curr. Opin. Genet. Dev.* **12**: 142-148.

Berggren, K., E. Chernokalskaya, T. H. Steinberg, C. Kemper, M. F. Lopez, Z. Diwu, R. P. Haugland & W. F. Patton, (2000) Background-free, high sensitivity staining of proteins in one- and two-dimensional sodium dodecyl sulfate-polyacrylamide gels using a luminescent ruthenium complex. *Electrophoresis* **21**: 2509-2521.

Betts, J. C., A. McLaren, M. G. Lennon, F. M. Kelly, P. T. Lukey, S. J. Blakemore & K. Duncan, (2003) Signature gene expression profiles discriminate between isoniazid-, thiolactomycin-, and triclosan-treated *Mycobacterium tuberculosis*. *Antimicrob. Agents Chemother.* **47**: 2903-2913.

Biagini, G. A., P. M. O'Neill, A. Nzila, S. A. Ward & P. G. Bray, (2003) Antimalarial chemotherapy: young guns or back to the future? *Trends Parasitol.* **19**: 479-487.

Binz, P. A., R. Barkovich, R. C. Beavis, D. Creasy, D. M. Horn, R. K. Julian, S. L. Seymour, C. F. Taylor & Y. Vandenbrouck, (2008) Guidelines for reporting the use of mass spectrometry informatics in proteomics. *Nat. Biotechnol.* **26**: 862-862.

Birkholtz, L.-M., G. Blatch, T. Coetzer, H. Hoppe, E. Human, E. Morris, Z. Ngcete, L. Oldfield, R. Roth, A. Shonhai, L. Stephens & A. Louw, (2008a) Heterologous expression of plasmodial proteins for structural studies and functional annotation. *Malaria J.l* **7**: 197.

Birkholtz, L., A. C. van Brummelen, K. Clark, J. Niemand, E. Marechal, M. Llinas & A. I. Louw, (2008b) Exploring functional genomics for drug target and therapeutics discovery in Plasmodia. *Acta Trop.* **105**: 113-123.

Birkholtz, L. M., O. Bastien, G. Wells, D. Grando, F. Joubert, V. Kasam, M. Zimmermann, P. Ortet, N. Jacq, N. Saidani, S. Roy, M. Hofmann-Apitius, V. Breton, A. I. Louw & E. Marechal, (2006) Integration and mining of malaria molecular, functional and pharmacological data: how far are we from a chemogenomic knowledge space? *Malaria J.* **5**.

Birkholtz, L. M., C. Wrenger, F. Joubert, G. A. Wells, R. D. Walter & A. I. Louw, (2004) Parasite-specific inserts in the bifunctional S-adenosylmethionine decarboxylase/ornithine decarboxylase of *Plasmodium falciparum* modulate catalytic activities and domain interactions. *Biochem. J.* **377**: 439-448.

Bistulfi, G., P. Diegelman, B. A. Foster, D. L. Kramer, C. W. Porter & D. J. Smiraglia, (2009) Polyamine biosynthesis impacts cellular folate requirements necessary to maintain S-adenosylmethionine and nucleotide pools. *FASEB J.* **23**: 2888-2897.

Bitonti, A. J., T. L. Byers, T. L. Bush, P. J. Casara, C. J. Bacchi, A. B. Clarkson, P. P. McCann & A. Sjoerdsma, (1990) Cure of *Trypanosoma brucei brucei* and *Trypanosoma brucei rhodesiense* infections in mice with an irreversible inhibitor of S-adenosylmethionine decarboxylase. *Antimicrob. Agents Chemother.* **34**: 1485-1490.

Blavid, R., P. Kusch, J. Hauber, U. Eschweiler, S. R. Sarite, S. Specht, S. Deininger, A. Hoerauf & A. Kaiser, (2010) Down-regulation of hypusine biosynthesis in plasmodium by inhibition of S-adenosyl-methionine-decarboxylase. *Amino Acids* **38**: 461-469.

Boitz, J. M., P. A. Yates, C. Kline, U. Gaur, M. E. Wilson, B. Ullman & S. C. Roberts, (2009) *Leishmania donovani* Ornithine Decarboxylase Is Indispensable for Parasite Survival in the Mammalian Host. *Infect. Immun.* **77**: 756-763.

Bojang, K., P. Milligan, M. Pinder, T. Doherty, A. Leach, O. Ofori-Anyinam, M. Lievens, K. Kester, K. Schaecher, W. R. Ballou & J. Cohen, (2009) Five-year safety and immunogenicity of GlaxoSmithKline's candidate malaria vaccine RTS,S/AS02 following administration to semi-immune adult men living in a malaria-endemic region of The Gambia. *Human Vaccines* **5**: 242-247.

Bonapace, C. R., J. A. Bosso, L. V. Friedrich & R. L. White, (2002) Comparison of methods of interpretation of checkerboard synergy testing. *Diagn. Microbiol. Infect. Dis.* **44**: 363-366.

Boshoff, H. I. M., T. G. Myers, B. R. Copp, M. R. McNeil, M. A. Wilson & C. E. Barry, (2004) The transcriptional responses of *Mycobacterium tuberculosis* to inhibitors of metabolism - Novel insights into drug mechanisms of action. *J. Biol. Chem.* **279**: 40174-40184.

Bozdech, Z., M. Llinas, B. L. Pulliam, E. D. Wong, J. C. Zhu & J. L. DeRisi, (2003) The transcriptome of the intraerythrocytic developmental cycle of *Plasmodium falciparum*. *PLoS Biol.* **1**: 85-100.

Bradford, M. M., (1976) Rapid and sensitive method for quantitation of microgram quantities of protein utilizing principle of protein-dye binding. *Anal. Biochem.* **72**: 248-254.

Braks, J. A. M., G. R. Mair, B. Franke-Fayard, C. J. Janse & A. P. Waters, (2008) A conserved U-rich RNA region implicated in regulation of translation in *Plasmodium* female gametocytes. *Nucleic Acids Res.* **36**: 1176-1186.

Brazas, M. D. & R. E. W. Hancock, (2005) Using microarray gene signatures to elucidate mechanisms of antibiotic action and resistance. *DDT* **10**: 1245-1252.

Brazma, A., P. Hingamp, J. Quackenbush, G. Sherlock, P. Spellman, C. Stoeckert, J. Aach, W. Ansorge, C. A. Ball, H. C. Causton, T. Gaasterland, P. Glenisson, F. C. P. Holstege, I. F. Kim, V. Markowitz, J. C. Matese, H. Parkinson, A. Robinson, U. Sarkans, S. Schulze-Kremer, J. Stewart, R. Taylor, J. Vilo & M. Vingron, (2001) Minimum information about a microarray experiment (MIAME) - toward standards for microarray data. *Nat. Genet.* **29**: 365-371.

Brobey, R. K. B. & L. Soong, (2007) Establishing a liquid-phase IEF in combination with 2-DE for the analysis of *Leishmania* proteins. *Proteomics* **7**: 116-120.

Bronner, U., P. C. S. Divis, A. Farnert & B. Singh, (2009) Swedish traveller with *Plasmodium knowlesi* malaria after visiting Malaysian Borneo. *Malaria J.* **8**.

Brown, H., G. Turner, S. Rogerson, M. Tembo, J. Mwenechanya, M. Molyneux & T. Taylor, (1999) Cytokine expression in the brain in human cerebral malaria. *J. Infect. Dis.* **180**: 1742-1746.

Buhlmann, C., O. Mueller, A. Schroeder & T. Ragg, (2004) RNA integrity number (RIN) - Towards standardization of RNA quality assessment for better reproducibility and reliability of gene expression experiments. *Tissue Antigens* **64**: 428-428.

Byers, T. L., J. R. Lakanen, J. K. Coward & A. E. Pegg, (1994) The role of hypusine depletion in cytostasis induced by S-adenosyl-L-methionine decarboxylase inhibition - new evidence provided by 1-methylspermidine and 1,12-dimethyspermine. *Biochem. J.* **303**: 363-368.

Caiafa, P. & M. Zampieri, (2005) DNA methylation and chromatin structure: The puzzling CpG islands. *J. Cell. Biochem.* **94**: 257-265.

Canas, B., D. Lopez-Ferrer, A. Ramos-Fernandez, E. Camofeita & E. Calvo, (2006) Mass spectrometry technologies for proteomics. *Brief. Funct Genom Proteom* **4**: 295-320.

Carrillo, C., N. S. Gonzalez & I. D. Algranati, (2007) *Trypanosoma cruzi* as a model system to study the expression of exogenous genes coding for polyamine biosynthetic enzymes. Induction of DFMO resistance in transgenic parasites. *Biochim. Biophys. Acta-General Subjects* **1770**: 1605-1611.

Carter, R. & K. N. Mendis, (2002) Evolutionary and Historical Aspects of the Burden of Malaria. *Clin. Microbiol. Rev.* **15**: 564-594.

Chaal, B. K., A. P. Gupta, B. D. Wastuwidyaningtyas, Y.-H. Luah & Z. Bozdech, (2010) Histone deacetylases play a major role in the transcriptional regulation of the *Plasmodium falciparum* life cycle. *PLoS Pathog* **6**: e1000737.

Chan, K. C. A., P. B. S. Lai, T. S. K. Mok, H. L. Y. Chan, C. M. Ding, S. W. Yeung & Y. M. D. Lo, (2008) Quantitative analysis of circulating methylated DNA as a biomarker for hepatocellular carcinoma. *Clin. Chem.* **54**: 1528-1536.

Chanda, S. K. & J. S. Caldwell, (2003) Fulfilling the promise: drug discovery in the post-genomic era. *Drug Discov. Today* **8**: 168-174.

Chattopadhyay, M. K., C. W. Tabor & H. Tabor, (2003) Spermidine but not spermine is essential for hypusine biosynthesis and growth in *Saccharomyces cerevisiae*: Spermine is converted

to spermidine in vivo by the FMS1-amine oxidase. *Proc. Natl. Acad. Sci. U. S. A.* **100**: 13869-13874.

Chattopadhyay, M. K., C. W. Tabor & H. Tabor, (2006) Polyamine deficiency leads to accumulation of reactive oxygen species in a spe2 Delta mutant of *Saccharomyces cerevisiae*. *Yeast* **23**: 751-761.

Chen, G., T. G. Gharib, D. G. Thomas, C. C. Huang, D. E. Misek, R. D. Kuick, T. J. Giordano, M. D. Iannettoni, M. B. Orringer, S. M. Hanash & D. G. Beer, (2003) Proteomic analysis of eIF-5A in lung adenocarcinomas. *Proteomics* **3**: 496-504.

Chen, G. A., T. G. Gharib, C. C. Huang, J. M. G. Taylor, D. E. Misek, S. L. R. Kardia, T. J. Giordano, M. D. Iannettoni, M. B. Orringer, S. M. Hanash & D. G. Beer, (2002) Discordant protein and mRNA expression in lung adenocarcinomas. *Mol. Cell. Proteomics* **1**: 304-313.

Chen, Y. C., P. H. Lu, S. L. Pan, C. M. Teng, S. C. Kuo, T. P. Lin, Y. F. Ho, Y. C. Huang & J. H. Guh, (2007) Quinolone analogue inhibits tubulin polymerization and induces apoptosis via Cdk1-involved signaling pathways. *Biochem. Pharmacol.* **74**: 10-19.

Chiogna, M., M. S. Massa, D. Risso & C. Romualdi, (2009) A comparison on effects of normalisations in the detection of differentially expressed genes. *BMC Bioinformatics* **10**.

Chiu, S. M. & N. L. Oleinick, (1997) Radioprotection against the formation of DNA double-strand breaks in cellular DNA but not native cellular chromatin by the polyamine spermine. *Radiat. Res.* **148**: 188-192.

Chiu, S. M. & N. L. Oleinick, (1998) Radioprotection of cellular chromatin by the polyamines spermine and putrescine: Preferential action against formation of DNA-Protein crosslinks. *Radiat. Res.* **149**: 543-549.

Choi, S. W., M. K. Keyes & P. Horrocks, (2006) LC/ESI-MS demonstrates the absence of 5-methyl-2 '-deoxycytosine in *Plasmodium falciparum* genomic DNA. *Mol. Biochem. Parasitol.* **150**: 350-352.

Chung, D. W. D., N. Ponts, S. Cervantes & K. G. Le Roch, (2009) Post-translational modifications in *Plasmodium*: More than you think! *Mol. Biochem. Parasitol.* **168**: 123-134.

Churchill, G. A., (2002) Fundamentals of experimental design for cDNA microarrays. *Nat. Genet.* **32**: 490-495.

Clark, I. A. & W. B. Cowden, (2003) The pathophysiology of *falciparum* malaria. *Pharmacol. Ther.* **99**: 221-260.

Clark, K., M. Dhoogra, A. I. Louw & L. M. Birkholtz, (2008) Transcriptional responses of *Plasmodium falciparum* to alpha-difluoromethylornithine-induced polyamine depletion. *Biol. Chem.* **389**: 111-125.

Clark, K., J. Niemand, S. Reeksting, S. Smit, A. C. van Brummelen, M. Williams, A. I. Louw & L. Birkholtz, (2010) Functional consequences of perturbing polyamine metabolism in the malaria parasite, *Plasmodium falciparum*. *Amino Acids* **38**: 633-644.

Clayton, C. E., (2002) Life without transcriptional control? From fly to man and back again (vol 21, pg 1881, 2002). *EMBO J.* **21**: 3917-3917.

Clyne, T., L. N. Kinch & M. A. Phillips, (2002) Putrescine activation of *Trypanosoma cruzi* S-adenosylmethionine decarboxylase. *Biochemistry* **41**: 13207-13216.

Coombs, G. H., D. E. Goldberg, M. Klemba, C. Berry, J. Kay & J. C. Mottram, (2001) Aspartic proteases of *Plasmodium falciparum* and other parasitic protozoa as drug targets. *Trends Parasitol.* **17**: 532-537.

Cooper, H. L., M. H. Park & J. E. Folk, (1982) Post-translational formation of hypusine in a single major protein occurs generally in growing cells and is associated with activation of lymphocyte growth. *Cell* **29**: 791-797.

Copois, V., F. Bibeau, C. Bascoul-Mollevi, N. Salvetat, P. Chalbos, C. Bareil, L. Candeil, C. Fraslon, E. Conseiller, V. Granci, P. Maziere, A. Kramar, M. Ychou, B. Pau, P. Martineau, F. Molina & M. Del Rio, (2007) Impact of RNA degradation on gene expression profiles: Assessment of different methods to reliably determine RNA quality. *J. Biotechnol.* **127**: 549-559.

Cortes, A., (2008) Switching *Plasmodium falciparum* genes on and off for erythrocyte invasion. *Trends Parasitol.* **24**: 517-524.

Coulson, R. M. R., N. Hall & C. A. Ouzounis, (2004) Comparative genomics of transcriptional control in the human malaria parasite *Plasmodium falciparum*. *Genome Res.* **14**: 1548-1554.

Cowman, A. F. & B. S. Crabb, (2002) The *Plasmodium falciparum* genome - a blueprint for erythrocyte invasion. *Science* **298**: 126-128.

Cowman, A. F. & B. S. Crabb, (2003) Functional genomics: identifying drug targets for parasitic diseases. *Trends Parasitol.* **19**: 538-543.

Cui, L., J. Miao, T. Furuya, Q. Fan, X. Y. Li, P. K. Rathod, X. Z. Su & L. W. Cui, (2008) Histone acetyltransferase inhibitor anacardic acid causes changes in global gene expression during in vitro *Plasmodium falciparum* development. *Eukaryot. Cell* **7**: 1200-1210.

Dahl, E. L., J. L. Shock, B. R. Shenai, J. Gut, J. L. DeRisi & P. J. Rosenthal, (2006) Tetracyclines specifically target the picoplast of the malaria parasite *Plasmodium falciparum*. *Antimicrob. Agents Chemother.* **50**: 3124-3131.

Daily, J. P., K. G. Le Roch, O. Sarr, X. M. Fang, Y. Y. Zhou, O. Ndir, S. Mboup, A. Sultan, E. A. Winzeler & D. F. Wirth, (2004) In vivo transcriptional profiling of *Plasmodium falciparum*. *Malaria J.* **3**.

Das Gupta, R., T. Krause-Ihle, B. Bergmann, I. B. Muller, A. R. Khomutov, S. Muller, R. D. Walter & K. Luersen, (2005) 3-aminooxy-1-aminopropane and derivatives have an antiproliferative effect on cultured *Plasmodium falciparum* by decreasing intracellular polyamine concentrations. *Antimicrob. Agents Chemother.* **49**: 2857-2864.

Date, S. V. & C. J. Stoeckert, (2006) Computational modeling of the *Plasmodium falciparum* interactome reveals protein function on a genome-wide scale. *Genome Res.* **16**: 542-549.

Davidson, E. A. & D. C. Gowda, (2001) Glycobiology of *Plasmodium falciparum*. *Biochimie* **83**: 601-604.

Davidson, E. A., D. C. Gowda, S. T. Yang, D. Nikodem & R. Naik, (1999) Glycobiology of the malaria parasite. *Glycobiology* **9**: 52.

De Jesus, J. B., P. Cuervo, M. Junqueira, C. Britto, F. C. Silva-Filho, L. Saboia-Vahia, L. J. Gonzalez & G. B. Domont, (2007) Application of two-dimensional electrophoresis and matrix-assisted laser desorption/ionization time-of-flight mass spectrometry for proteomic analysis of the sexually transmitted parasite *Trichomonas vaginalis*. *J. Mass Spectrom.* **42**: 1463-1473.

de Ridder, S., F. van der Kooy & R. Verpoorte, (2008) Artemisia annua as a self-reliant treatment for malaria in developing countries. *J. Ethnopharmacol.* **120**: 302-314.

Delibato, E., A. Gattuso, A. Minucci, B. Auricchio, D. De Medici, L. Toti, M. Castagnola, E. Capoluongo & M. V. Gianfranceschi, (2009) PCR experion automated electrophoresis system to detect *Listeria monocytogenes* in foods. *J. Sep. Sci.* **32**: 3817-3821.

Delport, R., J. B. Ubbink, H. Bosman, S. Bissbort & W. J. H. Vermaak, (1990) Altered vitamin-B6 homeostasis during aminophylline infusion in the Beagle dog. *Int. J. Vitam. Nutr. Res.* **60**: 35-40.

Deponte, M. & K. Becker, (2005) Glutathione S-transferase from malarial parasites: Structural and functional aspects. *Gluthione Transferases and Gamma-Glutamyl Transpeptidases* **401**: 241-253.

Djimde, A., O. K. Doumbo, J. F. Cortese, K. Kayentao, S. Doumbo, Y. Diourte, A. Dicko, X. Z. Su, T. Nomura, D. A. Fidock, T. E. Wellems, C. V. Plowe & D. Coulibaly, (2001) A molecular marker for chloroquine-resistant *falciparum* malaria. *New Engl. J. Med.* **344**: 257-263.

Doerig, C., O. Billker, T. Haystead, P. Sharma, A. B. Tobin & N. C. Waters, (2008) Protein kinases of malaria parasites: an update. *Trends Parasitol.* **24**: 570-577.

Doerig, C. & L. Meijer, (2007) Antimalarial drug discovery: targeting protein kinases. *Expert Opin. Ther. Targets* **11**: 279-290.

Dombkowski, A. A., B. J. Thibodeau, S. L. Starcevic & R. F. Novak, (2004) Gene-specific dye bias in microarray reference designs. *FEBS Lett.* **560**: 120-124.

Dondorp, A. M., F. Nosten, P. Yi, D. Das, A. P. Phyo, J. Tarning, K. M. Lwin, F. Ariey, W. Hanpithakpong, S. J. Lee, P. Ringwald, K. Silamut, M. Imwong, K. Chotivanich, P. Lim, T. Herdman, S. S. An, S. Yeung, P. Singhasivanon, N. P. J. Day, N. Lindegardh, D. Socheat & N. J. White, (2009) Artemisinin Resistance in *Plasmodium falciparum* Malaria. *New Engl. J. Med.* **361**: 455-467.

Dunlevy, L. P. E., K. A. Burren, L. S. Chitty, A. J. Copp & N. D. E. Greene, (2006) Excess methionine suppresses the methylation cycle and inhibits neural tube closure in mouse embryos. *FEBS Lett.* **580**: 2803-2807.

Duraisingh M., M.T. Fredig, C.J. Stoeckert, S.K. Volkman & V.P. McGovern, (2006) *Plasmodium* research in the postgenomic era. *TRENDS Parasitol.* **22**: 1-4.

Eckstein-Ludwig, U., R. J. Webb, I. D. A. van Goethem, J. M. East, A. G. Lee, M. Kimura, P. M. O'Neill, P. G. Bray, S. A. Ward & S. Krishna, (2003) Artemisinins target the SERCA of *Plasmodium falciparum*. *Nature* **424**: 957-961.

Engwerda, C. R., T. L. Mynott, S. Sawhney, J. B. De Souza, Q. D. Bickle & P. M. Kaye, (2002) Locally up-regulated lymphotoxin alpha, not systemic tumor necrosis factor alpha, is the principle mediator of murine cerebral malaria. *J. Exp. Med.* **195**: 1371-1377.

Fairfield, A. J. S., S. R. Meshnick & J. W. Eaton, (1983 (a)) Malarial parasites acquire host superoxide-dismutase. *Fed. Proc.* **42**: 2063-2063.

Fairfield, A. S. & S. R. Meshnick, (1984) Host superoxide dismutase incorporation by intraerythrocytic plasmodia. *Prog. Clin. Biol. Res.* **155**: 13-23.

Fairfield, A. S., S. R. Meshnick & J. W. Eaton, (1983 (b)) Malaria parasites adopt host-cell superoxide-dismutase. *Science* **221**: 764-766.

Falade, C. & C. Manyando, (2009) Safety profile of Coartem (R): the evidence base. *Malaria J.* **8**.

Fatumo, S., K. Plaimas, J. P. Mallm, G. Schramm, E. Adebiyi, M. Oswald, R. Eils & R. Konig, (2009) Estimating novel potential drug targets of *Plasmodium falciparum* by analysing the metabolic network of knock-out strains in silico. *Infect., Genet. Evol.* **9**: 351-358.

Fey, S. J. & P. M. Larsen, (2001) 2D or not 2D. *Curr. Opin. Chem. Biol.* **5**: 26-33.

Fisher, O., R. Siman-Tov & S. Ankri, (2004) Characterization of cytosine methylated regions and 5-cytosine DNA methyltransferase (Ehmeth) in the protozoan parasite Entamoeba histolytica. *Nucleic Acids Res.* **32**: 287-297.

Fisher, R. A., (1935) The logic of inductive inference. *J. Royal Statistical Society: Series A* **98**: 39-54.

Fivelman, Q. L., I. S. Adagu & D. C. Warhurst, (2004) Modified fixed-ratio isobologram method for studying in vitro interactions between atovaquone and proguanil or dihydroartemisinin against drug-resistant strains of *Plasmodium falciparum*. *Antimicrob. Agents Chemother.* **48**: 4097-4102.

Flohe, L., H. J. Hecht & P. Steinert, (1999) Glutathione and trypanothione in parasitic hydroperoxide metabolism. *Free Radical Biol. Med.* **27**: 966-984.

Florens, L., M. P. Washburn, J. D. Raine, R. M. Anthony, M. Grainger, J. D. Haynes, J. K. Moch, N. Muster, J. B. Sacci, D. L. Tabb, A. A. Witney, D. Wolters, Y. M. Wu, M. J. Gardner, A. A. Holder, R. E. Sinden, J. R. Yates & D. J. Carucci, (2002) A proteomic view of the *Plasmodium falciparum* life cycle. *Nature* **419**: 520-526.

Foth, B. J., S. A. Ralph, C. J. Tonkin, N. S. Struck, M. Fraunholz, D. S. Roos, A. F. Cowman & G. I. McFadden, (2003) Dissecting apicoplast targeting in the malaria parasite *Plasmodium falciparum*. *Science* **299**: 705-708.

Foth, B. J., N. Zhang, S. Mok, P. R. Preiser & Z. Bozdech, (2008) Quantitative protein expression profiling reveals extensive post-transcriptional regulation and post-translational modifications in schizont-stage malaria parasites. *Genome Biol.* **9**: R177.

Foucher, A. L., A. McIntosh, G. Douce, J. Wastling, A. Tait & C. M. R. Turner, (2006) A proteomic analysis of arsenical drug resistance in *Trypanosoma brucei*. *Proteomics* **6**: 2726-2732.

Freiberg, C. & H. Brotz-Oesterhelt, (2005) Functional genomics in antibacterial drug discovery. *Drug Discov. Today* **10**: 927-935.

Freiberg, C., H. Brotz-Oesterhelt & H. Labischinski, (2004) The impact of transcriptome and proteome analyses on antibiotic drug discovery. *Curr. Opin. Microbiol.* **7**: 451-459.

Fried, M., G. J. Domingo, C. D. Gowda, T. K. Mutabingwa & P. E. Duffy, (2006) *Plasmodium falciparum*: Chondroitin sulfate A is the major receptor for adhesion of parasitized erythrocytes in the placenta. *Exp. Parasitol.* **113**: 36-42.

Fritz-Wolf, K., A. Becker, S. Rahlfs, P. Harwaldt, R. H. Schirmer, W. Kabsch & K. Becker, (2003) X-ray structure of glutathione S-transferase from the malarial parasite *Plasmodium falciparum*. *Proc. Natl. Acad. Sci. U. S. A.* **100**: 13821-13826.

Fu, L. M., (2006) Exploring drug action on *Mycobacterium tuberculosis* using affymetrix oligonucleotide genechips. *Tuberculosis* **86**: 134-143.

Fu, L. M. & T. M. Shinnick, (2007) Understanding the action of INH on a highly INH-resistant *Mycobacterium tuberculosis* strain using GeneChips. *Tuberculosis* **87**: 63-70.

Gallup J.L. & J.D. Sachs, (2001) The economic burden of malaria. *Am J Trop Med Hyg.* **64**: 85-96.

Ganesan, K., N. Ponmee, L. Jiang, J. W. Fowble, J. White, S. Kamchonwongpaisan, Y. Yuthavong, P. Wilairat & P. K. Rathod, (2008) A Genetically Hard-Wired Metabolic Transcriptome in *Plasmodium falciparum* Fails to Mount Protective Responses to Lethal Antifolates. *PLoS Path.* **4**.

Garcia-Martinez, J., A. Aranda & J. E. Perez-Ortin, (2004) Genomic run-on evaluates transcription rates for all yeast genes and identifies gene regulatory mechanisms. *Mol. Cell* **15**: 303-313.

Garcia, C. R. S., M. F. de Azevedo, G. Wunderlich, A. Budu, J. A. Young & L. Bannister, (2008) *Plasmodium* in the postgenomic era: New insights into the molecular cell biology of malaria parasites. *Int. Rev. Cell Mol. Biol.* **266**: 85-+.

Gardiner D.L., McCarthy J.S. & Trenholme K.R., (2005) Malaria in the post-genomics era: light at the end of the tunnel or just another train? *Postgraduate Medical Journal* **81**: 505-509.

Gardner, M. J., N. Hall, E. Fung, O. White, M. Berriman, R. W. Hyman, J. M. Carlton, A. Pain, K. E. Nelson, S. Bowman, I. T. Paulsen, K. James, J. A. Eisen, K. Rutherford, S. L. Salzberg, A. Craig, S. Kyes, M. S. Chan, V. Nene, S. J. Shallom, B. Suh, J. Peterson, S. Angiuoli, M. Pertea, J. Allen, J. Selengut, D. Haft, M. W. Mather, A. B. Vaidya, D. M. A. Martin, A. H. Fairlamb, M. J. Fraunholz, D. S. Roos, S. A. Ralph, G. I. McFadden, L. M. Cummings, G. M. Subramanian, C. Mungall, J. C. Venter, D. J. Carucci, S. L. Hoffman, C. Newbold, R. W. Davis, C. M. Fraser & B. Barrell, (2002) Genome sequence of the human malaria parasite *Plasmodium falciparum*. *Nature* **419**: 498-511.

Gast, M. C. W., J. M. G. Bonfrer, E. J. van Dulken, L. de Kock, E. J. T. Rutgers, J. H. M. Schellens & J. H. Beijnen, (2006) SELDI-TOF MS serum protein, profiles in breast cancer: Assessment of robustness and validity. *Cancer Biomark.* **2**: 235-248.

Geall A.J., Baugh J.A., Loyevsky M., Gordeuk V.R., Al-Abed Y. & Bucala R., (2004) Targeting malaria with polyamines. *Bioconjugate Chemistry* **15**: 1161-1165.

Gelhaus, C., J. Fritsch, E. Krause & M. Leippe, (2005) Fractionation and identification of proteins by 2DE and MS: towards a proteomic analysis of *Plasmodium falciparum*. *Proteomics* **5**.

Gharahdaghi, F., C. R. Weinberg, D. A. Meagher, B. S. Imai & S. M. Mische, (1999) Mass spectrometric identification of proteins from silver-stained polyacrylamide gel: A method for the removal of silver ions to enhance sensitivity. *Electrophoresis* **20**: 601-605.

Gibson, F., L. Anderson, G. Babnigg, M. Baker, M. Berth, P. A. Binz, A. Borthwick, P. Cash, B. W. Day, D. B. Friedman, D. Garland, H. B. Gutstein, C. Hoogland, N. A. Jones, A. Khan, J. Klose, A. I. Lamond, P. F. Lemkin, K. S. Lilley, J. Minden, N. J. Morris, N. W. Paton, M. R. Pisano, J. E. Prime, T. Rabilloud, D. A. Stead, C. F. Taylor, H. Voshol, A. Wipat & A. R. Jones, (2008) Guidelines for reporting the use of gel electrophoresis in proteomics. *Nat. Biotechnol.* **26**: 863-864.

Gitan, R. S., H. D. Shi, C. M. Chen, P. S. Yan & T. H. M. Huang, (2002) Methylation-specific oligonucleotide microarray: A new potential for high-throughput methylation analysis. *Genome Res.* **12**: 158-164.

Goldberg, B., D. Rattendi, D. Lloyd, N. Yarlett & C. J. Bacchi, (1999) Kinetics of S-adenosylmethionine cellular transport and protein methylation in *Trypanosoma brucei brucei* and *Trypanosoma brucei rhodesiense*. *Arch. Biochem. Biophys.* **364**: 13-18.

Goldberg, B., D. Rattendi, D. Lloyd, N. Yarlett & C. J. Bacchi, (2000) Kinetics of methionine transport and metabolism by *Trypanosoma brucei brucei* and *Trypanosoma brucei rhodesiense*. *Arch. Biochem. Biophys.* **377**: 49-57.

Goldberg, B., D. Rattendi, N. Yarlett, D. Lloyd & C. J. Bacchi, (1997a) Effects of carboxylmethylation and polyamine synthesis inhibitors on methylation of *Trypanosoma brucei* cellular proteins and lipids. *J. Eukaryot. Microbiol.* **44**: 352-358.

Goldberg, B., N. Yarlett, D. Rattendi, D. Lloyd & C. J. Bacchi, (1997b) Rapid methylation of cell proteins and lipids in *Trypanosoma brucei*. *J. Eukaryot. Microbiol.* **44**: 345-351.

Goldberg B., D. Rattendi, D. Lloyd, N. Yarlett & C.J. Bacchi, (1999) Kinetics of S-adenosylmethionine cellular transport and protein methylation in *Trypanosoma brucei brucei* and *Trypanosoma brucei rhodesiense*. *Archiv Biochem Biophys* **364**: 13-18.

Goldberg B., D. Rattendi, N. Yarlett, D. Lloyd & C.J Bacchi, (1997) Effects of carboxylmethylation and polyamine synthesis inhibitors on methylation of Trypanosoma brucei cellular proteins and lipids. *J Eukar Microbiol* **44**: 352-358.

Gowda, D. C. & E. A. Davidson, (1999) Protein glycosylation in the malaria parasite. *Parasitol. Today* **15**: 147-152.

Grau, G. E., T. E. Taylor, M. E. Molyneux, J. J. Wirima, P. Vassalli, M. Hommel & P. H. Lambert, (1989) Tumor necrosis factor and disease severity in children with *falciparum*-malaria. *New Engl. J. Med.* **320**: 1586-1591.

Graves, P. & H. Gelband, (2006) Vaccines for preventing malaria (blood-stage). *Cochrane Database Syst Rev*: CD006199.

Greenwood, B., (2002) The molecular epidemiology of malaria. *Trop. Med. Int. Health* **7**: 1012-1021.

Greenwood, B. & T. Mutabingwa, (2002) Malaria in 2002. *Nature* **415**: 670-672.

Greenwood, B. M., K. Bojong, C. J. M. Whitty & G. A. Targett, (2005) Malaria. *Lancet* **365**: 1487-1498.

Gregson A. & C.V. Plowe, (2005) Mechanisms of resistance of malaria parasites to antifolates. *Pharmacol Rev* **57**: 117-145.

Griffin, T. J., S. P. Gygi, T. Ideker, B. Rist, J. Eng, L. Hood & R. Aebersold, (2002) Complementary profiling of gene expression at the transcriptome and proteome levels in *Saccharomyces cerevisiae*. *Mol. Cell. Proteomics* **1**: 323-333.

Grolleau, A., J. Bowman, B. Pradet-Balade, E. Puravs, S. Hanash, J. A. Garcia-Sanz & L. Beretta, (2002) Global and specific translational control by rapamycin in T cells uncovered by microarrays and proteomics. *J. Biol. Chem.* **277**: 22175-22184.

Guillemin, J., (2002) Choosing scientific patrimony: Sir Ronald Ross, Alphonse Laveran, and the mosquito-vector hypothesis. *J. Hist. Med. Allied Sci.* **57**: 385-409.

Gunasekera, A. M., A. Myrick, K. Le Roch, E. Winzeler & D. F. Wirth, (2007) *Plasmodium falciparum*: Genome wide perturbations in transcript profiles among mixed stage cultures after chloroquine treatment. *Exp. Parasitol.* **117**: 87-92.

Gunasekera, A. M., S. Patankar, J. Schug, G. Eisen & D. F. Wirth, (2003) Drug-induced alterations in gene expression of the asexual blood forms of *Plasmodium falciparum*. *Mol. Microbiol.* **50**: 1229-1239.

Gygi, S. P., Y. Rochon, B. R. Franza & R. Aebersold, (1999) Correlation between protein and mRNA abundance in yeast. *Mol. Cell. Biol.* **19**: 1720-1730.

Ha, H. C., N. S. Sirisoma, P. Kuppusamy, J. L. Zweier, P. M. Woster & R. A. Casero, (1998) The natural polyamine spermine functions directly as a free radical scavenger. *Proc. Natl. Acad. Sci. U. S. A.* **95**: 11140-11145.

Hagan, P. & V. Chauhan, (1997) Ronald Ross and the problem of malaria. *Parasitol. Today* **13**: 290-295.

Haider, N., M. L. Eschbach, S. D. Dias, T. W. Gilberger, R. D. Walter & K. Luersen, (2005) The spermidine synthase of the malaria parasite *Plasmodium falciparum*: Molecular and biochemical characterisation of the polyamine synthesis enzyme. *Mol. Biochem. Parasitol.* **142**: 224-236.

Hall, N., M. Karras, J. D. Raine, J. M. Carlton, T. W. A. Kooij, M. Berriman, L. Florens, C. S. Janssen, A. Pain, G. K. Christophides, K. James, K. Rutherford, B. Harris, D. Harris, C. Churcher, M. A. Quail, D. Ormond, J. Doggett, H. E. Trueman, J. Mendoza, S. L. Bidwell, M. A. Rajandream, D. J. Carucci, J. R. Yates, F. C. Kafatos, C. J. Janse, B. Barrell, C. M. R. Turner, A. P. Waters & R. E. Sinden, (2005) A comprehensive survey of the *Plasmodium* life cycle by genomic, transcriptomic, and proteomic analyses. *Science* **307**: 82-86.

Harris, L. R., M. A. Churchward, R. H. Butt & J. R. Coorssen, (2007) Assessing detection methods for gel-based proteomic analyses. *J Proteome Res*: 1418-1425.

Hattman, S., (2005) DNA-[adenine] methylation in lower eukaryotes. *Biochemistry (Mosc)* **70**: 550-558.

Hay, S. I., C. A. Guerra, P. W. Gething, A. P. Patil, A. J. Tatem, A. M. Noor, C. W. Kabaria, B. H. Manh, I. R. F. Elyazar, S. Brooker, D. L. Smith, R. A. Moyeed & R. W. Snow, (2009) A World Malaria Map: *Plasmodium falciparum* Endemicity in 2007. *Plos Medicine* **6**.

He, X., A. M. E. Reeve, U. R. Desai, G. E. Kellogg & K. A. Reynolds, (2004) 1,2-dithiole-3-ones as potent inhibitors of the bacterial 3-ketoacyl acyl carrier protein synthase III (FabH). *Antimicrob. Agents Chemother.* **48**: 3093-3102.

He, Z. X., L. L. Chen, J. L. You, L. Qin & X. P. Chen, (2009) Antiretroviral protease inhibitors potentiate chloroquine antimalarial activity in malaria parasites by regulating intracellular glutathione metabolism. *Exp. Parasitol.* **123**: 122-127.

Heby, O., L. Persson & M. Rentala, (2007) Targeting the polyamine biosynthetic enzymes: a promising approach to therapy of African sleeping sickness, Chagas' disease, and leishmaniasis. *Amino Acids* **33**: 359-366.

Hegde, P. S., I. R. White & C. Debouck, (2003) Interplay of transcriptomics and proteomics. *Curr. Opin. Biotechnol.* **14**: 647-651.

Hemingway J., (2004) The influence of genomics on the control of malaria and other vector-borne diseases. *South African J Sci* **100**: 475-479.

Hester, S. D., L. Reid, N. Nowak, W. D. Jones, J. S. Parker, K. Knudtson, W. Ward, J. Tiesman & N. D. Denslow, (2009) Comparison of comparative genomic hybridization technologies across microarray platforms. *J Biomol Tech* **20**: 135-151.

Hiller, N., K. Fritz-Wolf, M. Deponte, W. Wende, H. Zimmermann & K. Becker, (2006) *Plasmodium falciparum* glutathione S-transferase - Structural and mechanistic studies on ligand binding and enzyme inhibition. *Protein Sci.* **15**: 281-289.

Hockley, S. L., K. Mathijs, Y. C. M. Staal, D. Brewer, I. Giddings, J. H. M. van Delft & D. H. Phillips, (2009) Interlaboratory and Interplatform Comparison of Microarray Gene Expression Analysis of HepG2 Cells Exposed to Benzo(a)pyrene. *OMICS* **13**: 115-125.

Holt R.A., S. G., Halpern A, Sutton GG, Charlab R, Nusskern DR, Wincker P, Clark AG, Ribeiro JM, Wides R, Salzberg SL, Loftus B, Yandell M, Majoros WH, Rusch DB, Lai Z, Kraft CL, Abril JF, Anthouard V, Arensburger P, Atkinson PW, Baden H, de Berardinis V, Baldwin D, Benes V, Biedler J, Blass C, Bolanos R, Boscus D, Barnstead M, Cai S, Center A, Chaturverdi K, Christophides GK, Chrystal MA, Clamp M, Cravchik A, Curwen V, Dana A, Delcher A, Dew I, Evans CA, Flanigan M, Grundschober-Freimoser A, Friedli L, Gu Z, Guan P, Guigo R, Hillenmeyer ME, Hladun SL, Hogan JR, Hong YS, Hoover J, Jaillon O, Ke Z, Kodira C, Kokoza E, Koutsos A, Letunic I, Levitsky A, Liang Y, Lin JJ, Lobo NF,

Lopez JR, Malek JA, McIntosh TC, Meister S, Miller J, Mobarry C, Mongin E, Murphy SD, O'Brochta DA, Pfannkoch C, Qi R, Regier MA, Remington K, Shao H, Sharakhova MV, Sitter CD, Shetty J, Smith TJ, Strong R, Sun J, Thomasova D, Ton LQ, Topalis P, Tu Z, Unger MF, Walenz B, Wang A, Wang J, Wang M, Wang X, Woodford KJ, Wortman JR, Wu M, Yao A, Zdobnov EM, Zhang H, Zhao Q, Zhao S, Zhu SC, Zhimulev I, Coluzzi M, della Torre A, Roth CW, Louis C, Kalush F, Mural RJ, Myers EW, Adams MD, Smith HO, Broder S, Gardner MJ, Fraser CM, Birney E, Bork P, Brey PT, Venter JC, Weissenbach J, Kafatos FC, Collins FH, Hoffman SL.,, (2002) The genome sequence of the malaria mosquito Anopheles gambiae. *Science* **298**: 129-149.

Hu, G. A., A. Cabrera, M. Kono, S. Mok, B. K. Chaal, S. Haase, K. Engelberg, S. Cheemadan, T. Spielmann, P. R. Preiser, T. W. Gilberger & Z. Bozdech, (2010) Transcriptional profiling of growth perturbations of the human malaria parasite *Plasmodium falciparum*. *Nat. Biotechnol.* **28**: 91-U126.

Hu, Z. Q., W. H. Zhao, Y. Yoda, N. Asano, Y. Hara & T. Shimamura, (2002) Additive, indifferent and antagonistic effects in combinations of epigallocatechin gallate with 12 non-beta-lactam antibiotics against methicillin-resistant *Staphylococcus aureus*. *J. Antimicrob. Chemother.* **50**: 1051-1054.

Hyde, J. E., (2005) Drug-resistant malaria. *Trends Parasitol.* **21**: 494-498.

Hyde, J. E., (2007) Drug-resistant malaria - an insight. *FEBS J.* **274**: 4688-4698.

Icekson, I., M. Bakhanashvili & A. Apelbaum, (1986) Inhibition by ethylene of polyamine biosynthetic enzymes enhanced lysine decarboxylase activity and cadaverine accumulation in pea seedlings. *Plant Physiol.* **82**: 607–609.

Ignatenko, N. A., H. F. Yerushalmi, R. Pandey, K. L. Kachel, D. E. Stringer, L. J. Marton & E. W. Gerner, (2009) Gene Expression Analysis of HCT116 Colon Tumor-derived Cells Treated with the Polyamine Analog PG-11047. *Cancer Genom. Proteom.* **6**: 161-175.

Imbeaud, S., E. Graudens, V. Boulanger, X. Barlet, P. Zaborski, E. Eveno, O. Mueller, A. Schroeder & C. Auffray, (2005) Towards standardization of RNA quality assessment using user-independent classifiers of microcapillary electrophoresis traces. *Nucleic Acids Res.* **33**.

Iyer, J., A. C. Gruner, L. Renia, G. Snounou & P. R. Preiser, (2007) Invasion of host cells by malaria parasites: a tale of two protein families. *Mol. Microbiol.* **65**: 231-249.

Jambou, R., E. Legrand, M. Niang, N. Khim, P. Lim, B. Volney, M. T. Ekala, C. Bouchier, P. Esterre, T. Fandeur & O. Mercereau-Puijalon, (2005) Resistance of *Plasmodium falciparum* field isolates to in-vitro artemether and point mutations of the SERCA-type PfATPase6. *Lancet* **366**: 1960-1963.

Jana, S. & J. Paliwal, (2007) Novel molecular targets for antimalarial chemotherapy. *Int. J. Antimicrob. Agents* **30**: 4-10.

Jensen, L. J., M. Kuhn, M. Stark, S. Chaffron, C. Creevey, J. Muller, T. Doerks, P. Julien, A. Roth, M. Simonovic, P. Bork & C. von Mering, (2009) STRING 8-a global view on proteins and their functional interactions in 630 organisms. *Nucleic Acids Res.* **37**: D412-D416.

Jensen, O. N., M. Wilm, A. Shevchenko & M. Mann, (1999) *2-D Proteome Analysis Protocols*, p. 601. Humana Press Inc.,, Totowa, NJ.

Jiang, L., P. C. Lee, J. White & P. K. Rathod, (2000) Potent and selective activity of a combination of thymidine and 1843U89, a folate-based thymidylate synthase inhibitor, against Plasmodium falciparum. *Antimicrob. Agents Chemother.* **44**: 1047-1050.

Joet, T., U. Eckstein-Ludwig, C. Morin & S. Krishna, (2003) Validation of the hexose transporter of Plasmodium falciparum as a novel drug target. *Proc. Natl. Acad. Sci. U. S. A.* **100**: 7476-7479.

Johnson, J. R., L. Florens, D. J. Carucci & J. R. Yates, (2004) Proteomics in malaria. *J Proteome Res* **3**: 296-306.

Jones, A., A. Faldas, A. Foucher, E. Hunt, A. Tait, J. M. Wastling & C. M. Turner, (2006) Visualisation and analysis of proteomic data from the procyclic form of *Trypanosoma brucei*. *Proteomics* **6**: 259-267.

Jones, P. A. & P. W. Laird, (1999) Cancer epigenetics comes of age. *Nat. Genet.* **21**: 163-167.

Jung, I. L., T. J. Oh & I. G. Kim, (2003) Abnormal growth of polyamine-deficient *Escherichia coli* mutant is partially caused by oxidative stress-induced damage. *Arch. Biochem. Biophys.* **418**: 125-132.

Kahana, C., (2007) Ubiquitin dependent and independent protein degradation in the regulation of cellular polyamines. *Amino Acids* **33**: 225-230.

Kaiser, A., A. Gottwald, W. Maier & H. M. Seitz, (2003a) Targeting enzymes involved in spermidine metabolism of parasitic protozoa - a possible new strategy for anti-parasitic treatment. *Parasitol. Res.* **91**: 508-516.

Kaiser, A., I. Hammels, A. Gottwald, M. Nassar, M. S. Zaghloul, B. A. Motaal, J. Hauber & A. Hoerauf, (2007) Modification of eukaryotic initiation factor 5A from *Plasmodium vivax* by a truncated deoxyhypusine synthase from *Plasmodium falciparum*: An enzyme with dual enzymatic properties. *Biorg. Med. Chem.* **15**: 6200-6207.

Kaiser, A. E., A. M. Gottwald, C. S. Wiersch, W. A. Maier & H. M. Seitz, (2003b) Spermidine metabolism in parasitic protozoa - a comparison to the situation in prokaryotes, viruses, plants and fungi. *Folia Parasitol.* **50**: 3-18.

Kang, I. H., J. S. Kim, E. J. Kim & J. K. Lee, (2007) Cadaverine protects *Vibrio vulnificus* from superoxide stress. *J. Microbiol. Biotechnol.* **17**: 176-179.

Kerr, M. K., (2003) Design considerations for efficient and effective microarray studies. *Biometrics* **59**: 822-828.

Kerr, M. K. & G. A. Churchill, (2001) Statistical design and the analysis of gene expression microarray data. *Genet. Res.* **77**: 123-128.

Kester, K. E., J. F. Cummings, O. Ofori-Anyinam, C. F. Ockenhouse, U. Krzych, P. Moris, R. Schwenk, R. A. Nielsen, Z. Debebe, E. Pinelis, L. Juompan, J. Williams, M. Dowler, V. A. Stewart, R. A. Wirtz, M. C. Dubois, M. Lievens, J. Cohen, W. R. Ballou, D. G. Heppner, Rts & S. V. E. Grp, (2009) Randomized, Double-Blind, Phase 2a Trial of Falciparum Malaria Vaccines RTS,S/AS01B and RTS,S/AS02A in Malaria-Naive Adults: Safety, Efficacy, and Immunologic Associates of Protection. *J. Infect. Dis.* **200**: 337-346.

Kicska, G. A., P. C. Tyler, G. B. Evans, R. H. Furneaux, V. L. Schramm & K. Kim, (2002) Purine-less death in *Plasmodium falciparum* induced by immucillin-H, a transition state analogue of purine nucleoside phosphorylase. *J. Biol. Chem.* **277**: 3226-3231.

Kim, J. S., S. H. Choi & J. K. Lee, (2006) Lysine decarboxylase expression by *Vibrio vulnificus* is induced by SoxR in response to superoxide stress. *J. Bacteriol.* **188**: 8586-8592.

Kinoshita, E., E. Kinoshita-Kikutal, M. Matsubara, Y. Aoki, S. Ohie, Y. Mouri & T. Koike, (2009) Two-dimensional phosphate-affinity gel electrophoresis for the analysis of phosphoprotein isotypes. *Electrophoresis* **30**: 550-559.

Kitade, Y., A. Kozaki, T. Gotoh, T. Miwa, M. Nakanishi & C. Yatome, (1999) Synthesis of S-adenosyl-L-homocysteine hydrolase inhibitors and their biological activities. *Nucleic Acids Symp. Ser.*: 25-26.

Koncarevic, S., R. Bogumil & K. Becker, (2007) SELDI-TOF-MS analysis of chloroquine resistant and sensitive *Plasmodium falciparum* strains. *Proteomics* **7**: 711-721.

Koncarevic, S., S. Urig, K. Steiner, S. Rahlfs, C. Herold-Mende, H. Sueltmann & K. Becker, (2009) Differential genomic and proteomic profiling of glioblastoma cells exposed to terpyridineplatinum(II) complexes. *Free Radical Biol. Med.* **46**: 1096-1108.

Kreil, D. P., R. R. Russell & G. Inference, (2005) There is no silver bullet - a guide to low-level data transforms and normalisation methods for microarray data. *Brief. Bioinform.* **6**: 86-97.

Krishna, R. G. & F. Wold, (1993) Posttranslational modifications of proteins. *Adv. Enzymol. Relat. Areas Mol. Biol.* **67**: 265-298.

Krishna, S., C. J. Woodrow, H. M. Staines, R. K. HayneS & O. Mercereau-Puijalon, (2006) Re-evaluation of how artemisinins work in light of emerging evidence of in vitro resistance. *Trends Mol. Med.* **12**: 200-205.

Krungkrai, J., S. R. Krungkrai, N. Suraveratum & P. Prapunwattana, (1997) Mitochondrial ubiquinol-cytochrome C reductase and cytochrome C oxidase: Chemotherapeutic targets in malarial parasites. *Biochem. Mol. Biol. Int.* **42**: 1007-1014.

Kumar, S. & H. S. Banyal, (1997) Purification and characterisation of the hexokinase of *Plasmodium berghei*, a murine malaria parasite. *Acta Vet. Hung.* **45**: 119-126.

Lambros, C. & J. P. Vanderberg, (1979) Synchronization of *Plasmodium falciparum* erythrocytic stages in culture. *J. Parasitol.* **65**: 418-420.

Lanne, B. & O. Panfilov, (2005) Protein staining influences the quality of mass spectra obtained by peptide mass fingerprinting after separation on 2-D gels. A comparison of staining with coomassie brilliant blue and SYPRO Ruby. *J Proteome Res* **4**: 175-179.

Lasonder, E., Y. Ishihama, J. S. Andersen, A. M. W. Vermunt, A. Pain, R. W. Sauerwein, W. M. C. Eling, N. Hall, A. P. Waters, H. G. Stunnenberg & M. Mann, (2002) Analysis of the *Plasmodium falciparum* proteome by high-accuracy mass spectrometry. *Nature* **419**: 537-542.

Lauber, W. M., J. A. Carroll, D. R. Dufield, J. R. Kiesel, M. R. Radabaugh & J. P. Malone, (2001) Mass spectrometry compatibility of two-dimensional gel protein stains. *Electrophoresis* **22**: 906-918.

Law, P. J., C. Claudel-Renard, F. Joubert, A. I. Louw & D. K. Berger, (2008) MADIBA: A web server toolkit for biological interpretation of *Plasmodium* and plant gene clusters. *BMC Genomics* **9**.

Le Bras, J. & R. Durand, (2003) The mechanisms of resistance to antimalarial drugs in *Plasmodium falciparum*. *Fundam. Clin. Pharmacol.* **17**: 147-153.

Le Roch, K. G., J. R. Johnson, L. Florens, Y. Y. Zhou, A. Santrosyan, M. Grainger, S. F. Yan, K. C. Williamson, A. A. Holder, D. J. Carucci, J. R. Yates & E. A. Winzeler, (2004) Global analysis of transcript and protein levels across the *Plasmodium falciparum* life cycle. *Genome Res.* **14**: 2308-2318.

Lell, B., S. Agnandji, I. von Glasenapp, S. Haertle, S. Oyakhiromen, S. Issifou, J. Vekemans, A. Leach, M. Lievens, M.-C. Dubois, M.-A. Demoitie, T. Carter, T. Villafana, W. R. Ballou, J. Cohen & P. G. Kremsner, (2009) A randomized trial assessing the safety and immunogenicity of AS01 and AS02 adjuvanted RTS,S malaria vaccine candidates in children in Gabon. *Plos One* **4**: e7611.

Leonard, S. N., G. W. Kaatz, L. R. Rucker & M. J. Rybak, (2008) Synergy between gemifloxacin and trimethoprim/sulfamethoxazole against community-associated methicillin-resistant *Staphylococcus aureus*. *J. Antimicrob. Chemother.* **62**: 1305-1310.

Lin, J. F., Q. X. Chen, H. Y. Tian, X. Gao, M. L. Yu, G. J. Xu & F. K. Zhao, (2008) Stain efficiency and MALDI-TOF MS compatibility of seven visible staining procedures. *Anal. Bioanal. Chem.* **390**: 1765-1773.

Liu, J., E. S. Istvan, I. Y. Gluzman, J. Gross & D. E. Goldberg, (2006) *Plasmodium falciparum* ensures its amino acid supply with multiple acquisition pathways and redundant proteolytic enzyme systems. *Proc. Natl. Acad. Sci. U. S. A.* **103**: 8840-8845.

Llinas, M., Z. Bozdech, E. D. Wong, A. T. Adai & J. L. DeRisi, (2006) Comparative whole genome transcriptome analysis of three *Plasmodium falciparum* strains. *Nucleic Acids Res.* **34**: 1166-1173.

Lopez, M. F., (2000) Better approaches to finding the needle in a haystack: Optimizing proteome analysis through automation. *Electrophoresis* **21**: 1082-1093.

Lovaas, E. & G. Carlin, (1991) Spermine - an antioxidant and anti-inflammatory agent. *Free Radical Biol. Med.* **11**: 455-461.

Lowry, O. H., N. J. Rosebrough, A. L. Farr & R. J. Randall, (1951) Protein measurement with the Folin Phenol Reagent. *J. Biol. Chem.* **193**: 265-275.

Luersen, K., R. D. Walter & S. Muller, (2000) *Plasmodium falciparum*-infected red blood cells depend on a functional glutathione *de novo* synthesis attributable to an enhanced loss of glutathione. *Biochem. J.* **346**: 545-552.

MacBeath, G., (2002) Protein microarrays and proteomics. *Nat. Genet.* **32**: 526-532.

Mackinnon, M. J., J. G. Li, S. Mok, M. M. Kortok, K. Marsh, P. R. Preiser & Z. Bozdech, (2009) Comparative Transcriptional and Genomic Analysis of *Plasmodium falciparum* Field Isolates. *PLoS Path.* **5**.

Mackintosh, C. L., J. G. Beeson & K. Marsh, (2004) Clinical features and pathogenesis of severe malaria. *Trends Parasitol.* **20**: 597-603.

Mahajan, B., A. Selvapandiyan, N. J. Gerald, V. Majam, H. Zheng, T. Wickramarachchi, J. Tiwari, H. Fujioka, K. Moch, N. Kumar, L. Aravind, H. L. Nakhasi & S. Kumar, (2008) Centrins, Cell Cycle Regulation Proteins in Human Malaria Parasite *Plasmodium falciparum*. *J. Biol. Chem.* **283**: 31871-31883.

Mair, G. R., J. A. M. Braks, L. S. Garver, L. Wiegant, N. Hall, R. W. Dirks, S. M. Khan, G. Dimopoulos, C. J. Janse & A. P. Waters, (2006) Regulation of sexual development of *Plasmodium* by translational repression. *Science* **313**: 667-669.

Makanga, M., P. G. Bray, P. Horrocks & S. A. Ward, (2005) Towards a proteomic definition of CoArtem action in *Plasmodium falciparum* malaria. *Proteomics* **5**: 1-10.

Marverti, G., A. Ligabue, D. Guerrieri, G. Paglietti, S. Piras, M. P. Costi, D. Farina, C. Frassineti, M. G. Monti & M. S. Moruzzi, (2010) Spermidine/spermine N1-acetyltranferase modulation by novel folate cycle inhibitors in cisplatin-sensitive and -resistant human ovarian cancer cell lines. *Gynecol. Oncol.* **117**: 202-210.

Maubert, B., N. Fievet, G. Tami, C. Boudin & P. Deloron, (1998) *Plasmodium falciparum*-isolates from Cameroonian pregnant women do not rosette. *Parasite-Journal De La Societe Francaise De Parasitologie* **5**: 281-283.

McConkey, G. A., (1999) Targeting the shikimate pathway in the malaria parasite *Plasmodium falciparum*. *Antimicrob. Agents Chemother.* **43**: 175-177.

McLeod, R., S. P. Muench, J. B. Rafferty, D. E. Kyle, E. J. Mui, M. J. Kirisits, D. G. Mack, C. W. Roberts, B. U. Samuel, R. E. Lyons, M. Dorris, W. K. Milhous & D. W. Rice, (2001) Triclosan inhibits the growth of *Plasmodium falciparum* and *Toxoplasma gondii* by inhibition of apicomplexan Fab I. *Int. J. Parasitol.* **31**: 109-113.

McRobert, L., S. D. Jiang, A. Stead & G. A. McConkey, (2005) *Plasmodium falciparum*: Interaction of shikimate analogues with antimalarial drugs. *Exp. Parasitol.* **111**: 178-181.

Medzihradszky, K. F., Z. Darula, E. Perlson, M. Fainzilber, R. J. Chalkley, H. Ball, D. Greenbaum, M. Bogyo, D. R. Tyson, R. A. Bradshaw & A. L. Burlingame, (2004) O-sulfonation of serine and threonine - Mass spectrometric detection and characterization of a new posttranslational modification in diverse proteins throughout the eukaryotes. *Mol Cell Proteomics* **3**: 429-440.

Mehlin, C., E. Boni, F. S. Buckner, L. Engel, T. Feist, M. H. Gelb, L. Haji, D. Kim, C. Liu, N. Mueller, P. J. Myler, J. T. Reddy, J. N. Sampson, E. Subramanian, W. C. Van Voorhis, E. Worthey, F. Zucker & W. G. J. Hol, (2006) Heterologous expression of proteins from *Plasmodium falciparum*: Results from 1000 genes. *Mol. Biochem. Parasitol.* **148**: 144-160.

Meierjohann, S., R. D. Walter & S. Muller, (2002) Regulation of intracellular glutathione levels in erythrocytes infected with chloroquine-sensitive and chloroquine-resistant *Plasmodium falciparum*. *Biochem. J.* **368**: 761-768.

Meiklejohn, C. D. & J. P. Townsend, (2005) A Bayesian method for analysing spotted microarray data. *Brief. Bioinform.* **6**: 318-330.

Merchant, M. & S. R. Weinberger, (2000) Recent advancements in surface-enhanced laser desorption/ionization-time of flight-mass spectrometry. *Electrophoresis* **21**: 1164-1177.

Meshnick S.R., (2002) Artemisinin: mechanisms of action, resistance and toxicity. *International Journal for Parasitology* **32**: 1655-1660.

Miao, J., Q. Fan, L. Cui, J. S. Li, J. Y. Li & L. W. Cui, (2006) The malaria parasite *Plasmodium falciparum* histones: Organization, expression, and acetylation. *Gene* **369**: 53-65.

Misra, G. & R. Ramachandran, (2009) Hsp70-1 from *Plasmodium falciparum*: Protein stability, domain analysis and chaperone activity. *Biophys. Chem.* **142**: 55-64.

Molitor, I. M., S. Knobel, C. Dang, T. Spielmann, A. Allera & G. M. Konig, (2004) Translation initiation factor eIF-5A from *Plasmodium falciparum*. *Mol. Biochem. Parasitol.* **137**: 65-74.

Mons B., J.F. Trape, (1997) Malaria, Malaria and more Malaria. *Parasitology Today* **13**: 279-283.

Muller, I. B., R. Das Gupta, K. Luersen, C. Wrenger & R. D. Walter, (2008) Assessing the polyamine metabolism of *Plasmodium falciparum* as chemotherapeutic target. *Mol. Biochem. Parasitol.* **160**: 1-7.

Muller, S., (2004) Redox and antioxidant systems of the malaria parasite *Plasmodium falciparum*. *Mol. Microbiol.* **53**: 1291-1305.

Muller, S., G. H. Coombs & R. D. Walter, (2001) Targeting polyamines of parasitic protozoa in chemotheraphy. *Trends Parasitol.* **17**: 242-249.

Muller, S., A. Da'dara, K. Luersen, C. Wrenger, R. Das Gupta, R. Madhubala & R. D. Walter, (2000) In the human malaria parasite *Plasmodium falciparum,* polyamines are synthesized by a bifunctional ornithine decarboxylase, S-adenosylmethionine decarboxylase. *J. Biol. Chem.* **275**: 8097-8102.

Muller S., Coombs G.H. & Walter R.D., (2001) Targeting polyamines of parasitic protozoa in chemotheraphy. *TRENDS in Parasitology* **17**: 242-249.

Na-Bangchang, K. & J. Karbwang, (2009) Current status of malaria chemotherapy and the role of pharmacology in antimalarial drug research and development. *Fundam. Clin. Pharmacol.* **23**: 387-409.

Nair, S., B. Miller, M. Barends, A. Jaidee, J. Patel, M. Mayxay, P. Newton, F. Nosten, M. T. Ferdig & T. J. C. Anderson, (2008) Adaptive Copy Number Evolution in Malaria Parasites. *PLoS Genet.* **4**.

Nakanishi, M., A. Iwata, C. Yatome & Y. Kitade, (2001) Purification and properties of recombinant *Plasmodium falciparum* S-adenosyl-L-homocysteine hydrolase. *J. Biochem.* **129**: 101-105.

Nallan, L., K. D. Bauer, P. Bendale, K. Rivas, K. Yokoyama, C. P. Horney, P. R. Pendyala, D. Floyd, L. J. Lombardo, D. K. Williams, A. Hamilton, S. Sebti, W. T. Windsor, P. C. Weber, F. S. Buckner, D. Chakrabarti, M. H. Gelb & W. C. Van Voorhis, (2005) Protein farnesyltransferase inhibitors exhibit potent antimalarial activity. *J. Med. Chem.* **48**: 3704-3713.

Natalang, O., E. Bischoff, G. Deplaine, C. Proux, M. A. Dillies, O. Sismeiro, G. Guigon, S. Bonnefoy, J. Patarapotikul, O. Mercereau-Puijalon, J. Y. Coppee & P. H. David, (2008) Dynamic RNA profiling in *Plasmodium falciparum* synchronized blood stages exposed to lethal doses of artesunate. *BMC Genomics* **9**.

Naughton, J. A., R. Hughes, P. Bray & A. Bell, (2008) Accumulation of the antimalarial microtubule inhibitors trifluralin and vinblastine by *Plasmodium falciparum*. *Biochem. Pharmacol.* **75**: 1580-1587.

Nduati, E., A. Diriye, S. Ommeh, L. Mwai, S. Kiara, V. Masseno, G. Kokwaro & A. Nzila, (2008) Effect of folate derivatives on the activity of antifolate drugs used against malaria and cancer. *Parasitol. Res.* **102**: 1227-1234.

Nesvizhskii, A. I., O. Vitek & R. Aebersold, (2007) Analysis and validation of proteomic data generated by tandem mass spectrometry. *Nat. Methods* **4**: 787-797.

Neuhoff, V., N. Arold, D. Taube & W. Ehrhardt, (1988) Improved staining of proteins in polyacrylamide gels including isoelectric focusing gels with clear background at nanogram sensitivity using Coomassie Brilliant Blue G-250 and R-250. *Electrophoresis* **9**: 255-262.

Nirmalan, N., F. Flett, T. Skinner, J. E. Hyde & P. F. G. Sims, (2007) Microscale solution lsoelectric focusing as an effective strategy enabling containment of hemeoglobin-derived products for high-resolution gel-based analysis of the *Plasmodium falciparum* proteome. *J Proteome Res* **6**: 3780-3787.

Nirmalan, N., F. Flett, T. Skinner, J. E. Hyde & P. F. G. Sims, (2008) Off-line pre-fractionation of *P. falciparum* lysates provides a route to improved proteomic analysis. In., pp. S42-S42.

Nirmalan, N., P. F. G. Sims & J. E. Hyde, (2004a) Quantitative proteomics of the human malaria parasite *Plasmodium falciparum* and its application to studies of development and inhibition. *Mol. Microbiol.* **52**: 1187-1199.

Nirmalan, N., P. F. G. Sims & J. E. Hyde, (2004b) Translational up-regulation of antifolate drug targets in the human malaria parasite *Plasmodium falciparum* upon challenge with inhibitors. *Mol. Biochem. Parasitol.* **136**: 63-70.

Noedl, H., Y. Se, K. Schaecher, B. L. Smith, D. Socheat & M. M. Fukuda, (2008) Evidence of Artemisinin-Resistant Malaria in Western Cambodia. *New Engl. J. Med.* **359**: 2619-2620.

Noor, A. M., J. J. Mutheu, A. J. Tatem, S. I. Hay & R. W. Snow, (2009) Insecticide-treated net coverage in Africa: mapping progress in 2000-07. *Lancet* **373**: 58-67.

O'Farrell, P. H., (1975) High resolution two-dimensional electrophoresis of proteins. *J. Biol. Chem.* **250**: 4007-4021.

Oakeley E.J., (1999) DNA methylation analysis: a review of current methodologies. *Pharmacology and Therapeutics* **84**: 389-400.

Oakley, M. S. M., S. Kumar, V. Anantharaman, H. Zheng, B. Mahajan, J. D. Haynes, J. K. Moch, R. Fairhurst, T. F. McCutchan & L. Aravind, (2007) Molecular factors and biochemical pathways induced by febrile temperature in intraerythrocytic *Plasmodium falciparum* parasites. *Infect. Immun.* **75**: 2012-2025.

Oh, B. K., H. Kim, H. J. Park, Y. H. Shim, J. Choi, C. Park & Y. N. Park, (2007) DNA methyltransferase expression and DNA methylation in human hepatocellular carcinoma and their clinicopathological correlation. *Int. J. Mol. Med.* **20**: 65-73.

Ohkanda, J., J. W. Lockman, K. Yokoyama, M. H. Gelb, S. L. Croft, H. Kendrick, M. I. Harrell, J. E. Feagin, M. A. Blaskovich, S. M. Sebti & A. D. Hamilton, (2001) Peptidomimetic inhibitors of protein farnesyltransferase show potent antimalarial activity. *Bioorg. Med. Chem. Lett.* **11**: 761-764.

Olliaro, P. L. & W. R. J. Taylor, (2003) Antimalarial compounds: from bench to bedside. *J. Exp. Biol.* **206**: 3753-3759.

Olliaro, P. L. & Y. Yuthavong, (1999) An overview of chemotherapeutic targets for antimalarial drug discovery. *Pharmacol. Ther.* **81**: 91-110.

Olszewski, K. L., J. M. Morrisey, D. Wilinski, J. M. Burns, A. B. Vaidya, J. D. Rabinowitz & M. Linas, (2009) Host-Parasite Interactions Revealed by *Plasmodium falciparum* Metabolomics. *Cell Host & Microbe* **5**: 191-199.

Ong, S. E. & M. Mann, (2005) Mass spectrometry-based proteomics turns quantitative. *Nat. Chem. Biol.* **1**: 252-262.

Ong, S. E. & A. Pandey, (2001) An evaluation of the use of two-dimensional gel electrophoresis in proteomics. *Biomol. Eng.* **18**: 195-205.

Oshlack, A., D. Emslie, L. M. Corcoran & G. K. Smyth, (2007) Normalization of boutique two-color microarrays with a high proportion of differentially expressed probes. *Genome Biol.* **8**.

Owusu-Agyei, S., D. Ansong, K. Asante, S. Kwarteng Owusu, R. Owusu, N. A. Wireko Brobby, D. Dosoo, A. Osei Akoto, K. Osei-Kwakye, E. A. Adjei, K. O. Boahen, J. Sylverken, G. Adjei, D. Sambian, S. Apanga, K. Kayan, J. Vekemans, O. Ofori-Anyinam, A. Leach, M. Lievens, M.-A. Demoitie, M.-C. Dubois, J. Cohen, W. R. Ballou, B. Savarese, D. Chandramohan, J. O. Gyapong, P. Milligan, S. Antwi, T. Agbenyega, B. Greenwood & J. Evans, (2009) Randomized controlled trial of RTS,S/AS02D and RTS,S/AS01E malaria candidate vaccines given according to different schedules in Ghanaian children. *Plos One* **4**: e7302.

Paba, J., J. M. Santana, A. R. L. Teixeira, W. Fontes, M. V. Sousa & C. A. O. Ricart, (2004) Proteomic analysis of the human pathogen *Trypanosoma cruzi*. *Proteomics* **4**: 1052-1059.

Pal-Bhowmick, I., H. K. Vora & G. K. Jarori, (2007) Sub-cellular localization and post-translational modifications of the *Plasmodium yoelii* enolase suggest moonlighting functions. *Malaria J.* **6**.

Panpumthong, P. & P. Vattanaviboon, (2006) Improvement of proteomic profile of *Plasmodium falciparum* by two step protein extraction in two dimensional gel electrophoresis. *Thammasat Int. J. Sc. Tech.* **11**: 61-68.

Park, H. J., E. S. Yu & Y. H. Shim, (2006) DNA methyltransferase expression and DNA hypermethylation in human hepatocellular carcinoma. *Cancer Lett.* **233**: 271-278.

Park, M. H., (2006) The post-translational synthesis of a polyamine-derived amino acid, hypusine, in the eukaryotic translation initiation factor 5A (eIF5A). *J. Biochem.* **139**: 161-169.

Park, M. H., H. L. Cooper & J. E. Folk, (1981) Identification of hypusine, an unusual amino-acid, in a protein from human lymphocytes and of spermidine as its biosynthetic precursor. *Proc. Natl. Acad. Sci. U. S. A.* **78**: 2869-2873.

Park, M. H., Y. B. Lee & Y. A. Joe, (1997) Hypusine is essential for eukaryotic cell proliferation. *Biol. Signals* **6**: 115-123.

Park, M. H., E. C. Wolff, Z. Smitmcbride, J. W. B. Hershey & J. E. Folk, (1991) Comparison of the activities of variant forms of EIF-4D - the requirement for hypusine or deoxyhypusine. *J. Biol. Chem.* **266**: 7988-7994.

Pegg, A. E., K. Shuttleworth & H. Hibasami, (1981) Specificity of mammalian spermidine synthase and spermine synthase. *Biochem. J.* **197**: 315-320.

Perrot, M., S. Moes, A. Massoni, P. Jenoe & H. Boucherie, (2009) Yeast proteome map (last update). *Proteomics* **9**: 4669-4673.

Perrot, M., F. Sagliocco, T. Mini, C. Monribot, U. Schneider, A. Shevchenko, M. Mann, P. Jeno & H. Boucherie, (1999) Two-dimensional gel protein database of *Saccharomyces cerevisiae* (update 1999). *Electrophoresis* **20**: 2280-2298.

Pessi, G., G. Kociubinski & C. Ben Mamoun, (2004) A pathway for phosphatidylcholine biosynthesis in *Plasmodium falciparum* involving phosphoethanolamine methylation. *Proc. Natl. Acad. Sci. U. S. A.* **101**: 6206-6211.

Pietiainen, M., P. Francois, H. L. Hyyrylainen, M. Tangomo, V. Sass, H. G. Sahl, J. Schrenzel & V. P. Kontinen, (2009) Transcriptome analysis of the responses of *Staphylococcus aureus* to antimicrobial peptides and characterization of the roles of vraDE and vraSR in antimicrobial resistance. *BMC Genomics* **10**.

Pignatti C., Tantini B., Stefanelli C. & Flamigni F., (2004) Signal transduction pathways linking polyamines to apoptosis. *Amino Acids* **27**: 359-365.

Poetz, O., J. M. Schwenk, S. Kramer, D. Stoll, M. F. Templin & T. O. Joos, (2005) Protein microarrays: catching the proteome. *Mech. Ageing Dev.* **126**: 161-170.

Pogribny, I. P., A. G. Basnakian, B. J. Miller, N. G. Lopatina, L. A. Poirier & S. J. James, (1995) Breaks in genomic DNA and within the P53 gene are associated with hypomethylation in livers of folate/methyl-deficient rats. *Cancer Res.* **55**: 1894-1901.

Polhemus, M. E., A. J. Magill, J. F. Cummings, K. E. Kester, C. F. Ockenhouse, D. E. Lanar, S. Dutta, A. Barbosa, L. Soisson, C. L. Diggs, S. A. Robinson, J. D. Haynes, V. A. Stewart, L. A. Ware, C. Brando, U. Krzych, R. A. Bowden, J. D. Cohen, M. C. Dubois, O. Ofori-Anyinam, E. De-Kock, W. R. Ballou & D. G. Heppner, (2007) Phase I dose escalation safety and immunogenicity trial of *Plasmodium falciparum* apical membrane protein (AMA-1) FMP2.1, adjuvanted with AS02A, in malariu-naive adults at the Walter Reed Army Institute of Research. *Vaccine* **25**: 4203-4212.

Ponts, N., E. Y. Harris, J. Prudhomme, I. Wick, C. Eckhardt-Ludka, G. R. Hicks, G. Hardiman, S. Lonardi & K. G. Le Roch, (2010) Nucleosome landscape and control of transcription in the human malaria parasite. *Genome Res.* **20**: 228-238.

Price, R. N., (2000) Artemisinin drugs: novel antimalarial agents. *Expert Opin. Investig. Drugs* **9**: 1815-1827.

Prieto, J. H., S. Koncarevic, S. K. Park, J. Yates & K. Becker, (2008) Large-Scale Differential Proteome Analysis in *Plasmodium falciparum* under Drug Treatment. *Plos One* **3**.

Quackenbush, J., (2002) Microarray data normalization and transformation. *Nat. Genet.* **32**: 496-501.

Radfar, A., A. Diez & J. M. Bautista, (2008) Chloroquine mediates specific proteome oxidative damage across the erythrocytic cycle of resistant *Plasmodium falciparum*. *Free Radical Biol. Med.* **44**: 2034-2042.

Reguera, R. M., C. M. Redondo, Y. Perez-Pertejo & R. Balana-Fouce, (2007) S-adenosylmethionine in protozoan parasites: Functions, synthesis and regulation. *Mol. Biochem. Parasitol.* **152**: 1-10.

Rengarajan, K., S. M. Cristol, M. Mehta & J. M. Nickerson, (2002) Quantifying DNA concentrations using fluorometry: A comparison of fluorophores. *Mol. Vis.* **8**: 416-421.

Ricke, C. H., T. Staalsoe, K. Koram, B. D. Akanmori, E. M. Riley, T. G. Theander & L. Hviid, (2000) Plasma antibodies from malaria-exposed pregnant women recognize variant surface antigens on *Plasmodium falciparum*-infected erythrocytes in a parity-dependent manner and block parasite adhesion to chondroitin sulfate A. *J. Immunol.* **165**: 3309-3316.

Rider, J. E., A. Hacker, C. A. Mackintosh, A. E. Pegg, P. M. Woster & R. A. Casero, (2007) Spermine and spermidine mediate protection against oxidative damage caused by hydrogen peroxide. *Amino Acids* **33**: 231-240.

Ritchie, M. E., J. Silver, A. Oshlack, M. Holmes, D. Diyagama, A. Holloway & G. K. Smyth, (2007) A comparison of background correction methods for two-colour microarrays. *Bioinformatics* **23**: 2700-2707.

Roepstorff, P. & J. Fohlman, (1984) Proposal for a common nomenclature for sequence ions in mass-spectra of peptides. *Biomed. Mass Spectrom.* **11**: 601-601.

Rogerson, S. J., L. Hviid, P. E. Duffy, R. F. G. Leke & D. W. Taylor, (2007) Malaria in pregnancy: pathogenesis and immunity. *Lancet Infect. Dis.* **7**: 105-117.

Roggero, R., R. Zufferey, M. Minca, E. Richier, M. Calas, H. Vial & C. Ben Mamoun, (2004) Unraveling the mode of action of the antimalarial choline analog G25 in *Plasmodium falciparum* and *Saccharomyces cerevisiae*. *Antimicrob. Agents Chemother.* **48**: 2816-2824.

Rosenthal, P. J., J. E. Olson, G. K. Lee, J. T. Palmer, J. L. Klaus & D. Rasnick, (1996) Antimalarial effects of vinyl sulfone cysteine proteinase inhibitors. *Antimicrob. Agents Chemother.* **40**: 1600-1603.

Roth, E., (1990) *Plasmodium falciparum* carbohydrate metabolism - a connection between host cell and parasite. *Blood Cells* **16**: 453-460.

Roth, E., V. Joulin, S. Miwa, A. Yoshida, J. Akatsuka, M. Cohensolal & R. Rosa, (1988a) The use of enzymopathic human red-cell in the study of malarial parasite glucose metabolism. *Blood* **71**: 1408-1413.

Roth, E. F., M. C. Calvin, I. Maxaudit, J. Rosa & R. Rosa, (1988b) The enzymes of the glycolytic pathway in erythrocytes infected with *Plasmodium falciparum* malaria parasites. *Blood* **72**: 1922-1925.

Rychlik, W., W. J. Spencer & R. E. Rhoads, (1990) Optimization of the annealing temperature for DNA amplification *in vitro*. *Nucleic Acids Res.* **18**: 6409-6412.

Sacarlal, J., J. J. Aponte, P. Aide, I. Mandomando, Q. Bassat, C. Guinovart, A. Leach, J. Milman, E. Macete, M. Espasa, O. Ofori-Anyinam, J. Thonnard, S. Corachan, M. C. Dubois, M. Lievens, F. Dubovsky, W. R. Ballou, J. Cohen & P. L. Alonso, (2008) Safety of the RTS,S/AS02A malaria vaccine in Mozambican children during a Phase IIb trial. *Vaccine* **26**: 174-184.

Saliba, K. J., R. J. W. Allen, S. Zissis, P. G. Bray, S. A. Ward & K. Kirk, (2003) Acidification of the malaria parasite's digestive vacuole by a H+-ATPase and a H+-pyrophosphatase. *J. Biol. Chem.* **278**: 5605-5612.

Santos-Magalhaes, N. S. & V. C. F. Mosqueira, (2010) Nanotechnology applied to the treatment of malaria. *Adv. Drug Del. Rev.* **62**: 560-575.

Sarma, P. S. A., A. K. Mandal & H. J. Khamis, (1998) Allopurinol as an additive to quinine in the treatment of acute complicated *falciparum* malaria. *Am. J. Trop. Med. Hyg.* **58**: 454-457.

Savarin, P., A. Barbet, S. Delga, V. Joshi, L. Hamon, J. Lefevre, S. Nakib, J. P. De Bandt, C. Moinard, P. A. Curmi & D. Pastré, (2010) A Central Role for Polyamines in Microtubules Assembly in Cells. *Biochem. J.*

Scherl, A., P. Francois, Y. Charbonnier, J. M. Deshusses, T. Koessler, A. Huyghe, M. Bento, J. Stahl-Zeng, A. Fischer, A. Masselot, A. Vaezzadeh, F. Galle, A. Renzoni, P. Vaudaux, D. Lew, C. G. Zimmermann-Ivol, P. A. Binz, J. C. Sanchez, D. F. Hochstrasser & J. Schrenzel, (2006) Exploring glycopeptide-resistance in *Staphylococcus aureus*: A combined proteomics and transcriptomics approach for the identification of resistance-related markers. *BMC Genomics* **7**.

Schlitzer, M., (2008) Antimalarial drugs - What is in use and what is in the pipeline. *Arch. Pharm.* **341**: 149-163.

Shapiro R., B.I. Cohen & R.E. Servis, (1970a) Specific deamination of RNA by sodium bisulphite. *Nature* **227**: 1047-1048.

Shapiro R., R.E. Servis. & M. Welcher, (1970b) Reactions of uracil and cytosine derivatives with sodium bisulphite. *Journal of the American Chemical Society* **92**: 422-424.

Shevchenko, A., M. Wilm, O. Vorm & M. Mann, (1996) Mass spectrometric sequencing of proteins from silver-stained polyacrylamide gels. *Anal. Chem.* **68**: 850-858.

Shiio, Y. & R. Aebersold, (2006) Quantitative proteome analysis using isotope-coded affinity tags and mass spectrometry. *Nat. Protoc.* **1**: 139-145.

Shiraishi M. & Hayatsu H., (2004) High speed conversion of cytosine to uracil in bisulfite genomic sequencing analysis of DNA methylation. *DNA Research* **11**: 409- 415.

Shock, J. L., K. F. Fischer & J. L. DeRisi, (2007) Whole-genome analysis of mRNA decay in *Plasmodium falciparum* reveals a global lengthening of mRNA half-life during the intra-erythrocytic development cycle. *Genome Biol.* **8**.

Shuto, S., N. Minakawa, S. Niizuma, H. S. Kim, Y. Wataya & A. Matsuda, (2002) New neplanocin analogues. 12. Alternative synthesis and antimalarial effect of (6 ' R)-6 '-C-methylneplanocin A, a potent AdoHcy hydrolase inhibitor. *J. Med. Chem.* **45**: 748-751.

Silvie, O., M. M. Mota, K. Matuschewski & M. Prudencio, (2008) Interactions of the malaria parasite and its mammalian host. *Curr. Opin. Microbiol.* **11**: 352-359.

Sims, P. F. G. & J. E. Hyde, (2006) Proteomics of the human malaria parasite *Plasmodium falciparum*. *Expert Rev. Proteomics* **3**: 87-95.

Sinden, R. E. & P. F. Billingsley, (2001) *Plasmodium* invasion of mosquito cells: hawk or dove? *Trends Parasitol.* **17**: 209-212.

Singh, S., A. Mukherjee, A. R. Khomutov, L. Persson, O. Heby, M. Chatterjee & R. Madhubala, (2007) Antileishmanial effect of 3-aminooxy-1-aminopropane is due to polyamine depletion. *Antimicrob. Agents Chemother.* **51**: 528-534.

Smilkstein, M., N. Sriwilaijaroen, J. X. Kelly, P. Wilairat & M. Riscoe, (2004) Simple and inexpensive fluorescence-based technique for high-throughput antimalarial drug screening. *Antimicrob. Agents Chemother.* **48**: 1803-1806.

Smit, S., S. Stoychev, A. I. Louw & L.-M. Birkholtz, (2010) Proteomic profiling of *Plasmodium falciparum* through improved, semiquantitative two-dimensional gel electrophoresis. *J Proteome Res* **9**: 2170-2181.

Smith, P. K., R. I. Krohn, G. T. Hermanson, A. K. Mallia, F. H. Gartner, M. D. Provenzano, E. K. Fujimoto, N. M. Goeke, B. J. Olson & D. C. Klenk, (1985) Measurement of protein using Bicinchoninic acid. *Anal. Biochem.* **150**: 76-85.

Smyth, G. K., J. Michaud & H. S. Scott, (2005a) Use of within-array replicate spots for assessing differential expression in microarray experiments. *Bioinformatics* **21**: 2067-2075.

Smyth, G. K., M. Ritchie, N. Thorne & J. Wettenhall, (2008) limma:Linear Models for Microarray Data User's Guide. **2 January**.

Smyth, G. K. & T. Speed, (2003) Normalization of cDNA microarray data. *Methods* **31**: 265-273.

Smyth, G. K., N. Thorne & J. Wettenhall, (2005b) limma: Linear Models for Microarray Data User's Guide.

Smyth, G. K., Y. H. Yang & T. Speed, (2003) Statistical issues in cDNA microarray data analysis. *Methods Mol. Biol.* **224**: 111-136.

Sohn, K. J., J. M. Stempak, S. Reid, S. Shirwadkar, J. B. Mason & Y. I. Kim, (2003) The effect of dietary folate on genomic and p53-specific DNA methylation in rat colon. *Carcinogenesis* **24**: 81-90.

Spring, M. D., J. F. Cummings, C. F. Ockenhouse, S. Dutta, R. Reidler, E. Angov, E. Bergmann-Leitner, V. A. Stewart, S. Bittner, L. Juompan, M. G. Kortepeter, R. Nielsen, U. Krzych, E. Tierney, L. A. Ware, M. Dowler, C. C. Hermsen, R. W. Sauerwein, S. J. de Vlas, O. Ofori-Anyinam, D. E. Lanar, J. L. Williams, K. E. Kester, K. Tucker, M. Shi, E. Malkin, C. Long, C. L. Diggs, L. Soisson, M.-C. Dubois, W. R. Ballou, J. Cohen & D. G. Heppner, (2009) Phase 1/2a study of the malaria vaccine candidate apical membrane antigen-1 (AMA-1) administered in adjuvant system AS01B or AS02A. *Plos One* **4**: e5254.

Srivastava, P., S. K. Puri, K. K. Kamboj & V. C. Pandey, (1999) Glutathione-S-transferase activity in malarial parasites. *Trop. Med. Int. Health* **4**: 251-254.

Starnes, G. L., M. Coincon, J. Sygusch & L. D. Sibley, (2009) Aldolase Is Essential for Energy Production and Bridging Adhesin-Actin Cytoskeletal Interactions during Parasite Invasion of Host Cells. *Cell Host & Microbe* **5**: 353-364.

Steinberg, T. H., R. P. Haugland & V. L. Singer, (1996a) Applications of SYPRO Orange and SYPRO Red protein gel stains. *Anal. Biochem.* **239**: 238-245.

Steinberg, T. H., L. J. Jones, R. P. Haugland & V. L. Singer, (1996b) SYPRO Orange and SYPRO Red gel stains: One-step fluorescent staining of denaturing gels for detection of nanogram levels of protein. *Anal. Biochem.* **239**: 223-237.

Strahl, B. D. & C. D. Allis, (2000) The language of covalent histone modifications. *Nature* **403**: 41-45.

Sturm, N., E. Jortzik, B. M. Mailu, S. Koncarevic, M. Deponte, K. Forchhammer, S. Rahlfs & K. Becker, (2009) Identification of proteins targeted by the thioredoxin superfamily in *Plasmodium falciparum*. *PLoS Pathog* **5**: e1000383.

Tatem, A. J., D. J. Rogers & S. I. Hay, (2006) Estimating the malaria risk of African mosquito movement by air travel. *Malaria J.* **5**.

Taylor, C. F., P. A. Binz, R. Aebersold, M. Affolter, R. Barkovich, E. W. Deutsch, D. M. Horn, A. Huhmer, M. Kussmann, K. Lilley, M. Macht, M. Mann, D. Mueller, T. A. Neubert, J. Nickson, S. D. Patterson, R. Raso, K. Resing, S. L. Seymour, A. Tsugita, I. Xenarios, R. Zeng & R. K. Julian, (2008) Guidelines for reporting the use of mass spectrometry in proteomics. *Nat. Biotechnol.* **26**: 860-861.

Taylor, C. F., N. W. Paton, K. S. Lilley, P. A. Binz, R. K. Julian, A. R. Jones, W. M. Zhu, R. Apweiler, R. Aebersold, E. W. Deutsch, M. J. Dunn, A. J. R. Heck, A. Leitner, M. Macht, M. Mann, L. Martens, T. A. Neubert, S. D. Patterson, P. P. Ping, S. L. Seymour, P. Souda, A. Tsugita, J. Vandekerckhove, T. M. Vondriska, J. P. Whitelegge, M. R. Wilkins, I. Xenarios, J. R. Yates & H. Hermjakob, (2007) The minimum information about a proteomics experiment (MIAPE). *Nat. Biotechnol.* **25**: 887-893.

Teng, R. W., P. R. Junankar, W. A. Bubb, C. Rae, P. Mercier & K. Kirk, (2009) Metabolite profiling of the intraerythrocytic malaria parasite *Plasmodium falciparum* by H-1 NMR spectroscopy. *NMR Biomed.* **22**: 292-302.

Thingholm, T. E., O. N. Jensen & M. R. Larsen, (2009) Analytical strategies for phosphoproteomics. *Proteomics* **9**: 1451-1468.

Thomas, T. & T. J. Thomas, (2001) Polyamines in cell growth and cell death: molecular mechanisms and therapeutic applications. *Cell. Mol. Life Sci.* **58**: 244-258.

Tkachenko, A. G., (2004 (a)) Mechanisms of protective functions of *Escherichia coli* polyamines against toxic effect of paraquat, which causes superoxide stress. *Biochemistry (Mosc)* **69**: 188-194.

Tkachenko, A. G. & M. S. Shumkov, (2004 (b)) Role of putrescine in regulation of the sigma(S) subunit of RNA polymerase in *Escherichia coli* cells on transition to stationary phase. *Biochemistry (Mosc)* **69**: 876-882.

Trager, W. & J. B. Jensen, (1976) Human malaria parasites in continuous culture. *Science* **193**: 673-675.

Trelle, M. B., A. M. Salcedo-Amaya, A. M. Cohen, H. G. Stunnenberg & O. N. Jensen, (2009) Global Histone Analysis by Mass Spectrometry Reveals a High Content of Acetylated Lysine Residues in the Malaria Parasite *Plasmodium falciparum*. *J Proteome Res* **8**: 3439-3450.

Triglia, T., T. E. Wellems & D. J. Kemp, (1992) Towards a high-resolution map of the *Plasmodium falciparum* genome. *Parasitol. Today* **8**: 225-229.

Tyler, P. C., E. A. Taylor, R. F. G. Frohlich & V. L. Schramm, (2007) Synthesis of 5 '-methylthio coformycins: Specific inhibitors for malarial adenosine deaminase. *J. Am. Chem. Soc.* **129**: 6872-6879.

Van Brummelen, A. C., (2009) Functional genomics analysis of the effects of co-inhibition of the malarial S-adenosylmethionine decarboxylase/ornithine decarboxylase. In. Pretoria: University of Pretoria, pp.

van Brummelen, A. C., K. L. Olszewski, D. Wilinski, M. Llinás, A. I. Louw & L. Birkholtz, (2009) Co-inhibition of *Plasmodium falciparum* S-Adenosylmethionine Decarboxylase/Ornithine Decarboxylase Reveals Perturbation-specific Compensatory Mechanisms by Transcriptome, Proteome, and Metabolome Analyses. *J. Biol. Chem.* **284**: 4635-4646.

van Noort, V. & M. A. Huynen, (2006) Combinatorial gene regulation in *Plasmodium falciparum*. *Trends Genet.* **22**: 73-78.

Vangapandu, S., M. Jain, K. Kaur, P. Patil, S. R. Patel & R. Jain, (2007) Recent advances in antimalarial drug development. *Med. Res. Rev.* **27**: 65-107.

Vedadi, M., J. Lew, J. Artz, M. Amani, Y. Zhao, A. P. Dong, G. A. Wasney, M. Gao, T. Hills, S. Brokx, W. Qiu, S. Sharma, A. Diassiti, Z. Alam, M. Melone, A. Mulichak, A. Wernimont, J. Bray, P. Loppnau, O. Plotnikova, K. Newberry, E. Sundararajan, S. Houston, J. Walker, W. Tempel, A. Bochkarev, L. Kozieradzki, A. Edwards, C. Arrowsmith, D. Roos, K. Kain & R. Hui, (2007) Genome-scale protein expression and structural biology of *Plasmodium falciparum* and related Apicomplexan organisms. *Mol. Biochem. Parasitol.* **151**: 100-110.

Vivas, L., L. Rattray, L. B. Stewart, B. L. Robinson, B. Fugmann, R. K. Haynes, W. Peters & S. L. Croft, (2007) Antimalarial efficacy and drug interactions of the novel semi-synthetic endoperoxide artemisone in vitro and in vivo. *J. Antimicrob. Chemother.* **59**: 658-665.

Wagner, J. T., H. Ludemann, P. M. Farber, F. Lottspeich & R. L. Krauth-Siegel, (1998) Glutamate dehydrogenase, the marker protein of *Plasmodium falciparum* - Cloning, expression and characterization of the malarial enzyme. *Eur. J. Biochem.* **258**: 813-819.

Wallace, H. M., A. V. Fraser & A. Hughes, (2003) A perspective of polyamine metabolism. *Biochem. J.* **376**: 1-14.

Wang, P., F. G. Bouwman & E. C. M. Mariman, (2009) Generally detected proteins in comparative proteomics – A matter of cellular stress response? *Proteomics* **9**: 1-12.

Wang, P., Q. Wang, P. F. G. Sims & J. E. Hyde, (2002) Rapid positive selection of stable integrants following transfection of *Plasmodium falciparum*. *Mol. Biochem. Parasitol.* **123**: 1-10.

Wang, Y. L., C. Barbacioru, F. Hyland, W. M. Xiao, K. L. Hunkapiller, J. Blake, F. Chan, C. Gonzalez, L. Zhang & R. R. Samaha, (2006) Large scale real-time PCR validation on gene expression measurements from two commercial long-oligonucleotide microarrays. *BMC Genomics* **7**.

Wanidworanun, C., R. L. Nagel & H. L. Shear, (1999) Antisense oligonucleotides targeting malarial aldolase inhibit the asexual erythrocytic stages of *Plasmodium falciparum*. *Mol. Biochem. Parasitol.* **102**: 91-101.

Ward, P., L. Equinet, J. Packer & C. Doerig, (2004) Protein kinases of the human malaria parasite *Plasmodium falciparum*: the kinome of a divergent eukaryote. *BMC Genomics* **5**.

Washburn, M. P., A. Koller, G. Oshiro, R. R. Ulaszek, D. Plouffe, C. Deciu, E. Winzeler & J. R. Yates, (2003) Protein pathway and complex clustering of correlated mRNA and protein expression analyses in *Saccharomyces cerevisiae*. *Proc. Natl. Acad. Sci. U. S. A.* **100**: 3107-3112.

Weinberger, S. R., T. S. Morris & M. Pawlak, (2000) Recent trends in protein biochip technology. *Pharmacogenomics* **1**: 395-416.

Wells, G. A., L. M. Birkholtz, F. Joubert, R. D. Walter & A. I. Louw, (2006) Novel properties of malarial S-adenosylmethionine decarboxylase as revealed by structural modelling. *J. Mol. Graph. Model.* **24**: 307-318.

Wettenhall, J. M. & G. K. Smyth, (2004) limmaGUI: A graphical user interface for linear modeling of microarray data. *Bioinformatics* **20**: 3705-3706.

WHO, World Health Organization (WHO), www.who.int. *www.who.int*.

WHO Guidelines for the treatment of malaria, n. E., WHO, (2010) Guidelines for the treatment of malaria 2nd Edition

Willert, E. K. & M. A. Phillips, (2008) Regulated Expression of an Essential Allosteric Activator of Polyamine Biosynthesis in African Trypanosomes. *PLoS Path.* **4**.

Wilson, W., J. DeRisi, H. H. Kristensen, P. Imboden, S. Rane, P. O. Brown & G. K. Schoolnik, (1999) Exploring drug-induced alterations in gene expression in *Mycobacterium tuberculosis* by microarray hybridization. *Proc. Natl. Acad. Sci. U. S. A.* **96**: 12833-12838.

Winkler, C., K. Denker, S. Wortelkamp & A. Sickmann, (2007) Silver- and coomassie-staining protocols: Detection limits and compatibility with ESI MS. *Electrophoresis* **28**: 2095-2099.

Wirth, D. F., (2002) Biological relevations. *Nature* **419**: 495-496.

Witola, W. H. & C. Ben Mamoun, (2007) Choline induces transcriptional repression and proteasomal degradation of the malarial phosphoethanolamine methyltransferase. *Eukaryot. Cell* **6**: 1618-1624.

Wolber, P. K., P. J. Collins, A. B. Lucas, A. De Witte & K. W. Shannon, (2006) The agilent in situ-synthesized microarray platform. *DNA Microarrays Part A: Array Platforms and Wet-Bench Protocols* **410**: 28-57.

Wolff, E. C., K. R. Kang, Y. S. Kim & M. H. Park, (2007) Posttranslational synthesis of hypusine: evolutionary progression and specificity of the hypusine modification. *Amino Acids* **33**: 341-350.

World Malaria Report 2008, World Health Organization (www.who.int).

Wrenger, C., K. Luersen, T. Krause, S. Muller & R. D. Walter, (2001) The *Plasmodium falciparum* bifunctional ornithine decarboxylase, S-adenosyl-L-methionine decarboxylase, enables a well balanced polyamine synthesis without domain-domain interaction. *J. Biol. Chem.* **276**: 29651-29656.

Wright, P. S., T. L. Byers, D. E. Crossdoersen, P. P. McCann & A. J. Bitonti, (1991) Irreversible inhibition of S-adenosylmethionine decarboxylase in *Plasmodium falciparum* infected erythrocytes - growth inhibition *in virto*. *Biochem. Pharmacol.* **41**: 1713-1718.

Wu, Y. & A. Craig, (2006) Comparative proteomic analysis of metabolically labelled proteins from *Plasmodium falciparum* isolates with different adhesion properties. *Malaria J.* **5**: 67.

Wu, Y., M. M. Nelson, A. Quaile, D. Xia, J. M. Wastling & A. Craig, (2009) Identification of phosphorylated proteins in erythrocytes infected by the human malaria parasite *Plasmodium falciparum*. *Malaria J.* **8**.

Wu Y. & Craig A., (2006) Comparative proteomic analysis of metabolically labelled proteins from *Plasmodium falciparum* isolates with different adhesion properties. *Malaria J.* **5**: 67.

Wuchty, S., J. H. Adams & M. T. Ferdig, (2009) A comprehensive *Plasmodium falciparum* protein interaction map reveals a distinct architecture of a core interactome. *Proteomics* **9**: 1841-1849.

Wurtele, H. & A. Verreault, (2006) Histone post-translational modifications and the response to DNA double-strand breaks. *Curr. Opin. Cell Biol.* **18**: 137-144.

Xiao, Y. J., D. E. McCloskey & M. A. Phillips, (2009) RNA Interference-Mediated Silencing of Ornithine Decarboxylase and Spermidine Synthase Genes in *Trypanosoma brucei* Provides Insight into Regulation of Polyamine Biosynthesis. *Eukaryot. Cell* **8**: 747-755.

Yan, J. X., R. A. Harry, C. Spibey & M. J. Dunn, (2000 (a)) Postelectrophoretic staining of proteins separated by two-dimensional gel electrophoresis using SYPRO dyes. *Electrophoresis* **21**: 3657-3665.

Yang A.S., Estecio M.R.H., Doshi K., Kondo Y., Tajara E.H. & Issa J.P.J., (2004) A simple method for estimating global DNA methylation using bisulfite PCR of repetitive DNA elements. *Nucleic Acids Research* **32**: e38.

Yang, S. T., D. Nikodem, E. A. Davidson & D. C. Gowda, (1999) Glycosylation and proteolytic processing of 70 kDa C-terminal recombinant polypeptides of *Plasmodium falciparum* merozoite surface protein 1 expressed in mammalian cells. *Glycobiology* **9**: 1347-1356.

Yang, Y. H. & T. Speed, (2002) Design issues for cDNA microarray experiments. *Nat. Rev. Genet.* **3**: 579-588.

Yarlett, N., J. Garofalo, B. Goldberg, M. A. Ciminelli, V. Ruggiero, J. R. Sufrin & C. J. Bacchi, (1993) S-adenosylmethionine synthetase in blood-stream *Trypanosoma brucei*. *Biochim. Biophys. Acta* **1181**: 68-76.

Young J.A., Fivelman Q.L., Blair P.L., De la Vega P., Le Roch K.G., Zhou Y., Carucci D.J., Baker D.A. & Winzeler E.A., (2005) The *Plasmodium falciparum* sexual development transcriptome: A microarray analysis using ontology-based pattern identification. *Mol Biochem Parasit.* **143**: 67-79.

Yu, M., T. R. S. Kumar, L. J. Nkrumah, A. Coppi, S. Retzlaff, C. D. Li, B. J. Kelly, P. A. Moura, V. Lakshmanan, J. S. Freundlich, J.-C. Valderramos, C. Vilcheze, M. Siedner, J. H. C. Tsai, B. Falkard, A. B. S. Sidhu, L. A. Purcell, P. Gratraud, L. Kremer, A. P. Waters, G. Schiehser, D. P. Jacobus, C. J. Janse, A. Ager, W. R. Jacobs, J. C. Sacchettini, V. Heussler, P. Sinnis & D. A. Fidock, (2008) The fatty acid biosynthesis enzyme FabI plays a key role in the development of liver-stage malarial parasites. *Cell Host Microbe* **4**: 567-578.

Yuvaniyama, J., P. Chitnumsub, S. Kamchonwongpaisan, J. Vanichtanankul, W. Sirawaraporn, P. Taylor, M. D. Walkinshaw & Y. Yuthavong, (2003) Insights into antifolate resistance from malarial DHFR-TS structures. *Nat. Struct. Biol.* **10**: 357-365.

Zhang, K. & P. K. Rathod, (2002) Divergent regulation of dihydrofolate reductase between malaria parasite and human host. *Science* **296**: 545-547.

Zinellu, A., S. Sotgia, M. F. Usai, E. Zinellu, A. M. Posadino, L. Gaspa, R. Chessa, A. Pinna, F. Carta, L. Deiana & C. Carru, (2007) Plasma methionine determination by capillary electrophoresis-UV assay: Application on patients affected by retinal venous occlusive disease. *Anal. Biochem.* **363**: 91-96.

Appendix A

The List of proteins identified by MS/MS for Colloidal Coomassie Blue, MS compatible silver stain, SYPRO Ruby and Flamingo Pink

Spot nr[a]	Accession number[b]	PlasmoDB ID[c]	Name	Mr	pI	Mascot Score MS/MS[d]	Seq cov[e]	Match[f]
List of proteins identified by MS/MS for Colloidal Coomassie Blue								
C1	Q25883	PF07_0029	Heat shock protein 86	86468	4.94	866	20	18
C2	Q8I2X4	PFI0875w	Heat shock protein	72457	5.18	1344	32	17
C3	Q8I0V4	PFL1070c	Endoplasmin homolog, putative	95301	5.28	453	16	12
C4	Q8IB24	PF08_0054	Heat shock 70 kDa protein	74382	5.51	1296	35	21
C5	Q8II24	PF11_0351	Heat shock protein hsp70 homologue	73651	6.51	1084	33	19
C6	P02769	-	Bovine Serum albumin [Precursor]	71274	5.82	417	18	11
C7	Q8IJN9	PF10_0153	Hsp60	62911	6.71	371	20	11
C8	Q8I6S6	MAL8P1.17	Disulfide isomerase, putative	55808	5.56	906	32	14
C9	Q8IJN7	PF10_0155	Enolase	48989	6.21	391	20	7
C10	Q9GN14	PFI1090w	S-adenosylmethionine synthetase	45272	6.28	313	19	6
C11	Q6LFH8	PFF0435w	Ornithine aminotransferase	46938	6.47	258	19	7
C12	Q8II61	PF11_0313	Ribosomal phosphoprotein P0	35002	6.28	343	38	9
C13	Q8T6B1	PF14_0598	Glyceraldehyde-3-phosphate dehydrogenase	37068	7.59	453	32	10
C15	Q8IM15	PF14_0078	HAP protein	51889	8.05	442	20	9
C16	Q8IIR7	PF11_0098	Endoplasmic reticulum-resident calcium binding protein	39464	4.49	539	26	8
C17	Q8I3F3	PFE1590w	Early transcribed membrane protein	19132	5.26	80	7	1
C18	Q8I3F3	PFE1590w	Early transcribed membrane protein	19132	5.26	65	7	1
C19	Q8IKC8	PF14_0678	Exported protein 2	33619	5.1	201	15	6
C20	Q8I6U5	PF11_0161	Falcipain-2, putative	56281	8.14	276	10	5
C21	Q8IIU5	PF11_0069	Hypothetical protein	32112	4.91	148	20	5
C22	Q8IDQ9	MAL13P1.214	Phosphoethanolamine N-methyltransferase, putative	31309	5.43	522	39	9
C23	Q8I2Q0	PFI1270w	Hypothetical protein PFI1270w	24911	5.49	166	14	3
C24	Q8I2Q0	PFI1270w	Hypothetical protein PFI1270w	24911	5.49	137	14	3
C26	O97249	PFC0295c	40S Ribosomal protein S12, putative	15558	4.9	262	35	5
C27	Q8IIF0	PF11_0224	Circumsporozoite-related antigen	17285	5.64	278	22	5
C28	P00441	-	Human Superoxide dismutase	16154	5.7	217	27	4
C29	P32119	-	Human Peroxiredoxin-2	21918	5.67	371	32	8
C30	P32119	-	Human Peroxiredoxin-2	21918	5.67	351	35	9
C34	Q8IB17	MAL8P1.69	14-3-3 protein	30470	4.86	579	49	16
CM1	P00489	-	Rabbit Glycogen phosphorylase	97610	6.76	1348	29	24
CM2	P02769	-	Bovine Serum albumin [Precursor]	71274	5.82	762	20	14
CM3	P01012	-	Chicken ovalbumin	43196	5.19	913	40	14
CM4	P00921	-	Bovine carbonic anhydrase II	29096	6.41	517	45	8
CM5	1AVXB	-	Soybean trypsin inhibitor, chain B	19295	4.79	274	26	7
CM6	LABO	-	Bovine alpha lactalbumin	16692	4.93	48	7	1
List of proteins identified by MS/MS for the MS compatible silver stain								
M1	Q25883	PF07_0029	Heat shock protein 86	86468	4.94	848	20	16
M2	Q8I2X4	PFI0875w	Heat shock protein	72457	5.18	1639	39	20
M3	Q8I0V4	PFL1070c	Endoplasmin homolog, putative	95301	5.28	809	29	18
M4	Q8IB24	PF08_0054	Heat shock 70 kDa protein	74382	5.51	1455	39	21
M5	Q8II24	PF11_0351	Heat shock protein hsp70 homologue	73651	6.51	1060	29	18
M6	P02769	-	Bovine Serum albumin [Precursor]	71274	5.82	926	29	19
M7	Q8IJN9	PF10_0153	Hsp60	62911	6.71	333	11	5
M8	Q8I6S6	MAL8P1.17	Disulfide isomerase, putative	55808	5.56	939	38	16
M9	Q8IJN7	PF10_0155	Enolase	48989	6.21	1044	50	18
M10	Q9GN14	PFI1090w	S-adenosylmethionine synthetase	45272	6.28	488	28	9
M11	Q6LFH8	PFF0435w	Ornithine aminotransferase	46938	6.47	667	40	14
M12	Q8II61	PF11_0313	Ribosomal phosphoprotein P0	35002	6.28	519	40	10
M13	Q8T6B1	PF14_0598	Glyceraldehyde-3-phosphate dehydrogenase	37068	7.59	720	42	9
M16	Q8IIR7	PF11_0098	Endoplasmic reticulum-resident calcium binding protein	39464	4.49	1050	53	15
M22	Q8IDQ9	MAL13P1.214	Phosphoethanolamine N-methyltransferase, putative	31309	5.43	794	56	12
M23	Q8I2Q0	PFI1270w	Hypothetical protein PFI1270w	24911	5.49	244	25	5
M24	Q8I2Q0	PFI1270w	Hypothetical protein PFI1270w	24911	5.49	245	25	5
M25	Q8I3Z5	PFE0545c	Histamine releasing factor, putative	20024	4.48	189	26	4

M26	O97249	PFC0295c	40S Ribosom	15558	4.9	302	35	5
M27	Q8IIF0	PF11_0224	Circumsporozoite-related antigen	17285	5.64	357	22	6
M29	P32119	-	Human peroxiredoxin-2	21918	5.67	591	36	9
M30	P32119	-	Human peroxiredoxin-2	21918	5.67	381	26	7
M35	Q8IBP0	PF07_0087	Hypothetical protein PF07_0087	29631	8.76	271	31	8
M38	Q71T02	PF13_0141	L-lactate dehydrogenase	34314	7.12	582	35	12
M39	P00915	-	Human carbonic anhydrase 1	28778	6.63	568	48	9
M41	Q8IK90	PF14_0716	Proteosome subunit alpha type 1, putative	29219	5.51	309	23	4
M43	Q7Z0H0		Adenylate kinase 2	27822	8.97	518	45	10
MM1	P00489	-	Rabbit Glycogen phosphorylase	97610	6.76	275	15	11
MM2	P02769	-	Bovine Serum albumin [Precursor]	71274	5.82	510	16	10
MM3	P01012	-	Chicken ovalbumin	43196	5.19	922	40	15
MM4	P00921	-	Bovine carbonic anhydrase II	29096	6.41	469	38	6
MM5	1AVXB	-	Soybean trypsin inhibitor, chain B	19295	4.79	323	36	8
MM6	LABO	-	Bovine alpha lactalbumin	16692	4.93	57	7	1
List of proteins identified by MS/MS for SYPRO Ruby								
S1	Q25883	PF07_0029	Heat shock protein 86	86770	4.91	829	20	16
S2	Q8I2X4	PFI0875w	Heat shock protein					
S3	Q8I0V4	PFL1070c	Endoplasmin homolog, putative	95301	5.28	208	7	5
S4	Q8IB24	PF08_0054	Heat shock 70 kDa protein	74382	5.51	1345	38	19
S5	Q8II24	PF11_0351	Heat shock protein hsp70 homologue	73651	6.51	827	23	14
S6	P02769	-	Bovine Serum albumin [Precursor]	71274	5.82	745	22	14
S7	Q8IJN9	PF10_0153	Hsp60	62911	6.71	350	13	6
S8	Q8I6S6	MAL8P1.17	Disulfide isomerase, putative	55808	5.56	1075	40	16
S9	Q8IJN7	PF10_0155	Enolase	48989	6.21	727	31	10
S10	Q9GN14	PFI1090w	S-adenosylmethionine synthetase	45272	6.28	317	24	8
S11	Q6LFH8	PFF0435w	Ornithine aminotransferase	46938	6.47	378	19	8
S12	Q8II61	PF11_0313	Ribosomal phosphoprotein P0	35002	6.28	299	18	4
S13	Q8T6B1	PF14_0598	Glyceraldehyde-3-phosphate dehydrogenase	37068	7.59	425	30	7
S15	Q8IM15	PF14_0078	HAP protein	51889	8.05	494	25	10
S16	Q8IIR7	PF11_0098	Endoplasmic reticulum-resident calcium binding protein	39464	4.49	584	35	8
S18	Q8I3F3	PFE1590w	Early transcribed membrane protein	19132	5.26	202	20	2
S19	Q8IKC8	PF14_0678	Exported protein 2	33619	5.1	433	23	7
S20	Q8I6U5	PF11_0161	Falcipain 2, putative	56405	7.12	184	10	5
S21	Q8IIU5	PF11_0069	Hypothetical protein	32112	4.91	305	36	10
S22	Q8IDQ9	MAL13P1.214	Phosphoethanolamine N-methyltransferase, putative	31309	5.43	649	39	9
S23	Q8I2Q0	PFI1270w	Hypothetical protein PFI1270w	24911	5.49	116	15	3
S24	Q8I2Q0	PFI1270w	Hypothetical protein PFI1270w	24911	5.49	104	11	2
S25	Q8I3Z5	PFE0545c	Histamine releasing factor, putative	20024	4.48	129	11	3
S26	O97249	PFC0295c	40S Ribosomal protein S12, putative	15558	4.9	205	35	5
S27	Q8IIF0	PF11_0224	Circumsporozoite-related antigen	17285	5.64	293	21	4
S28	P00441	-	Human superoxide dismutase	16154	5.7	242	27	4
S32	Q8II72	PF11_0302	Hypothetical protein	52147	4.97	148	8	5
S33	Q7KQL5	PF10_0084	tubulin beta chain	50232	4.73	527	31	12
SM1	P00489	-	Rabbit Glycogen phosphorylase	97741	6.77	887	25	19
SM2	P02769	-	Bovine Serum albumin [Precursor]	71274	5.82	489	16	10
SM3	P01012	-	Chicken ovalbumin	43116	5.19	824	39	11
SM4	P00921	-	Bovine carbonic anhydrase II	28965	6.4	422	38	6
SM5	1AVXB	-	Soybean trypsin inhibitor, chain B	24346	4.99	265	26	6
List of proteins identified by MS/MS for Flamingo Pink								
F1	Q25883	PF07_0029	Heat shock protein 86	86770	4.91	848	17	16
F2	Q8I2X4	PFI0875w	Heat shock protein	72457	5.18	1518	36	18
F3	Q8I0V4	PFL1070c	Endoplasmin homolog, putative	95301	5.28	623	19	14
F4	Q8IB24	PF08_0054	Heat shock 70 kDa protein	74382	5.51	1401	42	23
F5	Q8II24	PF11_0351	Heat shock protein hsp70 homologue	73651	6.51	515	15	11
F6	P02769	-	Bovine Serum albumin [Precursor]	71274	5.82	612	20	11
F7	Q8IJN9	PF10_0153	Hsp60	62911	6.71	271	10	5
F8	Q8I6S6	MAL8P1.17	Disulfide isomerase, putative	55808	5.56	916	38	15
F9	Q8IJN7	PF10_0155	Enolase	48989	6.21	871	39	13
F10	Q9GN14	PFI1090w	S-adenosylmethionine synthetase	45272	6.28	678	40	13
F11	Q6LFH8	PFF0435w	Ornithine aminotransferase	46938	6.47	548	24	10
F12	Q8II61	PF11_0313	Ribosomal phosphoprotein P0	35002	6.28	569	45	13
F13	Q8T6B1	PF14_0598	Glyceraldehyde-3-phosphate dehydrogenase	37068	7.59	774	54	15
F15	Q8IM15	PF14_0078	HAP protein	51889	8.05	444	24	10
F16	Q8IIR7	PF11_0098	Endoplasmic reticulum-resident calcium binding protein	39464	4.49	849	48	13
F19	Q8IKC8	PF14_0678	Exported protein 2	33619	5.1	433	26	9
F20	Q8I6U5	PF11_0161	Falcipain 2, putative	56281	8.14	306	14	6
F21	Q8I2Q0	PFI1270w	Hypothetical protein PFI1270w	24911	5.49	299	31	7

F22	Q8IDQ9	MAL13P1.214	Phosphoetha	31309	5.43	910	59	13
F27	Q8IIF0	PF11_0224	Circumsporozoite-related antigen	17285	5.64	190	22	5
F28	DSHUCZ	-	Human superoxide dismutase	16154	5.7	198	37	4
F29	P32119	-	Human peroxiredoxin-2	21918	5.67	522	35	9
F30	P32119	-	Human peroxiredoxin-2	21918	5.67	523	29	8
F38	Q71T02	PF13_0141	L-lactate dehydrogenase	34314	7.12	622	43	13
F39	P00915	-	Human carbonic anhydrase 1	28778	6.63	624	55	11
F40	Q8IDQ9	MAL13P1.214	Phosphoethanolamine N-methyltransferase, putative	31309	5.43	499	39	9
F41	Q8IK90	PF14_0716	Proteosome subunit alpha type 1, putative	29218	5.51	100	5	1
F42	Q8IDQ9	MAL13P1.214	Phosphoethanolamine N-methyltransferase, putative	31309	5.43	632	44	10
F80	Q8IM15	PF14_0078	HAP protein	51889	8.05	288	21	9
F81	Q8IM15	PF14_0078	HAP protein	51889	8.05	629	35	13
F82	Q8IM15	PF14_0078	HAP protein	51889	8.05	614	30	12
F89	Q8I6U4	PF11_0165	Falcipain 2	56405	7.12	393	16	8
F90	Q8I6U5	PF11_0161	Falcipain 2, putative	56281	8.14	306	14	6
FM1	P00489	-	Rabbit Glycogen phosphorylase	97610	6.76	1375	34	28
FM2	P02769	-	Bovine Serum albumin [Precursor]	71274	5.82	807	19	13
FM3	P01012	-	Chicken ovalbumin	43196	5.19	922	40	15
FM4	P00921	-	Bovine carbonic anhydrase II	29096	6.41	583	47	9
FM5	1AVXB	-	Soybean trypsin inhibitor, chain B	24419	5	323	29	8
FM6	LABO	-	Bovine alpha lactalbumin	16692	4.93	57	7	1

[a]Spot number corresponds to marked spots on the various stain master images in Figure 3.4. [b]Accession number is obtained from the SwissProt UniProt database. [c]PlasmoDB ID is obtained from the PlasmoDB 6.0 database. [d]Mascot scores are based on MS/MS ion searches and is only taken when the score is significant ($p<0.05$). [e]Sequence coverage is given by Mascot for detected peptide sequences. [f]Matched is the number of peptides matched to the particular protein. C followed by number is indicative of spot number that was cut and identified by MS. CM is indicative of the standard molecular weight markers that was cut. M followed by number is indicative of spot number that was cut and identified by MS. MM is indicative of the standard molecular weight markers that was cut. S followed by number is indicative of spot number that was cut and identified by MS. SM is indicative of the standard molecular weight markers that was cut. F followed by number is indicative of spot number that was cut and identified by MS. FM is indicative of the standard molecular weight markers that was cut.

Appendix B

The differentially affected transcripts due to the inhibition of AdoMetDC

Total	Nr	PlasmoDB ID	Product Description	GO ID	Annotated GO Process	LogFC	FC	adj.P.Val
DNA metabolism								
1	1	MAL13P1.328	DNA topoisomerase VI, B subunit, putative	GO:0006259	Catalytic activity, ATP binding	1.48987	2.80864	1.32E-06
2	2	MAL13P1.346	DNA repair endonuclease, putative	GO:0006281	DNA repair	-1.0594	-2.084	0.001996
3	3	MAL13P1.42	recombinase, putative	GO:0015074	DNA recombination, DNA integration	-1.0702	-2.0997	0.001121
4	4	PF07_0023	DNA replication licensing factor mcm7 homologue, putative	GO:0006270	DNA replication initiation	-1.2721	-2.4151	3.61E-06
5	5	PF08_0126	DNA repair protein rad54, putative	GO:0006310	DNA recombination, double-strand break repair via homologous recombination	-0.8399	-1.7899	0.001887
6	6	PF10_0154	ribonucleotide reductase small subunit, putative	GO:0006260	DNA replication	-2.4224	-5.3606	1.14E-07
7	7	PF10_0165	DNA polymerase delta catalytic subunit	GO:0006260	DNA replication	-1.0257	-2.0359	0.000632
8	8	PF11_0061	histone H4	GO:0006334	nucleosome assembly, transcription initiation	-1.7751	-3.4225	4.76E-07
9	9	PF11_0062	histone H2B	GO:0006334	nucleosome assembly	-1.543	-2.914	0.000868
10	10	PF11_0087	Rad51 homolog	GO:0006281	DNA repair, DNA recombination	-0.7996	-1.7406	0.003805
11	11	PF11_0117	replication factor C subunit 5, putative	GO:0006271	DNA replication	-0.8698	-1.8275	0.001285
12	12	PF11_0241	Myb-like DNA-binding domain, putative	GO:0006259	null	0.75277	1.68502	0.034824
13	13	PF11_0282	deoxyuridine 5'-triphosphate nucleotidohydrolase, putative	GO:0006260	DNA replication	-2.6609	-6.3245	5.82E-06
14	14	PF13_0080	conserved Plasmodium protein, unknown function	GO:0006259	RNA-dependent DNA replication	-1.0513	-2.0724	0.002504
15	15	PF13_0095	DNA replication licensing factor MCM4-related	GO:0006268	DNA unwinding during replication	-1.631	-3.0973	3.24E-05
16	16	PF13_0149	chromatin assembly factor 1 subunit, putative	GO:0006333	chromatin assembly or disassembly	-1.5123	-2.8527	0.000207
17	17	PF13_0176	apurinic/apyrimidinic endonuclease Apn1	GO:0006281	DNA repair	-0.8765	-1.8359	0.023412
18	18	PF13_0291	replication licensing factor, putative	GO:0006270	DNA replication initiation	-1.3354	-2.5235	0.000325
19	19	PF13_0328	proliferating cell nuclear antigen	GO:0006275	regulation of DNA replication	-2.5146	-5.7144	1.51E-11
20	20	PF14_0053	ribonucleotide reductase small subunit	GO:0006260	DNA replication	-1.9647	-3.9034	6.96E-06
21	21	PF14_0148	uracil-DNA glycosylase, putative	GO:0006284	base-excision repair	-0.7987	-1.7395	0.015932
22	22	PF14_0177	DNA replication licensing factor MCM2	GO:0006270	DNA replication initiation	-1.0135	-2.0187	0.004041
23	23	PF14_0254	DNA mismatch repair protein Msh2p, putative	GO:0006298	mismatch repair	-0.9089	-1.8776	0.000548
24	24	PF14_0352	ribonucleoside-diphosphate reductase, large subunit	GO:0006260	DNA replication	-1.0587	-2.083	0.00041
25	25	PF14_0366	small subunit DNA primase	GO:0006269	DNA replication	-0.7398	-1.6699	0.044267
26	26	PF14_0374	CCAAT-binding transcription factor, putative	GO:0006259	null	0.78164	1.71908	0.029176
27	27	PF14_0602	DNA polymerase alpha subunit, putative	GO:0006269	DNA replication	-1.2062	-2.3073	0.000868
28	28	PFB0840w	replication factor C, subunit 2	GO:0006260	DNA replication	-1.7554	-3.3762	1.32E-06
29	29	PFB0895c	replication factor C subunit 1, putative	GO:0006260	DNA replication	-0.9455	-1.9259	0.001076
30	30	PFC0250c	AP endonuclease (DNA-[apurinic or apyrimidinic site] lyase), putative	GO:0006281	DNA repair	-0.776	-1.7123	0.00579
31	31	PFC0765c	conserved Plasmodium protein, unknown function	GO:0006260	DNA replication	-1.3613	-2.5691	0.006478
32	32	PFD0590c	DNA polymerase alpha	GO:0006260	DNA replication	-1.0291	-2.0407	0.000163
33	33	PFD0685c	chromosome associated protein, putative	GO:0006259	chromosome organization	-1.0345	-2.0484	0.005887
34	34	PFE0215w	ATP-dependent helicase, putative	GO:0006259	null	-0.7904	-1.7296	0.026565
35	35	PFE0270c	DNA repair protein, putative	GO:0006298	mismatch repair, DNA repair	-1.7925	-3.4641	0.000104
36	36	PFE0450w	chromosome condensation protein, putative	GO:0006259	chromosome organization	-1.381	-2.6045	0.001282

37	37	PFE0675c	deoxyribodipyrimidine photolyase (photoreactivating enzyme, DNA photolyase), putative	GO:0006281	DNA repair	-1.4742	-2.7783	0.000104
38	38	PFE1255w	conserved Plasmodium protein, unknown function	GO:0006259	chromosome organization	-0.7247	-1.6525	0.004461
39	39	PFE1345c	minichromosome maintenance protein 3, putative	GO:0006270	DNA replication initiation	-1.2134	-2.3189	0.000104
40	40	PFF0510w	histone H3	GO:0006333	nucleosome assembly	-2.1132	-4.3265	0.000524
41	41	PFF0865w	histone H3	GO:0006334	chromosome organization	-0.8174	-1.7622	0.000934
42	42	PFF1225c	DNA polymerase 1, putative	GO:0006260	DNA replication	-1.021	-2.0294	0.008609
43	43	PFF1470c	DNA polymerase epsilon, catalytic subunit a, putative	GO:0006261	DNA-dependent DNA replication	-0.812	-1.7556	0.000789
44	44	PFI0530c	DNA primase large subunit, putative	GO:0006269	DNA replication, synthesis of RNA primer	-1.9163	-3.7745	2.11E-06
45	45	PFL0150w	origin recognition complex 1 protein	GO:0006270	DNA replication initiation	-1.3542	-2.5565	0.00025
46	46	PFL0580w	DNA replication licensing factor MCM5, putative	GO:0006270	DNA replication initiation, DNA strand elongation	-1.8999	-3.7318	1.33E-05
47	47	PFL1180w	chromatin assembly protein (ASF1), putative	GO:0016458	gene silencing	-1.1375	-2.2	0.000169
48	48	PFL1285c	proliferating cell nuclear antigen 2	GO:0006275	regulation of DNA replication	-1.4194	-2.6748	0.011427
49	49	PFL1655c	DNA polymerase epsilon subunit B, putative	GO:0006260	DNA replication	-1.0389	-2.0546	0.015356
50	50	PFL2005w	replication factor C subunit 4	GO:0006260	DNA replication	-2.009	-4.0249	2.70E-07
Proteolysis								
51	1	MAL13P1.25	conserved Plasmodium protein, unknown function	GO:0006508	null	-1.2518	-2.3813	0.000944
52	2	MAL13P1.270	proteasome subunit, putative	GO:0006511	ubiquitin-dependent protein catabolic process	-0.8733	-1.8318	0.000339
53	3	MAL8P1.113	Peptidase family C50, putative	GO:0006508	proteolysis	-0.734	-1.6632	0.034431
54	4	MAL8P1.140	methionine aminopeptidase, putative	GO:0006508	proteolysis	-1.0168	-2.0234	0.003717
55	5	MAL8P1.75	ubiquitin-activating enzyme, putative	GO:0006464	protein modification process	-0.8558	-1.8098	0.03803
56	6	MAL8P1.99	GTPase, putative	GO:0006508	proteolysis	-1.0411	-2.0577	0.016593
57	7	PF11_0174	cathepsin C, homolog	GO:0006508	proteolysis	0.75926	1.69262	0.029384
58	8	PF13_0084	ubiquitin-like protein, putative	GO:0006464	protein modification process, modification-	0.72972	1.65832	0.010017
59	9	PF14_0348	ATP-dependent Clp protease proteolytic subunit, putative	GO:0006508	proteolysis	-1.0124	-2.0173	0.006525
60	10	PFB0330c	serine repeat antigen 7 (SERA-7)	GO:0006508	proteolysis	-0.7234	-1.6511	0.008836
61	11	PFC0855w	ubiquitin conjugating enzyme, putative	GO:0006464	regulation of protein metabolic process	-0.8927	-1.8567	0.012616
62	12	PFE0870w	transcriptional regulator, putative	GO:0006508	proteolysis, transcription	-0.7907	-1.7299	0.0263
63	13	PFE1355c	ubiquitin carboxyl-terminal hydrolase, putative	GO:0006511	ubiquitin-dependent protein catabolic process	-0.9467	-1.9275	0.006556
64	14	PFF0420c	proteasome subunit alpha type 2, putative	GO:0006511	ubiquitin-dependent protein catabolic process	-0.9812	-1.9741	4.01E-05
65	15	PFI0135c	serine repeat antigen 9 (SERA-9)	GO:0006508	proteolysis	-2.4916	-5.6239	1.21E-08
66	16	PFI0810c	apicoplast Ufd1 precursor	GO:0006511	ubiquitin-dependent protein catabolic process	-1.0179	-2.025	0.000159
67	17	PFL1465c	Heat shock protein hslv	GO:0006511	ubiquitin-dependent protein catabolic process	-1.0168	-2.0234	0.001997
Translation								
68	1	MAL8P1.110	apicoplast ribosomal protein L33 precursor, putative	GO:0006412	translation	-0.9003	-1.8664	0.002779
69	2	PF11_0113	mitochondrial ribosomal protein L11 precursor, putative	GO:0006412	translation	-1.0129	-2.018	0.002101
70	3	PF11_0181	tyrosine-tRNA ligase, putative	GO:0006437	tyrosyl-tRNA aminoacylation	-0.9572	-1.9416	0.005929
71	4	PF11_0182	conserved Plasmodium protein, unknown function	GO:0006415	translational termination	-0.8945	-1.8589	0.004045
72	5	PF11_0386	apicoplast ribosomal protein S14p/S29e precursor, putative	GO:0006412	translation	-1.0163	-2.0227	0.004578
73	6	PF14_0289	mitochondrial ribosomal protein L17-2 precursor, putative	GO:0006412	translation	-1.864	-3.64	3.49E-07
74	7	PF14_0606	mitochondrial ribosomal protein S6-2 precursor, putative	GO:0006412	translation	-1.1322	-2.192	0.000215
75	8	PF14_0709	mitochondrial ribosomal protein L20 precursor, putative	GO:0006412	translation	-1.0767	-2.1092	0.001788
76	9	PFB0390w	apicoplast ribosomal releasing factor precursor, putative	GO:0006412	translation	-0.9242	-1.8977	0.047945
77	10	PFB0645c	mitochondrial large ribosomal subunit, putative	GO:0006412	translation	-1.2275	-2.3417	0.003213
78	11	PFC0675c	mitochondrial ribosomal protein L29/L47 precursor, putative	GO:0006412	translation	-0.9066	-1.8747	0.00679
79	12	PFC0701w	mitochondrial ribosomal protein L27 precursor, putative	GO:0006412	translation	-1.32	-2.4967	2.29E-05
80	13	PFD0675w	apicoplast ribosomal protein L10 precursor, putative	GO:0006412	translation	-1.5395	-2.9069	0.048763
81	14	PFD0780w	glutamyl-tRNA(Gln) amidotransferase subunit A, putative	GO:0006412	translation	-0.9774	-1.969	0.002314
82	15	PFE0960w	mitochondrial ribosomal protein L14 precursor, putative	GO:0006412	translation	-0.9493	-1.9309	0.020063
83	16	PFF0495w	mitochondrial ribosomal protein L19 precursor, putative	GO:0006412	translation	-1.0037	-2.0051	0.003254
84	17	PFF0650w	apicoplast ribosomal protein L18 precursor, putative	GO:0042254	ribosome biogenesis, translation	-0.9535	-1.9366	0.001777
85	18	PFF1395c	glutamyl-tRNA(Gln) amidotransferase subunit B, putative	GO:0006424	glutamyl-tRNA aminoacylation, translation	-0.789	-1.7279	0.004166

86	19	PFI0380c	formylmethionine deformylase, putative	GO:0006412	translation	-0.8662	-1.8229	0.006232
87	20	PFI0890c	organelle ribosomal protein L3 precursor, putative	GO:0006412	translation	-1.1291	-2.1873	0.003978
88	21	PFI1240c	prolyl-t-RNA synthase, putative	GO:0006418	tRNA aminoacylation for protein translation	-1.4703	-2.7708	0.000225
89	22	PFI1575c	peptide release factor, putative	GO:0006415	translational termination	-1.4527	-2.7373	0.000503
90	23	PFI1585c	mitochondrial ribosomal protein S6 precursor, putative	GO:0006412	translation	-0.8202	-1.7657	0.01119
91	24	PFL1150c	mitochondrial ribosomal protein L24-2 precursor, putative	GO:0006412	translation, ribosome biogenesis	-0.7627	-1.6966	0.002721
92	25	PFL1590c	elongation factor G, putative	GO:0006414	translational elongation	-0.7568	-1.6898	0.006525
93	26	PFL1895w	mitochondrial ribosomal protein L23 precursor, putative	GO:0006412	translation	-0.7497	-1.6815	0.038466
Phosphorylation								
94	1	MAL13P1.278	serine/threonine protein kinase, putative	GO:0006468	protein amino acid phosphorylation	1.05398	2.07626	0.035788
95	2	MAL7P1.132	conserved Plasmodium protein, unknown function	GO:0006468	protein amino acid phosphorylation	-0.9639	-1.9505	0.019017
96	3	MAL7P1.144	Serine/Threonine protein kinase, FIKK family	GO:0006468	protein amino acid phosphorylation	0.98588	1.98052	0.016411
97	4	PF11_0377	casein kinase 1, PfCK1	GO:0006468	protein amino acid phosphorylation	-1.0443	-2.0623	0.009823
98	5	PF13_0258	serine/threonine protein kinase	GO:0006468	protein amino acid phosphorylation	-1.3263	-2.5076	0.000776
99	6	PF14_0142	serine/threonine protein phosphatase	GO:0006470	protein amino acid dephosphorylation	-1.328	-2.5106	0.000346
100	7	PFA0130c	Serine/Threonine protein kinase, FIKK family, putative	GO:0006468	protein amino acid phosphorylation	1.21443	2.32049	0.001022
101	8	PFB0815w	Calcium-dependent protein kinase 1	GO:0006468	protein amino acid phosphorylation	1.57348	2.97621	0.04031
102	9	PFC0485w	protein kinase, putative	GO:0006468	protein amino acid phosphorylation	-0.7621	-1.6959	0.005929
103	10	PFC0710w	inorganic pyrophosphatase, putative	GO:0006796	phosphate metabolic process	-1.4027	-2.6439	8.19E-05
104	11	PFC0755c	protein kinase, putative	GO:0006468	protein amino acid phosphorylation	-1.0395	-2.0555	0.009593
105	12	PFD1165w	Serine/Threonine protein kinase, FIKK family	GO:0006468	protein amino acid phosphorylation	0.99581	1.99421	0.016855
106	13	PFD1175w	Serine/Threonine protein kinase, FIKK family	GO:0006468	protein amino acid phosphorylation	1.23584	2.35518	1.84E-05
107	14	PFF0260w	serine/threonine protein kinase, Pfnek-5	GO:0006468	protein amino acid phosphorylation	-0.792	-1.7314	0.011966
108	15	PFF1370w	protein kinase PK4	GO:0006468	protein amino acid phosphorylation	0.74596	1.67709	0.012842
109	16	PFL1110c	CAMP-dependent protein kinase regulatory subunit, putative	GO:0006468	regulation of protein amino acid phosphorylation	-1.0569	-2.0804	0.007751
110	17	PFL1885c	calcium/calmodulin-dependent protein kinase 2	GO:0006468	protein amino acid phosphorylation	1.1697	2.24966	0.003213
Transport								
111	1	MAL13P1.16	SNARE protein, putative	GO:0006810	vesicle-mediated transport	-1.1293	-2.1875	0.020178
112	2	MAL13P1.23	CorA-like Mg2+ transporter protein, putative	GO:0030001	metal ion transport	0.82698	1.77397	0.021423
113	3	MAL7P1.340	ATP synthase subunit C, putative	GO:0015986	ATP synthesis coupled proton transport	-0.9988	-1.9984	0.001997
114	4	MAL8P1.32	nucleoside transporter, putative	GO:0015986	nucleoside transport	-1.4673	-2.765	1.67E-05
115	5	PF07_0065	zinc transporter, putative	GO:0030001	zinc ion transport	-2.2527	-4.7658	1.77E-07
116	6	PF11_0098	endoplasmic reticulum-resident calcium binding protein	GO:0006810	intracellular protein transport	-0.8198	-1.7652	0.011936
117	7	PF13_0041	conserved Plasmodium protein	GO:0006810	intracellular protein transport	-0.7443	-1.6752	0.026774
118	8	PF14_0211	Ctr copper transporter domain containing protein, putative	GO:0030001	copper ion transport	-1.2123	-2.3171	0.001022
119	9	PF14_0321	ABC transporter, putative	GO:0006810	transport	-0.8365	-1.7857	0.009928
120	10	PF14_0662	nucleoside transporter, putative	GO:0006810	transport	0.83567	1.78468	0.024563
121	11	PFA0590w	ABC transporter, (CT family), putative	GO:0006810	transport	-1.2602	-2.3953	2.17E-05
122	12	PFB0500c	Rab5a, GTPase	GO:0015031	protein transport	-0.8045	-1.7466	0.008088
123	13	PFC0125w	ABC transporter, (TAP family), putative	GO:0006810	multidrug transport	-0.915	-1.8856	0.003674
124	14	PFE0410w	triose phosphate transporter	GO:0006810	Transport	-0.7265	-1.6546	0.036221
125	15	PFE1510c	triose phosphate transporter	GO:0006810	transport	-1.327	-2.5088	0.00256
126	16	PFI0240c	Cu2+ -transporting ATPase, Cu2+ transporter	GO:0030001	metal ion transport, metabolic process	-0.9036	-1.8707	0.025984
127	17	PFI0300w	developmental protein, putative	GO:0015031	protein transport	-1.6875	-3.2211	4.07E-07
128	18	PFL1410c	ABC transporter, (CT family)	GO:0006810	transport	0.76578	1.70029	0.00209
129	19	PFL2220w	conserved Plasmodium protein, unknown function	GO:0006810	vesicle-mediated transport	0.75398	1.68644	0.019658
Polyamine methionine								
130	1	MAL13P1.214	phosphoethanolamine N-methyltransferase	GO:0006656	phosphatidylcholine biosynthetic process	-2.35	-5.0984	2.48E-05
131	2	PF10_0121	hypoxanthine phosphoribosyltransferase	GO:0006730	purine ribonucleoside salvage	-0.7731	-1.7089	0.014128
132	3	PF10_0289	adenosine deaminase, putative	GO:0009168	purine ribonucleoside monophosphate biosynthetic	-1.6534	-3.1458	5.35E-05
133	4	PF13_0016	methyl transferase-like protein, putative	GO:0006464	methylation	-0.9245	-1.898	0.001369
134	5	PF14_0309	protein-L-isoaspartate O-methyltransferase beta-aspartate	GO:0006464	protein modification process, protein repair	-1.9495	-3.8625	2.34E-07

135	6	PF14_0526	conserved Plasmodium protein, unknown function	GO:0016787	metabolic process, biological_process	-1.6173	-3.0681	1.05E-05
136	7	PFD0285c	lysine decarboxylase, putative	GO:0006554	lysine catabolic process	1.30051	2.46316	8.63E-06
137	8	PFE0660c	purine nucleotide phosphorylase, putative	GO:0009116	nucleoside metabolic process	-1.6031	-3.0379	1.14E-07
138	9	PFE1050w	adenosylhomocysteinase	GO:0006730	one-carbon compound metabolic process	-1.0572	-2.0808	4.40E-05
139	10	PFI1090w	S-adenosylmethionine synthetase	GO:0006730	one-carbon compound metabolic process	-1.2189	-2.3276	0.000462
140	11	PFL1475w	sun-family protein, putative	GO:0016787	metabolic process	-0.8098	-1.7529	0.011921
141	12	PFL1775c	s-adenosyl-methyltransferase, putative	GO:0006464	biological_process	-0.7291	-1.6576	0.023176
142	13	PFL2465c	thymidylate kinase	GO:0016787	dTDP biosynthetic process, dTTP biosynthetic process	-1.4418	-2.7166	3.17E-06
oxidative stress								
143	1	PF08_0071	Fe-superoxide dismutase	GO:0000679	response to oxidative stress	-1.0267	-2.0374	0.000597
144	2	PF08_0131	1-cys peroxiredoxin	GO:0000679	response to oxidative stress	-1.4511	-2.7341	0.000389
145	3	PF14_0187	glutathione S-transferase	GO:0000679	response to oxidative stress	-0.8293	-1.7768	0.010656
146	4	PF14_0192	glutathione reductase	GO:0000679	response to oxidative stress	-1.108	-2.1555	0.001222
147	5	PF14_0545	thioredoxin, putative	GO:0000679	response to oxidative stress	-1.6222	-3.0784	0.000829
148	6	PFL0595c	glutathione peroxidase	GO:0000679	response to oxidative stress	-1.1247	-2.1805	0.00664
Primary metabolism								
149	1	MAL13P1.218	UDP-N-acetylglucosamine pyrophosphorylase, putative	GO:0006047	UDP-N-acetylglucosamine metabolic process	-0.7698	-1.705	0.048791
150	2	MAL13P1.220	lipoate synthase, putative	GO:0009107	lipoate biosynthetic process	-0.7551	-1.6877	0.008278
151	3	MAL13P1.285	patatin-like phospholipase, putative	GO:0006629	lipid metabolic process	-0.8129	-1.7567	0.010297
152	4	MAL8P1.81	Phosphopantothenoylcysteine decarboxylase, putative	GO:0009152	null	0.96039	1.94584	0.000789
153	5	PF07_0129	acyl-coA synthetase, PfACS5	GO:0006631	fatty acid metabolic process	-0.956	-1.9399	0.000462
154	6	PF10_0016	acyl CoA binding protein, isoform 2, ACBP2	GO:0006631	fatty acid metabolic process	-1.5763	-2.9821	2.48E-05
155	7	PF10_0155	enolase	GO:0006096	glycolysis, gluconeogenesis	-1.4245	-2.6842	4.16E-06
156	8	PF10_0169	phosphomannomutase, putative	GO:0019307	GDP-mannose biosynthetic process	1.04627	2.06519	0.000254
157	9	PF10_0334	flavoprotein subunit of succinate dehydrogenase	GO:0006099	tricarboxylic acid cycle	-0.8543	-1.8079	0.008835
158	10	PF11_0257	ethanolamine kinase, putative	GO:0006629	lipid metabolic process, phosphatidylcholine	-1.3081	-2.4761	8.37E-06
159	11	PF13_0121	dihydrolipamide succinyltransferase component of 2-oxoglutarate dehydrogenase complex	GO:0006103	2-oxoglutarate metabolic process	-1.4046	-2.6475	0.000609
160	12	PF13_0141	L-lactate dehydrogenase	GO:0006100	anaerobic glycolysis	-0.8966	-1.8617	0.001996
161	13	PF13_0242	isocitrate dehydrogenase (NADP), mitochondrial precursor	GO:0006102	isocitrate metabolic process	-1.1511	-2.2209	1.05E-05
162	14	PF13_0349	nucleoside diphosphate kinase b, putative	GO:0009152	GTP biosynthetic process	-1.8054	-3.4954	0.009466
163	15	PF14_0378	triosephosphate isomerase	GO:0006096	glycolysis	-0.7757	-1.7121	0.023504
164	16	PFA0555c	UMP-CMP kinase, putative	GO:0006221	pyrimidine nucleotide biosynthetic process	-1.5145	-2.8571	0.003737
165	17	PFB0385w	apicoplast ACP	GO:0006633	fatty acid biosynthetic process	-1.4011	-2.6411	0.000326
166	18	PFB0505c	3-oxoacyl-(acyl carrier protein) synthase III, putative	GO:0006633	fatty acid biosynthetic process	-1.0612	-2.0866	0.002393
167	19	PFC0275w	FAD-dependent glycerol-3-phosphate dehydrogenase,	GO:0006072	glycerol-3-phosphate metabolic process	-0.8709	-1.8288	0.007514
168	20	PFC0395w	asparagine synthetase, putative	GO:0006529	asparagine biosynthetic process	-0.7346	-1.6639	0.003331
169	21	PFD0311w	cytosolic glyoxalase II	GO:0006089	Lactate metabolic process	0.78996	1.72902	0.03332
170	22	PFD0830w	bifunctional dihydrofolate reductase-thymidylate synthase	GO:0006730	one-carbon compound metabolic process	-2.2973	-4.9153	1.07E-08
171	23	PFE0555w	stearoyl-CoA Delta 9 desaturase, putative	GO:0006629	fatty acid biosynthetic process	-1.85	-3.605	0.000831
172	24	PFF0680c	thiamin-phosphate pyrophosphorylase, putative	GO:0009228	thiamin biosynthetic process	-1.629	-3.0931	1.52E-06
173	25	PFF0895w	malate dehydrogenase	GO:0006100	glycolysis, tricarboxylic acid cycle	-1.1707	-2.2513	0.017555
174	26	PFF1300w	pyruvate kinase	GO:0006096	glycolysis	-0.7933	-1.733	0.004025
175	27	PFI0960w	dolichyl-diphosphooligosaccharide-protein glycosyltransferase, putative	GO:0018279	protein amino acid N-linked glycosylation via asparagine	-0.7505	-1.6824	0.048293
176	28	PFL0415w	mitochondrial ACP precursor	GO:0006633	fatty acid biosynthetic process	-0.738	-1.6679	0.030195
177	29	PFL1720w	serine hydroxymethyltransferase	GO:0006544	one-carbon compound metabolic process	-2.2755	-4.8417	1.55E-06
178	30	PFL2030w	queuine tRNA-ribosyltransferase, putative	GO:0008616	queuosine biosynthetic process	-0.7346	-1.6639	0.031713
Cytoskeleton organization and								
179	1	PF10_0084	tubulin beta chain, putative	GO:0007017	microtubule cytoskeleton organization	-2.3862	-5.228	3.53E-07
180	2	PF10_0224	dynein heavy chain, putative	GO:0007017	microtubule-based movement	-1.3601	-2.5671	0.001384
181	3	PF11_0478	kinesin-like protein, putative	GO:0007018	microtubule-based movement	1.06545	2.09283	0.046894

182	4	PF14_0314	chromatin assembly factor 1 P55 subunit, putative	GO:0006334	nucleosome assembly	1.03554	2.04988	0.013309
183	5	PFA0520c	chromatin assembly factor 1 protein WD40 domain, putative	GO:0006334	nucleosome assembly	-2.2285	-4.6864	1.07E-08
184	6	PFE0165w	actin-depolymerizing factor, putative	GO:0030042	actin filament depolymerization	-1.1342	-2.195	5.88E-05
185	7	PFI0180w	alpha tubulin	GO:0007017	microtubule-based movement, protein	-2.8643	-7.2816	1.13E-11
186	8	PFI1565w	profilin, putative	GO:0007010	cytoskeleton organization	-1.5753	-2.9799	4.40E-05
187	9	PFL0925w	formin 2, putative	GO:0000910	actin cytoskeleton organization, cytokinesis	0.96744	1.95536	0.027169
188	10	PFL2215w	actin I	GO:0007010	cytoskeleton organization	-1.3261	-2.5073	4.14E-06
RNA metabolic process								
189	1	MAL13P1.303	polyadenylate-binding protein, putative	GO:0006396	RNA processing	-2.0479	-4.1351	2.23E-08
190	2	MAL8P1.101	RNA binding protein, putative	GO:0006396	RNA processing	-0.7539	-1.6864	0.01538
191	3	MAL8P1.72	high mobility group protein	GO:0006359	regulation of transcription from RNA polymerase III promoter	-0.7429	-1.6736	0.025947
192	4	PF08_0096	RNA helicase, putative	GO:0006396	RNA processing	-0.777	-1.7136	0.017932
193	5	PF10_0313	mitochondrial preribosomal assembly protein rimM	GO:0006364	rRNA processing	-0.9406	-1.9194	0.001973
194	6	PF13_0043	CCAAT-binding transcription factor, putative	GO:0006355	regulation of transcription, DNA-dependent	-0.8209	-1.7665	0.030195
195	7	PFD0750w	nuclear cap-binding protein, putative	GO:0006397	mRNA processing	-0.8402	-1.7903	0.04735
196	8	PFF1425w	RNA binding protein, putative	GO:0006396	RNA processing	-1.1017	-2.146	0.004767
197	9	PFL0465c	Zinc finger transcription factor (krox1)	GO:0006355	regulation of transcription, DNA-dependent	0.80926	1.75231	0.01026
198	10	PFL2115c	glucose inhibited division protein A homologue, putative	GO:0008033	tRNA processing	-1.5443	-2.9166	1.05E-05
Protein folding								
199	1	MAL13P1.283	TCP-1/cpn60 chaperonin family, putative	GO:0006457	protein folding	-0.7294	-1.6579	0.02857
200	2	PF11_0188	heat shock protein 90, putative	GO:0006457	protein folding, response to unfolded protein	-0.9595	-1.9447	0.016142
201	3	PF11_0352	protein disulfide isomerase	GO:0006467	cell redox homeostasis, protein folding	-0.8667	-1.8235	0.034431
202	4	PF11_0513	DNAJ protein, putative	GO:0006457	protein folding	0.77122	1.70671	0.004744
203	5	PFB0920w	DNAJ protein, putative	GO:0006457	protein folding	1.24227	2.3657	0.008609
204	6	PFL0120c	cyclophilin, putative	GO:0006457	protein folding	-0.8693	-1.8268	0.001361
205	7	PFL2550w	DNAJ domain protein, putative	GO:0006457	protein folding	-1.0136	-2.019	0.000707
Signal transduction								
206	1	MAL13P1.165	GPI transamidase subunit PIG-U, putative	GO:0006506	GPI anchor biosynthetic process	-0.7413	-1.6717	0.017537
207	2	MAL13P1.19	peptidase, putative	GO:0032012	null	-1.2705	-2.4125	0.001134
208	3	MAL13P1.205	Rab11b, GTPase	GO:0007264	small GTPase mediated signal transduction	-0.9526	-1.9353	0.004701
209	4	PF14_0317	Microsomal signal peptidase protein, putative	GO:0006465	signal peptide processing	-0.7569	-1.6899	0.020048
210	5	PFA0335w	Rab5c, GTPase	GO:0007264	small GTPase mediated signal transduction	-1.129	-2.1871	0.001276
211	6	PFE0690c	PfRab1a	GO:0007264	small GTPase mediated signal transduction	-0.8196	-1.7649	0.012142
212	7	PFI0155c	PfRab7, GTPase	GO:0007264	small GTPase mediated signal transduction	-0.777	-1.7136	0.003503
213	8	PFI0215c	signal peptidase, putative	GO:0006465	signal peptide processing	-0.8082	-1.7511	0.015665
214	9	PFI1005w	ADP-ribosylation factor-like protein	GO:0007264	small GTPase mediated signal transduction	-0.9795	-1.9718	0.017957
Coenzyme metabolic process								
215	1	MAL7P1.130	3-demethylubiquinone-9 3-methyltransferase, putative	GO:0006744	ubiquinone biosynthetic process	-0.7675	-1.7023	0.007692
216	2	PF13_0140	dihydrofolate synthase/folylpolyglutamate synthase	GO:0009396	folic acid and derivative biosynthetic process	-0.8106	-1.754	0.0165
217	3	PF14_0200	pantothenate kinase, putative	GO:0015937	coenzyme A biosynthetic process	-0.7489	-1.6805	0.014431
218	4	PF14_0415	dephospho-CoA kinase, putative	GO:0015937	coenzyme A biosynthetic process	-1.3524	-2.5533	0.000208
219	5	PFB0220w	ubiE/COQ5 methyltransferase family, putative	GO:0045426	quinone cofactor biosynthetic process	-1.23	-2.3456	0.000346
220	6	PFL1725w	ATP synthase beta chain, mitochondrial precursor, putative	GO:0006754	hydrogen transport, ATP synthesis coupled proton transport	-1.0458	-2.0646	0.003596
Hydrolase activity								
221	1	MAL13P1.121	adenosine-diphosphatase	GO:0016787	null	-0.8305	-1.7783	0.004701
222	2	PF14_0015	aminopeptidase, putative	GO:0016787	biological_process	1.30733	2.47483	0.032832
223	3	PF14_0017	lysophospholipase, putative	GO:0016787	biological_process	1.24572	2.37137	0.000344
224	4	PF14_0738	lysophospholipase, putative	GO:0016787	biological_process	0.84297	1.79374	0.026576

225	5	PFE1305c	ADP-ribosylation factor GTPase-activating protein, putative	GO:0043087	regulation of ARF GTPase activity, regulation of GTPase activity	-0.792	-1.7315	0.019802
Binding activity								
226	1	MAL13P1.122	SET domain protein, putative	GO:0008270	protein binding, zinc ion binding	0.74727	1.67861	0.030594
227	2	MAL13P1.337	Skp1 family protein, putative	GO:0005488	protein binding	-0.9096	-1.8785	0.010945
228	3	MAL8P1.69	14-3-3 protein, putative	GO:0019904	protein domain specific binding	-0.8588	-1.8136	0.015714
229	4	PF07_0035	cg1 protein	GO:0005488	protein binding	-1.4136	-2.664	0.000713
230	5	PF08_0054	heat shock 70 kDa protein	GO:0005488	response to unfolded protein, heat, ATP binding	-0.9421	-1.9213	0.012616
231	6	PF08_0063	ClpB protein, putative	GO:0005488	protein binding	-0.7873	-1.7259	0.014017
232	7	PF08_0118	conserved Plasmodium protein, unknown function	GO:0008270	zinc ion binding	1.16145	2.23682	0.034051
233	8	PF10_0271	centrin-3	GO:0005509	calcium ion binding	-1.4616	-2.7542	0.001222
234	9	PF11_0044	iron-sulfur assembly protein, sufD, putative	GO:0003674	protein binding	-0.8102	-1.7535	0.001205
235	10	PF11_0074	exonuclease, putative	GO:0005488	nucleic acid binding	-0.8399	-1.7899	0.03318
236	11	PF11_0486	MAEBL, putative	GO:0005488	binding	-0.8387	-1.7884	0.036834
237	12	PF13_0314	conserved Plasmodium protein, unknown function	GO:0008270	zinc ion binding, nucleic acid binding	1.98741	3.96525	0.000462
238	13	PF14_0061	PPR repeat protein	GO:0003674	nucleic acid binding	-0.9161	-1.887	0.011912
239	14	PF14_0257	conserved protein, unknown function	GO:0005515	protein binding	-1.5217	-2.8714	2.05E-06
240	15	PF14_0305	leucine-rich repeat protein 5, LRR5	GO:0005515	protein binding	-1.5022	-2.8327	0.000375
241	16	PF14_0413	CAF1 family ribonuclease, putative	GO:0005488	nucleic acid binding	-0.8857	-1.8477	0.006339
242	17	PF14_0443	centrin-2	GO:0005509	calcium ion binding	-2.2899	-4.8904	8.75E-09
243	18	PF14_0479	conserved Plasmodium protein, unknown function	GO:0008270	zinc ion binding, protein binding	0.83169	1.77977	0.036486
244	19	PFC0190c	EH (Eps15 homology) protein	GO:0005525	protein binding, GTP binding	0.7825	1.72011	0.01579
245	20	PFD0440w	peptidase, M22 family, putative	GO:0005488	zinc ion binding	-1.4319	-2.6981	0.000215
246	21	PFF0155w	Bcs1 protein, putative	GO:0005488	protein complex assembly	-0.8055	-1.7477	0.029559
247	22	PFF1180w	anaphase-promoting complex subunit, putative	GO:0005515	zinc ion binding, protein binding	-1.6559	-3.1512	6.96E-06
248	23	PFF1440w	SET domain protein, putative	GO:0005488	zinc ion binding	0.92613	1.90017	0.015665
249	24	PFI0235w	replication factor A-related protein, putative	GO:0003676	nucleic acid binding	-1.1043	-2.15	0.000713
250	25	PFI0490c	ran-binding protein, putative	GO:0005488	binding	-0.7284	-1.6568	0.007949
251	26	PFI0855w	conserved Plasmodium protein, unknown function	GO:0031072	heat shock protein binding	-0.9763	-1.9674	0.011163
Electron transport								
252	1	PF13_0353	NADH-cytochrome B5 reductase, putative	GO:0006118	electron carrier activity	-1.0751	-2.1068	0.042408
253	2	PF14_0248	ubiquinol-cytochrome c reductase hinge protein, putative	GO:0006122	mitochondrial electron transport, ubiquinol to cytochrome c	-0.839	-1.7888	0.011016
254	3	PF14_0597	cytochrome c1 precursor, putative	GO:0006118	electron carrier activity	-1.6755	-3.1943	0.001094
255	4	PFI1170c	thioredoxin reductase	GO:0006118	cell redox homeostasis	-0.9212	-1.8937	0.008668
256	5	PFI1250w	thioredoxin-like protein 2	GO:0045454	cell redox homeostasis	-0.8073	-1.7499	0.003539
257	6	PFL1550w	lipoamide dehydrogenase	GO:0006118	cell redox homeostasis	-1.2073	-2.309	0.013234
Host parasite								
258	1	MAL13P1.176	reticulocyte binding protein 2, homolog b	GO:0030260	entry into host cell	0.91731	1.88859	0.04735
259	2	PF07_0051	erythrocyte membrane protein 1, PfEMP1	GO:0002033	cell-cell adhesion, pathogenesis	0.96956	1.95824	0.000894
260	3	PF07_0138	rifin	GO:0002033	antigenic variation	-1.0778	-2.1108	0.024047
261	4	PF10_0002	rifin	GO:0002033	antigenic variation	-1.3987	-2.6366	2.65E-05
262	5	PF14_0138	conserved protein, unknown function	GO:0007155	null	-0.8143	-1.7585	0.006096
263	6	PFA0010c	rifin	GO:0002033	antigenic variation	-1.3952	-2.6303	0.029559
264	7	PFA0760w	rifin	GO:0002033	antigenic variation	-1.0321	-2.045	0.000896
265	8	PFD0015c	rifin	GO:0002033	antigenic variation	-0.8845	-1.8461	0.02176
266	9	PFD0995c	erythrocyte membrane protein 1, PfEMP1	GO:0002033	antigenic variation, pathogenesis, rosetting	0.83443	1.78316	0.002942
267	10	PFF0010w	erythrocyte membrane protein 1, PfEMP1	GO:0002033	pathogenesis, antigenic variation	-1.2507	-2.3796	0.000217
268	11	PFF0020c	erythrocyte membrane protein 1 (PfEMP1)-like protein	GO:0009405	pathogenesis	0.77516	1.71137	0.007514
269	12	PFL1420w	macrophage migration inhibitory factor homologue	GO:0020012	evasion or tolerance of host immune response	-1.0704	-2.1	0.000186
270	13	PFL1955w	erythrocyte membrane protein 1, PfEMP1	GO:0002033	cell-cell adhesion, pathogenesis, rosetting,	0.75069	1.68259	0.016669

Hypotheticals								
271	1	PF08_0060	asparagine-rich antigen	GO:0008150	biological_process	1.15728	2.23037	0.044795
272	2	PF10_0188	conserved Plasmodium membrane protein, unknown function	GO:0008150	biological_process	-1.3966	-2.6329	0.002101
273	3	PF10_0195	kinesin, putative	GO:0008150	biological_process	-0.8107	-1.7541	0.041116
274	4	PF10_0213	10b antigen, putative	GO:0008150	biological_process	-1.0633	-2.0896	0.000208
275	5	PF10_0246	conserved Plasmodium protein, unknown function	GO:0008150	biological_process	-1.1112	-2.1603	0.010342
276	6	PF11_0046	CPW-WPC family protein	GO:0008150	biological_process	-0.8724	-1.8307	0.010623
277	7	PF11_0049	NOT family protein, putative	GO:0008150	biological_process	-0.8906	-1.854	0.030109
278	8	PF11_0059	metabolite/drug transporter, putative	GO:0008150	biological_process	-1.0445	-2.0627	0.002158
279	9	PF11_0069	conserved Plasmodium protein, unknown function	GO:0008150	biological_process	-0.7906	-1.7298	0.002186
280	10	PF11_0146	conserved Plasmodium membrane protein, unknown function	GO:0008150	biological_process	-0.9831	-1.9768	0.008195
281	11	PF11_0215	conserved Plasmodium protein, unknown function	GO:0008150	biological_process	-1.353	-2.5544	0.002721
282	12	PF11_0231	conserved Plasmodium protein, unknown function	GO:0008150	biological_process	0.8138	1.75784	0.02359
283	13	PF11_0271	ThiF family protein, putative	GO:0008150	biological_process	-0.7408	-1.6711	0.03215
284	14	PF11_0307	phosphatidylinositol-4-phosphate-5-kinase,putative	GO:0008150	biological_process	0.81025	1.75352	0.032281
285	15	PF11_0319	mitochondrial rpoD precursor, putative	GO:0008150	biological_process	-0.9923	-1.9893	0.047682
286	16	PF11_0321	serpentine receptor, putative	GO:0008150	biological_process	1.00129	2.00179	0.00028
287	17	PF11_0355	conserved Plasmodium protein, unknown function	GO:0008150	biological_process	-1.7709	-3.4127	9.83E-06
288	18	PF11_0423	conserved Plasmodium protein, unknown function	GO:0008150	biological_process	-0.8207	-1.7662	0.002777
289	19	PF13_0011	plasmodium falciparum gamete antigen 27/25	GO:0008150	biological_process	-1.2549	-2.3865	0.008317
290	20	PF14_0014	Plasmodium exported protein, unknown function	GO:0008150	biological_process	-0.87	-1.8277	0.020408
291	21	PF14_0016	early transcribed membrane protein 14.1, etramp14.1	GO:0008150	biological_process	0.91963	1.89162	0.034832
292	22	PF14_0018	Plasmodium exported protein (PHISTb), unknown function	GO:0008150	biological_process	1.18603	2.27526	1.25E-05
293	23	PF14_0045	conserved Plasmodium protein, unknown function	GO:0008150	biological_process	1.04114	2.05786	0.001997
294	24	PF14_0105	conserved Plasmodium protein, unknown function	GO:0008150	biological_process	-1.2169	-2.3245	0.007714
295	25	PF14_0110	rhomboid protease ROM8	GO:0008150	biological_process	0.91907	1.8909	0.000993
296	26	PF14_0297	apyrase, putative	GO:0008150	biological_process	-1.0218	-2.0305	0.011507
297	27	PF14_0329	conserved protein, unknown function	GO:0008150	biological_process	-1	-2	0.024581
298	28	PF14_0463	chloroquine resistance marker protein	GO:0008150	biological_process	-0.7902	-1.7293	0.010523
299	29	PF14_0498	Degradation in the ER (DER1) like protein, putative	GO:0008150	biological_process	-1.0217	-2.0304	0.007714
300	30	PF14_0617	conserved Plasmodium protein, unknown function	GO:0008150	biological_process	-1.2055	-2.3061	5.88E-05
301	31	PF14_0680	conserved Plasmodium protein, unknown function	GO:0008150	biological_process	-1.6512	-3.141	1.54E-05
302	32	PF14_0696	conserved Plasmodium protein, unknown function	GO:0008150	biological_process	-0.9997	-1.9995	0.000519
303	33	PF14_0698	conserved Plasmodium protein, unknown function	GO:0008150	biological_process	1.32537	2.50598	0.034291
304	34	PF14_0758	Plasmodium exported protein (hyp17), unknown function	GO:0008150	biological_process	0.73928	1.66935	0.049948
305	35	PFB0075c	Plasmodium exported protein (hyp9), unknown function	GO:0008150	biological_process	0.82587	1.77261	0.015081
306	36	PFB0194w	conserved Plasmodium protein, unknown function	GO:0008150	biological_process	0.74353	1.67427	0.030454
307	37	PFB0365w	conserved Plasmodium protein, unknown function	GO:0008150	biological_process	-0.752	-1.6841	0.017957
308	38	PFB0590w	conserved Plasmodium protein, unknown function	GO:0008150	biological_process	-1.1625	-2.2385	0.001022
309	39	PFB0600c	conserved Plasmodium protein, unknown function	GO:0008150	biological_process	-1.1414	-2.2059	7.25E-05
310	40	PFB0923c	Plasmodium exported protein, unknown function	GO:0008150	biological_process	1.34746	2.54464	0.01753
311	41	PFB0953w	Plasmodium exported protein (hyp15), unknown function	GO:0008150	biological_process	-0.8516	-1.8045	0.001513
312	42	PFC0730w	HVA22/TB2/DP1 family protein, putative	GO:0008150	biological_process	-0.9235	-1.8967	0.019456
313	43	PFF1535w	Plasmodium exported protein (hyp5), unknown function	GO:0008150	biological_process	0.90252	1.86932	0.002996
314	44	PFL0065w	conserved Plasmodium protein, unknown function	GO:0008150	biological_process	0.79007	1.72916	0.012931
315	45	PFL0130c	conserved Plasmodium protein, unknown function	GO:0008150	biological_process	0.92295	1.89599	0.018093
316	46	PFL0170w	transporter, putative	GO:0008150	biological_process	-0.9434	-1.9231	0.03411
317	47	PFL0745c	conserved Plasmodium protein, unknown function	GO:0008150	biological_process	-1.0419	-2.0589	0.003161
318	48	PFL1065c	conserved Plasmodium protein, unknown function	GO:0008150	biological_process	-0.7318	-1.6607	0.032882
319	49	PFL1250c	conserved Plasmodium protein, unknown function	GO:0008150	biological_process	-1.0844	-2.1204	0.003737
320	50	PFL1330c	cyclin-related protein, Pfcyc-2	GO:0008150	biological_process	-1.4192	-2.6743	0.000309
321	51	PFL1630c	conserved Plasmodium protein, unknown function	GO:0008150	biological_process	-1.4052	-2.6485	0.000197

322	52	PFL1670c	conserved Plasmodium protein, unknown function	GO:0008150	biological_process	-1.9615	-3.8948	7.25E-05
323	53	PFL1685w	conserved Plasmodium protein, unknown function	GO:0008150	biological_process	-1.2729	-2.4164	2.35E-06
324	54	PFL2205w	conserved Plasmodium protein, unknown function	GO:0008150	biological_process	-0.8776	-1.8373	0.00567
325	55	PFL2240w	conserved Plasmodium protein, unknown function	GO:0008150	biological_process	-1.1238	-2.1791	0.00133
326	56	PFL2455w	conserved Plasmodium protein, unknown function	GO:0008150	biological_process	0.86553	1.82201	0.015428
327	57	PF13_0126	translation initiation factor EIF-2B subunit related	GO:0009987	cellular metabolic process	-0.8703	-1.8281	0.001361
328	58	PF10_0039	membrane skeletal protein IMC1-related	GO:0008150	cytoskeleton organization	1.07352	2.10456	0.003737
329	59	MAL13P1.307	conserved Plasmodium protein, unknown function	GO:0008150	iron-sulfur cluster assembly	-1.3596	-2.5661	0.000421
330	60	PF14_0557	conserved Plasmodium protein, unknown function	GO:0008152	metabolic process	0.96467	1.95162	0.036516
331	61	PFL0685w	Phosphatidylinositol-glycan biosynthesis class O protein,	GO:0008152	metabolic process	-0.9077	-1.8761	0.012798
332	62	MAL13P1.103	conserved Plasmodium protein, unknown function		null	-1.1218	-2.1762	0.019949
333	63	MAL13P1.138	conserved Plasmodium protein, unknown function		null	-1.1296	-2.1879	0.001072
334	64	MAL13P1.180	conserved Plasmodium protein, unknown function		null	-0.8791	-1.8393	0.002039
335	65	MAL13P1.188	conserved Plasmodium protein, unknown function		null	0.83428	1.78297	0.003813
336	66	MAL13P1.189	conserved Plasmodium membrane protein, unknown function		null	-0.8322	-1.7804	0.026901
337	67	MAL13P1.193	conserved Plasmodium protein, unknown function		null	-1.5222	-2.8723	1.54E-05
338	68	MAL13P1.203	conserved Plasmodium protein, unknown function		null	0.8874	1.84984	0.003737
339	69	MAL13P1.222	conserved Plasmodium protein, unknown function		null	0.7822	1.71975	0.00671
340	70	MAL13P1.239	conserved Plasmodium protein, unknown function		null	-0.8439	-1.7949	0.032832
341	71	MAL13P1.251	conserved Plasmodium protein, unknown function		null	-1.7989	-3.4795	1.42E-05
342	72	MAL13P1.260	conserved Plasmodium protein, unknown function		null	0.75977	1.69322	0.010017
343	73	MAL13P1.293	conserved Plasmodium protein, unknown function		null	0.82108	1.76673	0.016179
344	74	MAL13P1.298	conserved Plasmodium membrane protein, unknown function		null	0.72547	1.65344	0.028704
345	75	MAL13P1.332	conserved Plasmodium protein, unknown function	GO:0020011	apicoplast	1.05808	2.08216	0.000489
346	76	MAL13P1.470	Plasmodium exported protein (PHISTa), unknown function		null	0.78368	1.72152	0.013371
347	77	MAL13P1.57	conserved Plasmodium protein, unknown function		null	-0.8417	-1.7922	0.003543
348	78	MAL13P1.75	conserved Plasmodium protein, unknown function	GO:0020011	apicoplast	-0.7546	-1.6871	0.020825
349	79	MAL7P1.102	conserved Plasmodium protein, unknown function		null	-0.8471	-1.7989	0.005775
350	80	MAL7P1.107	conserved Plasmodium protein, unknown function		null	-1.331	-2.5158	0.000596
351	81	MAL7P1.124	conserved Plasmodium protein, unknown function		null	-1.1578	-2.2312	2.42E-05
352	82	MAL7P1.167	conserved Plasmodium protein, unknown function		null	-0.7703	-1.7056	0.017932
353	83	MAL7P1.173	Plasmodium exported protein, unknown function		null	0.87972	1.84002	0.042563
354	84	MAL7P1.174	Plasmodium exported protein (PHISTb), unknown function		null	1.04538	2.06391	0.000154
355	85	MAL7P1.208	rifin-like protein		null	0.78769	1.72631	0.045589
356	86	MAL7P1.23	RAP protein, putative	GO:0020011	apicoplast	-0.7512	-1.6832	0.021764
357	87	MAL7P1.230	hypothetical protein, pseudogene		null	0.75845	1.69167	0.015641
358	88	MAL7P1.3	Plasmodium exported protein (hyp5), unknown function		null	0.7584	1.69162	0.032281
359	89	MAL7P1.33	conserved Plasmodium protein, unknown function	GO:0020011	apicoplast	-1.3569	-2.5614	0.018747
360	90	MAL7P1.61	null		null	0.72546	1.65343	0.030195
361	91	MAL7P1.77	conserved Plasmodium protein, unknown function		null	-1.3846	-2.611	0.000755
362	92	MAL8P1.2	Plasmodium exported protein (PHISTb), unknown function		null	1.05545	2.07837	0.006518
363	93	MAL8P1.206	Plasmodium exported protein, unknown function		null	-1.5654	-2.9596	0.002017
364	94	MAL8P1.216	rifin		null	-1.2427	-2.3664	0.001369
365	95	MAL8P1.50	conserved Plasmodium protein, unknown function		null	-0.7268	-1.655	0.008317
366	96	MAL8P1.53	conserved Plasmodium protein, unknown function		null	-1.8738	-3.6651	2.70E-07
367	97	MAL8P1.74	conserved Plasmodium protein, unknown function		null	-1.0044	-2.0061	0.000755
368	98	MAL8P1.82	Vacuolar sorting protein VPS9, putative		null	0.8157	1.76015	0.043532
369	99	MAL8P1.86	Sel3 protein	GO:0020011	apicoplast	-1.2598	-2.3947	3.24E-05
370	100	PF07_0022	conserved Plasmodium protein, unknown function		null	-0.9995	-1.9993	0.00154
371	101	PF07_0039	conserved Plasmodium protein, unknown function		null	-0.8494	-1.8018	0.03388
372	102	PF07_0053	conserved Plasmodium protein, unknown function		null	0.86441	1.82059	0.01039
373	103	PF07_0078	transmembrane protein, putative	GO:0016020	membrane	-0.9754	-1.9662	0.000704

374	104	PF07_0082	conserved Plasmodium membrane protein, unknown function		null	0.85888	1.81363	0.024958
375	105	PF07_0084	conserved Plasmodium protein, unknown function		null	0.82274	1.76876	0.011456
376	106	PF07_0087	conserved Plasmodium protein, unknown function	GO:0020011	apicoplast	-1.3125	-2.4837	0.001103
377	107	PF07_0101	conserved Plasmodium protein, unknown function		null	-0.7944	-1.7344	0.017814
378	108	PF07_0106	conserved Plasmodium protein, unknown function		null	0.93347	1.90987	0.002223
379	109	PF08_0001	Plasmodium exported protein, unknown function	GO:0020011	apicoplast	1.10517	2.15124	7.72E-05
380	110	PF08_0002	surface-associated interspersed gene 8.2 (SURFIN8.2)		null	0.75416	1.68665	0.002869
381	111	PF08_0016	conserved Plasmodium protein, unknown function	GO:0020011	apicoplast	-1.0013	-2.0018	0.012775
382	112	PF08_0029	conserved Plasmodium protein, unknown function		null	-1.0739	-2.1051	0.019949
383	113	PF08_0030	conserved Plasmodium protein, unknown function		null	-1.3401	-2.5317	0.002264
384	114	PF08_0051	conserved Plasmodium protein, unknown function		null	-1.0001	-2.0001	0.003978
385	115	PF08_0134	conserved Plasmodium protein, unknown function		null	-0.8979	-1.8633	0.035574
386	116	PF10_0020	alpha/beta hydrolase, putative		null	-2.0211	-4.059	4.77E-06
387	117	PF10_0034	conserved Plasmodium protein, unknown function		null	1.21687	2.32442	9.59E-06
388	118	PF10_0052	conserved Plasmodium protein, unknown function		null	-1.4009	-2.6407	0.000515
389	119	PF10_0212	conserved Plasmodium protein, unknown function		null	-0.9745	-1.9649	0.002777
390	120	PF10_0243	conserved Plasmodium protein, unknown function		null	-0.7407	-1.671	0.03332
391	121	PF10_0253	conserved Plasmodium protein, unknown function		null	-0.7996	-1.7406	0.003791
392	122	PF10_0258	conserved Plasmodium protein, unknown function		null	0.91189	1.8815	0.010323
393	123	PF10_0286	conserved Plasmodium protein, unknown function		null	-1.2289	-2.3439	0.006304
394	124	PF10_0291	RAP protein, putative		null	-1.1628	-2.2388	0.015295
395	125	PF10_0307	conserved Plasmodium protein, unknown function		null	1.23334	2.35111	0.000298
396	126	PF10_0319	conserved Plasmodium protein, unknown function		null	0.85248	1.8056	0.011225
397	127	PF10_0336	conserved Plasmodium protein, unknown function		null	-1.4303	-2.6949	0.000934
398	128	PF10_0352	merozoite surface protein		null	0.7875	1.72609	0.017056
399	129	PF11_0035	Plasmodium exported protein, unknown function		null	0.78009	1.71724	0.002088
400	130	PF11_0093	IWS1-like protein, putative		null	0.73478	1.66415	0.023412
401	131	PF11_0206	conserved Plasmodium protein, unknown function		null	1.07565	2.10767	0.005257
402	132	PF11_0278	conserved Plasmodium protein, unknown function		null	0.7906	1.7298	0.0198
403	133	PF11_0290	conserved Plasmodium protein, unknown function		null	0.82433	1.77072	0.016387
404	134	PF11_0296	conserved protein, unknown function		null	0.76255	1.69649	0.019017
405	135	PF11_0371	conserved Plasmodium protein, unknown function		null	-1.0398	-2.0559	0.016977
406	136	PF11_0404	transcription factor with AP2 domain(s), putative		null	0.94238	1.9217	0.033309
407	137	PF11_0413	conserved Plasmodium protein, unknown function		null	0.74028	1.67049	0.048387
408	138	PF11_0425	conserved Plasmodium protein, unknown function		null	-1.213	-2.3182	0.000126
409	139	PF11_0508	Plasmodium exported protein, unknown function		null	-1.1405	-2.2046	0.021309
410	140	PF11_0514	Plasmodium exported protein (PHISTa), unknown function		null	0.96452	1.95141	0.017555
411	141	PF11_0560	conserved protein, unknown function		null	-0.9175	-1.8888	0.006687
412	142	PF13_0024	conserved Plasmodium protein, unknown function		null	-0.8017	-1.7431	0.045163
413	143	PF13_0032	hydrolase, putative	GO:0020011	apicoplast	-2.2264	-4.6797	0.002217
414	144	PF13_0097	transcription factor with AP2 domain(s), putative		null	0.78312	1.72084	0.007879
415	145	PF13_0104	conserved Plasmodium protein, unknown function		null	-0.7584	-1.6916	0.034431
416	146	PF13_0175	conserved protein, unknown function		null	0.89675	1.86186	0.015932
417	147	PF13_0189	conserved Plasmodium protein, unknown function		null	-0.8035	-1.7454	0.030161
418	148	PF13_0192	conserved Plasmodium protein, unknown function	GO:0016020	membrane	-2.0706	-4.2006	5.51E-08
419	149	PF13_0200	conserved Plasmodium protein, unknown function		null	-0.7553	-1.688	0.03309
420	150	PF13_0202	conserved Plasmodium protein, unknown function		null	-1.234	-2.3522	0.001512
421	151	PF13_0241	rhomboid protease ROM6, putative	GO:0016020	null	-0.7978	-1.7385	0.001088
422	152	PF13_0267	conserved Plasmodium protein, unknown function		null	0.7819	1.71939	0.003543
423	153	PF13_0296	splicing factor 3b subunit, putative		null	-0.8722	-1.8305	0.00434
424	154	PF13_0307	conserved Plasmodium protein, unknown function		null	-0.7945	-1.7345	0.001553
425	155	PF13_0338	cysteine-rich surface protein		null	-0.8841	-1.8456	0.039883

426	156	PF13_0348	rhoptry protein		null	-1.0309	-2.0432	0.001644
427	157	PF14_0031	conserved Plasmodium protein, unknown function		null	-1.4697	-2.7696	5.69E-06
428	158	PF14_0101	conserved Plasmodium protein, unknown function		null	-0.8496	-1.802	0.024125
429	159	PF14_0170	NOT family protein, putative		null	0.73112	1.65993	0.01662
430	160	PF14_0186	conserved Plasmodium protein, unknown function		null	-1.0318	-2.0446	0.000432
431	161	PF14_0226	conserved Plasmodium protein, unknown function		null	0.74205	1.67255	0.016411
432	162	PF14_0344	conserved Plasmodium protein, unknown function		null	0.85787	1.81236	0.003387
433	163	PF14_0347	conserved Plasmodium protein, unknown function		null	-0.8823	-1.8434	0.028026
434	164	PF14_0402	conserved Plasmodium protein, unknown function		null	0.83517	1.78407	0.024501
435	165	PF14_0430	mitochondrial ribosomal protein S29 precursor, putative		null	-0.8085	-1.7514	0.00671
436	166	PF14_0488	conserved Plasmodium protein, unknown function		null	-0.7861	-1.7244	0.039144
437	167	PF14_0502	conserved Plasmodium protein, unknown function		null	-0.8699	-1.8275	0.00671
438	168	PF14_0570	pyridoxal 5'-phosphate synthase, putative		null	-1.215	-2.3214	0.002779
439	169	PF14_0583	conserved Plasmodium protein, unknown function		null	-1.0339	-2.0476	0.005929
440	170	PF14_0609	conserved Plasmodium protein, unknown function		null	-0.9309	-1.9064	0.010137
441	171	PF14_0631	conserved Plasmodium protein, unknown function		null	0.7291	1.65761	0.04483
442	172	PF14_0703	conserved Plasmodium protein, unknown function		null	1.13702	2.19926	0.007252
443	173	PF14_0705	conserved Plasmodium protein, unknown function		null	-1.1044	-2.1501	0.017941
444	174	PF14_0706	conserved Plasmodium protein, unknown function		null	0.85094	1.80367	0.019075
445	175	PF14_0760	Plasmodium exported protein, unknown function		null	0.99433	1.99215	0.004045
446	176	PFA0115w	Plasmodium exported protein, unknown function	GO:0020011	apicoplast	-1.6653	-3.1717	0.000435
447	177	PFA0195w	conserved Plasmodium protein, unknown function		null	-1.0273	-2.0382	0.000405
448	178	PFA0245w	transporter, putative		null	-1.9419	-3.8421	6.97E-06
449	179	PFA0350c	conserved Plasmodium protein, unknown function		null	-0.7938	-1.7337	0.04735
450	180	PFA0385w	conserved Plasmodium membrane protein, unknown function	GO:0020011	apicoplast	-1.1384	-2.2013	0.000346
451	181	PFB0115w	conserved Plasmodium protein, unknown function		null	1.68929	3.22498	0.001885
452	182	PFB0161c	conserved Plasmodium protein, unknown function		null	-1.5041	-2.8365	0.003117
453	183	PFB0315w	41 kDa antigen		null	-1.0472	-2.0666	0.013449
454	184	PFB0475c	conserved Plasmodium protein, unknown function		null	1.61727	3.06794	0.00715
455	185	PFB0530c	conserved Plasmodium protein, unknown function		null	-1.1239	-2.1794	0.013309
456	186	PFB0535w	GDP-fructose:GMP antiporter, putative		null	-1.5443	-2.9167	0.001134
457	187	PFB0835c	conserved Plasmodium protein, unknown function		null	-2.094	-4.2693	1.55E-06
458	188	PFB0970c	Plasmodium exported protein, unknown function		null	0.75959	1.69301	0.009621
459	189	PFB0973c	hypothetical protein		null	0.83022	1.77796	0.015439
460	190	PFC0085c	Plasmodium exported protein, unknown function		null	0.85591	1.8099	0.003979
461	191	PFC0262c	conserved Plasmodium protein, unknown function		null	-1.798	-3.4773	6.80E-05
462	192	PFC0315c	conserved Plasmodium protein, unknown function		null	-1.3138	-2.486	0.003569
463	193	PFC0371w	conserved protein, unknown function		null	-1.0759	-2.1081	0.000328
464	194	PFC0390w	N2227-like protein, putative		null	0.72608	1.65413	0.046637
465	195	PFC0435w	conserved Plasmodium protein, unknown function	GO:0020011	apicoplast	-1.0274	-2.0383	0.000934
466	196	PFC0571c	conserved Plasmodium protein, unknown function		null	-0.9606	-1.9461	0.001222
467	197	PFC0590c	DER1-like protein, putative	GO:0020011	apicoplast	-1.4047	-2.6477	0.002903
468	198	PFC0715c	conserved Plasmodium protein, unknown function	GO:0020011	apicoplast	-1.4806	-2.7906	0.017237
469	199	PFC0760c	conserved Plasmodium protein, unknown function		null	0.77417	1.7102	0.015278
470	200	PFC0886w	conserved Plasmodium protein, unknown function		null	-1.1253	-2.1814	6.82E-05
471	201	PFC0912w	signal peptidase, putative		null	-1.6703	-3.1828	0.000131
472	202	PFC0965w	conserved Plasmodium protein, unknown function		null	0.73803	1.6679	0.002939
473	203	PFC0990c	conserved Plasmodium protein, unknown function		null	0.76261	1.69656	0.041639
474	204	PFC1110w	null		null	0.89672	1.86183	0.002216
475	205	PFD0080c	Plasmodium exported protein (PHISTb), unknown function		null	-0.9388	-1.9169	0.02204
476	206	PFD0225w	conserved Plasmodium membrane protein, unknown function		null	-0.9649	-1.9519	0.018337
477	207	PFD0495c	conserved Plasmodium protein, unknown function		null	0.85184	1.8048	0.00422

478	208	PFD0545w	conserved Plasmodium protein, unknown function		null	0.86339	1.81931	0.029731
479	209	PFD0550c	conserved Plasmodium protein, unknown function		null	-1.073	-2.1038	0.003745
480	210	PFD0655w	null		null	-0.7577	-1.6908	0.008418
481	211	PFD0670c	lysine decarboxylase-like protein, putative		null	-0.9665	-1.9541	0.002013
482	212	PFD0850c	Memo-like protein		null	-1.1069	-2.1538	0.017596
483	213	PFD0920w	conserved Plasmodium protein, unknown function		null	-0.9168	-1.888	0.013578
484	214	PFD1140w	Plasmodium exported protein (PHISTc), unknown function		null	1.06876	2.09763	0.001184
485	215	PFE0050w	Plasmodium exported protein, unknown function		null	0.83732	1.78673	0.00451
486	216	PFE0265c	conserved Plasmodium protein, unknown function	GO:0020011	apicoplast	-0.8716	-1.8297	0.03803
487	217	PFE0310c	conserved Plasmodium protein, unknown function		null	-1.0931	-2.1333	0.003117
488	218	PFE0340c	rhomboid protease ROM4	GO:0016020	membrane	1.12723	2.18438	0.032882
489	219	PFE0345c	conserved Plasmodium protein, unknown function	GO:0020011	apicoplast	-0.7931	-1.7328	0.022939
490	220	PFE0390w	conserved Plasmodium protein, unknown function		null	0.80204	1.74356	0.013578
491	221	PFE0500c	conserved Plasmodium protein, unknown function		null	-1.3206	-2.4978	9.55E-06
492	222	PFE0620c	conserved Plasmodium protein, unknown function		null	-1.0746	-2.1061	0.004441
493	223	PFE0635c	conserved Plasmodium protein, unknown function		null	-0.9004	-1.8666	0.001384
494	224	PFE1220w	conserved Plasmodium protein, unknown function		null	-0.7528	-1.685	0.020816
495	225	PFE1280w	conserved Plasmodium protein, unknown function		null	-1.1552	-2.2271	0.01052
496	226	PFE1365w	conserved Plasmodium protein, unknown function		null	0.9661	1.95355	0.010247
497	227	PFE1515w	conserved Plasmodium membrane protein, unknown function		null	-1.0758	-2.1079	0.004908
498	228	PFE1610w	Plasmodium exported protein, unknown function	GO:0020011	apicoplast	1.03126	2.04381	0.000462
499	229	PFF0075c	Plasmodium exported protein (PHISTb), unknown function		null	0.80949	1.75259	0.014759
500	230	PFF0205w	mitochondrial ribosomal protein L41 precursor, putative		null	-1.0659	-2.0935	0.001534
501	231	PFF0295c	conserved Plasmodium protein, unknown function		null	0.9298	1.90502	0.001297
502	232	PFF0480w	conserved Plasmodium protein, unknown function		null	0.9663	1.95382	0.000525
503	233	PFF0545c	conserved Plasmodium protein, unknown function		null	-0.9718	-1.9613	5.88E-05
504	234	PFF0550w	transcription factor with AP2 domain(s), putative		null	-0.8717	-1.8299	0.00671
505	235	PFF0630c	conserved Plasmodium protein, unknown function		null	-1.9912	-3.9756	2.70E-07
506	236	PFF0640w	conserved Plasmodium protein, unknown function		null	-1.6463	-3.1304	4.56E-05
507	237	PFF0725w	conserved Plasmodium protein, unknown function		null	0.72405	1.65182	0.003117
508	238	PFF0805c	conserved Plasmodium protein, unknown function		null	-0.902	-1.8687	0.004663
509	239	PFF0935c	conserved Plasmodium protein, unknown function		null	-1.175	-2.2579	0.007034
510	240	PFF1005w	conserved Plasmodium protein, unknown function		null	0.86301	1.81883	0.032073
511	241	PFF1160w	conserved Plasmodium protein, unknown function		null	-0.7971	-1.7376	0.031041
512	242	PFF1290c	conserved Plasmodium protein, unknown function		null	-0.7837	-1.7216	0.010045
513	243	PFF1460c	conserved Plasmodium protein, unknown function		null	0.91097	1.88031	0.003215
514	244	PFI0175w	conserved Plasmodium protein, unknown function		null	0.95386	1.93705	0.048791
515	245	PFI0210c	cysteine repeat modular protein, putative	GO:0020011	apicoplast	-0.9129	-1.8829	0.015639
516	246	PFI0405w	conserved Plasmodium protein, unknown function	GO:0020011	apicoplast	-1.1638	-2.2405	0.018385
517	247	PFI0765w	conserved Plasmodium protein, unknown function		null	0.86861	1.8259	0.007258
518	248	PFI0795w	conserved Plasmodium protein, unknown function		null	-0.8596	-1.8146	0.049904
519	249	PFI0880c	glideosome-associated protein 50		null	-1.5084	-2.8449	0.000146
520	250	PFI0905w	probable protein, unknown function		null	-2.6442	-6.2515	1.58E-09
521	251	PFI0975c	conserved Plasmodium protein, unknown function		null	-0.9179	-1.8894	0.005257
522	252	PFI1040c	conserved Plasmodium membrane protein, unknown function		null	0.992	1.98894	0.014819
523	253	PFI1185c	conserved Plasmodium protein, unknown function		null	0.75797	1.6911	0.030932
524	254	PFI1270w	conserved Plasmodium protein, unknown function		null	-1.5415	-2.911	0.01753
525	255	PFI1500w	conserved Plasmodium membrane protein, unknown function		null	-0.9484	-1.9297	0.041354
526	256	PFI1520w	asparagine-rich antigen, putative		null	0.96767	1.95569	0.027249
527	257	PFI1610c	calcyclin binding protein, putative		null	-0.8053	-1.7475	0.00457
528	258	PFI1630c	conserved Plasmodium protein, unknown function		null	-1.0553	-2.0782	0.048667
529	259	PFI1665w	transcription factor with AP2 domain(s), putative		null	-0.9113	-1.8808	0.004328

530	260	PFI1690c	conserved Plasmodium protein, unknown function		null	1.02675	2.03743	0.023976
531	261	PFI1770w	Plasmodium exported protein (PHISTb), unknown function		null	0.90449	1.87189	0.025947
532	262	PFI1780w	Plasmodium exported protein (PHISTc), unknown function		null	1.29911	2.46078	3.15E-05
533	263	PFL0235w	conserved Plasmodium protein, unknown function		null	-1.8419	-3.5847	9.93E-05
534	264	PFL0280c	histone binding protein, putative		null	-0.7982	-1.739	0.035574
535	265	PFL0975w	conserved Plasmodium protein, unknown function		null	-0.9113	-1.8807	0.032882
536	266	PFL1040w	conserved Plasmodium protein, unknown function		null	-0.7873	-1.7258	0.032281
537	267	PFL1300c	conserved Plasmodium protein, unknown function		null	-0.7312	-1.6601	0.003762
538	268	PFL1335w	cyclin related protein, putative		null	-1.2522	-2.382	0.001752
539	269	PFL1560c	conserved protein, unknown function		null	0.87151	1.82957	0.022843
540	270	PFL1645w	conserved Plasmodium protein, unknown function		null	0.76003	1.69352	0.002158
541	271	PFL1900w	transcription factor with AP2 domain(s), putative		null	-1.4485	-2.7293	0.000386
542	272	PFL2435w	conserved Plasmodium protein, unknown function		null	-0.8135	-1.7575	0.006073
543	273	PFL2535w	Plasmodium exported protein (PHISTb), unknown function		null	-1.4081	-2.6539	0.000375
544	274	MAL8P1.14	mitochondrial inner membrane translocase, putative	GO:0051205	protein insertion into membrane	-1.1011	-2.1452	4.56E-05
545	275	MAL8P1.330	conserved Plasmodium protein, unknown function		null	1.22718	2.3411	0.005232
546	276	PF14_0182	conserved Plasmodium protein, unknown function		null	1.68436	3.21398	0.007421
547	277	PFD1045w	conserved Plasmodium protein, unknown function		null	-1.5894	-3.0093	5.29E-06
548	278	PFE0240c	conserved Plasmodium protein, unknown function		null	-0.9274	-1.9019	0.01841
549	279	PFE0685w	conserved Plasmodium protein, unknown function		null	-1.3974	-2.6342	0.011921

Appendix C

The complete interacting binding partners of AdoMetDC, DHPS/HPPK and AdoMet synthase

Nr	PlasmoDB ID	Name	Score	Present in dataset
		AdoMetDC interactome		
1	PF11_0317	structural maintenance of chromosome protein, putative	9.53	
2	PFE0195w	P-type ATPase, putative	8.31	
3	PFA0390w	DNA repair exonuclease, putative	7.98	
4	MAL8P1.99	hypothetical protein	6.62	Yes
5	PF11_0427	dolichyl-phosphate b-D-mannosyltransferase, putative	6.62	
6	PF07_0129	ATP-dept. acyl-coa synthetase	6.62	Yes
7	PFA0590w	ABC transporter, putative	6.62	Yes
8	PF10_0260	hypothetical protein	5.90	
9	PF13_0348	PfRhop148,Rhoptry protein	5.90	Yes
10	PF14_0053	ribonucleotide reductase small subunit	5.70	Yes
11	PFD0685c	chromosome associated protein, putative	4.71	Yes
12	PFC0125w	ABC transporter, putative	4.71	Yes
13	PF14_0709	ribosomal protein L20, putative	4.71	Yes
14	PF08_0131	1-cys peroxidoxin	4.71	Yes
15	PF11_0117	replication factor C subunit 5, putative	4.71	Yes
16	PF11_0181	tyrosine --tRNA ligase, putative	4.71	Yes
17	PFB0180w	5'-3' exonuclease, N-terminal resolvase-like domain, putative	4.71	
18	PFL2180w	50S ribosomal protein L3, putative	4.71	
19	PF14_0097	cytidine diphosphate-diacylglycerol synthase	4.71	
20	PF14_0081	DNA repair helicase, putative	4.71	
21	PF11_0044	hypothetical protein	4.71	Yes
22	PF11_0197	hypothetical protein	4.71	
23	PF14_0338	hypothetical protein	4.52	
24	PF14_0397	hypothetical protein, conserved	4.52	
25	PF10_0362	DNA polymerase zeta catalytic subunit, putative	4.52	
26	PFB0605w	Ser/Thr protein kinase, putative	4.52	
27	PF08_0034	histone acetyltransferase Gcn5, putative	4.52	
28	PF10_0132	phospholipase C-like, putative	4.52	
29	PFI1310w	NAD synthase, putative	4.52	
30	PF13_0016	methyl transferase-like protein, putative	4.52	Yes
31	PFB0520w	protein kinase, putative	4.52	
32	PF11_0049	hypothetical protein, conserved	4.52	Yes
33	PF11_0074	hypothetical protein	4.52	Yes
34	PF14_0161	hypothetical protein, conserved	4.52	
35	PF14_0441	pyruvate dehydrogenase E1 beta subunit, putative	4.52	
36	PFE0040c	Mature parasite-infected erythrocyte surface antigen (MESA)	4.52	
37	MAL13P1.95	ferredoxin	4.52	
38	PFE0585c	myo-inositol 1-phosphate synthase, putative	4.52	
39	PF13_0021	small heat shock protein, putative	4.52	
40	PFC0915w	ATP-dependent RNA helicase, putative	4.52	
41	PFA0520c	chromatin assembly factor 1 protein WD40 domain, putative	4.52	Yes
42	PF08_0031	oxoglutarate/malate translocator protein, putative	4.52	
43	PFI0910w	DNA helicase, putative	4.52	
44	PF14_0200	hypothetical protein	4.52	Yes
45	PFL1545c	chaperonin cpn60	4.39	
46	PF11_0077	hypothetical protein	3.96	
47	MAL8P1.17	disulfide isomerase precursor, putative	3.96	
48	PF14_0570	hypothetical protein, conserved	3.96	Yes
49	PFE1155c	mitochondrial processing peptidase alpha subunit, putative	3.68	
50	PF14_0309	protein-L-isoaspartate O-methyltransferase beta-aspartate	3.68	Yes
51	PFC0955w	ATP-dependent RNA helicase	3.38	
52	PFI0490c	hypothetical protein	3.38	Yes
53	MAL8P1.157	hypothetical protein	3.38	
54	MAL13P1.138	hypothetical protein	3.38	Yes
55	PF14_0255	hypothetical protein	3.38	

56	PF13_0242	isocitrate dehyc rsor	3.38	Yes
57	PFE1320w	hypothetical protein	3.38	
58	PFL2245w	hypothetical protein	3.38	
59	PFI0670w	hypothetical protein, conserved	3.38	
60	PF14_0354	hypothetical protein	3.38	
61	PFB0215c	3'-5' exonuclease, putative	3.38	
62	PF14_0101	hypothetical protein	3.38	Yes
63	PFL0660w	dynein light chain 1, putative	3.38	
64	PF14_0112	POM1, putative	3.38	
65	PF14_0348	ATP-dependent Clp protease proteolytic subunit, putative	3.38	Yes
66	PF13_0322	falcilysin	3.38	
67	PF14_0192	glutathione reductase	3.38	Yes
68	PF10_0235	hypothetical protein	3.38	
69	PFE0675c	deoxyribodipyrimidine photolyase (photoreactivating enzyme, DNA	3.38	Yes
70	PFL1070c	endoplasmin homolog precursor, putative	3.38	
71	PFC0165w	hypothetical protein, conserved	3.38	
72	PF13_0117	hypothetical protein, conserved	3.38	
73	PF14_0318	hypothetical protein	3.34	
74	PFE0645w	hypothetical protein	3.34	
75	PFI1120c	hypothetical protein	3.34	
76	PF08_0010	hypothetical protein	3.34	
77	PF10_0234	hypothetical protein	3.34	
78	MAL13P1.107	hypothetical protein	3.34	
79	PF13_0077	DEAD box helicase, putative	3.34	
80	MAL13P1.180	hypothetical protein	3.34	Yes
81	PF11_0365	hypothetical protein	3.34	
82	PF14_0394	hypothetical protein	3.34	
83	MAL13P1.295	hypothetical protein	3.34	
84	PF14_0014	hypothetical protein	3.34	Yes
85	PF14_0471	hypothetical protein	3.34	
86	MAL13P1.90	hypothetical protein	3.34	
87	PF11_0219	hypothetical protein	3.34	
88	PFA0615w	hypothetical protein	3.34	
89	PFF0115c	elongation factor G, putative	3.34	
90	PFA0195w	hypothetical protein	3.34	Yes
91	PFA0175w	hypothetical protein	3.34	
92	PFL0485w	hypothetical protein	3.34	
93	PF14_0310	hypothetical protein	3.34	
94	PFI0610w	hypothetical protein	3.34	
95	MAL7P1.111	hypothetical protein	3.34	
96	PF11_0054	hypothetical protein	3.34	
97	PFE0310c	hypothetical protein	3.34	Yes
98	PF10_0226	hypothetical protein, conserved	3.34	
99	PF08_0046	hypothetical protein	3.34	
100	PFL0965c	hypothetical protein	3.34	
101	MAL13P1.332	hypothetical protein	3.34	Yes
102	PFF0655c	adapter-related protein, putative	3.34	
103	PF14_0176	hypothetical protein	3.34	
104	MAL8P1.55	hypothetical protein	3.34	
105	MAL13P1.127	hypothetical protein	3.34	
106	PFF0555w	hypothetical protein	3.34	
107	MAL8P1.11	hypothetical protein	3.34	
108	MAL8P1.86	hypothetical protein	3.34	Yes
109	MAL13P1.266	hypothetical protein	3.34	
110	PFL0605c	hypothetical protein	3.34	
111	PF13_0192	hypothetical protein	3.34	Yes
112	PF11_0248	hypothetical protein	3.34	
113	PFB0185w	hypothetical protein, conserved	3.34	
114	MAL13P1.325	hypothetical protein	3.34	
115	PF08_0067	hypothetical protein	3.34	
116	PFL1675c	hypothetical protein	3.34	
117	PFC0230c	hypothetical protein, conserved	3.34	
118	PFA0460c	tubulin-specific chaperone a, putative	3.34	
119	PF14_0306	hypothetical protein	3.34	
120	PF13_0134	hypothetical protein	3.34	
121	MAL7P1.114	P36-like protein homologue, putative	3.34	
122	PFI0585c	hypothetical protein	3.34	
123	PF14_0253	hypothetical protein	3.34	

124	PF13_0080	hypothetical pr	3.34	Yes
125	PFF0225w	DNA helicase, putative	3.34	
126	PFL1275c	hypothetical protein	3.34	
127	PF14_0498	hypothetical protein	3.34	Yes
128	PFF1175c	hypothetical protein, conserved	3.34	
129	PFF0770c	hypothetical protein with PP2C domain	3.34	
130	PFF1395c	glutamyl-tRNA(Gln) amidotransferase subunit B, putative	3.34	Yes
131	MAL7P1.157	hypothetical protein	3.34	
132	PFF0935c	hypothetical protein	3.34	Yes
133	PFF0400w	hypothetical protein	3.34	
134	PF14_0356	hypothetical protein	3.34	
135	PF14_0300	syntaxin, putative	3.34	
136	MAL7P1.74	hypothetical protein, conserved	3.34	
137	MAL13P1.390	#N/A	3.34	
138	PFF1140c	ATP-dependent DEAD box helicase, putative	3.34	
139	PF10_0032	hypothetical protein	3.34	
140	PF14_0186	hypothetical protein	3.34	Yes
141	PF14_0430	hypothetical protein	3.34	Yes
142	PFL0095c	hypothetical protein	3.34	
143	PF08_0080	hypothetical protein	3.34	
144	PFB0600c	hypothetical protein	3.34	Yes
145	PF13_0241	hypothetical protein	3.34	Yes
146	PF11_0258	co-chaperone GrpE, putative	3.00	
147	PFB0685c	acyl-CoA synthetase, PfACS9	3.00	

Nr	PlasmoDB ID	Name	Score	Present in dataset
		DHPS/HPPK interactome		
1	PF13_0140	dihydrofolate synthase/folylpolyglutamate synthase	10.32	Yes
2	PFL0740c	10 kd chaperonin, putative	8.31	
3	PF11_0258	co-chaperone GrpE, putative	8.31	
4	PF13_0180	chaperonin, putative	8.31	
5	PF08_0006	prohibitin, putative	7.98	
6	PFL1475w	sun-family protein, putative	7.98	Yes
7	PF13_0234	phosphoenolpyruvate carboxykinase	5.96	
8	PF11_0188	heat shock protein 90, putative	5.96	Yes
9	PF14_0656	U2 snRNP auxiliary factor, putative	5.96	
10	PF14_0242	arginine n-methyltransferase, putative	5.96	
11	PFB0953w	hypothetical protein	5.90	Yes
12	MAL7P1.209	#N/A	5.90	
13	PFF0945c	bi-functional enzyme: long-chain fatty- acid Co-A ligase and oxalyl Co-A	5.90	
14	PFE0060w	hypothetical protein	5.90	
15	PF11_0076	hypothetical protein	5.90	
16	PFF0775w	pyridoxal kinase-like protein, putative	5.90	
17	PF10_0013	hypothetical protein	5.90	
18	MAL8P1.124	hypothetical protein	5.90	
19	PF14_0705	hypothetical protein	5.90	Yes
20	PFE1230c	hypothetical protein, conserved	5.90	
21	PF13_0300	mitochondrial inner membrane translocase, putative	5.90	
22	MAL8P1.15	hypothetical protein	5.90	
23	PFE1245w	zinc finger protein, putative	5.90	
24	PF11_0511	hypothetical protein	5.90	
25	PFC0790w	hypothetical protein	5.90	
26	PF13_0015	hypothetical protein	5.90	
27	PFA0160c	hypothetical protein	5.90	
28	MAL13P1.73	hypothetical protein	5.90	
29	PF14_0674	hypothetical protein	5.90	
30	MAL13P1.318	hypothetical protein	5.90	
31	PFB0525w	asparagine -- tRNA ligase, putative	4.71	
32	PFL1210w	hypothetical protein	4.71	
33	PF07_0079	60S ribosomal protein L11a, putative	4.71	
34	PFL1425w	t-complex protein 1, gamma subunit, putative	4.71	
35	MAL13P1.284	pyrroline carboxylate reductase	4.71	
36	PFI1100w	Para-aminobenzoic acid synthetase	4.71	
37	PFE0475w	asparagine -- t RNA ligase, putative	4.71	
38	PF14_0370	RNA helicase, putative	4.71	
39	PFC0285c	T-complex protein beta subunit, putative	4.71	
40	PFL0705c	adrenodoxin-type ferredoxin, putative	4.52	

41	PFB0545c	ribosomal protei	4.52	
42	PF14_0023	hypothetical protein, conserved	4.52	
43	PF11_0339	hypothetical protein	4.52	
44	PFA0145c	aspartyl-tRNA synthetase	4.52	
45	PF14_0517	peptidase, putative	4.52	
46	PF14_0230	Ribosomal protein family L5, putative	4.52	
47	PF13_0345	aminomethyltransferase, mitochondrial precursor	4.52	
48	PFB0595w	heat shock 40 kDa protein, putative	4.52	
49	PFD0755c	adenylate kinase 1	4.52	
50	PF11_0077	hypothetical protein	4.52	
51	PF08_0018	translation initiation factor-like protein	4.52	
52	PFL2395c	dimethyladenosine transferase, putative	4.52	
53	PFL1150c	ribosomal protein L24, putative	4.52	Yes
54	PF10_0121	hypoxanthine phosphoribosyltransferase	4.52	Yes
55	PF10_0325	hypothetical protein, conserved	4.52	
56	PF14_0668	hypothetical protein	4.39	
57	PF14_0036	acid phosphatase, putative	4.39	
58	PFB0115w	hypothetical protein	4.39	Yes
59	PF14_0297	ecto-nucleoside triphosphate diphosphohydrolase 1, putative	4.39	Yes
60	PFE0605c	glutathione synthetase	4.39	
61	PFL0255c	uga suppressor tRNA-associated antigenic protein, putative	4.39	
62	PFL1310c	ATP-dependent RNA helicase, putative	4.39	
63	PF11_0264	DNA-dependent RNA polymerase	4.39	
64	PF11_0351	heat shock protein hsp70 homologue	4.39	
65	PF13_0243	hypothetical protein	4.39	
66	PFI1570c	aminopeptidase, putative	4.39	
67	PF14_0022	exopolyphosphatase, putative	4.39	
68	PFE0630c	orotate phosphoribosyltransferase, putative	3.38	
69	MAL13P1.54	hypothetical protein, conserved	3.38	
70	PF14_0378	triose-phosphate isomerase	3.38	Yes
71	PF10_0153	hsp60	3.38	
72	PFC0271c	glutaredoxin, putative	3.38	
73	PF11_0165	falcipain 2 precursor	3.38	
74	PFD0980w	holo-(acyl-carrier protein) synthase, putative	3.38	
75	PFB0200c	aspartate aminotransferase, putative	3.38	
76	PFE1080w	ribosomal large subunit pseudouridylate synthase, putative	3.38	
77	PF14_0381	delta-aminolevulinic acid dehydratase	3.38	
78	PF11_0507	antigen 332, putative	3.38	
79	PF14_0147	ATP-dependent protease, putative	3.38	
80	PFC0550w	hypothetical protein	3.38	
81	PF14_0166	lysine -- tRNA ligase, putative	3.38	
82	PF13_0141	L-lactate dehydrogenase	3.38	Yes
83	PFD0555c	hypothetical protein	3.38	
84	PF11_0301	spermidine synthase	3.38	
85	PFC0205c	PfGLP-1, 1-cys-glutaredoxin-like protein-1	3.38	
86	PFL1710c	tetQ family GTPase, putative	3.38	
87	PF10_0152	hypothetical protein	3.38	
88	PFL0690c	hypothetical protein conserved	3.38	
89	PF07_0100	hypothetical protein	3.38	
90	PF14_0341	glucose-6-phosphate isomerase	3.38	
91	PF14_0096	hypothetical protein	3.38	
92	PF14_0209	hypothetical protein	3.34	
93	PF10_0064	hypothetical protein	3.34	
94	MAL13P1.221	aspartate carbamoyltransferase	3.34	
95	PFI1750c	hypothetical protein	3.34	
96	PFF0105w	MYND finger domain protein	3.34	
97	PF13_0029	hypothetical protein	3.34	
98	PFF1330c	mitochondrial import inner membrane translocase subunit, putative	3.34	
99	PF08_0029	hypothetical protein	3.34	Yes
100	PFD0365c	hypothetical protein	3.34	
101	PF14_0410	hypothetical protein	3.34	
102	PFE0295w	hypothetical protein	3.34	
103	PF11_0319	hypothetical protein	3.34	Yes
104	PF13_0183	hypothetical protein	3.34	
105	PFB0470w	hypothetical protein	3.34	
106	PF14_0037	hypothetical protein	3.34	
107	PFA0630c	hypothetical protein	3.34	
108	PFF0820w	hypothetical protein	3.34	

109	PFL2355w	hypothetical pro	3.34	
110	PFB0620w	hypothetical protein	3.34	
111	PFB0560w	hypothetical protein	3.34	
112	PFF0120w	geranylgeranyltransferase, putative	3.34	
113	PF11_0404	malaria antigen	3.34	Yes
114	PFE1605w	DNAJ protein	3.34	
115	PF13_0098	hypothetical protein	3.34	
116	PF14_0312	hypothetical protein	3.34	
117	PF08_0051	hypothetical protein	3.34	Yes
118	PFE0670w	hypothetical protein	3.34	
119	MAL8P1.32	nucleoside transporter, putative	3.34	Yes
120	PFI1415w	Serine/Threonine protein kinase, putative	3.34	
121	PF13_0191	hypothetical protein	3.34	
122	MAL13P1.46	hypothetical protein	3.34	
123	PFI1615c	#N/A	3.34	
124	PF14_0180	hypothetical protein	3.34	
125	PFB0921c	hypothetical protein	3.34	
126	PF14_0687	hypothetical protein	3.34	
127	PFF1335c	4-methyl-5(B-hydroxyethyl)-thiazol monophosphate biosynthesis enzyme	3.34	
128	PFI0430c	hypothetical protein	3.34	
129	PFA0100c	hypothetical protein	3.34	
130	MAL13P1.333	hypothetical protein	3.34	
131	PFE0800w	hypothetical protein	3.34	
132	PFB0110w	hypothetical protein	3.34	
133	PF13_0281	hypothetical protein	3.34	
134	PFC0166w	#N/A	3.34	
135	PF13_0101	hypothetical protein	3.34	
136	PFF0590c	homologue of human HSPC025	3.34	
137	PF13_0252	nucleoside transporter 1	3.34	
138	PF11_0247	hypothetical protein	3.34	
139	PFC0085c	hypothetical protein, conserved	3.34	Yes
140	PF11_0254	hypothetical protein	3.34	
141	PF10_0324	hypothetical protein	3.34	
142	MAL7P1.225	#N/A	3.34	
143	PFF0435w	ornithine aminotransferase	3.34	
144	PFL0640w	hypothetical protein	3.34	
145	PF13_0097	hypothetical protein	3.34	Yes
146	PFB0930w	hypothetical protein	3.34	
147	MAL13P1.352	hypothetical protein	3.34	
148	PFF1400w	hypothetical protein	3.34	
149	PF07_0075	hypothetical protein, expressed	3.34	
150	PF11_0508	hypothetical protein	3.34	Yes
151	PF11_0506	hypothetical protein	3.34	
152	MAL7P1.31	hypothetical protein	3.34	
153	PF13_0071	hypothetical protein	3.34	
154	PF13_0099	hypothetical protein	3.34	
155	MAL7P1.201	#N/A	3.34	
156	PF10_0265	hypothetical protein	3.34	
157	PF10_0029	hypothetical protein	3.34	
158	PF13_0112	hypothetical protein	3.34	
159	PFE0595w	hypothetical protein	3.34	
160	PFA0255c	hypothetical protein	3.34	
161	MAL13P1.274	serine/threonine protein phosphatase pfPp5	3.34	
162	PFI1385c	hypothetical protein	3.34	
163	PF14_0308	hypothetical protein	3.34	
164	PFE1615c	hypothetical protein	3.34	

Nr	PlasmoDB ID	Name	Score	Present in dataset
		AdoMet synthase interactome		
1	PFE1345c	minichromosome maintenance protein 3, putative	11.69	Yes
2	PFB0895c	replication factor C subunit 1, putative	11.69	Yes
3	PFL0835w	GTP-binding protein, putative	8.31	
4	PFI1575c	peptide release factor, putative	8.31	Yes
5	PF13_0095	DNA replication licensing factor mcm4-related	8.31	Yes
6	PF14_0177	DNA replication licensing factor MCM2	8.31	Yes
7	PFB0795w	ATP synthase F1, alpha subunit, putative	8.31	

8	PFE0450w	chromosome cc	7.98	Yes
9	PFD0420c	flap exonuclease, putative	7.98	
10	MAL13P1.96	chromosome segregation protein, putative	7.98	
11	PFD0590c	DNA polymerase alpha	7.98	Yes
12	PFC0745c	proteasome component C8, putative	6.62	
13	PF13_0061	ATP synthase gamma chain, mitochondrial precursor, putative	6.62	
14	PF07_0023	DNA replication licensing factor mcm7 homologue, putative	6.62	Yes
15	MAL8P1.128	proteasome subunit alpha, putative	6.62	
16	PF13_0353	NADH-cytochrome b5 reductase, putative	5.96	Yes
17	MAL8P1.101	hypothetical protein	5.96	Yes
18	PF14_0063	ATP-dependent Clp protease, putative	5.96	
19	PFI0240c	E1-E2_ATPase/hydrolase, putative	5.96	Yes
20	PF11_0249	hypothetical protein	5.96	
21	MAL13P1.244	TBC domain protein, putative	5.96	
22	PFI0530c	DNA primase, large subunit, putative	5.96	Yes
23	PF14_0309	protein-L-isoaspartate O-methyltransferase beta-aspartate	5.96	Yes
24	PFB0750w	vacuolar protein-sorting protein VPS45, putative	5.96	
25	PFB0500c	rab5 protein, putative	5.96	Yes
26	PFI1240c	prolyl-t-RNA synthase, putative	5.96	Yes
27	PF14_0132	ribosomal protein S9, putative	5.96	
28	PFA0345w	centrin, putative	5.96	
29	MAL13P1.196	protein kinase, putative	5.96	
30	MAL8P1.138	hypothetical protein, conserved	5.96	
31	PF11_0352	protein disulfide isomerase related protein	5.96	Yes
32	PFF1190c	N-acetylglucosaminyl- phosphatidylinositol de-n-acetylase, putative	5.90	
33	MAL7P1.203	#N/A	5.90	
34	PFE0240c	hypothetical protein	5.90	Yes
35	PF11_0420	hypothetical protein	5.90	
36	MAL13P1.147	hypothetical protein	5.90	
37	MAL13P1.194	hypothetical protein	5.90	
38	PF11_0425	hypothetical protein	5.90	Yes
39	PFI0665w	hypothetical protein	5.90	
40	MAL13P1.103	hypothetical protein	5.90	Yes
41	MAL13P1.229	hypothetical protein	5.90	
42	PF13_0131	hypothetical protein	5.90	
43	PFD0465c	hypothetical protein, conserved	5.90	
44	PFB0835c	hypothetical protein	5.90	Yes
45	PF14_0351	hypothetical protein	5.90	
46	PF10_0133	hypothetical protein	5.90	
47	PF14_0105	hypothetical protein	5.90	Yes
48	PFL1430c	hypothetical protein	5.90	
49	MAL13P1.217	hypothetical protein	5.90	
50	PFD0175c	hypothetical protein	5.90	
51	PF11_0459	hypothetical protein	5.90	
52	PFB0530c	hypothetical protein	5.90	Yes
53	PF14_0138	hypothetical protein	5.90	Yes
54	PF10_0228	hypothetical protein, conserved	5.90	
55	PFB0170w	hypothetical protein, conserved	5.90	
56	MAL13P1.123	hypothetical protein	5.90	
57	PF10_0246	hypothetical protein	5.90	Yes
58	PFF1470c	DNA polymerase epsilon, catalytic subunit a, putative	5.90	Yes
59	PFF1225c	DNA polymerase 1, putative	5.90	Yes
60	PFC0320w	hypothetical protein	5.90	
61	PFB0590w	hypothetical protein	5.90	Yes
62	PF10_0249	hypothetical protein	5.90	
63	MAL7P1.77	hypothetical protein	5.90	Yes
64	PFE0760w	hypothetical protein	5.90	
65	PFL0265w	hypothetical protein	5.90	
66	PFB0535w	hypothetical protein	5.90	Yes
67	MAL13P1.161	unknown	5.90	
68	PFC0275w	FAD-dependent glycerol-3-phosphate dehydrogenase, putative	4.71	Yes
69	PFI0380c	formylmethionine deformylase, putative	4.71	Yes
70	MAL8P1.140	methionine aminopeptidase, putative	4.71	Yes
71	PF13_0291	replication licensing factor, putative	4.71	Yes
72	PF11_0317	structural maintenance of chromosome protein, putative	4.71	
73	PF13_0328	proliferating cell nuclear antigen	4.71	Yes
74	PF13_0251	DNA topoisomerase III, putative	4.71	
75	PFL0150w	origin recognition complex 1 protein	4.71	Yes

76	PF11_0087	Rad51 homolog	4.71	Yes
77	PFB0840w	replication factor C, subunit 2	4.71	Yes
78	PF14_0053	ribonucleotide reductase small subunit	4.52	Yes
79	PF11_0427	dolichyl-phosphate b-D-mannosyltransferase, putative	4.52	
80	PF11_0348	hypothetical protein	4.52	
81	MAL8P1.17	disulfide isomerase precursor, putative	4.52	
82	PF10_0362	DNA polymerase zeta catalytic subunit, putative	4.52	
83	PF11_0099	heat shock protein DnaJ homologue Pfj2	4.52	
84	MAL13P1.47	mitochondrial ATP synthase delta subunit, putative	4.52	
85	PF07_0105	exonuclease i, putative	4.52	
86	PFI1170c	Thioredoxin reductase	4.52	Yes
87	PF14_0064	vacuolar protein sorting 29, putative	4.52	
88	PFB0385w	acyl carrier protein, putative	4.52	Yes
89	PFL0595c	glutathione peroxidase	4.52	Yes
90	PFD0685c	chromosome associated protein, putative	4.52	Yes
91	PFD0790c	DNA replication licensing factor, putative	4.52	
92	PF13_0272	thioredoxin-related protein, putative	4.52	
93	MAL8P1.142	proteasome beta-subunit	4.52	
94	PF14_0695	DNA-directed RNA polymerase, alpha subunit, truncated, putative	4.52	
95	PFC0170c	dihydrolipoamide acyltransferase, putative	4.52	
96	PF14_0060	hypothetical protein	4.39	
97	PFL0090c	hypothetical protein	4.39	
98	PF14_0641	1-deoxy-D-xylulose 5-phosphate reductoisomerase	4.39	
99	PFB0365w	hypothetical protein, conserved	4.39	Yes
100	PFD0595w	hypothetical protein	4.39	
101	PFD0585c	hypothetical protein	4.39	
102	PF11_0112	vacuolar sorting protein 35, putative	4.39	
103	PF10_0140	hypothetical protein	4.39	
104	PF10_0360	hypothetical protein	4.39	
105	PFI0135c	papain family cysteine protease, putative	4.39	Yes
106	PF14_0252	hypothetical protein	4.39	
107	MAL13P1.105	hypothetical protein	4.39	
108	PFC0525c	glycogen synthase kinase, putative	4.39	
109	PF11_0098	endoplasmic reticulum-resident calcium binding protein	4.39	Yes
110	MAL13P1.42	hypothetical protein	4.39	Yes
111	MAL7P1.132	hypothetical protein	4.39	Yes
112	PF13_0189	hypothetical protein	4.39	Yes
113	PFE0090w	hypothetical protein	4.39	
114	PF14_0148	uracil-DNA glycosylase, putative	4.39	Yes
115	PFE1225w	50S ribosomal subunit protein L12, putative	4.39	
116	PF08_0014	plastid 50S ribosomal protein, putative	4.39	
117	PFC0510w	zinc finger protein, putative	4.39	
118	PF11_0131	hypothetical protein	3.96	
119	PF11_0282	deoxyuridine 5'-triphosphate nucleotidohydrolase, putative	3.38	Yes
120	PFE0270c	DNA repair protein, putative	3.38	Yes
121	PFI1360c	serine/threonine protein phosphatase, putative	3.38	
122	PF08_0126	DNA repair protein rad54, putative	3.38	Yes
123	PFL1180w	Chromatin assembly protein (ASF1), putative	3.38	Yes
124	PF13_0149	chromatin assembly factor 1 subunit, putative	3.38	Yes
125	PF14_0088	hypothetical protein	3.38	
126	PF11_0386	30S ribosomal protein S14, putative	3.38	Yes
127	PF14_0323	calmodulin	3.38	
128	MAL13P1.202	hypothetical protein	3.38	
129	PFI0155c	ras family GTP-ase, putative	3.38	Yes
130	PFC0310c	ATP-dependent CLP protease, putative	3.38	
131	PFC0710w	inorganic pyrophosphatase, putative	3.38	Yes
132	PFL1370w	NIMA-related protein kinase (Pfnek-1)	3.38	
133	PFL0630w	iron-sulfur subunit of succinate dehydrogenase	3.38	
134	PFA0225w	LytB protein	3.38	
135	PF11_0227	hypothetical protein	3.38	
136	PF14_0254	DNA mismatch repair protein Msh2p, putative	3.38	Yes
137	PFD0810w	small GTP-binding protein sar1	3.38	
138	PF07_0078	hypothetical protein, conserved	3.38	Yes
139	PF11_0061	histone H4, putative	3.38	Yes
140	PFC0250c	AP endonuclease (DNA-(apurinic or apyrimidinic site) lyase), putative	3.38	Yes
141	PF11_0145	glyoxalase I, putative	3.38	
142	PFC0955w	ATP-dependent RNA helicase	3.38	
143	PFA0545c	replication factor c protein, putative	3.38	

144	PF14_0142	serine/threonin	3.38	Yes
145	PFE0690c	Rab1 protein	3.38	Yes
146	PF11_0488	hypothetical protein	3.38	
147	PF07_0064	hypothetical protein	3.38	
148	MAL13P1.167	signal peptidase, putative	3.38	
149	PF10_0154	ribonucleotide reductase small subunit, putative	3.38	Yes
150	PF13_0349	nucleoside diphosphate kinase b; putative	3.38	Yes
151	PFB0220w	UbiE-like methlytransferase, putative	3.38	Yes
152	MAL13P1.141	hypothetical protein	3.34	
153	PFF0670w	hypothetical protein	3.34	
154	PFA0250w	hypothetical protein	3.34	
155	MAL13P1.124	hypothetical protein	3.34	
156	PF13_0249	hypothetical protein	3.34	
157	PF14_0488	hypothetical protein	3.34	Yes
158	PF10_0291	hypothetical protein	3.34	Yes
159	PFE0710w	hypothetical protein	3.34	
160	PFI0990c	hypothetical protein	3.34	
161	PF14_0435	hypothetical protein	3.34	
162	PFL0085c	hypothetical protein	3.34	
163	PFC1035w	hypothetical protein	3.34	
164	PF13_0336	hypothetical protein	3.34	
165	PFD0330w	hypothetical protein	3.34	
166	PFF1485w	hypothetical protein	3.34	
167	PFL2300w	hypothetical protein	3.34	
168	MAL13P1.336	hypothetical protein	3.34	
169	PF14_0153	hypothetical protein	3.34	
170	PF11_0448	hypothetical protein	3.34	
171	PF10_0236	hypothetical protein	3.34	
172	PFL0680c	hypothetical protein	3.34	
173	MAL13P1.307	hypothetical protein	3.34	Yes
174	PF11_0195	hypothetical protein	3.34	
175	MAL7P1.111	hypothetical protein	3.34	
176	PF13_0312	hypothetical protein	3.34	
177	PF11_0146	hypothetical protein	3.34	Yes
178	PFE0265c	hypothetical protein	3.34	Yes
179	PF14_0310	hypothetical protein	3.34	
180	PFI1665w	uncharacterised trophozoite protein	3.34	Yes
181	PFD0335c	hypothetical protein	3.34	
182	PF10_0164	hypothetical protein	3.34	
183	PF14_0445	hypothetical protein	3.34	
184	PF14_0666	hypothetical protein	3.34	
185	PFC0315c	hypothetical protein	3.34	Yes
186	PF11_0484	hypothetical protein	3.34	
187	PF10_0207	hypothetical protein	3.34	
188	PFF0940c	cell division cycle protein 48 homologue, putative	3.34	
189	PF14_0380	hypothetical protein	3.34	
190	PF11_0333	hypothetical protein	3.34	
191	PF13_0246	hypothetical protein	3.34	
192	PF11_0054	hypothetical protein	3.34	
193	PFE0490w	hypothetical protein	3.34	
194	PF13_0338	hypothetical protein	3.34	Yes
195	MAL13P1.57	hypothetical protein	3.34	Yes
196	MAL7P1.128	hypothetical protein	3.34	
197	PFD0655c	ubiquitin carboxyl-terminal hydrolase a, putative	3.34	
198	PFL2360w	hypothetical protein	3.34	
199	MAL13P1.311	hypothetical protein	3.34	
200	PF10_0050	hypothetical protein	3.34	
201	PF14_0444	hypothetical protein	3.34	
202	PFF0765c	hypothetical protein	3.34	
203	PFD0760c	hypothetical protein	3.34	
204	MAL13P1.160	unknown	3.34	
205	PF11_0075	hypothetical protein	3.34	
206	PFF0740c	hypothetical protein	3.34	
207	PF14_0270	ribosomal protein L15, putative	3.34	
208	PF14_0665	hypothetical protein	3.34	
209	PF08_0010	hypothetical protein	3.34	
210	PF14_0613	hypothetical protein	3.34	
211	PFI0565w	hypothetical protein	3.34	

212	PFF0650w	ribosomal prote	3.34	Yes
213	PFF0680c	thiamin-phosphate pyrophosphorylase, putative	3.34	Yes
214	PF14_0268	hypothetical protein	3.34	
215	PF10_0191	hypothetical protein	3.34	
216	PFE1025c	hypothetical protein	3.34	
217	PFL0615w	hypothetical protein	3.34	
218	PF14_0315	hypothetical protein	3.34	
219	PF11_0451	hypothetical protein	3.34	
220	PF14_0300	syntaxin, putative	3.34	
221	MAL13P1.131	hypothetical protein	3.34	
222	PFL0375w	hypothetical protein	3.34	
223	PFD0805w	prohibitin-like protein, putative	3.34	
224	MAL8P1.84	hypothetical protein	3.34	
225	PF14_0617	hypothetical protein	3.34	Yes
226	PFA0370w	hypothetical protein	3.34	
227	PFI0405w	hypothetical protein	3.34	Yes
228	PF14_0306	hypothetical protein	3.34	
229	PF13_0154	hypothetical protein	3.34	
230	MAL7P1.102	hypothetical protein	3.34	Yes
231	PFF0330w	coatomer alpha subunit, putative	3.34	
232	PFI0830c	hypothetical protein	3.34	
233	PFE1330c	hypothetical protein	3.34	
234	PF13_0333	hypothetical protein	3.34	
235	PFD0915w	hypothetical protein	3.34	
236	PFF0665c	syntaxin binding protein, putative	3.34	
237	PFE1165c	hypothetical protein	3.34	
238	PF14_0245	hypothetical protein	3.34	
239	PFI1525w	hypothetical protein	3.34	
240	PFL2045w	hypothetical protein	3.34	
241	PFI0160w	hypothetical protein	3.34	
242	PFE1280w	hypothetical protein	3.34	Yes
243	PFA0405w	hypothetical protein	3.34	
244	PFD0170c	hypothetical protein	3.34	
245	PF13_0155	hypothetical protein	3.34	
246	MAL7P1.74	hypothetical protein, conserved	3.34	
247	PF11_0440	hypothetical protein	3.34	
248	PF13_0200	hypothetical protein	3.34	Yes
249	PFC0500w	hypothetical protein	3.34	
250	PF10_0188	hypothetical protein	3.34	Yes
251	PF13_0188	hypothetical protein	3.34	
252	PF14_0169	hypothetical protein	3.34	
253	PFL0720w	hypothetical protein	3.34	
254	PF11_0324	hypothetical protein	3.34	
255	PF11_0482	hypothetical protein	3.34	
256	PFL1330c	hypothetical protein	3.34	Yes
257	PF11_0435	hypothetical protein	3.34	

Appendix D

Transcripts shared between the AdoMetDC inhibited transcriptome dataset, SpdS inhibition and the co-inhibition of AdoMetDC/ODC

Totall	Nr	PlasmoDB ID	Product Description	Fold change		
				AdoMetDC	A/O	SpdS
			DNA metabolism			
1	1	PF10_0154	ribonucleotide reductase small subunit, putative	-5.4	-1.5	-4.2
2	2	PF11_0087	Rad51 homolog	-1.7	-1.6	-3.5
3	3	PF11_0117	replication factor C subunit 5, putative	-1.8	-1.8	-4.5
4	4	PF11_0241	Myb-like DNA-binding domain, putative	1.7	1.8	2.1
5	5	PF11_0282	deoxyuridine 5'-triphosphate nucleotidohydrolase,	-6.3	-2.9	-2.8
6	6	PF13_0095	DNA replication licensing factor MCM4-related	-3.1	-1.4	
7	7	PF13_0291	replication licensing factor, putative	-2.5	-1.2	-3.5
8	8	PF13_0328	proliferating cell nuclear antigen	-5.7	-1.9	-4.2
9	9	PF14_0053	ribonucleotide reductase small subunit	-3.9	-1.4	-5.0
10	10	PF14_0254	DNA mismatch repair protein Msh2p, putative	-1.9	-1.4	-2.0
11	11	PF14_0366	small subunit DNA primase	-1.7		-2.1
12	12	PF14_0374	CCAAT-binding transcription factor, putative	1.7	2.1	
13	13	PFB0840w	replication factor C, subunit 2	-3.4		-2.8
14	14	PFB0895c	replication factor C subunit 1, putative	-1.9	-1.2	-2.7
15	15	PFD0685c	chromosome associated protein, putative	-2.0	-2.0	-2.0
16	16	PFE0215w	ATP-dependent helicase, putative	-1.7		-2.6
17	17	PFE0450w	chromosome condensation protein, putative	-2.6		-2.5
18	18	PFE0675c	deoxyribodipyrimidine photolyase (photoreactivating	-2.8	-1.5	-4.3
19	19	PFE1345c	minichromosome maintenance protein 3, putative	-2.3		-2.0
20	20	PFF1470c	DNA polymerase epsilon, catalytic subunit a, putative	-1.8	-1.5	
21	21	PFI0530c	DNA primase large subunit, putative	-3.8	-1.2	
22	22	PFL0580w	DNA replication licensing factor MCM5, putative	-3.7		-3.5
23	23	PFL1180w	chromatin assembly protein (ASF1), putative	-2.2		-2.4
24	24	PFL1285c	proliferating cell nuclear antigen 2	-2.7		-2.1
25	25	PFL1655c	DNA polymerase epsilon subunit B, putative	-2.1	-2.2	-2.2
26	26	PFL2005w	replication factor C subunit 4	-4.0		-3.8
			Proteolysis			
27	1	MAL8P1.113	Peptidase family C50, putative	-1.7	-1.6	
28	2	MAL8P1.99	GTPase, putative	-2.1	-2.2	-3.6
29	3	PF14_0348	ATP-dependent Clp protease proteolytic subunit,	-2.0	-1.6	
30	4	PFI0135c	serine repeat antigen 9 (SERA-9)	-5.6	-1.7	-4.0
31	5	PFL1465c	Heat shock protein hslv	-2.0		-2.5
			Translation			
32	1	MAL8P1.110	apicoplast ribosomal protein L33 precursor, putative	-1.9		-2.9
33	2	PF11_0113	mitochondrial ribosomal protein L11 precursor, putative	-2.0		-2.1
34	3	PF11_0181	tyrosine-tRNA ligase, putative	-1.9	-1.4	
35	4	PF11_0182	conserved Plasmodium protein, unknown function	-1.9	-1.9	
36	5	PF11_0386	apicoplast ribosomal protein S14p/S29e precursor,	-2.0		-2.6
37	6	PF14_0606	mitochondrial ribosomal protein S6-2 precursor,	-2.2	-1.7	
38	7	PF14_0709	mitochondrial ribosomal protein L20 precursor, putative	-2.1	-1.9	-2.4
39	8	PFC0675c	mitochondrial ribosomal protein L29/L47 precursor,	-1.9		-2.4
40	9	PFD0780w	glutamyl-tRNA(Gln) amidotransferase subunit A,	-2.0		-3.9
41	10	PFF0495w	mitochondrial ribosomal protein L19 precursor, putative	-2.0		-2.0
42	11	PFF0650w	apicoplast ribosomal protein L18 precursor, putative	-1.9		-2.6
43	12	PFI0380c	formylmethionine deformylase, putative	-1.8		-2.2
44	13	PFI0890c	organelle ribosomal protein L3 precursor, putative	-2.2	-1.6	-2.7
45	14	PFI1240c	prolyl-t-RNA synthase, putative	-2.8	-1.8	
46	15	PFI1585c	mitochondrial ribosomal protein S6 precursor, putative	-1.8	1.8	
47	16	PFL1895w	mitochondrial ribosomal protein L23 precursor, putative	-1.7		-3.0
			Phosphorylation			
48	1	PF13_0258	serine/threonine protein kinase	-2.5		2.2
49	2	PFA0130c	Serine/Threonine protein kinase, FIKK family, putative	2.3	1.8	
50	3	PFC0710w	inorganic pyrophosphatase, putative	-2.6		-2.2
51	4	PFC0755c	protein kinase, putative	-2.1		-2.1
52	5	PFD1165w	Serine/Threonine protein kinase, FIKK family	2.0	-2.0	

53	6	PFD1175w	Serine/Threonine protein kinase, FIKK family	2.4	1.7	2.5
54	7	PFF1370w	protein kinase PK4	1.7		2.0
55	8	PFL1110c	CAMP-dependent protein kinase regulatory subunit,	-2.1		-3.8
56	9	PFL1885c	calcium/calmodulin-dependent protein kinase 2	2.2	2.3	2.4
			Transport			
57	1	MAL13P1.23	CorA-like Mg2+ transporter protein, putative	1.8		2.0
58	2	MAL8P1.32	nucleoside transporter, putative	-2.8	-1.5	-3.0
59	3	PF07_0065	zinc transporter, putative	-4.8	-2.2	-3.4
60	4	PF14_0211	Ctr copper transporter domain containing protein,	-2.3		-3.4
61	5	PF14_0662	nucleoside transporter, putative	1.8	1.8	
62	6	PFA0590w	ABC transporter, (CT family), putative	-2.4	-1.7	
63	7	PFB0500c	Rab5a, GTPase	-1.7		-2.1
64	8	PFC0125w	ABC transporter, (TAP family), putative	-1.9	-1.9	-2.1
65	9	PFE0410w	triose phosphate transporter	-1.7	-1.9	-2.5
66	10	PFE1510c	triose phosphate transporter	-2.5		-3.2
67	11	PFI0240c	Cu2+ -transporting ATPase, Cu2+ transporter	-1.9		-4.4
68	12	PFI0300w	developmental protein, putative	-3.2		-2.7
69	13	PFL2220w	conserved Plasmodium protein, unknown function	1.7		3.3
			Polyamine methionine metabolism			
70	1	MAL13P1.214	phosphoethanolamine N-methyltransferase	-5.1	-2.7	-3.4
71	2	PF10_0289	adenosine deaminase, putative	-3.1	-2.4	-2.3
72	3	PF14_0309	protein-L-isoaspartate O-methyltransferase beta-	-3.9	-1.8	
73	4	PF14_0526	conserved Plasmodium protein, unknown function	-3.1	-2.1	-2.0
74	5	PFD0285c	lysine decarboxylase, putative	2.5	2.8	2.4
75	6	PFE0660c	purine nucleotide phosphorylase, putative	-3.0	-2.7	-3.6
76	7	PFE1050w	adenosylhomocysteinase(S-adenosyl-L-homocystein e	-2.1	-1.5	-1.0
77	8	PFI1090w	S-adenosylmethionine synthetase	-2.3	-1.5	-1.0
			Oxidative stress			
78	1	PF08_0131	1-cys peroxiredoxin	-2.7	-2.8	-4.5
79	2	PF14_0187	glutathione S-transferase	-1.8	-1.5	-2.1
80	3	PF14_0192	glutathione reductase	-2.2	-1.7	-2.6
81	4	PF13_0353	NADH-cytochrome B5 reductase, putative	-2.1		-2.4
82	5	PFI1170c	thioredoxin reductase	-1.9		-3.1
			Primary metabolism			
83	1	MAL8P1.81	Phosphopantothenoylcysteine decarboxylase, putative	1.9		3.1
84	2	PF07_0129	acyl-coA synthetase, PfACS5	-1.9	-1.6	-3.9
85	3	PF10_0016	acyl CoA binding protein, isoform 2, ACBP2	-3.0	-1.5	-6.3
86	4	PF10_0155	enolase	-2.7	-2.0	
87	5	PF10_0334	flavoprotein subunit of succinate dehydrogenase	-1.8		-3.1
88	6	PF11_0257	ethanolamine kinase, putative	-2.5	-1.4	-4.6
89	7	PF13_0121	dihydrolipamide succinyltransferase component of 2-	-2.6	-1.7	-2.5
90	8	PF13_0141	L-lactate dehydrogenase	-1.9	-1.5	-2.4
91	9	PF13_0242	isocitrate dehydrogenase (NADP), mitochondrial	-2.2		-2.1
92	10	PF13_0349	nucleoside diphosphate kinase b, putative	-3.5	-1.9	-4.4
93	11	PF14_0378	triosephosphate isomerase	-1.7	-1.1	
94	12	PFB0385w	apicoplast ACP	-2.6		-2.7
95	13	PFD0830w	bifunctional dihydrofolate reductase-thymidylate	-4.9	-1.6	-2.2
96	14	PFE0555w	stearoyl-CoA Delta 9 desaturase, putative	-3.6	-1.5	-2.9
97	15	PFF1300w	pyruvate kinase	-1.7	-1.5	-2.2
98	16	PF10_0084	tubulin beta chain, putative	-5.2	-1.3	-4.6
99	17	PF14_0314	chromatin assembly factor 1 P55 subunit, putative	2.0	2.4	
100	18	PFA0520c	chromatin assembly factor 1 protein WD40 domain,	-4.7	-1.6	
101	19	PFE0165w	actin-depolymerizing factor, putative	-2.2	-2.0	-2.5
102	20	PFI0180w	alpha tubulin	-7.3	-1.5	-4.5
103	21	PFI1565w	profilin, putative	-3.0	-2.0	-2.2
104	22	PFL0925w	formin 2, putative	2.0	1.9	
105	23	PFL2215w	actin I	-2.5		-2.3
			RNA metabolic process			
106	1	MAL13P1.303	polyadenylate-binding protein, putative	-4.1	-1.3	-3.1
107	2	MAL8P1.101	RNA binding protein, putative	-1.7		-2.8
108	3	PF08_0096	RNA helicase, putative	-1.7	-1.8	
109	4	PFF1425w	RNA binding protein, putative	-2.1		-2.8
110	5	PFL0465c	Zinc finger transcription factor (krox1)	1.8	2.0	
111	6	PFL2115c	glucose inhibited division protein A homologue, putative	-2.9	-1.3	
			Protein folding			
112	1	PFB0920w	DNAJ protein, putative	2.4		2.2
113	2	PFL2550w	DNAJ domain protein, putative	-2.0	-2.2	-2.2
			Signal transduction			

114	1	MAL13P1.165	GPI tran	-1.7		-2.0
115	2	MAL13P1.19	peptidase, putative	-2.4	-2.1	-1.0
116	3	PFE0690c	PfRab1a	-1.8	-3.2	-5.2
117	4	PFI0155c	PfRab7, GTPase	-1.7		-2.5
			Coenzyme metabolic process			
118	1	PF14_0200	pantothenate kinase, putative	-1.7		-2.2
119	2	PF14_0415	dephospho-CoA kinase, putative	-2.6	-1.4	-2.5
120	3	PF14_0570	pyridoxal 5'-phosphate synthase, putative	-2.3	-2.2	-2.5
121	4	PFL1725w	ATP synthase beta chain, mitochondrial precursor,	-2.1		-3.2
			Hydrolase activity			
122	1	MAL13P1.121	adenosine-diphosphatase	-1.8		-2.2
123	2	PF14_0015	aminopeptidase, putative	2.5	1.3	2.3
124	3	PF14_0017	lysophospholipase, putative	2.4		2.9
			Binding activity			
125	1	MAL13P1.122	SET domain protein, putative	1.7		3.1
126	2	PF07_0035	cg1 protein	-2.7		-2.3
127	3	PF14_0061	PPR repeat protein	-1.9	-1.6	-3.2
128	4	PF14_0257	conserved protein, unknown function	-2.9	-1.8	-2.4
129	5	PF14_0443	centrin-2	-4.9	-1.6	-2.0
130	6	PFD0440w	peptidase, M22 family, putative	-2.7	-1.8	-2.4
131	7	PFF1440w	SET domain protein, putative	1.9		2.1
132	8	PFI0235w	replication factor A-related protein, putative	-2.1	-1.8	-4.0
133	9	PFI0490c	ran-binding protein, putative	-1.7	-1.8	2.5
134	10	PFI0855w	conserved Plasmodium protein, unknown function	-2.0	-2.0	
			Host parasite			
135	1	MAL13P1.176	reticulocyte binding protein 2, homolog b	1.9	2.1	
136	2	PFF0020c	erythrocyte membrane protein 1 (PfEMP1)-like protein	1.7		3.4
137	3	PFL1420w	macrophage migration inhibitory factor homologue	-2.1	-2.0	-2.3
138	4	PFL1955w	erythrocyte membrane protein 1, PfEMP1	1.7		2.3
			Hypotheticals			
139	1	PF08_0060	asparagine-rich antigen	2.2	2.4	2.4
140	2	PF10_0188	conserved Plasmodium membrane protein, unknown	-2.6		-2.6
141	3	PF10_0195	kinesin, putative	-1.8		-3.2
142	4	PF10_0246	conserved Plasmodium protein, unknown function	-2.2		-2.4
143	5	PF11_0215	conserved Plasmodium protein, unknown function	-2.6	-1.3	-5.0
144	6	PF11_0231	conserved Plasmodium protein, unknown function	1.8		2.5
145	7	PF11_0321	serpentine receptor, putative	2.0		2.1
146	8	PF13_0011	plasmodium falciparum gamete antigen 27/25	-2.4	-3.9	-2.8
147	9	PF14_0014	Plasmodium exported protein, unknown function	-1.8		-2.5
148	10	PF14_0018	Plasmodium exported protein (PHISTb), unknown	2.3		2.2
149	11	PF14_0045	conserved Plasmodium protein, unknown function	2.1		3.4
150	12	PF14_0105	conserved Plasmodium protein, unknown function	-2.3		-3.2
151	13	PF14_0297	apyrase, putative	-2.0	-1.5	-2.1
152	14	PF14_0329	conserved protein, unknown function	-2.0	-2.1	-3.0
153	15	PF14_0680	conserved Plasmodium protein, unknown function	-3.1	-1.3	
154	16	PF14_0758	Plasmodium exported protein (hyp17), unknown	1.7	1.2	
155	17	PFB0075c	Plasmodium exported protein (hyp9), unknown function	1.8		3.9
156	18	PFB0365w	conserved Plasmodium protein, unknown function	-1.7		-2.9
157	19	PFB0590w	conserved Plasmodium protein, unknown function	-2.2	-2.1	
158	20	PFB0923c	Plasmodium exported protein, unknown function	2.5	2.1	2.2
159	21	PFB0953w	Plasmodium exported protein (hyp15), unknown	-1.8	-1.3	-3.9
160	22	PFC0730w	HVA22/TB2/DP1 family protein, putative	-1.9	-1.7	-2.7
161	23	PFL0130c	conserved Plasmodium protein, unknown function	1.9		2.1
162	24	PFL1330c	cyclin-related protein, Pfcyc-2	-2.7		
163	25	PFL2240w	conserved Plasmodium protein, unknown function	-2.2	-1.5	-2.3
164	26	PF10_0039	membrane skeletal protein IMC1-related	2.1	1.7	
165	27	PFL0685w	Phosphatidylinositol-glycan biosynthesis class O protein,	-1.9	-1.5	-2.3
166	28	MAL13P1.180	conserved Plasmodium protein, unknown function	-1.8		-2.2
167	29	MAL13P1.193	conserved Plasmodium protein, unknown function	-2.9	-1.4	-3.0
168	30	MAL13P1.293	conserved Plasmodium protein, unknown function	1.8		2.6
169	31	MAL13P1.298	conserved Plasmodium membrane protein, unknown	1.7		2.1
170	32	MAL13P1.332	conserved Plasmodium protein, unknown function	-0.5		-2.2
171	33	MAL13P1.57	conserved Plasmodium protein, unknown function	-1.8		-2.9
172	34	MAL7P1.173	Plasmodium exported protein, unknown function	1.8	-3.0	
173	35	MAL7P1.33	conserved Plasmodium protein, unknown function	-2.6	-1.6	-2.2
174	36	MAL7P1.61	null	1.7	-1.8	2.4
175	37	MAL7P1.77	conserved Plasmodium protein, unknown function	-2.6	-2.2	
176	38	MAL8P1.2	Plasmodium exported protein (PHISTb), unknown	2.1		2.1

177	39	MAL8P1.53	conserv ion	-3.7	-1.4	
178	40	MAL8P1.82	Vacuolar sorting protein VPS9, putative	1.8	1.8	
179	41	MAL8P1.86	Sel3 protein	-2.4	-1.7	
180	42	PF07_0039	conserved Plasmodium protein, unknown function	-1.8		-2.8
181	43	PF07_0087	conserved Plasmodium protein, unknown function	-2.5	-1.3	-3.4
182	44	PF07_0106	conserved Plasmodium protein, unknown function	1.9		2.6
183	45	PF08_0001	Plasmodium exported protein, unknown function	2.2	1.7	
184	46	PF08_0029	conserved Plasmodium protein, unknown function	-2.1		-3.7
185	47	PF08_0051	conserved Plasmodium protein, unknown function	-2.0	-1.7	
186	48	PF10_0020	alpha/beta hydrolase, putative	-4.1	-2.5	-6.3
187	49	PF10_0034	conserved Plasmodium protein, unknown function	2.3		-2.0
188	50	PF10_0243	conserved Plasmodium protein, unknown function	-1.7	-1.7	
189	51	PF10_0253	conserved Plasmodium protein, unknown function	-1.7	-2.0	-5.6
190	52	PF10_0286	conserved Plasmodium protein, unknown function	-2.3	-1.7	
191	53	PF10_0307	conserved Plasmodium protein, unknown function	2.4	2.1	
192	54	PF11_0035	Plasmodium exported protein, unknown function	1.7	2.4	-2.1
193	55	PF11_0371	conserved Plasmodium protein, unknown function	-2.1		2.1
194	56	PF11_0404	transcription factor with AP2 domain(s), putative	1.9		2.0
195	57	PF11_0425	conserved Plasmodium protein, unknown function	-2.3	-1.5	-2.2
196	58	PF11_0508	Plasmodium exported protein, unknown function	-2.2	-2.5	-2.5
197	59	PF13_0097	transcription factor with AP2 domain(s), putative	1.7		2.3
198	60	PF13_0192	conserved Plasmodium protein, unknown function	-4.2	-1.7	-8.1
199	61	PF13_0267	conserved Plasmodium protein, unknown function	1.7	1.8	4.8
200	62	PF13_0296	splicing factor 3b subunit, putative	-1.8	-1.8	
201	63	PF13_0338	cysteine-rich surface protein	-1.8		-2.1
202	64	PF14_0031	conserved Plasmodium protein, unknown function	-2.8		3.5
203	65	PF14_0101	conserved Plasmodium protein, unknown function	-1.8		2.0
204	66	PF14_0186	conserved Plasmodium protein, unknown function	-2.0	-1.2	-3.7
205	67	PF14_0402	conserved Plasmodium protein, unknown function	1.8	2.1	2.8
206	68	PF14_0430	mitochondrial ribosomal protein S29 precursor, putative	-1.8	-1.7	-1.0
207	69	PF14_0488	conserved Plasmodium protein, unknown function	-1.7		-2.7
208	70	PF14_0631	conserved Plasmodium protein, unknown function	1.7		2.0
209	71	PF14_0703	conserved Plasmodium protein, unknown function	2.2		3.3
210	72	PF14_0705	conserved Plasmodium protein, unknown function	-2.2		-2.2
211	73	PF14_0706	conserved Plasmodium protein, unknown function	1.8		2.2
212	74	PFA0115w	Plasmodium exported protein, unknown function	-3.2	-2.7	
213	75	PFA0245w	transporter, putative	-3.8	-1.3	
214	76	PFB0115w	conserved Plasmodium protein, unknown function	3.2	3.3	4.0
215	77	PFB0530c	conserved Plasmodium protein, unknown function	-2.2		-3.2
216	78	PFB0535w	GDP-fructose:GMP antiporter, putative	-2.9	-2.1	-3.0
217	79	PFB0835c	conserved Plasmodium protein, unknown function	-4.3	-1.6	-2.8
218	80	PFC0085c	Plasmodium exported protein, unknown function	1.8	1.7	2.1
219	81	PFC0262c	conserved Plasmodium protein, unknown function	-3.5		-2.4
220	82	PFC0571c	conserved Plasmodium protein, unknown function	-1.9		-3.1
221	83	PFC0590c	DER1-like protein, putative	-2.6	-1.5	
222	84	PFC0912w	signal peptidase, putative	-3.2	-1.5	-3.7
223	85	PFD0080c	Plasmodium exported protein (PHISTb), unknown	-1.9	-1.7	
224	86	PFD0225w	conserved Plasmodium membrane protein, unknown	-2.0	-2.2	
225	87	PFD0495c	conserved Plasmodium protein, unknown function	1.8		2.2
226	88	PFD0545w	conserved Plasmodium protein, unknown function	1.8		3.1
227	89	PFD0670c	lysine decarboxylase-like protein, putative	-2.0	-1.6	-3.1
228	90	PFD0850c	Memo-like protein	-2.2		-2.0
229	91	PFD0920w	conserved Plasmodium protein, unknown function	-1.9		2.3
230	92	PFD1140w	Plasmodium exported protein (PHISTc), unknown	2.1	1.3	
231	93	PFE0345c	conserved Plasmodium protein, unknown function	-1.7	-2.1	-2.5
232	94	PFE0500c	conserved Plasmodium protein, unknown function	-2.5	-1.8	-2.3
233	95	PFE1280w	conserved Plasmodium protein, unknown function	-2.2		-2.2
234	96	PFE1610w	Plasmodium exported protein, unknown function	2.0	1.8	
235	97	PFF0480w	conserved Plasmodium protein, unknown function	2.0		2.2
236	98	PFF0630c	conserved Plasmodium protein, unknown function	-4.0	-2.1	
237	99	PFF0935c	conserved Plasmodium protein, unknown function	-2.3	-1.7	
238	100	PFI0210c	cysteine repeat modular protein, putative	-1.9	-1.9	
239	101	PFI0405w	conserved Plasmodium protein, unknown function	-2.2		-4.1
240	102	PFI0880c	glideosome-associated protein 50	-2.8	-1.3	-2.2
241	103	PFI0975c	conserved Plasmodium protein, unknown function	-1.9	1.7	
242	104	PFI1520w	asparagine-rich antigen, putative	2.0		3.4
243	105	PFI1665w	transcription factor with AP2 domain(s), putative	-1.9		-2.2
244	106	PFI1770w	Plasmodium exported protein (PHISTb), unknown	1.9	-1.8	

245	107	PFI1780w	Plasmoc vn	2.5		2.2
246	108	PFL0280c	histone binding protein, putative	-1.7	-1.4	-2.2
247	109	PFL1040w	conserved Plasmodium protein, unknown function	-1.7		-3.5
248	110	PFL1300c	conserved Plasmodium protein, unknown function	-1.7	-0.6	
249	111	PFL1645w	conserved Plasmodium protein, unknown function	1.7	1.6	2.1
250	112	PFL1900w	transcription factor with AP2 domain(s), putative	-2.7	-1.4	-4.9
251	113	PFL2535w	Plasmodium exported protein (PHISTb), unknown	-2.7	-1.5	
252	114	PFE0685w	#N/A	-2.6	-1.9	-3.5

Appendix E

Unique transcripts found only with the inhibition of AdoMetDC

Nr	PlasmoDB ID	Product Description	FC
		DNA metabolism	
1	MAL13P1.328	DNA topoisomerase VI, B subunit, putative	2.8
2	PF14_0053	ribonucleotide reductase small subunit	-3.9
3	PFL1180w	chromatin assembly protein (ASF1), putative	-2.2
		Proteolysis	
4	PF13_0084	ubiquitin-like protein, putative	1.7
5	PF14_0348	ATP-dependent Clp protease proteolytic subunit, putative	-2.0
		Translation	
6	PF11_0113	mitochondrial ribosomal protein L11 precursor, putative	-2.0
7	PFC0675c	mitochondrial ribosomal protein L29/L47 precursor, putative	-1.9
8	PFC0701w	mitochondrial ribosomal protein L27 precursor, putative	-2.5
9	PFD0675w	apicoplast ribosomal protein L10 precursor, putative	-2.9
10	PFF0495w	mitochondrial ribosomal protein L19 precursor, putative	-2.0
11	PFL1150c	mitochondrial ribosomal protein L24-2 precursor, putative	-1.7
12	PFL1895w	mitochondrial ribosomal protein L23 precursor, putative	-1.7
		Phosphorylation	
13	PFC0485w	protein kinase, putative	-1.7
14	PFF0260w	serine/threonine protein kinase, Pfnek-5	-1.7
		Transport	
15	MAL13P1.16	SNARE protein, putative	-2.2
		polyamine methionine metabolism	
16	MAL13P1.214	phosphoethanolamine N-methyltransferase	-5.1
17	PF13_0016	methyl transferase-like protein, putative	-1.9
18	PF14_0526	conserved Plasmodium protein, unknown function	-3.1
		Primary metabolism	
19	MAL13P1.220	lipoate synthase, putative	-1.7
20	PFB0505c	3-oxoacyl-(acyl carrier protein) synthase III, putative	-2.1
21	PFI0960w	dolichyl-diphosphooligosaccharide-protein glycosyltransferase, putative	-1.7
		Cytoskeleton organization and biogenesis	
22	PF11_0478	kinesin-like protein, putative	2.1
		RNA metabolic process	
23	MAL8P1.72	high mobility group protein	-1.7
24	PF10_0313	mitochondrial preribosomal assembly protein rimM precursor, putative	-1.9
25	PF13_0043	CCAAT-binding transcription factor, putative	-1.8
26	PFD0750w	nuclear cap-binding protein, putative	-1.8
		Signal transduction	
27	PF14_0317	Microsomal signal peptidase protein, putative	-1.7
		Coenzyme metabolic process	
28	MAL7P1.130	3-demethylubiquinone-9 3-methyltransferase, putative	-1.7
29	PF14_0570	pyridoxal 5'-phosphate synthase, putative	-2.3
		Host parasite	
30	PF07_0138	rifin	-2.1
31	PFF0010w	erythrocyte membrane protein 1, PfEMP1	-2.4
32	PFF0020c	erythrocyte membrane protein 1 (PfEMP1)-like protein	1.7
		Hypotheticals	
33	PF11_0046	CPW-WPC family protein	-1.8
34	PF11_0355	conserved Plasmodium protein, unknown function	-3.4
35	PF14_0297	apyrase, putative	-2.0
36	PF14_0498	Degradation in the ER (DER1) like protein, putative	-2.0
37	PF14_0698	conserved Plasmodium protein, unknown function	2.5
38	PFB0953w	Plasmodium exported protein (hyp15), unknown function	-1.8

39	PFF1535w	Plasmod...own function	1.9
40	PFL0065w	conserved Plasmodium protein, unknown function	1.7
41	PFL1685w	conserved Plasmodium protein, unknown function	-2.4
42	PFL2455w	conserved Plasmodium protein, unknown function	1.8
43	MAL13P1.307	conserved Plasmodium protein, unknown function	-2.6
44	MAL13P1.188	conserved Plasmodium protein, unknown function	1.8
45	MAL13P1.251	conserved Plasmodium protein, unknown function	-3.5
46	MAL7P1.124	conserved Plasmodium protein, unknown function	-2.2
47	MAL7P1.173	Plasmodium exported protein, unknown function	1.8
48	MAL7P1.23	RAP protein, putative	-1.7
49	MAL7P1.230	hypothetical protein, pseudogene	1.7
50	MAL7P1.33	conserved Plasmodium protein, unknown function	-2.6
51	MAL7P1.61	conserved Plasmodium protein, unknown function	1.7
52	MAL8P1.206	Plasmodium exported protein, unknown function	-3.0
53	MAL8P1.216	rifin	-2.4
54	PF08_0030	conserved Plasmodium protein, unknown function	-2.5
55	PF08_0134	conserved Plasmodium protein, unknown function	-1.9
56	PF10_0034	conserved Plasmodium protein, unknown function	2.3
57	PF10_0258	conserved Plasmodium protein, unknown function	1.9
58	PF11_0514	Plasmodium exported protein (PHISTa), unknown function	2.0
59	PF11_0560	conserved protein, unknown function	-1.9
60	PF14_0226	conserved Plasmodium protein, unknown function	1.7
61	PF14_0488	conserved Plasmodium protein, unknown function	-1.7
62	PF14_0502	conserved Plasmodium protein, unknown function	-1.8
63	PF14_0705	conserved Plasmodium protein, unknown function	-2.2
64	PF14_0760	Plasmodium exported protein, unknown function	2.0
65	PFB0970c	Plasmodium exported protein, unknown function	1.7
66	PFB0973c	hypothetical protein	1.8
67	PFC0990c	conserved Plasmodium protein, unknown function	1.7
68	PFD0550c	conserved Plasmodium protein, unknown function	-2.1
69	PFD0655w	conserved Plasmodium protein, unknown function	-1.7
70	PFD0920w	conserved Plasmodium protein, unknown function	-1.9
71	PFD1140w	Plasmodium exported protein (PHISTc), unknown function	2.1
72	PFE1610w	Plasmodium exported protein, unknown function	2.0
73	PFF0075c	Plasmodium exported protein (PHISTb), unknown function	1.8
74	PFF0545c	conserved Plasmodium protein, unknown function	-2.0
75	PFF0630c	conserved Plasmodium protein, unknown function	-4.0
76	PFF0640w	conserved Plasmodium protein, unknown function	-3.1
77	PFF0725w	conserved Plasmodium protein, unknown function	1.7
78	PFF1005w	conserved Plasmodium protein, unknown function	1.8
79	PFF1160w	conserved Plasmodium protein, unknown function	-1.7
80	PFF1290c	conserved Plasmodium protein, unknown function	-1.7
81	PFI1630c	conserved Plasmodium protein, unknown function	-2.1
82	PFI1690c	conserved Plasmodium protein, unknown function	2.0
83	PFE0685w	conserved Plasmodium protein, unknown function	-2.6